# Optimisation of DNA vector activity and delivery for improved vaccination




Johanna K. Hettinga

Lincoln College

*Supervised by*

Prof. Robert C. Carlisle

Department of Engineering Science

University of Oxford

*A thesis presented for the degree of Doctor of Philosophy*

## Abstract

DNA-based vaccines represent a powerful technology that could be well-suited to the quick development and rapid, large-scale production needed for effective response to rapidly emerging or mutating pathogens. However, DNA vaccines have not yet been widely accepted or utilised as a vaccine technology due to the lack of immunogenicity observed. Intramuscular injection is the most commonly used vaccination dosing route but the skin represents an immune-rich environment that has been shown to enable significant dose-sparing and broader immunogenicity advantages. However, traditional needle and syringe methods are not adept at accessing this potentially powerful vaccination site. Cavitation has been shown to be able to permeabilise the stratum corneum and hence, provides a method for accessing the epidermis in a reliable and pain-free way. In this thesis, cavitation-mediated delivery of DNA vaccines into the dermal compartment is explored as a strategy for improved vaccination.

This thesis begins by exploring the formulation and ultrasound parameters of needle-free, cavitation-mediated delivery of DNA into the skin. Data shows that relatively low quantities of DNA are delivered into the skin compared to direct injection but that cavitation can be a mechanism to drive increased delivery into the skin. It is also demonstrated that, once cavitation is achieved, exposure of skin to higher ultrasound pressure amplitudes provides no additional benefit. It is also proposed that cavitation-mediated delivery targets a different cell population compared to intradermal injection, based on the observation that the balance of anti-transgene antibody isotypes is altered. Specifically, for cavitation mediated delivery an IgG1-dominant IgG profile is produced compared to a balanced IgG1/IgG2a response observed upon injection. An initial exploration of improved DNA vectors for vaccination, showcases the scope for improvement. Hence, subsequent chapters are devoted to three avenues of optimisation.

The potential of protein cavitation nuclei (p-CaN) is demonstrated, both as cavitation nuclei and as an immune-stimulatory particle. It is shown p-CaN can match delivery of DNA compared to polymeric cavitation nuclei produced to GMP standard, as well as induce an immune response against

the protein used to formulate the p-CaN. A number of p-CaN iterations are validated in this work, including p-CaN produced by the scalable technology of hydrodynamic shearing.

The second optimisation explored was an improved ultrasound set-up (V2). Crucially, the ultrasound transducer was inverted to enable easier handling and the scruff of the mouse is treated to prevent accidental ultrasound exposure of internal structures. Optimisation of delivery parameters using this improved set-up are determined and validated through reporter gene expression, anti-transgene antibody assays, as well as qPCR for DNA delivery quantification.

The final optimisation explored is in terms of DNA vectors used. In particular, perforin-encoding DNA was identified as a powerful adjuvant for cavitation-mediated delivery and shown to improve antibody titres and avidity compared to a non-adjuvanted DNA vaccine. A self-amplifying vector was also explored with the transgene expression profile defined and the immunogenic potential characterised. This showed that the self-amplifying vector has a marked increase in protein production after 5 days and can produce more reproducible antibody titres, higher avidity and a more IgG2a-skewed immune response compared to a non-amplifying vector.

In the final chapter, the potential of the self-amplifying vector and the perforin-encoding DNA vector are tested in a challenge study, which shows that the self-amplifying vector improves survival, and reduces symptomatic disease in a mouse model.

## Acknowledgements

This thesis would not have been possible without the help and support of so many people.

First and foremost, I will always be indebted to Prof. Robert Carlisle, my supervisor, for his expertise, hands-on help, lively scientific discussions and teaching me how to be scientist. Without his insight and quick adjustments to this project, the pandemic would have been much more difficult to navigate.

My gratitude also goes out the Synthetic Biology CDT for the world-class training I have been received and sponsoring both me and my research.

I must also express my thanks to Dr. Pramila Rijal for her expertise on influenza and her support with the microneutralisation titres and the challenge study.

From the Touchlight Genetics group, I would like to sincerely thank Lisa Caproni and Sarah Milsom for welcoming me at Touchlight Genetics and teaching me so much about how to look at research through an application perspective.

I am so thankful to the BUBBL group for welcoming me and providing me with an amazing scientific home, where I have learnt so much. In particular, I want to thank Cameron Smith for being a friend, teaching me acoustics from scratch and always accepting brownies as payment. Luca Bau cannot be thanked enough for his insight, help and his daily example of a dedicated scientist. A huge thank-you must go to Alex Martin for helping me through the *in vivo* hurdles and his advice on the home-stretch.

I must give a massive thank-you to all those of the TherOxImmune group. Particular mention must be given to Prof. Constantin Coussios for seeing potential in my research and the support to pursue it, as well as Brian Lyons for always taking the time to chat about new observations, the unending

supply of p-CaN and his perpetual optimism. Joel must also be thanked for his kindness, help with the ELISAs and his contribution to the p-CaN stocks. It has been an tremendous joy working with all of you.

A person who could not be missing from this list is Holly Wright, who was the most enthusiastic, engaged and clever M.Sc. student I have had the privilege to supervise.

To my friends, thank you for always helping me see the funny side and keeping me sane. In particular, Miranda, Paul and Toby have been the best dance partners a person could ask for. I have been lucky enough to call Claire a friend and I could not be happier to finish this life phase with her. To my Dutch friends, ontzettend bedankt voor alle steun door de jaren. Het was een stuk leuker met jullie erbij.

I would like to express my enormous gratitude to my parents for their unconditional support up to and throughout my DPhil. Thank you for believing in me and it is to them I dedicate this thesis.

Finally, I am forever grateful to my partner, Michael Newsome, who has selflessly supported me throughout every hurdle. His ability to always make me laugh has made every day better and I would not be here without him.

## Statement of Contribution

I gratefully acknowledge the following people who have kindly contributed to this doctoral research:

**Prof Robert Carlisle:** training and support in handling mice during *in vivo* studies, as well as providing feedback on this thesis.

**Dr. Brian Lyons:** fabricating the p-CaN used in this thesis.

**Joel Balkaran:** fabricating the p-CaN used in this thesis and performing the anti-luciferase ELISA.

**Dr. Michael Gray:** designing and calibrating the V2 set-up.

**Dr. Cameron Smith:** setting up the field calibration of the transducer and support on acoustic processing.

**Dr. Joshua Owen:** handling the ultrasound set-up for the pressure optimisation *in vivo* study.

**Dr. Pramila Rijal:** performing the intranasal administration of S-FLU and X-179A virus and performing the microneutralisation assay.

**Dr. Lisa Caproni & Sarah Milsom:** providing the dbDNA$^{TM}$ and facilities for DNA cloning.

**James Fisk:** fabricating the V2 set-up and maintenance of both the V1 and V2 set-up.

**Claire Coupland:** training on and support with Western Blots.

**Holly Wright:** contributing to the cloning work in Chapter 5.

**Mandy Poulter:** fixing and staining the mouse skin samples in Chapter 5.

**Jonathan Kantor:** consulting on the skin samples in Chapter 5.

# Dissemination

## Peer-Reviewed Journal Publications

**Hettinga, J.K.**, Carlisle, R.C. *'Vaccination into the dermal compartment: techniques, challenges and prospects'*, Vaccines, 8(3), 534 (2020)

**Hettinga, J.K.**, Lyons, B., Balkaran, J.P.R., Rijal, P., Caproni, L.J., Townsend, A.R., Suslick, K.S., Coussios, C.C., Carlisle, R.C. *'Cavitation-Mediated Transcutaneous Delivery of Protein and Nucleotide-Based Antigen for Rapid High-Level Immune Responses'* (in preparation)

## Conference Posters/Presentations

**Hettinga, J.K.**, Caproni, L.J., Carlisle, R.C., Coussios, C.C., *'Getting more bang for your buck: A DNA-encoded, self-amplifying RNA improves vaccine efficacy'*, Genetic Vaccine Development for Infectious Diseases Summit 2022, Boston, United States of America, 25-26 May 2022.

Balkaran, J.P.R., **Hettinga, J.K.**, Lyons, B., Carlisle, R.C., Coussios, C.C., *'Needle-free delivery of DNA using biodegradable cavitation nucleation'*, Genetic Vaccine Development for Infectious Diseases Summit 2022, Boston, United States of America, 25-26 May 2022.

Lyons, B, **Hettinga, J.K.**, Balkaran, J.P.R., Collins, A., Maardalen, M., Katti, P.S., Mannaris, C., Bau, L., Smith, C.A.B., Gray, M.D., Kwan, J.J., Carlisle, R.C., Coussios, C.C., *'Gas-stabilizing solid cavitation nuclei for systemic or transdermal ultrasound-enhanced drug and vaccine delivery and immunomodulation'*, The Journal of the Acoustical Society of America 150, A54 (2021)

**Hettinga, J.K.**, Carlisle, R.C. *'Transdermal delivery of DNA vaccines'*, Therapeutic Ultrasound Winter school, École de Physique des Houches, Les Houches, France, 3-8 March 2019.

# Contents


**1 Introduction** **1**

1.1 Vaccination . . . 1

1.2 Influenza . . . 3

1.3 Nucleotide vaccines . . . 5

1.4 Adjuvants . . . 9

1.5 The skin and its immune environment . . . 10

1.6 Rationale for vaccination into the dermal compartment . . . 12

1.7 Delivery of vaccines . . . 14

1.7.1 Ultrasound-mediated delivery . . . 14

1.8 Summary . . . 19

**2 Exploratory studies of ultrasound-mediated delivery of DNA** **21**

2.1 Introduction . . . 21

2.1.1 doggybone DNA . . . 21

2.1.2 DNA vectors . . . 22

2.2 Materials and Methods . . . 29

2.2.1 Ultrasound set-up . . . 29

2.2.2 Transducer calibration . . . 29

2.2.3 Acoustic data processing . . . 30

2.2.4 Statistics . . . 32

2.2.5 *In vivo* model . . . 33

2.2.6 *In vivo* imaging . . . 33

2.2.7 Blood sampling . . . 33

2.2.8 *In vivo* protocol for the optimisation of pressure . . . 33

2.2.9 Quantification of DNA delivery . . . 34

2.2.10 DNA vector design and construction . . . 35

2.2.11 Enzyme-linked immunosorbent assay (ELISA) . . . 40
2.2.12 Enzyme-linked immune absorbent spot (ELISpot) . . . 41
2.2.13 *In vivo* protocol to immunogenicity of the CMV-Cal09 vector . . . 43
2.2.14 *In vivo* protocol to assess DNA vaccines and adjuvants . . . 44
2.3 Results . . . 46
2.3.1 *In vivo* pressure optimisation . . . 46
2.3.2 DNA delivery assessed by qPCR . . . 52
2.3.3 Novel DNA vaccine and adjuvant vectors . . . 54
2.3.4 *In vivo* testing of DNA vectors by injection . . . 61
2.3.5 *In vivo* testing of novel DNA vectors . . . 63
2.4 Conclusions and Discussion . . . 71

**3 Protein Cavitation Nuclei 78**
3.1 Introduction . . . 78
3.2 Materials and Methods . . . 83
3.2.1 Plasmid purification . . . 83
3.2.2 ELISA . . . 83
3.2.3 *In vivo* protocol to assess the ability of BSA p-CaN to deliver luciferase-encoding pDNA . . . 84
3.2.4 *In vivo* protocol for assessing BSA p-CaN immunogenicity . . . 84
3.2.5 *In vivo* protocol for SARS-CoV-2 Spike protein p-CaN as a vaccine strategy . . . 85
3.2.6 Protein purification . . . 87
3.2.7 SDS-PAGE . . . 88
3.2.8 Western Blot . . . 88
3.2.9 BCA Assay . . . 90
3.2.10 Statistics . . . 90
3.3 Results . . . 91
3.3.1 *In vivo* study to assess the ability of BSA p-CaN to deliver luciferase-encoding pDNA . . . 91
3.3.2 *In vivo* to assess BSA p-CaN immunogenicity . . . 96
3.3.3 *In vivo* to investigate spike protein p-CaN as a vaccine strategy for COVID-19 . . . 98
3.3.4 Protein purification of FLT3L . . . 101
3.4 Conclusions and Discussion . . . 106

**4 New set-up** **110**

4.1 Introduction . . . 110

4.2 Materials and Methods . . . 112

4.2.1 V2 set-up . . . 112

4.2.2 Statistics . . . 114

4.2.3 Plasmid purification . . . 114

4.2.4 *In vivo* imaging . . . 114

4.2.5 Quantification of DNA delivery . . . 114

4.2.6 *In vivo* protocol to assess delivery and handling of the V2 set-up . . . 115

4.2.7 *In vivo* protocol for optimisations . . . 115

4.2.8 *In vivo* protocol for quantification of delivered DNA and BSA at 2 minutes and 24 hours . . . 117

4.2.9 *In vivo* protocol for assessing immunogenicity under optimised conditions . . . 117

4.3 Results . . . 119

4.3.1 *In vivo* comparison of SonoVue and nanocups . . . 119

4.3.2 *In vivo* p-CaN concentration optimisation . . . 122

4.3.3 *In vivo* pressure optimisation . . . 123

4.3.4 *In vivo* DNA concentration optimisation . . . 126

4.3.5 *In vivo* treatment time optimisation . . . 126

4.3.6 *In vivo* quantification of delivery with optimised parameters . . . 130

4.3.7 *In vivo* study on immunogenicity with optimised parameters . . . 135

4.4 Conclusions and Discussion . . . 138

**5 Second generation DNA vaccines** **142**

5.1 Introduction . . . 142

5.1.1 VEEV . . . 143

5.1.2 FLT3L . . . 145

5.1.3 CD80 . . . 146

5.1.4 Perforin . . . 146

5.1.5 p-CaN . . . 147

5.2 Materials and Methods . . . 149

5.2.1 Cloning . . . 149

5.2.2 Plasmid purification . . . 154

5.2.3 3G-H p-CaN . . . 154

5.2.4 Enzyme-linked immune absorbent spot (ELISpot) . . . 154
5.2.5 ELISA . . . 154
5.2.6 Histochemical staining with haematoxylin and eosin stain . . . 155
5.2.7 Statistics . . . 156
5.2.8 *In vivo* protocol for the optimisation of pressure and DNA dose with 3G-H p-CaN 157
5.2.9 *In vivo* protocol for the evaluation of a self-amplifying reporter plasmid . . . 158
5.2.10 *In vivo* protocol for the evaluation of a self-amplifying immunogenic vector . . . 159
5.2.11 *In vivo* protocol for the evaluation of the second generation DNA adjuvant vectors159
5.2.12 *In vivo* protocol to assess expression and immunogenicity with optimised parameters and an adjuvant . . . 161
5.3 Results . . . 162
5.3.1 *In vivo* for the optimisation of pressure and DNA dose with BSA 3G-H p-CaN . 162
5.3.2 Cloning of the self-amplifying vectors . . . 170
5.3.3 *In vivo* evaluation of a self-amplifying reporter plasmid . . . 175
5.3.4 *In vivo* evaluation of a self-amplifying immunogenic vector . . . 179
5.3.5 Cloning of the DNA adjuvant vectors . . . 183
5.3.6 *In vivo* evaluation of the second generation DNA adjuvant vectors . . . 189
5.3.7 *in vivo* to assess immunogenicity with optimised parameters and the addition of an adjuvant . . . 198
5.4 Conclusions and Discussion . . . 202

**6 Challenge Study 208**
6.1 Introduction . . . 208
6.2 Materials and Methods . . . 211
6.2.1 Plasmid purification . . . 211
6.2.2 Statistics . . . 211
6.2.3 *In vivo* model . . . 211
6.2.4 *In vivo* protocol for assessing delivery in DBA/2 mice . . . 211
6.2.5 *In vivo* protocol for influenza challenge . . . 212
6.3 Results . . . 215
6.3.1 *In vivo* for assessing pDNA delivery in DBA/2 mice . . . 215
6.3.2 *In vivo* influenza challenge study . . . 216
6.4 Conclusions and Discussion . . . 225

**7 Conclusions and Future Work** **229**

7.1 Research overview . . . . . 229

7.1.1 Ultrasound set-up and parameters . . . . . 230

7.1.2 p-CaN . . . . . 232

7.1.3 DNA vector optimisation . . . . . 233

7.1.4 Influenza challenge . . . . . 237

7.2 Research limitations and future directions . . . . . 241

7.2.1 Set-up . . . . . 241

7.2.2 Formulation . . . . . 242

7.2.3 Immunostimulatory p-CaN . . . . . 242

7.2.4 Challenge model . . . . . 243

7.2.5 Towards the clinic . . . . . 243

**A Plasmid maps** **XXXVIII**

# List of Figures


| | |
|---|---|
| 1.1 | Schematic representation of the skin. |
| 1.2 | Overview of techniques used for vaccination into the dermal compartment. |
| 2.1 | Schematic representation of the patented DNA amplification process of Touchlight Genetics Ltd. |
| 2.2 | Schematic of the ultrasound set-up used in the early immune studies (V1). |
| 2.3 | Calibration of the ultrasound transducer. |
| 2.4 | Summary of the treatment, blood sampling and spleen collection, as well as subsequent ELISA timeline for the *in vivo* to assess the immunogenicity of CMV-Cal09 dbDNA$^{TM}$ after intramuscular or intradermal injection. |
| 2.5 | Summary of the treatment, skin harvesting and blood sampling, as well as subsequent ELISA timeline for the *in vivo* to assess the immunogenicity of different DNA vaccine candidates and adjuvants. |
| 2.6 | IVIS images of the effect of scaling acoustic pressure on transfection of luciferase-encoding dbDNA$^{TM}$. |
| 2.7 | The effect of scaling acoustic pressure on transfection of dbDNA$^{TM}$-Luc. |
| 2.8 | Representative spectrograms for mice treated with nanocups at 0.5 MPa, 0.85 MPa, 1.0 MPa and 1.6 MPa. |
| 2.9 | The Total Acoustic Sensor Energy (TASE) or inertial component of TASE per treatment pressure compared to detected bioluminescence of luciferase. |
| 2.10 | Quantification of dbDNA$^{TM}$-Luc copies delivered into murine skin with or without ultrasound and with or without dbDNA$^{TM}$-Luc. |
| 2.11 | Schematic representation of the cloning of proTLx-$\kappa$ CD11c-Cal09 HA. |
| 2.12 | Agarose gel with the digest of proTLx-$\kappa$ B5X4 Cal09. |
| 2.13 | Agarose gel with the diagnostic PCR of proTLx-$\kappa$ CD11c-Cal09. |
| 2.14 | Schematic representation of the cloning of proTLx-$\kappa$ EF1$\alpha$ Cal09 HA. |
| 2.15 | Agarose gel with the diagnostic PCR of proTLx-$\kappa$ EF1$\alpha$ Cal09 HA. |

| | |
|---|---|
| 2.16 | Schematic representation of the cloning of proTLx-κ KCL27-Cal09 HA. |
| 2.17 | Agarose gel with the diagnostic PCR of proTLx-κ KCL27-Cal09 HA. |
| 2.18 | Schematic representation of the cloning of proTLx-κ IL1α-P2A-IL1β. |
| 2.19 | Agarose gel with the PCR product of the amplification of the proTLx-κ B5X4 mIL12 backbone. |
| 2.20 | Agarose gel with the diagnostic PCR of proTLx-κ IL1α-P2A-IL1β. |
| 2.21 | ELISA (a) and ELISpot (b) results for mice, which were injected with 50 µg CMV-Cal09 dbDNA$^{TM}$ intradermally or 25 µg intramuscularly. |
| 2.22 | ELISA data from blood samples taken at day 49 to assess the effect of promoter strength. |
| 2.23 | ELISA data from blood samples taken at day 49 to assess the effect of tissue specific promoters. |
| 2.24 | ELISA data from blood samples taken at day 7, 14, 20, 30, 42 and 49 to assess the effect of the CD11c promoter. |
| 2.25 | ELISA data from blood samples taken at day 49 to assess the effect of the first generation of DNA adjuvants. |
| 2.26 | Titred ELISA data from blood samples taken at day 49 for mice injected with CMV-IL1α-IL1β or treated with cavitation to deliver CMV-IL1α-IL1β. |
| 2.27 | Avidity and IgG1/IgG2a titres of CMV-Cal09 and CMV-IL1α-IL1β. |
| 3.1 | Summary of the treatment and blood sampling, as well as subsequent ELISA timeline for the *in vivo* to assess the use of BSA p-CaN to elicit immune responses. |
| 3.2 | Summary of the treatment and blood sampling timeline for the *in vivo* to assess the use of SARS-CoV-2 Spike p-CaN to elicit immune responses. |
| 3.3 | Comparison of pDNA delivery capability of BSA 1G p-CaN with nanocups in terms of pDNA expression. Total luminescence after 24 hours is compared. |
| 3.4 | TASE is plotted against luminescence for the comparison between BSA 1G p-CaN and nanocups. |
| 3.5 | *In vivo* imaging of the treated skin for the comparison between BSA 1G p-CaN and nanocups. |
| 3.6 | Spectrograms of the ultrasound treatments for the comparison between BSA 1G p-CaN and nanocups. |
| 3.7 | Levels of anti-BSA IgG antibodies generated by mice treated with 1G BSA p-CaN with or without ultrasound or injected with equivalent protein I.M., I.D or S.C. |
| 3.8 | Avidity of the anti-BSA IgG antibodies on day 28 generated by mice treated with 1G BSA p-CaN and ultrasound or injected with equivalent protein I.M., I.D or S.C. |

| | |
|---|---|
| 3.9 | ELISA to assess the anti-Spike antibodies in mice. Mice were I.D. injected with Spike protein with and without imiquimod or with Spike 1G p-CaN formulated with or without imiquimod. Alternatively, mice were treated with or without ultrasound and p-CaN formulated with or without imiquimod. |
| 3.10 | Isotyping of the anti-Spike antibodies in blood samples from mice on day 21 and 28 after prime. Mice were I.D. injected with protein and imiquimod or Spike 1G p-CaN formulated with imiquimod or PBS. Alternatively, mice were treated with ultrasound and Spike 1G p-CaN. |
| 3.11 | SDS-PAGE gel with the cell lysate of differently sonicated cell suspensions expressing FLT3L. |
| 3.12 | SDS-PAGE gels with fractions collected after purification of FLT3L from *E. coli*. |
| 3.13 | Western Blot of uninduced and induced cells of *E. coli* with an inducible FLT3L-encoding plasmid. |
| 3.14 | SDS-PAGE, 6xHIS Western Blot, FLT3L Western Blot for induced and uninduced cell lysates from *E. coli* with an inducible FLT3L-encoding plasmid. |
| 3.15 | SDS-PAGE and FLT3L Western Blot of fractions collected after protein purification of his-tagged FLT3L from FLT3L-expressing *E. coli*. |
| 4.1 | A schematic of the V2 set-up used for *in vivo* treatments. |
| 4.2 | A schematic summary of the RCV-mode and XMT-mode of the V2 set-up used for *in vivo* treatment. |
| 4.3 | Summary of the treatment and blood sampling, as well as subsequent ELISA timeline for the *in vivo* to assess the immunogenicity CMV-Luc plasmid DNA and 2G-U p-CaN. |
| 4.4 | Luminescence after 24 hours for mice treated with CMV-Luc pDNA, ultrasound and either MilliQ, SonoVue or nanocups or intradermally injected with an equivalent pDNA dose. |
| 4.5 | TASE values and spectrograms for ultrasound treatment with pDNA and MilliQ, SonoVue and nanocups. |
| 4.6 | Example spectrograms showing PCD data collected during treatment with 100% BSA 2G-U p-CaN dose, 50% BSA 2G-U p-CaN dose or 0% BSA 2G-U p-CaN dose (MilliQ). |
| 4.7 | Luminescence observed 24 hours after treatment with ultrasound, CMV-Luc pDNA and 100% BSA 2G-U p-CaN dose, 50% BSA 2G-U p-CaN dose or 0% BSA 2G-U p-CaN dose (MilliQ). |
| 4.8 | Luminescence after 24 hours for mice treated with BSA 2G-U p-CaN, CMV-Luc pDNA and ultrasound at scaling pressures (0.4 MPa, 1.5 MPa, 1.7 MPa, 2.0 MPa) or intradermally injected with an equivalent dose of pDNA. |

| | |
|---|---|
| 4.9 | TASE values for mice treated with BSA 2G-U p-CaN, CMV-Luc pDNA and ultrasound at scaling pressures (0.4 MPa, 1.5 MPa, 1.7 MPa, 2.0 MPa) or intradermally injected with an equivalent dose of pDNA. |
| 4.10 | Luminescence after 24 hours plotted against TASE for mice treated with BSA 2G-U p-CaN, CMV-Luc pDNA and ultrasound at scaling pressures (0.4 MPa, 1.5 MPa, 1.7 MPa, 2.0 MPa) or intradermally injected with an equivalent dose of pDNA. |
| 4.11 | Luminescence after 24 hours for mice treated with BSA 2G-U p-CaN, ultrasound and pDNA at scaling dose (71 µg, 142 µg and 284 µg). |
| 4.12 | Luminescence after 24 hours for mice treated with BSA 2G-U p-CaN, CMV-Luc pDNA and ultrasound at 1.7 MPa for a range of times (60, 120, 300 or 600 seconds). |
| 4.13 | Treatment time plotted against measured TASE for mice treated with BSA 2G-U p-CaN, CMV-Luc pDNA and ultrasound at 1.7 MPa for a range of times (60, 120, 300 or 600 seconds). |
| 4.14 | TASE values plotted against luminescence after 24 hours for mice treated with BSA 2G-U p-CaN, CMV-Luc pDNA and ultrasound at 1.7 MPa for a range of times (60, 120, 300 or 600 seconds). |
| 4.15 | Example pictures of the exposed skin regions taken directly after treatment and matching luciferase images captured 24 hours later. Mice were treated with BSA 2G-U p-CaN, CMV-Luc pDNA and ultrasound at 1.7 MPa for a range of times (60, 120, 300 or 600 seconds). |
| 4.16 | Luminescence and IVIS images of mice intradermally injected with 90 µg CMV-Luc pDNA or treated with ultrasound and a formulation with BSA 2G-U p-CaN and 90 µg CMV-Luc pDNA with optimised parameters. |
| 4.17 | DNA copies present in excised skin after 2 minutes or 24 hours as determined by qPCR after intradermal injection (I.D.) or cavitation (CAV) with 90 µg CMV-Luc pDNA. |
| 4.18 | The BSA protein equivalent detected in murine skin 2 min and 24 hours after intradermal injection of 100 µL BSA 2G-U p-CaN (I.D.) or ultrasound treatment (CAV) with 90 µg CMV-Luc pDNA and BSA 2G-U p-CaN, using an anti-BSA ELISA. |
| 4.19 | Luminescence 24, 48 and 72 hours after prime and 24 and 48 hours after boost for mice intradermally injected with 90 µg CMV-Luc pDNA and 100 µL BSA 2G-U p-CaN or treated with ultrasound, BSA 2G-U p-CaN and 90 µg CMV-Luc pDNA. |
| 4.20 | Levels of anti-BSA antibodies measured over time as assessed using an anti-BSA antibody ELISA for mice intradermally injected with 90 µg CMV-Luc pDNA and 100 µL BSA 2G-U p-CaN or treated with ultrasound, BSA 2G-U p-CaN and 90 µg CMV-Luc pDNA. |

| | |
|---|---|
| 4.21 | Levels of anti-Luc antibodies measured over time as assessed using an anti-Luc antibody ELISA for mice intradermally injected with 90 µg CMV-Luc pDNA and 100 µL BSA 2G-U p-CaN or treated with ultrasound, BSA 2G-U p-CaN and 90 µg CMV-Luc pDNA. |
| 5.1 | Schematic of the amplification process of a DNA-launched, self-replicating RNA for the amplification of Cal09 HA based on the non-structural proteins (nsP1-nsP4) derived from VEEV. |
| 5.2 | Summary of the treatment, blood sampling and spleen sampling, as well as subsequent ELISA timeline for the *in vivo* to assess the protection provided by DNA vaccines that are delivered by intradermal injection or by cavitation. |
| 5.3 | Summary of the treatment and blood sampling, as well as subsequent ELISA timeline for the *in vivo* to assess the expression and immunogenicity with optimised parameters and an adjuvant. |
| 5.6 | The effect of scaling acoustic pressure on cavitation energy (TASE in µJ), when treating with 3G-H p-CaN. |
| 5.4 | IVIS images of mouse skin showing the influence of pressure amplitude on the capability of 3G-H BSA p-CaN to deliver CMV-Luc pDNA. |
| 5.5 | Luminescence after 24 hours for mice treated with BSA 3G-H p-CaN, 90 µg CMV-Luc pDNA and ultrasound at scaling acoustic pressure. |
| 5.7 | DNA copies quantified by qPCR for murine skin harvested after 24 hours. Mice were treated with BSA 3G-H p-CaN, 90 µg CMV-Luc pDNA and ultrasound at scaling acoustic pressure. |
| 5.8 | The BSA protein equivalent detected in murine skin 24 hours after treatment, using an anti-BSA ELISA. Mice were treated with BSA 3G-H p-CaN, 90 µg CMV-Luc pDNA and ultrasound at scaling acoustic pressure or, for comparison, with 2G-U p-CaN, 90 µg CMV-Luc pDNA and ultrasound at 1.7 MPa. |
| 5.9 | IVIS images of mouse skin showing the influence of DNA dose on the delivery and expression of CMV-Luc pDNA by 3G-H BSA p-CaN-mediated cavitation. |
| 5.10 | Luminescence after 24 hours for mice treated with BSA 3G-H p-CaN, ultrasound at 1.7 MPa and CMV-Luc pDNA at scaling dose (20 µg, 90 µg or 142 µg). |
| 5.11 | DNA copies quantified by qPCR for murine skin harvested after 24 hours. Mice were treated with BSA 3G-H p-CaN, ultrasound at 1.7 MPa and CMV-Luc pDNA at scaling dose (20 µg, 90 µg or 142 µg). |
| 5.12 | Agarose gel with the PCR products of the temperature optimisation for the Luc-fragment. |

| | |
|---|---|
| 5.13 | Agarose gel with the PCR products of the temperature optimisation for the VEEV1-fragment and VEEV2-fragment. |
| 5.14 | Agarose gel with the diagnostic PCR for the proTLx-κ VEEV DREP Luc plasmid. |
| 5.15 | Schematic representation of the cloning of proTLx-κ VEEV DREP Luc plasmid. |
| 5.16 | Agarose gel with the PCR products of the temperature optimisation for the Cal09-fragment. |
| 5.17 | Agarose gel with the diagnostic PCR for the proTLx-κ VEEV DREP Cal09 plasmid. |
| 5.18 | Schematic representation of the cloning of proTLx-κ VEEV DREP Cal09 plasmid. |
| 5.19 | Example of a mouse intradermally injected with a non-amplifying CMV-Luc vector and a mouse intradermally injected with a self-amplifying CMV-VEEV-Luc vector. The IVIS images of the two mice over time is displayed. |
| 5.20 | Luminescence over time in mice intradermally injected with either 5 µg non-amplifying CMV-Luc plasmid or a copy-matched number of self-amplifying CMV-VEEV-Luc plasmid (9.4 µg). |
| 5.21 | Luminescence over time for mice treated by cavitation with 2G-U p-CaN and pDNA. Mice were either treated with 142 µg non-amplifying CMV-Luc plasmid (red circle), or with a 267 µg copy-matched dose of the self-amplifying CMV-VEEV-Luc plasmd (blue circle) or (µg-matched) 142 µg CMV-VEEV-Luc plasmid. |
| 5.22 | Analysis of the antibody levels, determined by ELISA, from the *in vivo* performed to evaluate non-amplifying versus amplifying Cal09-encoding vectors over time upon I.D. injection. |
| 5.23 | Titring and avidity of anti-Cal09 HA IgG antibodies generated, as determined by ELISA, from the *in vivo* performed to evaluate non-amplifying versus amplifying Cal09-encoding vectors over time upon I.D. injection. |
| 5.24 | Isotyping of anti-Cal09 HA IgG antibodies after 42 days (a) and 83 days (b), as determined by ELISA, from the *in vivo* performed to evaluate non-amplifying versus amplifying Cal09-encoding vectors over time upon I.D. injection. |
| 5.25 | Agarose gel with PCR products of the temperature optimisation for proTLx-κ B5X4 backbone. |
| 5.26 | Schematic representation of the cloning of proTLx-κ CMV-Perforin plasmid. |
| 5.27 | Agarose gel with the diagnostic PCR for the proTLx-κ CMV-Perforin plasmid. |
| 5.28 | Agarose gel with the PCR products of the temperature optimisation for the Fc-fragment. |
| 5.29 | Schematic representation of the cloning of proTLx-κ CMV-CD80-Fc plasmid. |
| 5.30 | Agarose gel with the diagnostic PCR for the proTLx-κ CMV-CD80-Fc. |
| 5.31 | Agarose gel with the PCR products of the Fc-fragment for the proTLx-κ CMV-Flt3l-Fc plasmid. |
| 5.32 | Agarose gel with the PCR products of the temperature optimisation for the Flt3l-fragment. |

| | |
|---|---|
| 5.33 | Schematic representation of the cloning of proTLx-κ CMV-Flt3l-Fc plasmid. |
| 5.34 | Analysis of the anti-Cal09 HA IgG antibody levels, determined by ELISA, from the *in vivo* experiment to evaluate the second generation of DNA adjuvant vectors over time upon I.D. injection. |
| 5.35 | Titring and avidity of anti-Cal09 HA IgG antibodies generated, as determined by ELISA, for mice I.D. injected with CMV-Cal09 pDNA with or without the adjuvant-encoding CMV-Perforin pDNA. |
| 5.36 | Isotyping of anti-Cal09 IgG antibodies after 42 days (a) and 83 days (b), as determined by ELISA, for mice I.D. injected with CMV-Cal09 pDNA with or without the adjuvant-encoding CMV-Perforin pDNA. |
| 5.37 | Analysis of the spot-forming units (SPU) per million cells, determined by ELISpot, from the *in vivo* experiment to evaluate the second generation of DNA adjuvant vectors upon I.D. injection. |
| 5.38 | Analysis of the anti-Cal09 HA IgG antibody levels, determined by ELISA, from the *in vivo* experiment to evaluate the second generation of DNA adjuvant vectors over time upon cavitation-mediated delivery with 3G-H p-CaN. |
| 5.39 | Titring and avidity of anti-Cal09 HA IgG antibodies generated, as determined by ELISA, for mice treated with ultrasound, 3G-H p-CaN and CMV-Cal09 pDNA with or without the adjuvant-encoding CMV-Perforin pDNA. |
| 5.40 | Isotyping of IgG antibodies after 42 days (a) and 83 days (b), as determined by ELISA, for mice treated with ultrasound, 3G-H p-CaN and CMV-Cal09 pDNA with or without the adjuvant-encoding CMV-Perforin pDNA. |
| 5.41 | Analysis of the spot-forming units (SPU) per million cells, determined by ELISpot, from the *in vivo* experiment to evaluate the second generation of DNA adjuvant vectors upon cavitation-mediated delivery with 3G-H p-CaN. |
| 5.42 | Luminescence after priming and boosting in mice intradermally injected with 90 µg CMV-Luc and 90 µg CMV-Perforin or treated with cavitation, 2G-U p-CaN and 90 µg CMV-Luc and 90 µg CMV-Perforin. |
| 5.43 | Cavitation levels during prime and boost treatment of mice treated with cavitation, 2G-U p-CaN and 90 µg CMV-Luc and 90 µg CMV-Perforin. Both the cavitation TASE and the inertial component of the cavitation TASE (iTASE) is displayed. |

| | |
|---|---|
| 5.44 | Analysis of the anti-Luc antibody levels on day 42, determined by ELISA. Mice were either I.D. injected with 90 µg CMV-Luc and 90 µg CMV-Perforin or treated with cavitation and 90 µg CMV-Luc and 90 µg CMV-Perforin for prime. Mice were boosted at 21 days. |
| 5.45 | Two example images of skin from mice treated with cavitation or intradermally injected 24 hours prior to harvesting. The skin was stained with haemotoxylin and eosin. |
| 6.1 | Summary of the treatment, blood sampling and challenge, as well as subsequent ELISA timeline for the study performed in DBA/2 mice to assess the protection provided by DNA vaccines that are delivered intradermally, intramuscularly, by cavitation or which are self-amplifying. |
| 6.2 | Groups of 4 mice were either treated with 142 µg CMV-Luc pDNA, 3G-H p-CaN and cavitation or intradermally injected with 142 µg CMV-Luc pDNA. (a) shows the IVIS image of each mouse. (b) shows the luminescence after 24 hours for each group. |
| 6.3 | Quantification of CMV-Luc pDNA copies delivered into DBA/2 mouse skin via cavitation with 3G-H p-CaN or intradermal injection after 48 hours. |
| 6.4 | Summary of the anti-Cal09 antibody levels 42 days after prime vaccination and 21 days after boosting. 6 groups are displayed. S-FLU is a positive control, which was intranasally administrated (IN). CMV-VEEV-Cal09 is a self-amplifying vector, of which 380 µg pDNA was intradermally injected. CMV-Cal09 is a non-self-amplifying vector, of which 142 µg was intradermally injected or delivered by cavitation or 0.182 µg was intramuscularly injected. CMV-Perforin is an adjuvant DNA vector added to each group, of which 142 µg was intradermally injected or delivered by cavitation or 0.182 µg was intramuscularly injected. The final group was an untreated control. |
| 6.5 | Titring of the anti-Cal09 antibodies from mice intradermally injected with either 142 µg non-amplifying CMV-Cal09 and 142 µg CMV-Perforin or 380 µg self-amplifying CMV-VEEV-Cal09 and 142 µg CMV-Perforin. |

| | |
|---|---|
| 6.6 | Microneutralisation titres, expressed as half maximal effective titre (EC50) for pooled (a) and individual (b) blood samples taken on day 42 after prime. 6 groups are displayed. S-FLU is a positive control, which was intranasally administrated (IN). CMV-VEEV-Cal09 is a self-amplifying vector, of which 380 µg pDNA was intradermally injected. CMV-Cal09 is a non-self-amplifying vector, of which 142 µg was intradermally injected or delivered by cavitation or 0.182 µg was intramuscularly injected. CMV-Perforin is an adjuvant DNA vector added to each group, of which 142 µg was intradermally injected or delivered by cavitation or 0.182 µg was intramuscularly injected. The final group was an untreated control. |
| 6.7 | Isotyping of blood samples taken on day 21 (a) or day 42 (b) after prime vaccination. The mice were intradermally injected with 142 µg CMV-Perforin pDNA and either 142 µg CMV-Cal09 pDNA or 380 µg of self-amplifying CMV-VEEV-Cal09 pDNA. |
| 6.8 | Avidity of blood samples taken on day 35 after prime vaccination. The mice were intradermally injected with 142 µg CMV-Perforin pDNA and either 142 µg CMV-Cal09 pDNA or 380 µg of self-amplifying CMV-VEEV-Cal09 pDNA. |
| 6.9 | Survival of DBA/2 mice after intransal exposure to 30xLD50 of X-179A virus. The mice were intradermally injected with 142 µg CMV-Perforin pDNA and either 142 µg CMV-Cal09 pDNA or 380 µg of self-amplifying CMV-VEEV-Cal09 pDNA. Mice dosed with S-FLU were used as a positive control and untreated mice as a negative control. |
| 6.10 | Relative weight changes in DBA/2 mice measured over a 13-day period after exposure to 30xLD50 of X-179A influenza virus. The mice were intradermally injected with 142 µg CMV-Perforin pDNA and either 142 µg CMV-Cal09 pDNA or 380 µg of self-amplifying CMV-VEEV-Cal09 pDNA. Untreated mice were used as a negative control. |

# List of Tables


| | |
|---|---|
| Table 2.1 | Ultrasound parameters used for *in vivo* studies. |
| Table 2.2 | qPCR primers and probe used for quantification of dbDNA™-Luc. |
| Table 2.3 | Overview of all elements of the genetic constructs described in Chapter 2. |
| Table 2.4 | Overview of all plasmids used as a template or created in Chapter 2. |
| Table 2.5 | Primers used for DNA vectors constructed in Chapter 2. |
| Table 2.6 | Summary of the *in vivo* to assess the immunogenicity of different DNA constructs. |
| Table 3.1 | Summary of the *in vivo* study to assess the use of BSA p-CaN to deliver CMV-Luc pDNA. |
| Table 3.2 | Summary of the *in vivo* study to assess the use of BSA 1G p-CaN to elicit immune responses. |
| Table 3.3 | Summary of the *in vivo* study to assess the use of SARS-CoV-2 Spike p-CaN to elicit immune responses with or without the addition of imiquimod. |
| Table 3.4 | Summary of different protocols for cell lysis using probe sonication ('on' and 'off' time relates to periods of probe sonication. It also noted whether froth was formed for each procedure. |
| Table 4.1 | Summary of the protocol to assess the V2 set-up, using commercial cavitation nuclei, SonoVue and nanocups. |
| Table 4.2 | Summary of the protocol to assess the effect of p-CaN dose on delivery. |
| Table 4.3 | Summary of the protocol to assess the optimal pressure for DNA delivery. |
| Table 4.4 | Summary of the protocol to assess the effect of DNA dose on delivery. |
| Table 4.5 | Summary of the protocol to assess the optimal time for DNA delivery. |
| Table 5.1 | Overview of all genetic elements used in chapter 5. |
| Table 5.2 | Overview of the plasmids used in chapter 5. |
| Table 5.3 | Overview of all primers used and created for second round of DNA cloning. |
| Table 5.4 | Overview of the DNA used to evaluate the expression of CMV-VEEV-Luc compared to CMV-Luc upon cavitation-mediated delivery of the DNA vectors. |

| | |
|---|---|
| Table 5.5 | Overview of the treatment to evaluate different DNA adjuvants upon I.D. injection. |
| Table 5.6 | Overview of the treatment to evaluate different DNA adjuvants upon cavitation-mediated delivery. |
| Table 6.1 | Overview of the treatment in the challenge study. |
| Table 7.1 | Summary of the content of the core and synthesis of the different p-CaN formulation evaluated in this thesis. |

## Acronyms and abbreviations

| | |
|---|---|
| ADCC | Antibody-dependent cellular cytotoxicity |
| anti-Luc | Anti-luciferase |
| APC | Antigen-presenting cells |
| BALB/c | Strain of albino laboratory mouse |
| Cal09 HA | Haemagglutinin of the A/California/07/2009 (H1N1) influenza virus |
| CAV | Cavitation |
| CDC | Complement-dependent cytotoxicity |
| CMV | Cytomegalovirus promoter |
| DAMP | Damage-associated molecular patterns |
| DBA/2 | Mouse model for influenza challenge |
| dbDNA$^{TM}$ | Doggybone DNA |
| DNA | Deoxyribonucleic acid |
| dsRNA | Double-stranded RNA |
| EF1$\alpha$ | Elongation factor 1 alpha |
| ELISA | Enzyme-Linked Immunosorbant Assay |
| ELISpot | Enzyme-Linked Immunospot |
| FFU | Focus forming units |
| Flt3l | Fms-like tyrosine kinase 3 ligand |
| Flu | Influenza |
| GM-CSF | Granulocyte-macrophage colony-stimulating factor |
| GMP | Good manufacturing practice |
| GSD | Geometric Standard Deviation |
| HA | Haemagglutinin |
| HBsAg | Hepatitis B surface antigen |
| HIFU | High Intensity Focused Ultrasound |
| HPV | Human papillomavirus |
| I.D. | Intradermal |

| | |
|---|---|
| IDT | Integrated DNA Technologies |
| i.e. | That is |
| IFN-γ | Interferon-gamma |
| IFN-I | Interferon I |
| IgG | Immunoglobulin G |
| IL1α | Interleukin 1 alpha |
| IL1β | Interleukin 1 beta |
| IL8 | Interleukin 8 |
| IL10 | Interleukin 10 |
| IL12 | Interleukin 12 |
| I.M. | Intramuscular |
| Imiq | Imiquimod |
| IPTG | isopropyl β-d-1-thiogalactopyranoside |
| iTASE | inertial component of TASE |
| IVIS | *In vivo* Imaging System |
| J | Joules |
| kDa | Kilodaltons |
| kHz | Kilohertz |
| L | Litre |
| LNP | Lipid nanoparticle |
| Luc | Luciferase |
| M1 | Matrix protein 1 |
| mg | Milligram |
| MHC-I | Major Histocompatibility Complex I |
| MHC-II | Major Histocompatibility Complex II |
| MHz | Megahertz |
| mL | Millilitre |
| MPa | Megapascal |
| MPL | Monophosphoryl lipid |
| mRNA | Messenger RNA |
| MW | Molecular weight |
| nJ | Nanojoules |
| N+S | Needle and syringe |

| | |
|---|---|
| NA | Neuramidase |
| NC | Nanocups |
| NEB | New England Biolabs |
| nsP | Non-structural protein |
| PAMP | Pathogen-associated molecular patterns |
| PBS | Phosphate-Buffered Saline |
| PCD | Passive Cavitation Detection |
| PCR | Polymerase Chain Reaction |
| pDNA | Plasmid DNA |
| PRF | Pulse Repetition Frequency |
| PRR | Pattern recognition receptors |
| qPCR | Quantitative Polymerase Chain Reaction |
| RNA | Ribonucleic acid |
| SARS-CoV-2 | Severe acute respiratory syndrome–related coronavirus 2 |
| S.C. | Subcutaneous |
| SD | Standard deviation |
| SDS | Sodium Dodecyl Sulphate |
| SFU | Spot-forming units |
| SFV | Semliki Forest Virus |
| TASE | Total Acoustic Sensor Energy |
| Th1 | T-helper cell type 1 |
| TLR | Toll-like receptor |
| TNF-$\alpha$ | Tumour Necrosis Factor alpha (TNF alpha) |
| US | Ultrasound |
| VEEV | Venezuelan Equine Encephalitis Virus |
| VLP | Virus-like particle |
| WHO | World Health Organization |
| w/v | Weight by volume |
| µg | Microgram |
| µJ | Microjoule |
| µL | Microlitre |

# Chapter 1

# Introduction

## 1.1 Vaccination

Vaccination is one of the most effective and cost-efficient measures to prevent illness and improve public health [1–3]. It has saved millions of lives and has even allowed for the complete eradication of devastating diseases such as smallpox [4]. As the world is finally emerging from the COVID-19 pandemic, with over 445 million cases and nearly 6 million deaths, the importance of vaccination has become painfully clear [5]. With over 10.7 billion vaccine doses administered globally [5], the global community has embarked on the most ambitious vaccination programme to date to curb the devastating effect of SARS-CoV-2. Indeed, within 28 months of the first SARS-CoV-2 cases, a remarkable number, 35 in total, of vaccines have already been approved by at least one country [6] and novel types of vaccines have even made their global debut, including mRNA and DNA vaccines.

Vaccines are commonly injected intramuscularly or subcutaneously and multiple doses may be required at set intervals to achieve sufficient protective immunity [7].

Preventative vaccination relies on presenting the body with a non-pathogenic version of a disease, typically containing signature target antigens, and thereby preparing the immune system for a real pathogenic infection. It is therefore important to first describe the process of immune response generation to a real pathogenic attack before describing how vaccination strategies co-opt this response in advance of such an attack.

When a pathogen enters the body, the first line of host defence it encounters is the innate immune system, which is comprised of complement, tissue resident leukocytes and the cytokines/chemokines

they release. Antigen will be generated either by the engulfment and degradation of the incoming material (exogenous) or the infection of host cells and production of progeny pathogen (endogenous). If pathogen-associated antigens are present in the cell, the cell will present these antigens on the major histocompatibility complex I (MHC-I) on the outside of its membrane. These antigens can contain conserved pathogen-associated molecular patterns (PAMPs) and if pathogens result in damage to the host cells or tissue, damage-associated molecular patterns (DAMPs) are released. PAMPs and DAMPS are recognized by germline-encoded pattern recognition receptors (PRRs), which are part of the innate immune system. These PRR-derived signals direct resident antigen-presenting cells (APC) to express costimulatory molecules (cytokines) on their cell surface and present specific pathogen-derived antigens on major histocompatibility complex II (MHC-II). These cytokines attract effector cells, such as eosinophils, macrophages, and natural killer cells. These cells engulf pathogens and kill infected host cells [8, 9].

Meanwhile, activated antigen-presenting dendritic cells migrate to lymph nodes, where they select for antigen-specific T lymphocytes. T cells need both the costimulatory molecules and the matching pathogen-antigen to be activated and hence, this adaptive response is dependent on the innate immune system [9, 10]. These lymphocytes travel to the infected tissue and seek to eliminate infected cells and microbes. This is called cellular immunity. In a similar manner, when antigen, free or bound to APC, is bound by the matching antigen-specific receptor on a B cell (the B-cell receptor), the B cell is activated. Cytokines expressed by T lymphocytes encourage proliferation of the B-cell, increase longevity and can drive isotype switching of the B cell. Upon stimulation by T cells and the antigen, the B cell develops into a plasma cell, which excretes antibodies matching the antigen-specificity of the B-cell receptor. These antibodies can bind to the antigens and directly neutralise the pathogen and also mark pathogen-infected cells for clearance from the body via antibody-dependent cellular cytotoxicity (ADCC). This antibody driven response is called humoral immunity, which is part of the adaptive immune system (which takes longer to develop but has greater specificity than the innate response). After infection or vaccination, memory B cells and memory T cells remain. These cells have a great proliferation potential. When their specific antigens are later encountered again by the body, a T and B cell response can be mounted much faster and reach higher antibody titres, enabling the body to clear the pathogen more efficiently [11, 12].

Vaccines utilise this method of generating immunity by presenting the body with non-pathogenic antigens that it can use to create memory B cells and memory T cells. Antigens can be presented as

live-attenuated whole pathogens, protein subunits or as DNA or RNA encoding the antigen, allowing for the *in situ* expression of the antigen. Often adjuvants that induce DAMPs or bind PRRs are added to increase the generated immune response. These can be a toxin attached to the antigen of interest (conjugate vaccine) or part of the vaccine formulation [8, 11, 13, 14].

A unique property of vaccination is herd immunity. Herd immunity refers to the indirect protection of susceptible individuals by being surrounded by immunised individuals; these vaccinated individuals prevent an infection from spreading to unprotected individuals [15]. Often children too young to be vaccinated and those who cannot be vaccinated due to medical conditions, rely on herd immunity. This has made vaccination not only an individual choice, but a societal decision [16].

## 1.2 Influenza

Influenza ('Flu') is predicted to affect 5-10% of adults and 20-30% of children [17] annually and it has been estimated that globally up to 645,000 people succumb to flu-associated respiratory disease every year [18]. This does not only have a human cost, but also imparts tremendous economic damage. The financial burden of flu has been projected to be $10.4 billion in medical costs and $16.3 billion in lost earnings annually based on the US population in 2003 [19]. This has led to the widespread implementation of national influenza vaccination programmes to protect vulnerable populations from severe disease [20].

Influenza is a pathogenic, negative-stranded RNA virus of the Orthomyxoviridae family. Influenza infection typically manifests as chills, fatigue, headache, muscle pain and muscle loss, runny nose and coughing. Flu can also lead to complications such as ear infections, pneumonia, croup, bronchiolitis, and cardiovascular complications [21–23].

Influenza is categorised into four types, denoted A, B, C and D [22, 24]. Influenza A is further subdivided based on its haemagglutinin (HA) and neuraminidase (NA) envelope glycoproteins. To date, there have been eighteen different HA proteins sequenced as well as nine subtypes of NA. The haemagglutinin protein is crucial for virus entry as it mediates attachment to the sialic acids on the cell surface, whilst the neuraminidase cleaves these sialic acids and enables the release of the virus from the cell once infection is complete [25, 26]. These proteins are the immune-dominant targets for the immune system, with HA proteins being the predominant target of neutralising antibodies. These

antibodies typically target the hypervariable regions that facilitate binding of the influenza virus to the cell membrane, applying a strong selection pressure. A small number of antibodies appear to prevent membrane fusion [27]. Antibodies, which target the neuraminidases, usually only reduce the severity of disease [28]. However, influenza gradually accrues mutations in the HA and NA proteins, preventing the immune system from recognising and neutralising the viral particles over the long-term. This antigenic drift is the consequence of a life cycle which is dependent on a proof-reading-free, error-prone RNA-dependent RNA polymerase which copies the flu genome and makes on average approximately one error per replication of the genome [29, 30].

A second occurrence evident in the infection cycle of influenza A, in particular, is antigenic shift, which is the replacement of one haemagglutinin and/or neuraminidase subtype with another subtype. This may be the consequence of the segmentation of the influenza genome, allowing recombination events, when a single cell is subject to simultaneous infection by more than one type of influenza [31]. This antigenic shift can result in a significant increase in the disease burden of influenza, resulting in epidemics and pandemics. It is estimated that a 'gain of pathogenicity' antigenic shift occurs approximately three times every hundred years, an estimate which does appear to correlate with the three pandemics which occurred in the $20^{th}$ century, namely in 1918, 1957 and 1968 [32]. These regular changes by antigenic shift and drift make it necessary to re-evaluate the components of the influenza vaccinations annually and provide appropriately adapted 'seasonal' flu vaccinations to vulnerable populations.

Indeed, the damage of these sudden, large epidemics led the World Health Organization (WHO) to name a "global influenza pandemic" as one of the "ten threats to global health in 2019" [33]. The consequences of a severe influenza outbreak became most vividly apparent during the pandemic of 1918-1920. It is estimated that 500 million people, which equated a third of the world's population, were infected and showed signs of illness [34]. The death toll resulting from that single pandemic may have been as high as 50-100 million people [35]. Hence, the WHO currently recommends that all health-care workers, pregnant women, children between the ages of six months and five years, the elderly (aged above 65 years) and people with underlying chronic health conditions are vaccinated against influenza each year [17]. In the United States during the 2017-2018 influenza season, these vaccinations prevented 7 million illnesses, 4 million medical visits, 109,000 hospitalizations and approximately 8000 deaths [36].

More broadly, the COVID-19 pandemic, impacting populations across the globe, has shown the necessity of planning, vigilance and the development of technologies that allow rapid, scalable deployment of vaccines to protect vulnerable populations from local outbreaks of new disease variants and prevent them from becoming pandemics.

## 1.3 Nucleotide vaccines

Nucleotide vaccines have long been heralded as the future of vaccine technology, due to the quick development times, the rapid production and possibility of fully synthetic, standardised production of vaccines. However, prior to 2020, no nucleotide-based vaccine had received regulatory approval for human use [37].

In the wake of the COVID-19 pandemic, as of March 2022, three nucleotide vaccines have received emergency regulatory approval by at least one country. Two RNA-based vaccines, mRNA-1273, also known as TAK-929 in Japan, by Moderna and BNT162b2 by Pfizer/BioNTech, have been rolled out globally, with the Pfizer/BioNTech vaccine having been approved in 138 countries [6]. The first DNA vaccine ZyCoV-D by Zydus Cadila has received approval in India on the 20th of August, 2021 [38]. ZyCoV-D is expected to be followed by INO-4800 by Inovio, which is currently in phase 3 trials [39].

#### RNA vaccines

The development of RNA vaccines was long overshadowed by DNA vaccines. This was probably due to the relative difficulty in production, cost and concerns regarding the instability of RNA during storage and *in vivo* [40]. However, RNA vaccines offer many advantages over DNA vaccines. These include the fact that RNA is expressed in the cytoplasm, circumventing the need for the payload to enter the nucleus as with DNA. Such nuclear delivery is a highly inefficient rate-limiting step in non-dividing cells. Indeed, it has been estimated that only around 1 in 1000 plasmid DNA constructs delivered to the cytoplasm can be detected in the nucleus 24-36 hours after addition of the DNA [41]. Some studies have put the proportion delivered plasmids higher in actively dividing cells, but still showed a 100-fold more DNA needed to be injected into the cytoplasm to get equivalent GFP fluorescence to DNA directly injected into the nucleus [42].

Use of RNA also alleviates the risk of genomic integration or cell transformation, which are safety

concerns for DNA vaccines [43]. The COVID-19 pandemic has also enabled the first mRNA vaccines to enter the market, with the lipid-encapsulated Pfizer-BioNTech BNT162b2 and Moderna's mRNA-1273 having been rolled out [44].

RNA vaccines were initially delivered intramuscularly using needle and syringe (N+S) [45], but as electroporation gained traction as a method for DNA vaccine delivery, RNA vaccines were also shown to elicit a broad immune response when delivered by electroporation [46]. In the context of cancer research *ex vivo* loading of dendritic cells via electroporation of RNA or *in vivo* injection with RNA is still being explored as a therapeutic vaccine approach [47]. However, the potential for combinatorial approaches, such as intradermal and intramuscular injection of mRNA encapsulated in lipid nanoparticles (LNP), has shown such promising results [48], it is now the leading delivery approach. Indeed, the mRNA vaccines by Moderna and Pfizer/BioNTech for COVID-19, which also rely on mRNA encapsulated in lipid nanoparticles, have shown high efficacy in protection from symptomatic illness, as well as severe disease (94.1% and 95% respectively). Similarly, Pfizer/BioNTech showed 97.4% efficacy in protection from severe, critical or fatal disease [49–51].

**DNA vaccines**

Vaccines based on mRNA will continue to make good progress and their application will undoubtedly be broadened to other pathogenic diseases. However, DNA vaccines still offer some important distinct advantages over all other approaches including mRNA. DNA is stable at room temperature and, hence, would not necessarily require a cold chain for transport or storage. Like RNA, DNA can be easily altered, enabling the quick development of different vaccines. The sequence can be precisely controlled, and so, in contrast to live attenuated vaccines, there is no risk of the growth adaptation observed in egg-based production. DNA vaccines only encode the antigen, their use prevents potential recombination of the attenuated vaccine strain with a wildtype strain. Furthermore, manufacturing for DNA vaccines can be standardised, as opposed to the inactivation or attenuation protocols needed for each pathogen in inactivated or live attenuated vaccines. Plasmid DNA has also been shown to be safe in humans, as well as enabling the presentation of antigens on both MHC-I and MHC-II complexes. The strength of the DNA vaccine approach appears to lie in the efficacy and general applicability of the technique, as well as its good safety profile [52].

The first study showing the potential of DNA vaccines was published as early as 1993. A plasmid encoding influenza A nucleoprotein was intramuscularly injected into BALB/c mice. The mice

injected with plasmid DNA encoding the antigen had a high titre of anti-nucleoprotein IgG antibodies and a 90% survival rate compared to 20% of the unvaccinated animals [53]. In 1996, DNA vaccines against influenza, expressing haemagglutinin, matrix protein (M1) and nucleoprotein were tested in non-human primates and shown to elicit levels of antibodies similar to approved vaccines. In a ferret challenge model, this DNA vaccine provided more cross-protection against other flu strains than the contemporary licensed vaccines, based on viral titre [54]. Crucially, DNA vaccines can mediate both humoral and cellular responses [55]. However, for a long time, despite this promising preclinical data, a lack of immunogenicity prevented clinical adoption. This could mainly be attributed to a suboptimal humoral response [52, 56, 57]. Multiple methods of increasing the immune response of DNA vaccines have been suggested, such as formulations that increase stability or distribution, co-expression of immunostimulatory molecules that trigger the immune system and the addition of adjuvants [58]. There has also been a study advocating a regime of combining DNA vaccines with boosting with a seasonal vaccine, as a method of increasing neutralizing capabilities [59].

Interestingly, both INO-4800 and the currently approved ZyCoV-D use non-traditional delivery methods. ZyCoV-D is administered with the liquid-jet device PharmaJet Tropis [60, 61] and requires three doses. INO-4800 uses the CELLECTRA 2000® Electroporation Device (Inovio Pharmaceuticals) to deliver a DNA vaccine intracellularly by electroporation after intradermal injection of the DNA vector [39]. The approach does not include adjuvants but it has been suggested that the destruction caused by electroporation does release DAMPs [62]. The ZyCoV-D and INO-4800 both utilise an IgE leader sequence to increase expression level and have optimised the antigen sequence, although the exact method of optimisation remains opaque. [63, 64].

INO-4800 was able to show T cell responses in mice as soon as 7 days after 25 µg of vaccine was administered by intradermal injection followed by electroporation. By 14 days humoral responses to SARS-CoV-2 were seen in mice, a result which was also observed in guinea pigs 14 days after intradermal administration of 100 µg of DNA and electroporation [64]. In a non-human primate model, the candidate vaccine showed two doses of vaccine reduced peak viral load in the throat (approximately 40-fold, $p \leq 0.05$) and reduced lesions in the lungs of the double vaccinated group compared to unvaccinated controls [39]. In the phase I trial, 1 mg or 2 mg DNA vaccine doses, delivered by intradermal injection plus electroporation and boosted after 4 weeks, were compared. After 6 weeks, 2 mg doses of DNA showed substantial advantages in terms of serum IgG binding titres to S1+S2 spike protein (1.5-fold for responders) and after 8 weeks, also in terms of T cell responses (1.6-fold

for responders) [65]. This 2 mg dosing is notably higher than the dosing used in the mRNA-based vaccines by Moderna (mRNA-1273) and Pfizer-BioNTech (BNT162b2), which are 100 µg and 30 µg respectively [66], at prime and boost. This may be a reflection on the relative difficulty in effectively delivering DNA to the nucleus, compared to the cytoplasm for RNA vaccines. Another consideration that may limit the ease of mass implementation, is the multi-step process of administration. Despite the ease of use of the CELLECTRA, two intradermal injections of 1.0 mg are needed, followed by the further painful application of the CELLECTRA. The pain of administration of the CELLECTRA has been described as up to 6.8/10 on a pain intensity scale, with an average of 2.5/10 upon intradermal application [67]. It is notable that whilst many delivery technologies are seeking to increase patient acceptance by removing the pain of N+S, this approach not only includes 2 N+S injections, but also application of electroporation which is judged to be even more painful than the injections.

The ZyCoV-D vaccine is based on the pVax-1 backbone by Thermo Fisher Scientific and encodes the amino acid sequence of SARS-CoV-2 from the Wuhan Hu-1 isolate and has an IgE signal peptide gene. Results showed cellular and humoral immunity in both mice and guinea pigs, after administering 3 doses of 25 µg and 100 µg intradermally with a 31G needle. Intradermal injection in rabbits was subsequently done with the PharmaJet Tropis [63]. Results were encouraging enough to proceed to phase 1 clinical trials, where a comparison was made between N+S administration and the PharmaJet Tropis. Similar to tests of the INO-4800 vaccine, 1.0 mg and 2.0 mg doses were compared. On day 84, the best geometric mean titre was observed after administration with the PharmaJet Tropis for both doses (1 mg: 38.84 (N+S) vs 96.49 (Tropis), 2 mg: 748.46 (N+S) vs 884.04 (Tropis)), with 2.0 mg showing a notably higher titre by day 84 compared to the 1.0 mg group (9.2-fold). In terms of seroconversion based on the generation of IgG antibodies (from undetectable to positive or a four-fold increase from baseline titre), the need for a high dose became further evident. In the 1.0 mg group injected by needle, only 2/11 subjects seroconverted, whereas in the 2.0 mg group injected by needle 5/10 subjects seroconverted. The Pharmajet injection further increased this to 8/10 subjects seroconverting in the 2.0 mg dosed group [60]. Unfortunately, only press releases are available for the phase 2 and 3 trials, limiting the amount of data available on efficacy, other than the reported 66.6% efficacy for symptomatic RT-PCR positive cases [38]. This is a relative low efficacy compared to the Moderna mRNA-1273 and Pfizer with an efficacy of 94% and 95% respectively [49, 50]. However, Pfizer has shown waning of immunity against infections over time, down to 47% after 4 months. The protection against hospital admissions remained high for at least 6 months at 93% [68]. Overall, the ZyCoV-D vaccine shows that a second booster and dermal administration could be the answer to

getting more DNA vaccines into the clinic. However, as the number of interventions goes up, compliance with the full vaccination schedule may decrease. Also, the relative delay in full protection, which was only detected after 84 days may limit its use in pandemics.

In order to develop DNA vaccines as a platform technology, a standardised, scalable method of production is necessary. For example, Touchlight Genetics has developed a DNA production platform that allows for the vector-free production of DNA sequences called doggyboneDNA$^{TM}$ (dbDNA$^{TM}$) [69] (section 2.1.1), similar to the backbone-free production of RNA. A fully chemical process of production would also speed-up and simplify production, as it would circumvent removal of bacterial components, such as lipopolysaccharide which can lead to toxicity [70]. Avoiding the reliance on bacteria for scale-up production has further advantages in terms of enabling sequence optimisation without compromising expression, the ability to methylate the DNA for instance in the case of CpG islands and the avoidance of sequences for antibiotic resistance, simplifying genetic constructs and enabling easier regulatory approval.

Overall, great strides have been made in getting DNA vaccines to the clinic. However, challenges remain in effective delivery. Although INO-4800 only requires two doses, the application method requires up to two intradermal injections as well as electroporation, which is cumbersome and imparts significant pain and could potentially compromise compliance. In contrast, ZyCoV-D utilising a liquid-jet for delivery as a quick and simple method, needs three interventions to achieve a level of protection lower than that achieved by mRNA vaccines, which could similarly decrease compliance. To enable large-scale roll-out of DNA vaccines, a need still exists for a pain-free delivery method, that only requires a two-dose regime. To further improve efficacy, the role of adjuvants, sequence optimisation and vector-free DNA still remain underexplored and could provide solutions to some of the challenges still faced.

## 1.4 Adjuvants

Adjuvants are a crucial component of conventional injectable vaccines and help stimulate effective immunity by inducing the innate immune system. They increase the efficacy of the vaccine leading to the generation of higher antibody titres and stimulation of a wider range of adaptive responses. It has been increasingly recognised that adjuvants may play a role in guiding the type of adaptive immune response [8]. They may also improve the immune response in the elderly, who generally have a

lower immune response to vaccines and infection [71]. From a safety perspective, adjuvants allow for less immunogenic purified antigen to be used instead of inactivated or attenuated virus, improving safety. Adjuvants can also enable dose-sparing, which could reduce the cost of vaccines. However, the development of adjuvants is challenging, as animal data often fails to predict the effect of an adjuvant accurately. Current licenced adjuvants include aluminium salts, oil-in-water emulsions and toll-like receptor agonist adsorbed on alum. Some adjuvants also show a synergistic effect, such as AS01, which consists of MPL (monophosphoryl lipid) and QS-21, which can induce novel pathways not induced by the individual components [72–74]. It has also been shown that double stranded RNA can function as an adjuvant, as it has PAMP structures associated with many viruses which at some point in their life cycle produce double stranded RNA [75]. Some DNA sequences (e.g. CpG dense sequences) also seem able to bind to the Toll-like Receptor 9 PPR, stimulating the secretion of cytokines [76].

## 1.5 The skin and its immune environment

When the large, distended and highly charged structure of plasmid DNA is considered, it is not surprising that its uptake *in vivo* is very inefficient, unless a method to facilitate its entry into cells is provided [77]. This has led to the evaluation of multiple methods to overcome the barrier presented by the plasma membrane. Initially, DNA was introduced using a needle and syringe intramuscularly [45], the unique electrophysiology of muscle cells appears to provide a mechanism for the entry of distended negatively charged DNA molecules which is not evident in other cell types. However, although amenable to the process of delivery, the muscle may not be ideal in terms of generating a robust and protective immune response from DNA vectors [78, 79].

The skin possesses multiple properties that make it an excellent site for vaccination; it is an easily accessible immune-rich environment and contains components that can induce both humoral and cellular immunity. It is also the natural route of infection for many pathogens so is evolutionarily primed to respond to challenge, an argument that may not hold true for the muscle.

The skin can be divided into three layers: The epidermis, dermis, and hypodermis (Figure 1.1). Vaccination to these layers are referred to as epidermal, intradermal, and subcutaneous, respectively, and distinct strategies exist for targeting the different layers [80].

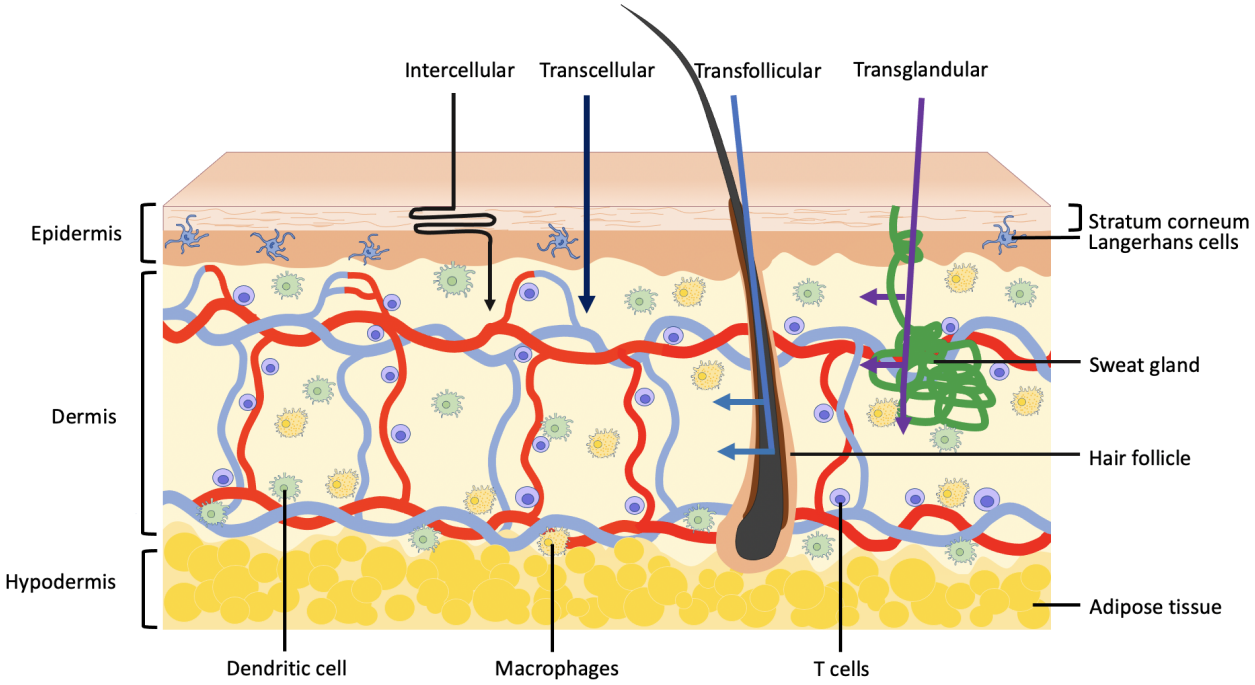



**Figure 1.1.** Schematic representation of the skin, the distribution of a variety of immune cells, and potential routes to bypass the stratum corneum.

The stratum corneum has a thickness averaging at around 20 µm, with the whole epidermis being around 85 µm thick, and it is the first and most formidable barrier against exposure to foreign substances and pathogens [81]. The stratum corneum is comprised of 10–20 layers of dead keratinocytes and intracellular lipids, proteins, and humectants [82, 83]. Typically, lipophilic molecules with a molecular weight below 500 Dalton are able to pass through the stratum corneum [84, 85]. Clearly, there are very few vaccine strategies that match these specifications.

As shown in Figure 1.1, there are four potential routes to bypass this layer: Intercellular, transcellular, transfollicular, and transglandular [86]. At the base of the stratum corneum are layers dominated by the keratinocytes, which will develop to form the stratum corneum. These keratinocytes form a crucial part of the innate immune system of the skin and express a variety of pattern recognition receptors (PRR) and cytokines. Langerhans cells reside between the keratinocytes in the suprabasal layer and function as professional antigen-presenting cells [82, 87]. Langerhans cells also possess the ability to sample the surface just below the stratum corneum by projecting dendrites through the keratinocyte junctions [88]. This has been shown to drive IgG1 responses in mice, activating humoral immunity against antigens [89].

The dermis is a fibroblast-rich environment with a network of elastin and collagen fibres to provide

both strength and elasticity [90]. It is also interspersed with a network of lymph and blood vessels, as well as dendritic cells, macrophages, and T cells. Approximately 20 billion T cells, i.e. twice as many T cells as in the entire blood volume, form perivascular layers throughout the entirety of the dermis [91]. Dendritic cells, however, are distributed interstitially near the epidermis and become progressively more numerous around the vasculature in the deeper layers of the dermis, similar to macrophages. The dendritic cells nearer the skin surface, which typically have a more branched morphology, form clusters and also express higher amounts of fascin, implying increased motility of these cells [91, 92].

The hypodermis consists of large pockets of adipose tissue, which both insulates and provides protection, and a vertically orientated network of fibres, which form vacuoles. It functions as a reservoir for interstitial fluid, which can be used to change the stiffness of the tissue. The loose matrix structure of the hypodermis enables the free diffusion of inflammatory and cascading cytokines [93].

The heterogeneity of immune cells and their organisation in the different skin layers reveal how a variety of immune responses may be induced by targeting different subsets of the skin. However, the composition and thickness of the skin is not a stationary state. It is influenced by age and body mass index, shows great inter- and intrapersonal variability, and is interconnected with the human microbiome.

## 1.6 Rationale for vaccination into the dermal compartment

In the last few decades, in the race to develop novel and improved vaccination technologies, there has been a renewed interest in the intradermal compartment as a target site, as it may enable dose sparing and broader immunogenicity compared to injections into the muscle. Transcutaneous and intradermal procedures have been developed for both therapeutic vaccinations, which are primarily geared towards cancer vaccines, and prophylactic vaccinations, which have centred around influenza vaccines but have also been investigated in the context of vaccines for hepatitis B, HIV, SARS-CoV-2, and dengue virus [94–98].

For instance, Arnou et al. demonstrated that intradermal injection of 9 µg of a trivalent inactivated split-virion influenza vaccine in humans achieved a similar immune response to intramuscular injection of 15 µg of the vaccine in adults aged 18 to 60 years [99]. Further influenza studies in healthy

young adults showed, a one fifth dose of trivalent subunit influenza vaccines delivered intradermally (I.D.) gave improved geometric mean titres and comparable seroconversion and seroprotection rates compared to a full dose delivered via intramuscular injection [100]. These data were in accordance with a subsequent study in the elderly ($\geq$65 years), who even showed a higher seroconversion after intradermal injection of inactivated vaccine compared to intramuscular injection, which may suggest further advantages for intradermal vaccination for vulnerable groups [101].

As the development of novel formulations of vaccines are explored, transcutaneous and intradermal delivery has also been investigated as a method of increasing the potency of these new vaccines. For example, as interest in nucleotide based vaccines increases, because they offer a method of rapidly producing cheap versatile vaccines, different intradermal injection techniques are being looked at to improve immunogenicity [102]. A comprehensive review on intradermal vaccinations and their application in low- and middle-income countries has been published by PATH and WHO and complemented by a subsequent WHO bulletin [103, 104]. A precis of these studies may conclude that the dermal compartment represents an immunologically attractive target allowing for robust responses from lower doses but that the process of intradermal delivery is a technically challenging and hard to standardise approach.

The ideal transcutaneous vaccine would provide protective immunity after a single dose and would be safe and cost-effective. The delivery method can significantly impact these factors, as well as affect patient compliance [105]. Considering pain is the biggest vaccine-related concern for parents and especially their children, alternatives to N+S, such as pain-free transcutaneous methods of vaccination, offer the possibility of reversing vaccine hesitancy, which was identified as one of the 10 threats to global health in 2019 according to the WHO [33, 106, 107]. A recent meta-analysis showed that up to 90% of young children have a fear of needles and 16% of adults avoid influenza vaccines because of needle fear [108]. This needle avoidance also carries through to parental vaccinations decisions and needle-sensitive parents are 9% more likely to delay HPV vaccinations for their children [109]. A situation where up to a fifth of the population may refuse a vaccine simply because of the method of its delivery has a substantial negative impact on the already challenging targets required to achieve effective herd immunity for many pathogens.

Furthermore, the issues of the risks associated with cross-infection and hazardous waste generation resulting from N+S use are also addressed by many of these alternative approaches. Indeed, a

study in the Academic Medical Centre in Amsterdam showed that 66% of occupational exposures to potentially infectious material were attributed to needle stick injuries and a study in Germany showed that up to 37% of needle stick injuries involving a hepatitis B-positive donor resulted in seroconversion in a non-immunised recipient [110, 111]. In total, it has been estimated that 16,000 infections of hepatitis C, 66,000 of hepatitis B, and about 1000 of HIV occur per year due to needle stick injuries in health care workers, which are unacceptably high numbers [112]. A review by Mannocci et al. also showed that significant costs are incurred in the management of needle stick injury, including lost productivity, laboratory testing, and potential treatments. These were estimated to equal $747 per needle stick injury in 2015 [113]. The risks of needle stick injuries do not only directly impact healthcare workers, but improper disposal also puts healthcare waste handlers at risk who may not have full knowledge of the risks associated with needle stick injuries [114].

It is no surprise therefore that a raft of new technologies has been developed, which aim to take advantage of the benefits of skin-targeted vaccination without the downsides associated with needle and syringe use. These technologies include microneedles and tattooing, jet and ballistic/particle-mediated delivery, and permeabilization approaches, which have relied upon thermal ablation, chemical enhancers, abrasion, iontophoresis, electroporation, or ultrasound [115–125]. This represents a huge variety of technologies, all applied with the common goal of circumventing the protective stratum corneum layer to access the immune rich milieu below (see Figures 1.1 and 1.2). It is notable that, in addition to providing enhanced levels of safety and patient acceptance, these methods are also increasingly being utilised to achieve higher immunogenicity or improved delivery of a new range of vaccines, such as those based on DNA and RNA.

## 1.7 Delivery of vaccines

For a further exploration of these alternative techniques, please refer to my review paper on the topic of "Vaccination into the dermal compartment" [126]. This thesis focuses on ultrasound-mediated delivery, which is discussed in more detail below.

### 1.7.1 Ultrasound-mediated delivery

Sonoporation refers to the generation of pores in cell membranes as a result of exposure to ultrasound [127]. Such pores are thought to be generated by cavitation events, which involves the expansion and collapse of gas bubbles in response to the alternating rarefactional and compressional

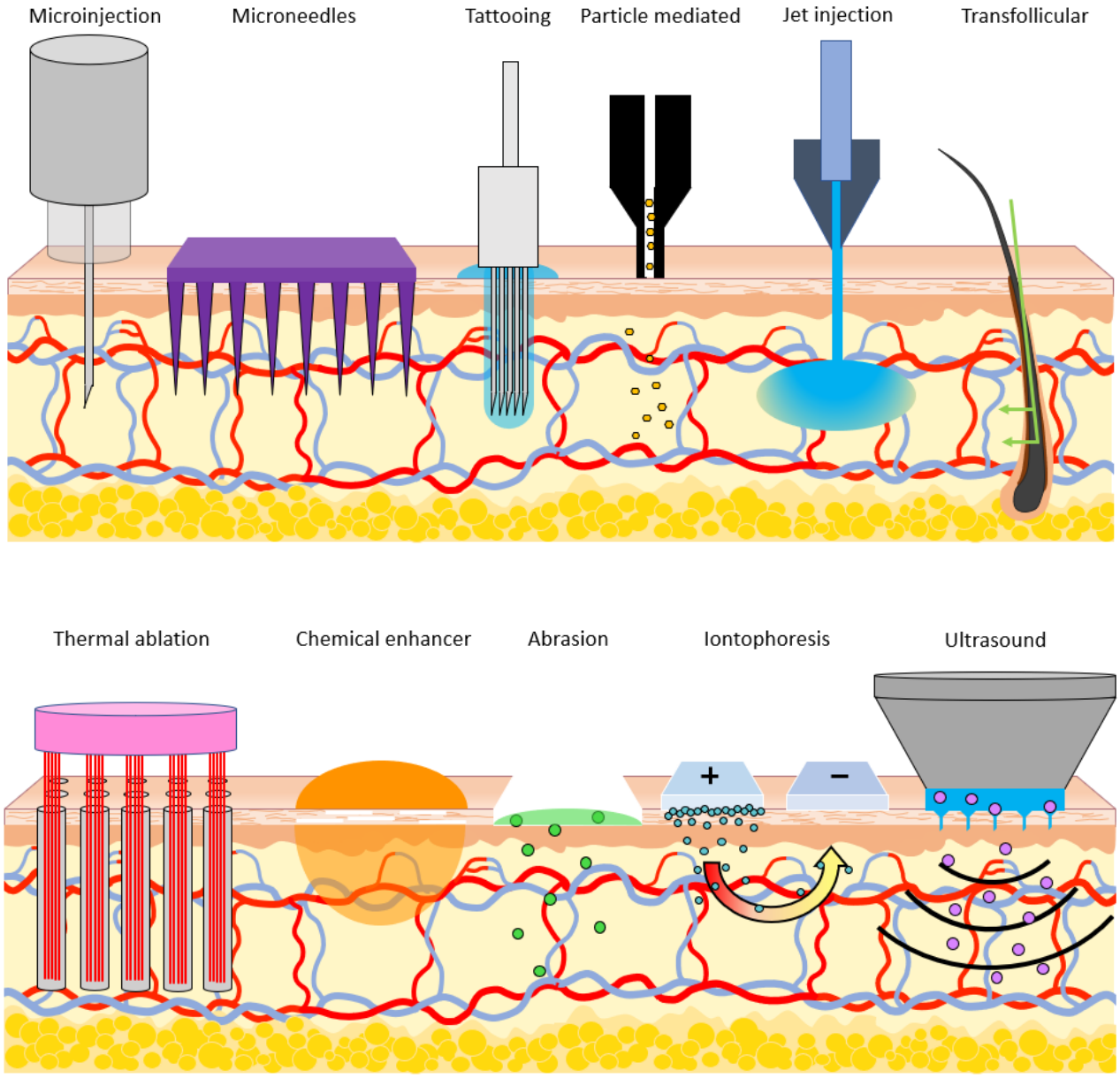



**Figure 1.2.** An overview of techniques used for vaccination into the dermal compartment.

cycles of an ultrasound wave [128]. If a bubble expands uncontrollably, it can reduce the pressure in the cavity to the point where the gas–liquid interface cannot support the inertia of the liquid around the bubble, causing it to collapse. Such events are associated with microstreaming and microjetting have been shown to increase the penetration and extravasation of free drugs in medical applications [129, 130]. The approach also holds potential for permeabilising the stratum corneum and allowing transport into the layers below [131].

The pores created by cavitation can furthermore provide a route for the passage of therapeutic agents into cells, circumventing the endocytosis pathway. The approach is particularly attractive for the delivery of nucleotide-based therapies, such as RNA and DNA, which are typically very effectively excluded from cells and can be degraded in the lysosome during endocytosis [130, 132]. Direct access to the cytoplasm by RNA and cytoplasm and then nucleus by DNA allows for the enhancement of expression, further demonstrating the role ultrasound can play in both successful delivery and improved expression of nucleotide vaccines in the skin [130].

Utilisation of cavitation for the transcutaneous delivery of DNA can hence provide both a means to cross the stratum corneum, as well as provide a mechanism to directly enter the cells in the immune-rich milieu of the dermal compartment.

Initial studies in this field applied the approach in two steps: Firstly, the skin would be exposed to ultrasound with or without gas-bubble cavitation nuclei to create pores, and then a second stage of drug application would be performed [133, 134]. More recently, pre-treatment with ultrasound and a SLS/PBS solution was used to successfully increase permeation of Q-starch/miRNA-197 for psoriasis treatment in a mouse model. The treatment required replenishing of the media every 30 seconds and subsequent application of a patch with the Q-starch/miRNA-197 for 24 hours [135]. Whilst encouraging results were produced for these type of preclinical trials, the process was somewhat suboptimal and is hard to standardise for clinical practice. Crucially, the convective flow and propulsion of drug that can be instigated by cavitation events was not utilised by temporal separation of the cavitation generation step and the drug exposure step. Hence, although the drug may be able to penetrate the barrier more easily, the process is still ultimately reliant on inefficient passive diffusion.

More recently, ultrasound-mediated cavitation has been shown to enhance drug penetration and extravasation in cancer therapy by providing a convective stimulus to push the drug into and through-

out solid tumours [136–138]. Notably, this happens without damage to the structure or activity of the drug [139, 140].

Cavitation as a means to achieve transcutaneous delivery is also gaining traction. Ultrasound-responsive liquid-core nuclei, containing a perfluorohexane core, were used to deliver a commercially available cosmetic product into the skin in a clinical trial. This showed that ultrasound in combination with these nuclei increased uptake by 1.9-fold and increased penetration depth by nearly two-fold. However, the methodology appears to imply that ultrasound was applied for 3 minutes, but the cosmetic/microbubble solution was applied for 30 minutes [141]. The short ultrasound exposure compared to solution application may be the consequence of the limited life-time of microbubbles. Analysis of cavitation data collected during the exposure would have been an interesting addition to these studies to help better understand the effect of ultrasound on the skin over time. Such cavitation measurement can even be used as a metric for successful delivery. The relatively long 30 min application of the solution could limit translation of this method to the clinic for vaccines, as often large-scale roll-out at speed is necessary to make vaccine roll-out practical and economically viable. This does not mean these ultrasound-responsive liquid-core nuclei could not be a useful tool in cosmetic research or enable improved delivery of medication to the skin. The use of the commercially available SONOCUBE does show how utilising existing ultrasound technology could speed up the route to clinic and that a concerted effort to align the device with the formulation is necessary for effective translation.

Ultrasound as an alternative to laser ablation, has also been shown to perforate murine skin in a controllable manner [142]. Using highly focused, high frequency ultrasound allowed for selective perforation of murine skin. The advantage of this method is that skin disruption is very well defined in terms of location and ultrasound pulse-echo imaging enables the monitoring of the channels. The combination of treatment and monitoring make ultrasound a unique competitor to microneedles and other transcutaneous techniques. However, the precision of ultrasound perforation does come at a cost in terms of equipment. Precisely defined ultrasound equipment is needed to accurately generate an array of channels through the stratum corneum. The formed channels allowed for a Hepatitis B surface antigen (HBsAg) to be delivered after ultrasound treatment by the application of a vaccine patch. This method successfully generated antibodies against the antigen and demonstrates the potential of transcutaneous vaccine delivery. Another risk of high frequency, highly focused ultrasound is skin heating which was reported to be 2.72 ℃ on average in a study by Hu et al., something

which may not be clinically acceptable. It does however induce HSP70 expression and may have further adjuvantal effects, as immune cells were observed to actively migrate to the perforation site [142].

A crucial step in improving cavitation-mediated transcutaneous delivery is the availability of gas nuclei that allow cavitation to be generated continuously over several minutes and thereby allow a one-step simultaneous poration-plus-delivery approach [129]. Our lab has developed such gas nuclei, which are denoted 'nanocups'. It is theorized that the sustained microstreaming and microjetting they create in response to ultrasound can permeabilize the stratum corneum, allowing penetration into the epidermis whilst also propelling the drug/vaccine and the nanocups themselves. Using these cavitation nuclei, enhanced transdermal delivery of the model protein OVA across the stratum corneum was shown and an immune response instigated [143, 144]. Crucially, these studies were performed in a single step procedure, with delivered drug co-formulated with the nanocups and present on the skin at the time of ultrasound exposure. These nanocups are a single-cavity polymeric nanoparticle that should have no immunogenic properties and are not biodegradable. Creating alternative nanocups from biodegrable material and even possibly immune-stimulatory nanocups could provide advantages both in immune outcomes as well as regulatory approval. Thus far, no biodegradable nanocup has been reported that can achieve sustained cavitation.

A further intriguing aspect of ultrasound application is the accumulating evidence low-frequency (20 kHz) ultrasound can function as a potent adjuvant, as it has been shown to directly activate immune cells [145]. Despite the advantages of utilizing ultrasound for transcutaneous delivery of vaccines, to date, no clinical trials have been conducted to establish the safety and efficacy in humans. This may be the consequence of the fact that until recently, there was a dearth of cavitation nuclei technology that would allow the generation of sustained cavitation events at relatively minor pressure amplitudes.

Notably, it has also been shown that sonophoresis has synergistic effects with the other transdermal techniques, such as microneedles and electroporation [146, 147]. However, the costs and complexities of bringing multimodal technologies into clinical practice may limit the translation of such combinations.

## 1.8 Summary

The COVID-19 pandemic and the effects vaccines have had on reducing mortality and reopening society, have served as a powerful reminder of the need for quickly deployable, effective vaccines.

Nucleotide vaccines have demonstrated they can provide the necessary speed of production, as they can be quickly designed and produced entirely synthetically and at scale. In response to the pandemic, the first nucleotide vaccines have received emergency regulatory approval. Where RNA vaccines were the first to reach the general public, the logistical complexity of maintaining a cold-chain has proven challenging. Hence, DNA vaccines, which are stable at ambient temperatures, have been suggested as a potential successor to RNA vaccines. However, as DNA needs to reach the nucleus, as opposed to the cytoplasm like RNA, the delivery challenges have been significant. Indeed, the first DNA vaccine to achieve approval notably relied on the unconventional delivery method of jet injection and still required two boosters to reach a desired immune effect.

Furthermore, there is a mounting body of literature which makes a compelling argument for selecting the dermal compartment as a target for vaccination as its immune cell-rich environment may allow for lower doses to have a larger effect compared to intramuscular delivery. Additionally, moving away from needles, may help address fear of needles and thus, increase vaccine uptake, as well as reduce the burden of needlestick injury currently affecting health workers. Cavitation-mediated delivery utilising ultrasound was suggested as a potential method for vaccination, as it is needle-free, has been shown to mediate dermal delivery and may have intrinsic adjuvant effects. Furthermore, it was proposed here that the use of immune-stimulatory cavitation nuclei could lead to better immune responses compared to polymeric nanocups.

Having established the benefits of nucleotide vaccines, particularly in response to pandemics, caused by rapidly mutating pathogens, as well as the advantages and challenges of the use of DNA vaccines, this thesis focuses on the use of DNA vaccines to generate a protective immune response and the role cavitation can play as a delivery method. Further, noting the merit of vaccination into the underutilised dermal compartment, ultrasound and cavitation are examined as a means of delivery into the (epi)dermal layer of the skin. To further enhance the effect of ultrasound, immunogenic cavitation nuclei are investigated and their potential as immune-stimulatory agents tested.

In summary, the aims of this thesis are:

- To improve delivery and increase reproducibility for cavitation-mediated delivery of DNA into the skin *in vivo*.
- To investigate the potential of immunogenic cavitation nuclei for mediating DNA plasmid delivery as well as generating immune responses *in vivo*.
- To assess the capability of different DNA constructs in eliciting an immune response against influenza haemagglutinin protein *in vivo*.
- To evaluate the utility of combining an optimised immunogenic cavitation nuclei, ultrasound and optimised DNA vectors as an effective vaccination strategy *in vivo*.

# Chapter 2

# Exploratory studies of ultrasound-mediated delivery of DNA

## 2.1 Introduction

It has previously been shown by authors including Dr. Van Blokland [143] and Dr. Bhatnagar [148] that drug and vaccine delivery can be enhanced using ultrasound-mediated cavitation. Whilst this work provided an important proof of concept, scope remains for improving both total delivery and increasing the immunogenicity of the vectors. The studies described in this chapter provide the first exploratory studies to establish potential improvements in delivery and efficacy.

From the ultrasound perspective, utilising the equipment and set-up used by Dr. Van Blokland, initial studies sought to optimise delivery parameters by considering different ultrasound exposure pressures. Furthermore, it was also clear that more robust comparison to more traditional needle and syringe modes of delivery was needed.

Whilst many DNA vaccines rely on the use of plasmids grown in, amplified in and purified from bacteria, the work here relied on the use of doggybone DNA™ as the DNA vector [69]. As such a vector is essentially produced 'cell-free', there should be a reduction in vector backbone-specific immunity and improvement in the ease of production and scale-up (as detailed below).

### 2.1.1 doggybone DNA

Touchlight Genetics Ltd. has developed a platform technique, marketed as Doggybone DNA$^{TM}$ (dbDNA$^{TM}$), which allows for the vector-free production of DNA sequences. dbDNA$^{TM}$ is a covalently

closed, linear DNA construct, produced in a cell-free way. This system allows the production of multi-grams of GMP DNA within 2 weeks of sequence identification. A template with 56 bp protelomerase binding sites flanking the sequence of interest, is amplified using rolling-circle amplification by Phi29 DNA polymerase. This results in a long concatameric DNA strand, which is cleaved by the protelomerase enzyme TelN [69, 149]. This protelomerase also catalyses the formation of covalently closed hairpin ends (Figure 2.1). These hairpins prevent exonuclease activity and illegitimate recombination events [150], which makes for a superior long-stranded DNA construct for clinical applications compared to PCR-amplified DNA. The leftover DNA strands are degraded with exonucleases. This process is both high-fidelity ($1/10^6$-$1/10^7$) and allows for high processing (approximately 70 kbp). As the protelomerase sequences only flank the relevant sequence, all vector sequences are removed during the production of the dbDNA$^{TM}$, preventing unwanted sequences, such as antibiotic resistance, being introduced into the host. It has already been shown that tail vein injection of naked dbDNA$^{TM}$ can achieve transfection of mice with a luciferase gene under the spleen focus-forming virus promoter, enabling higher whole-body expression than similar plasmid DNA [149].

### 2.1.2 DNA vectors

The poor delivery of DNA vaccines is recognised as a factor limiting their translational success (see section 1.3), and although nanocarriers have shown recent clinical success for mRNA delivery, such success has yet to be observed with DNA. One approach to addressing the inefficiency of DNA vaccines, which results from their limited delivery, is to ensure the low levels which do successfully reach the nucleus are as active as possible. Indeed, there have been multiple attempts to increase the immunogenicity and efficacy of individual DNA vaccines, including those for cancer. These have included promoter and coding sequence optimisations, incorporation of CpG islands (an approach which may increase TLR activation but may also cause rapid shutdown of transgene expression), co-encoding of cytokines, and use of heterogenous prime-boost strategies [152–154].

However, these strategies have not been evaluated for ultrasound-mediated delivery. In particular questions over the mechanism, efficiency and cell-type specificity of cavitation-mediated delivery have yet to be answered and so means of optimising the DNA sequence around these factors remains unaddressed. Hence, studies in this chapter aimed to design and test DNA constructs to answer some of the questions relating to the impact DNA vector design has on immunological outcomes.

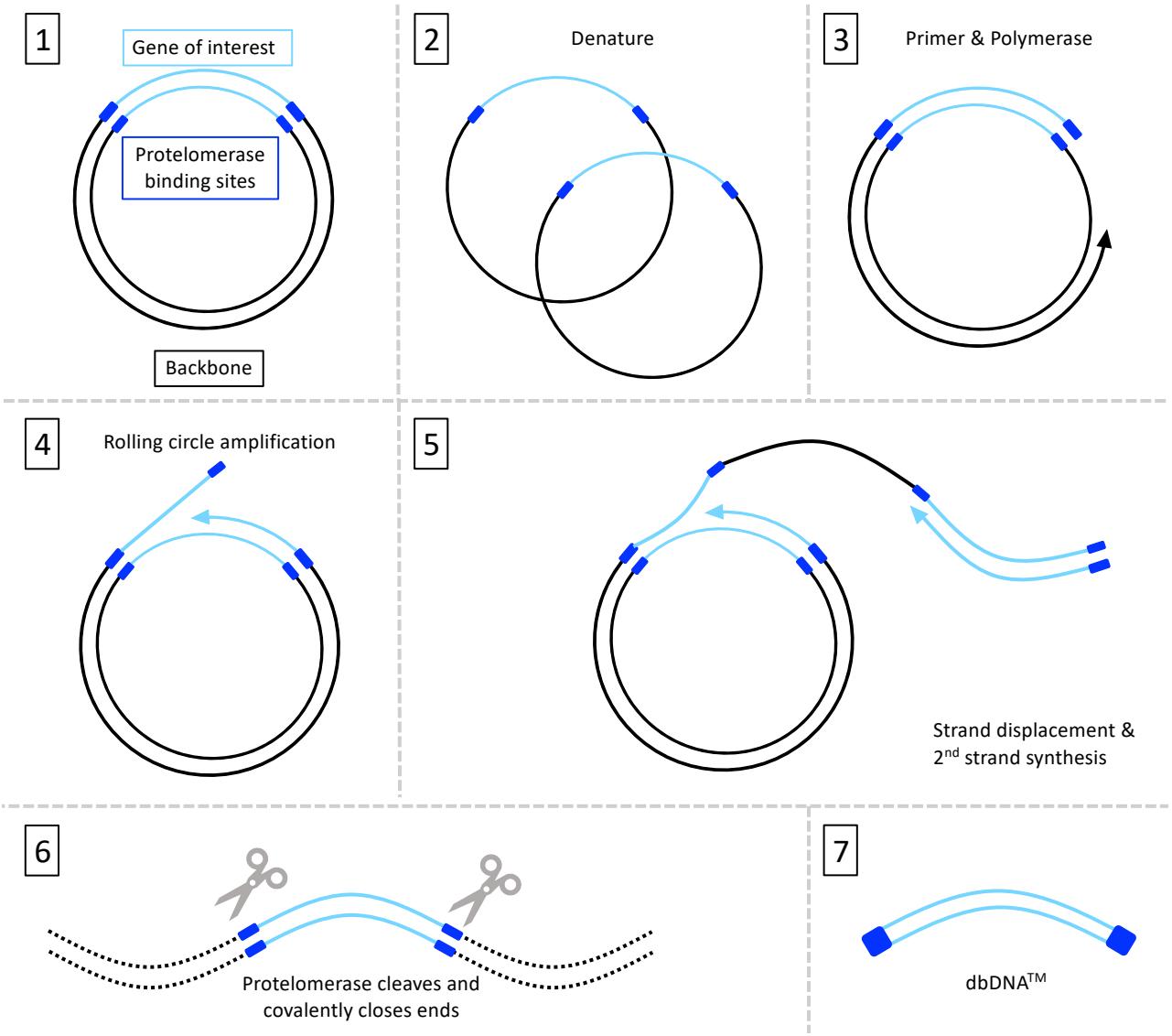



**Figure 2.1.** A schematic representation of the patented DNA amplification process of Touchlight Genetics Ltd. Adapted from [151]

### Promoters

Promoters play a crucial role in driving expression. Different considerations play into picking a promoter, in terms of level of expression, duration of expression and cell specificity.

#### CMV promoter

The CMV promoter is derived from the human cytomegalovirus. It is commonly used to drive mammalian gene expression, as it is widely applicable and shows high levels of expression in differentiated cells. A disadvantage of this promoter is that it can be downregulated by cells. For example, the CMV-promoter has been shown to be silenced by methylation in rats intramuscularly injected with an adenovirus encoding the human fibroblast growth factor 4 under the CMV-promoter. The authors reported, mRNA production peaked at 6 hours and then decreased rapidly with methylation of the

delivered DNA shown to be the largest contributing factor to the decreased expression [155].

In the context of the research in this thesis, where vectors are introduced to the skin, Vandermeulen et al. showed that upon electroporation, the CMV promoter drove higher levels of expression in skin (based on luciferase expression) compared to tissue specific promoters such as the CD11c promoter and the fascin promoter [156]. CMV promoter-driven expression of luciferase after intrapinna electroporation in mice also resulted in the highest induction of interferon-$\gamma$, showcasing the potential value of CMV as a promoter to successfully drive antigen production upon vaccination.

In the clinic, the ZyCoV-D DNA vaccine utilised the pVAX1 vector to express the Spike protein sequence [63]. This vector relies on the CMV promoter to drive protein expression [157], further demonstrating that the CMV promoter is a strong candidate for driving the antigen expression necessary for effective vaccination, but also highlighting a possible route to improvement of an approach which requires triple dosing to achieve efficacy.

Elongation factor 1 alpha (EF1$\alpha$) promoter

Where the CMV promoter can induce high expression, but potentially for a limited time due to downregulation, the EF1$\alpha$ promoter is derived from a household gene and is constitutively active in a wide variety of cells due to the role of the EF1$\alpha$ protein in delivery of aminoacyl tRNAs to the ribosome.

For example, the EF1$\alpha$ promoter maintains better transgene expression in long-term culture in CHO-K1 cells, based on recombinant protein expression after selection with geneticin of stably transfected cells ($p<0.05$) [158]. The EF1$\alpha$ promoter also showed expression stability after integration of eGFP constructs in undifferentiated human embryonic stem cells, whereas the CMV promoter showed significantly more downregulation ($p<0.0001$) [159]. Upon lentiviral transfer to P19 embryonic pluripotent carcinoma cells, a similar trend was observed. The CMV promoter was rapidly silenced (5 days) whereas the EF1$\alpha$ promoter had delayed silencing (20 days) and high-level gene expression for a CpG-rich GFP construct [160].

Despite not being in the clinic, the EF1$\alpha$ promoter is an interesting comparator to the CMV promoter in terms of ideal expression profile of an antigen. Where the CMV promoter may have advantages in terms of total protein expressed, the EF1$\alpha$ may provide benefit by giving longer expression of the antigen. Or on the contrary, such a long and low antigen expression profile may lead to tolerance.

**Targeted expression**

There is insufficient knowledge of the specific cell types transfected upon cavitation-mediated DNA delivery to the skin. Therefore testing of cell- or tissue-specific promoters may give more insight into the cells that are targeted and the types of cells that most effectively elicit immunity upon transfection.

Keratinocyte-specific expression

The KCL27 promoter has been identified by Touchlight Genetics Ltd. as resulting in effective gene expression in keratinocytes (personal communication). Keratinocytes form the majority of the epidermis, the layer targeted by cavitation-mediated delivery, and are considered an active participant in enabling immune responses. They possess different PRRs, including toll-like receptors and RIG-I-like receptors, and can express a range of cytokines [161].

If the KCL27 promoter can be used to limit expression to keratinocytes, their role in eliciting an immune response after cavitation-mediated delivery can be gauged.

Immune cell-specific expression

Immune cells form a relatively small proportion of the total cells in the epidermis. The predominant immune cell type in the epidermis is Langerhans cells. These are antigen-presenting dendritic cells. They patrol and sample their environment for antigens, which they then present to T cells, to mount an adaptive immune response [162]. CD11c is specific to dendritic cells and expressed by Langerhans cells and other dendritic cells in the dermis. Previous research by Vandermeulen et al. showed that a CD11c promoter could achieve $\sim$ 3% of the expression of CMV or CAG (CMV-actin-globin promoter) in mouse skin upon gene gun treatment, a low level which fits with the low proportion of immune cells in the skin [156]. Research by Moulin et al. also showed that CD11c is specifically expressed in immune cell lines [122].

Hence, using a CD11c promoter would restrict antigen expression to immune cells. If a successful antibody response could still be mounted, this could show that it is the direct transfection of immune cells that is crucial for raising an immune response, rather than the sampling of antigen eptiopes produced in keratinocytes, for example.

**Adjuvants**

As mentioned in the introduction (Section 1.4), adjuvants are a common addition to most vaccines to improve the immune responses generated. Hence, the effect of delivering adjuvants at the DNA level for production of protein in the target cells was investigated.

Interleukin-1

Interleukin-1 (IL-1) can strongly impact the innate immune system [163]. IL-1 can be present as $\alpha$ or $\beta$ [164]. The $\alpha$ form does not require further processing to function, whereas the $\beta$ variety needs to be cleaved by caspase 1 [165]. IL-1 is a systemic cytokine, which can also function as an adjuvant even when applied at a distance from the vaccine site [166]. The strength of IL-1$\beta$ can be seen in the number of auto-inflammatory diseases with which it is implicated [167]. It is also speculated that the release of pre-stored IL-1 could be one of the first signals for keratinocytes to be activated and excrete further cytokines [168].

Previous research on the adjuvant properties of interleukin-1 in mice, has shown that when delivered as recombinant protein, it significantly enhanced the antibody titres for inhalable influenza vaccines. Particularly IL-1$\beta$ and IL-18 provided complete protection [164]. IL-1 has also been shown to enhance the effect of weak vaccines and enable protection against fungal infections, even more so than lipopolysaccharides. In a study by Wüthrich et al., IL-1 specifically enhanced the expansion and differentiation of CD4+ T cells [169]. IL-1$\alpha$ can initiate a rapid activation of a cascade of inflammatory cytokines and chemokines, resulting in inflammation [165]. It is notable that many traditional adjuvants also greatly increase the secretion of IL-1$\beta$ [170, 171]. Hence, interleukin-1 seems to be a crucial cytokine which has previously been successfully used in recombinant protein form in the context of influenza vaccines, meriting further investigation in the research in this thesis.

Interleukin-12

Interleukin-12 (IL-12) is usually produced by activated inflammatory cells, such as macrophages, dendritic cells and neutrophils. IL-12 connects the innate to the adaptive immune systems and plays a role in the differentiation of T helper cell 1. It enhances IgG1, but downregulates IgE in humans [172], although other research by Metzger et al. has suggested IL-12 downregulates IgG1 and stimulates IgG2 in mice [173]. It has proven to be a strong enhancer of IFN-$\gamma$ and can be a successful adjuvant for tuberculosis treatment [174]. A DNA vaccine encoding the antigen and IL-12 also improved survival ($p<0.05$) in mice compared to a DNA vaccine encoding only the antigen, as well as significantly

reduced the metastases compared to untreated controls. [175]. CpG motifs in bacterially-produced DNA rapidly result in the excretion of interleukin-12 in mice [176]. Furthermore, it has been used as an adjuvant for an inhalable influenza vaccine in mice. This showed the potential for IL-12 in antiviral immunity [177]. A human trial for a cytomegalovirus vaccine with recombinant IL-12 protein as an adjuvant showed IL-12 was well tolerated and resulted in higher IgG peaks and CD4+ T cell proliferation [107]. These results make IL-12 an interesting candidate for a DNA-encoded adjuvant.

CpG islands

Unmethylated CpG motifs trigger toll-like receptor 9, which activates the innate immune response by the upregulation of proinflammatory genes [178]. Upon intraperitoneal administration in mice, upregulation of gene expression could be observed as soon as 30 minutes after injection [179]. The initial gene upregulation included genes involved in the B-cell receptor pathway, as well as induction of the innate immune system activators, such as interleukin-1$\alpha$ and interleukin-1$\beta$ [180]. CpG sequences have also been shown to be a valuable addition to vaccines and have been shown to boost the humoral immune response of vaccines against a plethora of pathogens, varying from anthrax to tetanus toxoid [181].

In a clinical trial, the addition of CpG oligodeoxynucleotide to a 1/10th dose of influenza vaccine resulted in significantly higher levels of IFN-$\gamma$ secretion compared to a 1/10th dose of influenza vaccine alone, and levels were similar to those achieved using a full-dose of vaccine. This dose-sparing activity shows the potential of CpG motifs to increase immunogenicity of vaccine where low-doses are delivered, such as with cavitation-mediated delivery [182]. In a different clinical trial, the addition of a CpG adjuvant to a Hepatitis B vaccine, the addition of the adjuvant resulted in both earlier (at 2 weeks 50% seroconversion in adjuvanted group vs 0% in the non-adjuvanted group) and higher antibody titres (4-fold at 26 weeks compared to the unadjuvanted control) [183]. More recently, a candidate COVID-19 vaccine combined recombinant Spike protein with a CpG adjuvant and aluminium hydroxide. This vaccine showed 99.8% seroconversion and successfully finished phase 2 trials [184]. The history of CpG as a valuable adjuvant in clinical trials, supports the exploration of the role CpG can play in the development of a DNA vaccine delivered by ultrasound-mediated cavitation.

RIG-I

RIG-I receptor is an RNA helicase that detects pathogen-associated molecular patterns (PAMPs) in the cytoplasm. It particularly plays a role in controlling virus infection by driving expression of inter-

feron and antiviral genes [185]. This includes playing a critical role in driving interferon expression upon influenza infection [186]. Apart from a helicase domain, it has two N-terminal caspase activation and recruitment domains. Upon binding of double-stranded RNA, RIG-I undergoes a conformational shift. This allows the caspase activation and recruitment domain to interact with interferon-β promoter stimulator. This interferon-β promoter stimulator starts an activation chain that results in pro-inflammatory cytokine production and NF-κB activation [187].

Two phase 1 clinical trials have been performed to investigate the efficacy of intratumoral injection of a RIG-I agonist in solid tumours and the agonist in combination with intravenous pembrolizumab for the treatment of solid tumours. Only abstracts are available on the results of these trials. These suggest that intratumoral injection resulted in increased chemokine levels in serum, as well as upregulation of genes involved in interferon signalling [188, 189].

The role RIG-I agonists can play in the upregulation of interferon can be a powerful tool in boosting the immunogenicity of vaccines and is tested in this chapter.

To begin assessing cavitation-mediated delivery of DNA vaccines, several exploratory studies were conducted, which are summarised in the aims of this chapter. These are to:

- Relate the pressure applied and cavitation detected to the level of transgene expression observed.
- Compare cavitation-mediated delivery of DNA to subcutaneous, intradermal and intramuscular injection.
- Quantify the total amount of DNA delivered to skin using cavitation.
- Construct and test DNA vectors to assess the effect of altering promoters, promoter specificity and adjuvant vectors on immunogenicity.

## 2.2 Materials and Methods

### 2.2.1 Ultrasound set-up

The ultrasound set-up (V1) used, was developed by Dr. Van Blokland and Dr. Bhatnagar, and the parameters used in this thesis are a development on their work [143, 148]. A signal was generated by a waveform generator (33250A, Agilent, United Kingdom), using the parameter set in Table 2.1.

**Table 2.1.** Summary of the ultrasound parameters used.

| Ultrasound parameters | Settings |
|---|---|
| Driving Frequency | 265 kHz |
| Duty cycle | 10% |
| Pulse Repetition Frequency (PRF) | 10 Hz |
| Pulse Length | 10 ms |

This was passed to a high-power radiofrequency (RF) amplifier (E&I 1040L RF Amplifier, Electronics & Innovation, Ltd, USA). A matching network (H-117 SIN-001, Sonic Concepts, USA) was used to match the impedance of the output of the amplifier to the transducer. The transducer (117D-01, Sonic Concepts, USA) was fitted with a Perspex coupling cone, filled with degassed water and covered with an acoustically transparent Mylar plastic. The coupling cone was designed to align with the outer envelope of the focused ultrasound beam. A formulation holder, containing the dbDNA™-Luc and nanocups (NC) solution, was placed on the murine skin and the transducer was placed on top of this, with the Mylar plastic acoustic window positioned to prevent air entering the acoustic path. A passive acoustic detector (PCD) was coaxially located inside the driving transducer, to allow the cavitation signal to be recorded. The PCD signal was passed through a 2.0 MHz high pass filter and amplified 25 times by a pre-amplifier (SR445A, Stanford Research Systems, USA). The signal was then digitised by an 8-bit digital oscilloscope (Handyscope HS3 100 MHz, TiePie Engineering, The Netherlands) and the data was saved on an external hard drive (Portable SSD T5, Samsung, Korea) (Figure 2.2). The sampling frequency was 50 MHz for the *in vivo* studies to optimise the treatment pressure with 2 ms sampled for each pulse and 25 MHz for all subsequent experiments with 4 ms sampled for each pulse to enable a larger proportion of the pulse to be captured.

### 2.2.2 Transducer calibration

The pressure field of the transducer (117D-01, Sonic Concepts, USA) with the attached custom coupling cone was measured. To this end, the coupling cone was sealed with a mylar sheet, filled with

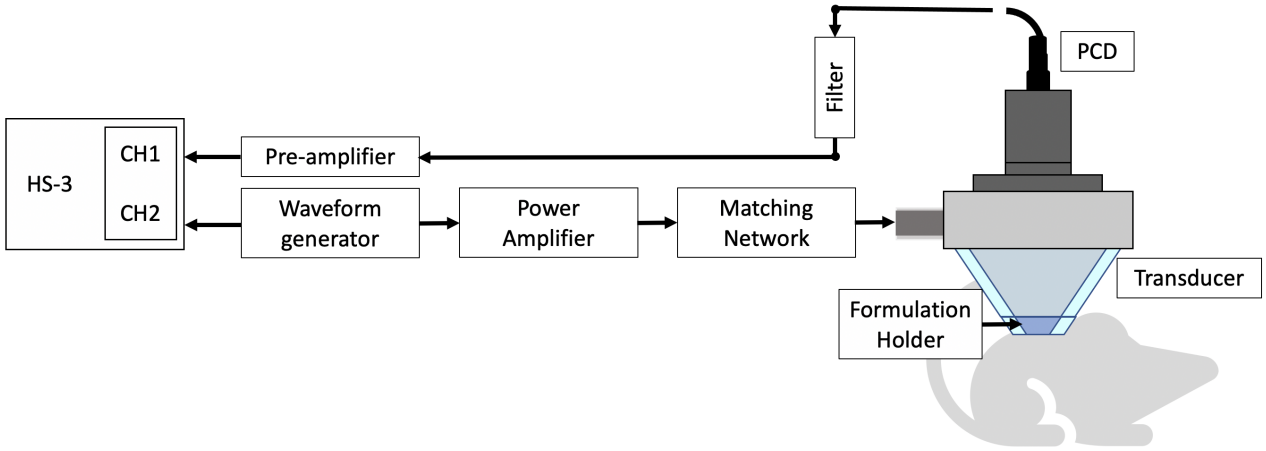



**Figure 2.2.** Schematic of the ultrasound set-up used in the early immune studies (V1), as described in section 2.2.1

degassed water, and placed above a water tank. The tank was filled with degassed water, to ensure the boundary conditions of the transducer were similar to those during treatment. The signal was generated by a waveform generator, which was connected to an amplifier. The amplifier signal was passed to a matching network (H-117 SIN-001, Sonic Concepts) that was attached to the transducer. A hydrophone (Onda HNA-0400, Onda Corporation, USA) was used for the pressure measurements. Measurements were collected with an oscilloscope (HDO4024 Teledyne Lecroy, USA) and the pressure profile was determined in the longitudinal and transverse plane. In the transverse plane two pressure profiles were measured, as seen in Figure 2.3. The focal point at 59.7 mm distance from the transducer was set as the origin. For each point, the root mean square of the signal was calculated. The pressure was normalised to the pressure at the focal point. The profiles are presented in Figure 2.3.

### 2.2.3 Acoustic data processing

The full acoustic signal of the burst could not be recorded, due to limitations of the software and data storage requirements. Instead, only two or four of a total of ten milliseconds were recorded. It was assumed that the acoustic signal recorded between 0.4 ms and 1.8 ms of each burst would be representative of the 10 ms pulse if 2 ms was recorded. If 4 ms were recorded, the signal between 0.4 and 3.5 ms was assumed to be representative.

Post-acquisition of the data, the data was resampled at 50,085,000 Hz if the original sampling frequency was 50 MHz and at 25,175,000 Hz if the original sampling frequency was 25 MHz to enable the easy separation of the inertial and non-inertial component. A digital high pass filter of 2.0

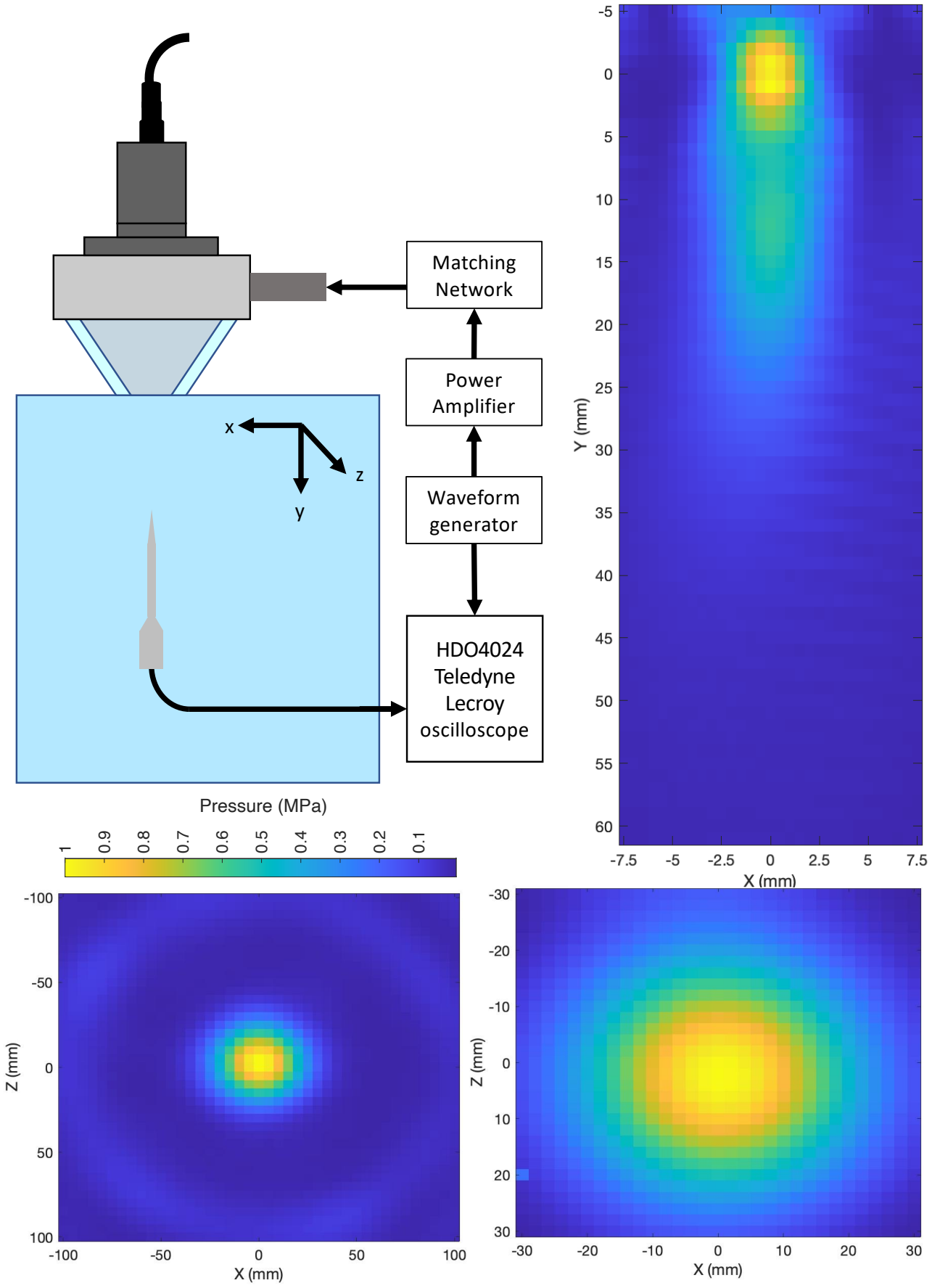



**Figure 2.3.** Top left: Experimental set-up used to determine the pressure field of the transducer with coupling cone. Top right: the pressure profile in the longitudinal plane. Bottom left: the pressure profile in the transverse plane. Bottom right: a zoomed in pressure profile in the transverse plane. Pressure was normalised to the pressure in the focus, which is located 59.7 mm below the coupling cone.

MHz was applied for the V1 set-up or 1.8 MHz in the V2 set-up. Subsequently, the data of each burst would be windowed for the appropriate time-interval and a Tukey window applied. The windowed data would be converted to the Fourier domain and the electrical energy for each frequency calculated. A spectrogram in dB re nJ was generated for each treatment, containing this electrical data per frequency for each pulse.

The total acoustic sensor energy (TASE) was calculated with the following formula:

$$TASE = \sum_{n}^{i=1} \frac{(V_{rms}(i))^2}{R} * T_{pulse} * R_{recorded} \tag{2.1}$$

The root mean square of the voltage measured in the time window was calculated. To calculate the total power, the root mean square of the voltage was squared and divided by the impedance, estimated at 50 Ω. This was multiplied with the actual pulse time to estimate the total energy of each pulse. Finally, as not every pulse was recorded, the TASE was corrected for the actual number of pulses ($R_{recorded}$).

To further analyse the acoustic emissions, the inertial cavitation was separated from the non-inertial cavitation. This was done by converting the windowed data to the Fourier frequency domain and applying a notching comb filter every 132.500 Hz (to account for the driving frequency of 265 kHz), with a width of 10.000 Hz to remove both harmonics and ultraharmonics. The TASE was calculated for this filtered dataset and an estimated inertial TASE (iTASE) was calculated by correcting the calculated TASE of the filtered dataset for the percentage of the frequency domain removed. Hence, for an original sampling frequency of 25 MHz, which was resampled at 25.175 MHz, and a filter width of 10 kHz, the iTASE would be equal to the TASE value of the filtered data divided by 0.9241 to compensate for the removal of 7.59% of the frequency domain by the notching comb-filter.

### 2.2.4 Statistics

Statistical analysis was done in Prism 9 (GraphPad Software, USA). A Welch's t-test was done when two groups were compared. Multiple independent groups were compared with a one-way ANOVA Tukey HSD post all group comparisons. Alternatively, groups were compared to a reference group with a one-way ANOVA with a Dunnett's test. Isotype changes (IgG1 and IgG2a) between groups were assessed with a two-way ANOVA with a post hoc test between isotypes for each group using the Šidák correction for multiple comparisons.

Luminescence and titres were log-transformed prior to statistical analysis and their geometric means $\times/\div$ geometric standard deviation (GSD) determined, as luminescence data was spread over orders of magnitude and titres were assessed across fold-changes.

### 2.2.5 *In vivo* model

Female BALB/c mice were obtained from Charles River Laboratories (USA) by the Biomedical Services at the John Radcliffe Hospital (Oxford, United Kingdom). All mice were kept in groups of up to 13 mice, in individually ventilated cages, under standardised and controlled living environments, under a Home Office approved project licence in line with Home Office Legislation and Oxford University Gold Standard. All procedures were performed by appropriately trained Home Office personal licence holders.

### 2.2.6 *In vivo* imaging

The mice were imaged after 24, 54 and/or 120 hours with an In Vivo Imaging System (IVIS, PerkinElmer, USA). They were anaesthetized with 2% isoflurane and 98% oxygen at 2 L/min flow rate. 100 µL of 15.8 mg/mL Pierce™ D-luciferin (88294, ThermoFisher Scientific, USA) was injected into the tail vein. The mice were imaged 3.5 minutes after injection and imaged for 30 seconds. The images were processed with Living Image® (PerkinElmer®, USA). The treatment area was digitally selected and the total luminescence (photons/sec) and the average radiance (photons/sec/cm$^2$/sr) were determined. The luciferase signal was displayed with bioluminescence intensity colour bars, scaled to cover the full range of intensity.

### 2.2.7 Blood sampling

10 µL blood samples were taken by tail-vein bleeds on a regular basis to assess antibody response. After culling, a 50 µL terminal bleed was taken. All blood samples were immediately diluted 10-fold in PBS. The cells were pelleted by centrifugation at 3000xg for 2 min. The serum was placed on ice and subsequently frozen at -20 ºC or -80 ºC .

### 2.2.8 *In vivo* protocol for the optimisation of pressure

#### Skin preparation

On the day of treatment, female BALB/c mice were anaesthetized with 2% isoflurane and 98% oxygen at 2 L/min flow rate. The treatment site was shaved with an electric razor. A depilatory cream

(VEET, Reckitt, UK) was applied to ensure full removal of the hair and rinsed off after 1 minute.

#### dbDNA™ delivery utilising ultrasound

For the transdermal delivery, approximately 2 mL of the formulation was placed in the formulation holder, equating a dose of 52.8 µg dbDNA™-Luc. The mice were placed under the ultrasound set-up for 10 minutes and treated with 0.5 MPa, 0.7 MPa, 0.85 MPa, 1 MPa or 1.6 MPa. After exposure, the excess formulation was removed by rinsing the treatment area with water and drying the skin with clean tissue. The treated area was encircled with a permanent marker pen.

#### dbDNA™ delivery with needle and syringe

For intramuscular injection, 22 µL was injected twice, which delivered a dose of 52.4 µg dbDNA™-Luc. For subcutaneous and intradermal injection, a total of 50 µg dbDNA™-Luc was delivered with a 100 µL injection.

### 2.2.9 Quantification of DNA delivery

#### Treatment

Mice were treated as described above in section 2.2.8 at 1.0 MPa for 10 minutes. Mice were imaged after 24 hours, as described in section 2.2.6. Directly after treatment, the mice were culled and the treated skin harvested.

#### Tissue preparation

The gross level of dbDNA™ delivered to the whole skin sample was measured. Skin tissue was cut in small pieces and 1x Promega Lysis Buffer (E1531,Promega, USA) was added to a final dilution of 125 mg skin per 1 mL of buffer. This was frozen at -80 ºC and then thawed. The thawed suspension was placed in a GentleMacs C tube (130-093-237, Miltenyi Biotec, Germany) and homogenised with a GentleMacs™ dissociator (Miltenyi Biotec, Germany) by running the predefined Multi_H_01 programme five times. This solution was spun down at 800xg for 1 minute.
100 µL of the homogenised supernatant was sampled and used for genomic DNA extraction. The rest of the homogenised solution and supernatant was stored at -80 ºC. 20 µL RNase from the GenElute™ Mammalian Genomic DNA Miniprep Kit (G1N350-1KT, Sigma-Aldrich, USA) was added to the homogenised supernatant and the cells were lysed with Lysis Solution C and proteinase K from the same kit. This solution was vortexed for 15 seconds and incubated at 70 ºC for 10 minutes.

Column preparation, binding, loading of samples, washing and eluting were performed according to manufacturer's instructions of the he GenElute™ Mammalian Genomic DNA Miniprep Kit (G1N350-1KT, Sigma-Aldrich, USA).

#### Standard curves

Standard curves were prepared by diluting various known amounts of dbDNA™-Luc in Promega Lysis Buffer (E1531, Promega, USA). These solutions were then added to untreated murine skin and processed exactly as described above.

#### qPCR conditions

A mastermix containing the primers, probe (Table 2.2), 2x qPCRBIO Probe Mix Hi-ROX (PB20.22-01, PCR Biosystems Ltd., UK) and nucleotide-free water was prepared, according to manufacturer's instructions. 5 µL of eluted DNA, which was either from a sample or a spiked control, was added to 15 µL of the mastermix. The solution contained a final concentration of 400 nM of forward and reverse primers, 200 nM of the TAM-FAMRA labelled probe, polymerase, nucleotides, buffers and ROX dye as a reference.

The plate was analysed on a StepOnePlus™ Real-Time PCR System (Applied Biosciences). The cycling conditions for the qPCR were 95 ℃ for two minutes for DNA denaturing and 40 cycles of 95 ℃ for five seconds and 60 ℃ for 30 seconds.

**Table 2.2.** Sequences of the probe, reverse and forward primer for the qPCR quantification of dbDNA™-Luc.

| | **Sequence (5'-3')** |
|---|---|
| Probe | [6FAM]TGCTGGTGCCCACACTATTTAGCT[TAMRA] |
| Reverse primer | GTCGTACTTGTCGATGAGAGTG |
| Forward primer | CTTCGAGGAGGAGCTATTCTTG |

### 2.2.10 DNA vector design and construction

#### Plasmid templates and custom gBlocks

The plasmids proTLx-κ B5X4 Cal09 HA, proTLx-κ B5X4 mIL12, TIVA-pUC EF1α-eGFP and proTLx-κ N3X2 KCL1-27 E6-E7 were kindly donated by Touchlight Genetics Ltd. gBlocks (Integrated DNA Technology (IDT), USA) were ordered for the sequences of:

- IL1$\alpha$ with overlapping sequences for the CMV promoter and P2A
- IL1$\beta$ with overlapping sequences for P2A and the proTLx-$\kappa$ B5X4 backbone
- The CD11c promoter with overlapping sequences for proTLx-$\kappa$ B5X4 Cal09 HA.

The following genetic elements are used in this chapter, Table 2.3, and the following genetic constructs are referenced, Table 2.4. The plasmid maps of all plasmids used in this chapter in *in vivo* studies are available in Appendix A.

**Table 2.3.** Overview of all elements of the genetic constructs described in this chapter.

| Name | Category | Function and origin |
|---|---|---|
| CMV | Promoter | The human cytomegalovirus (CMV) promoter used to drive gene expression – characterised as strong. Sequence is courtesy of Touchlight Genetics Ltd. |
| KCL27 | Promoter | Keratinocyte-specific promoter. Sequence is courtesy of Touchlight Genetics Ltd. |
| CD11c | Promoter | Promoter from the immune cell-specific gene CD11c. Sequence derived from [156]. |
| EF1$\alpha$ | Promoter | Promoter from the household gene eukaryotic translation elongation factor 1 alpha (EF1$\alpha$). Sequence is courtesy of Touchlight Genetics Ltd. |
| Cal09 HA | Antigen | The model antigen used to elicit an immune response. It is the haemagglutinin of the A/California/07/2009 (H1N1) influenza virus. Sequence is courtesy of Touchlight Genetics Ltd. |
| E6-E7 | Antigen | E6 and E7 genes of the human papillomavirus (HPV). |
| mIL12 | Adjuvant | Interleukin 12 is usually produced by activated inflammatory cells and plays a role in the differentiation of T helper cell 1. Sequence is courtesy of Touchlight Genetics. |

| | | |
|---|---|---|
| IL1α and IL1β | Adjuvant | A systemic cytokine. Sequences are derived from GenBack accession number: NM_010554 (IL1α) and NM_008361 (IL1β). |
| CpG | Adjuvant | CpG motifs stimulate the innate immune system through binding to TLR9. Sequence is courtesy of Touchlight Genetics Ltd. |
| RIG-I | Adjuvant | RNA sequence that binds to RIG-I, a cytosolic pattern recognition receptor (PRR) which can trigger a type-1 interferon (IFN1) response. Sequence is courtesy of Touchlight Genetics Ltd. |
| P2A | self-cleaving sequence | This sequence enables ribosomal skipping, which results in two individual proteins from a single RNA strand. Sequence is courtesy of Touchlight Genetics Ltd. |
| proTLx-κ | Vector backbone | A cloning vector compatible with the doggybone DNA production. Sequence is courtesy of Touchlight Genetics Ltd. |
| TIVA-pUC | Vector backbone | An *E. coli* compatible cloning vector. Sequence is courtesy of Touchlight Genetics Ltd. |

**Table 2.4.** Overview of all plasmids used as templates or created in this chapter. It lists the name, promoter, backbone and transgene of each construct

| **Plasmid name** | **Backbone** | **Promoter** | **Transgene** |
|---|---|---|---|
| proTLx-κ B5X4 Cal09 HA (CMV-Cal09) | proTLx-κ | CMV | Cal09 HA |
| TIVA-pUC EF1α-eGFP | TIVA-pUC | eF1α | eGFP |
| proTLx-κ N3X2 KCL-1-27 E6-E7 | proTLx-κ | KCL27 | E6-E7 |
| proTLx-κ EF1α-Cal09 HA (EF1α-Cal09) | proTLx-κ | EF1α | Cal09 HA |
| proTLx-κ KCL27-Cal09 HA (KCL27-Cal09) | proTLx-κ | KCL27 | Cal09 HA |
| proTLx-κ CD11c-Cal09 HA (CD11c-Cal09) | proTLx-κ | CD11c | Cal09 HA |
| proTLx-κ IL1α-P2A-IL1β (CMV-IL1α-IL1β) | proTLx-κ | CMV | IL1α & IL1β |
| proTLx-κ B5X4 mIL12 (CMV-IL12) | proTLx-κ | CMV | IL12 |
| proTLx-κ D3F2 CpG-C RIG-I (CpG-RIG1) | proTLx-κ | - | RIG-I activating RNA, CpG motifs |

### TOPO vector

gBlocks were cloned into a pCR™4-TOPO® TA vector using the TOPO™ TA Cloning™ Kit for Sequencing (K450002, ThermoFisher).

### Polymerase Chain Reaction (PCR)

All primers (Table 2.5) were purchased from Integrated DNA technologies (USA) and diluted to 10 µM in MilliQ water.

**Table 2.5.** Overview of all custom primers used for PCR in this chapter. The 5' and 3' termini are indicated. The sequences which do not overlap with their template are in lowercase.

| Primer name | Sequence (5'-3') |
|---|---|
| JKH_006 | 5'- GGTGAATTCGATATCAAGCTTATCGATAC - 3' |
| JKH_007 | 5'- CGGCCGCAGATCCAGAT - 3' |
| JKH_009 | 5'- gatatgtacacttaagGGCTCCGGTGCCCG - 3' |
| JKH_010 | 5'- tcatggtggcaagcttTCACGACACCTGAAATGGAAGAAAAAAAC - 3' |
| JKH_011 | 5'- gatatgtacacttaagTCGACTGTGCTCGGACC - 3' |
| JKH_012 | 5'- tcatggtggcaagcttGTTCCAGGAGATGAGAGGG - 3' |
| JKH_017 | 5'- GGCCTTTTTACGGTTCCTGG - 3' |
| JKH_019 | 5'- TTCCCAACCTTACCAGAGGG - 3' |
| JKH_021 | 5'- TACGGTTCCTGGCCTTTTG - 3' |
| JKH_022 | 5'- TATAGACTCTATAGGCACACCCCT - 3' |
| JKH_023 | 5'- ATATATCAGGATGTGGACAAACACTATCT - 3' |

### Agarose gels

PCR products and digestion products were analysed on a 1% agarose-TAE gel stained with SYBR Safe DNA gel stain (S33102, ThermoFisher Scientific, USA). 6x purple DNA loading dye (B7024S, NEB) was added to the DNA sample prior to loading. The gel was run at 70 V for 35 min.

### Gel/PCR clean-up

PCR products, digestion products and excised gel fragments were cleaned up with the NucleoSpin Gel & PCR clean-up kit (12303368, Macherey-Nagel) according to manufacturer's instructions.

**Infusion ligation**

DNA fragments were ligated using the In-Fusion Snap Assembly Master Mix (638943, Takara Bio USA, USA) according to manufacturer's instructions. Multiple fragments were ligated at a molar ratio of vector to insert of 1:2.

**Digestions**

Digestions with AflII (R0520S, New England Biolabs (NEB), USA) and HindIII-HF (R3104S, NEB) were performed according to manufacturer's instructions. Diagnostic digests with XhoI (R0146S, NEB) and SphI-HF (R3182L, NEB) for the EF1$\alpha$-Cal09 construct and with XmaI (R0180S, NEB) and SphI-HF (R3182L, NEB) for the KCL27-Cal09 construct were done according to manufacturer's instructions.

XmaI (R0180S, NEB) and SphI-HF (R3182L, NEB) digestions were performed according to manufacturer's instructions. Diagnostic digestion was done for the CD11c-Cal09 construct with AccI (R0161S, NEB) and NheI-HF (R3131S, NEB) according to manufacturer's instructions.

**Plasmid isolation**

DNA minipreparations were done with the QIAprep Spin Miniprep Kit (27106, Qiagen, Germany), according to manufacturer's instructions using a vacuum manifold. DNA mega-preparations were done with the HiSpeed Plasmid Mega EF Kits (1054578, Qiagen) using the QIAvac HiSpeed LS Vacuum set-up.

The DNA quantity and purity was assessed with a NanoDrop One (Thermo Scientific) using Ab260 and Ab280 values.

**Sequencing**

Purified plasmids were sent for Sanger sequencing to Source Bioscience (UK), using custom sequencing primers. Primers JKH_017 and JKH_019 were used for sequencing of CD11c-Cal09, EF1$\alpha$-Cal09 and KCL27-Cal09. Primers JKH_021 and JKH_023 were used for sequencing of CMV-IL1$\alpha$-P2A-IL1$\beta$.

**Cell line transformation**

Cells were transformed according to the manufacturer's instructions for 5-alpha Competent E. coli (High Effiency) (C2987H, NEB). In short, the competent cells were thawed for 10 minutes on ice. 1 pg-100 ng of plasmid DNA was added to the cell mixture, flicking to mix, and the mixture kept on ice for 30 minutes. The cells were heat shocked at 42 ℃ for 30 seconds and placed on ice for 5 minutes. 950 µL of SOC Outgrowth medium (B9020SVIAL, NEB) was added. The cells were placed at 37 ºC for 1 hour. Dilutions were plated on appropriate LB-agar plates.

**Cell culture**

Overnight cultures were grown in 5 mL of sterile liquid LB broth (luria low salt) (L3397, Sigma) or LB Broth, Vegitone (28713, Sigma) with 100 µg/mL ampicillin (A9393-5G, Sigma) or 50 µg/mL kanamycin (K4000-5G, Sigma). For large-scale purification of DNA, a starter culture was diluted 1:100 in 500mL-1L of broth with selection marker. This was grown in 3 x 1L Erlenmeyers. Cells were cultured at 37 ºC at 220 rpm in a shaking incubator. LB-agar plates were prepared by heating 7.5 g of agar in 500 mL of liquid LB broth until the agar was dissolved. The solution was then cooled until it was luke-warm, appropriate antibotics were added and plates were poured into sterile petri dishes (P5731-500EA, Sigma).

**Glycerol stocks**

Glycerol stocks were prepared for all completed DNA constructs. A 40% glycerol in MilliQ stock solution was made and filter-sterilised with a 0.2 µm filter. An overnight bacterial culture was mixed 1:1 with the glycerol stock and placed on ice for 10 minutes. The solutions were subsequently stored in a -80 ºC freezer.

### 2.2.11 Enzyme-linked immunosorbent assay (ELISA)

Nunc ImmunoPlates MaxiSorp 96-well plates (44-2404-21, ThermoFisher) were coated with 50 µL/well of a 10 µg/mL Cal09 protein (IT-003-SW12p, Immune Technology Corp., USA) and incubated overnight at 4 ºC. The plate was washed 6 times with PBS-0.05%Tween20. The plate was subsequently blocked with 50 µL/well of 10% FBS-PBS, sealed with SealPlate Sealing film (Z369667-100EA, Excel Scientific) and incubated for 1 hour at room temperature. After blocking, the plate was washed 6 times with PBS-0.05% Tween20. Serum samples were diluted a total of 10-1000 fold in PBS. 50 µL of diluted serum sample was added to the blocked plate. The plate was then sealed

again and incubated for 2 hours. The plate was then washed 6 times with PBS-0.05% Tween20. 50 µL/well of anti-mouse IgG secondary antibody HRP produced in goat (12-349, Sigma) was added at 1:10,000 in PBS. The plate was then sealed again and incubated for 1 hour. The plate was then washed 6 times with PBS-0.05%Tween20. 50 µL/well 1-Step™ Ultra TMB-ELISA Substrate Solution (34028, ThermoFisher Scientific) was added. The plate was sealed and incubated in the dark for 10-30 minutes. After developing, 50 µL/well stop solution of 0.5M $H_2SO_4$ was added. The absorbance was measured from 350 to 650 nm with a FLUOstar Omega (BMG LABTECH, Germany), with peak emission at 450 nm. Absorbance 450 nm was defined as the absorbance measured at 450 nm minus the absorbance at 600 nm to correct for background.

For titring, serum samples were diluted by 100, 200, 400, 800, 1000, 1500, 2000, 3000, 4000, 5000, 10,000, 15,000, 20,000, 25,000 or 30,000-fold in PBS. The titre was defined as the last dilution with a signal 3 times the standard deviation above the signal of negative-control serum. If no dilution was above this threshold, the titre was set as 10.

For measuring IgG1 and IgG2a ratio's, the secondary antibody was replaced with either Goat Anti-Mouse IgG1 (HRP) (ab97240, Abcam) or Goat Anti-Mouse IgG2a heavy chain (HRP) (ab97245, Abcam). Titre was defined as the last dilution with an absorbance above 0.1 AU.

To assess avidity, before adding the secondary antibody, sodium thiocynate (1066272500, Merck Millipore, USA) was added in increasing concentrations to the wells (0, 0.5, 1, 1.5, 2, 3, 4, 5 M) and incubated for 10 minutes. The plate was then washed 6 times with PBS-0.05%Tween20 before addition of secondary antibody. Avidity was measured as the concentration of sodium thiocyanate that reduced absorbance by 50%. This concentration was determined by fitting a "Five Parameters logistic regression" model [190] to the data and determining the NaSCN-50 concentration.

### 2.2.12 Enzyme-linked immune absorbent spot (ELISpot)

To determine the interferon-γ secretion by splenocytes upon stimulation with haemagglutinin Cal09, the mouse IFN-gamma ELISpot PLUS (HRP) (3321-4HST-2, Mabtech, Sweden) kit was used to perform an ELISpot.

15 mL falcon tubes with 5mL RPMI-1640 Medium (ThermoFisher Scientific, USA) with 10% Fetal Bovine Serum (qualified, Brazil) (10270106, ThermoFisher Scientific, USA) were prepared. For

collecting the spleen, a mouse was culled, its fur wetted with 70% ethanol, and the body cavity cut open and the spleen removed. The spleen was placed straight into the prepared falcon tubes with the RPMI-1640+10% FBS at room temperature.

In a tissue culture hood, a 70 µm cell strainer (10788201, ThermoFischer Scientific) was prewetted with 1 mL RPMI-1640+10% FBS media. The plunger end of a 3 mL syringe was used to mash the spleen through the cell strainer into a 55-60 mm petri dish to get a single cell suspension. Afterwards, the cell strainer was rinsed with 5 mL RPMI-1640+10% FBS to remove any remaining splenocytes.

The ELISpot plate with the required number of strips was assembled and washed four times with sterile PBS. This was conditioned with 200 µL of RPMI-1640+10% FBS/well whilst the splenocytes were processed.

The cell suspension was transferred from the petri dishes to 15 mL falcon tubes and spun down for 3 minutes at 800xg. The supernatant was then discarded and the pellet resuspended in 1 mL Red Blood Cell Lysis buffer (11814389001, Sigma). This was incubated for 5-10 minutes. 9 mL of RPMI-1640+10% FBS was added to this and the suspension spun down again at 800xg for 3 minutes. The supernatant was discarded and the cells resuspended in 3 mL RPMI-1640+10% FBS. A 4 µL cell suspension aliquot was dissolved 1:5 in RPMI-1640+10% FBS and mixed 1:1 with trypan blue solution, 0.4% (15250061, ThermoFisher Scientific). The cells were counted using a haemocytometer.

The positive control concanavalin A from Canavalia ensiformis (Jack bean) (L7647-25MG, Sigma) was dissolved to 1 µg/µL, the same concentration as the haemagglutinin Cal09 protein stock.

The media was removed from the ELISpot plate and for every splenocyte sample, 5 µL of media was added to two wells, 5 µL of haemagglutinin stock was added to two wells and 5 µL of concanavalin A solution was added to two wells. 62.500 splenocytes were then carefully added to each of these six wells per splenocyte sample.

The plate was incubated for 21.5 hours at 37 ºC in a humidified incubator with 5% $CO_2$, wrapped in cling film or aluminium foil to prevent evaporation. The following day, the cells were removed and the plate washed five times with 200 µL PBS per well. The interferon-$\gamma$ detection antibody (R4-6A2-biotin), which was part of the mouse IFN-gamma ELISpot PLUS (HRP) kit, was dissolved to 1 µg/mL

in PBS containing 0.5% fetal bovine serum (10270106, ThermoFisher Scientific, USA). 100 µL detection antibody was added to each well and incubated at room temperature for 2 hours. The plate was then washed again five times with 200 µL PBS per well. The streptavidin-HRP, also part of the kit, was dissolved 1:1000 in PBS containing 0.5% fetal bovine serum. A 100 µL/well of the streptavidin-HRP was added to each well and incubated at room temperature for 1 hour. The plate was again washed five times with 200 µL PBS per well. Then 100 µL/well of the supplied TMB substrate solution was added and the plate was left to develop until distinct spots emerged. The colour development was stopped by extensive washing with deionised water, including the undersides of the membrane. The plate and strips were left to dry overnight and then reassembled. The plate was imaged using AID ELISpot reader and software (AID Diagnostika GmbH, Germany).

The total number of spot forming units was calculated by subtracting the spots in the negative wells. The spots were then corrected to spot forming units/$10^6$ cells.

### 2.2.13 *In vivo* protocol to immunogenicity of the CMV-Cal09 vector

To understand the immunogenicity of the standard CMV-Cal09 vector to which promoter-modified vectors would be compared, an *in vivo* study was performed. Two groups of 6 mice were injected with 25 µg CMV-Cal09 dbDNA$^{TM}$ in PBS intramuscularly or with 50 µg CMV-Cal09 dbDNA$^{TM}$ in PBS intradermally. The mice were boosted with an identical dose after 20 days. Bleeds were taken on day 20, day 29, day 41 and day 48. The antibody content was assessed by ELISA, as described in section 2.2.11. On day 69 the mice were culled and an IFN-γ ELISpot was done on the collected splenocytes, as described in section 2.2.12. The timeline is summarised in Figure 2.4.

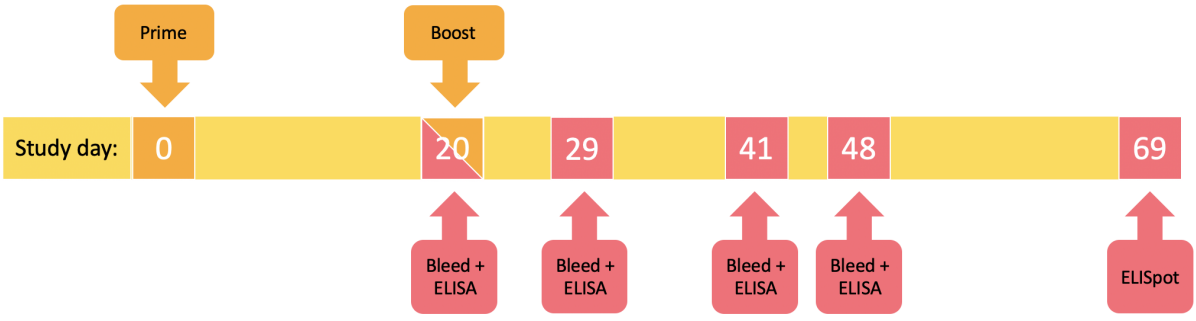



**Figure 2.4.** Summary of the treatment, blood sampling and spleen collection, as well as subsequent ELISA timeline for the *in vivo* to assess the immunogenicity of CMV-Cal09 dbDNA$^{TM}$ after intramuscular or intradermal injection.

### 2.2.14 *In vivo* protocol to assess DNA vaccines and adjuvants

To assess the immunogenicity of the different DNA vaccines and adjuvants, the following *in vivo* study was performed. 14 groups of 3 mice were treated, as summarised in Table 2.6. Mice were either treated with ultrasound in combination with nanocups or intramuscularly or intradermally injected.

For the mice treated by cavitation, a solution was prepared consisting of 52.8 µg dbDNA, 25% of nanocups to a final concentration of 26.4 µg/mL and MilliQ water. The mice were anaesthetised with 2% isoflurane and 98% oxygen. The fur of the mice was removed with an electric razor and subsequent application of depilatory cream VEET (Reckitt, UK) for 1 min. The formulation holder was placed on the flank of the mouse and filled with 2 mL of solution. Ultrasound was applied for 10 minutes, with the parameters as described in section 2.1. After treatment, the skin was thoroughly rinsed with water to remove any solution left behind and dried with tissue paper.

Mice were injected with 50 µg DNA dissolved in PBS intradermally. Intradermal injection had a total volume of 100 µL. Mice were injected intramuscularly with 20 µL containing 25 µg DNA dissolved in PBS.

The mice were boosted after 20 days. The mice were bled on day 7, day 14, day 20, day 30, day 42 and day 49 post-prime. The day 49 bleed was a terminal bleed. The protocol is summarised in Figure 2.5. The bleeds were analysed by ELISA, as described above, section 2.2.11.

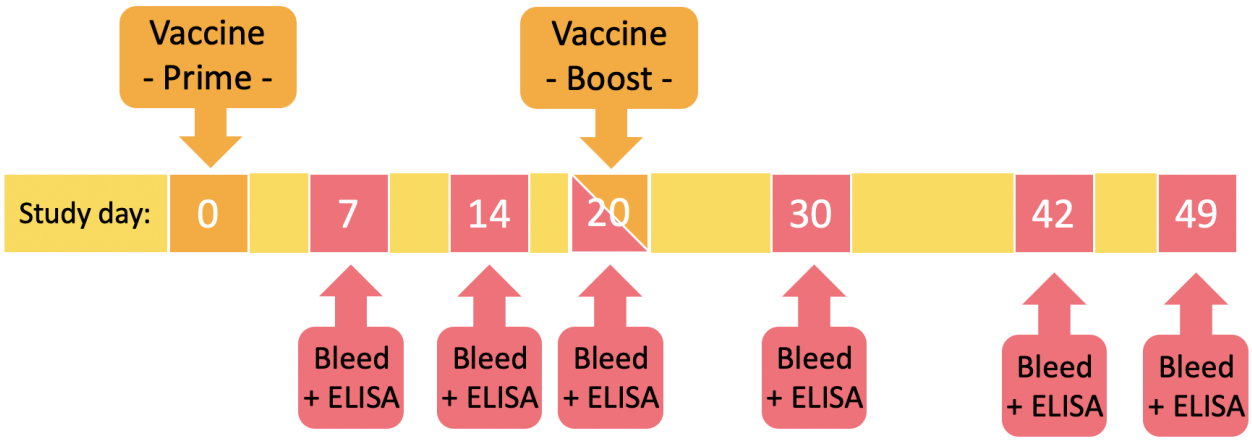



**Figure 2.5.** Summary of the treatment and blood sampling, as well as subsequent ELISA timeline for the *in vivo* to assess the immunogenicity of different DNA vaccine candidates and adjuvants.

**Table 2.6.** Summary of the *in vivo* to assess the immunogenicity of different DNA constructs. Per group, the number of mice, the DNA construct(s), whether they were treated with ultrasound or intradermally or intramuscularly injected, and dose per construct is noted.

| Group Name | Group size | DNA construct | Treatment | Dose |
|---|---|---|---|---|
| CMV-Cal09 | 3 | proTLx-κ B5X4 Cal09 HA | Ultrasound | 50 µg |
| EF1α-Cal09 | 3 | proTLx-κ EF1α-Cal09 | Ultrasound | 50 µg |
| KCL27-Cal09 | 3 | proTLx-κ KCL27-Cal09 | Ultrasound | 50 µg |
| CD11c-Cal09 | 3 | proTLx-κ CD11c-Cal09 | Ultrasound | 50 µg |
| CMV-Cal09<br>CMV-IL1α-IL1β | 3 | proTLx-κ B5X4 Cal09 HA<br>proTLx-κ CMV-IL1α-P2A-IL1β | Ultrasound | 50 µg<br>50 µg |
| CMV-Cal09<br>CMV-IL12 | 3 | proTLx-κ B5X4 Cal09 HA<br>proTLx-κ CMV-IL12 | Ultrasound | 50 µg<br>50 µg |
| CMV-Cal09<br>CpG-RIG1 | 3 | proTLx-κ B5X4 Cal09 HA<br>proTLx-κ D3F2 CpG-C RIG-I | Ultrasound | 50 µg<br>50 µg |
| CMV-Cal09 | 3 | proTLx-κ B5X4 Cal09 HA | Intramuscular | 25 µg |
| EF1α-Cal09 | 3 | proTLx-κ EF1α-Cal09 | Intradermal | 50 µg |
| KCL27-Cal09 | 3 | proTLx-κ KCL27-Cal09 | Intradermal | 50 µg |
| CD11c-Cal09 | 3 | proTLx-κ CD11c-Cal09 | Intradermal | 50 µg |
| CMV-Cal09<br>CMV-IL1α-IL1β | 3 | proTLx-κ B5X4 Cal09 HA<br>proTLx-κ CMV-IL1α-P2A-IL1β | Intramuscular | 12.5 µg<br>12.5 µg |
| CMV-Cal09<br>CMV-IL12 | 3 | proTLx-κ B5X4 Cal09 HA<br>proTLx-κ CMV-IL12 | Intramuscular | 12.5 µg<br>12.5 µg |
| CMV-Cal09<br>CpG-RIG1 | 3 | proTLx-κ B5X4 Cal09 HA<br>proTLx-κ D3F2 CpG-C RIG-I | Intramuscular | 12.5 µg<br>12.5 µg |

## 2.3 Results

### 2.3.1 *In vivo* pressure optimisation

In order to identify the optimal acoustic pressure for dbDNA$^{TM}$ delivery, groups of three mice were exposed to a range of ultrasound pressure amplitudes and a formulation containing nanocups (NC) and dbDNA$^{TM}$-Luc. As a control, one mouse was not exposed to ultrasound and the intention was to expose three mice to 'sub-cavitation' levels of ultrasound, i.e. levels which provided an acoustic exposure that was insufficient to trigger cavitation. However, at a pressure of 0.7 MPa, cavitation was observed and the pressure was dropped to 0.5 MPa for the remaining two mice in the 'sub-cavitation' group. Data was compared to subcutaneous, intramuscular and intradermal injection of similar DNA doses, (intramuscular injection was limited in dose due to welfare restrictions on the permitted injectable volume). After 24 hours, 54 hours and 120 hours the luciferase expression was measured to give a metric of the level of transfection and therefore DNA delivery. The results are displayed in Figures 2.6 and 2.7.

From Figure 2.6 it is apparent that luciferase transgene expression was achieved in all mice where the pressure applied exceeded 0.7 MPa, but not in control mice or those treated with lower pressure amplitude (0.5 MPa). It is notable that the area of expression in ultrasound treated mice appeared to extend over the entire exposed area and was very reproducible between mice exposed to the same pressure. This was especially evident at 1 MPa which provided evenly distributed luciferase expression across the exposed area in all 3 mice (geometric mean of $2.28 \times 10^6$ p/s). The higher pressure amplitude of 1.6 MPa appeared to be associated with lower expression in the central area of the exposed circle which may relate to cell damage. Notably, needle-dependent approaches gave much more localised and variable levels of expression (e.g. geometric standard deviation (GSD) for I.D. injection 17.6 vs 1.4 for 1 MPa).

Figure 2.7 represents the findings of Figure 3 in numeric form. After 24 hours, the mice treated with sub-cavitation ultrasound, i.e. a pressure amplitude insufficient to instigate cavitation, and the control mouse (DNA and cavitation nuclei but no ultrasound) have substantially less (on average 112-fold) luminescence (p/s) than the mice treated with ultrasound-mediated cavitation (t-test with Welch's correction, $p<0.0001$). Indeed, the level detected ($1.6 \times 10^4$ p/s) is considered equivalent to background, as may be expected when no mechanism for permeation of the stratum corneum or transport of the DNA is provided. The expression across the cavitation groups was similar at each

timepoint. Based on these results, it was decided to continue experiments with 1.0 MPa, as occasionally mild damage to the skin could be observed at 1.6 MPa. Compared to alternative needle-based techniques, cavitation-mediated delivery also gave more consistent expression with lower standard deviations. Furthermore, cavitation-mediated delivery showed greater levels of expression than subcutaneous injection (Geometric means: $1.66x10^6$ for cavitation-treated groups vs $1.66x10^5$ for subcutaneous (S.C.) injection at 24 hours, Welch's t-test, $p<0.0005$).

The acoustic emissions were recorded with a PCD. Representative spectrograms for each group are displayed in Figure 2.8. In order to relate the acoustic dose to luciferase expression, the energy detected by the PCD per burst was quantified and summed, as described in section 2.2.3 and expressed as total acoustic sensor energy in microjoules (μJ). It was expected that the energy measured would be proportional to the acoustic emissions from within the formulation during ultrasound exposure.

The TASE value was plotted against the detected bioluminescence of luciferase for each mouse (Figure 2.9). There is an approximate 100-fold difference between the luminescence observed for the mice treated at sub-cavitation pressures and those treated with cavitation. Once the 0.7 MPa threshold was crossed, further increases in pressure amplitude applied did not increase the observed luminescence (p/s), despite increases in TASE values being achieved. The transition between sub-cavitation and cavitation appears to be between 1.7 μJ (0.5 MPa) and 4.3 μJ (0.7 MPa). Frequency analysis of the acoustic emissions permits the component of the total emission energy which relates to broadband (inertial) emissions and the component which relates to harmonics and sub-harmonics of the driving frequency (non-inertial) emissions to be calculated. When the TASE values were determined for only the inertial cavitation component, the same stepwise change was observed. Interestingly, a smaller inertial energy difference exist for the transition between sub-cavitation (no luciferase expression) and cavitation (luciferase expression) at 1.0 μJ and 2.3 μJ from 0.5 MPa to 0.7 MPa respectively. This transition could reflect a tipping point, which could imply that inertial cavitation is the crucial mechanism. Alternatively, there may be other phenomena which are not picked up by the PCD or limitations may exist in the subsequent analysis of the cavitation. The intention is to compare this to other, future experiments with the same ultrasound set-up and NC content to determine if the TASE values calculated at the time of delivery can be utilised to predict effective delivery and expression of dbDNA$^{TM}$ as measured 24 hours later.

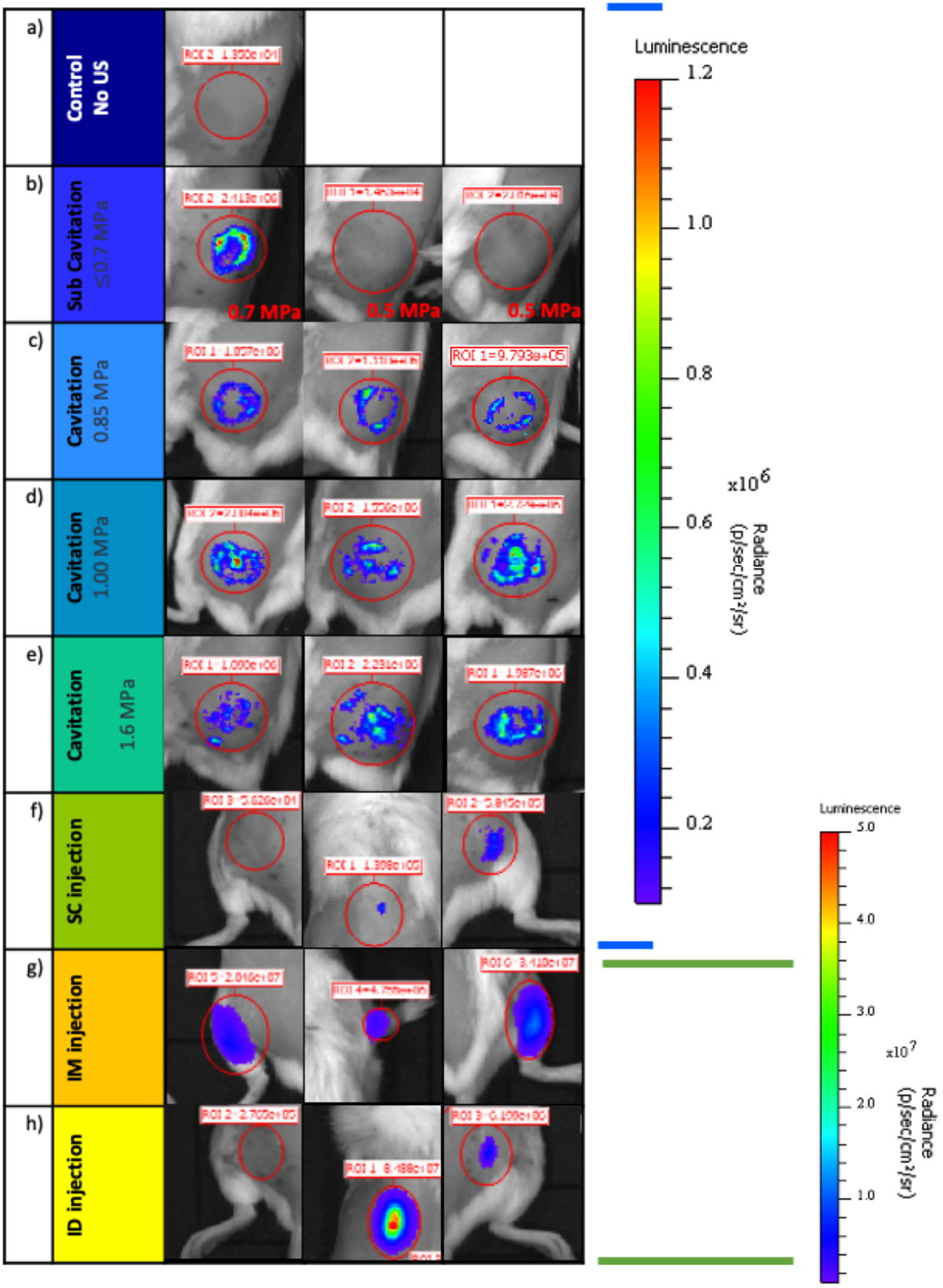



**Figure 2.6.** The impact of scaling acoustic pressure and delivery route on transfection of dbDNA$^{TM}$ encoding luciferase. Approximately 50 µg of dbDNA$^{TM}$ was used per treatment and administered by exposing the skin to a sample formula containing the DNA and a cavitating agent (NC) for 10 min and applying ultrasound at different pressures or by injecting the DNA by needle and syringe intradermally (I.D.), intramuscularly (I.M.) or subcutaneously (S.C.). The luminescence and radiance produced by luciferase was imaged *in vivo* after 24 h. The ROI displayed are not corrected for surface area and are in photons/second. N=3, except for the control where n=1.

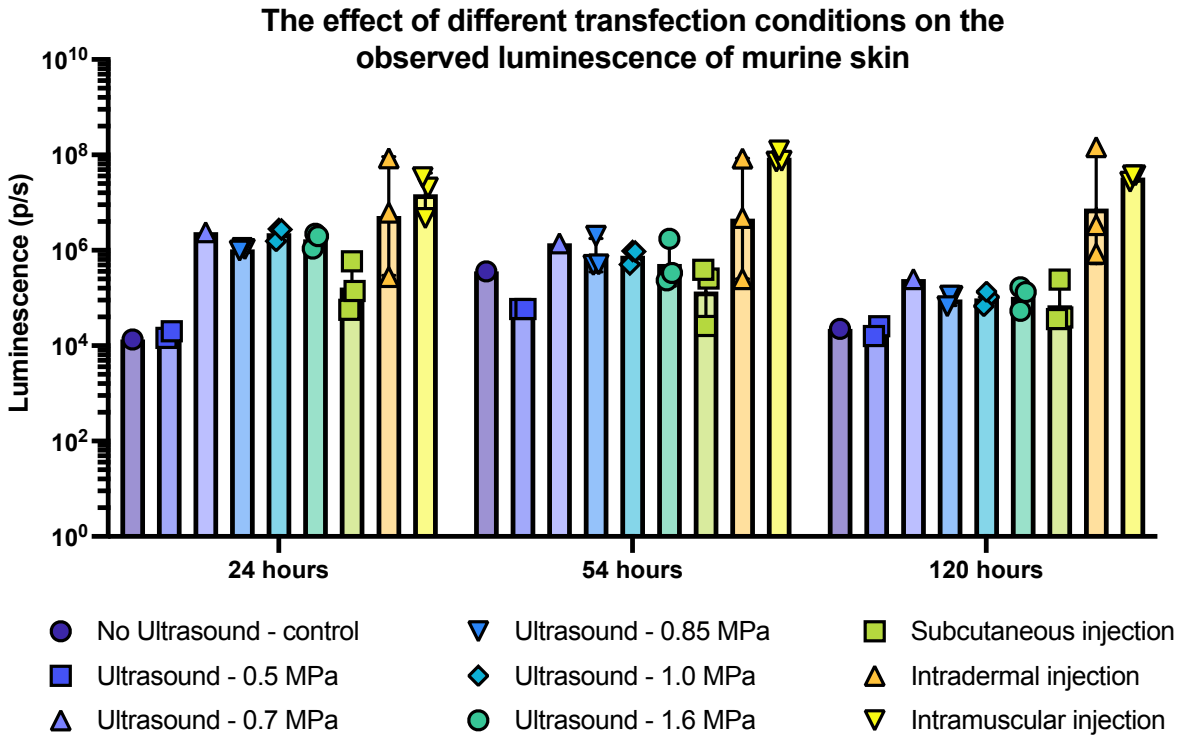
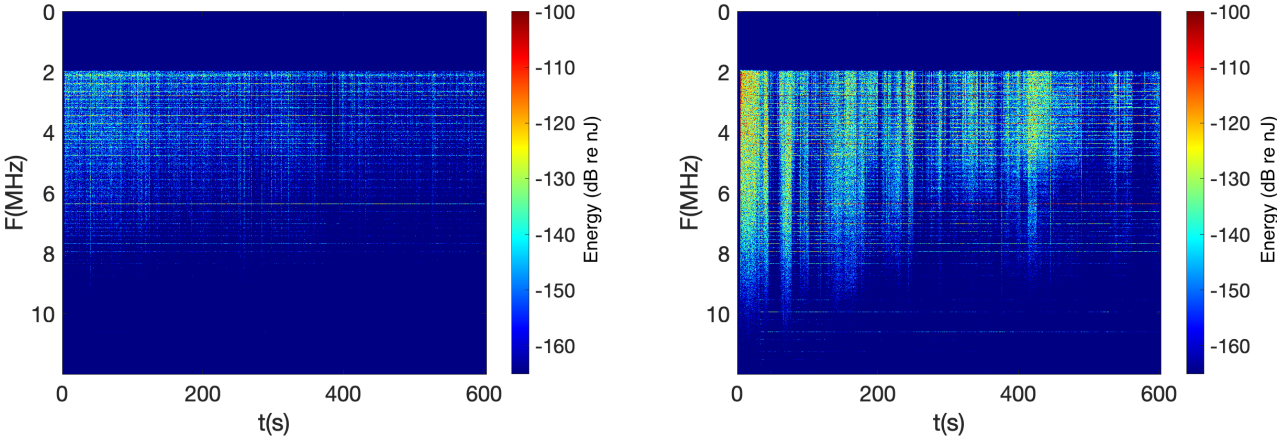



**Figure 2.7.** The effect of varying acoustic pressure on transfection of dbDNA$^{TM}$-Luc. Approximately 50 µg of dbDNA$^{TM}$ was used per treatment and administered by exposing the skin to a formula containing the DNA and a cavitating agent (NC) for 10 min and exposing to ultrasound at different pressures or by injecting the DNA by needle and syringe intradermally (I.D.), intramuscularly (I.M.) or subcutaneously (S.C.). The luminescence produced by luciferase was imaged *in vivo* after 24 h, 54 h and 120 h. The geometric average luminescence $\times/\div$ the geometric standard deviation of the treated skin is plotted in photons/second per treatment group. N=3, except for the control and sub-cavitation group. N=1 for the control and the mouse treated with 0.7 MPa and n=2 for the sub-cavitation group as cavitation was detected for the mouse treated with 0.7 MPa.



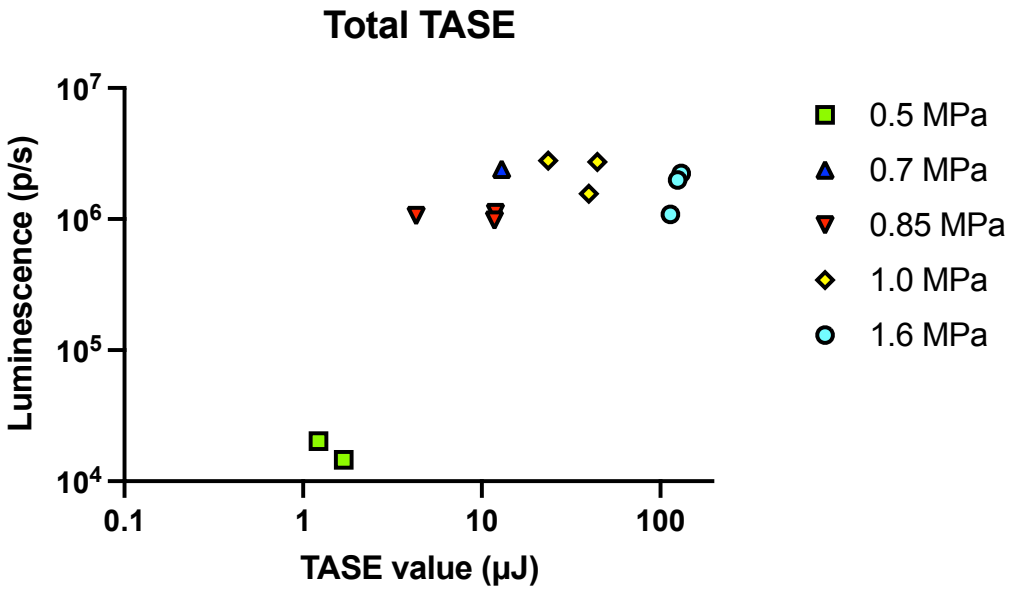

**(a)** Sub-cavitation - 0.5 MPa

**(b)** Cavitation - 0.85 MPa

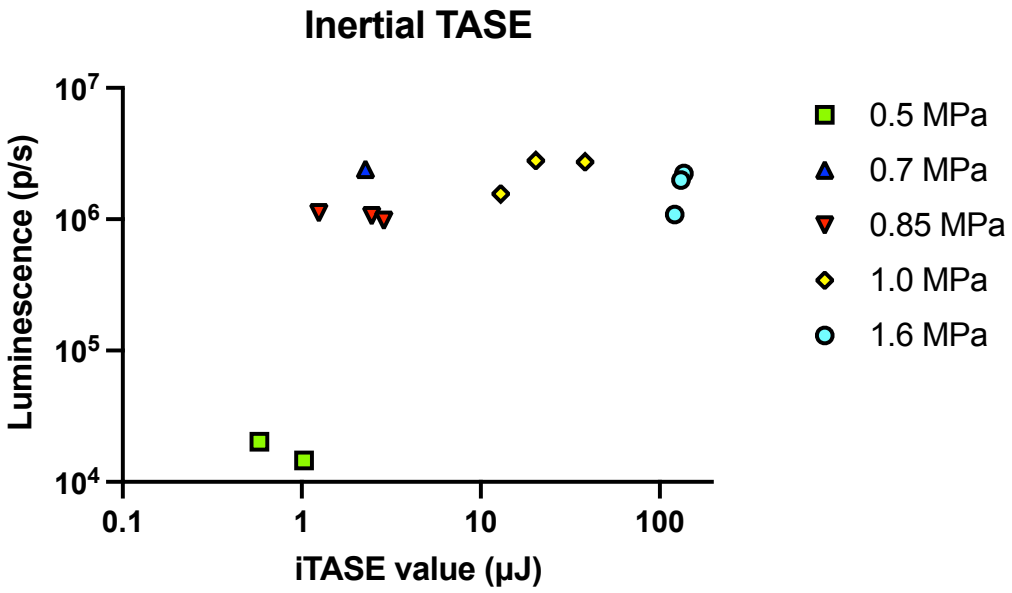
**(c)** Cavitation - 1.0 MPa

**(d)** Cavitation - 1.6 MPa

**Figure 2.8.** Representative spectrograms for mice treated at 0.5 MPa (Sub-cavitation), 0.85 MPa, 1.0 MPa and 1.6 MPa (Cavitation). Approximately 50 µg of dbDNA$^{TM}$ was used per treatment and administered by exposing the skin and a formula containing the DNA and NC for 10 min to ultrasound at different pressures. The colour bar on the right represents the power spectral density in dB re nJ. Data was processed as described in section 2.2.3.




**(a)** Total Tase




**(b)** Inertial TASE

**Figure 2.9.** The total TASE (top) or inertial component of TASE (bottom) per treatment condition compared to detected bioluminescence of luciferase. Approximately 50 µg of dbDNA$^{TM}$ was used per treatment and administered by exposing the skin and a formula containing the DNA and NC for 10 min to ultrasound at 0.5 MPa (Sub-cavitation), 0.7 MPa, 0.85 MPa, 1 MPa, 1.6 MPa (Cavitation). Cavitation data was processed as described in section 2.2.3.

### 2.3.2 DNA delivery assessed by qPCR

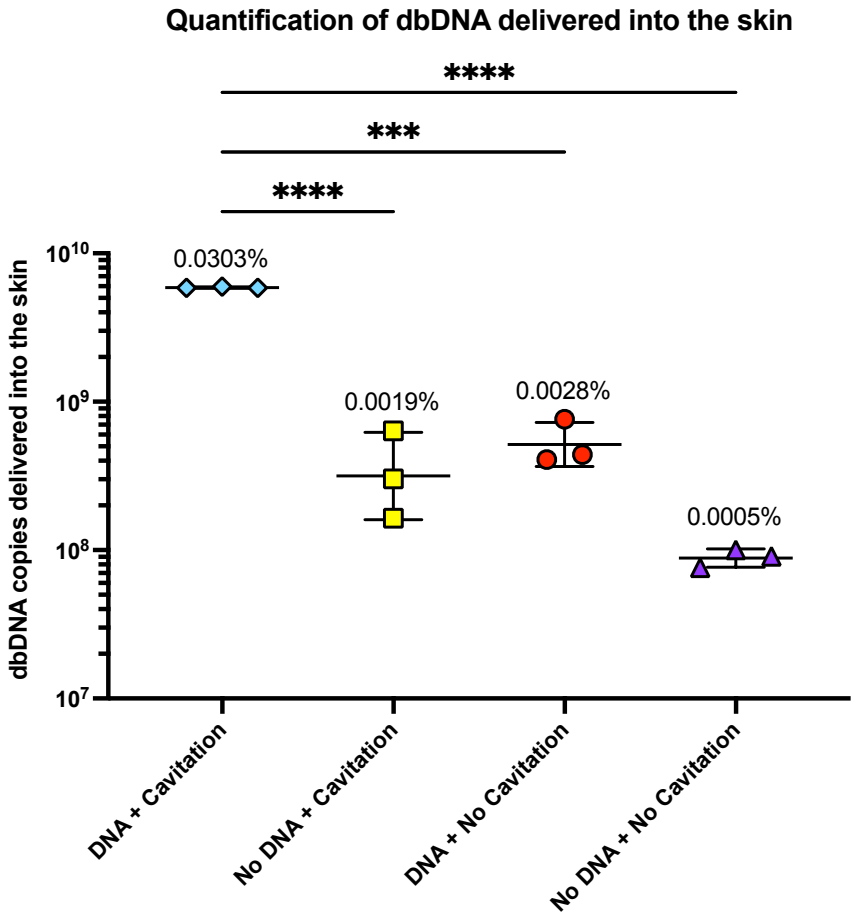



**Figure 2.10.** Quantification of dbDNA$^{TM}$-Luc copies delivered into differently treated murine skin after 24 hours. The mice were treated with formulations containing NC and with or without DNA placed on the skin and were or were not exposed to ultrasound. The geometric mean (horizontal bar) $\times/\div$ geometric standard deviation (error bars) is displayed. The individual measurements are displayed as points on the graph. Above each treatment, the percentage of the original dose placed on the skin during exposure is displayed. N=3 for all samples. A one-way ANOVA was used to assess the difference with a post-hoc test with the 'DNA + Cavitation' group, using the Šidák correction for multiple comparisons, *** = p<0.0005. **** = p<0.0001.

Assessment of gross dbDNA$^{TM}$ delivery 24 hours post-treatment to the whole skin segment, as shown in Figure 2.10, demonstrates that cavitation-mediated transcutaneous delivery can deliver DNA into the skin and up to 0.0303% of the 50 µg dose present in the exposure chamber remains after 24 hours. This equates to a geometric mean of 5.88x10$^9$ dbDNA$^{TM}$ copies. The recovery of <0.002% of dbDNA$^{TM}$ for the remaining groups is likely within the background of the assay, and therefore does not represent a true positive signal. This is supported by the lack of bioluminescence observed in these mice (<1.9x10$^4$ p/s). This further shows that cavitation is a crucial component to enable delivery of dbDNA$^{TM}$ into the skin, as in the presence of DNA but absence of cavitation, a background signal was obtained (i.e. that was similar to 'No DNA + Cavitation' signal). This further demonstrates the potential of cavitation as a new and effective way of delivering DNA into the skin. It also highlights that cavitation results in strong luciferase expression, even for very low levels of DNA

delivered. Indeed, for these ultrasound exposure conditions each million DNA copies led to $3.93x10^2$ p/s at 24 hours. This p/s/$10^6$ DNA copies can be used for subsequent comparisons with intradermal (I.D.) and intramuscular (I.M.) injection.

### 2.3.3 Novel DNA vaccine and adjuvant vectors

In total four plasmids were constructed, each expressing the influenza haemagglutinin antigen Cal09 HA under the control of a different promoter or encoding an adjuvant:

- proTLx-κ CD11c-Cal09 HA,
- proTLx-κ EF1α-Cal09 HA,
- proTLx-κ KCL27-Cal09 HA,
- proTLx-κ CMV-IL1α-P2A-IL1β.

These plasmids also contained the telRL sequences necessary for dbDNA™ production. The plasmid maps of all plasmids used in this chapter are available in Appendix A.

#### proTLx-κ CD11c-Cal09 HA (CD11c-Cal09)

In order to assemble proTLx-κ CD11c-Cal09 HA, a custom gBlock was ordered with the CD11c promoter and overlapping sequences the proTLx-K backbone and Cal09 HA (Figure 2.11), with Cal09 HA being the DNA sequence encoding the haemagglutinin of the A/California/07/2009 (H1N1) influenza virus.

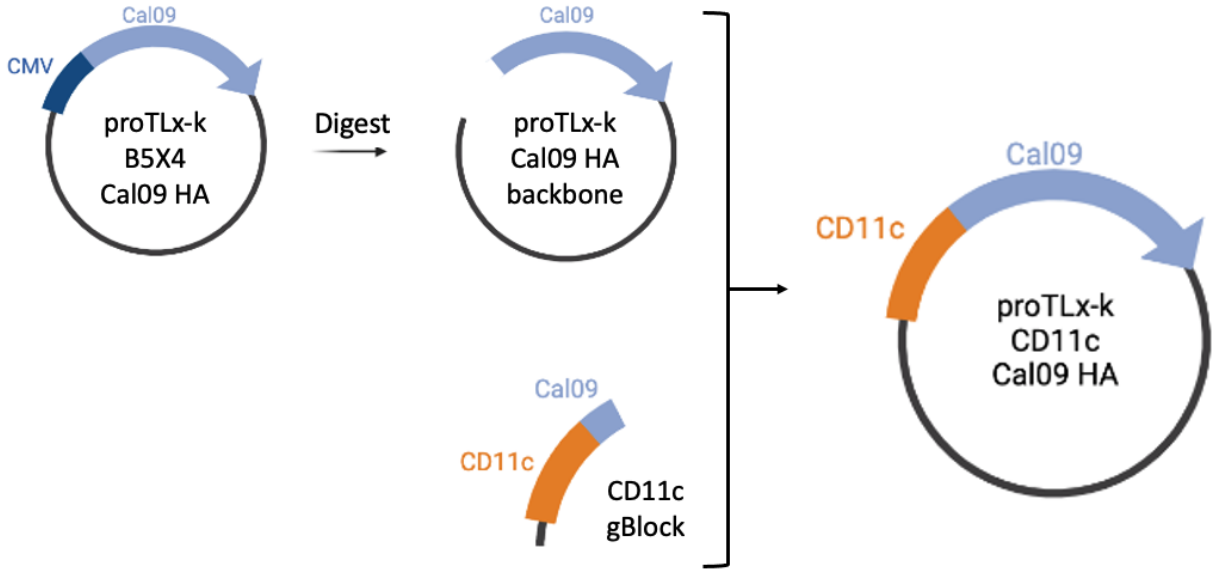



**Figure 2.11.** Schematic representation of the cloning of the proTLx-κ CD11c-Cal09 plasmid. The proTLx-κ B5X4 Cal09 HA plasmid was digested. The CD11c promoter was ordered as a gBlock, with overlapping sequences with the Cal09 HA gene and the proTLx-κ B5X4 backbone. The CD11c promoter and the proTLx-k Cal09 HA vector were ligated together to form proTLx-κ CD11c-Cal09 HA.

The plasmid proTLx-κ B5X4 Cal09 HA was digested with AflII (NEB) and HindIII-HF (NEB) according to manufacturer's instructions to remove the CMV promoter from the Cal09 HA gene and the backbone from proTLx-κ B5X4 Cal09 HA. In accordance with predicted molecular weights of the fragments, bands were evident at 4079 bp (proTLx-κ Cal09 HA) and 582 bp (CMV promoter) (Figure 2.12).

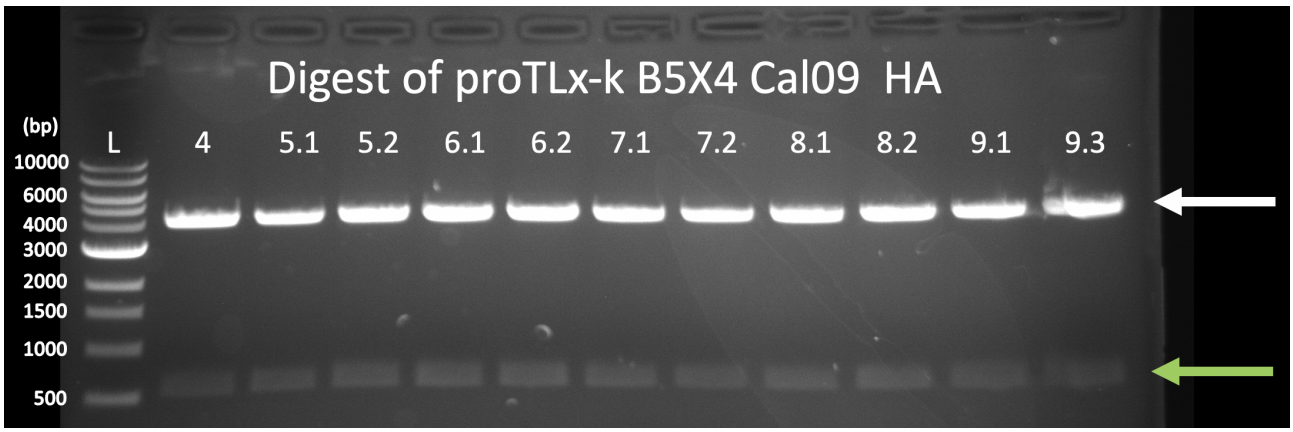



**Figure 2.12.** A 1% agarose gel with the enzymatic digest products of the digestion of proTLX-κ B5X4 Cal09 HA with AflII and HindIII-HF. The white arrow indicates the proTLx-K Cal09 HA backbone and the green arrow indicates the CMV promoter fragment. Colonies are numbered at the top of the wells. On the left, a 1 kb DNA ladder was run and the molecular weight of the bands in basepairs is depicted. The gel was run as described in section 2.2.10.

The CD11c gBlock and proTLx-κ B5X4 Cal09 HA backbone were ligated to generate proTLx-k CD11c-Cal09 HA (Figure 2.11). A diagnostic digest was done for the proTLx-κ CD11c-Cal09 HA construct with AccI (NEB) and NheI-HF (NEB) according to manufacturer's instruction. Correct assembly was confirmed as the predicted fragment sizes of 780 bp, 1564 bp and 2452 bp were observed on an agarose gel for 6 of 7 colonies tested, whereas proTLx-k B5X4 Cal09 HA template would result in 2 fragments of 780 bp and 3881 bp (Figure 2.13). Results were subsequently confirmed by Sanger sequencing, as described in section 2.2.10.

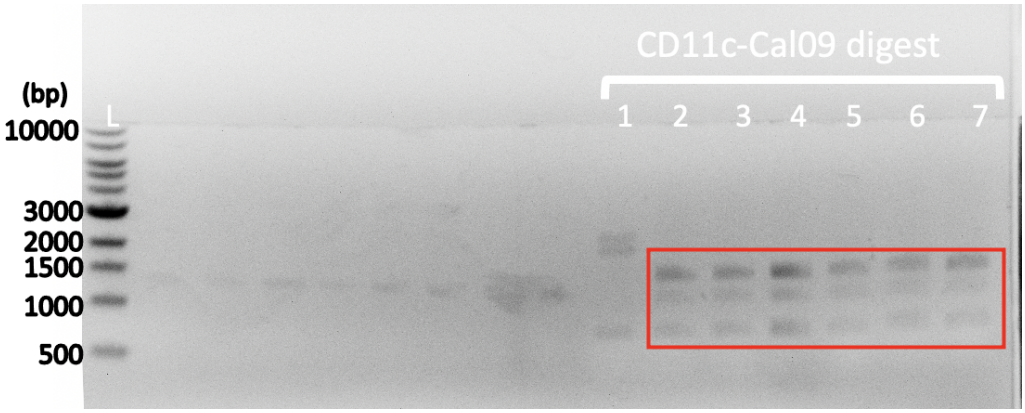



**Figure 2.13.** Agarose gel with the digest products of the enzymatic digest of proTLx-κ CD11c-Cal09 HA with AccI and NheI-HF (right). In red are the correctly assembled proTLx-κ CD11c-Cal09 HA. Colonies are numbered at the top of the wells. On the left, a 1 kb DNA ladder was run and the molecular weight of the bands in basepairs is depicted.

**proTLx-κ EF1α-Cal09 HA**

To amplify the EF1α promoter from TIVA-pUC EF1α-eGFP, 113 µL CloneAmp™ HiFi PCR Premix (Takara Bio) was mixed with 11.5 µL of primer JKH_009, 11.5 µL of primer JKH_010, 1 µL of TIVA-pUC EF1α-eGFP and 90 µL MilliQ water to form the PCR mix. 25 µL of this PCR mix was aliquoted into 8 tubes. The cycling parameters were 98 ºC for 30 seconds, 35 cycles of 98 ºC for 30 seconds, a gradient from 50-72 ºC across the 8 tubes for 20 seconds and 72 ºC for 25 seconds, followed by 72 ºC for 2 minutes.

The PCR-amplified EF1α fragment was ligated into the plasmid proTLx-κ B5X4 Cal09 HA, which had been digested as described above (Section 2.3.3 - CD11c-Cal09). This resulted in proTLx-κ EF1α-Cal09 HA (Figure 2.14).

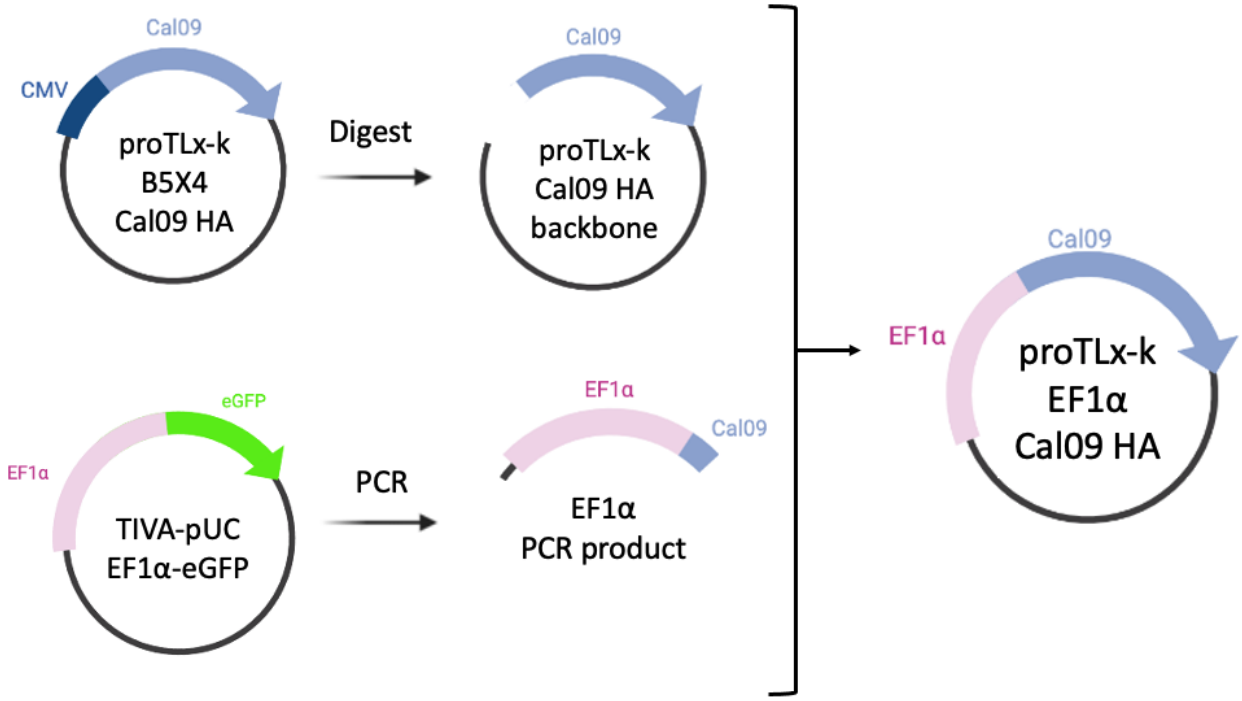



**Figure 2.14.** Schematic representation of the cloning of the proTLx-κ EF1α-Cal09 HA plasmid. The proTLx-κ B5X4 Cal09 HA plasmid was digested to remove the CMV promoter. The EF1α promoter was PCR amplified from the TIVA-pUC EF1α-eGFP plasmid with overlapping sequences with the Cal09 HA gene and the proTLx-κ B5X4 backbone. The EF1α promoter and the proTLx-κ Cal09 HA vector were ligated together to form proTLx-κ EF1α-Cal09 HA.

A diagnostic digest was performed for the proTLX-κ EF1α Cal09 HA construct with XhoI (NEB) and SphI-HF (NEB) according to manufacturer's instructions. Successful assembly of the plasmid would result in a band at 2946 bp and 2318 bp. Digestion of TIVA-pUC EF1α-eGFP would result in 6 bands, all equal or smaller than 1325 bp. Digestion of proTLx-κ B5X4 Cal09 HA would result

in 2 bands at 3407 bp and 1254 bp. The agarose gel showed that 4/8 colonies were correctly assembled and the other four contained the TIVA-pUC EF1α-eGFP plasmid (Figure 2.15). Results were subsequently confirmed by Sanger sequencing, as described in section 2.2.10.

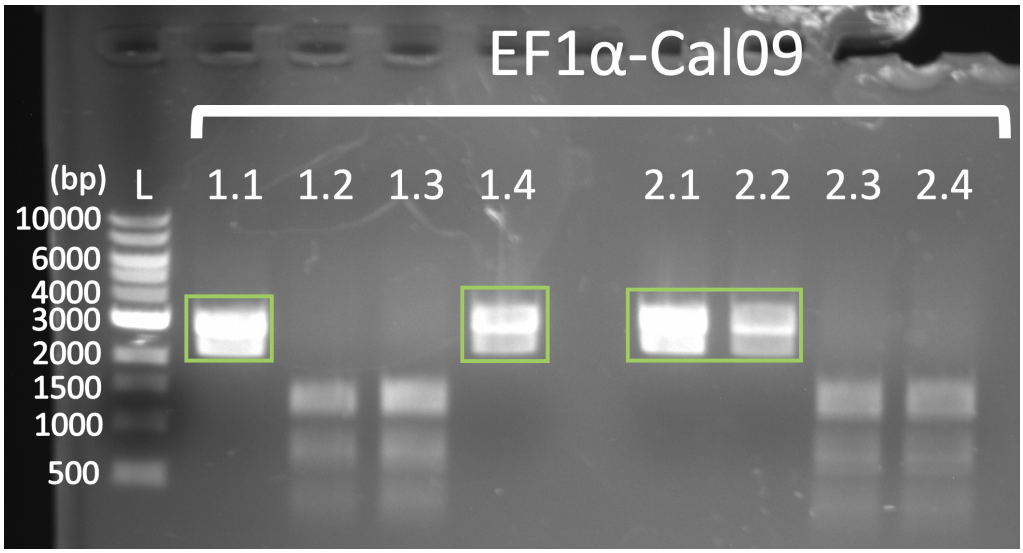



**Figure 2.15.** Agarose gel with the diagnostic enzymatic digest products of the digestion of proTLX-κ EF1α Cal09 HA with XhoI and SphI-HF. Correct assembly of proTLX-κ EF1α Cal09 HA would result in a band at 2946 bp and 2318 bp, indicated in green. Colonies are numbered at the top of the wells. On the left, a 1 kb DNA ladder was run and the molecular weight of the bands in basepairs is depicted.

**proTLx-κ KCL27-Cal09 HA**

To amplify the KCL1-27 promoter from proTLx-k N3X2 KCL1-27 E6-E7, 113 µL CloneAmp™ HiFi PCR Premix (Takara Bio) was mixed with 11.5 µL of primer JKH_011, 11.5 µL of primer JKH_012, 1 µL of proTLx-k N3X2 KCL1-27 E6-E7 and 90 µL MilliQ water. This was aliquoted into 25 µL over 8 tubes. The cycling parameters were 98 ºC for 30 seconds, 35 cycles of 98 ºC for 10 seconds, a gradient from 50-72 ºC for 20 seconds across the 8 tubes and 72 ºC for 12 seconds, followed by 72 ºC for 2 minutes. The PCR-amplified KCL27-1 fragment was ligated into the plasmid proTLx-κ B5X4 Cal09 HA, which had been digested as described above (Section 2.3.3 - CD11c-Cal09). This resulted in proTLx-κ KCL27-Cal09 HA (Figure 2.16).

A diagnostic digest was done for the proTLx-κ KCL27-Cal09 HA construct with XmaI (NEB) and SphI-HF (NEB) according to manufacturer's instructions. Successful assembly would result in 3 bands, at 179 bp, 1439 bp and 2952 bp. The proTLx-k B5X4 Cal09 HA template would result in a band of 4661 bp and the proTLx-K N3X2 KCL-1-27 E6-E7 plasmid would result in 4 bands of 173 bp, 179 bp, 1304 bp and 2099 bp. The gel in Figure 2.17 demonstrates the successful generation of the proTLx-κ KCL-Cal09 HA construct. Results were confirmed by Sanger sequencing, as described in section 2.2.10.

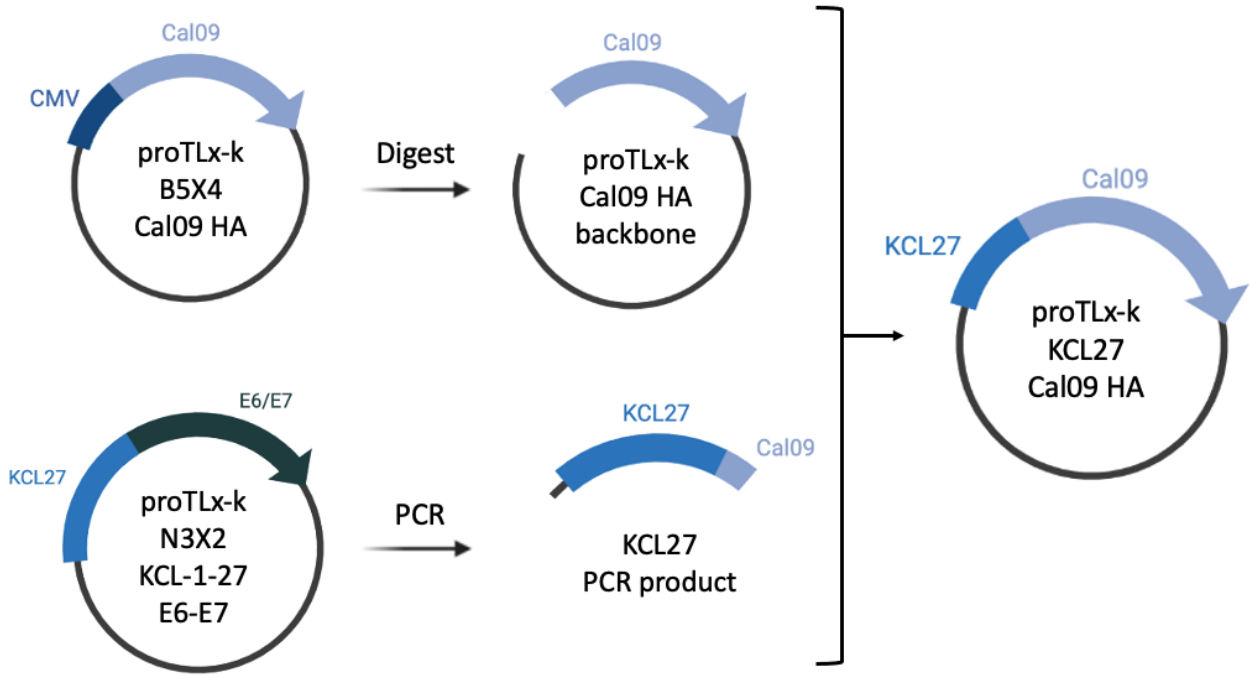



**Figure 2.16.** Schematic representation of the cloning of the proTLx-κ KCL27-Cal09 plasmid. The proTLx-κ B5X4 Cal09 HA plasmid was digested. The KCL27 promoter was PCR amplified from the proTLx-κ N3X2 KCL-1-27 E6-E7 plasmid with overlapping sequences with the Cal09 gene and the proTLx-κ B5X4 backbone. The KCL27 promoter and the proTLx-κ Cal09 HA vector were ligated together to form proTLx-κ KCL27-Cal09 HA.

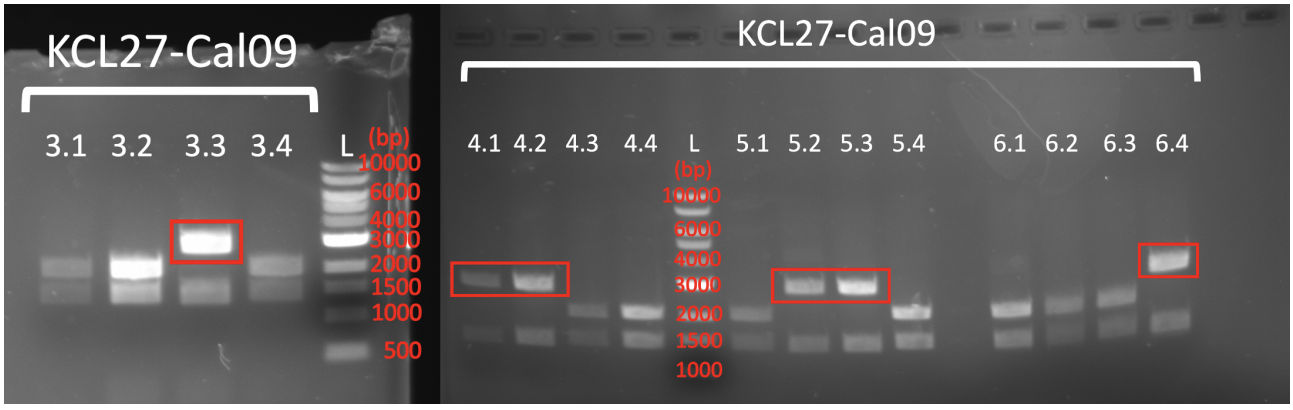



**Figure 2.17.** Agarose gel with the diagnostic enzymatic digest products of the digestion of proTLX-κ KCL27-Cal09 HA with XmaI and SphI-HF. Correct assembly of proTLX-κ KCL27-Cal09 HA would result in bands at 173, 1439 and 2952 bp. The bands at 2952 bp, indicating correct assembly, are marked in red. Colonies are numbered at the top of the wells. Two 1 kb DNA ladders were run and the molecular weight of the bands in basepairs is depicted in red.

**proTL-κ CMV-IL1α-P2A-IL1β**

In addition to the range of Cal09 HA expression vectors driven by a range of different promoters, a set of vectors expressing immunomodulators driven by the CMV promoter were also assessed. proTLx-κ B5X4 mIL12 and proTLx-κ D3F2 CpG-C RIG-I were kindly donated by Touchlight Genetics. The proTLx-κ IL1α-P2A-IL1β was cloned as described below.

To amplify the backbone from proTLx-k B5X4 mIL12, 122 µL Q5 Mastermix (NEB) was mixed with 25 µL of primer JKH_006, 25 µL of primer JKH_007, 1 µL of proTLx-κ B5X4 mIL12 and 47 µL MilliQ water. This was aliquoted into 25 µL. The cycling parameters were 98 ºC for 30 seconds, 35 cycles of 98 ºC for 10 seconds, a gradient from 50-72 ºC for 20 seconds across 8 tubes and 72 ºC for 85 seconds, followed by 72 ºC for 2 minutes (Figure 2.19).

The PCR-amplified proTLx-k B5X4 mIL12 backbone was ligated with the IL1α and IL1β gBlocks, which had overlapping sequences with the CMV promoter, the P2A sequence (ribosomal skipping sequence) or the backbone (Figure 2.18).

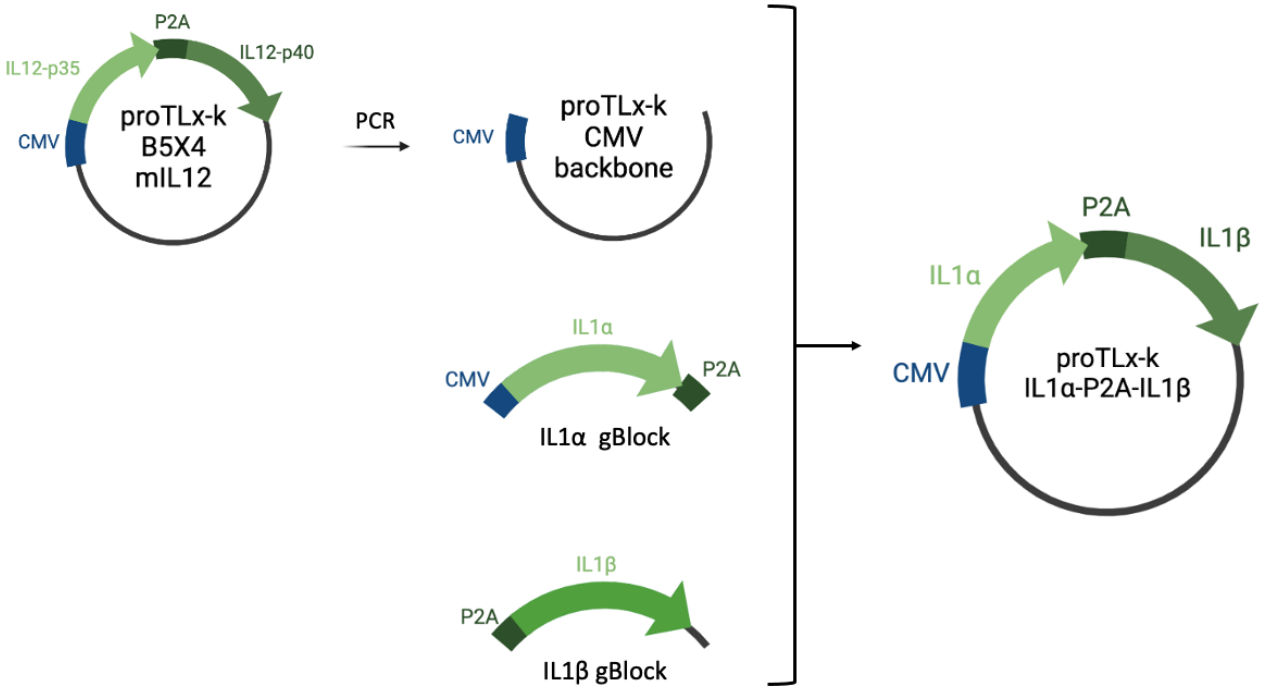



**Figure 2.18.** Schematic representation of the cloning of the proTLx-κ IL1α-P2A-IL1β plasmid. The proTLx-κ B5X4 Cal09 HA plasmid was digested. gBlocks of IL1α and IL1β were ordered with overlapping sequences with the CMV promoter, P2A sequence and the proTLx-κ B5X4 backbone. The IL1α and IL1β gBlocks and the proTLx-kCal09 HA vector were ligated together to form proTLx-κ IL1α-P2A-IL1β.

A diagnostic colony PCR was done to assess the correct incorporation of IL1α and IL1β. To this end, colonies were picked with a pipette tip from a plate with cells transformed with a ligation mixture




**Figure 2.19.** Agarose gel of the PCR amplification of the backbone from proTLx-κ B5X4 mIL12. Successful amplification would result in a band at 3385 bp, indicated in green. Colonies are numbered at the top of the wells. On the left, a 1 kb DNA ladder was run and the molecular weight of the bands in basepairs is depicted.

containing linearised backbone, gBlock IL1α and gBlock IL1β . This pipette tip was swirled in the PCR mix. This PCR mix consisted of 225 µL of Q5 Mastermix (NEB), 27.5 µL primer JKH_019, 27.5 µL primer JKH_022 with 270 µL MilliQ water. This was aliquoted into 25 µL. The cycling parameters were 98 ºC for 6 minutes, 35 cycles of 98 ºC for 10 seconds, 66 ºC for 20 seconds and 72 ºC for 40 seconds, followed by 72 ºC for 2 minutes. A fragment of 1632 bp would imply correct assembly of the plasmid (Figure 2.20). This showed 6 correctly assembled clones. These results were subsequently confirmed by Sanger sequencing, as described in section 2.2.10.

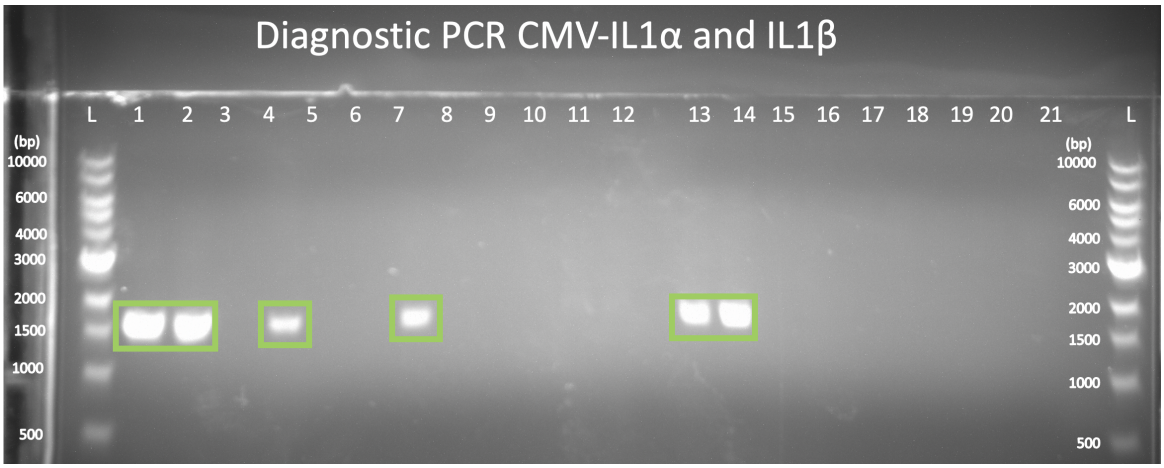



**Figure 2.20.** Agarose gel with the diagnostic colony PCR of proTLX-κ CMV-IL1α-P2A-IL1β. Correct assembly would result in a band at 1632 bp, indicated in green. Colonies are numbered at the top of the wells. On the left, a 1 kb DNA ladder was run and the molecular weight of the bands in basepairs is depicted.

### 2.3.4 *In vivo* testing of DNA vectors by injection

The CMV-Cal09 (proTLx-κ B5X4 Cal09 HA) vector was the standard vector to which subsequently designed vectors would be compared. An *in vivo* study was performed to assess the immunogenicity of this vector after intramuscular injection or intradermal injection. Regular bleeds were taken to assess anti-Cal09 HA antibody levels by ELISA and an IFN-γ ELISpot (see section 2.2.11 and section 2.2.12 for methods) was performed to assess cellular responses against the Cal09 HA protein on day 69 (Figure 2.21).

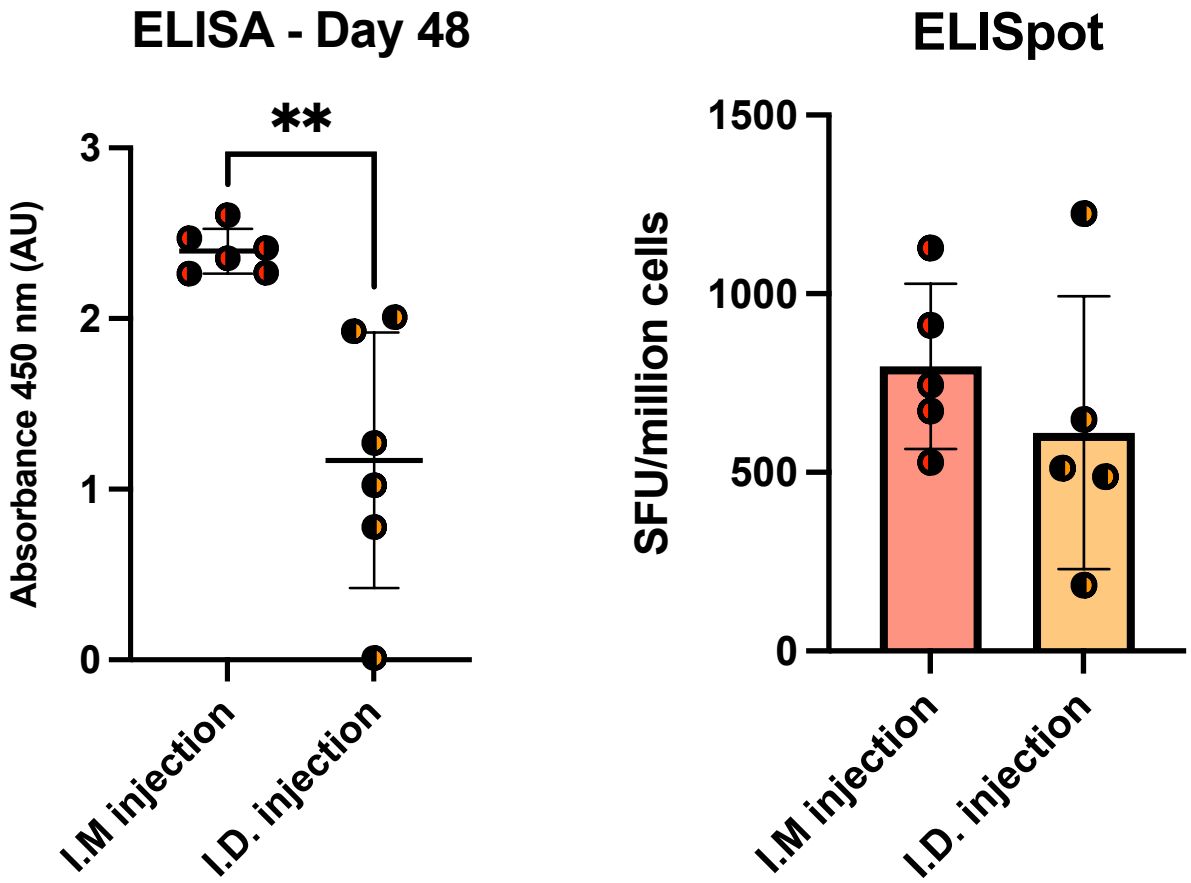



**Figure 2.21.** Mice were injected with 50 µg CMV-Cal09 dbDNA$^{TM}$ intradermally (I.D). or 25 µg intramuscularly (I.M.). A Welch's t-test was used to assess the difference. Left: anti-Cal09 HA IgG ELISA data from blood samples taken at day 48. Relative absorbance is plotted for all groups, n=6, ** = $p<0.01$. Right: ELISpot results from splenocytes taken on day 69. Spot forming units (SFU) are plotted per group, n=5, $p>0.05$.

Comparing the ELISA with the ELISpot, intramuscular (I.M.) injection appears to give more robust immune responses compared to the intradermal (I.D.) injection. For I.M. injection, there is a smaller standard deviation and a significantly higher ($p<0.01$) level of antibodies compared to I.D. injection. The technically challenging nature and poor reproducibility of intradermal injection has prevented its widespread clinical use. This is reflected in these results where a wider spread in immune responses is seen, likely a consequence of varied amounts being successfully delivered to the most

appropriate cells during injection. Notably, the cellular response achieved by I.D. injection relatively outperforms the antibody response generated, and the SFU (spot-forming units)/million cells produced (611 SPU/million cells) is not statistically different from the level produced by I.M. injection (797 SPU/million cells). Despite the differences shown here, it is apparent that the DNA vector encoding Cal09 HA is functional and both delivery routes can successfully elicit immune responses and can be used as 'control' references for future optimisations of ultrasound-mediated delivery.

### 2.3.5 *In vivo* testing of novel DNA vectors

The plasmids described in section 2.3.3 , which were constructed as described in 2.3.3, as well as three plasmids donated by Touchlight Ltd. were assessed for their *in vivo* efficacy. Experiments aimed to address three questions, namely:

- Does the promoter strength impact the observed immune response?
- Does targeting antigen production to certain cells by the use of promoters increase the observed immune response for ultrasound mediated delivery?
- Can the co-delivery of DNA-encoded cytokines result in an increased immune response?

To assess these questions, groups of three mice were injected with DNA or treated with ultrasound and a solution of dbDNA$^{TM}$ and nanocups for cavitation-mediated delivery. The mice were homologously boosted on day 20 and bleeds were taken regularly. A terminal bleed was taken on day 49. The anti-Cal09 HA IgG antibody levels were assessed by ELISA, and the isotype subclass of the antibody response was profiled.

#### Impact of promoter strength

To assess if promoter strength would impact immune responses, two vectors were compared, namely proTLx-$\kappa$ B5X4 Cal09 (CMV-Cal09) and proTLx-$\kappa$ EF1$\alpha$-Cal09 (EF1$\alpha$-Cal09). The CMV-Cal09 vector has a promoter derived from the cytomegalovirus, which results in constitutively high expression in mammalian cells. This was compared with the EF1$\alpha$ promoter, a ubiquitous mammalian promoter, which has shown to drive long-term expression compared to the CMV promoter ([159, 160]). The antibody levels after 49 days (Figure 2.22) show that vaccination with ultrasound resulted in lower average antibody titres for both CMV-Cal09 dbDNA$^{TM}$ and EF1$\alpha$-Cal09 dbDNA$^{TM}$ ($p<0.05$). However, the highest antibody level in the ultrasound-treated group matched the average level of antibodies detected by direct intramuscular injection of CMV-Cal09, despite cavitation-mediated delivery depositing a much lower total amount of DNA into the skin (approximately 0.03% of the dose placed on the skin remains after 24 hours, i.e. approximately 3300-fold less than was injected (see section 2.3.2). This showcased the potential of ultrasound-mediated delivery to match the antibody responses achieved by direct injection and even allow dose sparing, whilst also highlighting the need to improve the reliability of the process to gain optimal benefit from the approach.

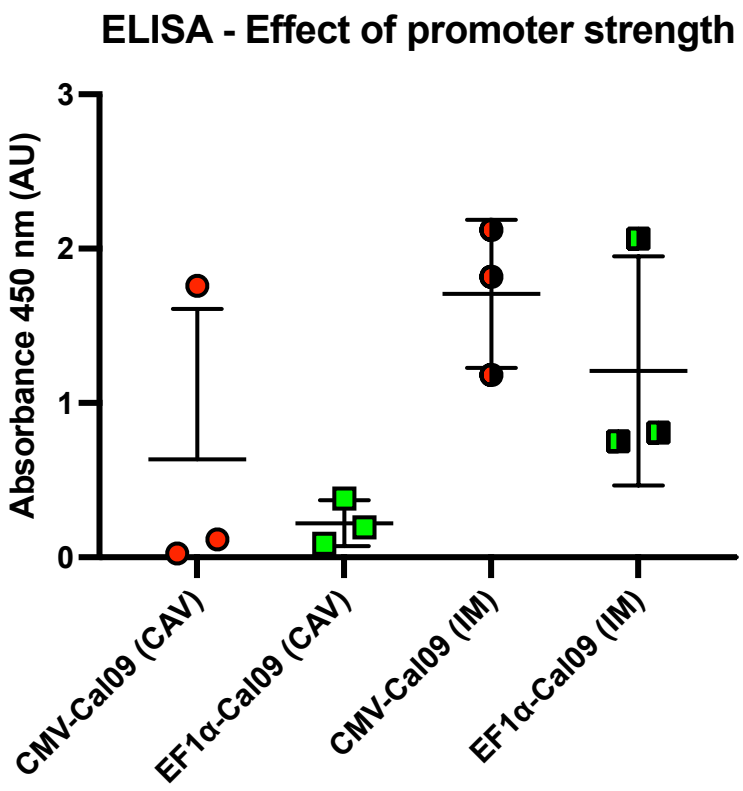



**Figure 2.22.** ELISA to detect anti-Cal09 HA IgG antibodies in blood samples of mice taken at day 49. Absorbance is plotted for all groups. The mice were I.M. injected with 50 µg dbDNA$^{TM}$ or treated with a formulation containing 25% nanocups, MilliQ and 50 µg dbDNA$^{TM}$ with ultrasound. The mice were treated with either CMV-Cal09 dbDNA$^{TM}$ or EF1$\alpha$-Cal09, n=3. Mean (horizontal line) and standard deviation (error bars) are displayed. A two-way ANOVA (vector x treatment) was done with a post hoc test between vectors for the different treatments using the Šidák correction for multiple comparisons. A significant effect of treatment was observed, $p<0.05$. No significant effect of vector or the interaction was observed ($p>0.05$). Multiple comparisons showed $p>0.05$ for all vector groups.

Interestingly, cavitation-mediated delivery of CMV-Cal09 resulted in 2/3 mice generating an immune response above background, whilst EF1$\alpha$-Cal09 generated an immune response in 3/3 mice. The CMV-Cal09 vector however has a much greater variance in the level of antibody levels, compared to EF1$\alpha$-Cal09. This illustrates that despite the ability of cavitation-mediated delivery to match intramuscular injection, it cannot be reproducibly done with the current set-up. In the intramuscularly injected groups, there is a non-significant difference in the antibody levels between the two vectors, implying there is no marked advantage of the CMV promoter over the EF1$\alpha$ promoter at this time point. Based on these results, there was little compelling rationale to develop the EF1$\alpha$-Cal09 vector over the CMV-Cal09 vector.

### Impact of targeting expression to different tissues

The impact of targeting expression to specific cell types was then assessed. There is yet to be consensus on whether optimal vaccination is achieved by initial expression and/or presentation of antigen directly by immune cells or by non-immune cells or by both, or on how the nature of the

vaccine or the vaccination site alters this [191, 192]. The ability to use cavitation to deliver the DNA specifically to the dermal compartment and to utilise cell-specific promoters allowed these questions to be probed. Hence, proTLx-κ B5X4 Cal09 HA (CMV-Cal09), proTLx-κ KCL27-Cal09 (KCL27-Cal09) and proTLx-κ CD11c-Cal09 (CD11c-Cal09) were compared. The KCL27 promoter is specific for keratinocytes, the majority of cells in the skin, and the CD11c promoter is specific for dendritic cells [156]. If cavitation-mediated delivery resulted in targeted delivery to a subset of cells, only one of these constructs would be expected to induce immunity. Similarly, if I.D. injection predominantly targets keratinocytes rather than dendritic cells, then the proTLx-κ KCL-Cal09 (KCL-Cal09) would be expected to outperform the proTLx-κ CD11c-Cal09 and vice versa. The ability of these constructs to raise immune responses to Cal09 HA was therefore compared to standard (non-cell selective) CMV-Cal09 vector delivered via I.M. injection. Data showed that according to the antibody levels after 49 days (Figure 2.23), none of the mice in the cavitation treated groups showed any substantial immune response after treatment with KCL27-Cal09 or CD11c-Cal09. Notably, after intradermal injection of the KCL27-Cal09 vector, an immune response comparable to CMV-Cal09 pDNA injected I.M. was observed. This confirmed that the KCL27-Cal09 vector was functional and could successfully express Cal09 haemagglutinin, but notably it failed to do so after cavitation-mediated delivery. At this time-point there was still not assurance that the CD11c-Cal09 vector was even functional or had produced any transgene or consequent immune response.

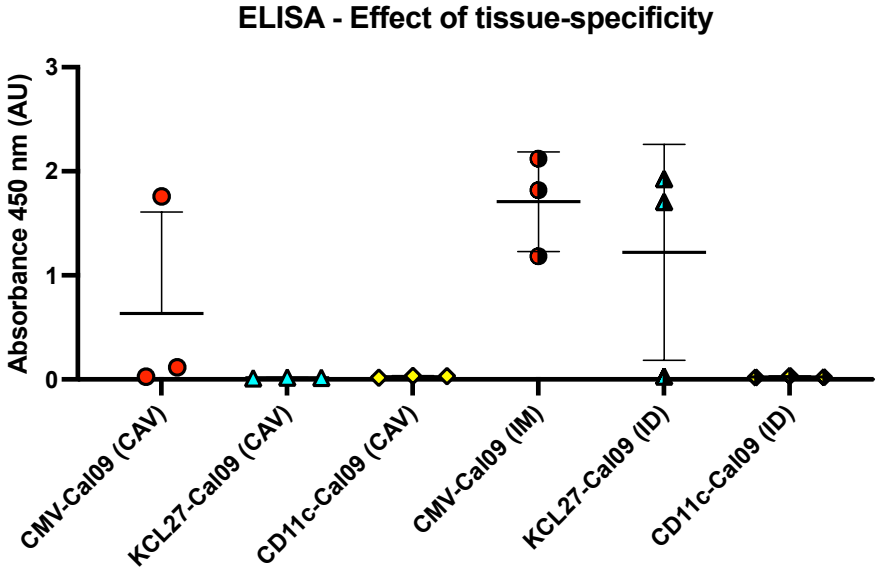



**Figure 2.23.** ELISA to detect anti-Cal09 HA IgG antibodies in blood samples of mice taken at day 49. Relative absorbance of the anti-Cal09 ELISA is plotted for all groups. The mice were injected with 50 µg dbDNA$^{TM}$ or treated with a formulation containing 25% nanocups, MilliQ and 50 µg dbDNA$^{TM}$ with ultrasound. The mice were treated with either CMV-Cal09 dbDNA$^{TM}$, KCL27-Cal09 or CD11c-Cal09, n=3. Mean (horizontal bars) and standard deviation (error bars) are displayed. A two-way ANOVA (vector x treatment) was done with a post hoc test between vectors for the different treatments using the Šidák correction for multiple comparisons. A significant effect of treatment was observed, as well as for vector, $p<0.05$. No significant effect of the interaction was observed ($p>0.05$). Multiple comparisons showed $p>0.05$ for all vector groups.

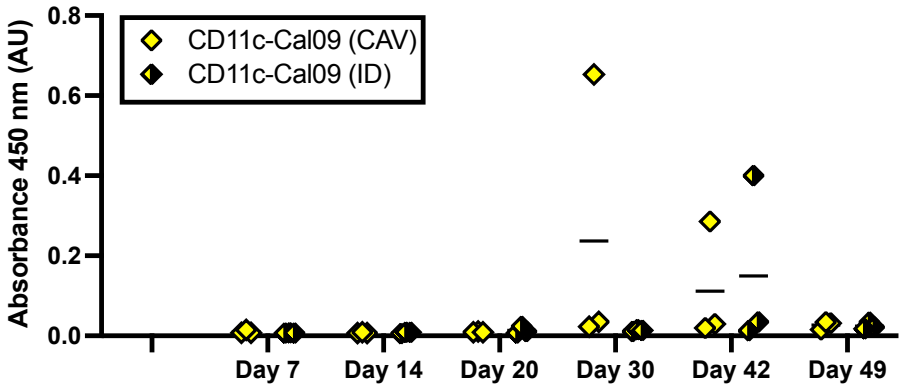



**Figure 2.24.** ELISA to detect anti-Cal09 HA IgG antibodies in blood samples of mice taken at day 7, 14, 20, 30, 42 and 49. Relative absorbance is plotted for all groups. The mice were injected with 50 µg CD11c-Cal09 dbDNA$^{TM}$ or treated with a formulation containing 25% nanocups, MilliQ and 50 µg CD11c-Cal09 dbDNA$^{TM}$ with ultrasound. N = 3, mean is displayed.

However, when immune response development over time was profiled by assaying anti-Cal09 HA antibodies in bloods taken at intervals prior to 49 days a response was observed, confirming functionality (Figure 2.24). After ultrasound treatment, in one mouse a low transient immune response was observed, which peaked on day 30, dropped on day 42 and then became undetectable on day 49. Notably, this response exceeded that achieved by intradermal injection of the CD11c-Cal09 vector which was later, lower and more transient. This showed that the vector did elicit an immune response (albeit transient), showcasing that cavitation-mediated delivery can transfect immune cells. As the KCL27 promoter-driven plasmid and therefore keratinocytes did not appear to elicit an immune response when treated with DNA and cavitation at any time point sampled (day 7, 14, 20, 30, 42, 49 - data not shown), this may imply that immune cells play a crucial role in the expression of and immunisation observed with cavitation-mediated DNA delivery. Further studies with larger groups would be required to build on these intriguing suggestions.

Overall, this data showed some evidence for successful transfection of immune cells by cavitation-mediated delivery of dbDNA$^{TM}$ but no evidence of the targeting of keratinocytes. However, targeting of specific tissues for expression of antigen did not have demonstrable advantage for improving the immune response against the encoded antigen. These vectors may therefore have greater utility in helping define target cell populations and helping probe the mechanisms underlying immunisation by cavitation, rather than in clinical translation. Indeed, it should be noted that the recently approved ZyCoV-D SARS-CoV-2 DNA vaccine relies on nothing more sophisticated than the CMV promoter [63].

**Impact of the addition of adjuvants**

A common strategy to improve poorly immunogenic vaccines, particularly those based on recombinant protein or DNA vaccines, has been the addition of adjuvants. Hence, the adjuvant efficacy of two DNA-encoded cytokines and a CpG island and RIG-I activating RNA containing DNA vector was explored. Three vectors were assessed, namely proTL-κ CMV-IL1α-P2A-IL1β (CMV-IL1α-IL1β), proTLx-κ CMV-IL12 (CMV-IL12) and proTLx-κ D3F2 CpG-C RIG-I (CpG-RIG1).

To assess whether for the same total 50 µg DNA quantity, a stronger immune response could be achieved, half the Cal09 HA-encoding DNA was replaced by the adjuvant-encoding DNA vector and a comparison was made to the use of 50 µg of CMV-Cal09 dbDNA$^{TM}$ only. The impact of the delivery route was assessed by comparing cavitation-mediated transcutaneous delivery to delivery via I.M. injection. After 49 days, the anti-Cal09 HA antibody levels showed there to be no significant difference in antibody levels after I.M. injection (Figure 2.25) (t-test with Welch's correction, p=0.91). This means there was no detectable benefit upon addition of the adjuvant-encoding DNA vectors. After ultrasound-mediated delivery, the average antibody level was lower after addition of CpG-RIG1 and CMV-IL12. However, the addition of CMV-IL1α-IL1β resulted in 3/3 responders compared to 2/3 responders in the CMV-Cal09, as well as a higher average absorbance level and a smaller standard deviation. Hence, the antibody responses for CMV-IL1α-IL1β in combination with CMV-Cal09 were further characterised.

Titring, i.e. serial dilution of sample until absorbance signal is lost, can give a more refined comparison of the relative antibody levels than absorbance readings alone. Titring (Figure 2.26) further corroborated that mice treated with CMV-IL1α-IL1β and CMV-Cal09 had higher (geometric means of 2520 vs 342) and more reproducible antibody titres (GSD of 3.6 vs 31.7) than those treated with only CMV-Cal09 in the ultrasound-treated groups, despite the mice only being exposed to half the dose of CMV-Cal09 vector. A similar difference was not observed for I.M. injected mice.

Immunoglobulin molecules exist in different isotypes with different effector functions and levels. In mice, IgG1 antibodies are indicative of a Th2 lymphocyte response and have limited activation of antibody-dependent cellular cytotoxicity (ADCC) and complement-dependent cytotoxicity (CDC). IgG2 antibodies are indicative of a T-helper cell type 1 (Th1) lymphocyte response and strongly activate ADCC and CDC [193–195]. Isotyping of anti-Cal09 HA IgG1 and IgG2a antibodies generated in the mice in these studies showed a marked difference in immune response after treatment by

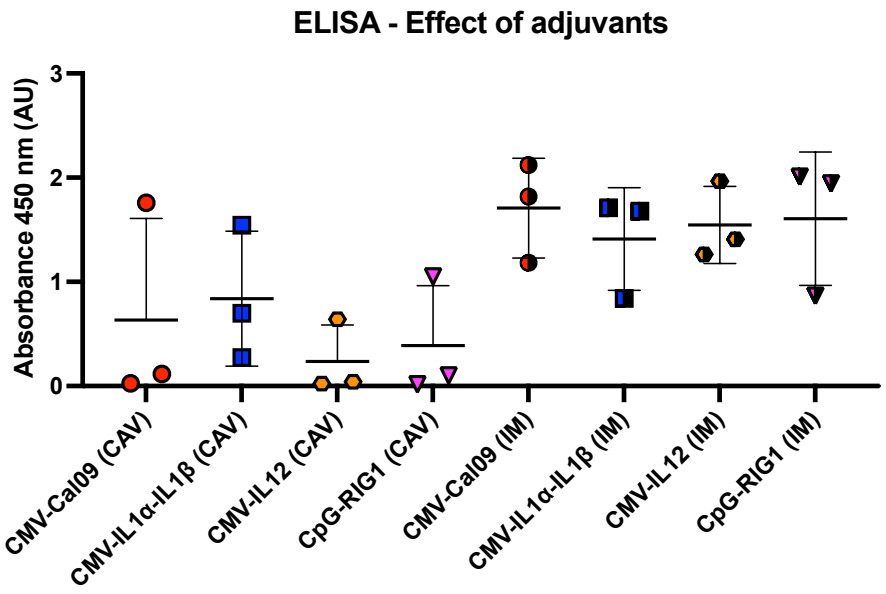



**Figure 2.25.** ELISA to detect anti-Cal09 HA IgG antibodies in blood samples of mice taken at day 49. Relative absorbance is plotted for all groups. The mice were injected with 25 µg dbDNA$^{TM}$ or treated with a formulation containing 25% nanocups, MilliQ and 50 µg dbDNA$^{TM}$ with ultrasound. The mice were treated with either only CMV-Cal09 dbDNA$^{TM}$ or 50% CMV-Cal09 dbDNA$^{TM}$ in combination with 50% CMV-IL1$\alpha$-IL1$\beta$, CMV-IL12 or CpG-RIG1 dbDNA$^{TM}$, n=3. Mean (horizontal bars) and standard deviation (error bars) are displayed). A two-way ANOVA (vector x treatment) was done with a post hoc test between vectors for the different treatments using the Šidák correction for multiple comparisons. A significant effect of treatment was observed, $p<0.001$. No significant effect of the interaction or vector was observed ($p>0.05$). Multiple comparisons showed $p>0.05$ for all vector groups.

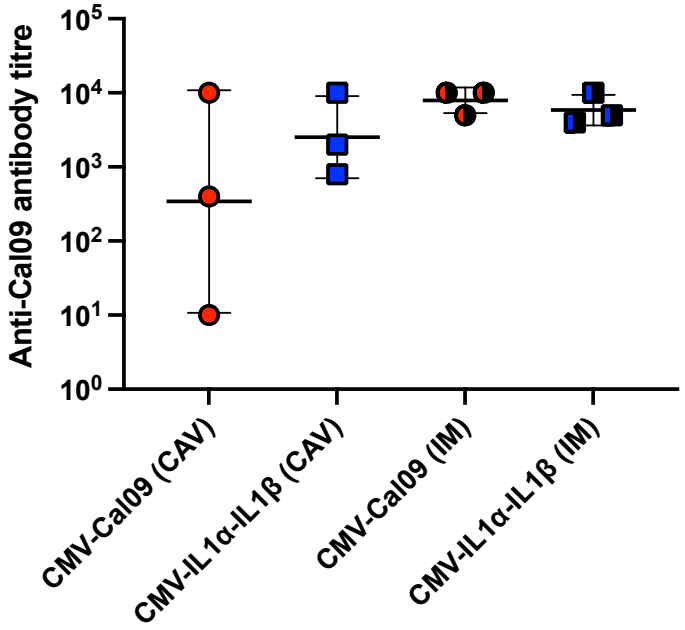
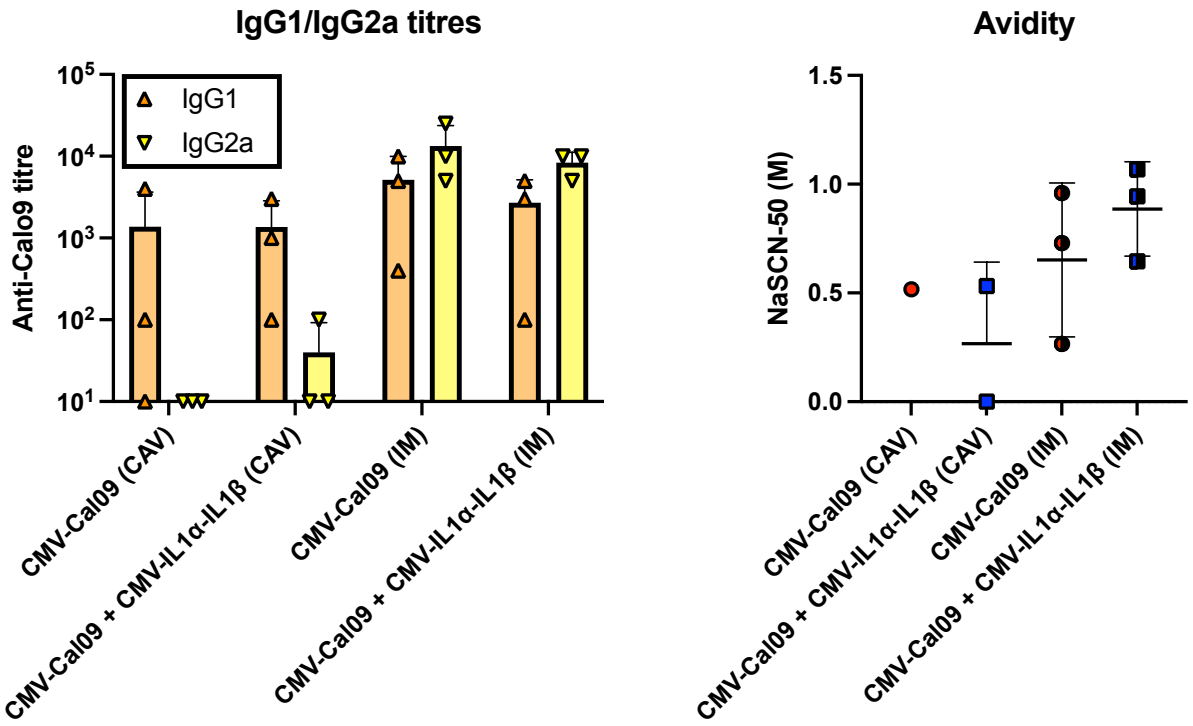



**Figure 2.26.** ELISA to detect anti-Cal09 HA IgG antibodies in blood samples of mice taken at day 49. The samples were titred as described in section 2.2.11. Final titre (last dilution where the signal was above 3xSD above the signal of negative-control serum) is plotted for all groups. The mice were injected with 25 µg dbDNA$^{TM}$ or treated with a formulation containing 25% nanocups, MilliQ and 50 µg dbDNA$^{TM}$ with ultrasound. The mice were treated with either only CMV-Cal09 dbDNA$^{TM}$ or 50% µg CMV-Cal09 dbDNA$^{TM}$ in combination with 50% µg of CMV-IL1$\alpha$-IL1$\beta$ dbDNA$^{TM}$, n=3. Geometric mean titre (horizontal bars) $\times/\div$ geometric standard deviation (error bars) are displayed. A two-way ANOVA (vector x treatment) was done with a post hoc test between vectors for the different treatments using the Šidák correction for multiple comparisons. No significant effect of treatment, vector or interaction was observed ($p>0.05$). Multiple comparisons showed $p>0.05$ for both vector groups.

cavitation compared to I.M. injection (Figure 2.27a). There was a significant ($p<0.005$) difference in IgG1/IgG2a between cavitation and intradermal injection. After ultrasound-mediated delivery, there was a clear preference for IgG1 antibodies, whereas injection gave a more balanced distribution of IgG1 and IgG2a antibodies. This further supports the notion that ultrasound-mediated delivery targets different cells and activates different immune branches compared to I.M. injection.

Finally, the avidity as a measure of binding strength was measured. Sodium thiocyanate (NaSCN) was added in increasing concentrations and the NaSCN concentration at which the absorbance reading was halved was used as a measure of avidity. Only three samples in the ultrasound-treated group showed high enough antibody titres to measure avidity accurately. Although limited data is available from the ultrasound groups, a higher avidity of antibodies was associated with I.M. injection (Figure 2.27b). Interestingly, a higher mean avidity was associated with the 'CMV-Cal09 + CMV-IL1$\alpha$-IL1$\beta$ (IM)' group than the 'CMV-Cal09 (IM)' group (0.89 M vs 0.65 M), despite there being half the amount of Cal09 HA-encoding DNA ($p>0.05$).




**(a)** Isotyping **(b)** Avidity

**Figure 2.27.** ELISA data to detect anti-Cal09 HA IgG antibodies in blood samples of mice taken at day 49. The mice were injected with 25 µg dbDNA$^{TM}$ or treated with a formulation containing 25% nanocups, MilliQ and 50 µg dbDNA$^{TM}$ with ultrasound. The dbDNA$^{TM}$ dose consisted of either CMV-Cal09 dbDNA$^{TM}$ alone or 50% CMV-Cal09 dbDNA$^{TM}$ and 50% CMV-IL1α-IL1β dbDNA$^{TM}$. N=3. (a) Titring of the isotype-specific ELISA for anti-Cal09 HA antibodies from blood samples taken at day 49, as described in section 2.2.11. Geometric means (bar height) $\times/\div$ geometric standard deviation (error bars) are displayed. A two-way ANOVA (isotype x treatment) was done with a post hoc test between isotypes for each group using the Šidák correction for multiple comparisons. A significant effect of treatment was observed, $p<0.005$. Multiple comparisons showed $p>0.05$ for all groups. (b) Avidity of anti-Cal09 antibodies from blood samples of mice taken at day 49. NaSCN concentration at which the absorbance was halved are plotted for all groups, calculated as described in section 2.2.11. Mean (horizontal bar) and standard deviation (error bars) are displayed. A two-way ANOVA (vector x treatment) was done with a post hoc test between vectors for the different treatments using the Šidák correction for multiple comparisons. No significant effect of treatment, vector or interaction, $p>0.05$. Multiple comparisons showed $p>0.05$ for both vector groups.

## 2.4 Conclusions and Discussion

The aim of this chapter was to explore the potential of cavitation-mediated DNA delivery, and how it may be enhanced by vector modification. The foundation for this, was work by Dr. Van Blokland and Dr. Bhatnagar which showed that cavitation is an effective method of delivering substances into the skin and cavitation can deliver reporter-encoding DNA into the skin [143, 144]. There is strong evidence that the skin presents a potentially powerful site for vaccine delivery if it can be reliably targeted [196]. The advantages of cavitation-mediated DNA delivery include that it provides a pain-free method for dermal delivery, compared to other technologies, such as electroporation. Utilising DNA vaccines instead of RNA vaccines could reduce production costs and would also negate the need for cold-chain storage [197]. Scalable, essentially cell-free technologies such as dbDNA$^{TM}$ open up the possiblity of harnessing the power of DNA without the need to rely on viral vectors as agents to achieve delivery of the DNA, improving manufacturing safety and regulatory concerns.

In this chapter, an initial study was done to assess the effect of ultrasound pressure amplitude on delivery. A passive cavitation detector (PCD) was used to capture and quantify the cavitation energy, which was represented as Total Acoustic Sensor Energy (TASE), so that the relationship between TASE and gene delivery/expression could be profiled. A clear relationship was found between cavitation and delivery, where pressures insufficient to instigate cavitation ($\leq$ 0.5 MPa) resulted in negligible DNA delivery and transgene expression, whereas beyond a threshold (4.3 µJ TASE) whereby the pressure applied gave sustained substantial cavitation, there was reliable expression from the DNA reporter vector. This has also been observed by Dr. Van Blokland who recorded similar bioluminescence levels sub-cavitation and above cavitation levels as in this work, namely 3.5x$10^4$ p/s sub-cavitation and 1.3x$10^6$ p/s above cavitation, compared to 1.7x$10^4$ p/s for sub-cavitation and 1.7x$10^6$ p/s for 0.7 MPa and above in this work [143]. Interestingly, once the threshold of cavitation was passed, increasing pressure provided no additional luciferase protein expression, implying that cavitation is the crucial mechanism for delivery but that its effect saturates beyond a certain level. This effect was not directly investigated or described previously by Dr. Van Blokland with this set-up, however, she did report that increasing delivery time from 10 minutes to 15 minutes provided no additional delivery benefit [143]. Saturation of cavitation has been previously observed by Qiu et al. [198], who observed that a linear relationship exists between inertial cavitation dose and DNA transfection until 1670 V µs, beyond which cavitation dose no further improvement was observed in transfection efficiency for a PEI/DNA complex delivered to a MCF-7 cell suspension.

This potential for real-time confirmation of delivery using a non-invasive integratable technology is a notable advantage of the cavitation-mediated delivery approach compared to other dermal delivery techniques, and the need for feedback on delivery has been highlighted by the public in focus groups on the use of microneedles [199]. Furthermore, analysis of the frequency content of the acoustic emissions even allows the importance of the presence and relative levels of broadband and harmonic emissions to be gauged [200]. It could be observed that the broadband ('inertial') energy component showed the same stepwise change in levels (1.0 μJ to 2.3 μJ) in going from 0.5 MPa to 0.7 MPa which was observed for the expression of luciferase ($1.7x10^4$ p/s vs $2.4x10^6$ p/s) (Figure 2.7). The importance of inertial cavitation for delivery into the skin has previously been shown by Feiszthuber et al., who showed that broadband acoustic emissions, which are generated by inertial cavitation, were detected for enhanced delivery of insulin across two skin models. They also observed a 23% increase in penetration distance and 40% increase at 1.4 MPa in an agar model [201]. The effect of improving delivery with inertial cavitation has also been observed in different contexts, such as cancer. For instance, a 60-fold improvement in delivery of luciferase-expressing adenovirus into breast cancer cells embedded in a hydrogel tumour model has been described [202]. This has been further supported by *in vivo* studies. One of these has shown that ultrasound and SonoVue significantly ($p=0.0167$) improve the tumour/blood ratio of $^{111}$In-EGFP-LP in tumour-bearing mice, showcasing the potential of cavitation to deliver drugs locally [136]. Another study by Graham et al. demonstrated that a 30% increase in payload release was seen for liposomes with a high proportion of DSPE lipids used in combination with SonoVue and ultrasound above the cavitation threshold *in vitro* and a 16-fold increase in luminescence *in vivo* for luciferin-loaded liposomes in B16F10-luciferase tumours on C57BL6 mice ($p<0.001$).

Another observation made, was that compared to other techniques, such as I.M. injection, S.C. injection and I.D. injection, cavitation had a very different expression footprint on the skin. Cavitation resulted in either a ring of expression within the treated area or diffuse expression across the treated area (depending on the pressure applied), whereas injection resulted in localised peaks restricted to the site of injection only. In terms of total level of expression of the luciferase protein, cavitation-mediated delivery outperformed S.C. injection and showed lower variability than I.D. injection (suggesting it may be a more reliable way to reach the dermal compartment). However, cavitation-mediated delivery was unable to match the luciferase protein expression achieved by I.M. injection ($1.66x10^6$ vs $1.49x10^7$). It is also noticeable that whereas I.D. injection leads to little diminishment of signal over the subsequent 5 days, there was a loss of between 5 and 10–fold for

cavitation mediated delivery over the same duration. This may reflect the targeting of different cell populations and a consequently different silencing, destruction or lymph node shuttling of the vector or the cells it has entered. For instance, DNA/PEIm nanoparticles targeted to Langerhans cells in the epidermis can be detected in the skin-draining lymph nodes in a rabbit-model after topical application to exfoliated skin [203]. These findings make the immunisation data in section 2.3.5 more tantalising in terms of antibodies generated by the different techniques.

Previous work by Dr. Van Blokland shows only 0.011% of the original dose is delivered to the skin by cavitation which decreases to 0.004% after 24 hours, as assessed by qPCR immediately after treatment, whereas without cavitation <0.001% is delivered [143]. In the work in this thesis, a larger percentage of dbDNA$^{TM}$ remained after 24 hours, namely 0.0303%, which is also higher than the delivered dose observed by Dr. Van Blokland directly post-treatment. This probably reflects the improvements made to the delivery parameters and set up. The coordinated quantification of the amount of DNA actually delivered into the skin and the level of cavitation, which occurred during delivery in section 2.3.2, similarly provided confirmation that cavitation was the enabling stimulus required for delivery, rather than just ultrasound exposure per-se. This also showed that compared to needle-and-syringe approaches where the complete dose in the formulation is delivered (i.e. complete depression of the syringe plunger ensures 100% of the dose enters the mouse), using this ultrasound set-up and these parameters, cavitation likely only delivers a relatively very low proportion of the dose placed on the skin and just 0.03% of this dose remains after 24 hours. Hence, it does appear a much better luminescence/dbDNA$^{TM}$ ratio can be achieved with cavitation. The reason for the greater 'expression per DNA copy delivered' efficiency with cavitation, may be that although needle and syringe can provide an entry mechanism for DNA into the body, the vast majority of this DNA is not provided with a mechanism to traverse the cell or nuclear membranes so is degraded in the extracellular space and goes to waste [204]. This could imply that small improvements in the level of delivery achieved via cavitation, could have a relatively large impact on transgene expression.

This demonstrates how little DNA is needed upon cavitation-mediated delivery to result in strong expression, as assessed by luminescence.

These delivery and expression data therefore served to confirm that cavitation could be used to reliably achieve DNA delivery and expression, and that the spatial and temporal profile of the expression differed dramatically from expression resulting from needle and syringe delivery in ways that could

suggest benefit if used in vaccination. It was also clear that demonstration of such utility would require a better understanding of the cell populations involved, improved levels of delivery/expression and an output of the ability to raise immune responses against an antigen rather than just reporter gene expression. Hence, these requirements were explored using a DNA vector expressing haemaglutinin antigen from a 2009 influenza outbreak in California, proTLX-k B5X4 Cal09 HA (CMV-Cal09), in combination with a range of DNA vectors designed to enhance activity and provide insight into cell specificity.

To verify that the control DNA vector (proTLX-κ B5X4 Cal09 HA (CMV-Cal09)) used for subsequent comparisons could elicit humoral and cellular immunity, a pilot study was performed to assess the immune responses after the I.D. and I.M. injection of the CMV-Cal09 vector. This showed that this vector was capable of eliciting both humoral (as assessed by anti-Cal09 HA antibody ELISA) and cellular immune responses (as assessed by ELISpot). It further showed that I.M delivery provides higher antibody titres and more reproducible cellular responses compared to I.D. responses. This is in line with work of Donnelly et al., who showed that I.M. injection of 100 µg of nucleoprotein-encoding pDNA resulted in higher survival than I.D. injection in BALB/c mice upon challenge with a cross-strain ($p<0.002$) [205]. However, Best et al. described that gene gun-mediated delivery into the epidermis resulted in higher antibody responses and cellular responses, as well as a higher percentage of tumour-free C57BL/6 mice upon inoculation with tumour cells after prime and boost DNA vaccination compared to I.M. vaccination [206]. In another study by Alarcon et al., 1 µg HA-encoding pDNA delivered by microneedle did result in higher antibody titre compared to the same dose delivered by intramuscular injection in rats. However, similar titres were observed for doses higher than 5 µg [207]. It is possible that had a much lower dose been administered, the dose-sparing benefits of I.D. shown by Alarcon et al. would have been observed in this chapter. It should also be noted that I.M. injection in mice may produce an overestimate of the efficacy of vaccines due to the disparity in injected volume to tissue mass ratio and associated hydrostatic pressure [77] in going from mice I.M. injection to I.M. injection in rhesus monkeys. For instance, McCluskie observed that after two boosters, I.M. resulted in higher anti-HBsAg titres than I.D. in mice, but no significant difference was observed in rhesus monkeys [208]. These results further emphasise how route, volume, species and the exact skin layer targeted may impact on antibody responses and (cross-)protection from disease. Furthermore, it should be taken from this data that no ideal comparitor exists for cavitation-mediated delivery. From the data presented, it could be seen that I.D. injection is a difficult technique, which lacks the reproducibility seen from I.M. injection but it does target the same cell populations as

cavitation-mediated delivery. However, I.M. injection targets a completely different cell population but shows greater reproducibility and is the standard vaccine administration route. In this thesis, either an I.D. or I.M. control is included in the *in vivo* studies depending on which is most appropriate, as including both in all studies would results in an unsustainably high number of animals per study.

Four questions were then addressed through the use of seven different DNA constructs, namely the effect of promoters, the effect of cell type specific expression, and the impact of DNA-based adjuvants and the importance of route of delivery. Substantial cloning work was performed to generate four novel DNA vectors and a further three were kindly donated by Touchlight Genetics Ltd.

Firstly, the virus-derived, high-expressing CMV promoter was compared to the household EF1$\alpha$ promoter to assess whether such a swap would negatively impact immune responses. Data showed that in terms of anti-HA antibody titre the CMV-Cal09 vector delivered by cavitation was able to match I.M. injection of the CMV-Cal09 vector, albeit inconsistently. This is particularly intriguing when the substantially lower peak and duration of DNA expression evident with cavitation compared to I.M. in Figure 2.7 is considered. In comparison, for the EF1$\alpha$-Cal09 vector, all mice in the cavitation group were shown to produce an anti-HA antibody response but at low levels.

With no obvious benefit to the use of the EF1$\alpha$ promoter the CMV-Cal09 vector was therefore chosen as the promoter for further work. However, even though CMV can provide high levels of response, more work is needed to increase reproducibility of immunisation with CMV-Cal09. This could be through an improved ultrasound set-up, through improved sample formulation or the addition of DNA adjuvants.

Secondly, cell type specific promoters were assessed to gain some insight into the type of cells transfected by cavitation. Notably, the keratinocyte-specific promoter (KCL27) could elicit anti-HA antibodies upon I.D. injection, but not upon cavitation-mediated delivery. This implies that keratinocytes may not play a big role in generating immunity upon cavitation-mediated delivery. The dendritic cell-specific promoter (CD11c) showed low, late (30 days) and transient generation of an anti-HA antibody response which was more pronounced in the case of cavitation delivery vs I.D. injection. Again indicating that these two delivery approaches may target different cell populations, with cavitation leading to the transfection of immune cells as a driver of immune responses rather than keratinocytes. This preferential uptake has been observed for the aforementioned DNA/PEIm nanoparticles, which were

inefficiently loaded by keratinocytes but captured by over 90% of MHCII-positive Langerhans cells based on *ex vivo* cultures of murine epidermal cells [203]. Despite the tantalising clues provided by the cell type specific promoters, they showed no improvement in terms of total antibody levels compared to the CMV promoter. So may be of most use in continuing to probe cell population deposition and processing.

Finally, three adjuvant constructs were tested, namely proTLx-κ CMV-IL1α-P2A-IL1β (CMV-IL1α-IL1β), proTLx-κ CMV-IL12 (CMV-IL12) and proTLx-κ D3F2 CpG-C RIG-I (CpG-RIG1). Half the CMV-Cal09 DNA dose was replaced by the DNA adjuvants and the antibody titres compared to the non-adjuvanted CMV-Cal09 vector, based upon the principle that the addition of another plasmid would have to be warranted by at least a halving of the dose of the CMV-Cal09 needed. Upon I.M. injection the adjuvants showed no beneficial effect to the anti-HA antibody levels generated. However, the DNA-encoded CMV-IL1α-IL1β adjuvant increased the number of mice which produced a positive response, and the antibody titres compared to unadjuvanted CMV-Cal09 in combination with cavitation-mediated delivery. Further highlighting the difference between delivery by cavitation and direct I.M. injection, the avidity upon I.M. injection was higher than upon cavitation-mediated delivery. This could be related to the different cell types transfected by the different delivery methods. The different immunological routes were also highlighted by the isotyping of the antibodies. IgG1 and IgG2a titring showed that I.M. injection of the DNA vectors led to a balanced IgG1/IgG2a response, whereas a clear skewing towards IgG1 was seen for cavitation-mediated delivery. This fits well with work by Kwissa et al., which showed that intradermal injection with a gene gun resulted in IgG1/IgG2a ratio >100, whereas I.M. resulted in an IgG1/IgG2a ratio of 0.4-0.7 [209]. The underlying mechanism may be related to the observation of the enhanced CD11c promoter activity seen with cavitation-mediated delivery (Figure 2.24) and the fact that Langerhans cells have been shown to drive predominantly IgG1 responses [89]. Interestingly, one mouse in the CMV-Cal09 + CMV-IL1α-IL1β did also generate IgG2a responses, which could imply that it is possible to elicit IgG2a antibodies upon cavitation-mediated delivery, but that a better understanding of the level, type and duration of cavitation is needed to understand how a particular response profile may be chosen. As IgG2a antibodies are related to a Th1 response, complement activation and antibody-dependent cellular cytotoxicity [194, 195, 210], the ability to generate IgG2a antibodies would likely be beneficial in terms of generating a robust immune response to future infections.

This chapter focused on exploring the potential of cavitation-mediated DNA delivery. To drive this

research forwards, three areas have been identified that require further work. These include:

- Increasing the IgG2a antibody responses for cavitation-mediated delivery
- Improving reproducibility by improving the design of the ultrasound set-up
- Investigating the potential of biodegradable cavitation nuclei

As the ability to elicit both IgG1 and IgG2a antibodies would likely relate to a more robust immune response, strategies to enable more IgG2a antibodies are of interest. In Chapter 5, different DNA vaccines are assessed for their ability to generate a more balanced antibody response.

As the ultrasound set-up (see Figure 2.2) used in this chapter is limited by poor reproducibility in the positioning of mice and exposes underlying tissue to ultrasound in addition to skin, it is speculated that an easier to manage set-up could enable better reproducible delivery into the epidermis and by extension better immunological reproducibility. Chapter 4 investigates an alternative set-up and seeks to optimise parameters for use.

Finally, all experiments in this chapter were performed with nanocups, a single-cavity polymeric nanoparticle [129]. In the introduction (Section 1.7.1) it was speculated that a biodegradable alternative might have advantages in terms of regulatory barriers, as well as offering the potential of being immune-stimulatory. In the following chapter (Chapter 3), biodegradable cavitation nuclei are investigated. Ultimately, the aim is that optimisations in DNA vectors, ultrasound set-up and cavitation nuclei will lead to an improved vaccination strategy.

# Chapter 3

# Protein Cavitation Nuclei

## 3.1 Introduction

Data presented in Chapter 2 of this thesis demonstrate that utilising cavitation for transcutaneous delivery of dbDNA$^{TM}$ results in effective, reproducible delivery and expression of a luciferase-encoding vector. Specifically, using quantitative PCR (qPCR), it was shown that 0.03% of the dbDNA$^{TM}$ dose present in the sample holder during exposure of the skin to ultrasound could still be detected 24 hours later. In addition, quantification of the acoustic output of the system showed the enabling role cavitation played in achieving successful expression from the DNA vector upon its delivery into the skin. In the absence of cavitation, bioluminescence was akin to background, non-transfected skin, whereas a stepwise increase of bioluminescence could be observed beyond a defined cavitation threshold (between 1.7 μJ and 4.3 μJ an approximate 100-fold increase in luminescence was observed). The ability to deliver DNA to the skin, and elicit remarkably high levels of expression for each plasmid delivered ($3.93x10^2$ photons/second/$10^6$ DNA copies), highlights the potential of this approach as a vaccine delivery route. However, this study relied on the use of polymeric cups as the cavitation nuclei which, although inert, still create a concern due to their poor biodegradability. It is therefore hypothesised that a formulation of protein-based cavitation nuclei may provide for a biodegradable alternative to replace the polymeric cups. Furthermore, careful selection of the protein used may allow for the cavitation and delivery properties of the polymeric cups to be recapitulated, whilst also achieving immunomodulatory effects to enhance the immune response generated against the DNA-encoded antigen.

**Protein cavitation nuclei (p-CaN)**

In much of the published work on ultrasound-mediated delivery, the skin would be permeabilised before application of the therapeutic, or cavitation agents would be mixed with the therapeutic [133–135]. Our previous studies have moved the field forward by utilising cavitation nuclei with sufficiently sustained cavitation to allow concurrent ultrasound exposure and delivery. However, a concern has been raised that the deposition of these polymeric cavitation particles in the skin may cause toxicity and regulatory issues. It was therefore postulated that changing from methacrylamide-based polymer [129] to a protein-based cavitation nuclei may provide important advantages. Firstly, protein would be less xenogenic and more biodegradable, removing potential safety and regulatory barriers. Furthermore, if the protein chosen could provide an immunogenic stimulus in its own right, it may help enhance the effect of the nucleotide vector, and if a platform method of production could be used, the protein could be chosen to match the disease indication being addressed.

This chapter reports work performed towards development and validation of a methodology to allow proteins to be formulated as protein cavitation nuclei (p-CaN), a process which is the basis of a recently filed patent family, which includes Dr. Lyons and the current author as inventors. In short, this is achieved by firstly sonicating a solution of protein in the presence of a volatile solvent and optionally an oil as well. This creates spherical protein particles with an oil and volatile core. As the volatile is removed by vacuum, the particles collapse and become indented. These protein particles can entrap air and function as cavitation nuclei. These p-CaN have sizes varying from tens of nanometres up to several micron. It is postulated that formulating p-CaN from an antigen could result in a formulation that is both ultrasound responsive and immunogenic. Furthermore, the oil core allows for the loading of therapeutics into the core of the particles. As different formulations of p-CaN are discussed in this thesis, the p-CaN formulated with an oil/hexane core are referred to as 1G p-CaN. The protein that these p-CaN are made of can be either BSA (BSA 1G p-CaN) or Spike protein from SARS-CoV-2 (Spike 1G p-CaN).

The size of the particles may also have the added benefit of mimicking the size of viral particles and have benefits similar to virus-like particles (VLP) based vaccines, which can lower the amount of antigen needed to stimulate an immune response [211].

**Adjuvants**

Adjuvants are a crucial component of conventional injectable vaccines and help stimulate the immune system by inducing the innate immune system. They increase the efficacy of the vaccine leading to the generation of higher antibody titres and stimulating a wider range of adaptive responses.

**Imiquimod**

Imiquimod is a synthetic molecule developed by 3M Pharmaceuticals (USA). Its mechanism of action involves activation of Toll-like receptor 7 on immune cells, which leads to secretion of cytokines. These cytokines include interferon-$\alpha$, tumour necrosis factor $\alpha$ (TNF-$\alpha$), IL-1$\beta$, GM-CSF, interleukin 10 and interleukin 12. These cytokines work together to create an environment encouraging Th1-cell mediated immune responses [212, 213]. In the clinic, imiquimod has been used as a topically applied treatment for human papillomavirus infection [214]. However, its ability to engage the immune system has also made it of interest as a potent adjuvant (section 1.4 contains further discussion on adjuvants).

In the context of DNA vaccines, a mouse study has shown that the subcutaneous injection of imiquimod after particle immunisation by PowderJect$^{TM}$ with an OVA-encoding DNA plasmid resulted in cytokine production by antigen-specific T cells and extended the duration of the immune responses of these T cells (peak at 14 days without vs 21 days with imiquimod), as well as increasing the total proportion of CD4+ and CD8+ T cells [215]. Similarly, a DNA vaccine encoding the DAMP calreticulin (CRT) linked to human papillomavirus type 16 (HPV-16) E7 antigen (CRT/E7) delivered via gene gun, showed a significant ($p<0.05$) increase in E7-specific CD8+ T cells and significantly ($p<0.05$) longer survival for tumour bearing mice in combination with regular topical imiquimod application than without imiquimod (approximately 57 days vs 47 days) [216].

The beneficial effect of imiquimod used as an adjuvant to a trivalent influenza vaccine was also demonstrated in a clincial trial (NCT01508884). Specifically, the pre-treatment of skin with imiquimod before intradermal injection of the vaccine resulted in 90% seroconversion, compared to 38.7% when pre-treated with an aqueous cream without imiquimod before intradermal injection [217].

**FLT3L**

Dendritic cells are an important antigen-presenting cell, crucial for the induction of the adaptive immune system [218]. Fms-like tyrosine kinase 3 ligand (FLT3L) is a haemopoietic progenitor growth factor that can induce mobilisation of haemopoietic progenitors and stem cells *in vivo* [219] by engaging with FLT3. FLT3 is necessary for homeostatic development of dendritic cells by controlling division of progenitors in the periphery [220]. Mice treated with FLT3L expand immature B cells, natural killer (NK) cells and dendritic cells (DC) *in vivo* [219] and injection of FLT3L in mice has been shown to results in an increase in cells, which express dendritic cell markers [221]. The dendritic cells also help activate T cell responses to parasites after induction by inflammatory FLT3L [222]. Furthermore, during acute infection, FLT3L is necessary for dendritic cells to activate and stimulate expansion of natural killer cells upon viral infection [223].

FLT3L has also been shown to play a role in effective vaccination. It is secreted within 1 hour after subcutaneous vaccination and enhances T cell and humoral responses. Immunity to subcutaneously injected protein vaccines is also dependent on classical lymphoid-resident dendritic cells, which are FLT3L dependent [224]. A pre-clinical study in mice showed that the co-delivery of FLT3L, with a Chlamydia trachomatis vaccine, resulted in enhanced immunity [225]. In mice studies comparing microneedle vaccination with pVAX-S encoding HBV small envelope protein alone or this construct with the addition of a plasmid encoding FLT3L also showed increased antibody responses (approximately 1.5-fold) with the FLT3L included. This also resulted in increased survival, as the p-Vax-S vector alone delivered by microneedle array resulted in 40% survival, whereas the addition of FLT3L resulted in 70% survival after challenge with CT26/S cell expressing HBV antigen [226]. Notably, this study suggests that the presence of the FLT3L does not have to precede the presence of the antigen, and that both elements can be delivered at the DNA level. *Flt3l* has also been shown to improve the effects of a plasmid HPV16 E6/E7 vaccine with granulocyte macrophage colony-stimulating factor (GM-CSF) on the rate of tumour growth and metastasis in mice [227]. In a similar study, utilising recombinant protein, the linkage of FLT3L to HPV15 E6/E7 antigen enhanced E7-specific CD8+ T cell responses, as well as providing an anti-tumour effect [228]. In a recent clinical trial (NCT01634503), a HPV DNA vaccine, designed to co-expresses FLT3L, achieved complete regression in seven out of nine patients after 36 weeks through the induction of type 1 T cell-mediated immunity after 3 doses of intramuscular injected vaccine, delivered in weeks 0, 4 and 12 in combination with electroporation [229]. Hence, as dendritic cells are an important factor in generating an immune response and the skin represents an immune-rich environment, FLT3L is an interesting adjuvant candidate for cavitation-mediated delivery.

The aims of this chapter are:

- To probe the feasibility of using p-CaN to deliver DNA into the epidermis, and thereby achieve protein expression from the DNA.
- To investigate the simultaneous utility of p-CaN as cavitation nuclei and immunogenic antigen, using bovine serum albumin as a model antigen.
- To characterise the immunogenic potential of p-CaN delivered by ultrasound and compare this to intradermally injected p-CaN or free protein.
- To assess the added benefit of the addition of imiquimod.
- To develop a protocol for the purification of FLT3L, as an immune stimulatory protein.

## 3.2 Materials and Methods

### 3.2.1 Plasmid purification

pGL4.50[*luc2*/CMV/Hygro] Vector (#E1310, Promega, USA) (CMV-Luc) was purchased and transformed into NEB® Turbo Competent E. coli cells (C2984H, NEB). Cells were transformed according to the manufacturer's instruction for 5-alpha Competent E. coli (High Efficiency) (NEB). In short, the competent cells were thawed for 10 minutes on ice. 1 pg-100 ng of plasmid DNA was added to the cell mixture, flicking to mix, and the mixture kept on ice for 30 minutes. The cells were heat shocked at 42 ℃ for 30 seconds and placed on ice for 5 minutes. 950 µL of SOC medium (2% Vegetable Peptone, 0.5% Yeast Extract, 10 mM NaCl, 2.5 mM KCl, 10 mM $MgCl_2$, 10 mM $MgSO_4$, 20 mM Glucose) (NEB) was added. The cells were placed at 37 ºC for 1 hour. Dilutions were plated on appropriate LB-agar plates. Glycerol stocks were prepared for all completed DNA constructs. A 40% glycerol in MilliQ stock solution was made and filter sterilised with a 0.2 µm filter (Thermo Scientific Nalgene, USA). An overnight bacterial culture was mixed 1:1 with the glycerol stock and placed on ice for 10 minutes. The solutions were subsequently stored in a -80 ºC freezer.

Overnight cultures were grown in 5 mL of sterile liquid LB broth (luria low salt) (L3397, Sigma) or LB Broth, Vegitone (28713, Sigma) with 100 µg/mL ampicillin (Sigma) from picked colonies or from frozen glycerol stocks. For large-scale purification of DNA, a starter culture was diluted 1:100 in 1L of broth with selection marker. This was grown in 3x1L Erlenmeyers. Cells were cultured at 37 ºC at 220 rpm in a SI-300R shaking incubator (Medline Scientific™).

DNA mega-preparations were made with the GenElute™ HP Endotoxin-Free Plasmid Megaprep Kit (NA0600, Sigma), according to manufacturer's instructions for maximal final concentration. The DNA was quantified with a NanoDrop One (ND-ONE-W, Thermo Scientific).

### 3.2.2 ELISA

ELISA, including avidity assays, were done as described in section 2.2.11, with the exception that the plate was blocked with 50 µL/well of Pierce Protein-free blocking buffer (37572, ThermoFisher Scientific), instead of 10%FBS-PBS.

The antigen with which the ELISA plate was coated was either Spike protein (RayBiotech, USA or GenScript, USA) or Bovine Serum Albumin (Sigma) depending on the antibodies characterised.

### 3.2.3 *In vivo* protocol to assess the ability of BSA p-CaN to deliver luciferase-encoding pDNA

In order to assess the potential for Bovine Serum Albumin (BSA) p-CaN to deliver DNA, a luciferase plasmid (pGL4.50[*luc2*/CMV/Hygro] Vector, Promega) was delivered by BSA 1G p-CaN or nanocups as a cavitation agent. 8 mice were treated on both flanks. Four treatments were compared, as seen in Table 3.1. The p-CaN were kindly formulated and provided by Dr. Lyons. The pressure was adjusted to achieve an appropriate level of cavitation. The mice were imaged after 24 hours and the bioluminescence quantified.

**Table 3.1.** Summary of the *in vivo* testing to assess the use of BSA p-CaN to deliver CMV-Luc pDNA. Per group, the number of mice, whether they were treated with ultrasound (US or no US), which type of cavitation nuclei (BSA 1G p-CaN or nanocups), which pressure and for how long they were treated with the formulation of CMV-Luc pDNA with cavitation nuclei, is noted.

| Group size | Treatment | Cavitation nuclei | Pressure | Treatment time |
|---|---|---|---|---|
| 4 | No US | Nanocups | - | 10 min |
| 4 | US | Nanocups | 1.2 MPa | 10 min |
| 4 | US | BSA 1G p-CaN | 1.3-1.4 MPa | 10 min |
| 4 | US | BSA 1G p-CaN | 1.3 MPa | 2 min |

### 3.2.4 *In vivo* protocol for assessing BSA p-CaN immunogenicity

Having established the ability of p-CaN to mediate plasmid delivery, the ability of BSA 1G p-CaN to elicit an immune response following cavitation-mediated delivery or direct N+S delivery into the subcutaneous (S.C.), intramuscular (I.M.) or intradermal (I.D.) compartments was assessed. Groups of 3 mice were treated, except for the ultrasound group where 4 mice were treated, as summarised in Table 3.2. Mice were prepared as described in section 2.2.8. The p-CaN were kindly formulated and provided by Dr. Lyons. All treatments were performed with the set-up as displayed in Figure 2.2 and a pressure of 1.4 MPa was used for the ultrasound group using the set-up described in methods 2.2.1. 2 mL of formulation solution was placed on the skin per exposure site in the control and ultrasound group. For the no-ultrasound and the ultrasound groups, the formulation had a concentration of 18 mg/mL BSA 1G p-CaN in MilliQ with the cavitation nuclei making up 25% of the total of 2 mL. For the remaining groups, mice were injected with 25 µL of a 360 mg/mL BSA protein solution in PBS, either intramuscularly, subcutaneous or intradermally. The mice were bled every week for 4 weeks, as described in section 2.2.7 and the immune response were assessed by ELISA, as decribed in section 3.2.2, as summarised in Figure 3.1.

**Table 3.2.** Summary of the *in vivo* to assess the use of BSA 1G p-CaN to elicit immune responses. Per group, the number of mice, whether they were treated with ultrasound or with which injection technique, at which pressure and what BSA p-CaN concentration in which volume is noted.

| Group size | Delivery | Pressure | BSA p-CaN concentration | Volume p-CaN |
|---|---|---|---|---|
| 3 | No Ultrasound | 0 MPa | 18 mg/mL | 500 µL BSA 1G p-CaN per 2 mL formulation |
| 4 | Ultrasound | 1.4 MPa | 18 mg/mL | 500 µL BSA 1G p-CaN per 2 mL formulation |
| 3 | Intramuscular | - | 360 mg/mL | 25 µL |
| 3 | Subcutaneous | - | 360 mg/mL | 25 µL |
| 3 | Intradermal | - | 360 mg/mL | 25 µL |

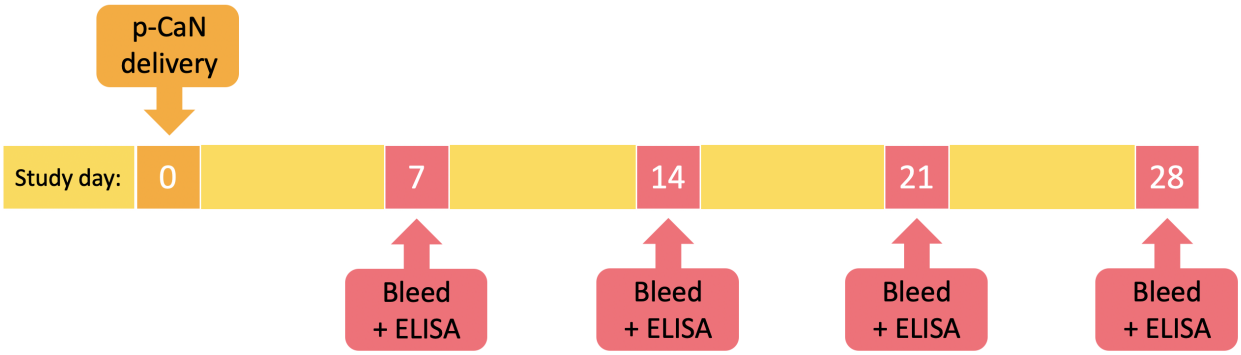



**Figure 3.1.** Summary of the treatment and blood sampling, as well as subsequent ELISA timeline for the *in vivo* to assess the use of BSA p-CaN to elicit immune responses.

### 3.2.5 *In vivo* protocol for SARS-CoV-2 Spike protein p-CaN as a vaccine strategy

Eight groups of mice were treated with spike protein (RayBiotech, 230-30162) or spike protein formulated into ultrasound-sensitive particles (Spike 1G p-CaN), optionally co-formulated with the adjuvant imiquimod in the core (Spike 1G p-CaN Imiq). The p-CaN were kindly formulated and provided by Dr. Lyons. Optionally, imiquimod (Imiq) was co-injected with the protein as a control comparator for the p-CaN Imiq group. The mice treated with ultrasound and Spike 1G p-CaN were treated using the set-up described in methods 2.2.1 at 1.35 MPa and those with ultrasound and Spike 1G p-CaN Imiq were treated at 1.43 MPa (due to a slight loss in cavitation nucleation activity upon inclusion of the imiquimod). The final group was placed in the ultrasound set-up, without application of ultrasound, as a negative control. The mice were boosted by retreatment after 16 days and bled weekly (Table 3.3 and Figure 3.2).

**Table 3.3.** Summary of the *in vivo* to assess the use of SARS-CoV-2 Spike 1G p-CaN to elicit immune responses with or without the addition of imiquimod. Per group, the number of mice, whether they were treated with spike protein or spike 1G p-CaN, whether they were treated with ultrasound or with which injection technique, whether imiquimod was added to the formulation and at what dosage, is noted.

| Group size | Protein/p-CaN | Adjuvant | Dosage | Route |
|---|---|---|---|---|
| 1 | PBS | - | 100 µL | Intradermal |
| 4 | Protein | - | 5 µg Spike protein in 100 µL PBS | Intradermal |
| 4 | Protein | Imiquimod | 5 µg Spike protein in 100 µL PBS, 0.1 µg Imiq in 100 µL | Intradermal |
| 4 | Spike 1G p-CaN | - | 5 µg Spike 1G p-CaN in PBS to a total of 100 µL | Intradermal |
| 4 | Spike 1G p-CaN Imiq | Imiquimod | 5 µg Spike 1G p-CaN Imiq in PBS to a total of 100 µL | Intradermal |
| 3 | Spike 1G p-CaN | | 2 mL Spike 1G p-CaN (50 µg spike protein/mL) | Ultrasound |
| 4 | Spike 1G p-CaN Imiq | Imiquimod | 2 mL Spike 1G p-CaN Imiq (50 µg Spike protein /mL) | Ultrasound |
| 3 | p-CaN | Imiquimod | 2 mL p-CaN Imiq (50 µg spike protein/mL) | No Ultrasound |

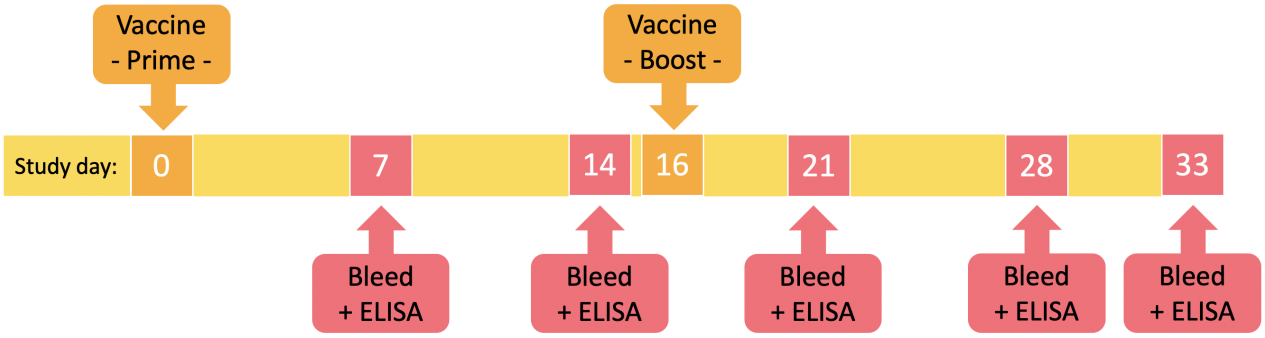



**Figure 3.2.** Summary of the treatment and sampling timeline for the *in vivo* to assess the use of SARS-CoV-2 Spike p-CaN to elicit immune responses.

### 3.2.6 Protein purification

The rationale for the use of FLT3L as a protein to form into p-CaN was established in section 3.1. As this protein is not available at scale commerically, it had to be produced in-house. A *Mus musculus* optimised *Flt3l* gene (NM_013520) with a 6xHIS-tag in a pET151/D-TOPO plasmid backbone was ordered from Invitrogen (USA). This was transformed into a BL21(DE3) T7 Express Competent E. coli (High efficiency) (NEB), as described above. 250 mL of cells were grown as described in section 3.2.1 and induced after 4 hours with a final concentration of isopropyl β-d-1-thiogalactopyranoside (IPTG) of 1 mM IPTG.

250 mL of IPTG-induced cell culture was harvested by centrifugation at 3234xg for 5 minutes at 4 ºC. The cell pellets were resuspended in 8 mL Native Binding Buffer (50 mM NaH2PO4, 10mM imidazole, pH8.0) (denoted here-on as 'native conditions') or 8 mL Guanidium Lysis Buffer (6 M Guanidine HCl, 20 mM sodium phosphate, pH7.8) for 'denaturing' conditions. 8 mg of lysozyme was added, and the solution was incubated on ice for at least 10 min whilst slowly rocking. Optionally, the cells were frozen and thawed three times in liquid nitrogen. The cells were sonicated on ice by exposure of 8 mL to 50% amplitude for three 20 seconds on/20 seconds off cycles using a Qsonica Q125 Sonicator with a CL-18 ultrasound probe.

Protein purification was based on the ProBond™ Purification system (Life technologies) according to the purification procedure for bacterial lysates. A 'native' purification for bacterial lysates was performed according to manufacturer's instructions.

Protein purification under 'denaturing' conditions was performed with a ProBond™ column (Life Technologies) or Econo-Pac® Chromatography Column (Biorad). 400 µL - 2 mL resin (Nickel-chelating 50% slurry in 20% ethanol) was allowed to settle to the bottom of the column and was subsequently washed with 6 mL of MilliQ water, followed by two washes with 6 mL of denaturing binding buffer (Life technologies). 8 mL of cell lysate was added to the column and mixed. This was incubated for 15-30 minutes at room temperature with gentle agitation. The unbound cell lysate was either poured off or allowed to flow through, and retained for analysis. 4 mL of denaturing binding buffer was added and the column was gentle rocked for two minutes. The supernatant was then removed either by centrifugation of the resin (500xg for 1 min) and pipetting off the supernatant or by allowing the liquid to flow through the column. This step was done twice. 4 mL of denaturing wash buffer at pH 6.0 was added and the column was gently rocked for two minutes. The supernatant was

then removed either by centrifugation of the resin (500xg for 1 min) and discarding the supernatant or by allowing the liquid to flow through the column. This step was done twice. 4 mL of denaturing wash buffer at pH 5.3 was added and the column was gently rocked for two minutes. The supernatant was then removed either by centrifugation of the resin (500xg for 1 min) and pipetting of the supernatant or by allowing the liquid to flow through the column. This step was done twice. The protein was eluted by addition of 5 mL of denaturing elution buffer, pH 4.0. Fractions of 1 mL were collected into 1.5 mL Eppendorfs and stored at 4 ºC for further analysis by SDS-PAGE and Western Blot. At all stages supernatants/eluates were collected for later analysis. Analysis was performed by BCA assay (section 3.2.9) for total protein content and by SDS-PAGE (section 3.2.7) and Western Blot (section 3.2.8) for protein identification.

### 3.2.7 SDS-PAGE

In order to assess levels of FLT3L expression and purification, SDS-PAGE gels were prepared. 27 µL of sample was mixed with 4x Laemmli Sample buffer (1610747, Bio-rad, USA) with or without the addition of the reducing agent β-mercaptoethanol. The samples were heated for 20 min at 95 ºC at 300 rpm in a heating block (HM100-Pro Digital Thermal Mixer, Scilogex, USA). 4–20% or 12% Mini-PROTEAN® TGX™ Precast Protein Gels (Bio-rad) were prepared and loaded into a Mini-PROTEAN Tetra Vertical Electrophoresis Cell (Bio-rad). 1 L of running buffer was prepared by diluting 10x Tris/Glycine/SDS (Bio-rad) ten-fold with MilliQ and added to the chamber. 10 µL of Precision Plus Protein™ Dual Color Standards (#1610374EDU, Bio-rad) was loaded onto the gel as a reference and 10-30 µL of each prepared sample. The gel was run for 35 min at 200 Volts using a PowerPac™ HC High-Current Power Supply (Bio-rad). Once the gel had completed running, the running buffer was discarded, and the gel carefully removed from the cartridge. The gel was rinsed with MilliQ water and stained using QC Colloidal Coomassie solution (#1610803, Bio-rad) for 16-72 hours at 240 rpm on a KS 130 Basic orbital shaker (IKA, Germany). The gel was then washed 3-5 times in MilliQ water.

### 3.2.8 Western Blot

For a Western Blot, the Mini-PROTEAN Tetra Vertical Electrophoresis Cell (Bio-rad) in combination with the Mini TRANS-Blot® Electrophoretic Transfer Cell (Bio-rad) was used. Transfer buffer was prepared by mixing 100 mL 10x Tris-Glycine buffer (25 mM Tris, 192 mM glycine) (#1610734EDU, Bio-rad) and 200 mL ethanol. This was topped off to 1 L with MilliQ water. The pads, 0.2 µm nitrocellulose/filter paper sandwich (Bio-rad) were soaked in transfer buffer for at least 10 min. A protein gel was prepared as described in section 3.2.7 for SDS-PAGE, except instead of staining the gel, a

gel sandwich was made for blotting. To this end, a fibre pad, filter paper, the gel, the membrane, the second piece of filter paper and second fibre pad were sandwiched into the TRANS-Blot® cassette. The bubbles were removed by gently rolling a stripette over the sandwich before closing the cassette. The cassette was placed inside the module, which was put inside the buffer chamber. A pre-chilled cooling unit was added, and transfer buffer was used to fill the chamber. A stir bar was added and the assembled set-up placed on a stirrer at maximum speed to ensure even cooling. A high intensity field of 100 V, 350 mA for 1 hour was run using the PowerPac™ HC High-Current Power Supply (Bio-rad). Once transfer was completed, the gel sandwich was disassembled, and the membrane placed in a new container. 15 mL of Pierce protein-free blocking buffer (37572, ThermoFisher Scientific) was added or a 3% BSA solution (Sigma) in phosphate buffer solution (PBS) (Sigma, USA). The membrane was blocked for one hour.

For detection of a 6xHistidine tag, the membrane was added to a solution of 1:1000 dilution of an anti-6x-His Tag Monoclonal Antibody (4E3D10H2/E3) linked to horseradish peroxidase (HRP) enzyme (ThermoFisher) in 0.05%Tween20 in either Pierce protein-free blocking buffer (37572, ThermoFisher Scientific) or a 3% BSA solution (Sigma) in PBS. The membrane was incubated in this primary antibody for one hour at 80 rpm on a KS 130 Basic orbital shaker (IKA). The membrane was then rinsed twice with PBS and washed thrice in PBS for 5 min at 80 rpm on the orbital shaker.

For detection of FLT3L, the membrane was incubated for one hour in a solution of 1:1000 dilution of anti-FLT3LG polyclonal antibody (PA5-47603, ThermoFisher) in 0.05%Tween20 in either Pierce protein-free blocking buffer (37572, ThermoFisher Scientific) or a 3% BSA solution (Sigma) in PBS. After incubation, the membrane was then rinsed twice with PBS-0.05%Tween20 and washed thrice in PBS-0.05%Tween20 for 5 min at 80 rpm on the orbital shaker. A 1:5000 dilution of secondary antibody Anti-Rabbit IgG (whole molecule)–Peroxidase antibody produced in goat (A0545, Sigma) in Pierce blocking buffer (ThermoFisher) or a 3% BSA solution (Sigma) in PBS was added. This was incubated for an hour. The membrane was then rinsed twice with PBS-0.05%Tween20 and washed thrice in PBS for 5 min at 80 rpm on the orbital shaker. After adding the antibodies and subsequent washing, the membrane was carefully dried. 1 mL of SuperSignal™ West Dura Extended Duration Substrate (34075, ThermoFisher Scientific) was prepared according to manufacturer's instructions. The membrane was placed on an acetate sheet and the substrate added. A second piece of acetate was placed over the membrane and any excess substrate was removed. The membrane was visualised with a ChemiDoc™ MP Imaging System (Bio-rad).

### 3.2.9 BCA Assay

BCA assay was performed with the QuantiPro™ BCA assay kit (QPBCA, Sigma), according to manufacturer's instructions. In short, ten, hundred or thousand-fold dilutions of cell lysate samples in PBS were prepared. A protein standard curve containing 0 µg/mL, 0.5 µg/mL, 5 µg/mL, 10 µg/mL, 20 µg/mL and 30 µg/mL was prepared using 1.0 mg/ml bovine serum albumin in 0.15 M NaCl with 0.05% sodium azide. The QuantiPro working reagent for a 96 well-plate was prepared, and 150 µL of sample was mixed with 150 µL of working reagent. The 96 well-plate was sealed with SealPlate Sealing film (Excel Scientific) and incubated at 60 ºC for 1 hour. The absorbance was measured at 562 nm with a FLUOstar Omega (BMG LABTECH, Germany).

### 3.2.10 Statistics

Statistical analysis was done in Prism 9 (GraphPad Software, USA). Significance between groups was assessed with a one-way ANOVA with a post hoc test with a Šidák correction for multiple comparisons. A two-way ANOVA (treatment x time) was done with a Tukey post hoc test between treatments for the different timepoints.

Luminescence was log-transformed prior to statistical analysis and the geometric mean and geometric standard deviation (GSD) determined, as luminescence data was spread over orders of magnitude.

## 3.3 Results

### 3.3.1 *In vivo* study to assess the ability of BSA p-CaN to deliver luciferase-encoding pDNA

Whilst polymeric nanocups have now reached the stage of clinical testing in the field of oncology, they are not ideally suited to this transcutaneous delivery application. Indeed, both the composition of the polymeric nanocups and the exposure duration (10 minutes) they have been used at [230], restrict potential future clinical translation. To assess the capability of the 1G p-CaN as effective alternative cavitation nuclei, their capacity to instigate cavitation-mediated transcutaneous delivery of Luc-pDNA was tested and compared to polymeric nanocups in an *in vivo* pilot study. Groups of four mice were treated with a mixture of BSA 1G p-CaN with luciferase-encoding pDNA for 10 or 2 minutes with or without ultrasound. This was compared to delivery of the luciferase-encoding DNA using nanocups at a pressure shown previously to be optimal. Testing p-CaN at either 2 or 10 minute exposure durations helped establish whether a shorter, more patient acceptable exposure time could be used. Luminescence was measured 24 hours after exposure. The luminescence and cavitation results are summarised in Figure 3.3, 3.4, 3.5 and 3.6.

The data presented in Figure 3.3 demonstrates that the cavitation produced by the p-CaN (see Figure 3.4) can successfully deliver luciferase-encoding pDNA transcutaneously. Crucially the observed geometric mean luminescence level ($2.46 \times 10^6$ p/s) is not significantly different ($p>0.05$) from the level achieved by using nanocups ($0.79 \times 10^6$ p/s) technology which has been subject to more than 7 years of development and is produced to GMP. Furthermore, 2 minute treatment does not result in a significantly different ($p>0.05$) mean luciferase expression level ($0.73 \times 10^6$ p/s) than achieved with 10 minute exposure, an encouraging aspect when ultimate translation is considered.

When comparing the observed acoustic energy detected by the passive cavitation detector (PCD) during delivery (calculated as described in section 2.2.3) with the luminescence measured by IVIS at 24 hours (Figure 3.4), it can be seen that the 1G p-CaN can deliver DNA into murine skin and a comparable amount of luminescence is detected for both p-CaN and nanocup-mediated delivery. Notably, no increase in luciferase expression is seen for higher TASE values, further supporting the theory that beyond a threshold, no further expression is achieved. This provides encouragement regarding ultimate translation, as the frequency (265 kHz) and pressure (1.3 MPa) settings required to obtain these TASE levels sit within the typical parameters of currently used medical ultrasound

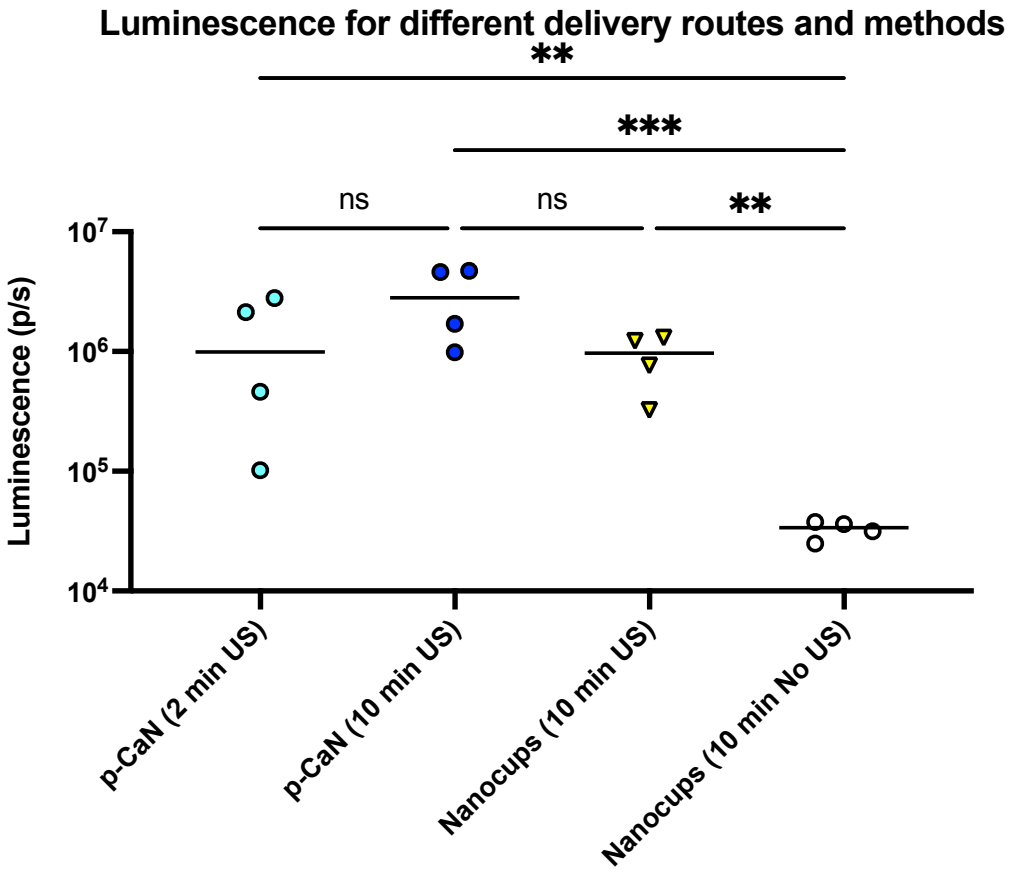



**Figure 3.3.** Total luminescence after 24 hours. Luciferase-encoding DNA was delivered in a formulation containing either nanocups or BSA 1G p-CaN. The mouse skin was treated with or without ultrasound for 10 minutes. A group with p-CaN and a 2 minute exposure was also included. N=4, bar height represents the geometric mean value. Significance was analysed by a one-way ANOVA with a post-hoc test for the groups displayed, using the Šidák correction for multiple comparisons, ** = $p<0.005$, *** = $p=0.0001$.

equipment.

Notably, delivery was still observed for low TASE values (<16 μJ) after exposure for 2 minutes using these p-CaN, even though significant non-inertial cavitation (as evidenced by horizontal lines on the spectrograms in Figure 3.6) was evident. This implies that even short treatments with ultrasound could be sufficient for successful delivery of DNA. The presence of significant non-inertial cavitation (up to 64%) does warrant further investigation into the ultrasound set-up to improve reproducibility between similar treatments. Indeed, although a general pattern of increasing luciferase expression with increasing TASE is observed more refinement and characterisation of this relationship is needed before TASE can be used as a real-time proxy to inform the operator when a sufficient dose of cavitation and therefore DNA has been delivered.

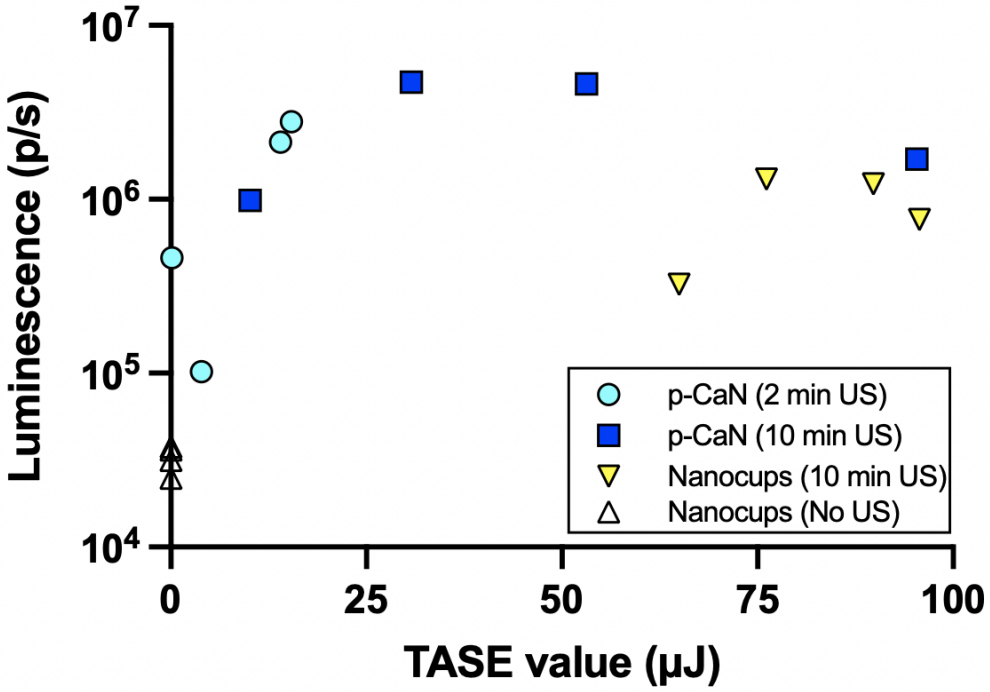



**Figure 3.4.** Total luminescence after 24 hours plotted against the total acoustic sensor energy (TASE). Luciferase-encoding DNA was delivered in a formulation with nanocups or BSA 1G p-CaN. Mice were treated for 2 or 10 min with ultrasound (US) or without ultrasound (No US). They were imaged at 24 hours, as described in methods 3.2.3. The processing of acoustic data was performed as described in material and methods section 2.2.3.

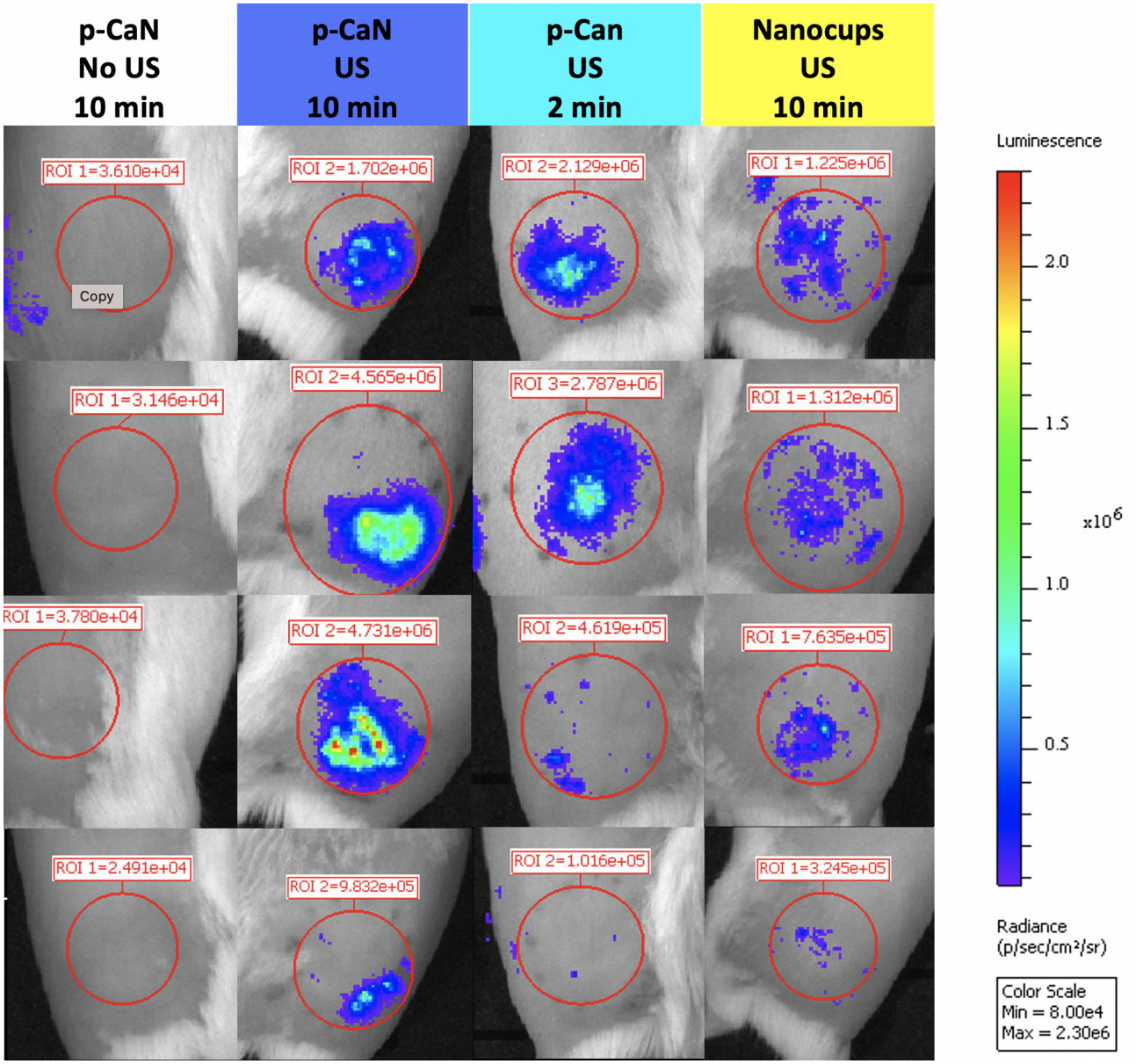



**Figure 3.5.** *In vivo* imaging of luciferase expression after 24 hours. Groups of 4 mice were treated with luciferase-encoding DNA in a formulation with nanocups or BSA 1G p-CaN. The mice were treated for 2 or 10 min with ultrasound (US) or without ultrasound (No US), using the set-up and parameters shown in the schematic in methods section 2.2.1. The ROI value represents the total photon emission per second. Imaging was performed as described in methods section 2.2.6. The treated area is circled in red according to the exposure perimeter as marked using pen directly after exposure.

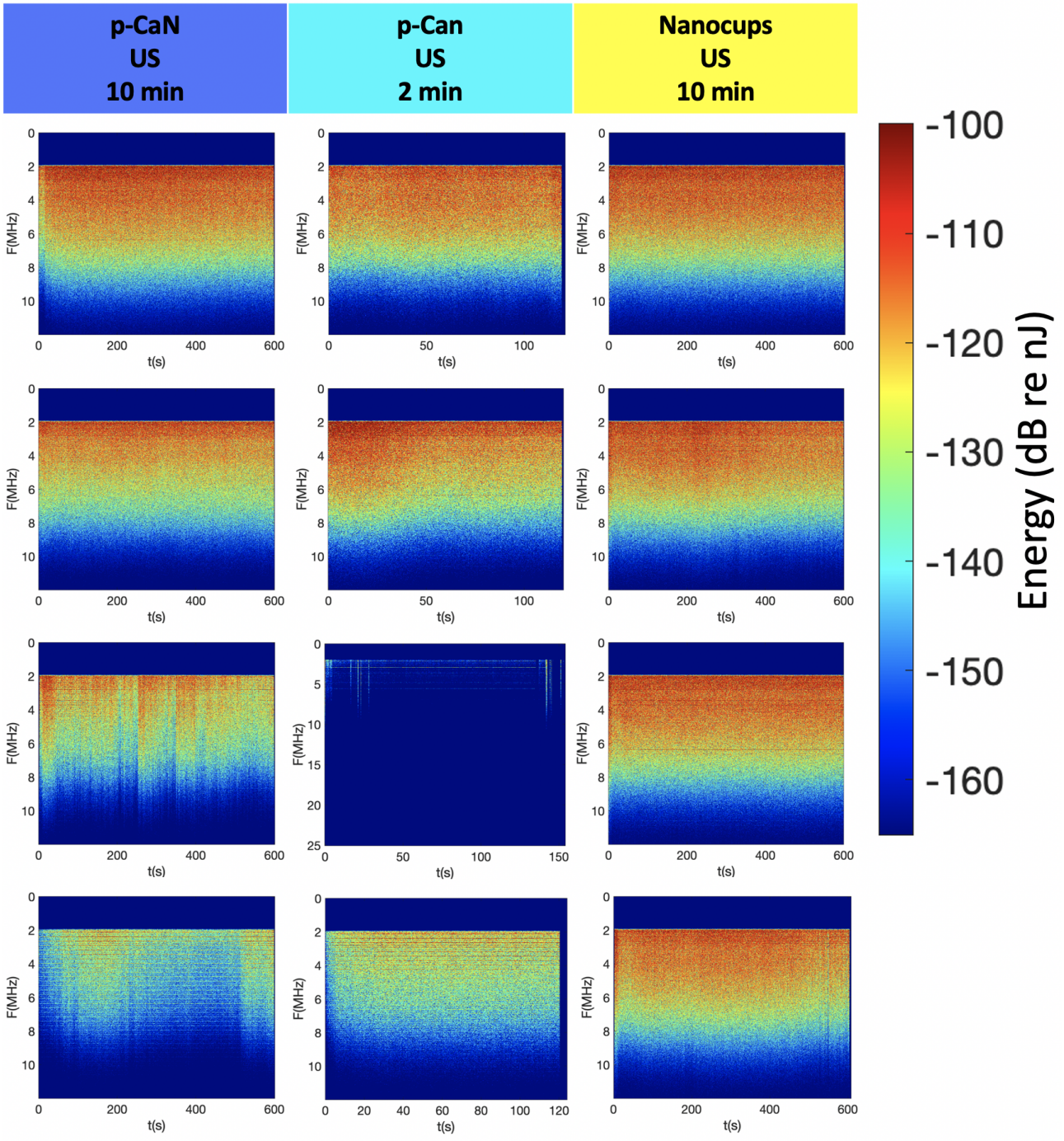



**Figure 3.6.** Spectrograms of the acoustic emissions during treatment. Groups of 4 mice were treated with luciferase-encoding DNA in a formulation with nanocups or BSA 1G p-CaN. Mice were treated for 2 or 10 minutes with ultrasound. The colour bar on the right represents the power spectral density in dB re nJ. Data was processed as described in section 2.2.3.

### 3.3.2 *In vivo* to assess BSA p-CaN immunogenicity

Having established the utility of p-CaN in replacing the polymeric nanocups as the cavitation nuclei used to drive delivery, the second potentially useful facet of p-CaN, i.e. as an immune modulator, could be probed. It was hypothesised that the simple act of creating a 'particle' of antigen rather than using free protein would enhance immunogenicity, in the same way a virus-like particle (VLP) may act. Furthermore, delivery of such a particle using cavitation to the immune-rich milieu of the I.D. compartment may also enhance immunogenicity. A pilot study was performed to address these questions. In this study, groups of three mice were injected with 9 mg of BSA protein, either intramuscularly, intradermally or subcutaneously. Alternatively, 9 mg of BSA protein formulated as p-CaN (BSA 1G p-CaN) was placed in the formulation holder on the skin for 10 minutes and ultrasound was applied or not (see table 2.1 for parameters). The mice were bled every week and the IgG titres were determined using an ELISA (see methods section 3.2.2). On day 28 a terminal bleed was performed, and the antibody level and avidity assessed (Figure 3.7).

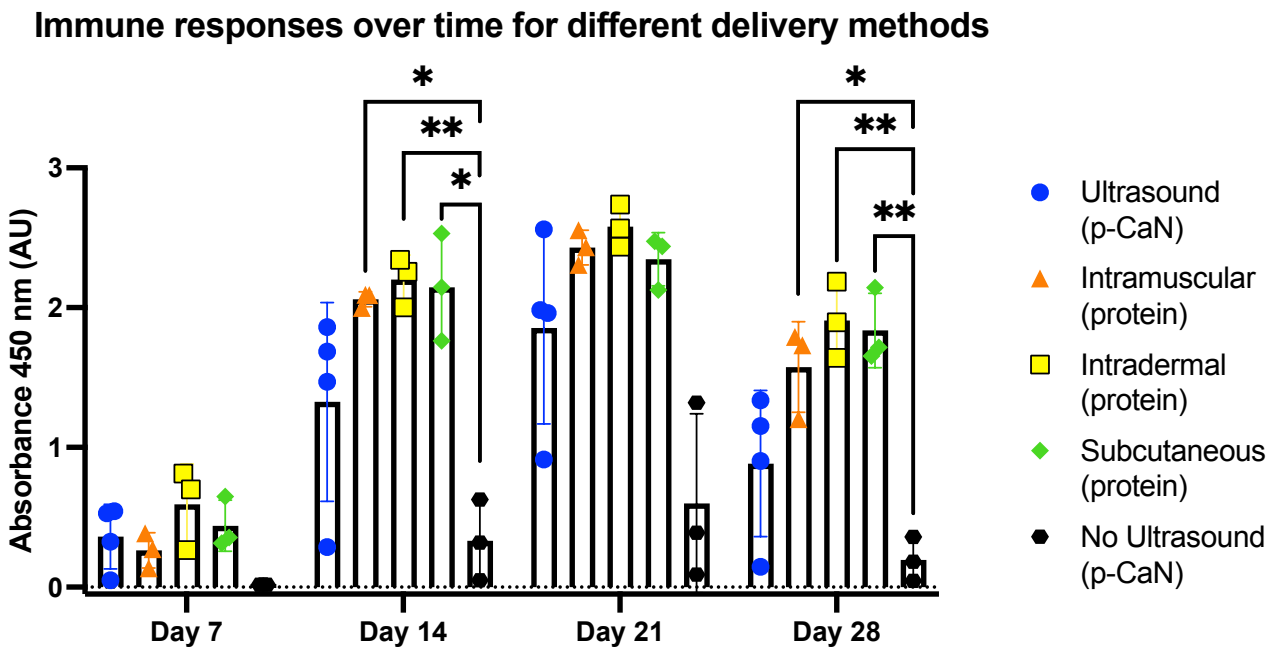



**Figure 3.7.** Level of anti-BSA IgG antibodies in blood samples taken at day 7, 14, 21 and 28 as assessed by ELISA. Absorbance (450 nm) is plotted for all groups at each day. Mice were injected with 9 mg BSA protein via conventional I.M., I.D. or S.C. routes or treated with a formulation with 9 mg BSA protein (BSA 1G p-CaN) with or without ultrasound. ELISA was performed as described in methods 3.2.2, bar height represents mean absorbance and error bars represent standard deviations, n = 3 or 4. A two-way ANOVA (treatment x time) was done with a Tukey post hoc test between treatments for the different timepoints. A significant effect of subject ($p<0.0001$), treatment ($p=0.0006$), time ($p<0.0001$) and their interaction ($p<0.0001$) was observed.

By 14 days a high anti-BSA IgG level was observed for all mice which received injected protein. Notably, high mean responses were seen following I.D. delivery, as well as I.M. or S.C. delivery (2.20,

2.06 and 2.15). For the ultrasound-delivered p-CaN group (blue circles), a lower mean absorbance and a wider spread of values was seen compared to the levels achieved with direct injection. This wide spread of values is hard to reconcile with the consistent and similar cavitation which was seen in the mice in this group, with an average TASE of 19.77±0.77 µJ. However, differences in the TASE values were seen during the first 15 seconds. Regardless, considering these TASE values and as a calculated 55%±3% of this total cavitation energy was the result of inertial cavitation and the findings of Figure 3.4, it is suggested that had a DNA vector been included in these experiments, these levels and types of cavitation would have been sufficient to achieve delivery of the DNA. It is important to note that the total level of BSA protein actually entering the mouse skin during ultrasound exposure is likely to be a small fraction of the amount delivered by injection.

A much lower, although non-negligible, anti-BSA immune response was detected in the group which was exposed to BSA p-CaN sample on the skin without application of ultrasound (black circles) (two-way ANOVA with a Tukey HSD post all groups, $p<0.05$ for 'No Ultrasound' compared to I.M., I.D. and S.C. injection on day 14 and 28). This non-negligible response could be a result of the sampling by the Langerhans cells in the epidermis, which may have resulted in a low-level immune response despite an absence of an effective active delivery mechanism. Regardless, of such 'passive' delivery, the benefit of the addition of ultrasound is substantial.

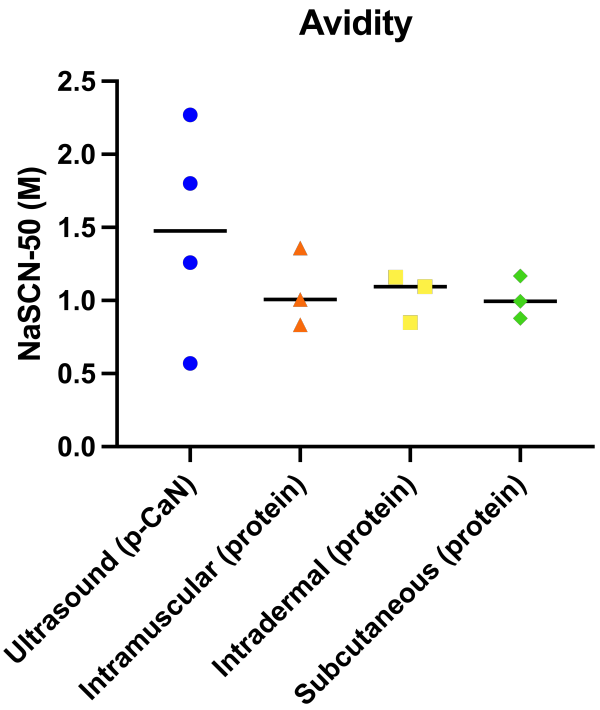



**Figure 3.8.** Avidity data from blood samples taken at day 28. Mice were injected with 9 mg BSA protein or treated with a formulation with 9 mg BSA protein formulated as p-CaN (BSA 1G p-CaN) with ultrasound (Ultrasound (p-CaN)). Avidity was assessed by the concentration of NaSCN that resulted in a 50% reduction in absorbance, as described in methods 3.2.2, bar height represents mean absorbance, n = 3 or 4.

By day 28 (Figure 3.7) antibody levels seem to be declining in all groups compared to day 21, but study of the avidity of the antibodies present revealed interesting findings. Specifically, the avidity of the antibodies from the terminal 28 day bleed were assessed (Figure 3.8). Sodium thiocyanate (NaSCN) was added in increasing concentration to determine the avidity (see methods 3.2.2). Although the total IgG levels achieved following I.D. and S.C. injection appeared increased compared to I.M. injection on day 28 in Figure 3.7, the analysis of avidity indicated that all 3 routes produced IgG with similar mean avidity for their target (I.D.: 1.03, S.C.:

1.01, I.M.: 1.07). Notably, the very low levels of antibody produced by simply resting the sample on the skin were not sufficient to allow avidity analysis. For ultrasound delivered p-CaN the picture was very different, with the highest overall mean value and 3 of the 4 mice demonstrating higher avidity antibodies than all but one of the 9 mice that were injected. This increase in avidity was an unexpected but potentially important aspect of ultrasound-mediated delivery. As with total IgG levels in Figure 3.7, one ultrasound-treated mouse performed comparatively poorly. Upon probing the cavitation and treatment, the only difference that could be observed was relatively low TASE in the first 15 seconds of treatment, as the pressure was increased to achieve cavitation. However, total delivered TASE was equal to the other mice in the group (20.3 µJ vs 19.6 µJ±0.8 µJ). This highlights that there are still aspects of cavitation-mediated delivery that impact immunity which are not fully understood and would require further research to elucidate.

### 3.3.3 *In vivo* to investigate spike protein p-CaN as a vaccine strategy for COVID-19

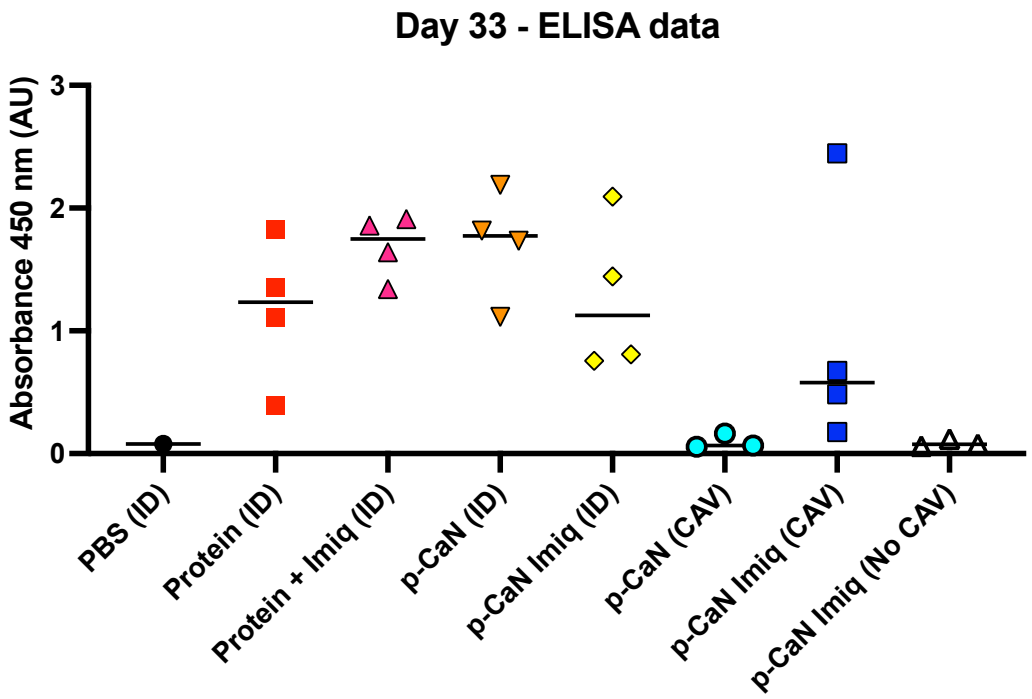



**Figure 3.9.** ELISA to detect anti-Spike antibodies in blood samples taken at day 33. Mice were intradermally injected (ID) with spike protein without imiquimod (protein) or with imiquimod (protein + imiq). Alternatively, mice were injected intradermally with p-CaN formulated from spike protein without imiquimod (p-CaN) or with imiquimod in the core (p-CaN Imiq). P-CaN and p-CaN Imiq were also delivered transcutaneously with ultrasound (CAV) or without ultrasound (No CAV). ELISA was performed as described in methods 3.2.2. Mean is displayed as a horizontal bar, n = 3 or 4.

In the wake of the COVID-19 pandemic, eight groups of mice were treated with spike protein or spike protein formulated as Spike 1G p-CaN, optionally co-formulated with the adjuvant imiquimod in

the core (Spike 1G p-CaN Imiq). Optionally, imiquimod (Imiq) was co-injected with the protein as a control comparator for the p-CaN Imiq group. Two groups were treated with ultrasound in combination with Spike 1G p-CaN with or without imiquimod in its core (Table 3.3 and Figure 3.2).

After 33 days, all injected protein and p-CaN formulations with and without imiquimod resulted in a substantial immune response (Figure 3.9). In line with previous work using nanoparticulate vaccines, the delivery of p-CaN I.D. appeared to give higher mean (1.71 vs 1.17) and more reproducible (SD: 0.45 vs 0.60) antibody levels than the delivery of protein I.D. (orange triangles vs red squares), although this difference was not significant (Welch's t-test, $p>0.05$) and lost when imiquimod was included in both formulations (p-CaN+Imiq (ID), mean: 1.28, SD: 0.63. Protein+Imiq (ID), mean 1.69, SD: 0.26).

Notably, the p-CaN formulation without imiquimod did not result in detectable antibody levels when delivered by ultrasound (light blue circles - p-CaN (CAV)), whilst substantial antibody levels could be detected in the p-CaN Imiq (CAV) group (blue squares). As similar acoustic responses were detected for both groups, it is implied that the imiquimod had a beneficial effect on the immune responses generated after cavitation-mediated delivery. This could be due to the immune-stimulatory effect of imiquimod. No immune response was detected for these same p-CaN when placed on the skin without the application of ultrasound ('p-CaN Imiq (No CAV)', white triangles), suggesting the need for cavitation-mediated delivery to elicit an immune response. Remarkably, one mouse treated with 'p-CaN Imiq (CAV)' had the highest detectable antibody response of all treated mice (Abs = 2.45). This suggests that there is potential for the transcutaneously delivered p-CaN to achieve similar immune responses to injected protein, despite the vastly lower level of protein that is likely to be delivered transcutaneously when compared to direct injection. The disparity between the dose delivered by I.D. injection vs transcutaneously using ultrasound, is explored further in chapter 4.

Exploration of the isotype profile of the antibodies produced can provide useful information about the nature of the response generated. After 21 and 28 days, the IgG1 and IgG2a content was assessed for the imiquimod containing groups (i.e. those that had showed the strongest total IgG response in Figure 3.9) (Figure 3.10). In mice, IgG2a antibodies are associated with antibody-dependent cellular cytotoxicity (ADCC) and complement-dependent cytotoxicity (CDC) activation in mice [194, 195]. There were minimal differences in the level or profile of antibodies raised as a result of I.D. injection of p-CaN Imiq (yellow diamonds) vs transcutaneous delivery of p-CaN Imiq

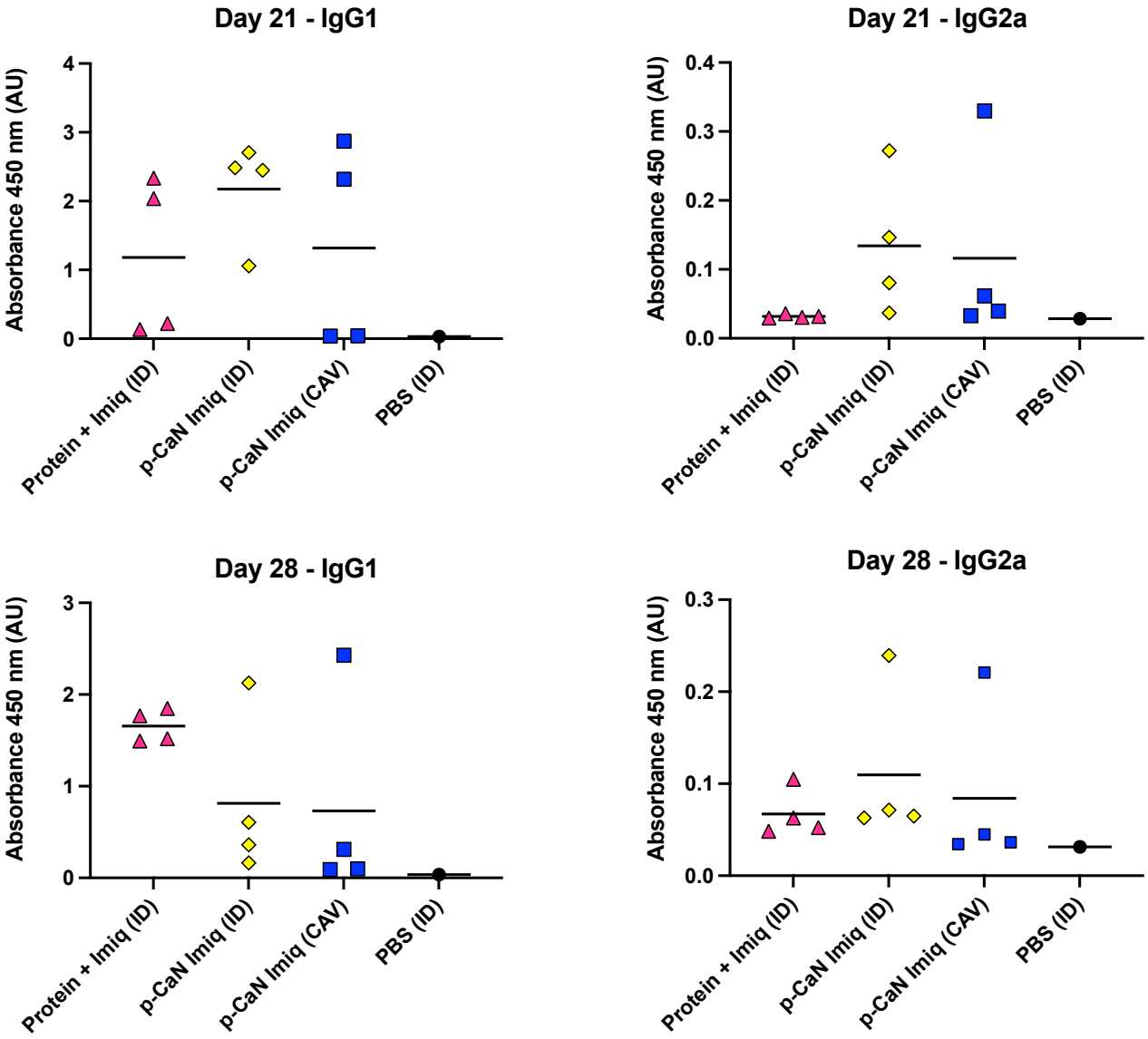



**Figure 3.10.** anti-Spike antibody IgG1 and IgG2a ELISA data from blood samples taken at day 21 and 28 to assess the antibody isotype distribution. Mice were intradermally injected with spike protein mixed with imiquimod (protein + imiq). Alternatively, mice were injected intradermally with p-CaN formulated with spike protein with imiquimod in the core (p-CaN Imiq). P-Can Imiq were also delivered transcutaneously with ultrasound (CAV). IgG1 and IgG2a ELISAs were performed as described in methods 3.2.2. Mean (horizontal line) is displayed. N=4 in all cases except the PBS control.

(blue squares) on day 28. Notably, on day 21, the p-CaN Imiq treated mice, both intradermally injected and transcutaneous delivered samples produced a relatively strong IgG2a immune response, whereas in the protein+imiq group, an IgG2a response was not observed until day 28, which was still comparatively low compared to the IgG1 response (IgG1/IgG2a = 24.7, paired t-test, $p<0.0005$).

### 3.3.4 Protein purification of FLT3L

Results in section 3.3.3 showed that formulation of p-CaN from target antigen and delivery via ultrasound-mediated cavitation has potential for further development, as the scale of response in relation to the relatively minor amount of antigen actually delivered is impressive. However, in terms of ultimate translation, a situation whereby a 'platform' p-CaN formulation comprised of a standard immunomodulatory protein, which can be stored and then easily paired with a rapidly synthesised DNA vector produced in response to a pathogen outbreak, is a more attractive approach. For the rationale described in section 3.1, FLT3L was chosen as the immunomodulatory protein to test this approach. As this protein was not commercially available, it had to be synthesised before such testing could be performed.

BL21(DE3) *E. coli* cells were grown in 5 mL fresh media and induced as described in 3.2.6. These cultures were incubated overnight at 30 ºC. These cells were spun down and resuspended in 1 mL PBS before being sonicated on ice. Multiple protocols were tested to assess different sonication protocols, as well as a sample in 5x lysis buffer for comparison (Table 3.4). The lysed cells were analysed by SDS-PAGE. The results are displayed in Figure 3.11.

**Table 3.4.** Summary of different protocols for cell lysis using probe sonication ('on' and 'off' time relates to periods of probe sonication. It also noted whether froth was formed for each procedure.

| Protocol number | Induced/ uninduced | Seconds on | Seconds off | Repeats | Froth formation |
|---|---|---|---|---|---|
| 1 | Induced | 10 | 20 | 11x | frothy |
| 2 | Induced | 20 | 20 | 10x | frothy |
| 3 | Induced | 20 | 30 | 10x | frothy |
| 4 | Induced | 10 | 20 | 3x | no froth |
| 5 | Induced | 20 | 20 | 3x | no froth |
| 6 | Induced | 20 | 30 | 3x | no froth |
| 7 | Induced | 20 | 20 | 6x | frothy |
| 8 | Induced | 10 | 30 | 10x | no froth |
| 9 | Induced | 10 | 30 | 20x | no froth |
| 10 | Induced | 0 | 0 | 0 | 5x lysis buffer |
| C | Uninduced | 10 | 20 | 11x | no froth |

The expected size for FLT3L is 21.9 kDa (see white arrow, Figure 3.11). For all IPTG induced,

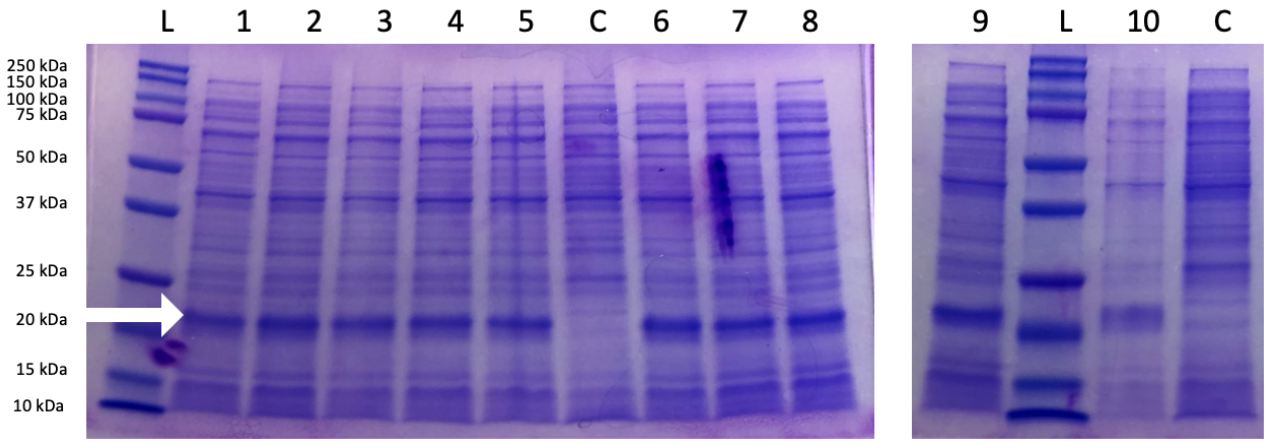



**Figure 3.11.** SDS-PAGE with the cell lysate of differently sonicated cells suspensions. L = ladder, C = uninduced control (i.e. no IPTG), 1-10 = different samples, sonicated according to Table 3.4. For the ladder, the different molecular weights are displayed per band. The white arrow shows the band at correct molecular weight for FLT3L.

sonicated samples a clear band is visible at 20-25 kDa, which is not visible for the non-induced sample (C). This supports the successful expression of FLT3L and that the sonication process does not negatively affect the protein size. On the basis of these results, subsequent purification was performed on samples which has been subject to sonication of 20 seconds on/20 seconds off, repeated three times (i.e. protocol '5'). For protein purification, the native protocol was compared to the denaturing protocol. A native protocol would allow for the protein to be isolated in its native state, minimising misfolding. If the FLT3L was expressed in inclusion bodies, a denaturing protocol would allow for the extraction of these proteins at the expense of its folding. The results were analysed on an SDS-PAGE gel (Figure 3.12). This showed no detectable protein between 20-25 kDa after native purification, but multiple other proteins had been eluted in the first three fractions. For the denaturing protocol, a band was observed between 20-25 kDa in fraction 2, 3 and to a lesser extent 4. This implied that the protein could be purified, however the gel also showed that several other proteins were being eluted in the fractions and so the purity of the sample was not yet sufficient for use in p-CaN production.

Whilst coomassie staining provides a guide to the presence of the desired FLT3L protein, a Western Blot was done to confirm expression in induced and uninduced cells (Figure 3.13). Contrary to expectations, an initial Western Blot with an anti-6xHIS antibody for detection, only showed 2 bands at approximately 15 kDa. This implies some cross-reactivity with similar histidine rich proteins, some degradation of the 21 kDa FLT3L and/or level of leaky expression of the protein in non-induced cells.

A second expression experiment was performed, combining a BCA assay, SDS-PAGE gel and

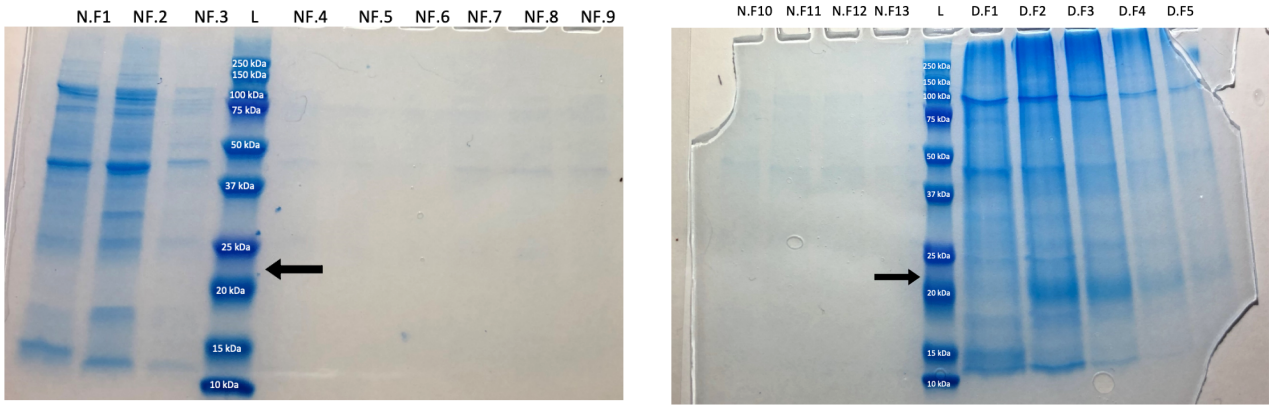



**Figure 3.12.** FLT3L was purified from *E. coli* by his-tag column affinity. The expected size of FLT3L is 21.9 kDa, indicated by the black arrows. After loading of sample onto the column, washing was performed and then elution with 8 mL of Native Elution Buffer. Thirteen 1 mL fraction were taken during this elution according to a native protocol (N.F1-N.F13), as described in methods 3.2.6. Alternatively, five 1-mL fractions were taken after purification according to a denaturing protocol (D.F1-D.F5), as described in methods 3.2.6. An SDS-PAGE, according to methods 3.2.7, was done for the fractions. L = ladder. For the ladder, the different molecular weights are displayed per band.

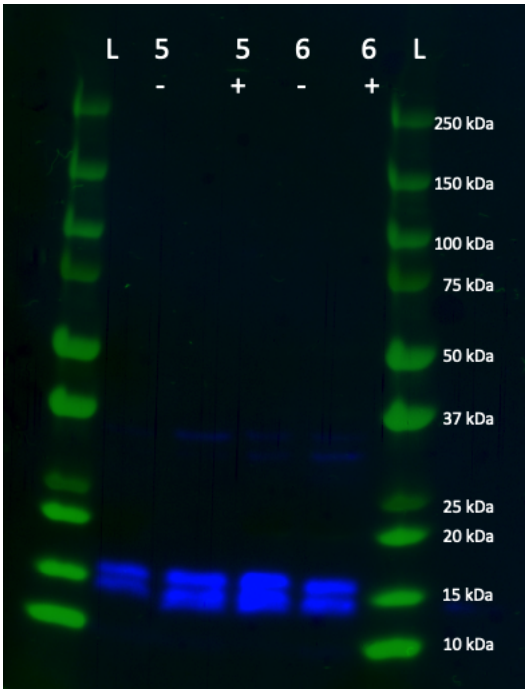



**Figure 3.13.** Western Blot of uninduced cells (-) and induced cells (+) of two different colonies (5 and 6). An anti-6x-HIS antibody conjugated to a HRP enzyme was used to visualise the FLT3L protein. For the ladder, (L) the different molecular weights are displayed per band.

Western Blots using an anti-FLT3L specific antibody for detection as well as an anti-6xHIS antibody (in case the anti-6xHIS was cross reacting with non-target protein).

Four different colonies (colony 1, 2, 5 and 6) of FLT3L-plasmid containing cells were grown overnight and two tubes of each colony were reinoculated 1:100 in fresh medium. One tube of each colony was IPTG induced (+) and the other tube was not induced (-). These cells were lysed by sonication. A 1:100 dilution of the cells lysates was made to quantify the protein concentration in the cell lysate. The total concentration was determined to be 2202 µg/mL ± 191 µg/mL of protein in the cell lysate based on a standard curve. Approximately 24 µg of protein was loaded onto the SDS-PAGE gels used for the coomassie staining and Western Blots (Figure 3.14)

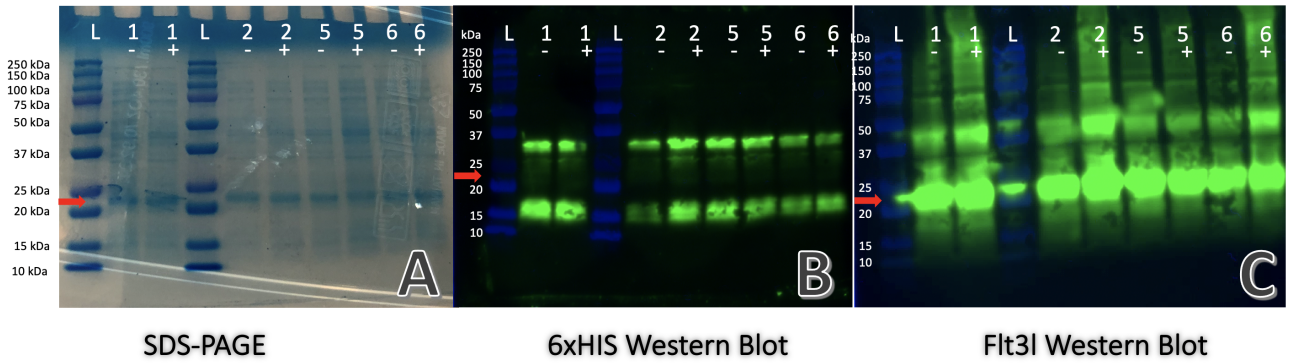



**Figure 3.14.** SDS-PAGE (A), Western Blot with anti-6xHIS antibody (B) and a Western Blot with an anti-FLT3L antibody (C) were performed on IPTG uninduced (-) and induced (+) cell lysates from colony 1, 2, 5, 6, which were transformed with a FLT3L expression vector. The red arrow indicates the desired fragment of 21.9 kDa. For the ladder, (L) the different molecular weights are displayed per band.

On the SDS-PAGE, stained by Coomassie stain (panel A), a clear band was visible between 20-25 kDa (A - red arrow), which corresponds to the calculated size of FLT3L. A similar band could be seen on the Western blot using the anti-FLT3L antibody (panel C), which implies the presence of FLT3L, although this antibody shows much off-target binding. The anti-6xHIS antibody (panel B), however, shows two distinct bands between 15-20 kDa and just below 37 kDa. A similar 15-20 kDa band was observed in Figure 3.13. This could have been the consequence of degradation of the HIS-tag fragment, which could be a potential problem when purifying the protein, or an artifact of the blotting. A further concerning aspect of these results is the failure of IPTG addition to instigate induced-colony specific expression.

In order to prevent potential degradation of the protein and increase the proportion of FLT3L protein versus other proteins in the fractions, a number of optimisations were trialled. These included decreasing the resin in the column from 2 mL to 400 µL and using 250 mL of cell culture instead of

50 mL and the addition of protease inhibitors. The SDS-PAGE running speed was adjusted to 120 V for 70 min to prevent any artifacts and provide better resolution. A Western Blot (Figure 3.15 – right) was performed with an anti-FLT3L antibody. On the SDS-PAGE (Figure 3.15 – left) two bands are visible at 25 kDa in fraction 6 and 7 and to a lesser degree in fractions 3, 4 and 5. At the same migration distance, a band is visible in the Western Blot with the FLT3L specific antibody, which further supports the successful purification of FLT3L. However, the SDS-PAGE shows that there are clearly still other proteins present after purification. It is encouraging that the sample of the first wash step (W1, Figure 3.15) does not show the presence of FLT3L in either the SDS-PAGE or the Western Blot. Indicating that the column can be washed of contaminatory proteins without loss of FLT3L, and that more thorough washing may be required. The total protein content of the fractions was determined with a BCA kit. The protein content of the fractions was calculated to be between 676 and 872 µg/mL compared to approximately 5500 µg/mL in the original cell lysate, implying over 84% of protein was removed. If a more robust washing procedure can be optimised, the conditions will be in place to achieve production and purification of high levels of high purity FLT3L for use in p-CaN formulation.

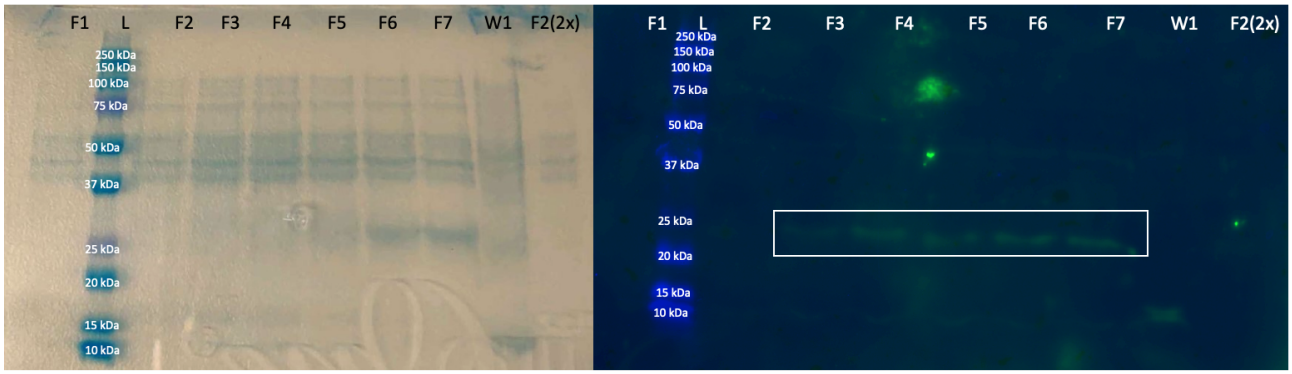



**Figure 3.15.** SDS-PAGE (top) and Western Blot (bottom) for fractions collected after protein purification (F1-F7). One fraction was diluted twice and also run on the gel (F2(2x)), as well as the flow-through after the first wash step (W1). An anti-FLT3L antibody was used for the Western Blot. For the ladder, (L) the different molecular weights are displayed per band.

## 3.4 Conclusions and Discussion

The work in this chapter aimed to examine the unique potential of p-CaN (a novel cavitation nuclei, subject to a recent patent filing), as both cavitation nuclei to deliver DNA and as an immunogenic formulation in its own right. Commonly used cavitation nuclei are phospholipid-coated microbubbles, such as Definity and SonoVue or solid cavitation nuclei, such as polymeric cups [231, 232], which are designed to be inert and non-immunogenic. When utilising these cavitation agents, it is necessary to either load or co-deliver the therapeutic. By combining both therapeutic and cavitation nuclei, p-CaN offer the opportunity to ensure effective co-delivery, as well as reduction in resources needed. This has huge potential beneficial ramifications for both the efficacy of therapy and the cost and regulation involved in translation.

To assess the utility of the p-CaN formulation as cavitation nuclei, it was tested for the effective transcutaneous delivery of luciferase-encoding pDNA. The resulting expression of luciferase transgene was shown to be equivalent to the level achieved by nanocups and substantially ($\sim$100x) and significantly ($p<0.0001$) higher than the luminescence observed without the application of ultrasound (geometric mean $2.46 \times 10^6$ p/s for p-CaN with ultrasound versus a geometric mean of $0.032 \times 10^6$ p/s without ultrasound). Also, in terms of area and level of luciferase expression the transcutaneous approach did show good reproducibility. Based on the TASE values, the hypothesis was further supported that beyond a threshold, a higher TASE does not result in more luminescence. Interestingly, this appears to enable shorter treatment times, as it was seen that 2 min ultrasound exposure with p-CaN and luciferase-encoding pDNA resulted in similar expression of luciferase as a 10 min ultrasound exposure. It is notable that although nanocup-mediated delivery of protein [144] and nucleotide has been shown previously (Chapter 2), there is no published literature showing the successful delivery of nucleotide constructs into the skin using protein cavitation nuclei.

In addition, it was shown that cavitation-mediated delivery of p-CaN could result in an immune response to the protein used to formulate the p-CaN, although a greater variability in antibody titre was observed compared to directly injected free protein. This greater variability may be expected as the needle and syringe approach does offer instant assurance of delivery. It is notable that the 4 mice in the immunisation study showed similar cavitation levels. The variability in immune responses may be explained by mouse handling, alignment inconsistencies, making it clear a more reproducible exposure set-up is needed. The fact that a response was generated is encouraging, as previous work has suggested that a comparatively very low dose is actually delivered by cavitation-mediated

delivery compared to direct injection [143]. This indicates a multiplier of efficacy must be occurring due to the site or cells reached by transcutaneous delivery. Furthermore, the antibodies generated after cavitation-mediated delivery showed a greater avidity distribution and higher average avidity compared to the antibodies generated upon needle and syringe injection.

In response to the COVID-19 pandemic, p-CaN were formulated from SARS-CoV-2 spike protein with or without imiquimod formulated into the core. Due to the cost of spike protein, much lower levels of p-CaN could be formulated and used compared to the model BSA antigen. Hence, to mitigate against the decreased dosing it was postulated that the addition of imiquimod could enhance the immunogenicity of the vaccine. Injected spike 1G p-CaN formulated with or without imiquimod showed no markedly increased immunogenicity compared to injected protein with or without imiquimod. Interestingly, p-CaN formulated with imiquimod delivered transcutaneously by ultrasound did generate immune responses, whilst p-CaN without imiquimod did not. No responses were generated for p-CaN Imiq when no ultrasound was applied. This implied some beneficial effect of imiquimod when these p-CaN were delivered by ultrasound. Notably, it was a mouse in the 'p-CaN Imiq (CAV)' group that actually outperformed all other mice in all other groups. Imiquimod is a well-recognised and powerful immunomodulator and is even approved as a therapeutic in its own right [214]. The data shown here is the first to be reported on the combination of spike protein and imiquimod for transcutaneous immunisation. It should be noted that previous analysis ([143]) and studies later in this thesis (section 4.3.6 and 5.3.1) have demonstrated the percentage of dose delivered transcutaneously is dramatically lower than following needle and syringe injection, but as previously seen, biological outputs can match those achieved by needle and syringe injection. Interestingly, the injection of p-CaN with imiquimod in the core resulted in a stronger IgG2a response compared to protein co-injected with imiquimod, which only showed a modest IgG2a response after 28 days.

Overall, these studies demonstrate the potential of p-CaN and open up questions relating to how to improve the reproducibility of immunogenicity when p-CaN are transcutaneously delivered, as well as regarding adjuvants that may increase immunogenicity.

One approach to enhancing the system is to ensure that both the protein cavitation nuclei and the DNA work in tandem to produce the most marked response. Hence, in anticipation of formulating p-CaN with immune stimulatory compounds, a protocol was developed for the production and purification of FLT3L, a potentially powerful immune modulator [226]. In particular, FLT3L has been

shown to be a potent adjuvant. Zhou et al. showed increased IFN-γ and IL-12 production after co-injection of a plasmid encoding FLT3L with a plasmid encoding a hepatitis B virus (HBV) small envelope protein compared to injection of the HBV small envelope protein expressing plasmid alone. It also showed that the addition of the FLT3L-expressing plasmid resulted in significantly higher antibody titres. Notably, peak antibody titres were reported to be higher after intradermal vaccination using microneedles than after intramuscular injection, further supporting the application of FLT3L in modalities using the transcutaneous delivery route [226].

It is hoped that FLT3L p-CaN could be a 'platform' technology used to deliver a range of DNA encoding disease-specific antigens (such as spike protein), and enhance responses generated against them. To date, whilst Novavax has reported promising protective immunity against SARS-CoV-2 infection [233] using a protein nanoparticle [234], the vast majority of other approaches that have shown similar success, have encoded the spike protein within RNA or DNA. Indeed, nucleotide approaches certainly provide quicker (see Moderna's 42 days from sequencing to clinical batch [235]) and more readily adaptable production (for example if mutation-driven resistance develops) than approaches which deliver the antigen as protein. Such rationale drove the 'general immune-stimulatory protein p-CaN' plus 'specific antigen DNA vector' approach followed here, but the system has sufficient flexibility to allow the reverse to be pursued in future.

A custom cell line was created which expressed FLT3L upon induction with IPTG. The presence of FLT3L was demonstrated with both an SDS-PAGE and a 6xHIS-tag and FLT3L Western Blot. Different sonication protocols were considered and the comparative merits of a native purification and a denaturing purification protocol were explored. It was shown that FLT3L could only be isolated with a denaturing purification protocol, a requirement which may relate to the need to free the protein from inclusion bodies [236]. The presence of FLT3L in the resulting fractions was shown with an anti-FLT3L antibody on a Western Blot. There are still challenges to ensuring adequate purity of the FLT3L protein before formulating p-CaN with this immune stimulatory protein. Once sufficient purity is achieved, FLT3L p-CaN could be combined with DNA vaccines. This could result in cavitation nuclei, which create an immune-rich environment. This could ultimately result in increased uptake, processing and presentation of the antigens produced by the DNA vaccines, resulting in more potent immunity.

To move this work forward, further work is needed:

- To improve reproducibility of the transcutaneous ultrasound set-up
- To investigate the effect of adjuvants loaded into the core of p-CaN, as well as the effect of p-CaN formulated from immune stimulatory proteins
- To formulate p-CaN from FLT3L to investigate its potential as an adjuvant.

Subsequent chapters will introduce a new ultrasound set-up to improve the reproducibility and determine optimal pressure, DNA concentration and treatment time for the expression of DNA. The potential of FLT3L as an adjuvant will be investigated in the context of an adjuvant-encoding pDNA vector. Ultimately, the aim is to conduct a challenge study combining optimised DNA vectors with p-CaN as instigators of ultrasound-mediated cavitation.

# Chapter 4

# New set-up

## 4.1 Introduction

In Chapter 2, an ultrasound exposure set-up was introduced for the delivery of DNA into the skin. This set-up required the alignment of a mouse flank, formulation holder and the ultrasound transducer including coupling cone for successful delivery. This proved a difficult to handle set-up, with limited clinical translational potential.

Hence, in this chapter an optimised set-up (V2) was designed, built and tested (Figure 4.1). The goal of this set-up was to improve the handling, increase reproducibility and ensure that the correct coupling of the ultrasound transducer to the skin could be verified by the addition of a pulser-receiver system. The ease of the ultimate translation to the clinical situation was also considered in the design. The largest design change introduced was the inversion of the transducer. By inverting the transducer, the need for manipulating this large piece of equipment onto a small animal model is removed. Furthermore, it was considered that as p-CaN or other cavitation nuclei may demonstrate buoyancy and could float to the surface of the formulation holder, inversion of the transducer, would increase the concentration of nuclei at the sample-skin interface. The advantage of concentrating cavitation agents near the skin to improve delivery has previously been shown by Park et al. ([237]), who used sinking cavitation agents to show that their concentration on the skin substantially improved delivery. The addition of the pulser-receiver allowed for verification of a clear acoustic path to the target skin before treatment commenced, hopefully resulting in better reproducibility within and between experiments. Finally, a new formulation holder, incorporating a treatment bed was added to the set-up. In this new set-up (V2), the scruff of the mouse was treated, rather than its flank. Treatment of the scruff allowed for treatment of skin only, preventing any unintended impact of the ultrasound on

other parts of the animal and unexpected acoustic reflections (a situation further improved by the use of an acoustic absorber to hold the skin flap in place). The size of the formulation holder was also reduced from 2 mL to 1.8 mL to enable dose-sparing.

The aims of this chapter are:

- optimisation of the treatment parameters within this new set-up (V2), including pressure, treatment time, DNA dose and p-CaN dose.
- assessment of the delivery of DNA and p-CaN under these optimised conditions.
- investigation of the resulting immune responses *in vivo*.

## 4.2 Materials and Methods

### 4.2.1 V2 set-up

In line with the requirements and aims discussed in section 4.1, a new set-up (V2) was developed in discussion with Dr. Michael Gray and used for all subsequent experiments.

The ultrasound coupling cone was filled with degassed water and the bed lowered on the coupling cone (Figure 4.1). The scruff of the mouse was secured with a bobby pin and placed over the filled formulation holder, incorporated into the bed. The scruff was secured by an acoustic absorber.

In this V2 set-up, the same parameters were used as described in section 2.2.1, as well as the same transducer with coupling cone, passive cavitation detector, matching network, amplifier, hard drive and 8-bit digital oscilloscope.

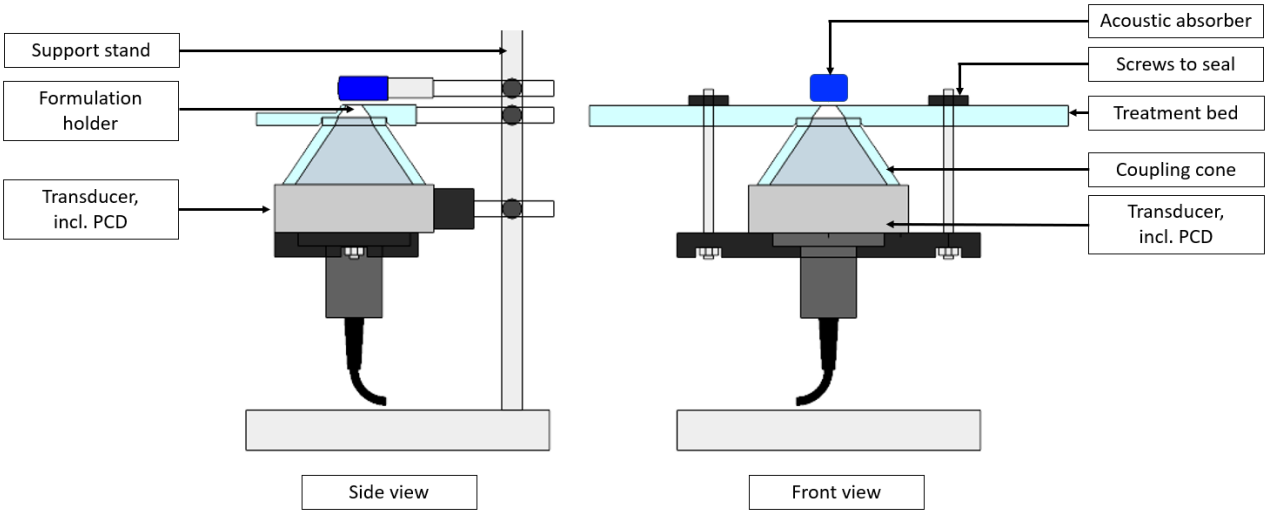



**Figure 4.1.** A schematic of the V2 set-up used for *in vivo* treatments. Adapted from Dr. Michael Gray.

In order to better assess the acoustic path, a pulser-receiver (DPR300 ultrasonic pulser/receiver, JSR Ultrasonics, Imaginant, USA) was introduced into the set-up. This allowed both for potential disruptions in the path of the acoustic beam to be detected, as well as amplification of the signal from the transducer. To assess disruptions, the set-up was used in RCV-mode (Figure 4.2, top) and for delivery of treatments the set-up was used in XMT-mode (Figure 4.2, bottom). Other adjustments, included replacing the 2.0 MHz filter with a 1.8 MHz filter (EF509, Thorlabs, USA). The acoustic processing, as described in section 2.2.3 was also adjusted to accommodate the 23 dB relative gain of the pulser-receiver and the digital highpass filter was set at 1.8 MHz.

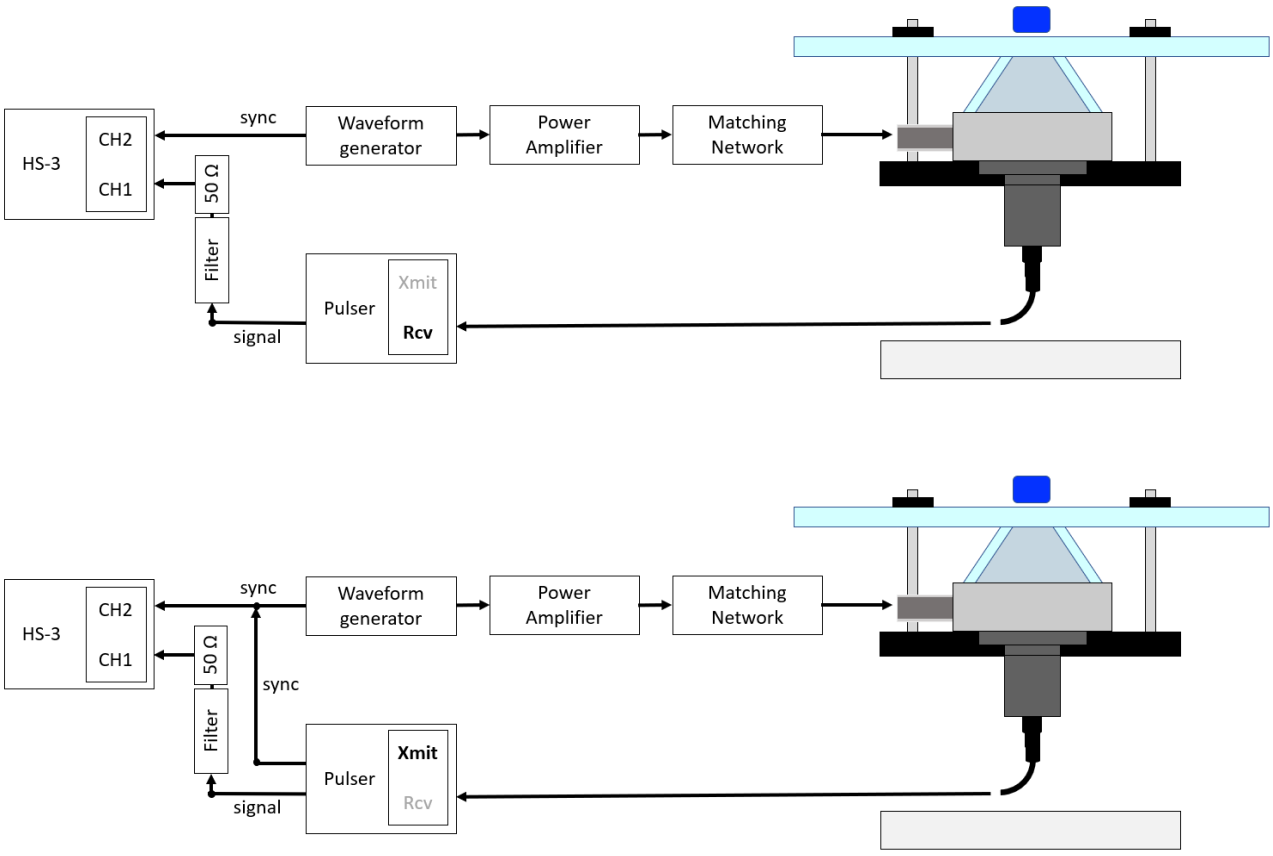



**Figure 4.2.** A schematic summary of the V2 set-up used for *in vivo* treatment. Top: RCV-mode for the assessment of a clear beampath. Bottom: XMT-mode used for treatment with p-CaN and DNA. Adapted from Dr. Michael Gray.

### 4.2.2 Statistics

Statistics were done as described in section 2.2.4. For DNA dose a linear regression was fitted and the p-value and slope determined.

### 4.2.3 Plasmid purification

Cells for plasmid isolation were grown up as described in section 3.2.1. Cell broth was spun down in a 5804R centrifuge (Eppendorf, UK) in 250 mL bottles. The supernatant was disposed off and the cell pellet used for subsequent purification. The cell pellets were stored at -80 ºC until used. Plasmid DNA was isolated as described in section 3.2.1 or, alternatively, a DNA giga-preparation was done from 2 L of cell broth with the GenElute™ HP Endotoxin-Free Plasmid Gigaprep Kit (Sigma), according to manufacturer's instructions for maximal final concentration.

### 4.2.4 *In vivo* imaging

Mice were imaged as described in 2.2.6 after 24 hours and/or 48 hours and/or 72 hours.

### 4.2.5 Quantification of DNA delivery

Excised skin was homogenised as described in section 2.2.9. 200 µL of the homogenised supernatant was sampled and used for genomic DNA extraction and quantification. The skin was subsequently processed with the GenElute$^{TM}$ Mammalian Genomic DNA Miniprep Kit (Sigma-Aldrich). In short, the 20 µL RNAse was added and the cells were lysed with 200 µL of Lysis Solution C and 20 µL proteinase K solution (20 mg/mL). This was vortexed for 15 seconds and incubated at 70 ºC for 10 minutes. All subsequent steps, column preparation, binding, washing and elution, were done exactly according to manufacturer's instructions. 5 µL of this elution was used for qPCR quantification. If the qPCR values were not within the standard curve, the elution was diluted 10,000-fold and 5 µL of the dilution was used.

Standard curves were prepared by spiking untreated skin with known number of CMV-Luc DNA copies. The skin was then processed in an identical way to the samples as described above.

The qPCR sample preparation and cycling conditions were as described in 2.2.9.

### 4.2.6 *In vivo* protocol to assess delivery and handling of the V2 set-up

Three groups of 4 mice were treated with ultrasound, CMV-Luc pDNA and either MilliQ, 25% SonoVue or 25% nanocups, as summarised below (Table 4.1). 11 mice were intradermally injected with 50 µg pDNA. Female BALB/c mice (section 2.2.5) were prepared as described in section 2.2.8. They were placed in the set-up as described above (Section 4.2.1).

Due to the short lifetime for SonoVue, samples with SonoVue were prepared as follows. The vial with SonoVue was agitated just before use. The DNA was added to the formulation holder and the SonoVue was used to top up the formulation holder. The scruff of the mouse was overlaid on the solution. The time for adding the solution and overlaying the skin was limited to two minutes before the ultrasound was turned on for 3 minutes. The pulser-receiver was used afterwards instead of beforehand to check for correct alignment. These precautions were not required for nanocups due to their greater stability.

**Table 4.1.** Summary of the protocol to assess the V2 set-up. Mice were treated with ultrasound (US) for 3 min with 50 µg CMV-Luc plasmid DNA and 25% SonoVue or 25% nanocups supplemented with MilliQ to maintain a constant volume or MilliQ alone.

| Group size | Treatment | Cavitation nuclei | Pressure | DNA concentration | Treatment time |
|---|---|---|---|---|---|
| 4 | US | MilliQ | 1.3-1.4 MPa | 50 µg | 3 min |
| 4 | US | 25% SonoVue, 75% MilliQ | 1.3 MPa | 50 µg | 3 min |
| 4 | US | 25% nanocups, 75% MilliQ | 1.3 MPa | 50 µg | 3 min |
| 11 | ID | PBS | - | 50 µg | - |

### 4.2.7 *In vivo* protocol for optimisations

In total four parameters were optimised, pressure, treatment time, DNA dose and p-CaN dose. Female BALB/c mice (section 2.2.5) were prepared as described in section 2.2.8. They were placed in the set-up as described above (Section 4.2.1). The protocols are summarised in Table 4.2-4.5.

In this chapter, BSA 2G-U p-CaN are used. These are p-CaN with a 100% hexane core instead of a oil/hexane core. The BSA 2G-U p-CaN were kindly formulated by Dr. Brian Lyons.

**Table 4.2.** Summary of the protocol to assess the effect of p-CaN dose on delivery. Mice were treated with ultrasound (US) for 5 min with 142 µg CMV-Luc plasmid DNA and 100% or 50% or 0% of BSA 2G-U p-CaN supplemented with MilliQ to maintain a constant volume.

| Group size | Treatment | Cavitation nuclei | Pressure | DNA concentration | Treatment time |
|---|---|---|---|---|---|
| 4 | US | 100% 2G-U p-CaN | 1.5 MPa | 142 µg | 2 min |
| 4 | US | 50% 2G-U p-CaN | 1.5 MPa | 142 µg | 2 min |
| 4 | US | none | 1.5 MPa | 142 µg | 2 min |

**Table 4.3.** Summary of the protocol to assess the optimal pressure for DNA delivery. Mice were either injected intradermally (ID) with 142 µg of CMV-Luc plasmid DNA or treated with ultrasound (US) at scaling pressures with 142 µg CMV-Luc plasmid DNA for 5 min with or without BSA 2G-U p-CaN.

| Group size | Treatment | Cavitation nuclei | Pressure | DNA concentration | Treatment time |
|---|---|---|---|---|---|
| 4 | US | 2G-U p-CaN | 0.4 MPa | 142 µg | 5 min |
| 4 | US | 2G-U p-CaN | 1.5 MPa | 142 µg | 5 min |
| 4 | US | 2G-U p-CaN | 1.7 MPa | 142 µg | 5 min |
| 4 | US | 2G-U p-CaN | 2.0 MPa | 142 µg | 5 min |
| 4 | ID | none | 0 MPa | 142 µg | 5 min |

**Table 4.4.** Summary of the protocol to assess the effect of DNA dose on delivery. Mice were treated with ultrasound (US) for 5 min with scaling amounts of CMV-Luc plasmid DNA and BSA 2G-U p-CaN.

| Group size | Treatment | Cavitation nuclei | Pressure | DNA concentration | Treatment time |
|---|---|---|---|---|---|
| 4 | US | 2G-U p-CaN | 1.7 MPa | 284 µg | 5 min |
| 4 | US | 2G-U p-CaN | 1.7 MPa | 142 µg | 5 min |
| 4 | US | 2G-U p-CaN | 1.7 MPa | 71 µg | 5 min |

**Table 4.5.** Summary of the protocol to assess the optimal time for DNA delivery. Mice were treated with ultrasound (US) for varying amount of time with 142 µg CMV-Luc plasmid DNA and BSA 2G-U p-CaN.

| Group size | Treatment | Cavitation nuclei | Pressure | DNA concentration | Treatment time |
|---|---|---|---|---|---|
| 4 | US | 2G-U p-CaN | 1.7 MPa | 142 µg | 10 min |
| 4 | US | 2G-U p-CaN | 1.7 MPa | 142 µg | 5 min |
| 4 | US | 2G-U p-CaN | 1.7 MPa | 142 µg | 2 min |
| 4 | US | 2G-U p-CaN | 1.7 MPa | 142 µg | 1 min |
| 4 | No US | - | - | - | 0 min |

### 4.2.8 *In vivo* protocol for quantification of delivered DNA and BSA at 2 minutes and 24 hours

An *in vivo* study was conducted to understand the delivery and expression under optimised conditions.

For this *in vivo* study, two groups of 4 mice were treated with ultrasound. All mice were treated with 2G-U p-CaN made from bovine serum albumin (BSA) at the maximal concentration, 90 µg of CMV-Luc plasmid DNA, at 1.7 MPa for 2 min on the right flank and were intradermally injected with 90 µg of CMV-Luc plasmid DNA on their left flank.

The first group was culled after 2 min and their treated skin excised. The luminesence of both flanks of the second group was IVIS imaged after 24 hours. They were subsequently culled and their treated skin excised. The DNA content of the excised skin was quantified by qPCR as described in section 4.2.5. Part of the homogenised skin was used for the quantification of the BSA delivery into the skin. Hence, using just 8 mice this study provided information on the amount of DNA delivered, the amount of pCaN delivered, the persistence of the DNA over the subsequent 24 hours and the transgene expression that results.

A third and fourth group of mice was intradermally injected with 100 µL BSA 2G-U p-CaN. One group was culled after 2 minutes and the other group was culled after 24 hours. The skin was homogenised as described in section 2.2.9.

The amount of BSA p-CaN delivered into the skin was assessed by measuring the BSA protein content in the skin by ELISA using a BSA ELISA kit (abx150325, Abbexa, UK). A standard curve of BSA protein was used, so the concentration determined is in BSA equivalent. The skin was homogenised as described in section 2.2.9 and diluted two-fold in 0.01 mol/L PBS.

### 4.2.9 *In vivo* protocol for assessing immunogenicity under optimised conditions

For the subsequent *in vivo* experiment, the expression and related immunogenicity under the identified optimised conditions was assessed. To this end, 8 mice were treated with BSA 2G-U p-CaN at the maximal concentration, 90 µg of CMV-Luc plasmid DNA, at 1.7 MPa for 2 min on the right-hand flank. A second group of 4 mice was intradermally injected with 100 µL pCaN and 90 µg CMV-Luc plasmid DNA. Both groups were homologously boosted after 21 days and blood was

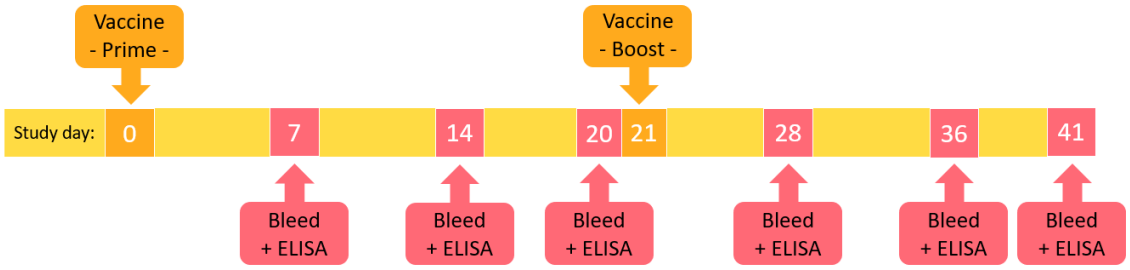



**Figure 4.3.** Summary of the treatment and blood sampling, as well as subsequent ELISA timeline for the *in vivo* to assess the immunogenicity CMV-Luc plasmid DNA and 2G-U p-CaN.

sampled at 7, 14, 20, 28, 36 and 41 days (Figure 4.3). The mice were also imaged 24, 48 and 74 hours after the prime vaccination and 24 and 48 hours after the boost vaccination.

Immunogenicity was evaluated by ELISA as described in section 2.2.11, with the exception that the plate was blocked with 50 µL/well of Pierce Protein-free blocking buffer (37572, ThermoFisher Scientific), instead of 10% FBS-PBS. Furthermore, the plate was coated with 10 µg/mL luciferase protein (ab100961, Abcam) to quantify luciferase antibody concentration or with 10 µg/mL Bovine Serum Albumin (Sigma-Aldrich) to quantify antibody responses against BSA. Luciferase standard curves were prepared with firefly luciferase antibody (anti-Luc) (MA1-80225, ThermoFisher).

## 4.3 Results

### 4.3.1 *In vivo* comparison of SonoVue and nanocups

To assess the potential of the V2 set-up (see schematics 4.1 and 4.2), a preliminary *in vivo* was performed. In this experiment, a solution containing SonoVue (microbubbles with a shell formulated from phospholipids and polyethyleneglycol shell and a sulphur hexafluoride core), nanocups or the negative control MilliQ water was used to deliver CMV-Luc pDNA. The reliance on cavitation nuclei with a longer history of use than p-CaN allowed better comparison to historical data collected with the V1 ultrasound exposure set-up. Both SonoVue and nanocups were shown to be able to deliver the pDNA. However, overall the nanocups had a higher average luminescence and reduced variability than SonoVue (geometric mean: $3.34 \times 10^5$ p/s vs $1.50 \times 10^5$, geometric SD: 1.849 vs 2.626) (Figure 4.4). The higher luminescence achieved with nanocups may be attributed to the longer periods of sustained cavitation induced, compared to SonoVue (see cavitation diagrams below - figure 4.5). Indeed, it could be argued that 3 of the 4 luminescence values produced using SonoVue did not exceed levels achieved with water alone. This could have been expected as SonoVue consists of microbubbles, which are less amenable to the generation of sustained cavitation [144]. This is further emphasised in the TASE values, which are much more reproducible for nanocups than for SonoVue in this context (8.13±0.62 μJ vs 7.11±2.57 μJ). The alignment between luciferase and total TASE level is encouraging for further translation but there is also a suggestion that features such as peak TASE and duration above a certain TASE level should be probed further. Interestingly, one mouse in the MilliQ-group had successful delivery of the DNA ($2.46 \times 10^5$ p/s) despite a relatively low TASE value (0.85 μJ), which may have been caused by some skin abrasions from shaving, allowing passage of the DNA into the skin.

Intradermal injection showed a higher average luciferase expression level which was the result of 2 very high readings (exceeding $5 \times 10^6$ p/s) amongst a very wide range ($1.36 \times 10^4$ to $7.54 \times 10^6$ p/s). Hence, these data show that in accordance with the previous iteration of the ultrasound set-up, this V2 set-up was also capable of delivering pDNA into the skin and cavitation could be effectively monitored. In Chapter 2 section 2.3.1, a TASE threshold for delivery was observed between 1.7 μJ and 4.3 μJ. In this dataset, the MilliQ-treated mice all have TASE-values below 1.1 μJ and the nanocups-treated mice all have a TASE-value above 7.5 μJ. Hence, the measurements from this experiment still agree with the previously determined threshold. Furthermore, the SonoVue treated mouse with the highest luminescence had a TASE value of 8.3 μJ, compared to its groupmates which

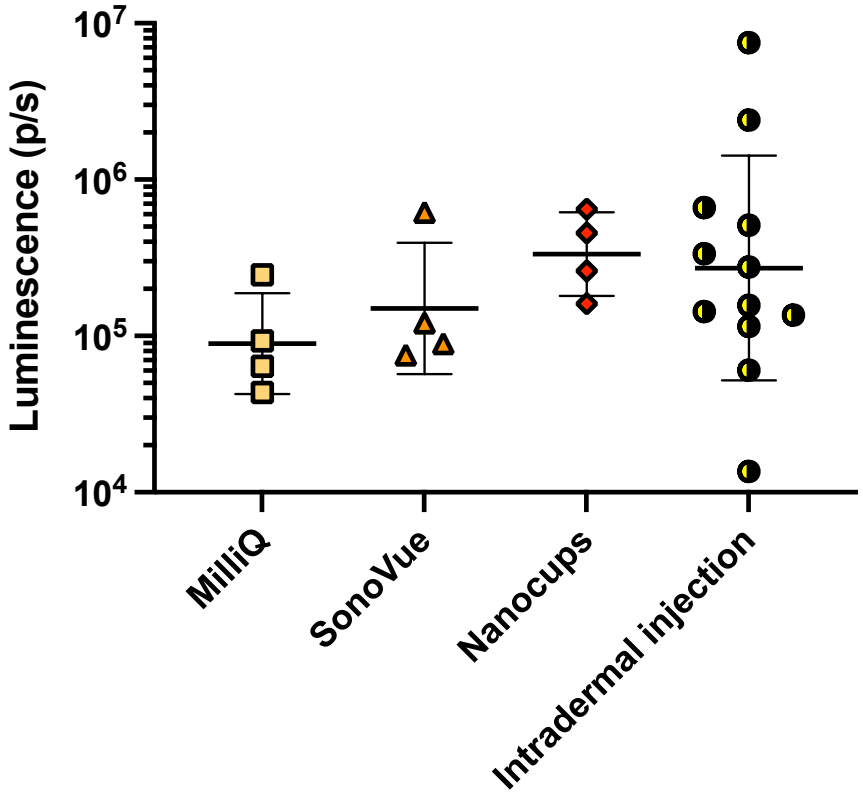
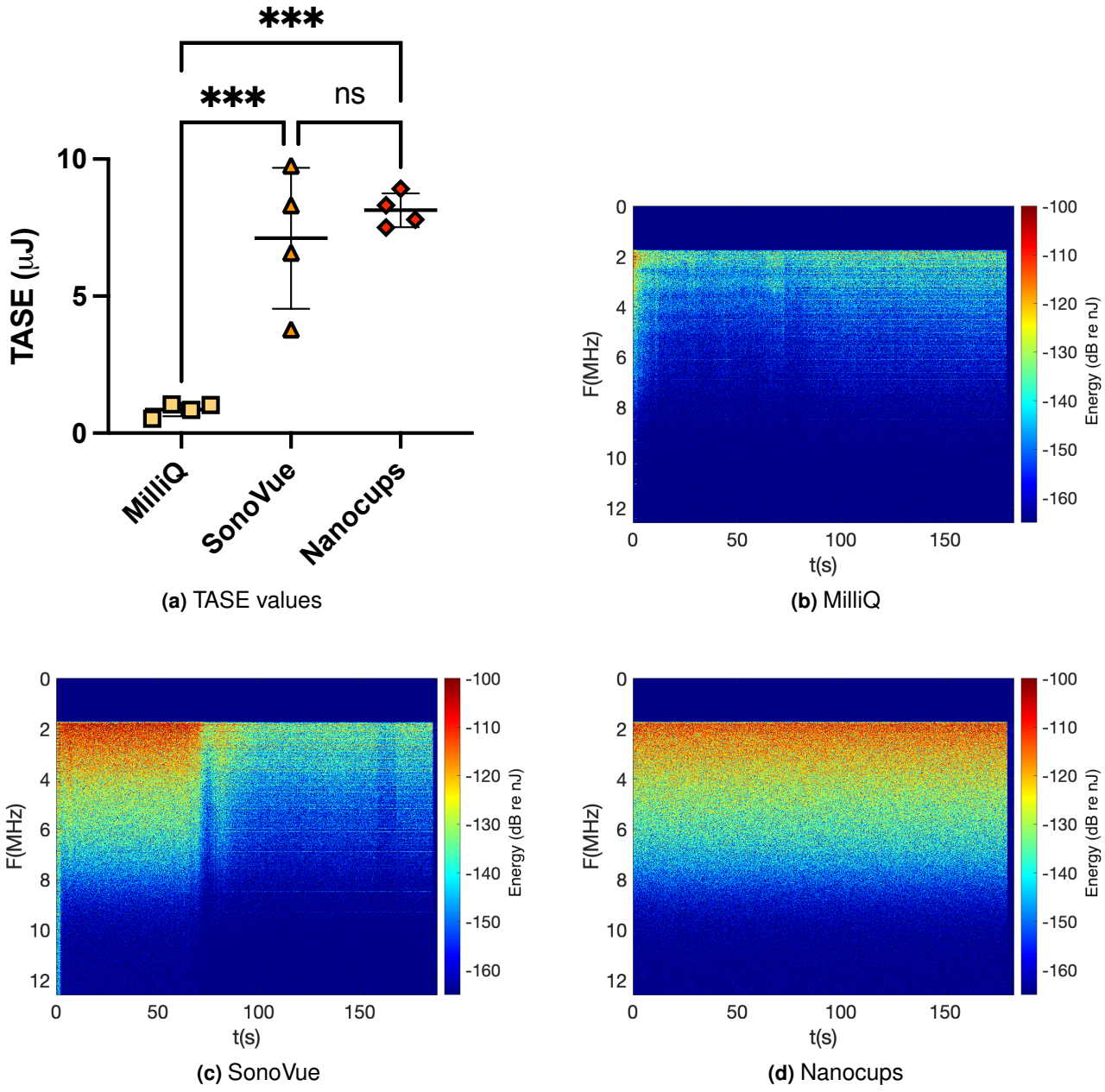



**Figure 4.4.** Total luminescence quantified after 24 hours. Groups of 4 mice were dosed with CMV-Luc pDNA combined with either MilliQ, 25% SonoVue or 25% nanocups. 11 mice were intradermally injected for comparison. Geometric mean $\times/\div$ geometric standard deviation are displayed. Significance was assessed by an ordinary one-way ANOVA with a Dunnett's test compared to 'MilliQ', $p>0.05$ for all tested groups.

had lower luminescence and TASE values of 6.6 µJ, 9.7 µJ and 3.8 µJ. In this study upon 3 minutes of sonication at 1.3 MPa, the luciferase expression had a geometric mean of $3.3\text{x}10^5$ p/s. Compared with the luciferase-encoding pDNA delivered in section 3.3.1, where $7.95\text{x}10^5$ p/s geometric mean was observed upon 10 minutes of sonication at 1.2 MPa, a lower luminescence was observed. This may be related to the lack of treatment time optimisation for sonication with nanocups.




**(a)** TASE values

**(b)** MilliQ

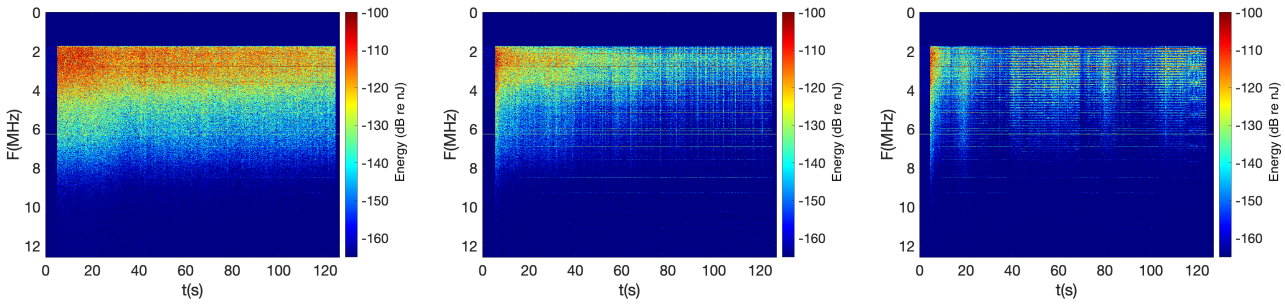
**(c)** SonoVue

**(d)** Nanocups

**Figure 4.5.** TASE readings and spectrograms from treatments of mice in the experiment assessing MilliQ, SonoVue or nanocups mediated-delivery of CMV-Luc pDNA. Panel (a) displays TASE for the different treatments. Mean (horizontal bars) and standard deviation (error bars) are displayed. Significance was assessed by an ordinary one way ANOVA with a Tukey HSD post all group comparisons. *** = $p<0.001$. Panel (b) shows an exemplar spectrogram for treatments with MilliQ. Panel (c) shows an exemplar spectrogram for treatments with SonoVue. Panel (d) shows an exemplar spectrogram for treatments with nanocups.

### 4.3.2 *In vivo* p-CaN concentration optimisation

Having validated that the V2 set-up could replicate levels of cavitation-mediated delivery seen previously with well-established cavitation nuclei, the set-up could then be tested with the novel cavitation nuclei p-CaN made from BSA. The first relationship to characterise and optimise was the one between p-CaN concentration and cavitation and delivery. It was speculated that, if very high levels of p-CaN led to prefocal acoustic shielding (as has been observed in cancer treatment with cavitation [238]), a decrease in their concentration would not necessarily lead to a decrease in cavitation on the skin surface and may still result in effective delivery. Hence, an *in vivo* study was performed, where a maximal concentration of p-CaN (43.9 mg/mL) was compared to a 50% reduction as well as a no p-CaN control, at 1.5 MPa with 142 µg of luciferase-encoding DNA for 2 minutes of exposure. The data (Example spectrograms are displayed in Figure 4.6) showed that the addition of 100% p-CaN was necessary to achieve sustained cavitation at a total level of above 3.4 µJ for all treated mice and therefore also needed for reliable delivery and expression of the luciferase plasmid. Furthermore, although a 50% p-CaN dose did result in lower cavitation levels (0.6-3.6 µJ), the mouse with $1.4x10^6$ p/s luminescence still reached the threshold with a TASE of 3.6 µJ and as a result showed greater expression than was evident in the controls. However, with the p-CaN dose of 50%, a wider range of luminescence values was seen across the 4 mice compared to the 4 mice treated with formulation with the 100% p-CaN dose (GSD: 4.16 vs 2.80) (Figure 4.7). Hence, for the sake of reproducibility, it was decided to continue with a maximal p-CaN concentration in the formulation to maximise the cavitation level to effectively deliver the pDNA.




**(a)** 100% p-CaN **(b)** 50% p-CaN **(c)** 0% p-CaN

**Figure 4.6.** Example spectrograms showing PCD data collected during treatment. Mice were treated with CMV-Luc pDNA and MilliQ or 50% p-CaN or 100% p-CaN in the formulation applied to the skin. One representative example from each group of 4 mice is shown. The y-axis represents the frequency spectra of the acoustic emissions, x-axis the time post-commencement of ultrasound and the colourbar shows the energy in dB re nJ as calculated as described in section 2.2.3.

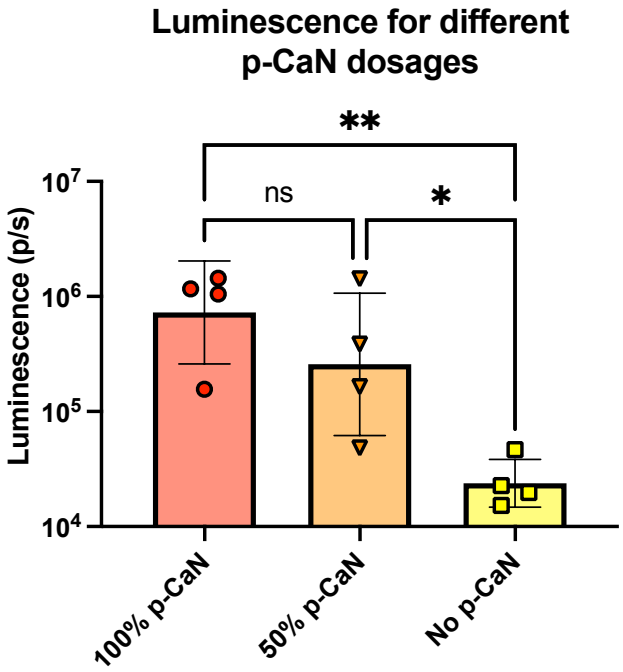



**Figure 4.7.** Expression from the luciferase reporter gene as measured 24 hours after delivery. Groups of 4 mice were treated with 142 µg CMV-Luc pDNA, and a range of 2G-U p-CaN (0%, 50% or 100%) and ultrasound. Delivery was performed as summarised in Table 4.2 and IVIS imaging as described in section 2.2.6. Geometric means (bar height) $\times/\div$ geometric standard deviation (error bars) are displayed. Significance was assessed with a one-way ANOVA with Tukey HSD post all group comparisons. * = p<0.05, ** = p<0.005.

### 4.3.3 *In vivo* pressure optimisation

In order to assess the effect of pressure amplitude on delivery using the V2 set-up, a pressure optimisation was conducted. Groups of four mice were treated with CMV-Luc pDNA at 0.4 MPa, 1.5 MPa, 1.7 MPa or 2.0 MPa ultrasound pressure amplitude with 2G-U p-CaN as cavitation nuclei. As a control, dose-matched intradermal injections of the luciferase vector were administered. The luciferase expression was measured by IVIS after 24 hours and used as a measure of successful delivery. The results show that at a sub-cavitation pressure of 0.4 MPa, very little expression could be observed (geometric mean of $1.63\text{x}10^4$ p/s) (Figure 4.8). Enhanced expression levels could be seen at 1.5 MPa and 1.7 MPa (geometric means of $2.95\text{x}10^5$ p/s and $3.62\text{x}10^5$ p/s). However, when the pressure was increased to 2.0 MPa, 3/4 mice showed reduced expression compared to 1.5 and 1.7 MPa pressure amplitudes. This may be attributed to damage of the skin observed at this higher pressure, which results in lower expression from the DNA plasmids. Notably, the I.D. control showed the greatest intra-group variability (GSD: 8.99).

Interestingly, the mean TASE values for 1.5 MPa and 1.7 MPa (18.23 µJ and 19.18 µJ) were very similar. However, a marked increase was observed when the pressure was increased to 2.0 MPa

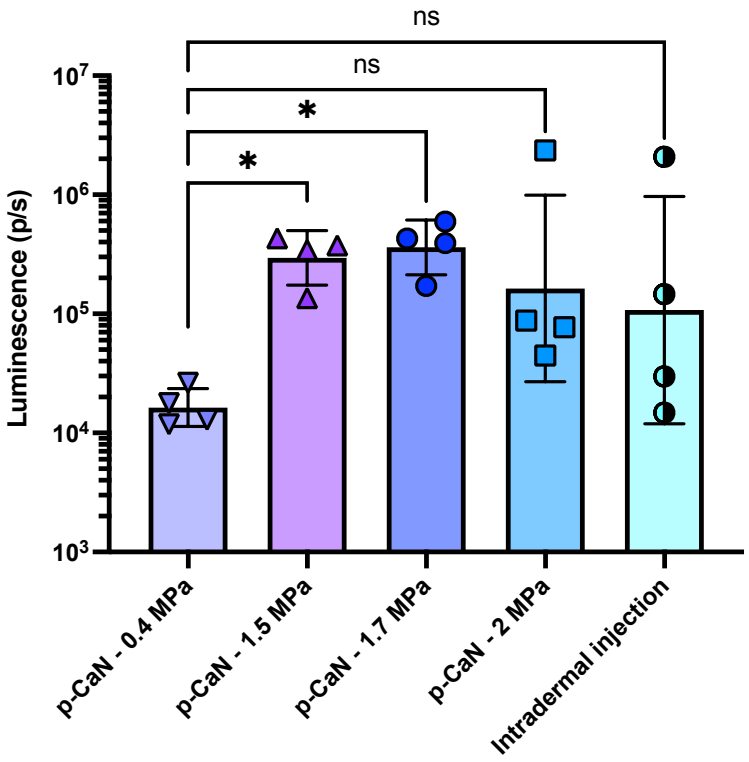



**Figure 4.8.** The measured luminescence 24 hours after treatment. Groups of 4 mice were treated with 142 µg CMV-Luc pDNA, BSA 2G-U p-CaN and ultrasound at different pressure amplitudes for 5 minutes or intradermally injected with 142 µg CMV-Luc pDNA. Geometric means (bar height) $\times/\div$ geometric standard deviation (error bars) are displayed. Significance was analysed by one-way ANOVA with Dunnett test compared to 'p-CaN - 0.4 MPa', * = $p<0.05$, ns = $p>0.05$.

(31.66 µJ) (Figure 4.9 and 4.10). This could imply that going above a certain TASE threshold results in adverse effects both in terms of skin damage as well as DNA expression. The approximate doubling of TASE between 1.7 and 2.0 MPa suggests a threshold for cavitation of endogenous gas bubbles may have been crossed [201]

A pressure of 1.7 MPa was selected for subsequent experiments on the basis of the level and reproducibility of the transgene expression achieved.

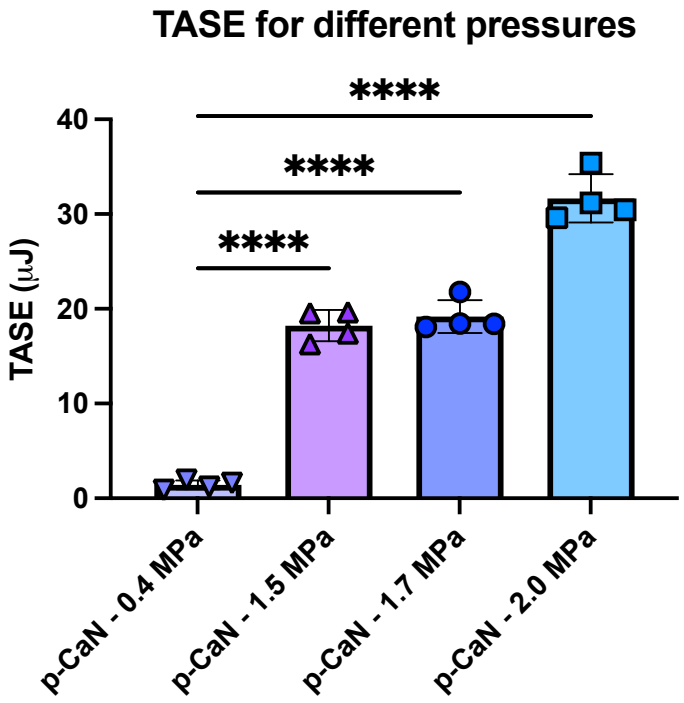



**Figure 4.9.** The measured cavitation in TASE for different treatment pressures. n=4 mice were treated with 142 µg CMV-Luc pDNA, p-CaN and ultrasound at different pressures for 5 minutes or intradermally injected with 142 µg CMV-Luc pDNA. N=4, mean value (bar height) and standard deviation (error bars) are displayed. Significance was analysed by one-way ANOVA with Dunnett's test compared to 'p-CaN - 0.4 MPa'. **** = p<0.0001.

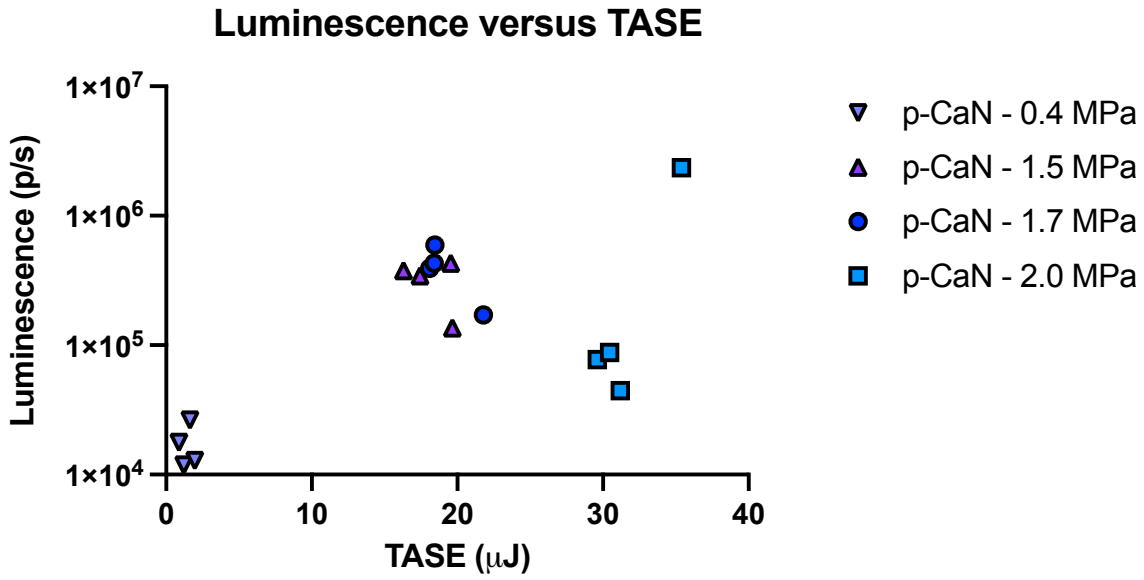



**Figure 4.10.** The measured cavitation in TASE for different treatment pressures and the measured luminescence after 24 hours. n=4 mice were treated with 142 µg CMV-Luc pDNA, p-CaN and ultrasound at different pressures for 5 minutes.

### 4.3.4 *In vivo* DNA concentration optimisation

Having refined p-CaN concentration and exposure pressure parameters, the effect of scaling DNA concentration was studied. Mice were treated with 100% p-CaN (45.5 mg/mL) and 71 µg, 142 µg or 284 µg at 1.7 MPa for 5 minutes. The following day the luminescence was quantified using IVIS as a measure for delivery. The results are summarised in Figure 4.11. A linear regression was fitted, which showed a fold increase of 1.003 in luminescence per µg of pDNA, which was not statistically significant (p = 0.1). Hence, no dose-relationship between pDNA and luminescence could be observed for this pDNA dose range. Although no significance could be observed when a linear regression was fitted, there was an upward trend in luminescence for higher doses. This may mean there is a delivery or uptake limit to the skin. As a dose of DNA of 71 µg and 142 µg showed the least intra-group variability (GSD: 1.58 vs 1.32 vs 2.37) and permitted dose sparing compared to 284 µg, DNA doses between 70-142 µg were chosen for subsequent experiments.

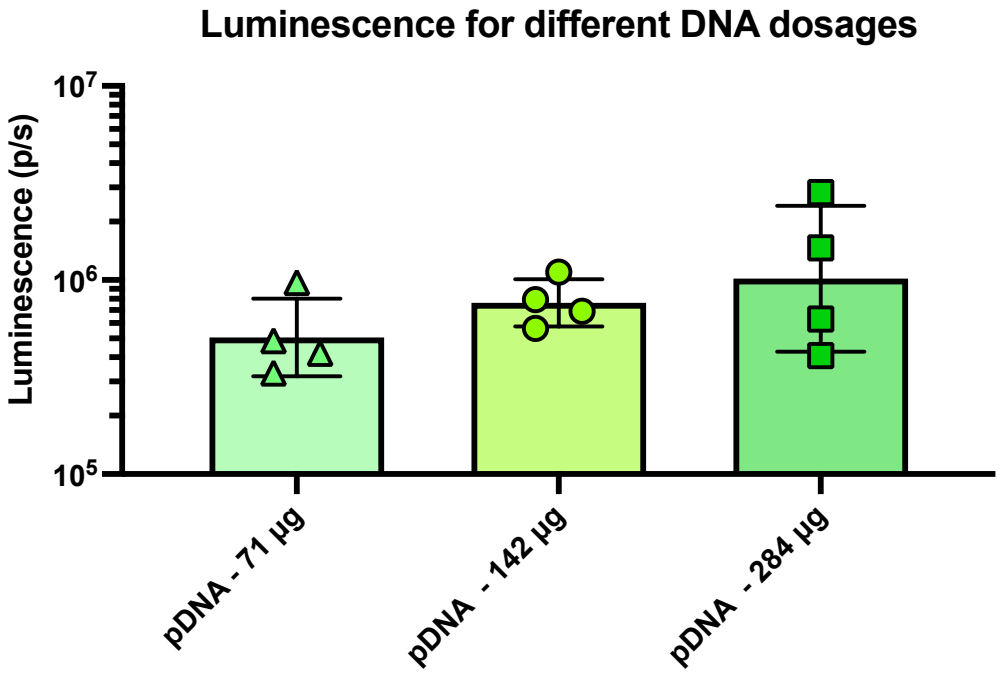



**Figure 4.11.** The luciferase expression 24 hours after treatment with 71 µg, 142 µg or 284 µg CMV-Luc pDNA, BSA 2G-U p-CaN and ultrasound at 1.7 MPa for 5 minutes. N=4. Geometric mean (bar height) $\times/\div$ geometric standard deviation (error bars) is displayed. A linear regression was fitted, which showed a fold increase of 1.003 in luminescence per µg of pDNA with p = 0.1.

### 4.3.5 *In vivo* treatment time optimisation

Having optimised the p-CaN dose, the DNA dose and the pressure amplitude, the issue of treatment time was addressed. Reducing the exposure time without decreasing delivery is important for the translatability of the approach. In order to assess the effect of treatment time, groups of four

mice were treated for 1, 2, 5 or 10 minutes with all the other optimised parameters or untreated and the following day the luciferase expression was measured. The results are displayed in Figure 4.12. All treated groups had significantly more luminescence than the untreated control. Intriguingly, the 2 minute-treatment showed the highest geometric mean total luminescence in photons/second of all the groups ($4.23x10^5$ p/s) and lowest geometric standard deviation of the treated groups (GSD: 1.59 (60 sec) vs 1.36 (120 sec) vs 1.68 (300 sec) vs 1.53 (600 sec)). Hence, for subsequent experiments, a 2-minute-treatment was applied. This standard deviation compares favourably with the nanocups treatment in section 4.3.1 and the p-CaN treatment at 1.7 and 1.5 MPa in section 4.3.3, which showed a GSD of 1.8 and 1.7 respectively. This could be a reflection of the treatment time, as those experiments had treatment times of 3 minutes and 5 minutes respectively.

To further evaluate the possible underlying mechanism for this optimum, the cavitation energy was analysed and compared to the *in vivo* observations.

As expected, a linear relationship could be observed between cavitation energy (TASE) and the treatment time (Figure 4.13). This means that more energy is deposited as the treatment time is increased, this confirms the maintenance of cavitation by this preparation of p-CaN. Such sustained cavitation is also a feature of nanocups but is not observed with microbubble formulation (section 4.3.1). However, this increase in energy with time does not necessarily lead to an increase in observed total luciferase expression (Figure 4.14). Examination of the mouse skin after treatment, revealed that increasing duration of exposure increased the level and area over which reddening of the skin was evident (Figure 4.15). This increased damage may therefore align with the decreased luciferase at longer exposure times, i.e. if too much energy is deposited on the skin, the skin cells are damaged and this leads to a decrease in the capacity to take up and express DNA. This observation is supported by the evident horseshoe pattern of expression at the highest pressure; the luminescence is no longer present in the centre and only as a circle around the damaged cells in the focus of the transducer (white arrow in Figure 4.15 depicts the centre without luminescence). Notably, in almost all cases the reddening evident directly after treatment was fully resolved the following day.

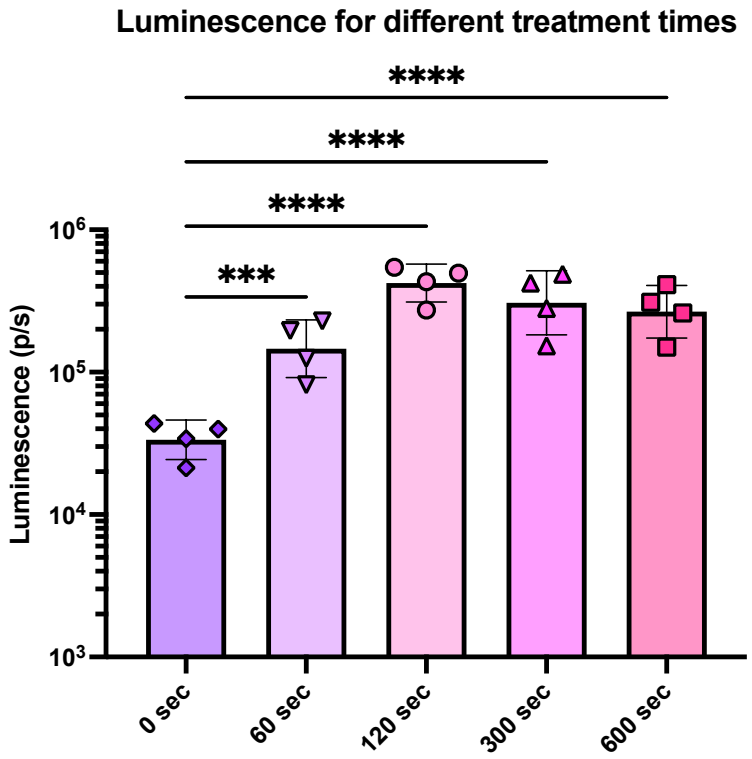



**Figure 4.12.** The measured lumiferase expression 24 hours after treatment. Groups of mice were treated for 60, 120, 300 or 600 seconds with 142 µg CMV-Luc pDNA, BSA 2G-U p-CaN and ultrasound at 1.7 MPa. Untreated skin ('0 sec') was used as a control. N=4, geometric mean (bar height) ×/÷ geometric standard deviation (error bars) are displayed. A one-way ANOVA with a Dunnett's test compared to '0 sec' was used to assess the difference, * = p<0.05.

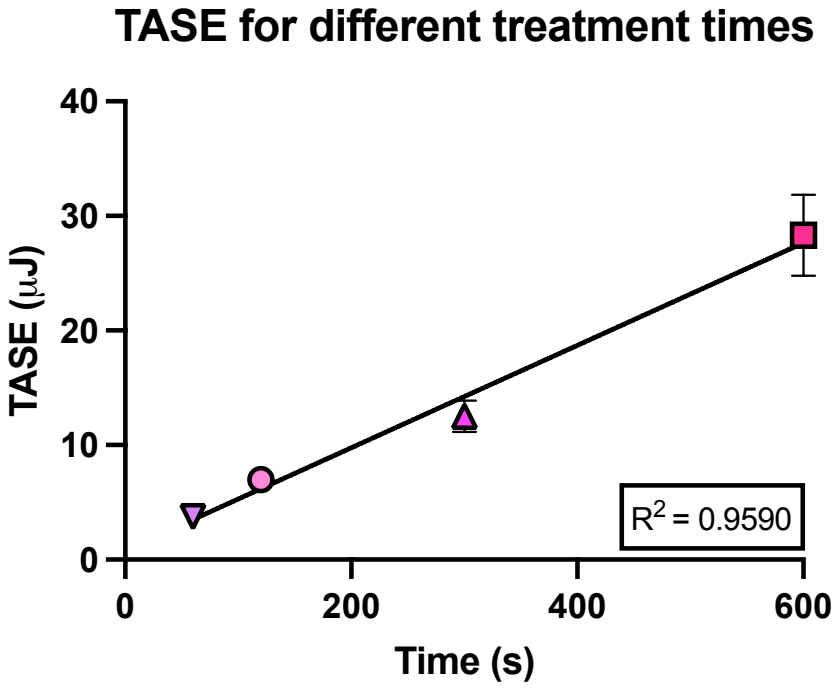



**Figure 4.13.** The measured TASE values for different treatment times. Mice were treated for 60, 120, 300 or 600 seconds with 142 µg CMV-Luc pDNA, BSA 2G-U p-CaN and ultrasound at 1.7 MPa. n = 4 mice and the mean and standard deviation are displayed. A linear fit is shown. TASE was calculated as described in section 2.2.3.

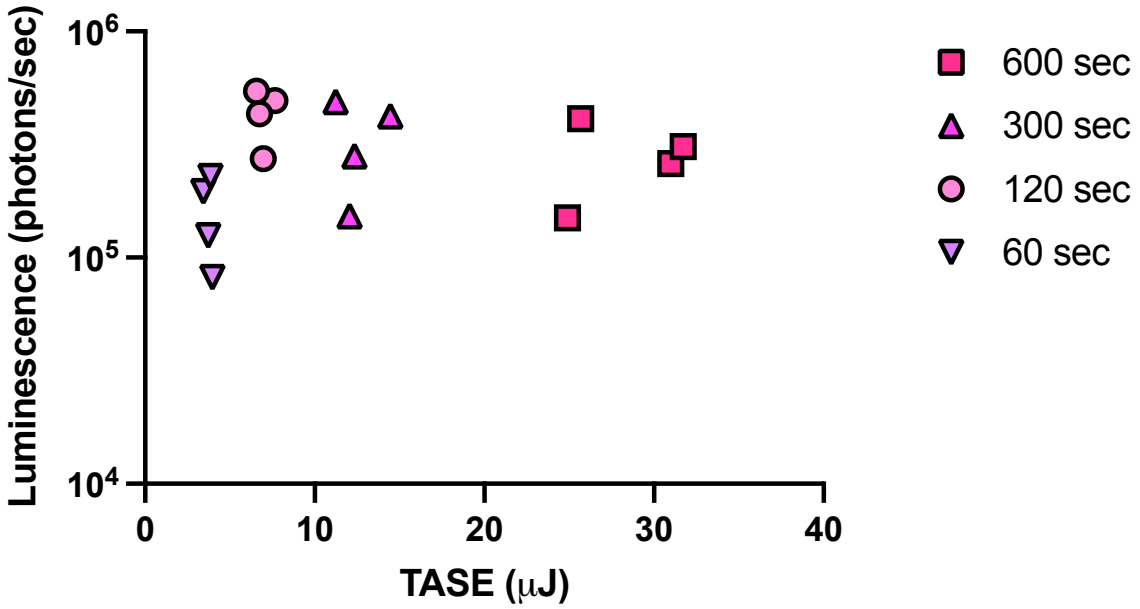



**Figure 4.14.** The measured luciferase expression 24 hours after treatment plotted against the TASE values captured during exposure and calculated, as described in section 2.2.3. Mice were treated for 0, 60, 120, 300 or 600 seconds with 142 µg CMV-Luc pDNA, BSA 2G-U p-CaN (2G-U) and ultrasound at 1.7 MPa.

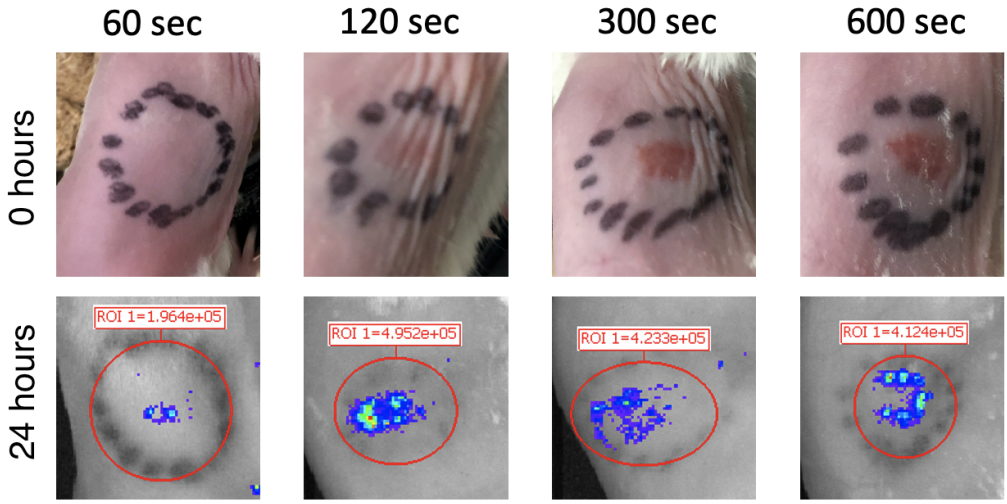



**Figure 4.15.** Representative pictures of the exposed skin regions taken directly after treatment and matching luciferase images captured 24 hours later. Representative mice are displayed for each group that received either 60 sec, 120 sec, 300 sec or 600 sec of ultrasound treatment. The white arrow indicates the region without any luciferase expression.

### 4.3.6 *In vivo* quantification of delivery with optimised parameters

To bring together all the optimisations, an *in vivo* study was performed with CMV-Luc and BSA 2G-U p-CaN in the V2 set-up. In addition to measurement of luciferase expression, more in depth analysis of the level of delivery of both the p-CaN and the DNA was performed. Two groups of mice were treated with BSA 2G-U p-CaN, ultrasound and 90 µg of CMV-Luc pDNA on their right flank and intradermally injected with 90 µg of CMV-Luc pDNA on their left flank. Another two groups of mice were injected with 100 µL of 2G-U BSA p-CaN.

One group treated with ultrasound and I.D. injected with pDNA was culled 2 minutes after treatment and the treated areas of skin excised. The second group was IVIS imaged after 24 hours and then culled with the treated areas of skin excised after imaging. One group of the BSA 2G-U p-CaN injected mice was culled after 2 minutes and the other group after 24 hours to assess the BSA in the skin upon intradermal injection. This therefore permitted, delivery directly after exposure as well as the amount remaining at 24 hours to be quantified. The DNA content and BSA content of the skin could be determined by qPCR and ELISA respectively (section 4.2.8) to assess the delivery with these optimised parameters.

#### Cavitation

The cavitation was quantified for these optimised conditions. This was determined to be between 3.5 µJ and 10.8 µJ for all mice. This is in line with the mean TASE values observed during the pressure optimisation at 1.7 MPa, which was 19.2 µJ over 5 min, which equals 7.7 µJ over 2 minutes. It also shows that as little as 3.5 µJ of TASE is sufficient for delivery of pDNA. Notably, the luminescence observed in this study was 3.9-fold higher than in the pressure optimisation study ($1.41 \times 10^6$ vs $3.62 \times 10^5$). This implies more refinement may be needed to link cavitation to delivery and expression of a DNA plasmid.

#### *In vivo* Imaging

The raw IVIS images and measured luciferase expression of the treated mice are displayed in Figure 4.16. This data shows that there was no significant difference in luminescence between intradermally injected mice and cavitation-treated mice with these optimised conditions ($1.41 \times 10^6$ p/s vs $1.12 \times 10^6$ p/s, p=0.87). The observed luminescence also shows that the cavitation-treated group has a smaller standard deviation compared to I.D. injection (GSD: 1.518 vs 2.61) as well as

a more similar and homogenous area of expression compared to injection. This shows the potential for increasing the delivery of DNA by ultrasound by increasing the treatment area; this would enable a potentially scalable delivery technology. Notably, this mean is ~3-fold higher than in the exposure time optimisation study (section 4.3.5) ($1.41x10^6$ vs $4.23x10^5$). The reason for this increase when all conditions and exposure parameters are intended to be identical, may be the inertial and non-inertial component of the cavitation. In the time optimisation study, inertial cavitation represented nearly all the cavitation detected by PCD, whereas in this study only approximately 50% of the cavitation signal detected by PCD was inertial cavitation. This showcases there may still be aspects of cavitation-mediated delivery that need to be elucidated, in particular the contribution of inertial and non-inertial cavitation.

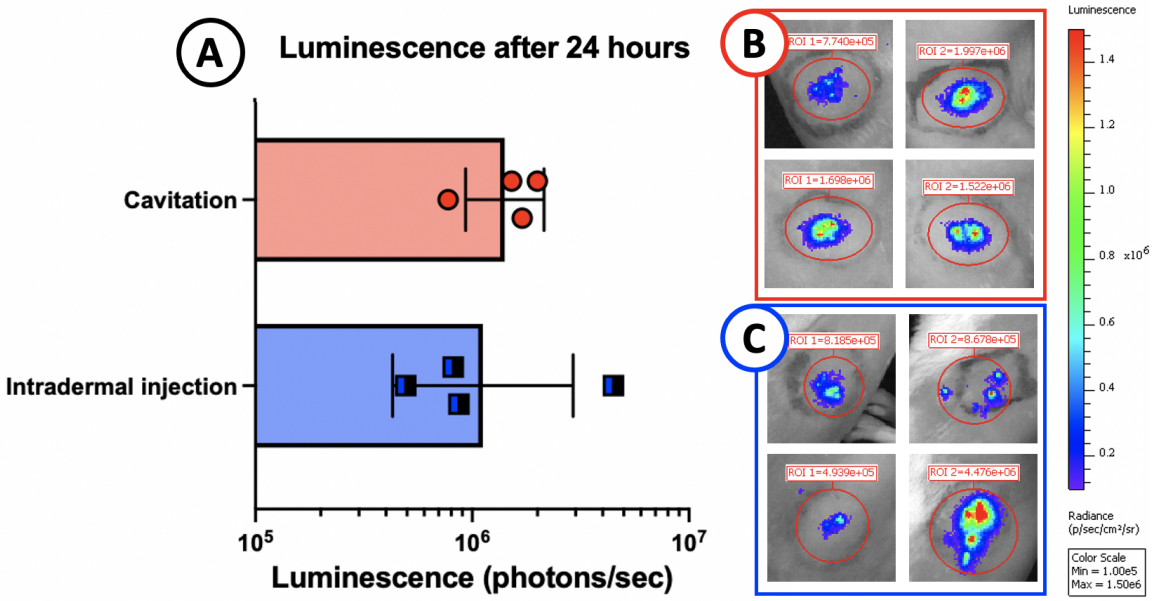



**Figure 4.16.** Panel A: Luciferase expression after 24 hours for intradermal injection of 90 µg of CMV-Luc pDNA or after application of 90 µg of CMV-Luc pDNA with ultrasound-mediated cavitation. N = 4 and the geometric mean (bar height) ×/÷ geometric standard deviation (error bars) are displayed. Significance was assessed by an unpaired t-test with Welch's correction, p>0.05. Panel B: IVIS images 24 hours after treatment for the mice treated with ultrasound-mediated cavitation. Panel C: IVIS images 24 hours after treatment for the mice intradermally injected.

### qPCR quantification of DNA copies delivered

The number of DNA copies delivered into skin was quantified by qPCR. The results show that as may be expected immediately after intradermal injection, the majority of the dose was present in the skin (92.27%). A comparatively much lower pDNA dose was delivered by ultrasound, specifically 0.08%. This implies ultrasound delivers substantially less (~513-fold, p<0.0001) than direct injection. However, after 24 hours, 0.03% of pDNA is present after ultrasound-mediated delivery and 0.18%

pDNA after intradermal injection (Figure 4.17). This also means the amount of pDNA present after ultrasound-mediated delivery decreases by only 2.7 fold. In contrast the level in I.D. injected mice decreases 1150-fold over the 24 hours post-injection. This may reflect that the majority of the dose from intradermal injection does not penetrate the cells and is degraded and cleared in the extracellular space, whereas the pDNA delivered by cavitation gets cleared at a much lower rate, perhaps indicating that a higher proportion of the dose delivered into the skin by cavitation actually achieves entry into cells. Furthermore, the finding that 0.03% of the pDNA dose is present after 24 hours is identical to the percentage dbDNA$^{TM}$ delivered, as assessed in section 2.3.2. This further highlights the reproducibility of cavitation, as a consistent amount of DNA delivery is observed two years after the original measurements with completely different reagents, different cavitation nuclei and a different ultrasound set-up, but for all treatments cavitation above the 3.5 µJ TASE threshold (16.9-28.2 µJ and 3.5-10.8 µJ).

Interestingly, after 24 hours there are very similar levels of luminescence by IVIS between the ultrasound-treated group and the intradermally injected group. This is despite a 5.6-fold difference ($p<0.01$) in DNA copy number detected ($4.29x10^9$ vs $2.41x10^{10}$) at 24 hours.

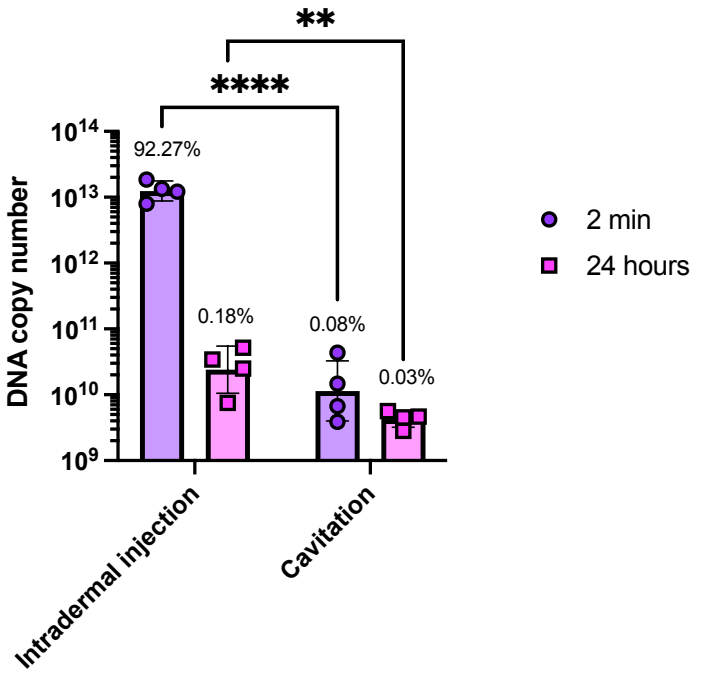



**Figure 4.17.** DNA copies present in excised skin after intradermal injection or cavitation treatment with 90 µg CMV-Luc pDNA. The results are for skin excised directly after treatment (2 min) or after 24 hours. The DNA copy number was determined by qPCR, as described in section 4.2.5. The proportion of the original dose is displayed above each column. N = 4, geometric mean (bar height) $\times/\div$ geometric standard deviation (error bars) are displayed. Significance was analysed by two-way ANOVA (time x treatment) with post-hoc tests between 2 minutes and 24 hours for each treatment method, using the Šidák correction for multiple comparisons. **** = $p<0.0001$, ** = $p<0.01$. A statistically significant effect was observed for time, treatment and their interaction ($p<0.0001$).

**ELISA quantification of BSA protein delivered**

The use of protein to form p-CaN raises the prospect of using immunogenic protein to both deliver the DNA and enhance the response against the encoded protein. To gauge the potential of this approach, the amount of protein delivered into the skin in p-CaN form should be defined. Hence, the BSA concentration in the skin was measured. Mice were either treated with cavitation and BSA 2G-U p-CaN or 100 µL of BSA 2G-U p-CaN was intradermally injected. Mice were culled at 2 minutes or after 24 hours. A BSA ELISA kit was used to quantify the BSA in the skin. The results are summarised in Figure 4.18 in BSA equivalents. As BSA p-CaN rely on crosslinking of protein, it is expected that not all the BSA in the skin can be detected by the existing and available techniques. Hence, the BSA concentration is expressed in BSA equivalent on a BSA standard curve, but the true dose is expected to be higher. The ELISA showed that as expected, the highest amount of BSA was detected directly after intradermal injection ($1.59x10^6$ ng BSA equivalent). The BSA concentration decreased approximately 5.8-fold over 24 hours to $2.76x10^5$ ng BSA equivalent. In comparison, cavitation delivered a much lower amount of BSA ($4.79x10^4$ ng BSA equivalent), but this concentration then only decreased 2-fold over 24 hours ($2.48x10^4$ ng BSA equivalent). This could imply that similar to DNA, the protein delivered by cavitation gets cleared more slowly than when it is directly injected.

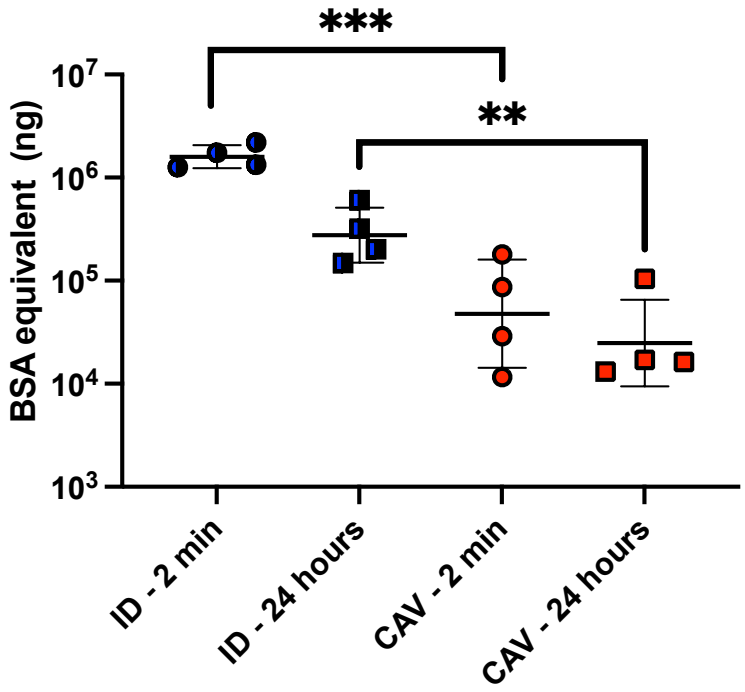



**Figure 4.18.** The BSA protein equivalent detected in murine skin 2 min and 24 hours after treatment, using an anti-BSA ELISA. Groups of 4 mice were treated with BSA 2G-U p-CaN and 90 µg CMV-Luc pDNA for 2 minutes at 1.7 MPa or intradermally injected with 100 µL BSA 2G-U p-CaN. N=4, geometric means (horizontal bar) $\times/\div$ geometric standard deviation (error bars) are displayed. A two-way ANOVA (treatment x time) was done with a post hoc test between treatments for the different timepoints using the Šidák correction for multiple comparisons. A significant effect of treatment ($p<0.001$) and time ($p<0.05$) was observed. No effect of the subject or the interaction was observed ($p>0.05$).

### 4.3.7 *In vivo* study on immunogenicity with optimised parameters

Having determined the cavitation, luminescence, DNA and BSA delivery with the optimised parameters, the system was sufficiently characterised and optimised to assess whether an immune response could be generated against a DNA vector and BSA formulated as p-CaN. 8 mice were treated with 90 µg CMV-Luc, BSA 2G-U p-CaN and ultrasound and 4 mice were intradermally injected with 90 µg CMV-Luc and 100 µL BSA 2G-U p-CaN, all mice were homologously boosted after 21 days. Luminescence was monitored and anti-Luc and anti-BSA antibody levels were measured.

#### Cavitation and IVIS

Cavitation for all mice was above 5.45 µJ for the prime and above 4.2 µJ for the boost, i.e. for both treatments levels, were above the 3.5 µJ threshold for successful delivery of the DNA vectors shown in section 4.3.6. The successful delivery was further supported by the observed luminescence, all the cavitation-treated mice and all the intradermally injected mice showed luciferase expression after 24 hours (prime: $5.01 \times 10^5$ p/s for cavitation vs $1.08 \times 10^6$ p/s for ID, boost: $2.62 \times 10^5$ p/s vs $2.86 \times 10^6$ p/s) (Figure 4.19). Whilst for the 'prime' intradermal delivery luciferase levels matched those shown in Figure 4.16 (Welch's t-test, p=1.00), the levels achieved at 'prime' (Welch's t-test, p=0.03) and 'boost' (Welch's t-test, p=0.02) with cavitation were substantially lower than in Figure 4.16. This may be related to the total TASE, which had a mean of 16.3 µJ and 24.3 µJ for the prime and boost respectively compared to 5.3 µJ in section 4.3.6. As previously noted, when too much energy is deposited, a negative effect on luciferase expression can be observed. However, the cavitation-treated groups did show improved intra-group reproducibility compared to I.D. injection (GSD prime: 1.79 vs 3.28, GSD boost: 1.45 vs 2.90), which is a reflection of the technically challenging nature of I.D. injection as a technique, and the reproducibility of the cavitation technique. As expected the luciferase expression dropped over time and 72 hours after prime treatment, it had decreased 8-fold for the cavitation group and 2.5-fold for the intradermally injected group.

#### anti-BSA ELISA

The anti-BSA antibody levels were quantified at 7, 14, 20, 28, 36 and 41 days (Figure 4.20). This showed that all mice in both the ultrasound-treated group and the intradermally injected group had high anti-BSA antibody levels after 14 days. These levels did not increase dramatically after boosting compared to day 14 and remained high for the entire duration of the *in vivo* study (two-way ANOVA (time x treatment) with post-hoc tests between 2 min and 24 hrs for each treatment, using

the Šidák correction for multiple comparisons show p>0.19 between day 14 and 20 for both cavitation and intradermal. No significant effect (p>0.8) of time or treatment was seen. Interaction (p<0.05) and mouse (p<0.0005) had a significant effect). So, despite the low levels of BSA detected in the skin after cavitation-mediated delivery (section 4.3.6), the p-CaN elicited a strong immune responses on par with direct injection.

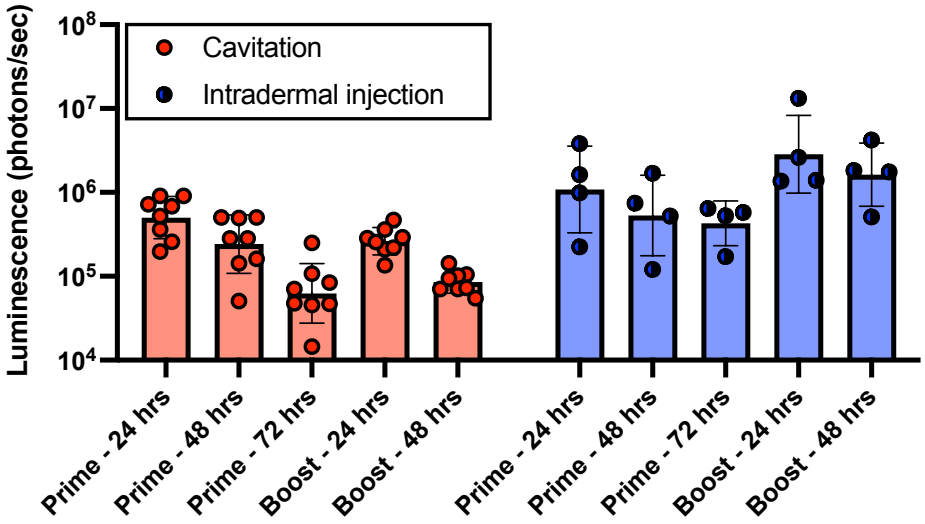



**Figure 4.19.** Luminescence 24, 48 and 72 hours after prime and 24 and 48 hours after boost. 8 mice were treated with 90 µg of CMV-Luc pDNA. It was administered by exposing the skin to a sample formula containing the DNA and BSA 2G-U p-CaN and applying ultrasound at 1.7 MPa for two minutes. For comparison, mice were injected intradermally with an equivalent dose of CMV-Luc pDNA and 100 µL BSA 2G-U p-CaN. The luminescence flux was measured as described in section 2.2.6. N=4, geometric means (bar height) ×/÷ geometric standard deviation (error bars) are displayed.

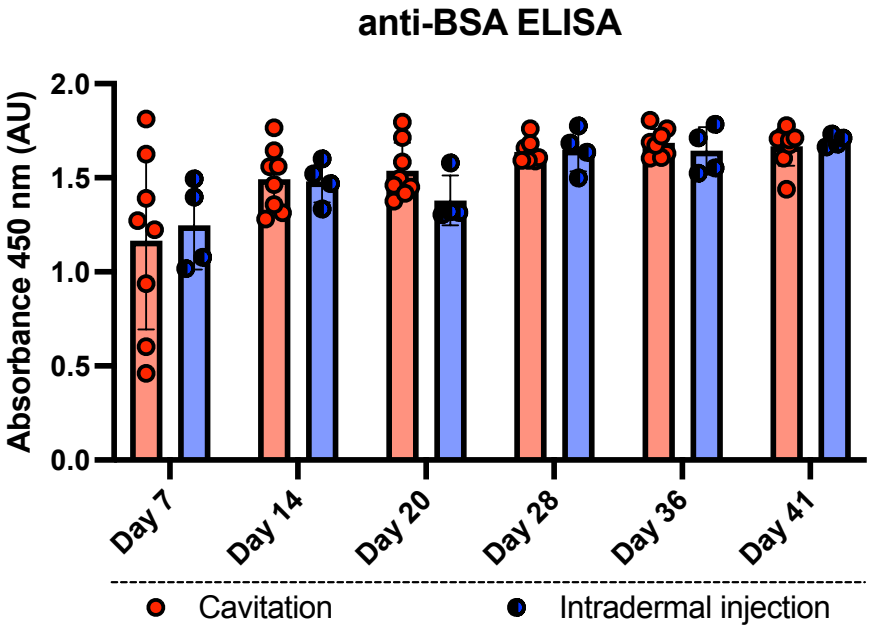



**Figure 4.20.** Levels of anti-BSA antibodies measured over time as assessed using an anti-BSA antibody ELISA. The anti-BSA antibody levels were assessed as described in section 4.2.9. 8 mice were treated with 90 µg DNA, 2G-U p-CaN and cavitation at 1.7 MPa for 2 minutes. 4 mice were intradermally injected with 100 µg 2G-U p-CaN. The mean (bar height) and standard deviation (error bars) are displayed.

**anti-Luciferase ELISA**

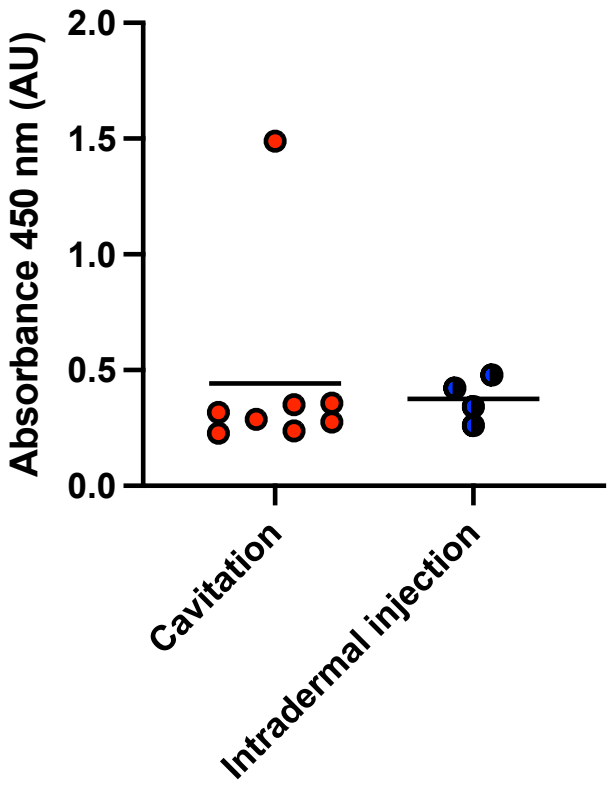



**Figure 4.21.** Antibody levels, determined by anti-Luc ELISA, as described in section 4.2.9. 8 mice were treated with 90 µg of CMV-Luc pDNA. It was administered by exposing the skin to a sample formula containing the DNA and BSA 2G-U p-CaN and applying ultrasound at 1.7 MPa for two minutes. For comparison, mice were injected intradermally with an equivalent dose of CMV-Luc pDNA and 100 µL BSA 2G-U p-CaN. N=4 and means (bar height) are displayed.

Quantification of the anti-Luc antibody levels using an anti-Luc antibody ELISA, showed that the only mouse with a strong antibody response (1.49 AU) to luciferase, which equates approx 8.4 µg/mL anti-luciferase antibody, was a cavitation-treated mouse (Figure 4.21). Upon further investigation of IVIS images and cavitation data, the only noteworthy difference between this mouse and the other ultrasound-treated mice, was the relatively high and sustained expression of luciferase after the prime and to a lesser extent after the boost. No significant difference could be observed in cavitation data compared to the other mice in the group. This could imply that the prolonged expression of the luciferase protein resulted in stronger immune responses, which agrees with previous literature where it was shown that the delivery of antigen through sustained hydrogel release increases immunogenicity [239]. This longer expression may be attributable to the transfection of a specific cell-group, which shows high retention of DNA, or a decrease in shuttling of DNA to other parts of the body or reduced degradation.

Interestingly, the I.D. injected control mice were unable to generate an immune response, despite having higher protein expression over a longer duration than the ultrasound-treated mice. This implies that expression of the antigen does not reliably predict immunogenicity against luciferase protein and poses interesting questions on the effect of ultrasound delivery and expression compared to intradermal injection. For example, the question is raised; does ultrasound-delivered CMV-Luc DNA have a lower expression threshold for immunogenicity due to an adjuvant effect or a selective delivery effect?

## 4.4 Conclusions and Discussion

The aims of this chapter were to assess, amongst other aspects, a redesigned ultrasound set-up. The need for a V2 set-up was driven by the poor reproducibility of the original set-up, the challenge of aligning the beampath and the difficulty in handling. Hence, a number of improvements were introduced, including the addition of a pulser-receiver and inversion of the ultrasound cone and transducer.

In terms of handling, the set-up showed pronounced advantages, as it was no longer necessary to lower the entire ultrasound transducer and cone onto the mouse, as the mouse could simply be placed on the transducer. To mitigate the risk of bubbles aggregating at the cone-formulation interface, the introduction of the pulser-receiver enabled checking of the beampath.

To assess whether the V2 set-up was capable of delivering DNA into skin, GMP-standard cavitation nuclei, SonoVue and nanocups, were tested. This demonstrated that nanocups in particular were able to effectively deliver DNA into murine skin, to achieve transgene expression levels similar to I.D. injection. This also showed that the sustained cavitation produced by nanocups resulted in 2.2-fold higher luminescence than the shorter cavitation produced by SonoVue. This experiment also agreed with the threshold determined in chapter 2, i.e. no expression was achieved below 1.7 μJ.

To assess the ideal parameters for treatment in the V2 set-up in combination with p-CaN, a number of optimisation were done. The expression of luciferase was used as a correlate for delivery and expression of pDNA-encoded protein. These optimisations showed that a higher amount of p-CaN in the formulation is beneficial for delivery. It was also shown that delivery and expression were very similar at 1.5 MPa and 1.7 MPa, as was the TASE at these pressures (18.23 μJ and 19.18 μJ). At a pressure of 2.0 MPa an effect detrimental to delivery was observed, as well as a much higher TASE (31.66 μJ). This may be related to damage to the skin; as greater amounts of energy are deposited, cells are damaged, and so are less able to express DNA. The ability to define a 'TASE-window' where successful delivery can be achieved without causing damage could be useful for clinical translation. No significant difference in luminescence was detected when DNA concentration was increased, although there was a slight upward trend as concentration increased. This may imply there is some limit in the amount of DNA that can be expressed or delivered by cavitation. The treatment time was assessed to determine if treatment time could be decreased to allow for better clinical translation. This showed that luminescence was highest at 2 minutes of treatment and that the TASE values directly correlated with the treatment time, as would be expected for 2G-U p-CaN which can generate

cavitation continuously for at least 10 minutes. As TASE increased, luminescence reduced and a relationship could be seen between skin damage and expression. In conclusion, optimal conditions were determined as treatment at 1.7 MPa for 2 minutes with a high concentration (>43 mg/mL) of p-CaN. The effect of DNA concentration was low, although a slight effect could be observed, it was not deemed substantial enough to warrant the extra cost associated with the use of higher levels.

The skin damage as well as the observed subsequent DNA expression provide intriguing glimpses into the underlying mechanisms of ultrasound. Typically, skin reddening would appear within 10 minutes of treatment (Figure 4.15), and be fully resolved within 24 hours (Figure 5.45). This is in line with the reported estimated time for skin resistance to recover from ultrasound-permeabilisation [240]. The reddening of the skin is an indicator of an inflammatory response. Due to the short time after treatment, it is unlikely to be the consequence of the expression of the encoded antigen, but rather a more immediate response to the physical disruption of the skin. Tezel et al. showed that ultrasound can be a potent physical adjuvant by activating langerhans cells, the predominant immune cells in the epidermis [145] and hence, it is the physical pertubation that results in the erythema of the skin. If this physical assault of the skin may have also resulted in the death of cells, the danger signals (damage associated molecular patterns – DAMPs) released by these cells may have also contributed to the observed inflammation. Overall, this erythema in my experience has resulted in subsequently better luciferase expression in the treated skin and an indication sufficient acoustic energy had been applied. Furthermore, it is known from other transcutaneous techniques that the release of danger signals by the cells and the activation of immune cells are powerful adjuvants that can enhance immune responses generated [191].

However, although a sufficient energy deposition is necessary to facilitate adequate permeability for skin penetration, a too high deposition of energy on the skin, would result in a 'dead' zone without expression of the DNA. This dead zone would typically be observed in the focus of the ultrasound beam and on occasion result in a wound that would not resolve quickly. It is speculated that on these occasions, the cavitation had a strong local destructive effect upon the cells. These regions would subsequently also not show any expression of the luciferase plasmid, as marked in Figure 4.15 by the white arrow. A lack of viable cells capable of expressing the plasmid would account for the lack of luminescence seen. In terms of translating the technique, the erythema could translate into some mild discomfort after treatment but the powerful message that pain will be specifically avoided as it would be counterproductive for successful treatment may entice more people to get vaccinated.

Once these optimal parameters were determined, two *in vivo* studies were performed. In the first study, the delivery of the BSA protein formulated as p-CaN was quantified as well as the CMV-Luc p-DNA, and the IVIS and cavitation evaluated. These were compared to intradermally injected mice. No significant difference could be observed in terms of luminescence for intradermally injected mice and cavitation-treated mice after 24 hours. Interestingly, quantification of the pDNA in the skin immediately after treatment, revealed that only 0.08% of the original dose is present in the skin after cavitation-mediated delivery compared to 92.27% of the dose after injection. The difference in delivery was also apparent after 24 hours, where a $\sim$500-fold drop in CMV-Luc pDNA copies could be observed after I.D. injection and only a 2.7-fold drop in the cavitation-treated group. The difference in pDNA copies at 24 hours between the 'ID' and 'CAV' group was significant, implying that the very low copy number delivered by cavitation is sufficient for efficient expression of the protein. Certainly in terms of photons/second per DNA copy delivered into skin, cavitation far surpasses intradermal injection. This enhanced efficiency per delivered DNA copy suggests even small improvements to cavitation-mediated delivery will produced notable changes in immune responses. Also, a surprisingly low amount of BSA protein was observed in the skin after 24 hours ($2.48 \times 10^4$ ng BSA equivalent for cavitation and $2.76 \times 10^5$ ng BSA equivalent for I.D. injection). Again, it showed that a relatively low amount of BSA was initially delivered by cavitation compared to direct injection ($4.79 \times 10^4$ vs $1.59 \times 10^6$ ng BSA equivalent.

In the second *in vivo* experiment, the immunogenic effect over time was observed for these optimised conditions by priming and boosting mice with BSA 2G-U p-CaN and CMV-Luc pDNA both by cavitation and intradermal injection. To verify delivery, the cavitation was observed and luminescence quantified after the prime and boost. This showed that intradermal injection showed higher luminescence levels for both prime and boost but the cavitation-mediated delivery showed higher consistency. Despite the low BSA delivered by cavitation compared to injection, a strong antibody response could be observed against the BSA from the BSA 2G-U p-CaN. Interestingly, only one mouse showed substantial anti-Luc antibody levels, which was treated with cavitation. The only observed difference between this mouse and other cavitation-treated mice was a prolonged expression of luciferase after the prime. However, this expression was still well below the levels observed upon intradermal injection (1.7-fold), implying that cavitation-mediated delivery delivered the DNA to a compartment that enabled an effective immune response from a low level of gene expression.

Overall, in this chapter, the new, more easy to handle ultrasound set-up was assessed and a set of parameters was identified that could effectively deliver pDNA into murine skin. In the following chapters, this V2 set-up and the optimised parameters were used to deliver different DNA constructs into the skin and assess their immunogenic potential as vaccines or adjuvants.

# Chapter 5

# Second generation DNA vaccines

## 5.1 Introduction

In Chapter 2, a first iteration of DNA vaccine vectors was assessed for their ability to initiate an immune response against their encoded antigen and antibody and cell responses were observed. It was also shown that cavitation-mediated delivery of DNA vectors could give an immune response which was strong relative to the amount of DNA actually delivered. However, the antibodies generated had lower avidity and a higher IgG1/IgG2a ratio, as well as lower overall titres, than the alternative needle and syringe delivery approach. Optimisation was therefore necessary if protective immunity was to be achieved. Three areas of potential further improvements were identified:

1. the ultrasound set-up
2. the DNA vector activity
3. the reproducibility of protein cavitation nuclei production and activity.

In chapter 4, the first of these was addressed with the successful design and deployment of a new ultrasound exposure set-up to improve reproducibility of mouse placement and ease of handling of the ultrasound equipment.

In this chapter, areas 2 and 3 are addressed. For area 2, DNA vector modification and addition was explored to help improve the immune response. Specifically, a vector enabling self-amplification of the antigen within the target cells was created to achieve a higher number of copies of antigen protein produced per DNA vector delivered, with the intention of increasing overall antibody titres. A vector, encoding self-amplification of the reporter gene luciferase was used to assess the expression-time profile of the self-replication machinery. Furthermore, three DNA vectors encoding protein ad-

juvants were designed and produced to try and generate a higher and more balanced antibody and cellular immune response, namely vectors encoding FLT3L, CD80 and Perforin.

### 5.1.1 VEEV

Recently the ability of nucleotide sequences, borrowed from viruses, to self-amplify has become of interest to researchers seeking ways to enhance the efficacy of nucleotide-based vaccines. Hence, nucleotide vaccines can now be split into two categories: self-amplifying and non-amplifying [241]. Non-amplifying nucleotide vaccines contain only the sequence of interest with the untranslated regions [242]. Self-amplifying vaccines utilise non-structural proteins borrowed from alphaviruses, including Venezuelan Equine Encephalitis Virus (VEEV) and the Semliki Forest Virus (SFV). Alphaviruses encode RNA replicase, which facilitates the amplification of their RNA genome. When used to make vaccines, cells can either be transfected directly with RNA transcripts or a plasmid DNA containing the sequence for the self-amplifying RNA transcript can be used. In the second instance, the RNA polymerase of the host is used to make an initial RNA strand [40]. These self-amplifying constructs can be delivered directly as 'naked' plasmid DNA, as RNA/LNP or as 'naked' RNA [243].

In this chapter, the focus has been on the use of sequences from Venezuelan equine encephalitis virus (VEEV) which is an alphavirus that can cause serious disease and high mortality in equines [244]. The virus consists of 4 non-structural proteins (nsP1-nsP4) and several structural proteins (capsid, E3, E2, 6K and E1). These proteins are encoded by its single-stranded plus-sense RNA genome [245]. nsP1 appears to have a role in initiation of the synthesis of the minus-RNA strand from the positive strand template, as well as capping RNA during transcription. nsP2 is necessary to synthesise the 26S subgenomic mRNA and cleave the polyprotein. nsP3 is a necessary part of the RNA synthesis process, although the details of its function have yet to be fullly defined. nsP4 is an RNA replicase, which drives production of multiple copies of positive strand RNA from the negative strand [245]. Overall, these four non-structural proteins play a crucial role in replicating the genome of VEEV, and providing multiple positive strand templates in the cytoplasm of transfected cells for high levels of encoded protein production.

As early as 1999, Ying et al. showed that intramuscular vaccination with a self-replicating RNA vaccine provided increased survival compared to a non-replicating RNA vaccine upon challenge

with an established CT26.CL25 tumour. They proposed that the induction of apoptotic cell death by replicase-containing RNA vaccines resulted in the enhanced uptake of components of these cells by antigen-presenting cells, potentially by increasing the production of 'danger signals' due to the presence of dsRNA (a well-recognised pathogen-associated molecular pattern (PAMP) and toll-like receptor agonist). Hence, it was not specifically the increase in antigen levels per-se, but the production mechanism of self-amplifying vectors that resulted in effective immunisation [246]. Another interesting discovery made by Zhang et al. was the impact of the innate immune system on the expression of the antigen from a self-amplifying RNA vector. They showed that the presence of dsRNA resulted in activation of the innate immune system, including expression of type I interferons, which suppressed the expression of the antigen. The addition of corticosteroids or the removal of dsRNA when preparing the self-replicating RNA was then able to improve expression again [247]. When utilising a DNA-launched, self-amplifying RNA, a potential risk is that the presence of dsRNA may decrease its efficacy.

Other examples of the investigation of self-amplifying vectors include needle and syringe delivery of a nanoparticle/self-replicating multi-epitope DNA vaccine construct in mice which showed higher antibody levels. An increase of 1.2-fold was observed without encapsulation in a nanoparticle and 1.3-fold increase in antibody concentration was observed upon encapsulation [248]. The delivery of two separate vectors, one encoding the replicon and a second encoding the antigen of interest showed that as little as 0.05 µg of haemagglutinin-encoding RNA and 20 µg of replicon-encoding RNA provided BALB/c mice, who were needle and syringe I.D. prime-boosted, with complete protection upon challenge with 10x lethal dose 50 (LD50) of A/California/4/2009 [249]. Indeed, Vogel et al. showed similar protection could be achieved with 1.25 µg self-amplifying RNA as with 80 µg non-amplifying RNA upon I.M. injection, based on haemagglutinination inhibition assay, viral neutralising titre and weight 3 days post-infection [250]. In light of the COVID-19 pandemic, McKay et al. showed significantly higher antibody levels (>$10^6$ ng/mL) could be elicited in mice upon prime and boosting with 10 µg of self-amplifying RNA/LNP encoding the SARS-CoV-2 spike protein compared to 10 µg non-amplifying DNA vector encoding the same protein delivered by intramuscular injection (approximately $10^5$) with p=0.0036 [251]. This technology has even reached a phase 1 clinical trial, where it was shown to be safe at the low dose levels tested when primed and then boosted 4 weeks later with 5 µg self-amplifying RNA vaccine, but it only achieved 87% conversion based on binding antibody by immunoblot or 48% based on neutralisating antibody after 6 weeks post-prime, (i.e. a level which may have been deemed sufficient at the start of the pandemic, but not now there are so

many vaccines already available) [252].

The literature seems to support the efficacy of self-amplifying vectors to boost immunity, although the precise nature of the increased efficacy could be either attributed to the increase in antigen production or an adjuvant effect by the generation of dsRNA and virus-associated proteins. In this chapter, the behaviour of a DNA vector encoding self-amplifying RNA, based on VEEV, is investigated via a reporter gene and its ability to generate a humoral immune response (Figure 5.1).

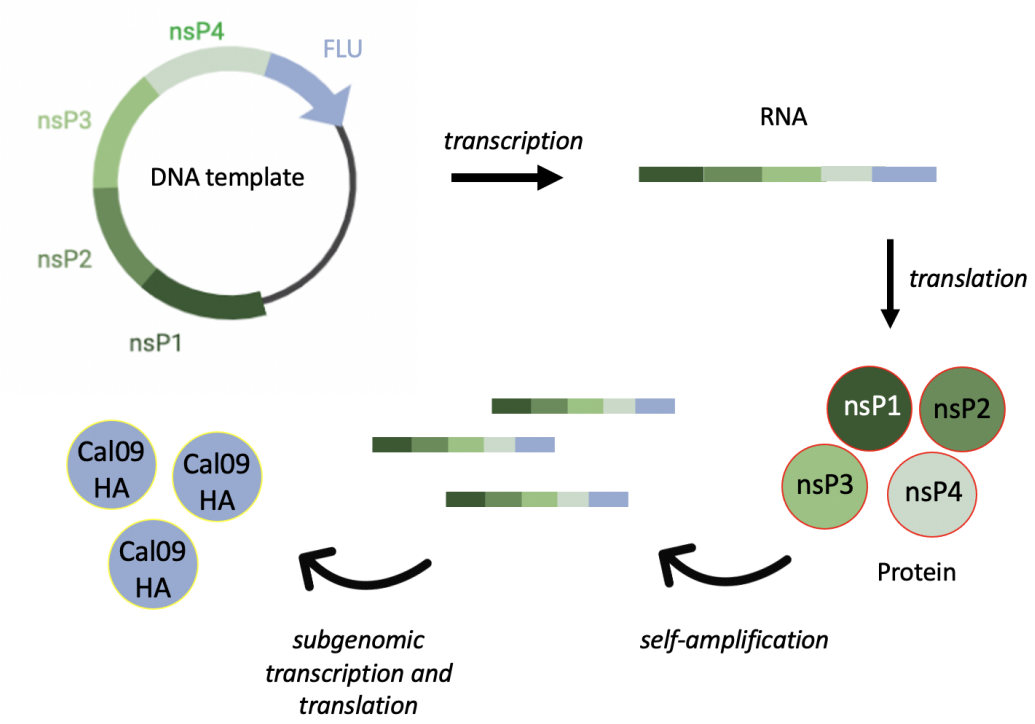



**Figure 5.1.** Schematic of the amplification process of a DNA-launched, self-replicating RNA for the amplification of Cal09 HA based on the non-structural proteins (nsP1-nsP4) derived from VEEV.

### 5.1.2 FLT3L

The potential of FLT3L as an adjuvant has already been discussed in section 3.1. In short, FLT3L can induce the mobilisation of haemopoietic progenitors and stem cells [219] and is necessary for the activation of dendritic cells and stimulation to expand natural killer cells upon viral infection [223]. In vaccination, FLT3L-expressing plasmid has been tested in combination with a antigen-encoding plasmid vector and microneedles in mice. This addition increased survival from 40% to 70% in mice [226]. Other successful studies have included combining a FLT3L-encoding plasmid with a HPV16 E6/E7 plasmid vaccine [227, 228]. It has even been tested in a clinical trial for HPV. The vaccine encoding both the antigen and FLT3L resulted in complete regression in 7/9 patients [229].

### 5.1.3 CD80

CD80 is expressed by antigen-presenting cells, which include dendritic cells, macrophages and B cells. It can interact with the CD28 receptor on T cells, which is a costimulatory signal that activates T cells [253]. It was hoped such direct interaction with T cells, would allow the addition of CD80 to drive a more balanced IgG1/IgG2a immune response.

In the context of vaccination, the CD80/86-CD28 pathway has already been identified as having a crucial role in the generation of an anti-tumour response after neoantigen vaccination by Yamauchi et al. [254]. Multiple vaccine candidates have also been shown to result in CD80 expression, including an oral microparticulate vaccine for murine prostate cancer [255], a pseudorabies virus vaccine in mice [256] and an intranasal vaccine against vesceral leishmaniasis in mice [257].

A CD80-encoding plasmid has been shown to improve the T cell responses to the cancer DNA vaccine candidate STEAP1. The treatment was intramuscularly applied using the CELLECTRA 3P device and resulted in significantly more antigen-specific cells, which expressed IFN-$\gamma$, TNF$\alpha$ and CD107a in mice [258]. Thorne et al. showed in the same paper that the addition of CD80 plasmid to STEAP1 resulted in significantly reduced tumour burden compared to the STEAP1 vaccine alone ($p<0.001$ on day 20) [258]. Similarly, Maue et al. showed that the addition of plasmid encoding CD80 and CD86 (a closely related molecule) to a DNA vaccine against bovine tuberculosis resulted in significantly ($p<0.05$) reduced lymph node weight in cows upon challenge [259].

Overall, the effect of the addition of CD80 is a stronger T cell response against vaccine encoded peptide/proteins. As cellular immunity plays a crucial role in viral clearance, combining CD80 with an antigen-encoding plasmid may improve protective immunity achieved by the vaccine.

### 5.1.4 Perforin

Perforin is a pore-forming protein, which bears similarities to the complement membrane attack complex. It is excreted by cytotoxic T lymphocytes and natural killer cells. These cells release their toxic cargo, including perforin, upon conjugating to a target cell. The perforin forms large pores in the membrane that allow the entry of other granzymes, which initiate apoptosis within and the release of DAMPs from, the target cell [260].

Gargett et al. [261] speculated that the induction of necrosis would increase the immunogenicity of DNA vaccines. Perforin was proposed as a candidate capable of inducing necrosis. The necrotic capability of perforin is supported by a study by Wijesunda et al., which showed that after transfection of HEK293T cells with a truncated perforin, signs of necrotic/lytic cell death were evident. This truncated perforin was created by deletion of the 12 C-terminal basepairs (G(D/E)PPGNRSGAVWstop). Dendritic cells from C57BL/6 mice exposed to this lytic cell debris then upregulate CD80 [262, 263], a factor associated with dendritic cell maturation as mentioned above (section 5.1.3), further emphasising the value of necrotic signals in stimulating the immune response. Gargett et al. were able to show that the addition of truncated perforin under the SV40 promoter to the DNA vector with the HIV antigen GAG under the CMV promoter resulted in an increase of $CD8^+$ TNF$\alpha$+ IFN-$\gamma$+ cells ($p=0.03$) compared with the same CMV GAG DNA vector without perforin, as well as reduced Eco-HIV (a chimeric HIV) viral load in the spleen and peripheral blood upon challenge. An interesting observation was that the perforin had to be on a weaker promoter than the antigen. It was postulated that sufficient expression of the antigen needed to occur prior to the effects of perforin [261]. In the studies reported in this chapter, for the sake of simplicity the perforin gene is delivered on a separate DNA vector to the haemagglutinin (HA) antigen. Hence, the assumption is that the perforin and antigen-expression will not necessarily co-locate and different expression strength should have a lesser impact. Studies on hepatitis C Virus, have also shown that the addition of the perforin gene to a NS3 (non-structural protein 3) DNA vaccine, derived from Hepatitis C Virus, resulted in a stronger cellular immune response in both mice and pigs [264, 265]. The strong precedent in different species makes perforin an interesting DNA adjuvant candidate to test in the context of cavitation-mediated delivery.

### 5.1.5 p-CaN

The progression from inert polymer-based to potentially immune-modulatory protein-based cavitation nuclei (p-CaN) is described in Chapter 3. As the work in this thesis aligned with the development process of the p-CaN, it was possible for the work here to benefit from improvements to the scale-up and batch-production process of p-CaN. This therefore helped address area 3 for potential improvement and so in this chapter a new iteration of p-CaN are assessed, denoted '3G-H'. These p-CaN are expected to be structurally similar to 2G-U p-CaN but are produced using hydrodynamic shearing instead of an ultrasound horn. Hydrodynamic shearing provides the advantage that it is a much more reproducible and scalable production process [266]. The cavitation behaviour of these p-CaN and their DNA delivery potential is investigated in this chapter to merit their utility for future

cavitation studies with p-CaN.

Overall, the aims of this chapter are:

- Validate the cavitation of 3G-H p-CaN
- Investigate the behaviour and potential advantages of a self-amplifying vector with a reporter gene and an immunogenic self-amplifying DNA construct.
- Assess the potential of DNA vectors encoding FLT3L, CD80 or Perforin to improve the immunogenicity of the haemagglutinin-encoding CMV-Cal09 vector.

## 5.2 Materials and Methods

### 5.2.1 Cloning

The following genetic elements are used in this chapter, Table 5.1, and the following genetic constructs are referenced, Table 5.2. The plasmid maps of all plasmids used in this chapter are available in Appendix A.

**Table 5.1.** Overview of all elements of the genetic constructs described in this chapter.

| Name | Category | Function and origin |
|---|---|---|
| CMV | Promoter | The human cytomegalovirus (CMV) promoter used to drive gene expression – characterised as strong. Sequence courtesy of Touchlight Genetics Ltd. |
| FLT3L | Immune stimulator | Fms-like tyrosine kinase 3 ligand is a hemapoietic progenitor growth factor, which induces B cell maturation, natural killer cells and dendritic cells. [219]. Sequence is courtesy of Touchlight Genetics Ltd. |
| CD80 | Immune stimulator | Enhances T cell responses, showing promise as an adjuvant [258], sequence derived from GenBank accession number: NM_001359898. |
| Perforin | Immune stimulator | Pore-forming protein, which results in enhanced immunogenicity when used as an adjuvant [267]. The last 12 bp deleted, based on the work of Gargett et al. [261]. Sequence derived from GenBank accession number: XM_006513370 [248-1873]. |
| Fc | Stabilising factor | The Fc-component of murine IgG2a, increases half-life of the protein [268]. Sequence is courtesy of Touchlight Genetics Ltd. |
| Luc | Reporter protein | Luciferase reporter gene (luc2) derived from fireflies. Allows for *in vivo* imaging of protein expression, available from Promega (USA) (#E1310) |

| | | |
|---|---|---|
| Cal09 | Antigen | Haemagglutinin from the influenza strain H1N1 Cal/09. Sequence is courtesy of Touchlight Genetics Ltd. |
| VEEV DREP | Four non-structural proteins | DNA-launched, self-replicating RNA platform, derived from the Venezuelan Equine Encephalitis Virus. This allows for the self-amplification of the RNA produced from the DNA strand. Sequence is courtesy of Touchlight Genetics Ltd., based on GenBank: MH891622.1 |
| eGFP | Fluorescent reporter protein | Enhanced Green Fluorescent Protein. Sequence is courtesy of Touchlight Genetics Ltd. |
| SV40 late poly(A) region | PolyA tail region | PolyA tail. Sequence is courtesy of Touchlight Genetics Ltd. |
| kan | Resistance gene | Kanamycin resistance gene, necessary for selection of *E. coli* colonies. Sequence is courtesy of Touchlight Genetics Ltd. |
| amp | Resistance gene | Ampicillin resistance gene, necessary for selection of *E. coli* colonies, part of the pcDNA™ 3.1 vector by ThermoFisher. |
| hygro | Resistance gene | Hygromycin resistance gene, part of the pGL4.50 vector by Promega (USA). |
| pGL4.50 | Vector backbone | A mammalian expression vector, available from Promega (USA). |
| pcDNA™ 3.1 | Vector backbone | A mammalian expression vector, which is commercially available from ThermoFisher (USA). |
| proTLx-κ | Vector backbone | A cloning vector compatible with the doggybone DNA production, courtesy of Touchlight Genetics Ltd. |

**Table 5.2.** Overview of all plasmids used as templates or created in this chapter. It lists the name, promoter, backbone and transgene of each construct

| Plasmid name | Backbone | Promoter | Transgene |
|---|---|---|---|
| proTLx-κ CMV-Flt3l-Fc | proTLx-κ | CMV | Flt3l-Fc |
| proTLx-κ CMV-CD80-Fc | proTLx-κ | CMV | CD80-Fc |
| proTLx-κ CMV-Perforin | proTLx-κ | CMV | Perforin |
| proTLx-κ VEEV DREP Luc | proTLx-κ | CMV | VEEV DREP (nsP1-4), Luc2 |
| proTLx-κ VEEV DREP Cal09 | proTLx-κ | CMV | VEEV DREP (nsP1-4), Cal09 |
| proTLx-κ VEEV DREP eGFP | proTLx-κ | CMV | VEEV DREP (nsP1-4), eGFP |
| proTLx-κ B5X4 Cal09 | proTLx-κ | CMV | Cal09 |
| proTLx-κ Flt3l-Flex-C Ag | proTLx-κ | CMV | Flt3l, hepatitis 3 core protein |
| proTLx-κ N3X2 Mouse Chimaera | proTLx-κ | CMV | Humira (anti-TNFα) |
| pGL4.50[*luc2*/CMV/Hygro] Vector (CMV-Luc) (#E1310) | pGL4.50 | CMV | Luc2 |

### Plasmid templates

The plasmids proTLx-κ VEEV DREP eGFP, proTLx-κ B5X4 Cal09 HA, proTLx-κ Flt3L-Flex-C Ag, proTLx-κ N3X2 Mouse Chimaera Humira Heavy were kindly donated by Touchlight Genetics Ltd. pGL4.50[*luc2*/CMV/Hygro] vector was purchased from Promega (USA). The gBlocks for cloning CD80 and Perforin were purchased from Integrated DNA Technologies (IDT) (USA).

### PCR with Q5 polymerase

All primers were ordered from IDT and diluted to 10 µM. All PCR mixtures were made up with 122 µL Q5® High-Fidelity 2X Master Mix (M0491S, NEB), 11.2 µL of each primer, 1 µL template DNA and 78.6 µL nuclease-free water and aliquoted over 8 PCR-compatible tubes. For colony PCR, a sterile pipette tip was used to pick a colony. This tip was swirled in 10 µL MilliQ water. 1 µL of this solution was used as template DNA.

### Agarose gels

PCR products and digestion products were analysed on a 1% agarose-TAE gel (TAE buffer, B49, ThermoFisher, USA) stained with SYBR Safe DNA gel stain (S33102, ThermoFisher Scientific). The gel was run at 70 V for 60 min. 10 µL of a 1 kb plus DNA ladder (N3200S, New England Biolabs (NEB), USA) was used as a size-reference. 6x purple DNA loading dye (B7024S, NEB) was added

to the DNA sample prior to loading.

**Ligation**

The DNA fragments were ligated with Gibson Assembly® Master Mix (E2611L, NEB), according to manufacturer's instructions, with a 1:2 ratio for vector:insert and increasing the incubation time to 60 min at 50 ℃.

**Digestion**

DpnI is a restriction enzyme which only cleaves when its recognition site is methylated, it is therefore often added to PCR products to degrade the methylated DNA template, isolated from bacteria. For digestion with DpnI (R0176S, NEB), 25 µL PCR mix was combined with 5 µL 10x CutSmart buffer (NEB), 1 µL DpnI (NEB) and topped up to 50 µL with MilliQ water. This was incubated at 37 ºC for 15 minutes.

For digestion with SphI-HF (R3182S, NEB), 1 µg plasmid DNA was mixed with 5 µL 10x CutSmart buffer (NEB), 1 µL SphI-HF (NEB) and topped up to 50 µL with MilliQ water. This was incubated at 37 ºC for 15 minutes.

**Sequencing**

Purified plasmids were sent for Sanger sequencing to Source Bioscience (UK), using custom primers or the stock primers CMVF_pCDNA3 (5'- CAA CGG GAC TTT CCA AAA TG – 3') or EGFP C R (5' - GTT CAG GGG GAG GTG TG – 3') (See Table 5.3).

**Cell line transformation, culture and glycerol stocks**

NEB® 5-alpha Competent E. coli (High Efficiency) (C2987H, NEB) cells were transformed as described in section 2.2.10. The cells were cultured as described in section 2.2.10. Glycerol stocks were prepared as described in section 2.2.10.

**Table 5.3.** Overview of all custom primers used for PCR in this chapter. The 5' and 3' termini are indicated. The sequences which do not overlap with their template are highlighted in blue.

| Primer name | Sequence (5'-3') |
|---|---|
| JKH_031 | 5'- TCTCGTCGATGGCATTCTG - 3' |
| JKH_041 | 5'- ATACAGCAGCAATTGGCAAGCTG - 3' |
| JKH_042 | 5'- GGTGCGATACTTGGCGGACTAG - 3' |
| JKH_043 | 5'- GCCAAGTATCGCACCATGAAGGCCATCCTGGTGGTG - 3' |
| JKH_045 | 5'- CAATTGCTGCTGTATTCAGATGCAGATCCGGCACTG- 3' |
| JKH_050 | 5'- GAATTCCAGACATGATAAGATAC- 3' |
| JKH_051_alt | 5'- GAATTCCAGACATGATAAGATACATTGATGA- 3' |
| JKH_057_alt | 5'- GCCAAGACAGCCCAGAGGCCCCAC - 3' |
| JKH_058 | 5'- TCTTATCATGTCTGGAATTCTCATCACTTGCCGGGGGTTC - 3' |
| JKH_059 | 5'- ACCGTCAGAAGCTTGCCACCATGGACGCCATGAAGAGGGG - 3' |
| JKH_060 | 5'- GGCCTCTGGGCTGTCTTGGCCTTGGCTCAG- 3' |
| JKH_073 | 5'- CGTCTTCCTTCCCAGAGGCCCCACCATC- 3' |
| JKH_074 | 5'- TCTTATCATGTCTGGAATTCTCATCACTTGCCGGGGGTTC - 3' |
| JKH_083 | 5'- TAGGACTACGAGATAGACAG - 3' |
| JKH_092 | 5'- GCCTTATTTCTGTGGAGGGTT - 3' |
| JKH_094 | 5'- CCATTGCCGGCTTTATCGAG - 3' |
| JKH_096 | 5'- CCATCCAGTTTACTTTGCAGG - 3' |
| JKH_106 | 5'- CACTCCTCTATCGTGGCAGT - 3' |
| JKH_111 | 5'- ATGATACACTTGATGTACTGCCAAG - 3' |
| JKH_114 | 5'- GATTGGAGAGTGGGAAAAGTAACAA - 3' |
| JKH_117 | 5'- GGTAGAGAAGTCAGCTTTGATGG - 3' |
| HW_006 | 5'- GCCAAGTATCGCACCATGGAAGATGCCAAAAACATT- 3' |
| HW_007 | 5'- CAATTGCTGCTGTATTTACACGGCGATCTTGCCG - 3' |
| HW_010 | 5'- TCATCATCATGGATAGCAAG - 3' |
| HW_012 | 5'- AAGAGCTACCAACTCTTTTTCCG - 3' |
| HW_013 | 5'- AGTCTGAGAACACGACCAGC - 3' |
| HW_014 | 5'- GCTGGTCGTGTTCTCAGACT - 3' |
| EGFP_C_R | 5'- GTT CAG GGG GAG GTG TG - 3' |
| CMVF_pCDNA3 | 5'- CAA CGG GAC TTT CCA AAA TG - 3' |

### 5.2.2 Plasmid purification

For large-scale isolation of DNA for use in *in vivo* studies, overnight cultures were grown up from glycerol stocks stored at -80 ºC. Overnight cultures were grown in 5 mL of sterile liquid LB broth (luria low salt) (L3397, Sigma) or LB Broth, Vegitone (28713, Sigma) with 100 µg/mL ampicillin (A9393-5G, Sigma) or 50 µg/mL kanamycin (K4000-5G, Sigma). The following day, a starter culture was prepared by diluting 5 µL of overnight culture in 5 mL fresh liquid LB broth, Vegitone, with the appropriate antibiotic. After four hours of incubation, the 5 mL of starter culture was added to 350-400 mL of LB broth with the appropriate antibiotic in a 1L Erlenmeyer. For mega- and giga-preparations, 3x1L flasks were grown at a time overnight. All cells were cultured at 37 ºC at 220 rpm in a SI-300R (Medline Scientific™) shaking incubator.

1 L of cell broth was used for mega-preparations, as described in section 3.2.1 and 2 L of cell broth was used for giga-preparations, as described in section 4.2.3.

### 5.2.3 3G-H p-CaN

3G-H p-CaN were formulated and produced by Dr. Brian Lyons and comprised of a core of 50% hexane and 50% cyclohexane. These p-CaN are produced via hydrodynamic shearing instead of ultrasonic horn and freeze-drying.

### 5.2.4 Enzyme-linked immune absorbent spot (ELISpot)

An ELISpot was performed as described in section 2.2.12. The cell number was increased to 100,000 splenocytes/well. Futhermore, concanavalin A (L7647-25MG, Sigma) was prepared by dissolving the powder to 1 µg/µL in PBS and dissolving this 1:10 in RPMI-1640+10% FBS (A1049101, 10270106, ThermoFisher). The haemagglutinin stock was similarly diluted 1:10 in RPMI-1640+10% FBS. PBS was diluted 1:10 in RPMI-1640+10% FBS media to be used as a negative control.

### 5.2.5 ELISA

Antibodies from serum samples were analysed by ELISA, as described in section 2.2.11 except the secondary anti-mouse IgG was replaced by the secondary antibody Goat Anti-Mouse IgG H&L (HRP) (ab6789,Abcam) at 1:20,000 and protein-free blocking buffer (37572, ThermoFisher Scientific) was used.

For titring, serum samples were diluted 100-fold and subsequently diluted two-fold until the absorbance from the ELISA dropped below the background threshold. The threshold was defined as the last dilution with a signal 3 times the standard deviation above the signal of control serum from an untreated mouse.

Isotyping was done as described in section 2.2.11, replacing the 10%FBS-PBS blocking buffer with 100 µL/well protein-free protein buffer.

Avidity was assessed, as described in section 2.2.11, except the concentrations range was changed. Sodium thiocynate (NaSCN) was added at increasing concentrations: 0 M, 0.333 M, 0.667 M, 1.0 M, 1.333 M, 1.667 M, 2.0 M, 3.0 M NaSCN.

### 5.2.6 Histochemical staining with haematoxylin and eosin stain

In order to obtain sections of mouse skin, mice were culled 24 hours after treatment and the treated skin harvested. The skin was immediately placed in a 10% formalin solution, neutral buffered (HT501128, Sigma) for fixing and transferred to 70% ethanol after 24 hours. The skin was subsequently dehydrated and penetrated by paraffin overnight using an Excelsior AS (Thermo Scientific). The wax-penetrated skin was then embedded in a paraffin block and left to set.

Sections of 4 µm were cut with a HM 355 S rotary microtome (Epredia$^{TM}$, USA). The slices were floated and attached to microscope slides. This was left to cool and stained after 2 days with haematoxylin and eosin. To stain the sections, the slides were submerged twice for 5 minutes in histoclear, then twice in absolute ethanol for 3 minutes, 90% ethanol for 1 minute, 70% ethanol for 1 minute and then washed in tap water to rehydrate.

Then the slides were rinsed in water for 4 minutes. The slides were then stained with haematoxylin (Hematoxylin Solution, Harris Modified, HHS-16, Merck) for 3 minutes. The slides were again rinsed in tap water for 4 minutes and rinsed with water. The samples were then differentiated with 1% acid alcohol (1 mL hydrochloric acid in 100 mL 70% ethanol) and washed in tap water for 4 minutes and rinsed in water. Scotts' Water (2% $NaHCO_3$) was used for 30 seconds to blue the haematoxylin stain. This was then rinsed in tap water again. The slides were then stained with eosin stain (1 g Eosin Y disodium salt, E-6003, Sigma in 100 mL 70% ethanol) for 5 minutes. Any excess eosin was removed by rinsing the slides in tap water.

To dehydrate the samples, the slides were submerged in 70% ethanol for 30 seconds, 90% ethanol for 30 seconds, absolute ethanol for 1 minute, a second time in absolute ethanol for 2 minutes, histoclear for 5 minutes and a second time in histoclear for 5 minutes. The slides were then mounted using VectaMount Mounting Medium (H-5000).

The slides were imaged by light microscope (Leica DM500, Leica Microsystems).

### 5.2.7 Statistics

Statistics were done as described in section 2.2.4. For DNA dose a linear regression was fit and a 95% confidence interval, p-value and slope determined. A two-way ANOVA (treatment x time) was done with a Tukey post hoc test between treatments for the different timepoints.

### 5.2.8 *In vivo* protocol for the optimisation of pressure and DNA dose with 3G-H p-CaN

#### Pressure optimisation

To assess whether p-CaN produced by hydrodynamic shearing behaved similarly to those made with an ultrasound horn and could successfully deliver DNA, 3G-H p-CaN were prepared, as described in section 5.2.3. Using the ultrasound set-up described in section 4.2.1, the effect of pressure amplitude was assessed. The 3G-H p-CaN were mixed with 90 µg in-house produced CMV-Luc pDNA (pGL4.50[luc2/CMV/Hygro] Vector (#E1310, Promega, USA), as described in section 5.2.2.

12 mice were treated with ultrasound in groups of 4. Each mouse was treated with a 3G-H p-CaN/DNA formulation and ultrasound for 2 minutes at a scale of pressure amplitudes. 5 mice were also intradermally injected with 90 µg CMV-Luc pDNA in their flank. Three pressures were assessed, namely 0.8 MPa, 1.2 MPa and 1.7 MPa. After 24 hours, the mice were imaged by IVIS and luminescence quantified, as described in section 2.2.6. The treated skin was harvested and the DNA content analysed by qPCR, as described in section 4.2.5.

#### DNA dose optimisation

Based on luminescence the optimal pressure was chosen. The DNA dose was then varied and two groups of 4 mice were treated with 3G-H p-CaN made from bovine serum albumin (BSA) and ultrasound. Using the set-up described in section 4.2.1, mice were treated for 2 minutes at 1.7 MPa with 20 µg or 142 µg of CMV-Luc pDNA.

After 24 hours, the mice were imaged by IVIS and luminescence quantified, as described in section 2.2.6. The treated skin was harvested and the DNA content analysed by qPCR, as described in section 4.2.5. The amount of BSA p-CaN delivered into the skin was assessed by measuring the BSA protein content in the skin by ELISA using a BSA ELISA kit (abx150325, Abbexa, UK). A standard curve of BSA protein was used, so the concentration determined is in BSA equivalent. The skin was homogenised as described in section 2.2.9 and diluted four-fold in 0.01 mol/L PBS.

### 5.2.9 *In vivo* protocol for the evaluation of a self-amplifying reporter plasmid

Two *in vivo* experiments were conducted to assess the expression pattern of a self-amplifying vector. In the first experiment, mice were intradermally injected and in the second experiment, the vectors were delivered by cavitation.

#### Intradermal injection

Two groups of 4 mice were intradermally injected with 5 µg CMV-Luc or a DNA copy-matched amount (9.4 µg) of CMV-VEEV-Luc. The mice were then imaged by IVIS, as described in section 2.2.6 on day 1, 3, 5, 7, 10, 14 and finally day 41.

#### Cavitation-mediated delivery

Three groups of mice were treated for 2 min at 1.7 MPa with BSA 2G-U p-CaN, cavitation and DNA, with the set-up as described in section 2.2.1 as summarised in Table 5.4. The mice were subsequently imaged by IVIS, as described in section 2.2.6 after 1, 2, 3, 8 and 15 days.

**Table 5.4.** Overview of group size, the DNA and the DNA quantity used to evaluate the expression of CMV-VEEV-Luc compared to CMV-Luc upon cavitation-mediated delivery of the DNA vectors

| Group size | DNA vector | Quantity | Copy- or dose-matched |
|---|---|---|---|
| 4 | CMV-VEEV-Luc | 142 µg | dose-matched |
| 3 | CMV-VEEV-Luc | 267 µg | copy-matched |
| 4 | CMV-Luc | 142 µg | - |

### 5.2.10 *In vivo* protocol for the evaluation of a self-amplifying immunogenic vector

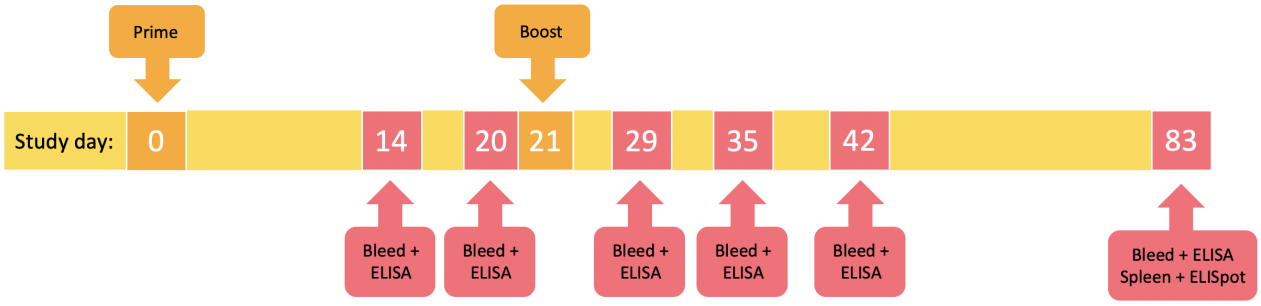



**Figure 5.2.** Summary of the treatment and blood and spleen sampling, as well as subsequent ELISA and ELISpot timeline for the *in vivo* to assess the protection provided by DNA vaccines that are delivered by intradermal injection or by cavitation.

To assess whether a self-amplifying immunogenic vector was able to elicit an immune response, groups of four mice were intradermally injected with 142 µg CMV-Cal09 (non-amplifying) plasmid or 380 µg CMV-VEEV-Cal09 (self-amplifying) plasmid. Both plasmids encode the HA1(A/California/07/2009) (H1N1) haemagglutinin antigen (Cal09). The plasmids were copy-matched to correct for their different sizes and mice were boosted homologously after 21 days. Regular bleeds were taken as described in section 2.2.7 on day 14, 20, 29, 35, 42 and day 83 and as visualised in Figure 5.2.

### 5.2.11 *In vivo* protocol for the evaluation of the second generation DNA adjuvant vectors

#### Intradermal injection

To evaluate the different DNA vaccines and adjuvants, 4 groups of mice were dosed by intradermal injection, as summarised in Table 5.5.

**Table 5.5.** Overview of the treatment to evaluate different DNA vaccines and adjuvants upon I.D. injection.

| Group size | DNA vector | DNA adjuvant | Administration route |
|---|---|---|---|
| 4 | 142 µg CMV-Cal09 | - | Intradermal injection |
| 4 | 142 µg CMV-Cal09 | 142 µg CMV-Flt3l-Fc | Intradermal injection |
| 4 | 142 µg CMV-Cal09 | 142 µg CMV-CD80-Fc | Intradermal injection |
| 4 | 142 µg CMV-Cal09 | 142 µg CMV-Perforin | Intradermal injection |

For intradermal injection, the antigen DNA vector and if relevant, the adjuvant DNA vector, were mixed prior to intradermal injection.

The mice were homologously boosted after 21 days. Regular bleeds were taken as described in section 2.2.7 on day 14, 20, 29, 35, 42 and day 83. Spleens were harvested at 83 days for ELISpot assays, as visualised in Figure 5.2.

**Cavitation-mediated delivery**

Mice were treated with ultrasound in combination with BSA 3G-H p-CaN. For cavitation-treated mice, a solution was prepared consisting of 76.6% p-CaN and 23.4% DNA and MilliQ water. This resulted in the doses as described in Table 5.6. Mice were prepared as described in section 2.2.8. Treatment was performed by placing the mice in the set-up, as described in section 4.2.1. The mice were treated at 1.7 MPa for 2 minutes. Skin disruptions were recorded.

The mice were homologously boosted after 21 days. Regular bleeds were taken as described in section 2.2.7 on day 14, 20, 29, 35 and 42, as visualised in Figure 5.2. A terminal bleed was taken on day 83, as well as spleens harvested for ELISpot assays.

**Table 5.6.** Overview of the treatment to evaluate different DNA vaccines and adjuvants upon cavitation-mediated delivery

| Group size | DNA vector | DNA adjuvant | Administration route |
|---|---|---|---|
| 4 | 142 µg CMV-Cal09 | - | Cavitation |
| 4 | 142 µg CMV-Cal09 | 142 µg CMV-Flt3l-Fc | Cavitation |
| 4 | 142 µg CMV-Cal09 | 142 µg CMV-CD80-Fc | Cavitation |
| 4 | 142 µg CMV-Cal09 | 142 µg CMV-Perforin | Cavitation |

### 5.2.12 *In vivo* protocol to assess expression and immunogenicity with optimised parameters and an adjuvant

Two groups of 6 mice were treated either with cavitation or were intradermally injected with DNA. The mice treated with cavitation were exposed to ultrasound at 1.7 MPa in combination with 2G-U p-CaN and 90 µg CMV-Luc pDNA and 90 µg CMV-Perforin. Mice were prepared as described in section 2.2.8. Treatment was performed by placing the mice in the set-up, as described in section 4.2.1. The mice were treated at 1.7 MPa for 2 minutes. Skin disruptions were recorded.

After 24 hours, the mice were imaged and two mice from each group were culled and the treated area harvested. These skin samples were then fixed, as described in section 5.2.6.

The remaining groups of four mice were boosted after 21 days and imaged after 24 hours. Regular bleeds were taken as described in section 2.2.7 on day 14, 20, 28, 35 and 42 (Figure 5.3).

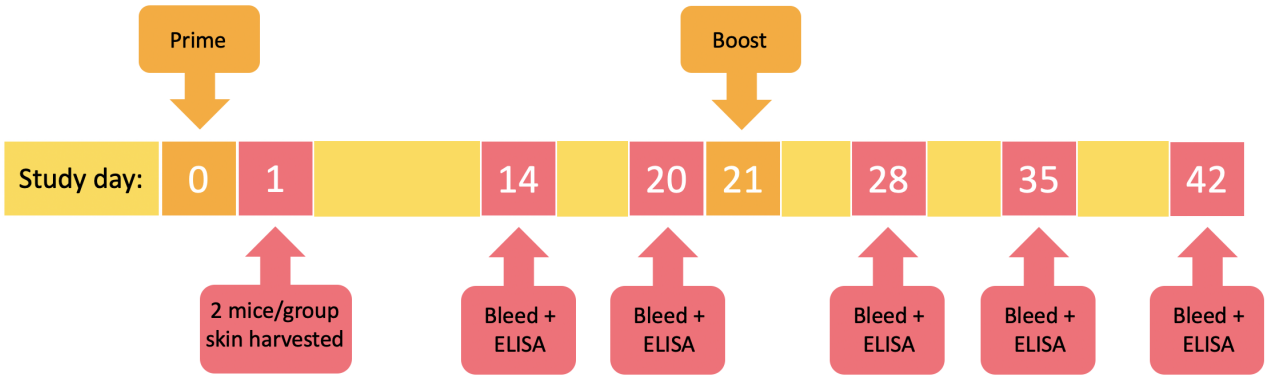



**Figure 5.3.** Summary of the treatment, skin harvesting and blood sampling, as well as subsequent ELISA timeline for the *in vivo* to assess the expression and immunogenicity with optimised parameters and an adjuvant.

## 5.3 Results

### 5.3.1 *In vivo* for the optimisation of pressure and DNA dose with BSA 3G-H p-CaN

A more scalable production method for p-CaN production was developed (utilising high-dynamic sheering meaning the resulting p-CaN are annotated as 3G-H p-CaN), so initial studies were required to profile the pressure-, time- and concentration-related response of this new formulation.

#### Pressure optimisation

To assess the cavitation behaviour and DNA delivery capabilities of BSA 3G-H p-CaN, groups of four mice were treated with ultrasound at a scale of pressure amplitudes and a formulation containing 3G-H p-CaN and 90 µg CMV-Luc pDNA. As a control, five mice were I.D. injected with a similar dose of CMV-Luc pDNA. After 24 hours, the mice were imaged by IVIS and luminescence quantified. The area of treated skin was subsequently harvested. The BSA protein content was then quantified by ELISA and the CMV-Luc pDNA content quantified by qPCR.

Figures 5.4 and 5.5 show the IVIS data from the pressure optimisation and the intradermal injection of an equivalent DNA dose. This shows that 0.8 MPa, which is at the cusp of the cavitation threshold for these p-CaN, resulted in negligible luciferase expression (average $8x10^4$ p/s in 3 of 4 mice), apart from in one mouse which reached $5.70x10^5$ p/s. In comparison, exposure pressures of 1.2 MPa and 1.7 MPa showed substantial widespread and similar levels of luciferase expression (geometric mean: $4.10\ x10^5$ p/s and $5.05\ x10^5$ p/s). The absence of difference seen when comparing luciferase expression agrees well with the observation in section 4.3.3, where no difference in luminescence was observed between 1.5 and 1.7 MPa. As previously seen, a difference was observed when cavitation levels were compared, which showed that 1.2 MPa exposure achieved 3.47 µJ compared to 16.01 µJ at 1.7 MPa (Figure 5.6). A linear regression could be fitted to the log(TASE) and pressure, implying that over the pressure range 0.8 MPa (which is at the cusp of cavitation) to 1.7 MPa a relationship exists between TASE and pressure. Notably, these measurements also mean as little as 3.47 µJ cavitation is sufficient for effective delivery of the DNA, as was also seen in section 4.3.6 with 2G-U p-CaN.

Interestingly, when the amount of CMV-Luc pDNA present at 24 hours after exposure was quantified by PCR, the level of the CMV-Luc pDNA vector scaled with the pressure applied so that 1.7 MPa achieved 3.1-fold greater delivery than 1.2 MPa and 1.2 MPa achieved 3.5-fold more delivery than 0.8

MPa ($9.06x10^8$ vs $2.96x10^8$ vs $8.54x10^7$ mean pDNA copies), and a linear regression could be fitted (Figure 5.7). This level equated to 0.007% of the available dose, compared to 0.03% in section 2.3.2 and 4.3.6. This could indicate that 3G-H p-CaN have a reduced capacity to deliver pDNA. However, as 3.1-fold more DNA was delivered at 1.7 MPa, but no greater transgene expression was observed, this may indicate a metabolic limit for expressing the luciferase vector in the target cells and/or saturation of the target cell population within the area of exposure, or cell damage at the higher pressure negating gains made in delivery. Regardless of the causative factor(s) the data is in accordance with section 4.3.3 showing higher cavitation does not necessarily lead to higher expression.

This same stepwise increase in delivery with increasing pressures was not observed upon quantifying the amount of BSA protein delivered to the skin in the form of p-CaN (Figure 5.8). Though it should be noted that the quantities of BSA detected are at the lower detection limit of the assay, which makes it difficult to separate the true signal from the noise of the assay and make firm conclusions. Notably, the mean level of cavitation energy was higher with 3G-H (16.0 µJ) vs 2G-U (6.0 µJ) (Welch's t-test, $p<0.01$), whilst the delivery of BSA with 3G-H p-CaN appears to be similar to that achieved with 2G-U p-CaN. Overall, 3G-H p-CaN at 1.7 MPa showed DNA delivery in line with what has previously been seen in Chapter 4 with BSA 2G-U p-CaN, a similar level of BSA delivery and a similar but less variable level of luciferase expression after 24 hours compared to 1.2 MPa. Hence, 1.7 MPa was chosen for subsequent experiments. However, it should be noted that intradermal injection resulted in higher DNA copy number delivery (as expected) and higher luminescence compared to cavitation-mediated delivery ($2.0x10^6$ p/s vs $4.1x10^5$ p/s at 1.7 MPa).

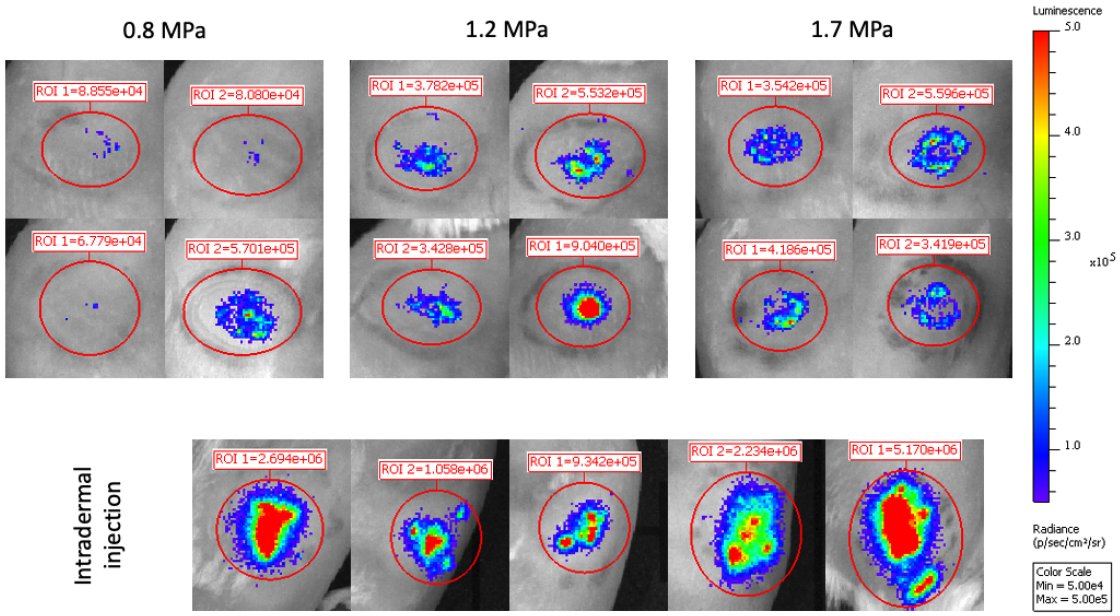



**Figure 5.4.** IVIS images of mouse skin showing the influence of pressure amplitude on the capability of 3G-H BSA p-CaN to deliver CMV-Luc pDNA. Approximately 90 µg of pDNA was used per treatment and administered by exposing the skin to a sample formula containing the DNA and 3G-H p-CaN for 2 min and applying ultrasound at 1.7 MPa, 1.2 MPa or 0.8 MPa. For comparison, mice were injected intradermally with an equivalent dose of pDNA. The luminescence flux produced by luciferase was imaged *in vivo* after 24h (with luciferin administration and IVIS image capture as described in Section 2.2.6). Scale bar was set to 5e4-5e5 p/s/cm$^2$/sr for all images.

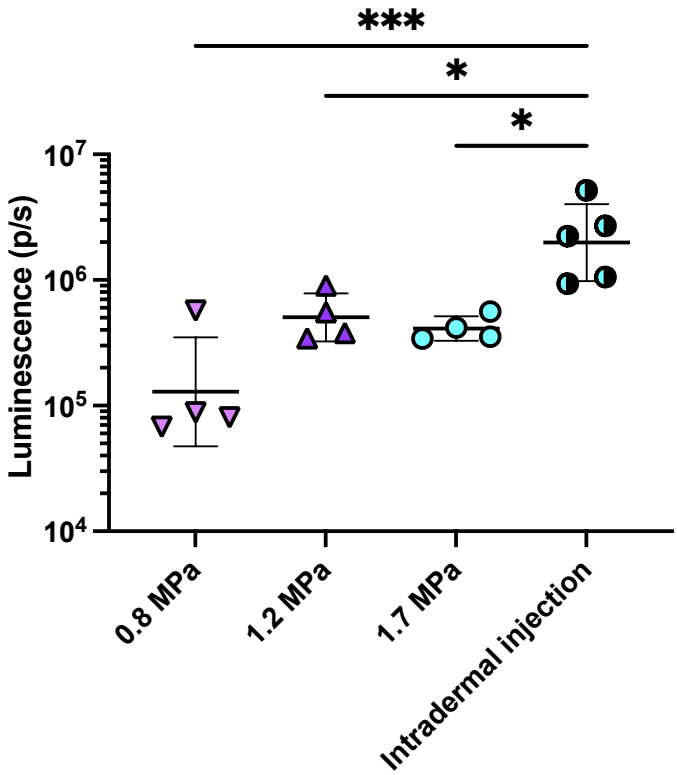
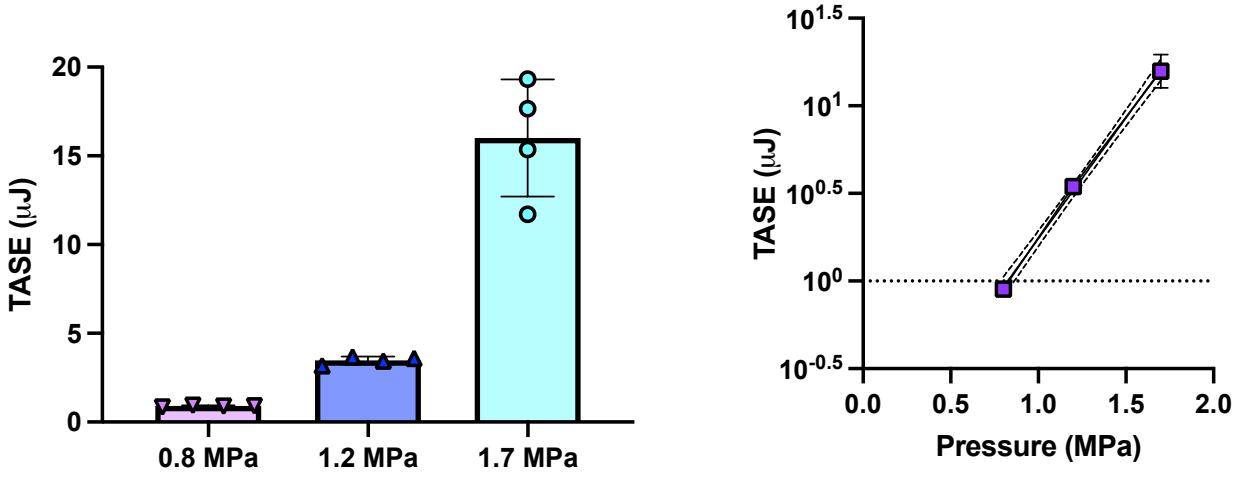
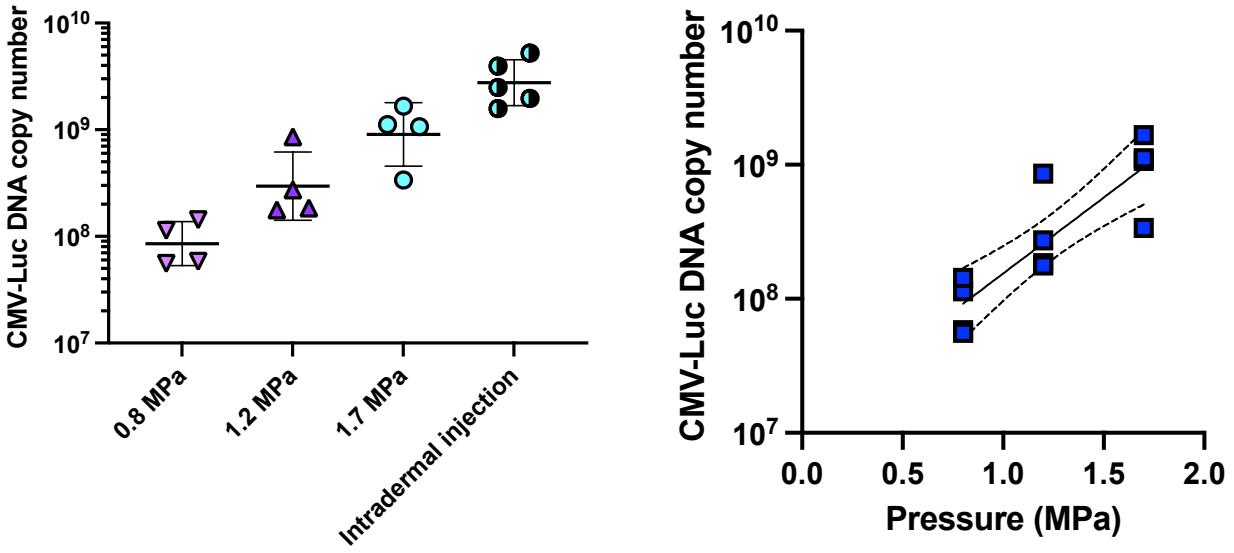



**Figure 5.5.** The effect of scaling acoustic pressure on transfection and expression of CMV-Luc pDNA. Approximately 90 µg of pDNA was used per treatment and administered by exposing the skin to a sample formula containing the DNA and 3G-H p-CaN for 2 min and applying ultrasound at 0.8 MPa, 1.2 MPa or 1.7 MPa. For comparison, mice were injected intradermally with an equivalent dose of CMV-Luc pDNA. The luminescence flux produced by luciferase was imaged *in vivo* after 24 h. N=4, geometric means (horizontal bar) $\times/\div$ geometric standard deviation (error bars) are displayed. A one-way ANOVA with Tukey HSD post all groups was used to assess significance, *=p<0.05, ***=p<0.0005. Non-significant differences are not displayed.




**(a)** TASE vs Pressure **(b)** Linear Regression

**Figure 5.6.** The effect of scaling acoustic pressure on cavitation energy (TASE in μJ) (a). Approximately 90 μg of pDNA was used per treatment and administered by exposing the skin to a sample formula containing the DNA and 3G-H p-CaN for 2 min and applying ultrasound at 0.8 MPa, 1.2 MPa or 1.7 MPa. N=4, mean and standard deviation are displayed. A linear regression was fitted (b), which shows a fold increase of 24.0 in TASE value (μJ) per MPa, which is statistically significant ($p<0.0001$) for this pressure range (0.8-1.7 MPa). The 95% confidence interval is plotted for the linear regression.




**(a)** CMV-Luc pDNA copy number vs treatment **(b)** Linear Regression

**Figure 5.7.** CMV-Luc pDNA copies present in excised skin after cavitation-mediated delivery with 3G-H p-CaN for 2 minutes at 0.8 MPa, 1.2 MPa or 1.7 MPa and 90 μg CMV-Luc pDNA in the formulation holder. The DNA copy number after intradermal injection with 90 μg CMV-Luc pDNA is also displayed (a). The skin was excised after 24 hours. The DNA copy number was determined with qPCR, as described in 4.2.5. N=4. A linear regression (b) with 95% confidence interval is plotted, which shows a fold increase of 13.5 in copy number per MPa, which is statistically significant ($p=0.0003$) for this pressure range (0.8-1.7 MPa).

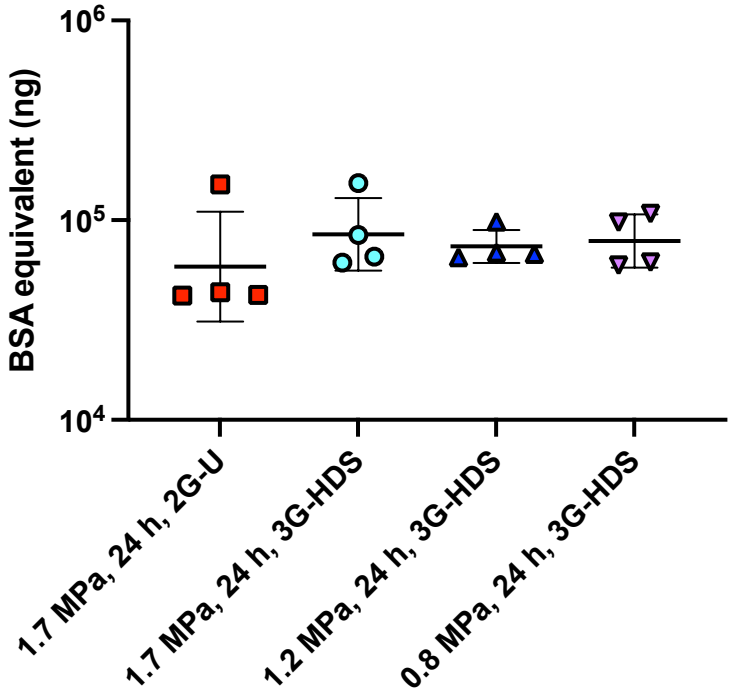



**Figure 5.8.** The BSA protein equivalent detected in murine skin 24 hours after treatment, using an anti-BSA ELISA. Groups of 4 mice were treated with 3G-H p-CaN and 90 µg CMV-Luc pDNA for 2 minutes at 1.7 MPa, 1.2 MPa or 0.8 MPa. The BSA equivalent of 2G-U is displayed for comparison. N=4, geometric mean (horizontal bar) $\times/\div$ geometric standard deviation (error bars) are displayed. No statistically significant differences were seen between groups by one-way ANOVA with Tukeys HSD test, p=0.63.

**DNA dose optimisation**

To assess the effect of the pDNA dose placed on the skin on the level of transgene expression achieved, groups of four mice were treated with ultrasound at 1.7 MPa, (which was determined to be optimal above (section 5.3.1 - Pressure optimisation)), and a formulation containing 3G-H p-CaN and a scale of CMV-Luc pDNA. 24 hours later, the mice were imaged by IVIS and the luminescence was quantified. The treated skin was harvested and the CMV-Luc pDNA quantified by qPCR and the BSA protein content quantified by ELISA.

Figure 5.9 and Figure 5.10 show the results from the IVIS imaging after 24 hours. The images show that a stepwise increase is observed when the pDNA dose is increased. When data from the IVIS imaging was plotted in Figure 5.10 a clear DNA dose-luciferase expression level relationship can be seen. This shows that higher levels of DNA in the formulation chamber results in a higher luminescence flux after 24 hours. Indeed, a linear regression could be fitted, which showed a fold increase of 1.01 in luminescence per µg of pDNA dose, which was statistically significant ($p<0.0001$). This is in contradiction with the data presented in section 4.3.4, where no linear regression could be fitted and no clear difference could be observed between the different doses of DNA (although an upward trend was seen). This may be attributed to the fact that chapter 4 covered a range of doses at a higher concentration (71-284 µg/mouse) compared to this chapter (20-142 µg/mouse). Hence, it may be that studies in chapter 4 suffered from saturation and a plateuing of effect not observed here, so this further supports the hypothesis of saturation in the amount of DNA that can be delivered into the skin by cavitation. Interestingly, this increase in luminescence was not reflected in the qPCR data (Figure 5.11), where no statistically significant linear regression could be fitted to relate CMV-Luc pDNA present in the skin at 24 hours to the pDNA dose in the formulation holder. This may be a reflection of the clearance of the pDNA from the skin. If an initial higher DNA dose was present, it may have resulted in a high initial burst of expression before being cleared relatively quickly compared to lower DNA doses. As overall an increase in dose results in an increase of expression in the dose range explored here, 142 µg of DNA is used for subsequent experiments.

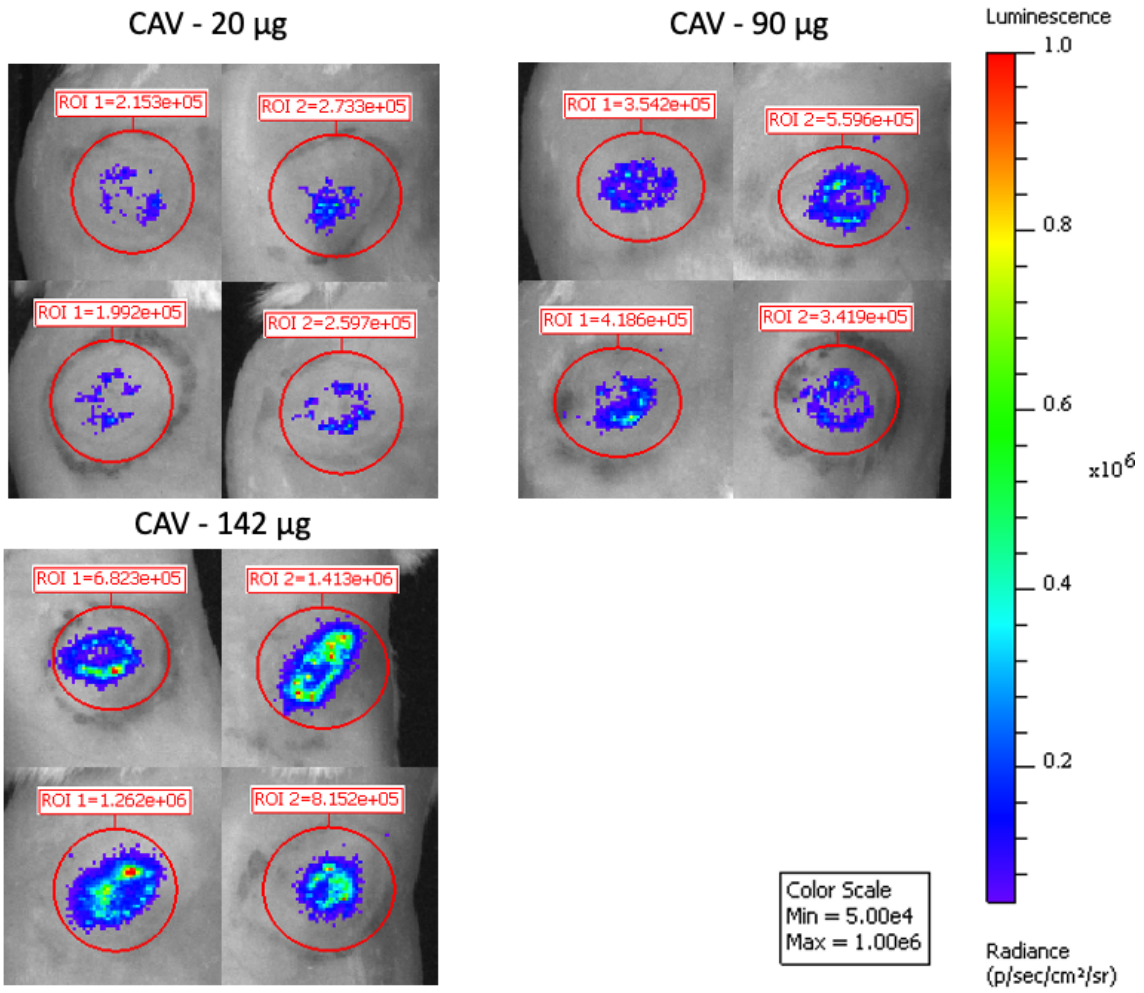



**Figure 5.9.** IVIS images of mouse skin showing the influence of DNA dose on the delivery of CMV-Luc pDNA by 3G-H BSA p-CaN-mediated cavitation. Approximately 20 µg, 90 µg or 142 µg of pDNA was used per treatment and administered by exposing the skin to a sample formula containing the DNA and 3G-H p-CaN for 2 min and applying ultrasound at 1.7 MPa. The luminescence flux produced by luciferase was imaged *in vivo* after 24 h (with luciferin administration and IVIS image capture as described in Section 2.2.6). Scale bar was set to 5e4-1e6 p/s/cm$^2$/sr for all images.The luminescence flux produced by luciferase was imaged *in vivo* after 24 hours.

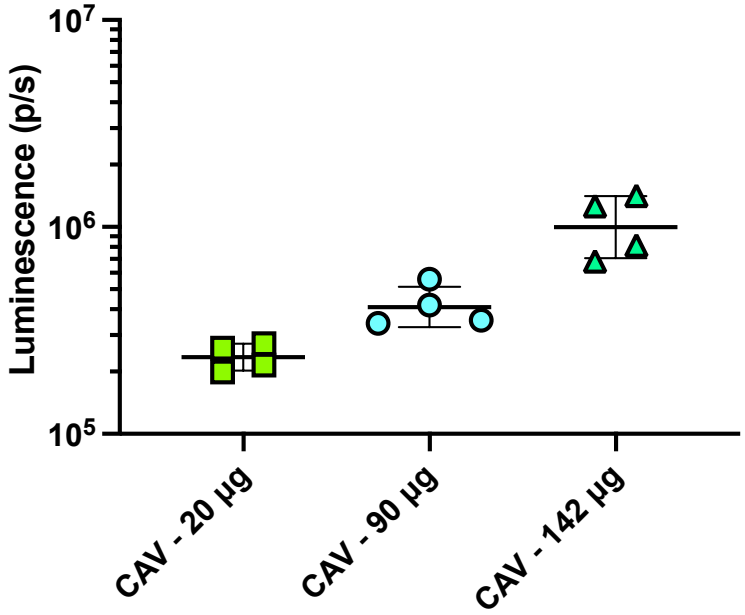



**Figure 5.10.** The effect of increasing DNA dose on transfection and expression of CMV-Luc pDNA with BSA 3G-H p-CaN and ultrasound. Approximately 20, 90 or 142 µg of pDNA was used per treatment and administered by exposing the skin to a sample formula containing the DNA and 3G-H p-CaN for 2 min and applying ultrasound at 1.7 MPa. N=4, geometric means (horizontal bars) $\times/\div$ geometric standard deviation (error bars) are displayed. A linear regression was fitted, which shows a fold increase of 1.01 in luminescence per µg of pDNA, which is statistically significant ($p<0.0001$) for this dose range (20-142 µg).

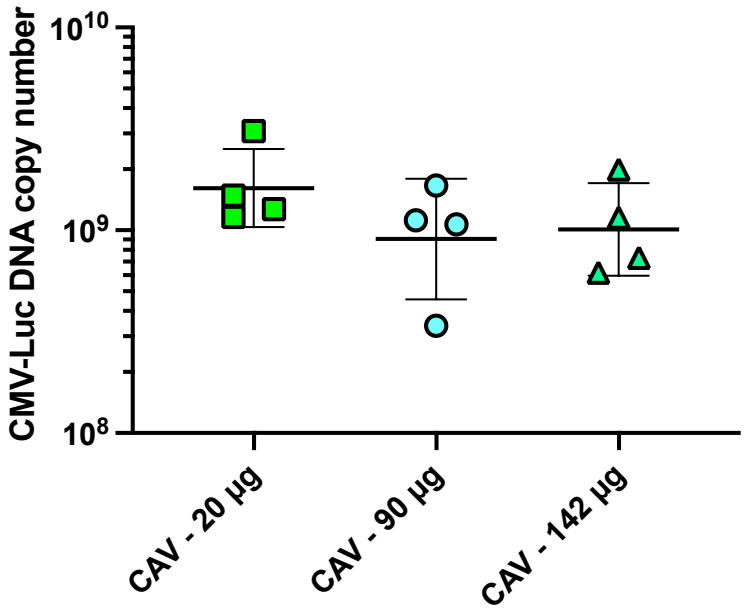



**Figure 5.11.** CMV-Luc pDNA copies present in excised skin after cavitation-mediated delivery with 3G-H p-CaN (CAV) for 2 minutes at 1.7 MPa with 20 µg, 90 µg or 142 µg CMV-Luc pDNA in the formulation applied to the skin. The skin was excised 24 hours after treatment. The DNA copy number was determined with qPCR. N=4, geometric mean (horizontal bars) $\times/\div$ geometric standard deviation (error bars) are displayed. A linear regression was fitted, which showed a fold increase of 1.0 in luminescence per µg of pDNA, which was not statistically significant ($p = 0.24$).

### 5.3.2 Cloning of the self-amplifying vectors

Having optimised the pressure and DNA dose, two novel self-amplifying vectors were then created to explore the potential means of enhancing expression and immunogenicity utilising the self-replicating mechanism from VEEV.

#### proTLx-κ VEEV DREP Luc (CMV-VEEV-Luc)

Firstly, the annealing temperature for the amplification of the luciferase fragment from pGL4.50[*luc2*/CMV/Hygro] was determined with a temperature gradient PCR. A PCR with pGL4.50[*luc2*/CMV/Hygro], HW_006 and HW_007 was prepared. The cycling parameters were 98 ºC for 30 seconds, 35 cycles of 98℃ for 10 seconds, 50-72 ºC for 20 seconds and 72 ºC for 45 seconds, followed by 72 ºC for 2 minutes. The PCR products for annealing temperature 50 ºC and 72 ℃ were run on an agarose gel (Figure 5.12). Both worked and an annealing temperature of 65 ºC was selected. The PCR was run again and the PCR product purified. The fragment was Sanger sequenced with primer HW_010.

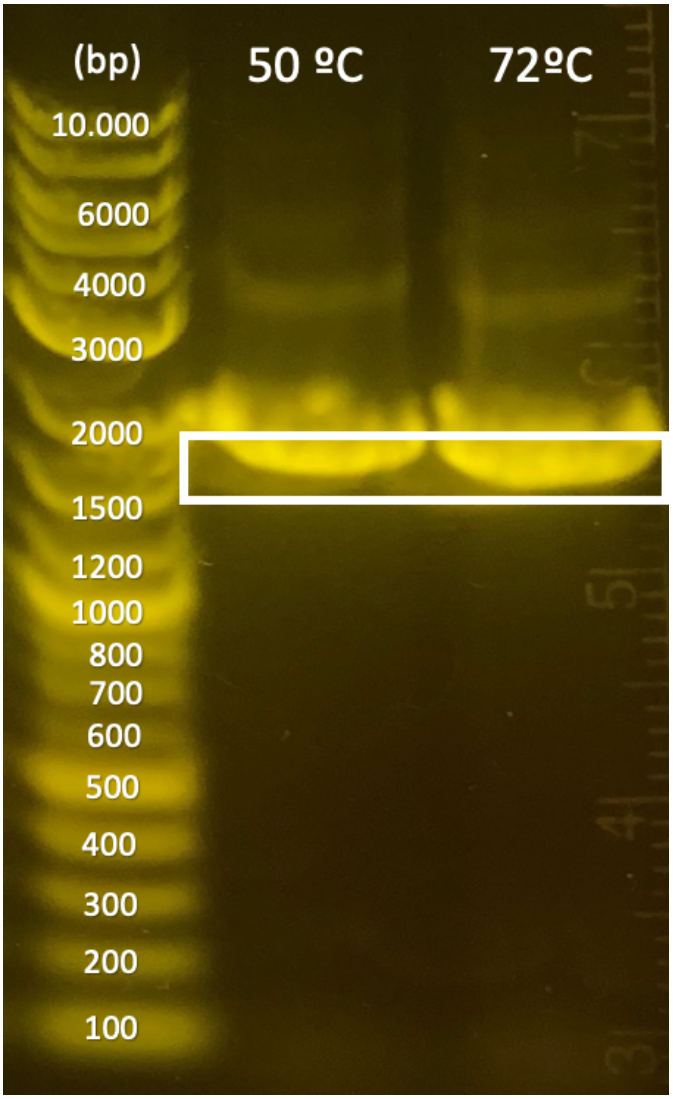



**Figure 5.12.** Agarose gel with the PCR products for two different annealing temperatures of the luciferase fragment. On the left, a 1 kb plus DNA ladder was run and the molecular weight of the bands in basepairs is depicted. The annealing temperature is displayed at the top of the wells. The white box indicates the desired fragment of 1683 bp.

The VEEV backbone was amplified in two parts. The first part (VEEV1) contained the kanamycin resistance, origin, nsP1 and part of nsP2. The second part (VEEV2) contained the sequence for the remaining non-structural proteins (nsP2-4). For both, a temperature gradient PCR was run to determine the optimal annealing temperature. Fragment VEEV1 was amplified from proTLx-κ VEEV DREP eGFP

with primers HW_014 and JKH_041. Fragment VEEV2 was amplified from the same plasmid with primers HW_013 and JKH_042. The cycling parameters were 98 ºC for 30 seconds, 35 cycles of 98℃ for 10 seconds, 50-72 ºC for 20 seconds and 72 ºC for 2 minutes and 30 seconds, followed by 72 ºC for 2 minutes. A selection of the PCR products were run on a gel (Figure 5.13). An annealing temperature of 70.3 ºC was selected for VEEV1 and 72 ºC for VEEV2. The PCR were run again with the optimised conditions. Half of the sample was DpnI-treated. Both the PCR-purified and DpnI-treated fragments were Sanger sequenced with primers JKH_096 and JKH_083 for VEEV1 and JKH_092 and JKH_106 for VEEV2.

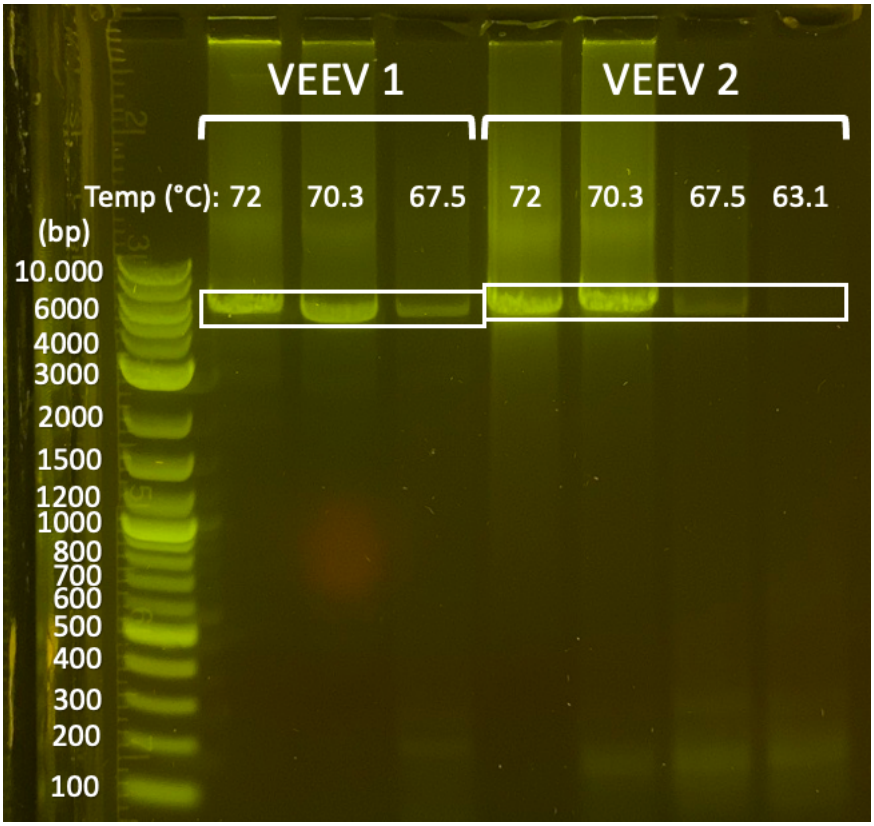



**Figure 5.13.** Agarose gel with the PCR products for different annealing temperatures of the VEEV1 and VEEV2 fragments. On the left, a 1 kb plus DNA ladder was run and the molecular weight of the bands in basepairs is depicted. The annealing temperature is displayed at the top of the wells, as well as whether the product was for VEEV1 or VEEV2. The white box indicated the desired fragment of 5384 bp for VEEV1 and 5420 bp for VEEV2.

The construct was assembled by Gibson Assembly of VEEV1, VEEV2 and Luc, both DpnI-treated and non-DpnI-treated (Figure 5.15). Correct assembly was verified with a diagnostic colony PCR. A colony PCR reaction was run with primers HW_010 and JKH_096 and cycling conditions: 98 ºC for 10 minutes, 35 cycles of 98 ºC for 10 seconds, 50-72 ºC for 30 seconds and 72 ºC for 1 minute, followed by 72 ºC for 2 minutes. One colony showed the desired band at 1840 bp (Figure 5.14). Insertion was confirmed by Sanger sequencing with primer EGFP_C_R. The successful clone was glycerol stocked.

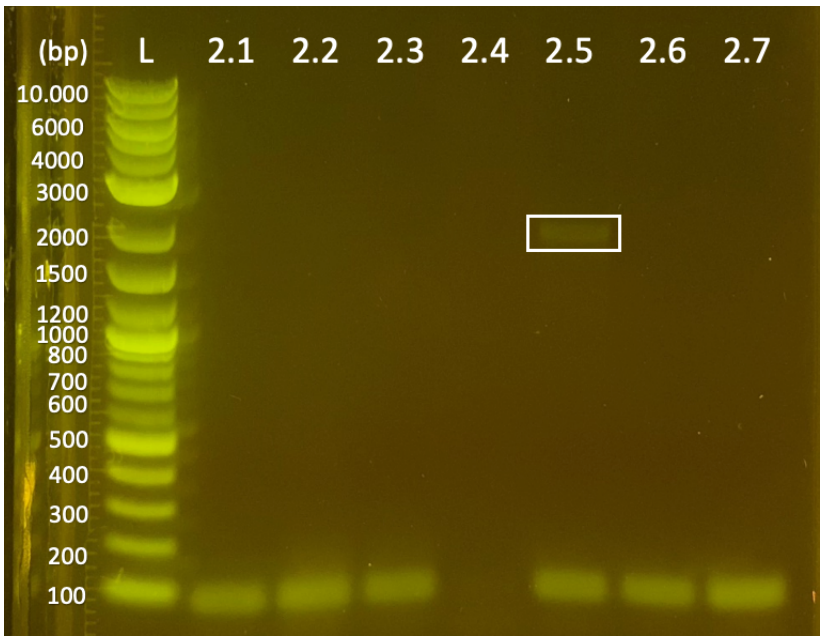



**Figure 5.14.** PCR products of a diagnostic colony PCR of proTLx-κ VEEV DREP Luc, prepared with DpnI-treated VEEV1 and VEEV2, were run on an agarose gel. On the right side a 1 kb plus DNA ladder was loaded and the weight in basepairs is indicated. The numbers on top indicate the numbers assigned to different colonies which were assessed. Successful construction of proTLx-κ VEEV DREP Luc would result in a 1840 bp band, indicated in white.

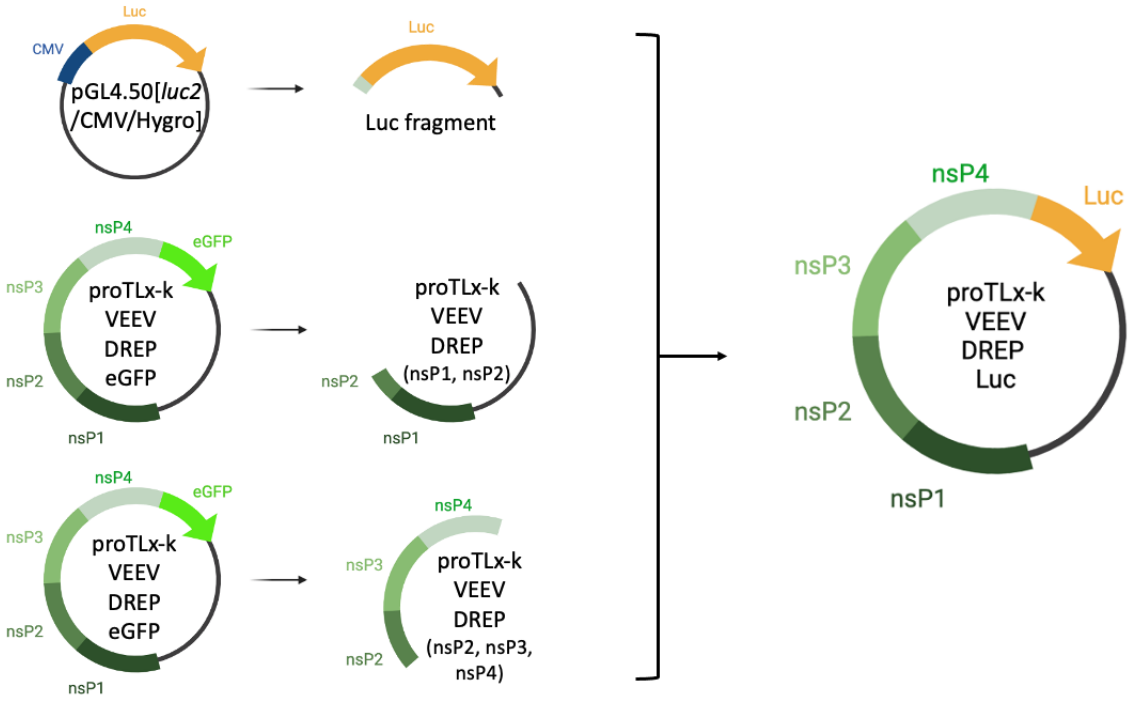



**Figure 5.15.** Schematic representation of the cloning of the proTLx-κ VEEV DREP Luc plasmid. The Luc-fragment (top) was PCR-amplified of the pGL4.50[luc2/CMV/Hygro] plasmid. The proTLx-κ VEEV DREP backbone and VEEV non-structural proteins were PCR-amplified in two parts. The VEEV1-fragment (middle) was PCR-amplified of the proTLx-κ VEEV DREP eGFP and included the backbone and non-structural protein 1 and part of 2. The VEEV2-fragment (bottom) was PCR-amplified of the proTLx-κ VEEV DREP eGFP and included non-structural protein 3, 4 and part of 2. These three fragments were ligated together to form proTLx-κ VEEV DREP Luc.

**proTLx-κ VEEV DREP Cal09 HA (CMV-VEEV-Cal09)**

The Cal09 HA fragment was amplified from proTLx-κ B5X4 Cal09 HA with primers JKH_043 and JKH_045. A gradient temperature PCR was used to optimise the annealing temperature. The cycling parameters were 98 ºC for 30 seconds, 35 cycles of 98 ℃ for 10 seconds, 50-72 ºC for 20 seconds and 72 ºC for 2 minutes, followed by 72 ºC for 2 minutes. The resulting PCR products of 1731 bp were run on an agarose gel (Figure 5.16) and an annealing temperature of 65 ℃ was selected. The PCR was run again and the product was DpnI treated. This fragment was verified by Sanger sequencing with primer JKH_031.

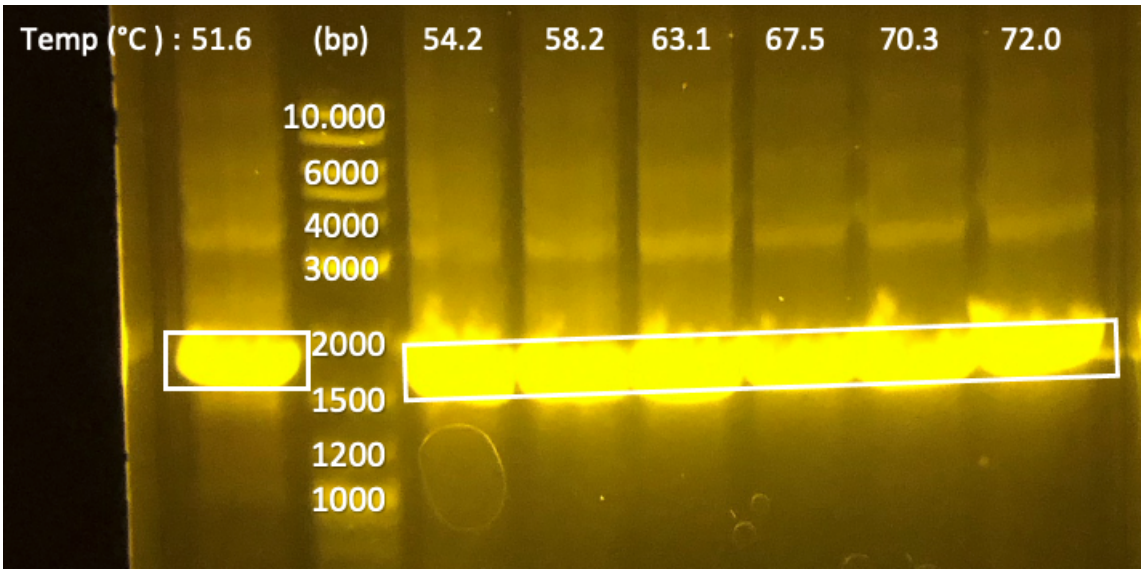



**Figure 5.16.** Agarose gel with the PCR products for different annealing temperatures of the Cal09 HA fragment. On the second lane, a 1 kb plus DNA ladder was run and the molecular weight of the bands in basepairs is depicted. The annealing temperature is displayed at the top of the wells. The white box indicates the desired fragment of 1731 bp.

The VEEV1 and VEEV2 fragment were generated as described under VEEV DREP Luc for DpnI-treated samples.

The construct was assembled by Gibson Assembly of the VEEV1, VEEV2 and Cal09 HA fragments. The construct was verified by a diagnostic PCR with primers JKH_094 and JKH_096, which anneal to Cal09 and the backbone respectively (Figure 5.18). proTLx-κ VEEV DREP Cal09 HA would result in a band at 1332 bp, whilst the template proTLx-κ B5X4 Cal09 HA would result in a band at 1062 bp. This showed 2/7 colonies had correctly assembled (Figure 5.17). This was subsequently confirmed by Sanger sequencing with primer EGFP_C_R and a correct colony was glycerol stocked.

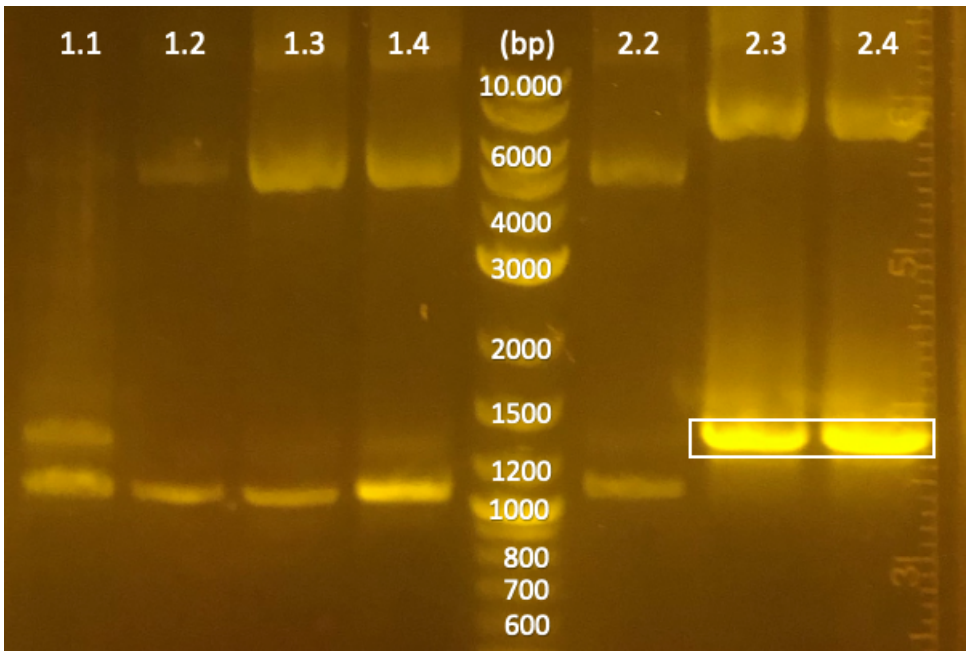



**Figure 5.17.** The products of a diagnostic PCR of proTLx-κ VEEV DREP Cal09 HA, prepared with DpnI-treated Cal09 HA fragment, VEEV1 and VEEV2, was run on an agarose gel. On the fifth lane, a 1 kb plus DNA ladder was loaded and the weight in basepairs is indicated. The numbers on top indicate the numbers assigned to the different colonies which were assessed. Successful construction of proTLx-κ VEEV DREP Cal09 HA would result in a 1332 bp band, indicated in white, as opposed to 1069 bp, which indicates the template proTLx-κ B5X4 Cal09 HA.

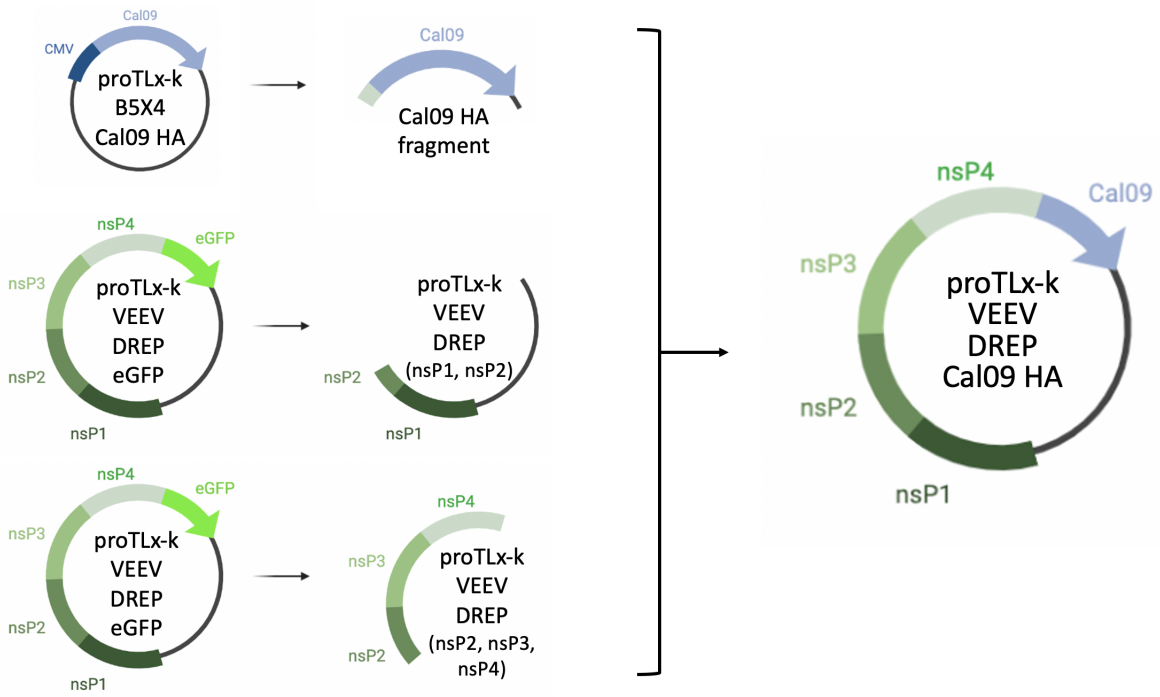



**Figure 5.18.** Schematic representation of the cloning of the proTLx-κ VEEV DREP Cal09 HA plasmid. The Cal09-fragment (top) was PCR-amplified of the proTLx-κ B5X4 Cal09 HA plasmid. The proTLx-κ VEEV DREP backbone and VEEV non-structural proteins were PCR-amplified in two parts. The VEEV1-fragment (middle) was PCR-amplified of the proTLx-κ VEEV DREP eGFP and included the backbone and non-structural protein 1 and part of 2. The VEEV2-fragment (bottom) was PCR-amplified of the proTLx-κ VEEV DREP eGFP and included non-structural protein 3, 4 and part of 2. These three fragments were ligated together to form proTLx-κ VEEV DREP Cal09 HA.

### 5.3.3 *In vivo* evaluation of a self-amplifying reporter plasmid

#### Intradermal injection comparison

Once the proTLx-κ VEEV DREP Luc plasmid (CMV-VEEV-Luc) reporter vector had been created and its sequence validated, an experiment was performed to determine its reporter gene expression profile *in vivo*. To this end, two groups of 4 mice were injected intradermally with either 5 µg CMV-Luc or 9.4 µg CMV-VEEV-Luc (i.e. to achieve an equal copy number). The luciferase expression was then monitored over time.

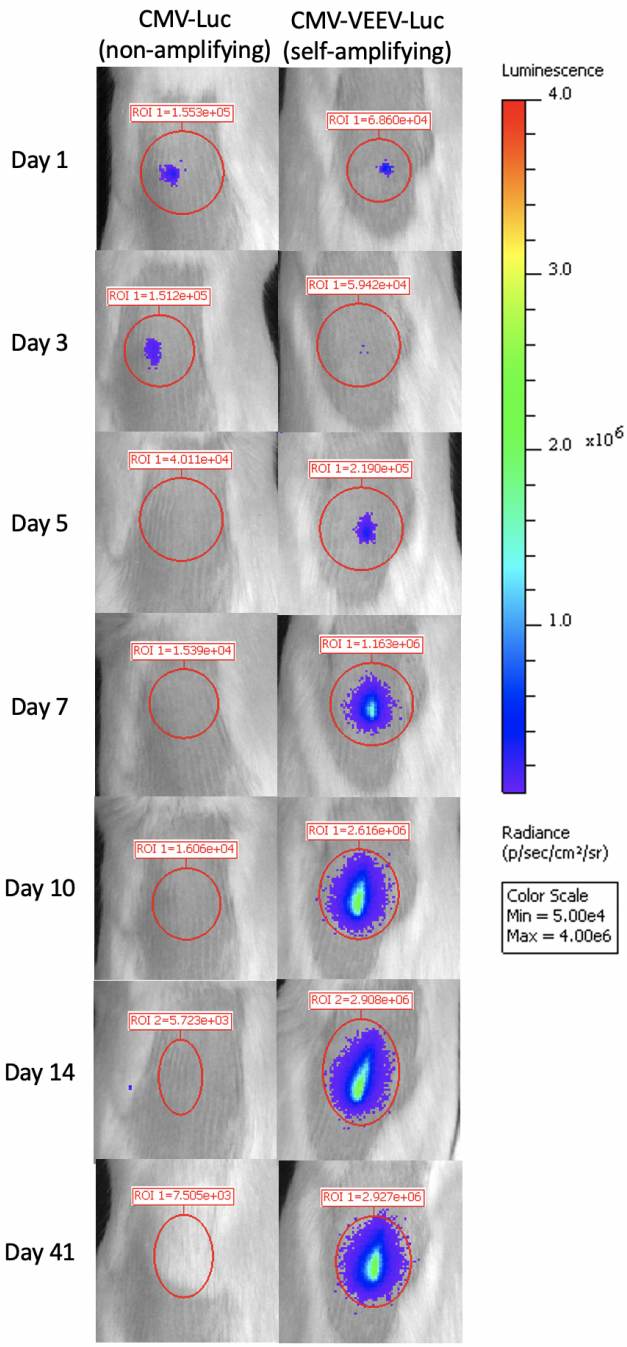



**Figure 5.19.** Example of a mouse intradermally injected with a non-amplifying CMV-Luc vector and a mouse intradermally injected with a self-amplifying CMV-VEEV-Luc vector. The IVIS images of the two mice over time is displayed.

Although 4 mice were injected in each group, only 1 mouse from each group was deemed to have a level of luciferase expression at 24 hours which was similar enough to each other to provide confidence that any subsequent differences in expression profile were the consequence of the differences in the composition of the vector rather than the effectiveness of the initial I.D. injection. The expression over time of these two mice is shown in Figure 5.19 and is also plotted in Figure 5.20. The mouse injected with the non-amplifying vector showed slightly higher expression after 24 hours and then a gradual decline down to background level ($10^4$ p/s) by day 5 (in accordance with the time-expression profile seen in Chapter 2, Figure 2.7). However, the mouse with the self-amplifying vector, initially (24 h) showed a similar but lower level of expression ($6.86 \times 10^4$ p/s), perhaps reflecting production

of a limited amount of luciferase protein at the point where the mRNA transcript produced from the CMV-VEEV-Luc pDNA is first translated along with the VEEV proteins required for further RNA amplification. The expression remained consistent for a few days, (perhaps reflecting a pause for generation of negative strand then self-amplified positive strand RNA transcript) before an uptick was seen at 5 days, when the self-amplified transcript begins to be translated exponentially. Hence, whilst this mouse initially showed low expression ($<10^5$ p/s), after 5 days a marked uptick in expression was seen and expression remained high ($>5x10^5$ p/s) for at least 1 month.

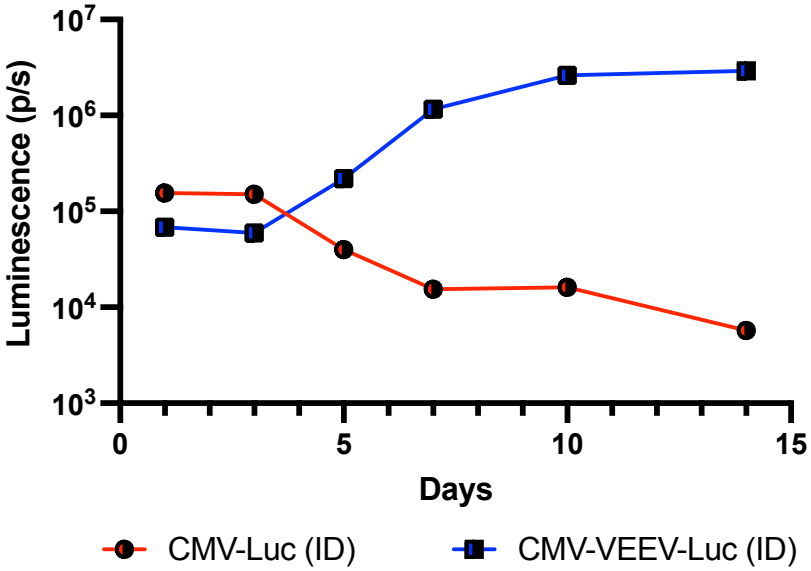



**Figure 5.20.** Luminescence over time in mice intradermally injected with either 5 µg non-amplifying CMV-Luc plasmid or a copy-matched number of self-amplifying CMV-VEEV-Luc plasmid (9.4 µg). IVIS imaging was performed as described in section 2.2.6. Each line represents a single mouse (n=1).

The IVIS images of these two mice over time have been plotted (Figure 5.19). The unique expression pattern of the self-amplifying vector may be a consequence of the self-amplification mechanism and the lower initial level of expression from the self-amplifying vector may be the consequence of the self-amplification mechanism, this requires the transcription and translation of the non-structural proteins and then replication of the mRNA before an increased amount of luciferase can be translated. Both the size of the self-amplifying vector (12437 bp), as well as the metabolic load of expressing five proteins (nsP1-4 plus luciferase) instead of just luciferase, may have further contributed to the pause/delay between 24 hours and 5 days. For instance, it is possible that the self-amplifying vector has a lower delivery efficiency due to its size and more self-replication cycles are needed to compensate for this lower DNA delivery efficiency. Notably, two mice responded from the self-amplifying group and showed increased expression after 5 days irrespective of their initial expression after 24 hours. This implies that the self-amplification process starts to ramp up around this timepoint and overcomes competing silencing or degradation processes in the cell. Comparing this to the literature,

Huysman et al. observed a peak of expression of luciferase between 8-10 days after intradermal electroporation with self-amplifying RNA in mice [269]. This aligns well with an observed peak around day 10 in the experiment reported in this thesis.

The distinctive behaviour of the self-amplifying vector was a confirmation of the expected behaviour, whilst providing encouragement for the further testing of its potential.

**Ultrasound-mediated delivery comparison**

After the intriguing results from the Figures 5.19 and 5.20, where the self-amplifying vector was intradermally injected, the next question investigated was whether this expression profile would be mimicked for cavitation-mediated delivery of the self-amplifying vector to the skin. This may allow the initially lower level of delivery achieved with cavitation to be compensated for by enhanced activity of the vector. To assess this, mice were treated with either the self-amplifying reporter vector or a non-amplifying reporter vector and cavitation using parameters as described in section 5.2.9. The self-amplifying vector was either matched in nanograms to the non-amplifying control or in copy-number, as described in the methods 5.2.9, to give three treatment groups. The luciferase expression was monitored using IVIS for two weeks following exposure of the skin to pDNA, p-CaN and ultrasound. The results are summarised in Figure 5.21. Analysis of cavitation data confirmed all three groups had been exposed to low but equivalent mean levels of cavitation (2.89±0.41 μJ vs 5.03±2.33 μJ vs 3.3±0.64 μJ).

At 24 hours, low levels of luciferase expression were observed for both the ng and copy-matched self-amplifying groups compared to the group treated with non-self-amplifying vector (means of $2.2x10^5$ and $7.3x10^5$ vs $2.9x10^6$ respectively)(two-way ANOVA Tukey HSD post all group comparisons, $p<0.01$ for CMV-Luc (CAV) vs CMV-VEEV-Luc (copy-matched) and CMV-Luc (CAV) vs CMV-VEEV-Luc (ng-matched)). In contrast to the experiments with self-amplifying vector delivered I.D. (see Figure 5.20), the level of expression continued on a downward trend, so that by day 15, levels were only marginally above background. This is surprising considering the strong expression seen after I.D. injection of this self-amplifying vector by day 14 (Figure 5.20). There may be some difference in the cells transfected by cavitation compared to intradermal injection that make the cell populations targeted by cavitation more likely to silence the CMV-VEEV-Luc vector or less likely to support the VEEV machinery or less able to express the encoded antigen and VEEV non-structural proteins sufficiently to allow a beneficial effect. Alternatively, the cells transfected may be more transient, and hence, not allow enough

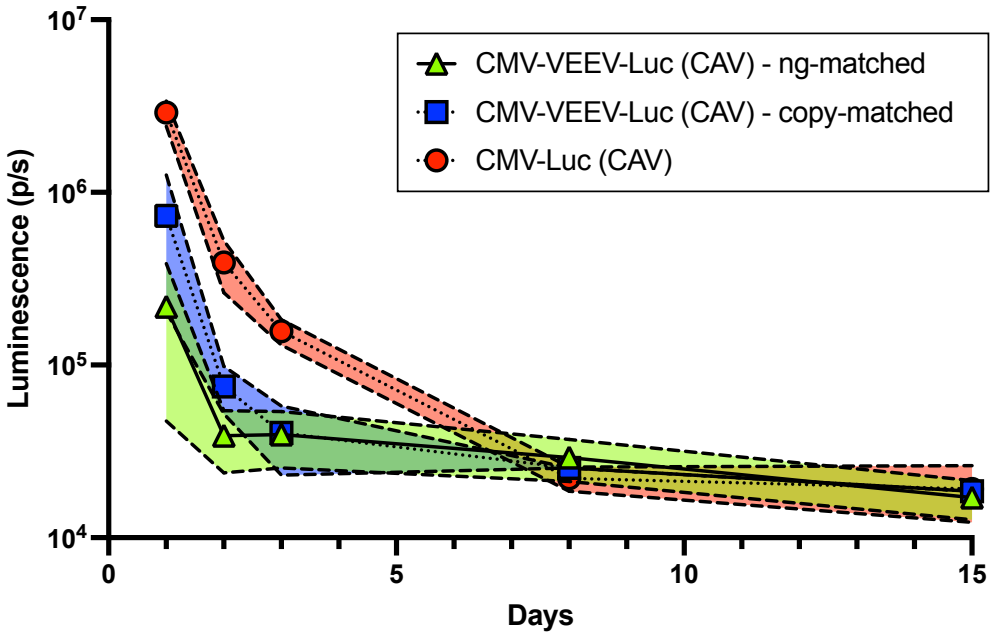



**Figure 5.21.** Luminescence over time for mice treated by cavitation with 2G-U p-CaN and pDNA. Mice were either treated with 142 µg non-amplifying CMV-Luc plasmid (red circle), or with a 267 µg copy-matched dose of the self-amplifying CMV-VEEV-Luc plasmid (blue square) or 142 µg CMV-VEEV-Luc plasmid (green triangles). N=3 for CMV-VEEV-Luc (CAV) - copy-matched and n=4 for the other groups. Mean (line) and standard deviation (shaded area) are displayed. A two-way ANOVA (treatment x time) was done with a Tukey post hoc test between treatments for the different timepoints. A significant effect of treatment ($p<0.0001$), time ($p<0.0001$) and their interaction ($p<0.0001$) was observed. No significant effect ($p>0.05$) of subject was observed. A significant difference ($p<0.05$) between 'CMV-VEEV-Luc (CAV) - copy-matched' and 'CMV-Luc (CAV)' was observed for day 1,2 and 3, as well as for 'CMV-VEEV-Luc (CAV) - ng -matched' and 'CMV-Luc (CAV)' for day 1,2 and 3.

time for the self-expression to come to its full fruition. Overall, these results did not show enough potential for the self-amplifying vector to be pursued further for cavitation-mediated delivery. These data did serve to support the hypothesis that cavitation and injection may target different cell populations.

### 5.3.4 *In vivo* evaluation of a self-amplifying immunogenic vector

Whilst the mode or cell target of cavitation-mediated delivery did not appear compatible with the VEEV self-amplifying mechanism of/requirements for action, it was clear that the approach still had potential for enhancement of needle and syringe injection efficacy. To explore whether, when using I.D. injection, the enhanced profile of luciferase expression with the CMV-VEEV-Luc vector could be reproduced for a pathogen-associated antigen, the proTLx-κ VEEV DREP Cal09 HA (CMV-VEEV-Cal09) construct (see section 5.3.2) was compared to CMV-Cal09. To test the *in vivo* effect of this vector, mice were intradermally injected with either the non-amplifying CMV-Cal09 vector or a copy-matched amount of the self-amplifying CMV-VEEV-Cal09 pDNA vector. They were subsequently homologously boosted on day 21. Blood was sampled on day 14, 20, 29, 35 and 42 and a terminal bleed was taken on day 83. The results of the IgG ELISA performed on these bloods are summarised in Figure 5.22.

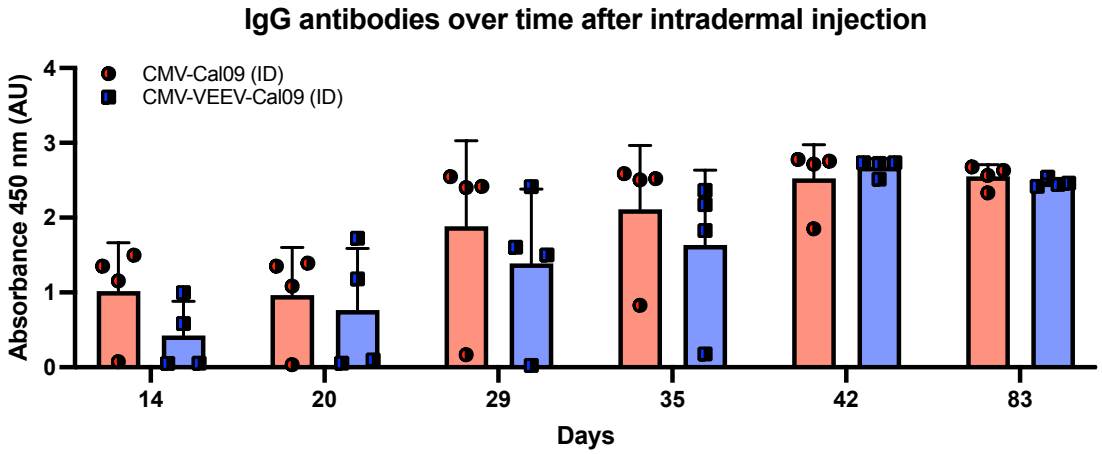



**Figure 5.22.** Analysis of the anti-Cal09 HA antibody levels, determined by ELISA, from the *in vivo* study performed to evaluate non-amplifying versus self-amplifying Cal09-encoding vectors over time. Mice were intradermally injected (ID) with 142 µg CMV-Cal09 or 380 µg CMV-VEEV-Cal09. N = 4, mean (bar height) and SD (error bars) are displayed. A two-way ANOVA (vector x time) was done with a post hoc test between vectors for the different treatments using the Šidák correction for multiple comparisons. A significant effect of time ($p=0.0002$) and subject ($p<0.0001$) was observed. No significant effect of vector was observed ($p>0.05$). Multiple comparisons showed $p>0.05$ for all vector groups.

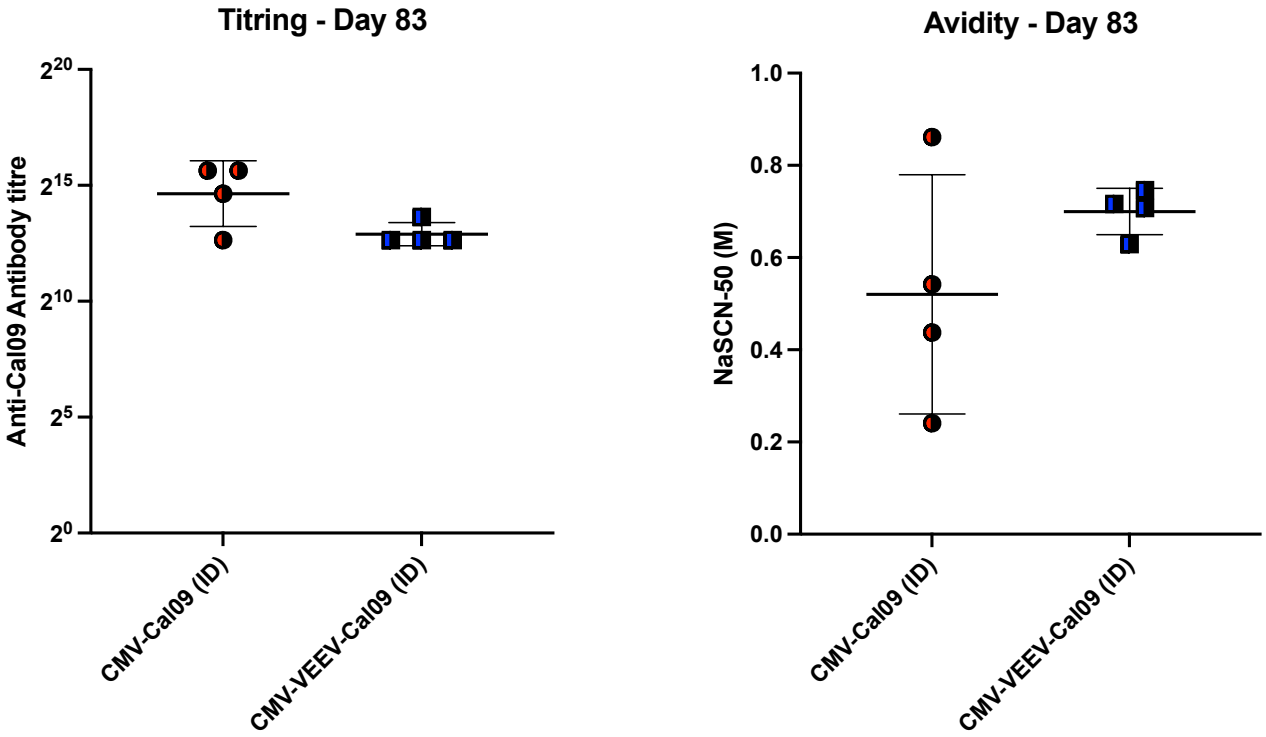
Notably, although no significant difference was observed between the response generated by the CMV-Cal09 and the self-amplifying antigen group (CMV-VEEV-Cal09) at any timepoint, there were differences to the time profile and the intragroup variability. Specifically, a delayed response from the CMV-VEEV-Cal09 group becomes apparent, as the average antibody level is still rising and the variability still high until day 42 in this group, whereas the average antibody level of 3 of 4 mice changes very little in the CMV-Cal09 group from day 28 onwards. This may be attributable to the delay in in-

creased protein expression achieved with the self-amplifying vector. However, once the antibody level stabilises around day 42 for the self-amplifying vector, the antibody levels show high reproducibility (SD = 0.11 AU for self-amplifying vs 0.45 AU for non-amplifying vector on day 42), which may be due to the relatively high expression of antigen in that group. This provides more confidence that reproducible protection could be achieved if a challenge experiment was performed.

The antibody responses were further probed by titring the antibody levels, determining the avidity and measuring the IgG1 and IgG2a isotype levels. The titring further confirmed the high reproducibility of the self-amplifying vector, albeit showed lower (although not significantly so) antibody levels compared to the CMV-Cal09 vector (7611 for the CMV-VEEV-Cal09 and 25600 for CMV-Cal09, p=0.099) (Figure 5.23a). In contrast, the avidity of the CMV-VEEV-Cal09 group was 1.34-fold higher at 0.70 M NaSCN-50 than the non-amplifying vector at 0.52 M NaSCN-50 (Figure 5.23b), and greater reproducibility was again seen. This implies that the antibodies generated by the self-amplifying vector bind more tightly to their antigen, which could be advantageous in terms of protection against disease.

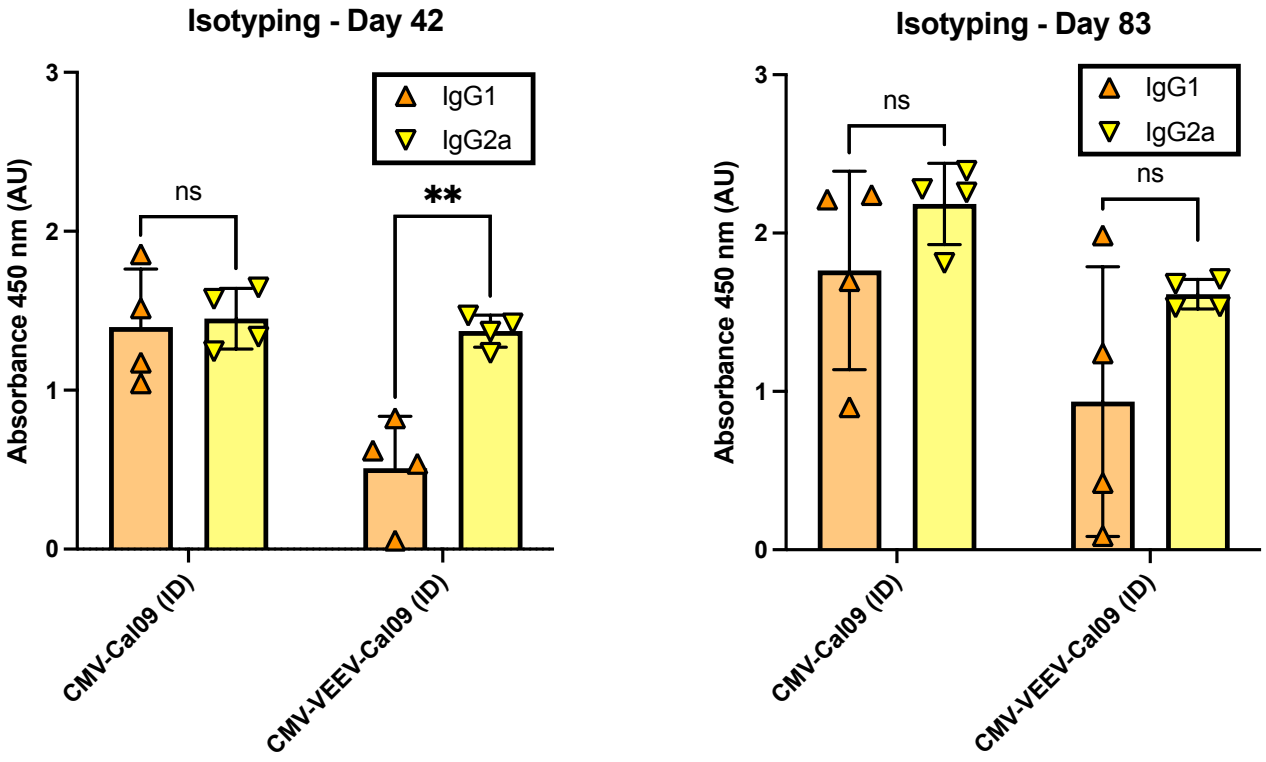
Finally the IgG1 and IgG2a levels of the generated antibodies were determined (Figure 5.24). Interestingly, the self-amplifying vector had a lower IgG1/Ig2a ratio on both day 42 (0.99 vs 0.37) and day 83 (0.86 vs 0.58). Overall, the CMV-VEEV-Cal09 vector resulted in an IgG2a-skewed antibody response. The effect of the vector depends on the treatment method used, which was significant ($p<0.05$). As IgG2a is associated with T-helper cell type 1 (Th1) [210], complement activation [195] and antibody-dependent cellular cytotoxity [194], the generation of IgG2a antibodies has been correlated to increased protection from a lethal influenza challenge [270]. This improved IgG2a response may be related to the 'danger' signals produced by cells due to the presence of dsRNA during the self-amplification process of VEEV, as discussed in the section 5.1.1.

Based on this data, the self-amplifying vector appeared a strong candidate for improving immunogenicity upon intradermal injection.




**(a)** Titring **(b)** Avidity

**Figure 5.23.** Titring and avidity of anti-Cal09 HA IgG antibodies generated, as determined by ELISA. Groups of 4 mice were intradermally injected (ID) with 142 µg CMV-Cal09 or copy-matched 380 µg CMV-VEEV-Cal09. N=4. a) Titred antibody levels upon intradermal injection with different DNA vectors. Geometric means $\times/\div$ geometric standard deviation are displayed. Significance was assessed with a Welch's t-test, $p>0.05$. b) Avidity of the antibodies generated upon intradermal injection with different DNA vectors. Significance was assessed with a Welch's t-test, $p>0.05$. Mean and standard deviation are displayed.




**(a)** Day 42 **(b)** Day 83

**Figure 5.24.** Isotyping of anti-Cal09 HA IgG antibodies after 42 days (a) and 83 days (b), as determined by ELISA. Groups of 4 mice were intradermally injected (ID) with 142 µg CMV-Cal09 or copy-matched 380 µg CMV-VEEV-Cal09. n=4, SD displayed. A two-way ANOVA (vector x isotype) was done for both day 42 and 83 with a post-hoc test between isotypes for each group using the Šidák correction for multiple comparisons. ** = $p<0.01$, ns = $p>0.05$ for all other groups. No significant effect ($p>0.45$) of vector, isotype or their interaction could be observed for either timepoint.

### 5.3.5 Cloning of the DNA adjuvant vectors

To assess the effect of three DNA adjuvants, three plasmids were constructed as described below.

#### proTLx-κ CMV-Perforin (CMV-Perforin)

To create the CMV-Perforin plasmid, the proTLx-κ B5X4 Cal09 HA plasmid backbone including the CMV promoter was amplified with the primers JKH_050 and JKH_051_alt. The annealing temperature was optimised by running a temperature gradient. The cycling parameters for optimisation were 98 ºC for 30 seconds, 35 cycles of 98℃ for 10 seconds, 50-72 ºC gradient for 20 seconds and 72 ºC for 1 minute, followed by 72 ºC for 2 minutes. A gradient of annealing temperatures was run because at this stage the optimal temperature was unknown. Gel analysis of the products (Figure 5.25) demonstrated that there was minimal desired product (2960 bp band) above 63 ℃, and the optimum intensity was evident at 58 ℃, which was therefore selected.

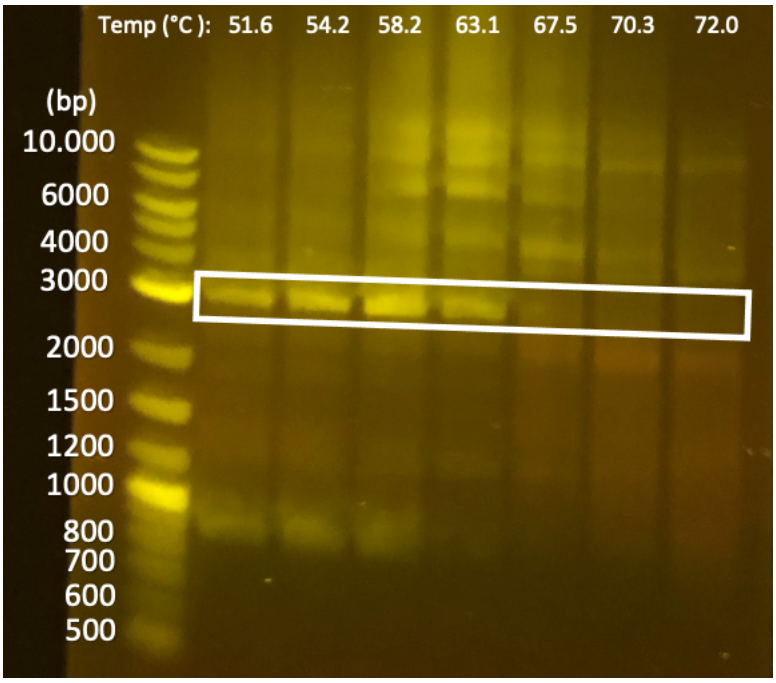



**Figure 5.25.** Agarose gel with the PCR products for different annealing temperatures for the proTLx-κ B5X4 backbone was run as described in Section 5.2.1. On the left, a 1 kb plus DNA ladder was run and the molecular weight of the bands in basepairs is depicted. The annealing temperature is displayed at the top of the wells. The white box indicated the desired fragment of 2960 bp.

The cycling parameters for generating the backbone cloning fragment were therefore 98 ºC for 30 seconds, 35 cycles of 98℃ for 10 seconds, 58 ºC for 20 seconds and 72 ºC for 1 minute, followed by 72 ºC for 2 minutes. The PCR product was run on an agarose gel, excised and purified. This fragment was checked by Sanger sequencing with primer JKH_111. This backbone was ligated with the custom perforin gBlock, which had overlapping sequences with the backbone, see Figure 5.26.

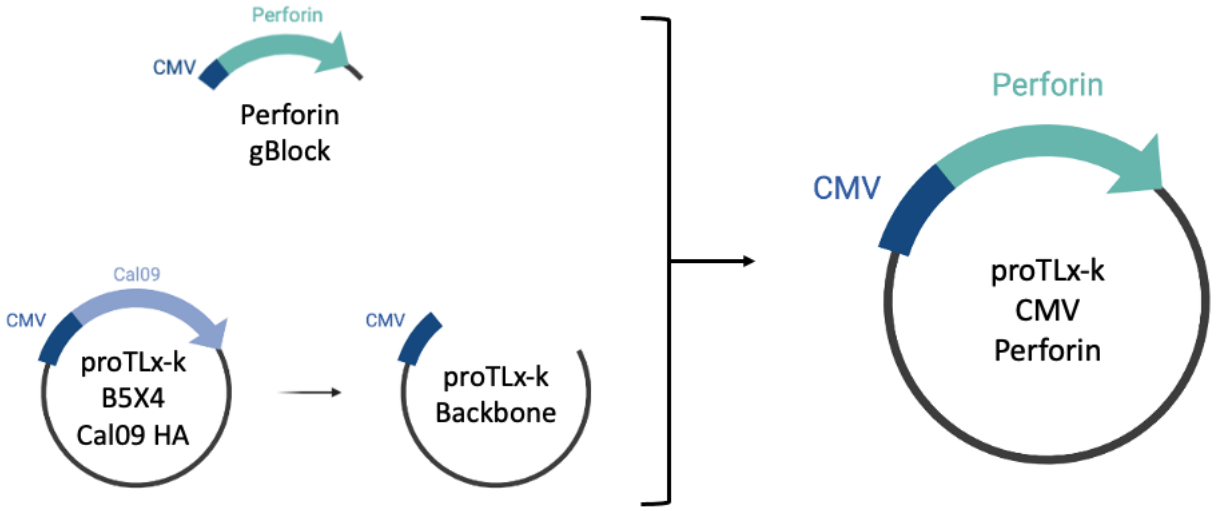



**Figure 5.26.** Schematic representation of the cloning of the proTLx-κ CMV-Perforin plasmid. The proTLx-κ B5X4 backbone, including the CMV promoter, was PCR-amplified. The perforin gene with ends overlapping the backbone was ordered as a gBlock. These two fragments were ligated together to form proTLx-κ CMV-Perforin.

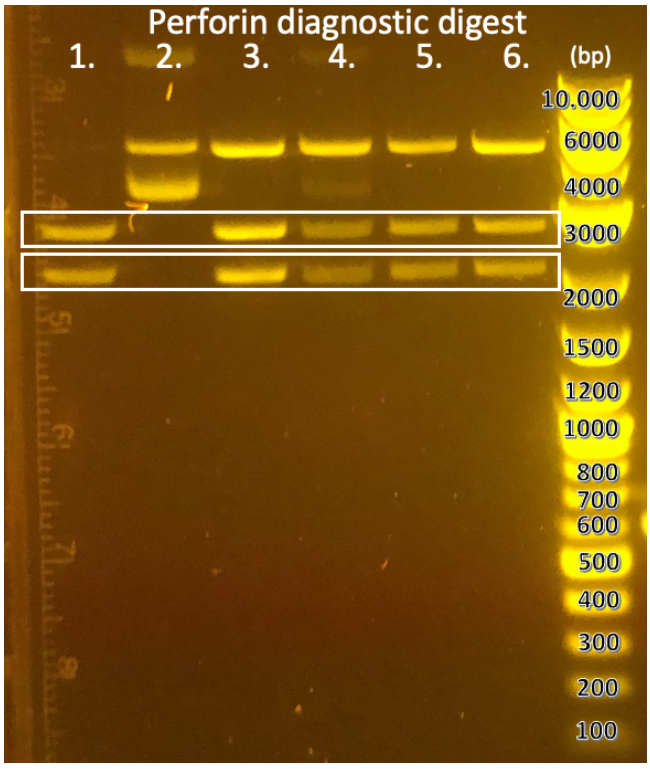



**Figure 5.27.** Products of a diagnostic digest of proTLx-κ CMV-Perforin with SphI-HF were run on an agarose gel. On the right side a 1 kb plus DNA ladder was loaded and the weight in basepairs is indicated. Samples with DNA isolated from each of 6 colonies positive for kanamycin resistance, were assigned a number 1-6 and run in wells 1-6. Successful construction of proTLx-κ CMV-Perforin would result in two bands, at 2021 bp and 2568 bp, indicated in white.

Correct assembly was confirmed with a diagnostic digest with restriction enzyme SphI-HF. Correct incorporation of perforin would result in two bands at 2021 bp and 2568 bp, instead of a singular band at 4661 bp. The diagnostic gel (Figure 5.27) showed 5 of the 6 plasmids had been correctly engineerd. Correct integration was subsequently confirmed with Sanger sequencing with primer CMVF_pCDNA3 and a glycerol stock was created, as described in section 2.2.10.

**proTLx-κ-CMV CD80-Fc (CMV-CD80-Fc)**

The fraction crystallisable (Fc) region of immunoglobulin can confer enhanced stability upon recombinant protein. Hence, the mouse Fc was added to the CD80 sequence used here. To create the proTLx-κ CMV-CD80-Fc plasmid (CMV-CD80-Fc), the Fc fragment was amplified with the primers JKH_073 and JKH_074 from proTLx-κ N3X2 Mouse Chimaera. The cycling parameters for generating the Fc cloning fragment were 98 ºC for 30 seconds, 35 cycles of 98℃ for 10 seconds and 72 ºC for 35 seconds, followed by 72 ºC for 2 minutes. The PCR product of 723 bp was run on an agarose gel (Figure 5.28), cut out and purified. The fragment was confirmed by Sanger sequencing with primer JKH_116. The proTLx-κ backbone, generated as described in the CMV-Perforin section above, was ligated with this Fc fragment and the custom CD80 gBlock, which had overlapping sequences with the backbone and Fc fragment to enable effective ligation (Figure 5.29).

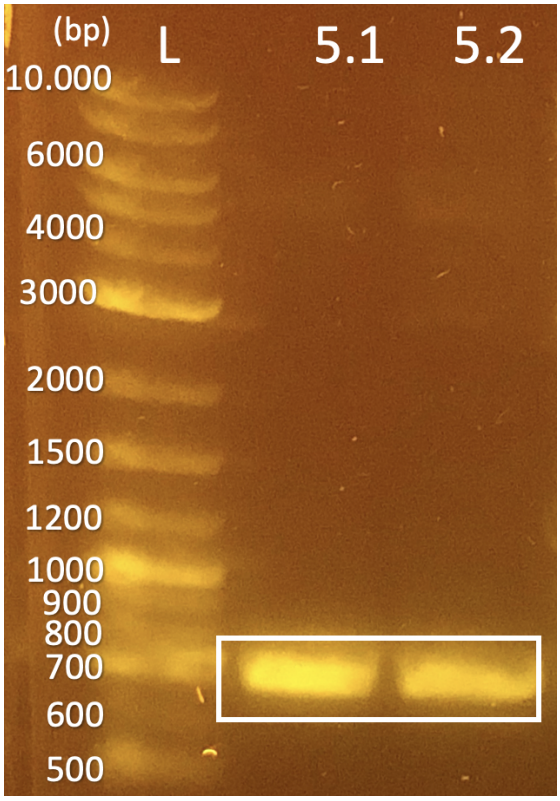



**Figure 5.28.** Agarose gel with the PCR products for amplification of the Fc fragment from proTLx-κ N3X2 Mouse Chimaera for the construction of proTLx-κ CMV-CD80-Fc. On the left, a 1 kb plus DNA ladder was run and the molecular weight of the bands in basepairs is depicted. Two samples were assessed. The white box indicated the desired fragment of 723 bp.

Correct assembly was confirmed by diagnostic PCR with the primers HW_012 and JKH_117, which annealed on the backbone and the CD80 fragment respectively. The cycling parameters were 98 ºC for 30 seconds, 35 cycles of 98℃ for 10 seconds and 72 ºC for 55 seconds, followed by 72 ºC for 2 minutes. Correct assembly would result in a fragment of 1688 bp. All clones showed a band at the correct migration distance, with colonies 2 and 3 showing the greatest intensity of signal at the migration distance for 1688 bp (Figure 5.30). Correct integration was subsequently confirmed with Sanger sequencing with CMVF_pCDNA3 and a glycerol stock was created.

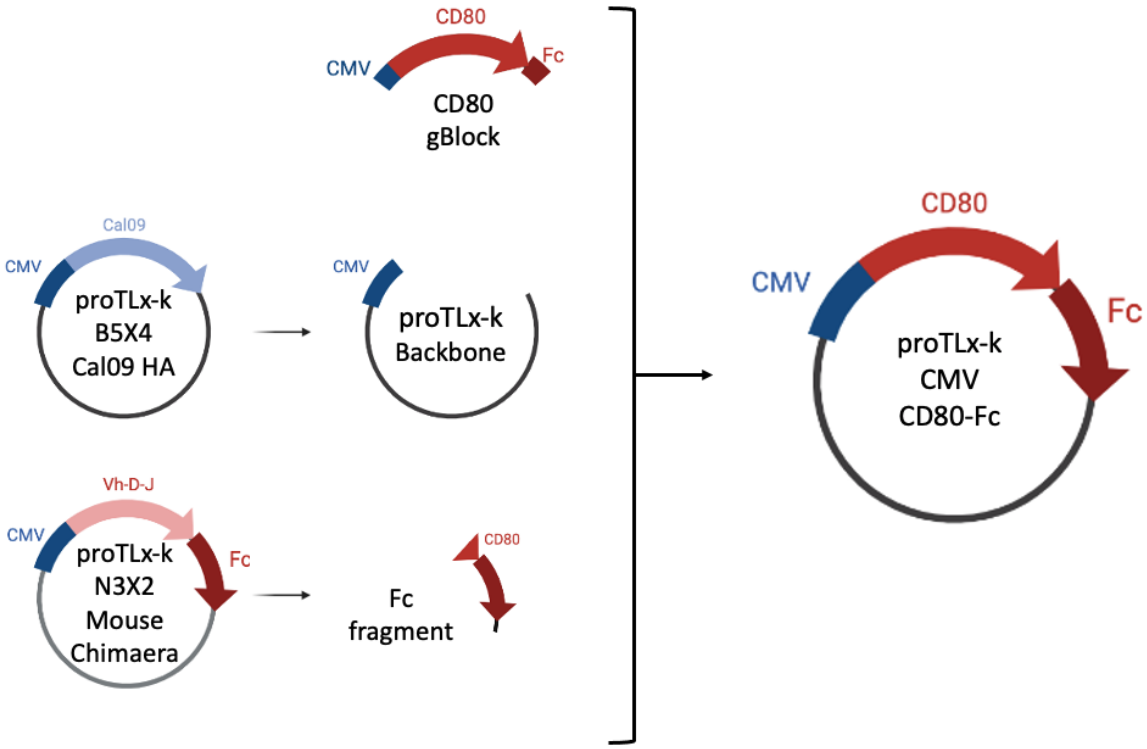



**Figure 5.29.** Schematic representation of the cloning of the proTLx-κ CMV-CD80-Fc plasmid. The proTLx-κ B5X4 backbone, including the CMV promoter, was PCR-amplified. The CD80 gene with ends overlapping the backbone and the Fc fragment was ordered as a gBlock. The Fc-fragment was PCR-amplified of the proTLx-κ N3X2 Mouse Chimaera. These three fragments were ligated together to form proTLx-κ CMV-CD80-Fc plasmid.

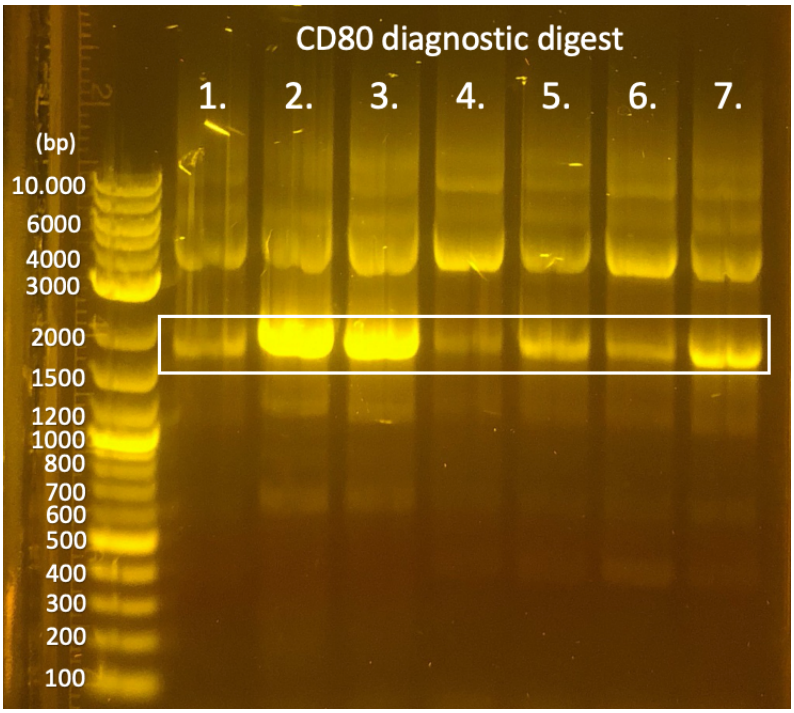



**Figure 5.30.** Products of a diagnostic PCR of proTLx-κ CMV-CD80-Fc were run on an agarose gel. On the left side a 1 kb plus DNA ladder was loaded and the weight in basepairs is indicated. The numbers on top indicate the different colony numbers which were assigned to colonies positive for kanamycin resistance. Successful construction of proTLx-κ CMV-CD80-Fc would result in a 1688 bp band, indicated by the white box.

**proTLx-κ CMV-Flt3l-Fc (CMV-Flt3l-Fc)**

To create the proTLx-κ CMV-Flt3l-Fc plasmid (CMV-Flt3l-Fc), the Fc fragment was amplified from proTLx-κ N3X2 Mouse Chimaera with the primers JKH_057_alt and JKH_058. The cycling parameters for generating the Fc fragment were 98 ºC for 30 seconds, 35 cycles of 98℃ for 10 seconds and 72 ºC for 35 seconds, followed by 72 ºC for 2 minutes. The PCR product of 732 bp was run on an agarose gel, cut out and purified (Figure 5.31). This fragment was checked by Sanger sequencing with primer JKH_116.

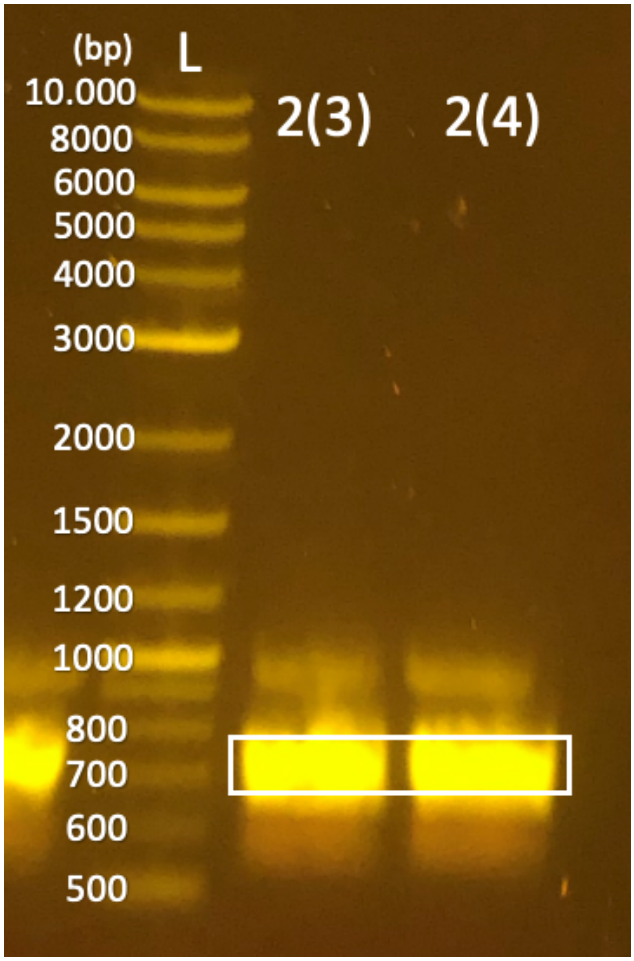



**Figure 5.31.** Agarose gel with the PCR products for amplification of the Fc fragment from proTLx-κ N3X2 Mouse Chimaera for the construction of proTLx-κ CMV-Flt3l-Fc. On the left, a 1 kb plus DNA ladder was run and the molecular weight of the bands in basepairs is depicted. Two samples were assessed. The white box indicates the desired fragment of 732 bp.

For the Flt3l fragment, the annealing temperature was determined by a temperature gradient with primers JKH_059 and JKH_060 and template proTLx-κ Flt3L-Flex-C Ag. The cycling parameters were 98 ºC for 30 seconds, 35 cycles of 98 ºC for 10 seconds, 50-72 ºC for 20 seconds and 72 ºC for 12 seconds, followed by 72 ℃ for 2 minutes. The PCR product of 594 bp was run on an agarose gel (Figure 5.32). All temperatures showed good annealing. An annealing temperature of 69 ºC was selected. A new PCR reaction was run with the optimised annealing temperature, the correct band cut out and purified. This fragment was sent for Sanger sequencing with primer JKH_114.

The proTLx-κ backbone, as described in the CMV-Perforin section above, was ligated with this Fc fragment and Flt3l fragment (Figure 5.33). Correct assembly was confirmed with Sanger sequencing with primer CMVF_pCDNA3.

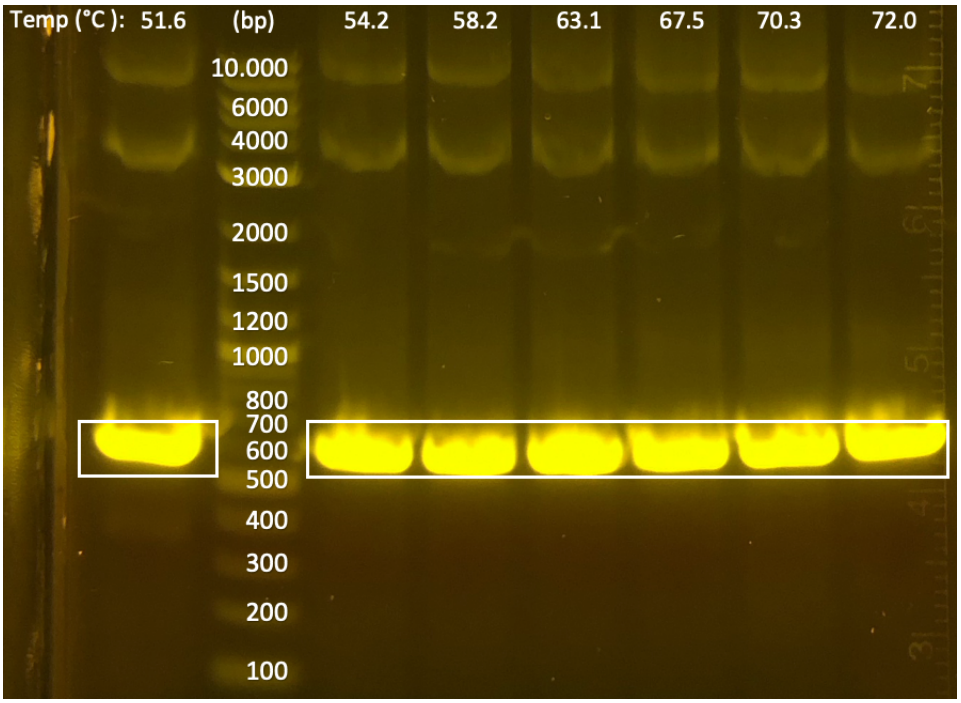



**Figure 5.32.** Agarose gel with the PCR products for different annealing temperatures of the Flt3l fragment. In the second lane from the left, a 1 kb plus DNA ladder was run and the molecular weight of the bands in basepairs is depicted (L). The annealing temperature is displayed at the top of the wells. The white box indicates the desired fragment of 594 bp.

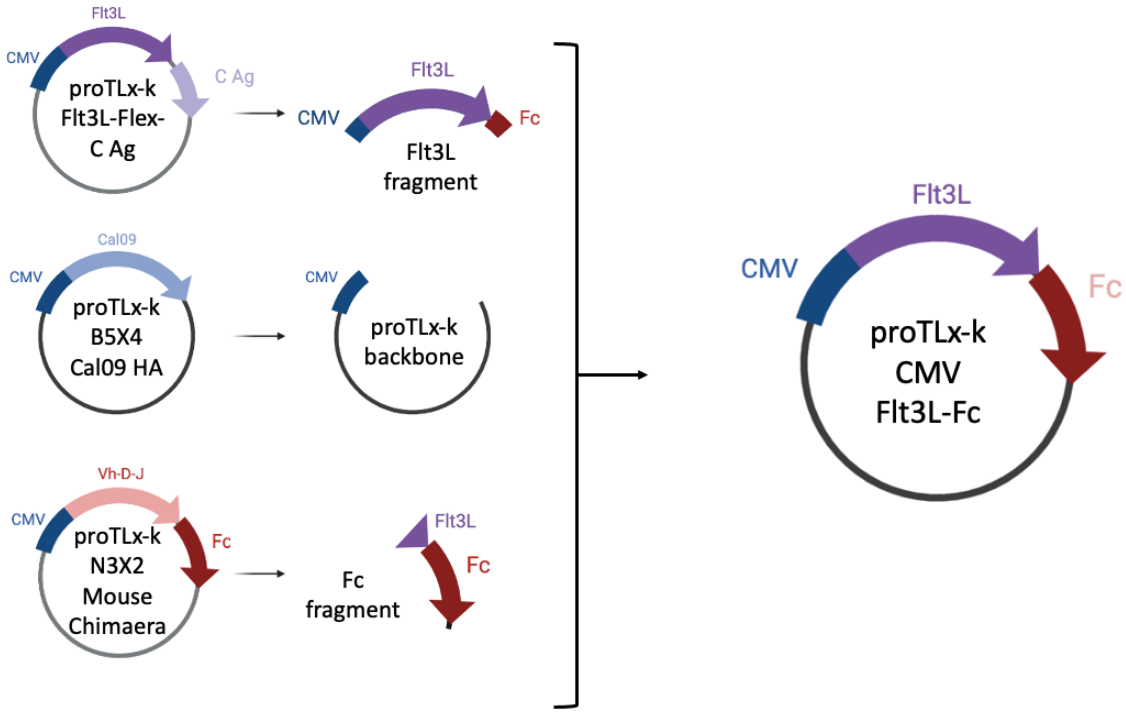



**Figure 5.33.** Schematic representation of the cloning of the proTLx-κ CMV-Flt3l-Fc plasmid. The proTLx-κ B5X4 backbone, including the CMV promoter, was PCR-amplified. The Flt3l-fragment was PCR-amplified of the proTLx-κ Flt3L-Flex-C Ag. The Fc-fragment was PCR-amplified of the proTLx-κ N3X2 Mouse Chimaera. These three fragments were ligated together to form proTLx-κ CMV-Flt3l-Fc plasmid.

### 5.3.6 *In vivo* evaluation of the second generation DNA adjuvant vectors

#### Intradermal injection

To test the *in vivo* effect of the novel adjuvant DNA vectors, which include the vectors CMV-Flt3l-Fc, CMV-CD80-Fc and CMV-Perforin, mice were intradermally injected and subsequently homologously boosted on day 21. Blood was sampled on day 14, 20, 29, 35, 42 and a terminal bleed was taken on day 83. The results of the IgG ELISA are summarised in Figure 5.34.

As can be seen from Figure 5.34, intradermal injection elicited relatively high levels of antibodies. Within the intradermally injected groups, mice treated with adjuvant DNA vectors (CMV-Flt3l-Fc, CMV-CD80-Fc and CMV-Perforin) did not have an improved antibody level compared to the antigen pDNA-only group (CMV-Cal09). The adjuvant CMV-Perforin does not seem to have particular benefit upon intradermal injection (mean 2.42 AU vs 2.55 AU) and had a greater standard deviation than the control CMV-Cal09 (SD: 0.38 AU vs 0.15 AU).

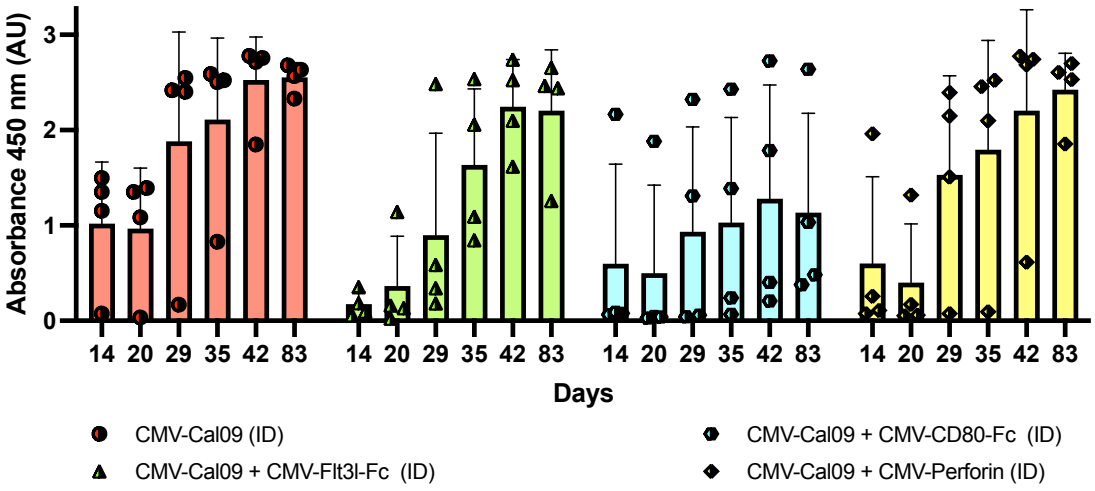
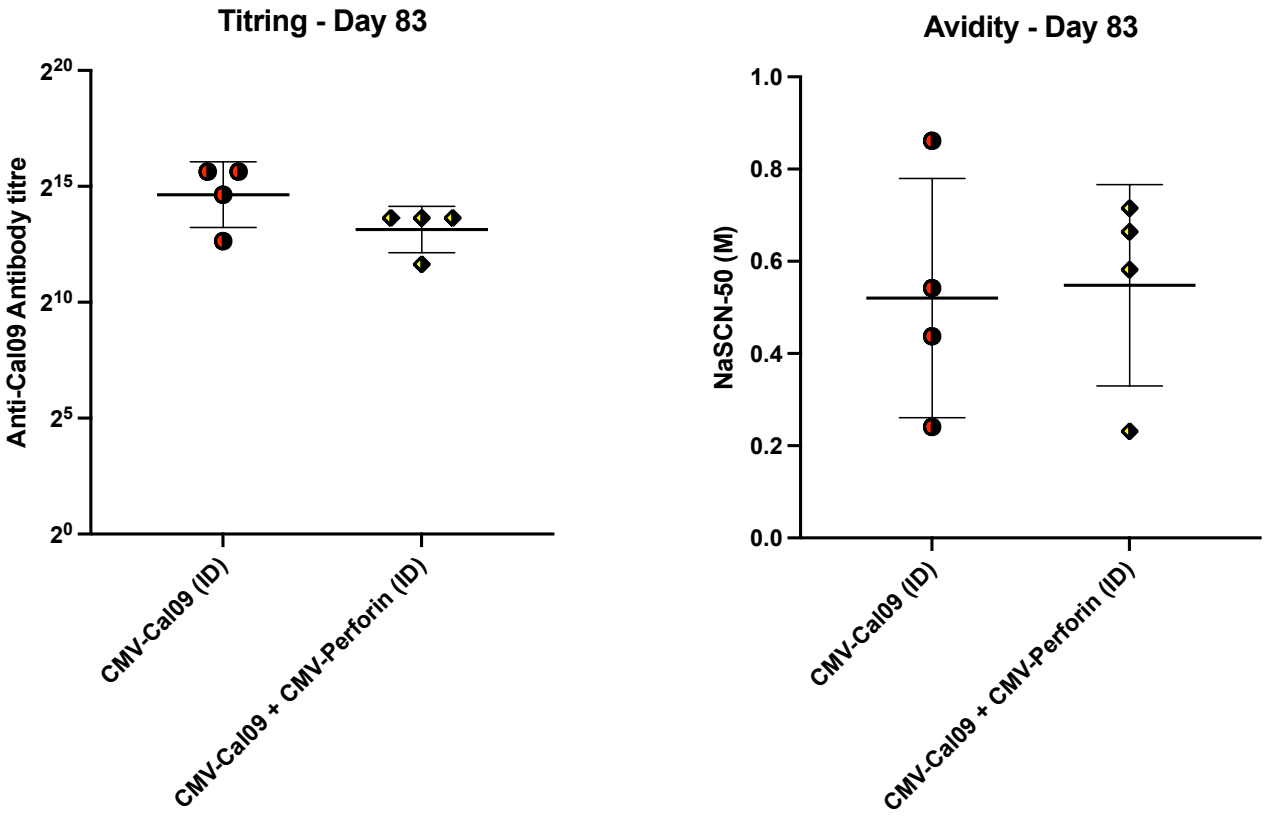



**Figure 5.34.** Analysis of the anti-Cal09 HA antibody levels, determined by ELISA, from the *in vivo* experiment to evaluate the second generation of DNA adjuvants over time. Mice were intradermally injected (ID) with 142 µg CMV-Cal09, and optionally 142 µg CMV-Flt3l-Fc or 142 µg CMV-CD80-Fc or 142 µg CMV-Perforin. N = 4, mean (bar height) and SD (error bars) are displayed. A two-way ANOVA (vector x time) was done with a Tukey post hoc test between treatments for the different timepoints. A significant effect of time ($p<0.0001$), subject ($p<0.0001$) and interaction between vector and time ($p<0.05$) was observed. No significant effect of vector was observed ($p=0.41$). Multiple comparisons showed $p>0.05$ for all vector comparisons for each timepoint.

To confirm the difference in antibody levels, serum samples of the 'CMV-Cal09' and 'CMV-Cal09 + CMV-Perforin' groups were titred (Figure 5.35a). CMV-Perforin appeared to have a negative effect on the titre in the intradermally injected group with a 2.8-fold lower antibody titre compared to CMV-Cal09 (ID). However, the avidity for the antibodies shows no difference upon inclusion of the CMV-Perforin



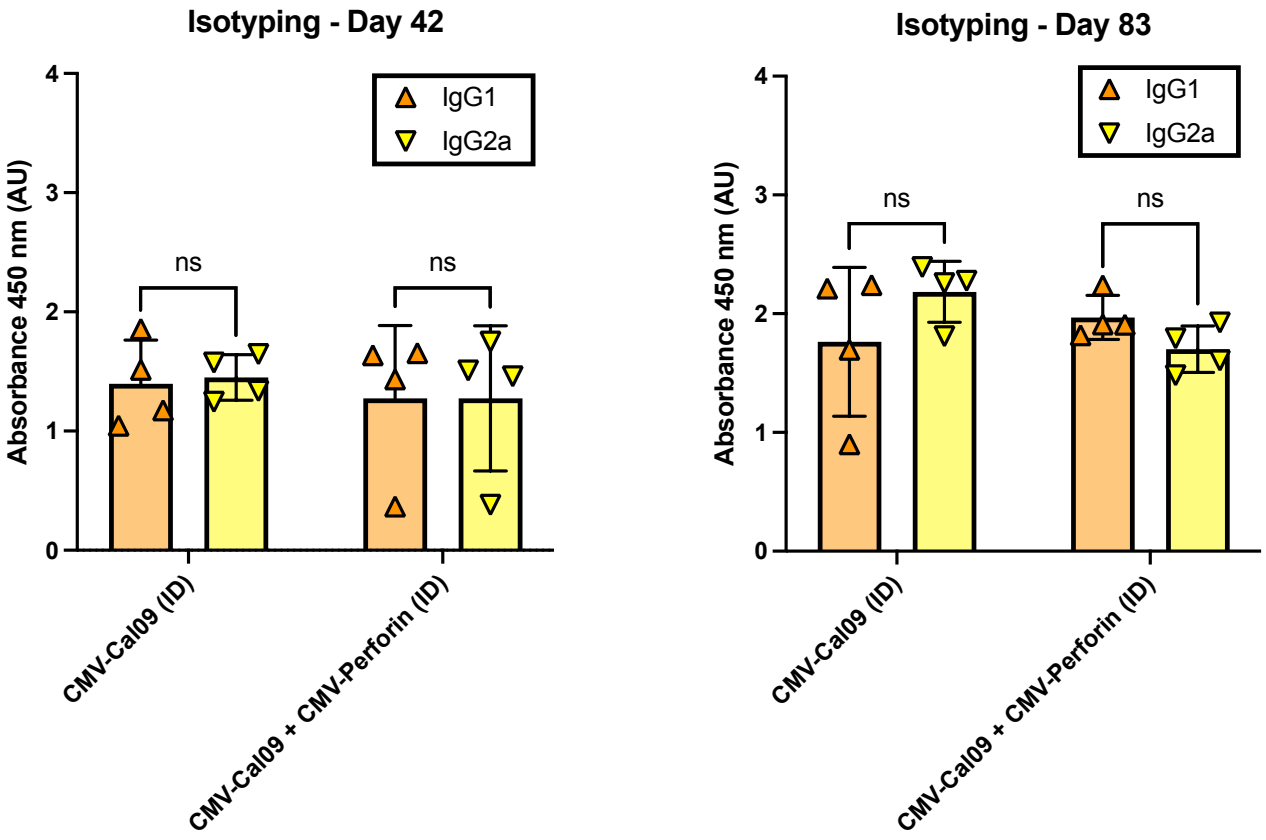

**(a)** Titring **(b)** Avidity

**Figure 5.35.** Titring and avidity of anti-Cal09 HA IgG antibodies generated, as determined by ELISA. Groups of 4 mice were intradermally injected (ID) with 142 µg CMV-Cal09, and optionally 142 µg CMV-Perforin. N=4. Significance was assessed with a Welch's t-test, p>0.05 a) Titred antibody levels upon intradermal injection with different DNA vectors. Geometric means (horizontal bars) $\times/\div$ geometric SD (error bars) are displayed. b) Avidity of the antibodies generated upon intradermal injection with different DNA vectors. Means (horizontal bars) and SD (error bars) are displayed.

vector in the treatment (0.52 M vs 0.55 M) (Figure 5.35b).

Furthermore, the IgG1 and IgG2a isotypes of the antibodies for these groups was determined on day 42 and day 83 (Figure 5.36). As seen in chapter 2, upon intradermal injection of CMV-Cal09, a balanced IgG1/IgG2a antibody response is seen. This is also the case when CMV-Perforin is added.

Finally, the cellular immune response was assessed for 'CMV-Cal09' and 'CMV-Cal09 + CMV-Perforin' (Figure 5.37). This showed that the addition of CMV-Perforin resulted in a (non-significant p>0.05) 1.4-fold increase in spot-forming units. This could be a reflection of the mechanism of CMV-Perforin, which is normally part of the arsenal of cytotoxic T cells and forms pores in cells. This agrees with previous work, which showed that the addition of CMV-Perforin increases the number of CD8+ TNF$\alpha$+ IFN-$\gamma$+ cells [261]. Hence, it appears that CMV-Perforin can stimulate the cellular immune response but shows no marked benefit in terms of the humoral antibody response.




**(a)** Day 42 **(b)** Day 83

**Figure 5.36.** Isotyping of anti-Cal09 HA IgG antibodies after 42 days (a) and 83 days (b), as determined by ELISA. Groups of 4 mice were intradermally injected (ID) with 142 µg CMV-Cal09 or 142 µg CMV-Cal09 with 142 µg CMV-Perforin. N=4, mean (bar) and SD (error bars) displayed. A two-way ANOVA (vector x isotype) was done with a post-hoc test between isotypes for each group using the Šidák correction for multiple comparisons. $p>0.05$ for all groups. No significant effect ($p>0.65$) of isotype, vector or their interaction was observed for either timepoint. A significant effect of the subject was observed ($p=0.01$) for day 42, but not day 83 ($p=0.48$).

Based on this data, both CMV-Flt3l-Fc and CMV-CD80-Fc appeared to have a detrimental effect upon intradermal injection and CMV-Perforin appeared to have a neutral to slightly decreased effect on total antibody levels but increased cellular immunity. However, as accumulated evidence in this thesis indicates that cavitation targets different cell populations, all three adjuvants were also tested with cavitation rather than I.D. injection.

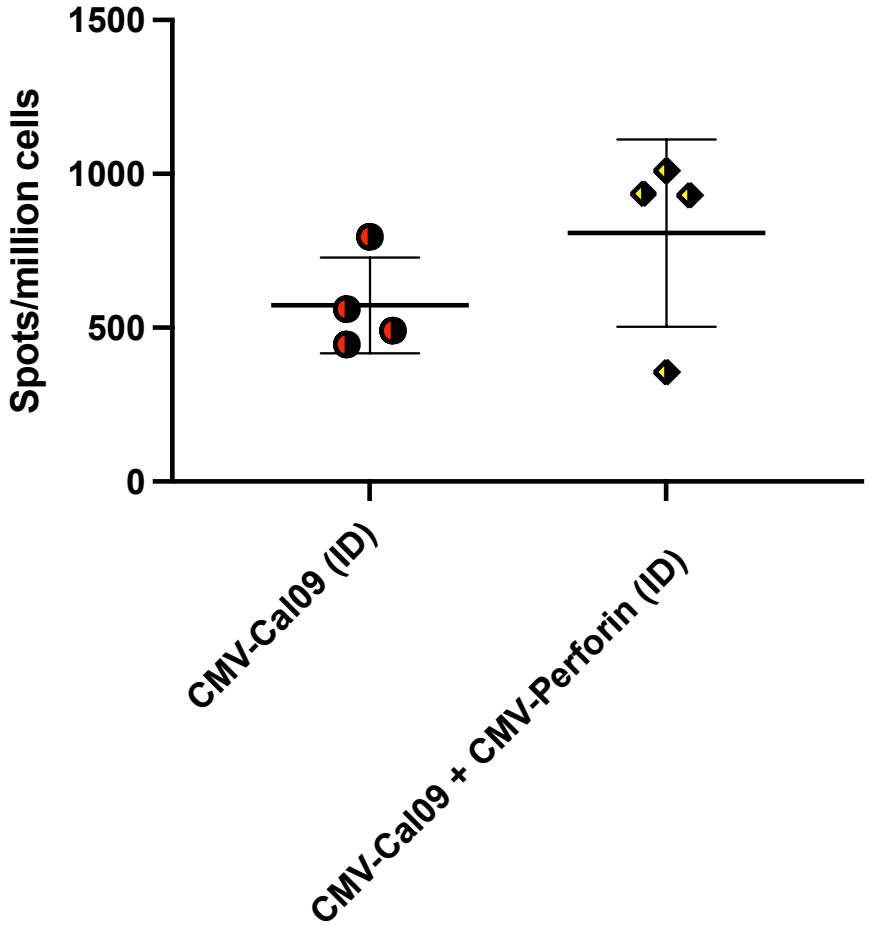



**Figure 5.37.** Analysis of the spot-forming units (SPU) per million cells, determined by ELISpot, from the *in vivo* experiment to evaluate the second generation of DNA adjuvants. Mice were intradermally injected (ID). N = 4, mean (horizontal line) and SD (error bars) are displayed. Significance was assessed with a Welch's t-test, $p>0.05$.

**Cavitation-mediated delivery**

Having verified that DNA could effectively be delivered by 3G-H p-CaN in section 5.2.3, the different adjuvant DNA vectors were tested *in vivo* with cavitation. Mice were primed and then homologously boosted on day 21. Blood was sampled on day 14, 20, 29, 35 and 42. A terminal bleed was taken on day 83, as well as spleens for an ELISpot. The results of the IgG ELISA from the bleeds are summarised in Figure 5.38.

Compared to the intradermal groups (Figure 5.38), lower mean antibody levels were observed in the cavitation groups for CMV-Cal09 without and with CMV-Flt3l-Fc or CMV-CD80-Fc ($p<0.001$, two-way ANOVA (vector x treatment)). The addition of the DNA adjuvants CMV-Flt3l-Fc and CMV-CD80-Fc showed barely any antibody response and no benefit compared to 'CMV-Cal09 (CAV)' (Welch's t-test for day 83, $p>0.05$). Interestingly, the addition of CMV-Perforin did result in all mice generating an immune response, as well as 1.7-fold higher mean antibody levels compared to 'CMV-Cal09 (CAV)', showcasing the benefit of the CMV-Perforin vector as an adjuvant, when used in combination with cavitation. In the cavitation-treated mice, both the 'CMV-Cal09 (CAV)' and the 'CMV-Cal09 + CMV-Perforin (CAV)' group showed an increase in antibody levels at least until day 83, when the experiment was concluded. Compared to the intradermally injected mice (Figure 5.34), the increase is more gradual and does not reach the same levels. This may be a reflection of the lower levels of DNA delivered by cavitation and the additional time needed for a lower amount of expressed protein to induce an immune response.

To confirm the difference in antibody levels, serum samples of the 'CMV-Cal09' and 'CMV-Cal09 + CMV-Perforin' groups for the cavitation-treated mice were titred (Figure 5.39a). This further confirmed the benefit of CMV-Perforin as an adjuvant, as CMV-Cal09 + CMV-Perforin (CAV) had a 10.6-fold higher average geometric mean titre compared to CMV-Cal09 (CAV) alone (672.7 vs 63.3). Interestingly, where the addition of CMV-Perforin appeared to have a negative effect on the titre in the intradermally injected group with a 2.8-fold lower antibody titre compared to 'CMV-Cal09 (ID)', the addition of CMV-Perforin provided advantage in combination with cavitation-mediated delivery.

In terms of avidity (Figure 5.39b), the addition of CMV-Perforin increased the avidity by 1.5-fold compared to 'CMV-Cal09 (CAV)' in the cavitation-treated mice. As poor avidity has been related to disease susceptibility [271], the higher avidity seen upon the addition of CMV-Perforin, could result in better protection from disease. This is in contrast to the results from intradermal injection (Figure

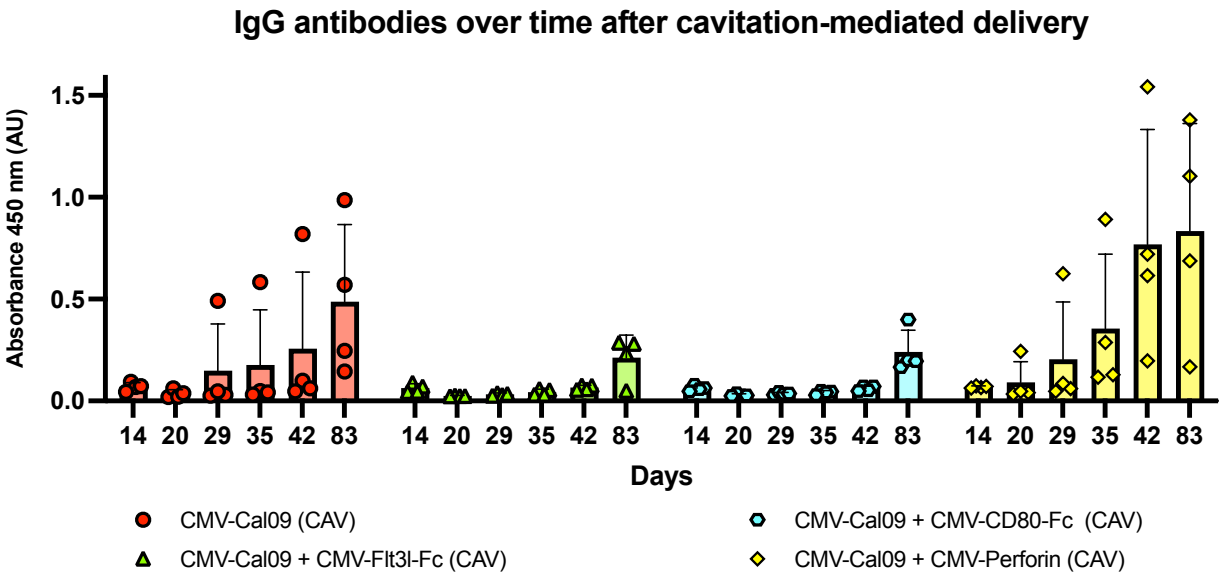
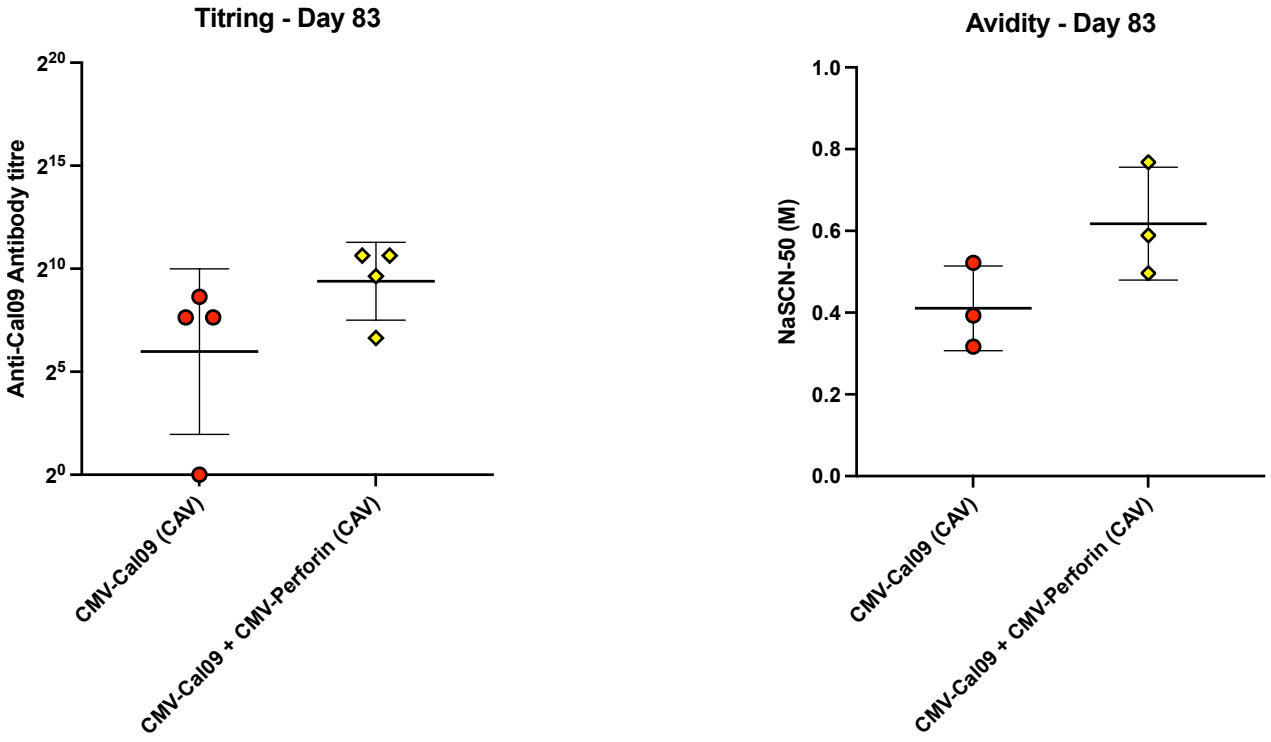



**Figure 5.38.** Analysis of the anti-Cal09 HA antibody levels, determined by ELISA, from the *in vivo* experiment to evaluate the second generation of DNA adjuvants over time. Mice were treated by 3G-H p-CaN and ultrasound-mediated cavitation (CAV) at 1.7 MPa for 2 minutes with 142 µg CMV-Cal09 and optionally 142 µg CMV-Flt3l-Fc or CMV-CD80-Fc or CMV-Perforin vector. N = 4, mean (horizontal lines) and SD (error bars) are displayed. A two-way ANOVA (vector x time) was done with a Tukey post hoc test between treatments for the different timepoints. A significant effect of time ($p=0.0002$), subject ($p<0.0001$) and interaction between vector and time ($p=0.001$) was observed. No significant effect of vector was observed ($p>0.05$). Multiple comparisons showed $p>0.05$ for all vector comparisons for each timepoint.

5.35b), where CMV-Perforin provided no advantage in terms of avidity.

The IgG1 and IgG2a isotypes of the antibodies for the 'CMV-Cal09 (CAV)' and 'CMV-Cal09 + CMV-Perforin (CAV)' groups was measured on day 42 and day 83 (Figure 5.40). As seen in Chapter 2, the cavitation-treated group do not show any IgG2a antibodies and generated only IgG1 antibodies. As previously mentioned, this may be related to cavitation delivering to the Langerhans cells in the epidermis, whereas intradermal injection results in delivery to the dermis. As seen in chapter 2, upon intradermal injection of CMV-Cal09, a balanced IgG1/IgG2a antibody response was seen. This is also the case when CMV-Perforin was added to an intradermally injected dose (Figure 5.36b). However, even the addition of CMV-Perforin does not improve the IgG1/IgG2a antibody balance for cavitation-delivered pDNA, implying that upon cavitation-mediated delivery a predominantly humoral response with Th2 immune response is generated.

Finally, the cellular response was probed for the 'CMV-Cal09' and 'CMV-Cal09 + CMV-Perforin' groups after I.D. injection and cavitation-mediated delivery. Only the mice with clear antibody responses on day 42 were analysed. As there was only one mouse in the 'CMV-Cal09 (CAV)' group, no strong conclusions can be drawn from the remarkably high SFU/million cells (Figure 5.41). For

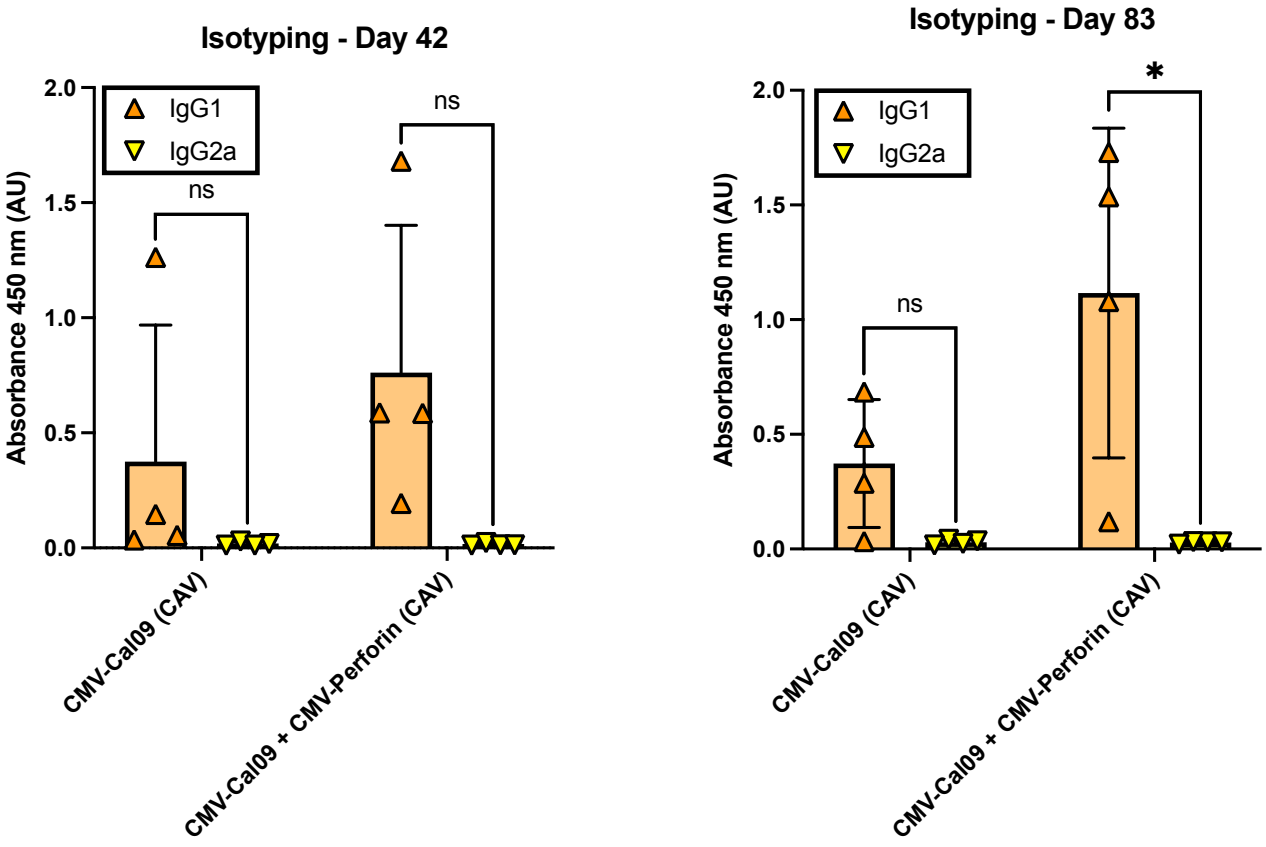



**(a)** Titring **(b)** Avidity

**Figure 5.39.** Titring and avidity of anti-Cal09 HA IgG antibodies generated, as determined by ELISA. Mice were treated by 3G-H p-CaN and ultrasound-mediated cavitation (CAV) at 1.7 MPa for 2 minutes with 142 µg CMV-Cal09 or 142 µg CMV-Cal09 and 142 µg CMV-Perforin vector. N=4. Significance was assessed with a Welch's t-test. a) Titred antibody levels upon cavitation-mediated delivery of different DNA vectors. Geometric means (horizontal line) $\times/\div$ geometric SD (error bars) displayed. $p>0.05$. b) Avidity of the antibodies generated upon cavitation-mediated delivery of different DNA vectors. Means (horizontal line) and SD (error bars) are displayed. $p>0.05$.

the 'CMV-Cal09 + CMV-Perforin', cavitation-mediated delivery resulted in lower cellular immunity than intradermal injection (mean 337.5 vs 807.5 SFU) (Figures 5.41 and 5.37). A similar trend was seen in the antibody levels and the lower SFU/million cells may be related to the relatively low levels of DNA delivered with cavitation compared to direct injection as discussed in section 5.3.1 or a reflection of the immune cascade set into motion by Langerhans cells, which results in a more humoral and Th2-skewed immune response.

Despite not generating a strong cellular immune response, the addition of CMV-Perforin resulted in higher antibody titres and higher avidity. This shows that CMV-Perforin may be a valuable adjuvant for increasing antibodies levels upon cavitation-mediated delivery.




**(a)** Day 42 **(b)** Day 83

**Figure 5.40.** Isotyping of anti-Cal09 HA IgG antibodies after 42 days (a) and 83 days (b), as determined by ELISA. Mice were treated by 3G-H p-CaN and ultrasound-mediated cavitation (CAV) at 1.7 MPa for 2 minutes with 142 µg CMV-Cal09 or 142 µg CMV-Cal09 and 142 µg CMV-Perforin vector. n = 4, mean (horizontal line) and SD (error bars) are displayed. A two-way ANOVA (isotype x vector) was done with a post-hoc test between isotypes for each group using the Šidák correction for multiple comparisons. ns = $p>0.05$, * = $p<0.05$. No significant effect of vector, subject or the interaction between vector and isotype was observed for either timepoint. A significant effect of isotype was observed ($p<0.05$) for both days.

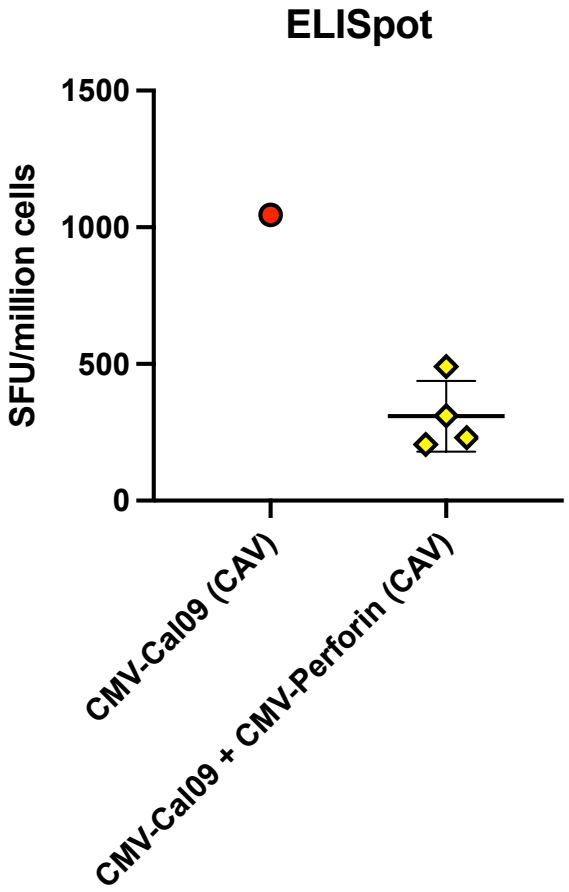



**Figure 5.41.** Analysis of the spot-forming units (SPU) per million cells, determined by ELISpot, from the *in vivo* experiment to evaluate the second generation of DNA adjuvants. Mice were treated by ultrasound-mediated cavitation (CAV). N = 4, mean and SD are displayed. No further statistics could be done due to the low number of mice in the 'CMV-Cal09 (CAV)' group (n=1).

### 5.3.7 *in vivo* to assess immunogenicity with optimised parameters and the addition of an adjuvant

In the previous section, the CMV-Perforin vector was identified as a useful adjuvant to boost the immunogenicity of the cavitation-delivered CMV-Cal09 vector. To further demonstrate the potential of CMV-Perforin as an adjuvant, the experiment from the previous chapter (section 4.3.7) was repeated with the addition of CMV-Perforin.

Two groups of mice were treated with 90 µg of CMV-Luc and 90 µg CMV-Perforin. One group was intradermally injected and the other group was treated with 2G-U p-CaN and ultrasound. The mice were imaged after 24 hours. Two mice from each group were then culled and skin sections fixed to assess any damage resulting from the perforin or the ultrasound. The four remaining mice in each group were subsequently boosted homologously after 21 days and again imaged after 24 hours.

#### IVIS

The levels of luminescence are displayed in Figure 5.42 and show that after the prime, the cavitation-treated mice had a slightly higher, although not significant, mean level of luminescence than the injected group (mean levels: $2.63x10^5$ p/s vs $1.23x10^5$ p/s) (Welch's t-test, $p>0.05$). Similar levels of luminescence were achieved in the cavitation group upon boosting ($2.72x10^5$ p/s) compared to prime (Welch's t-test, $p>0.05$). Levels were more variable after boosting for the intradermally injected group, which showed very strong luminescence in 3 out of 4 mice (mean of $3.73x10^7$ p/s). Indeed, these levels were 10-fold higher than any previously seen in experiments in this thesis. The huge variability in the I.D. levels following prime and boost is hard to reconcile.

#### Cavitation

The cavitation levels were comparable between the mice during the prime treatment (range: 3.76-6.86 µJ, mean: 5.67 µJ, SD: 1.36 µJ). However, the boost showed greater variability with a mean cavitation of 17.05 µJ TASE and a standard deviation of 15.43 µJ (range 7.10-39.83 µJ). It should be noted though, that despite the high standard deviation, all TASE values were above 7.0 µJ for the boost. All these TASE values were above the 3.5 µJ threshold for delivery (Figure 5.43), as was also evident from luminescence seen after 24 hours. Notably, if the inertial components (wide frequency spectra) of TASE are compared, the prime and boost show very similar mean values (3.24 µJ vs 3.95 µJ). A possible source for the stable cavitation may be p-CaN which did not collapse to form a cup

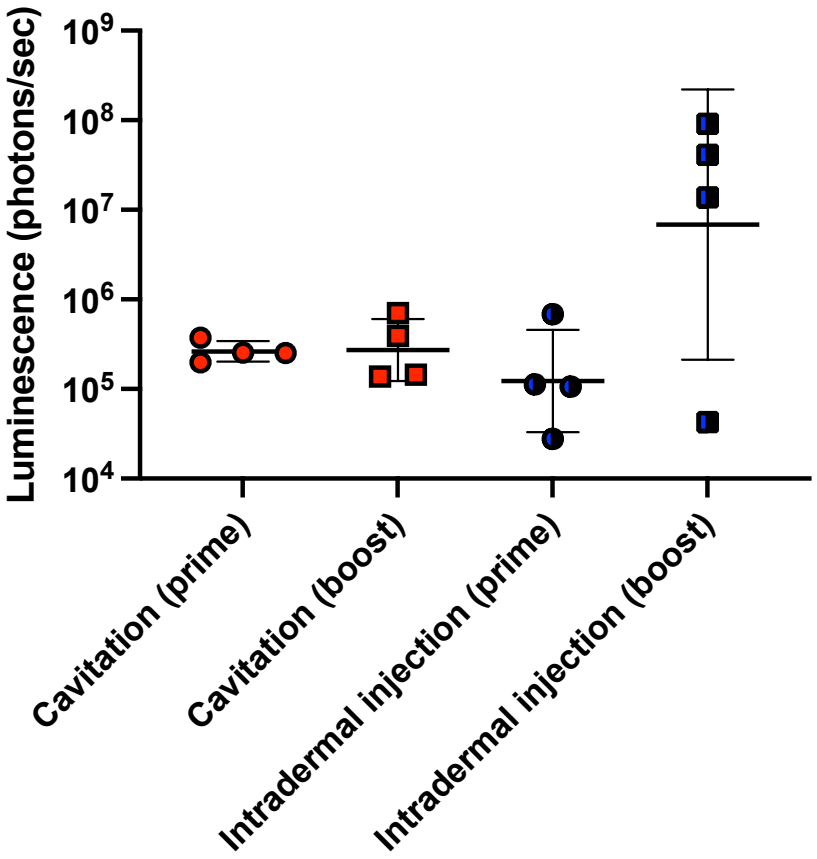



**Figure 5.42.** Luminescence after priming and boosting in mice intradermally injected with 90 µg CMV-Luc and µg CMV-Perforin or treated with cavitation, BSA 2G-U p-CaN and 90 µg CMV-Luc and 90 µg CMV-Perforin. IVIS imaging was performed as described in section 2.2.5. N = 4, geometric means (horizontal line) ×/÷ geometric SD (error bars) are displayed.

during manufacture and became large protein bubbles or alternatively may represent gas dissolved in the water.

### Anti-Luciferase ELISA

In this *in vivo* study, the DNA adjuvant CMV-Perforin was added to improve the immunogenicity of the CMV-Luc vector. The anti-Luc ELISA (Figure 5.44) shows the anti-Luc antibody concentration was significantly ($p<0.05$) higher in the cavitation-treated group compared to the intradermally injected group (mean 1114 ng/mL vs 81 ng/mL). This is surprising considering the mean luminescence levels from the intradermally injected group were over 100-fold higher compared to the cavitation-treated group after the boost. This does further emphasise that total protein expression does not necessarily directly relate to effective immunity and cavitation-mediated delivery of a fractional dose can elicit high antibody levels. It also further showcases the ability of CMV-Perforin to increase antibody levels in combination with cavitation-mediated delivery of a DNA vaccine.

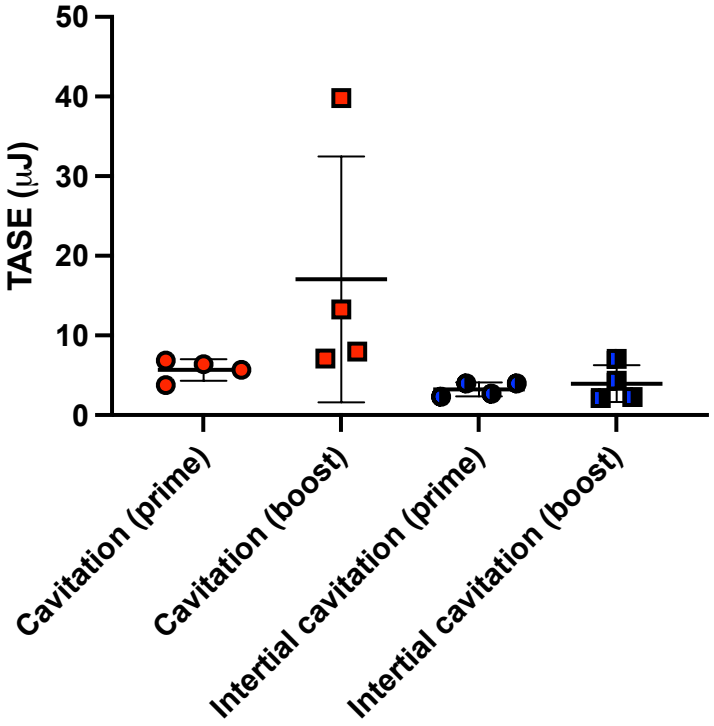



**Figure 5.43.** Cavitation levels during prime (circles) and boost (squares) treatment of mice treated with cavitation and 90 µg CMV-Luc and 90 µg CMV-Perforin. Both the cavitation TASE (red) and the inertial component of the cavitation TASE (blue) are displayed. N = 4, mean (horizontal bars) and SD (error bars) are displayed.

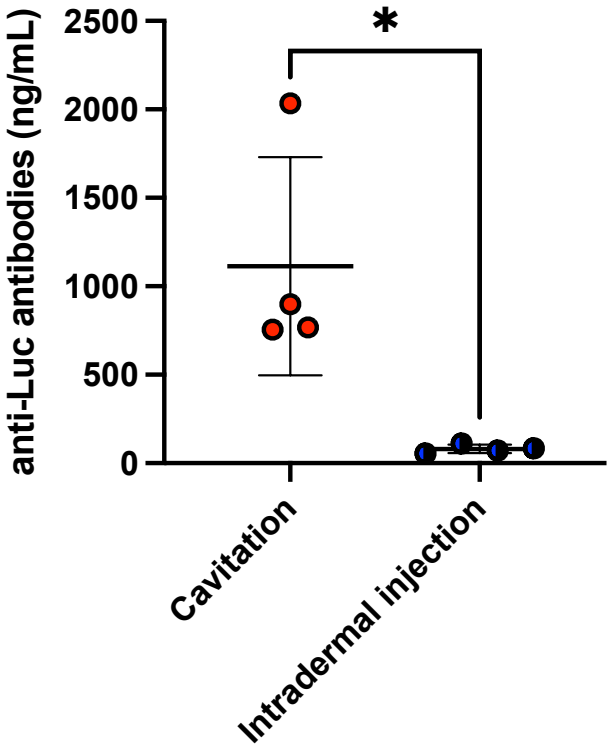



**Figure 5.44.** Analysis of the anti-Luc antibody levels on day 42, determined by ELISA for serum samples diluted 1:100 in PBS. Mice were either intradermally injected with 90 µg CMV-Luc and 90 µg CMV-Perforin or treated with cavitation and 90 µg CMV-Luc and 90 µg CMV-Perforin. They were boosted after 21 days. N = 4, mean (horizontal lines) and SD (error bars) are displayed. Significance was assessed with a Welch's t-test, * = $p<0.05$.

### Histology

The skin sections 24 hours after treatment with cavitation or intradermal injection were assessed for skin damage, and compared to some untreated control skin. The sections were stained with haematoxylin and eosin and the section evaluated under a microscope. These showed no significant impact from either the injection or ultrasound treatment after 24 hours. No acute inflammatory response or collagen remodelling was apparent after 24 hours. Exemple skin sections are displayed below (Figure 5.45).

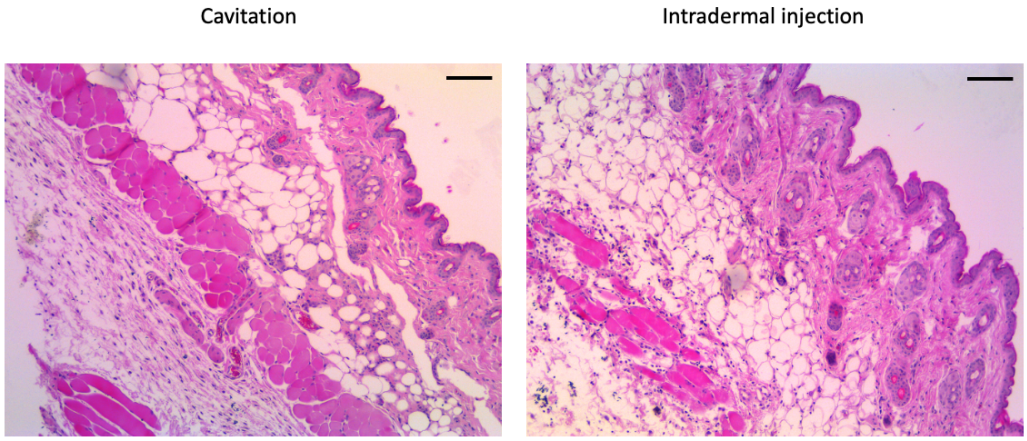



**Figure 5.45.** Two example images of skin from mice treated with cavitation or intradermally injected 24 hours prior to harvesting. The skin was stained with haemotoxylin and eosin, as described in section 5.2.6. Scalebar represents 100 µm.

## 5.4 Conclusions and Discussion

The aims of this chapter were to validate the cavitation of 3G-H p-CaN, to assess three DNA adjuvants and investigate the behaviour and merits of a self-amplifying vector.

Previous iteration of p-CaN had relied on an ultrasonic horn to generate spherical particles, which is not a scalable process. Hydrodynamic shearing, however, is a commonly used technique in industry and allows for easy upscaling of production [266]. Hence, the cavitation behaviour of this new generation of BSA 3G-H p-CaN, which was produced through hydrodynamic shearing, was assessed. Data showed that the p-CaN produced by this new method were capable of effectively delivering DNA at pressures above 1.2 MPa and that the DNA copy number retrieved from the skin was proportional to the pressure applied, based on qPCR data for the CMV-Luc pDNA. Interestingly, this relationship did not hold for the BSA protein delivered into the skin by the BSA p-CaN. This could indicate that the BSA protein delivered is independent of the pressure of ultrasound applied. The amount of BSA was also very similar to the amount observed when using 2G-U p-CaN. Overall, it appeared these 3G-H p-CaN would be a suitable alternative to the previously used 2G-U p-CaN and 1.7 MPa was selected as the pressure for future experiments. Indeed, the two could be used interchangeably for these development studies, in the knowledge that consistent results could be produced.

To further probe the relationship between DNA dose and protein expression, a lower and higher dose of pDNA was tested and the luminescence quantified. In terms of expression, a relationship was seen between pDNA dose and luminescence. Peculiarly, this same relationship could not be seen in the qPCR data, which did not show a dose-relationship between the DNA in the formulation holder and the level of pDNA recovered from the skin at 24 hours. Two possible explanations for this observation are, DNA was delivered to the cell nucleus proportional to the original dose and expresses luciferase. However, there is also a level of DNA that has not yet been cleared from the skin which remains present so can be detected by qPCR but does not express. However, this is contradicted by the short half-life of DNA in the cytoplasm. DNA in the cytoplasm has a half-life as low as 50-90 minutes due to degradation by cytosolic nuclease [272] and up to 99% of injected DNA into muscle has been reported to be cleared within 90 minutes of injection [273, 274]. The DNA clearance rate upon cavitation-mediated delivery could be tested by assessing luminescence and pDNA copy number at multiple time points, as it is still unknown where the DNA is deposited. An alternative explanation could be that although the DNA may be rapidly cleared, luciferase protein remains present in the skin for more extended periods. Luciferase has a half-life of approximately 3 hours [275]. Hence, an early

burst of expression of luciferase may explain why luminescence may be related to the DNA dose in the formulation holder but not the pDNA copy number in the skin after 24 hours. As a relationship was seen in expression and DNA dose, a dose of 142 µg of DNA was selected for the subsequent experiments.

Next, the characteristics of a self-amplifying vector based on the non-structural proteins from VEEV were investigated. To this end, two self-amplifying vectors were constructed: one with a reporter gene and one encoding haemagglutinin. Upon intradermal injection of the self-amplifying vector, a delay in increased expression of luciferase was seen. However, after 5 days, a marked increase in expression was observed, which remained high for over a month. This initial expression, followed by a second burst of protein expression is also reminiscent of a traditional prime/boost regime. In contrast the control non-amplifying vector remained at the same level or showed a decrease in expression. However, when this experiment was repeated with cavitation-mediated delivery, no increase (delayed or otherwise) was observed in luciferase expression for the self-amplifying vector. This could be related to the different cell types that are transfected by cavitation, which likely targets the epidermis, compared to the cells in the dermis, which are targeted by intradermal injection. It may be that the cells transfected in the epidermis by cavitation, lack the longevity needed for the self-amplifying vector to be expressed. Despite the lack of suitability of the self-amplifying vector for cavitation-mediated delivery, it showed promise as an intradermally injected vaccine candidate. Hence, it was further pursued by intradermally injecting the Cal09 HA antigen-encoding, self-amplifying vector into a mouse model. The self-amplifying vector showed remarkable high titre reproducibility, as well as very reproducible and higher avidity than the 'CMV-Cal09 (ID)' group. The self-amplifying vector also showed a lower IgG1/IgG2a ratio, implying a stronger cellular response than with the 'CMV-Cal09 (ID)' and greater ability to trigger CDC and ADCC. These distinct characteristics of the self-amplifying vector made it a compelling candidate for further investigation, as it may be more potent in protecting from disease despite lower overall antibody titres (see Chapter 6).

To assess the DNA vectors expressing potential adjuvants, the addition of the pDNA encoding adjuvants Flt3l-Fc, CD80-Fc and perforin was investigated over 83 days, following intradermal injection. No clear advantage of the adjuvants CMV-Flt3l-Fc and CMV-CD80-Fc was observed.

These results are surprising considering the number of studies that have reported the benefit of the addition of FLT3L. For instance, Zhang et al. showed that a recombinant rabies virus vaccine ex-

pressing mouse FLT3L resulted in a virus-neutralising antibody titre increase from 20.09 international units/mL to 33.53 international units/mL at 5 weeks post immunisation compared to a recombinant rabies virus without FLT3L, as well as increased survival (80% vs 45%) upon intramuscular injection of $10^6$ FFU and challenge after 21 days with 50% mouse intracerebral lethal dose 50 (MICLD50) of a pathogenic RABV strain (CVS-24) injected intracerebrally [276]. Also in the context of DNA vaccines, the addition of the *Flt3l* gene led to an increase in antibody titre in combination with a HPV16 E6/E7 DNA vaccine after I.M. delivery [227]. Addition of a FLT3L-encoding plasmid has also been beneficial when administered with microneedles into the epidermis of the skin, where a signficantly higher titre of HBsAg antibodies was observed upon addition of the FLT3L-encoding plasmid by Zhou et al. [226]. The plasmid used by Zhou et al. had the *Flt3l*-gene under the same promoter as in the study reported in this thesis, implying that the DNA vector should have successfully resulted in the expression of FLT3L in the epidermis. As no beneficial or clear detrimental effect was observed, this could mean that even though enough FLT3L was expressed, the protein had no added benefit. This may be related to the timescales of expression. If the effects of FLT3L are delayed compared to when antigen expression is maximised, an optimised dosing regime that takes advantage of this property may be necessary. Notably, Zhou et al. dosed three times with two week intervals. This may have allowed for the expression and mobilisation of haemapoietic progenitors for the boost treatments. To further probe this, additional work would be needed to assess how FLT3L is expressed upon I.D. injection and the timescales of its effect on mobilisation of haemopoietic progenitors to understand how FLT3L can optimally increase the immunogenicity of the antigen.

CD80 expression is commonly associated with vaccine efficacy [255–257] and a promising candidate for improving T cell responses [258] and protection against challenge [259]. It is specifically expressed by antigen-presenting cells and is a co-stimulatory signal for T cells [253]. However, there is less precedent for its function as an adjuvant and predominantly reported in the context of cancer vaccines and not in the context of dermal vaccination [258, 277]. It may be that CD80 expression is not beneficial in the dermal compartment as an adjuvant due to the large number of dendritic cells already present in the dermis, whereas in the muscle the addition of CD80 may have a greater relative impact or, alternatively, again timescales between expression of the CD80 and the expression of the adjuvant may not be well coordinated.

The final adjuvant assessed, CMV-Perforin ('CMV-Cal09 + CMV-Perforin (ID)' group) had lower antibody titres than the 'CMV-Cal09 (ID)' group. The CMV-Perforin vector showed no clear benefit in

combination with intradermal injection in terms of antibody levels, although it did increase the cellular immunity (808±304 SFU vs 573±156 SFU by ELISpot). This may be a reflection on the mechanism of perforin. Perforin forms pores in cells [260] and induces necrosis, which is a powerful signal for the mobilisation of the cellular immune response. Despite necrosis being the likely underlying mechanism, no evidence of necrosis or physical skin damage caused by the application of ultrasound could be observed after 24 hours on stained skin slides (Figure 5.45), which could suggest most of the acute inflammatory response has been resolved within 24 hours or the effects of perforin are not yet apparent due to the delay in transcription and translation. Further observation of skin collagen remodelling over time could also provide further insights on the impact cavitation and transgene expression may have on skin.

As there has been mounting evidence presented in this thesis that cavitation targets a different cell population compared to intradermal injection, the adjuvant-expressing DNA vectors were also assessed for their efficacy upon cavitation-mediated delivery. A potentially detrimental effect was observed for CMV-Flt3l-Fc and CMV-CD80-Fc after cavitation-mediated delivery. In the context of cavitation-mediated delivery, the lack of activity observed may, however, be related to the dose administered. Mice were dosed three times with 50 µg of FLT3L-encoding plasmid in the microneedle study by Zhou et al. In Chapter 4, section 4.3.6, it was shown that a fraction of the DNA in the formulation holder is delivered to the skin (0.08%). Even though the low level of DNA delivered by cavitation may result in sufficient antigen expression to elicit an immune response, the FLT3L or CD80 expressed may not be sufficient to result in an *in vivo* effect. If the amount of DNA delivered by cavitation is limited or the metabolic ability of the cells transfected becomes limited, the addition of the adjuvant may have been detrimental as it would have decreased the level of antigen expressed without providing an adjuvant effect. Quantification of the FLT3L and CD80 in the skin may provide some insight into levels expressed and levels needed for an adjuvant effect.

In contrast, the CMV-Perforin vector increased average antibody titre and avidity upon cavitation-mediated delivery, making it a useful adjuvant in this context. Notably, where 'CMV-Cal09 + CMV-Perforin' results in a balanced IgG1/IgG2a response upon intradermal injection, only IgG1 antibodies were generated upon cavitation-mediated delivery. This may be a reflection of the different cells transfected by cavitation. Langerhans cells specifically drive IgG1 responses ([89]) and may be targeted by cavitation. The observation that Langerhans cells specifically drive IgG1 responses, is supported by Stoecklinger et al., who showed that Langerin$^{+}$ dendritic cells are crucial of the induction of IgG1

antibodies, but not IgG2a antibodies [278]. The hypothesis that Langerhans cells may be targeted by cavitation is in line with observations from solid microneedles, which have been reported to stimulate Langerhans cells in human skin *ex vivo* and result in changes in Langerhans cell morphology and distribution [279]. In contrast, a study on gene gun delivery has shown that langerin$^+$ dermal dendritic cells are responsible for the IgG1 antibody response to gene guns but not Langerhans cells [278], which does raise the question which cell subpopulation is targeted by cavitation. An experiment looking into the transfection of different cell populations in the skin by cavitation would provide some insight into which cells drive the observed immune responses, as well as allow for more informed decisions on other potentially valuable adjuvants. The second question is then whether Langerhans cells are an appropriate vaccination target, to which the answer is not yet clear, as reports exist that Langerhans cells may induce tolerance [280]. Interestingly, a report by Berger et al. suggests that Langerhans cells are capable of both immunity and tolerance, and factors such as level of cell death and danger signals may determine which response is elicited [281]. This would align with the findings reported here that the addition of perforin, which increases the amount of cell death and danger signals, increases the immune response, as Langerhans cells targeting may then improve immunity and downregulate a tolerance response.

Having observed a predominant IgG1 response, and little IgG2a antibodies by cavitation-mediated delivery, strategies to improve the IgG2a proportion in IgG antibodies would also be of interest. In particular as IgG2a has been shown to be associated with whole virus vaccination and natural infection in mice and enhanced immune responses [282, 283]. IgG2a antibodies are characteristic of a Th1 immune responses, which have been recognised as important for ADCC and complement fixation and the most protective against infection [284]. IgG2a antibodies have also been correlated with clearance of virus and better protection against challenge [270], which fits with the role the complement plays in inducing specific immunity through the promotion of T cell responses [285]. Hence, the induction of IgG2a may enable stronger protective immune responses to be observed for cavitation-mediated delivery. However, IgG1 antibodies have been correlated to protection against plague in BALB/c mice [286]. Also, passive administration of a 3E5 IgG1 instead of a 3E5 IgG3 antibodies has been shown to increase survival upon challenge with *Cryptococcus neoformans* [287] in a murine model. Hence, a vaccination-strategy inducing IgG1 antibodies, as presented here, may provide protection from certain pathogens, despite not being optimal for protection from influenza.

Overall, the 3G-H p-CaN were characterised as effective cavitation nuclei and a pressure ampli-

tude of 1.7 MPa and a DNA dose of 142 µg were selected for subsequent experiments. Upon intradermal injection, the self-amplifying vector was shown to exhibit an initially lower expression of the gene of interest followed by high levels of expression for sustained periods. This self-amplifying vector was also shown to have advantages for vaccination, as it showed high reproducibility, increased avidity and a lower IgG1/IgG2a antibody isotype ratio. The adjuvant CMV-Perforin was identified as increasing antibody responses and avidity upon cavitation-mediated delivery of DNA. In the following chapter, these 3G-H p-CaN and DNA vectors are put to the test in an influenza challenge study to assess if these DNA optimisations provide better protection against disease than the CMV-Cal09 vector alone.

# Chapter 6

# Challenge Study

## 6.1 Introduction

Throughout this thesis, the ultimate goal has been to create an effective DNA vaccine delivered by ultrasound-mediated cavitation into the skin. Having:

1. improved the ultrasound set-up and associated parameters to optimise delivery (Chapter 4),
2. tested and validated protein cavitation nuclei (p-CaN) as a biodegradable, potentially immunostimulatory alternative to polymeric nanocups (Chapter 3),
3. and optimised DNA vaccine vectors and their combination with DNA-encoded adjuvants to boost immunogenicity (Chapter 2 and 5),

this final chapter is focused on bringing the learnings and most promising findings together to test protection from pathogenic challenge. As BALB/c mice are not susceptible to the A/California/07/2009 strain [288], and the haemagglutinin encoded by the CMV-Cal09 and CMV-VEEV-Cal09 vectors is from this virus strain, an alternative Cal09 compatible mouse strain (DBA/2) was selected for the challenge study. This strain has previously been used for influenza challenge studies and is susceptible to disease upon inoculation with H1N1 influenza A, which includes A/California/07/2009 [289]. Challenge with H1N1pdm09 vaccine virus X-179A, which contains the haemagglutinin and neuraminidase of A/California/07/2009, is lethal to this mouse strain and represents a model previously used to assess the efficacy of a lentiviral influenza vaccine [290]. In this challenge study, different treatments were compared to assess the benefits of cavitation-mediated delivery of a non-amplifying vector and needle and syringe delivery of a self-amplifying vector.

The original purpose of the challenge study was three-fold. These were:

- To compare the protection provided by ultrasound-mediated delivery of a DNA vaccine with an intradermally injected control.
- To compare the protection provided by the low dose delivered by ultrasound-mediated delivery of a DNA vaccines with an equivalent dose injected intramuscularly.
- To investigate the difference in protection provided by a non-amplifying DNA vaccine and a self-amplifying DNA vaccine when injected intradermally.

The challenge study had therefore 6 groups in total:

1. Positive control, dosed intranasally with S-FLU
2. CMV-Cal09 + CMV-Perforin, cavitation-mediated delivery with 3G-H p-CaN
3. CMV-Cal09 + CMV-Perforin, I.D. injected
4. CMV-VEEV-Cal09 (copy-matched) + CMV-Perforin, I.D. injected
5. CMV-Cal09 + CMV-Perforin (0.1% dose), I.M. injected
6. Untreated, negative control

The positive control was treated with S-FLU. S-FLU has been developed by the Townsend group in Oxford as an inhalable vaccine. It is a replication-deficient influenza virus, which can infect cells once, as the HA signal sequence has been inactivated, as described by Powell et al. [291]. Its efficacy is derived from inducing powerful T cell responses against the core proteins, which are expressed in the cytosol of infected cells. However, minimal antibodies against haemagglutinin are generated as these are only present on the protein envelope of S-FLU, but not expressed by the infected cells [291]. S-FLU has been shown to provide protection from lethal challenge with both homologous and heterologous influenza strains in mice and ferrets [291, 292]. It has also been tested in pigs where it showed reduced lung pathology and induced memory T cells [293].

In Chapter 4 it was shown that only a fraction of the DNA dose applied in the sample holder on the skin is delivered by cavitation compared to direct injection. More specifically, cavitation delivered 0.08% of a 142 µg DNA dose, whereas an average 92.3% of the same dose could be detected immediately after intradermal injection. To showcase the dose-sparing potential of cavitation-mediated delivery, a second control group was injected intramuscularly (the standard clinical route of vaccine dosing) with the equivalent of the cavitation-delivered dose (i.e. $\sim$0.18 µg/vector). The choice

was made to inject intramuscularly to give the pDNA the highest chance of generating an immune response, as it was shown in Chapter 2 that intramuscular injection generated higher antibody levels and a stronger cellular immune response compared to intradermal injection, which also showed greater variability.

## 6.2 Materials and Methods

### 6.2.1 Plasmid purification

Plasmid DNA was isolated as described in section 5.2.2. In order to achieve sufficient concentration of plasmid DNA. The eluted plasmid DNA was spun down to remove any pollutants at 3234xg for 5 minutes and the supernatant transferred to a clean 15 mL falcon tube. This was spun down in the Concentrator Plus - Centrifuge Concentrator (Eppendorf, Germany) until the desired concentration was reached. The falcon tube was then vortexed and the final concentration measured with a NanoDrop One (Thermo Scientific). An agarose gel was run to confirm purity, as described in section 2.2.10.

### 6.2.2 Statistics

Statistics were done as described in section 2.2.4.

### 6.2.3 *In vivo* model

6 week old, female, DBA/2OlaHsd mice were obtained from Envigo and kept at the John Radcliffe Hospital (Oxford, United Kingdom). All mice were kept in groups of up to 10 mice, in individually ventilated cages, under standardised and controlled living environments, under a Home Office approved project licence in line with Home Office Legislation and Oxford University Gold Standard. All procedures were performed by appropriately trained Home Office personal licence holders.

### 6.2.4 *In vivo* protocol for assessing delivery in DBA/2 mice

To establish whether the ultrasound delivery of DNA achieved in DBA/2 mice could match that achieved in BALB/c mice (as reported in Chapter 4 and 5), a preliminary study was performed with CMV-Luc pDNA. Two groups of 4 mice were treated either with 142 µg CMV-Luc pDNA, 3G-H p-CaN and ultrasound (1.7 MPa, 2 min) or intradermally injected with 142 µg CMV-Luc pDNA. Female DBA/2 mice were prepared as described in section 2.2.8 and treated with ultrasound. They were placed in the set-up as described previously (Section 4.2.1). The mice were imaged after 24 and 48 hours by IVIS, as described in section 2.2.6. The treated skin was harvested after 48 hours. The DNA content in the skin was quantified by qPCR, as described in 4.2.5.

### 6.2.5 *In vivo* protocol for influenza challenge

#### Dosing of the mice

For the challenge study, six groups of mice were dosed as summarised in Table 6.1. Mice were either treated with ultrasound in combination with 3G-H p-CaN, intramuscularly injected, intradermally injected or intranasally dosed with S-FLU (a replication-deficient influenza virus positive control).

For mice treated by cavitation, a solution was prepared consisting of 4.5% DNA and 95.5% 3G-H p-CaN at 50 mg/mL. This equalled a dose of 142 µg CMV-Cal09 and 142 µg CMV-Perforin in the 1.8 mL in the formulation bed. Mice were prepared as described in section 2.2.8. Treatment was performed by placing the mice in the set-up described in section 4.2.1. The mice were then treated at 1.7 MPa for 2 minutes. Cavitation data was captured during exposure and any skin disruptions apparent after exposure were recorded.

For intranasal dosing, mice were anaesthetised with isoflurane. They were subsequently scruffed and 50 µL S-FLU [S-eGFP-PR8/N1(Eng 195)]/H1 (Eng 195)], which equates $3.40 \times 10^5$ TCID50, was administered by placing the pipette on the nasal cavity. For intradermal injections, the antigen DNA vector and the adjuvant DNA vector were mixed before injection. For intramuscular injection, a 100-fold dilution was prepared of the DNA stocks in PBS. This was then intramuscularly injected into the hind limb.

The mice were homologously boosted after 21 days and regular bleeds were taken as described in 2.2.7 and summarised in Figure 6.1.

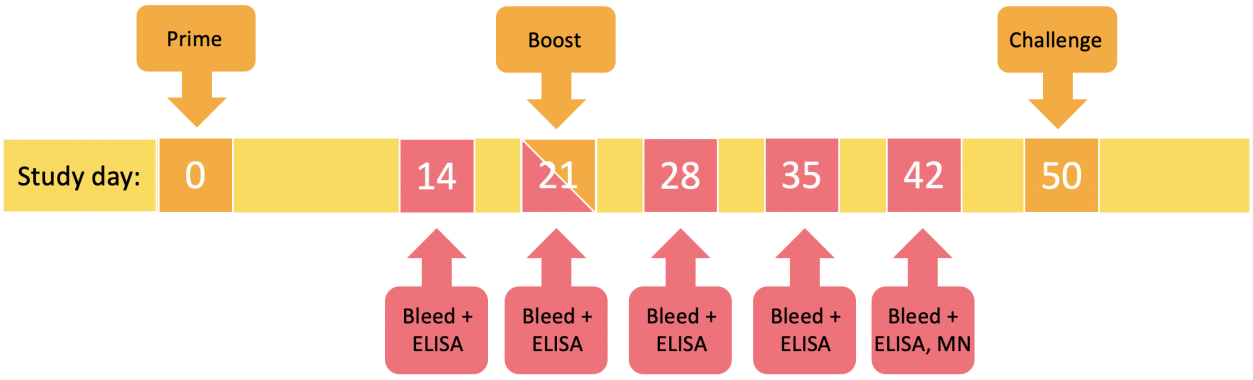



**Figure 6.1.** Summary of the treatment, blood sampling and challenge, as well as subsequent ELISA timeline for the study performed in DBA/2 mice to assess the protection provided by DNA vaccines that are delivered intradermally, intramuscularly, by cavitation or which are self-amplifying.

**ELISA**

The blood samples were analysed by ELISA, as described in section 2.2.11 except the secondary anti-mouse IgG was replaced by the secondary antibody Goat Anti-Mouse IgG H&L (HRP) (ab6789) (Abcam) at 1:20,000 and protein-free blocking buffer (37584, Thermo Fisher) was used.

For titring, serum samples were diluted 100-fold and subsequently diluted two-fold until the absorbance dropped below the threshold. The threshold was defined as the last dilution with a signal 3 times the standard deviation above the signal of negative-control serum.

Isotyping was done as described in section 2.2.11, replacing the 10%FBS-PBS blocking buffer with protein-free protein buffer. The threshold was defined as the last dilution with a signal 3 times the standard deviation above the signal of negative-control serum. Avidity was determined as described in section 5.2.5.

**Microneutralisation assay for influenza**

To perform a microneutralisation assay, a flat-bottomed 96-well plate was coated with 50 µL of serial diluted serum in duplicates. Serum was diluted at 1:40 and subsequently diluted two-fold up to 20,480 fold. Pseudotyped eGFP-expressing influenza virus was diluted in virus growth media (DMEM with 0.1%BSA, 1% 10mM HEPES, 1%100 U Pen/Strep, 1% 2mM glutamine). 50 µL of virus (2 HAU: $\sim 4 \times 10^4$ 50% tissue culture infectious dose of eGFP-encoding S-FLU virus [291]) was added to each well. The plate was then incubated for 2 hours at 37 ºC.

40 min before the end of the incubation period, 12 mL of trypsin was added to MDCK-SIAT1 cells in a T175 flask and incubated for 15 minutes. The trypsinized cells and media were then topped up to 50 mL with virus growth media. The cells were collected by spinning down for 5 minutes at 1400 rpm. The supernatant was removed and the pellet washed with 50 mL virus growth medium. The washed pellet was resuspended in 50 mL of virus growth media and the cells were counted. The cells were diluted to a final density of $3x10^5$ cells/mL.

100 µL of MDCK-SIAT1 cells was added to each column of wells on the 96 well plate containing the serum dilutions plus a standard amount (2 HAU). The plate was then incubated for a further 24 hours at 37 ºC.

The following day, the supernatant was removed and 100 µL of 10% formalin was added to the wells. The plate was then left to incubate at 4℃ for at least 30 minutes. The wells were washed once with 200 µL of PBS and then 100 µL of PBS was added to each well. The plate was then read by a Clariostar platereader (BMG Labtech). A lack of expression of GFP-labelled nucleoprotein is indicative of their successful protection from virus infection via antibody neutralisation of the virus.

The limit of detection was a 1:40 dilution. If no signal was detected, the EC50 was set at 10.

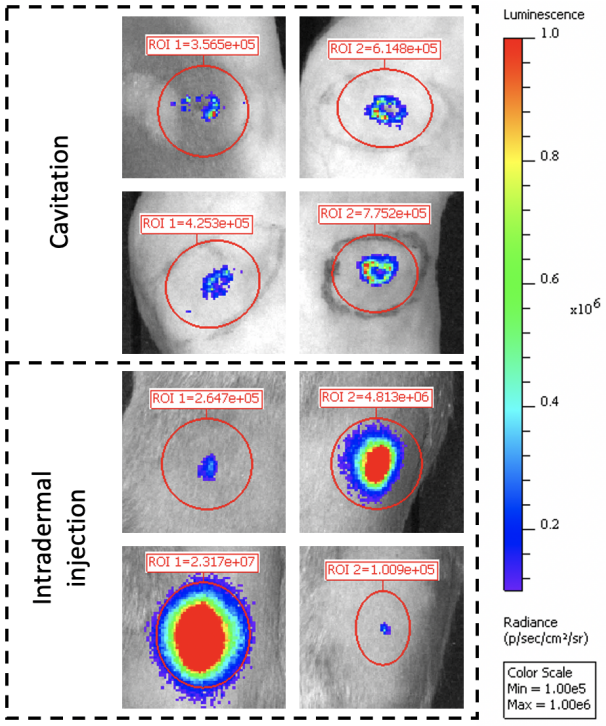
**Challenge**

In the interests of animal welfare and in line with the wording of the project licence under which this experiment was performed, from the DNA-dosed groups, only mice from which serum with an influenza antibody titre of at least 200 was obtained, were enrolled into the challenge study. This titre stipulation was in place on the advice of the Townsend group who have demonstrated that titres below this level do not provide protection and so it is ethically unacceptable to subject mice to a challenge knowing that it will succumb. Mice were challenged 50 days after their 'prime' dose by intranasal administration of 50 µL of the H1N1pdm09 vaccine virus X-179A, which is an infectious H1N1 virus and contains the haemagglutinin and neuraminidase of A/California/07/2009, at 30 times the LD50 dose (0.04 HAU/1500 TCID50). The mice were weighed immediately after administration and their weight was monitored twice daily for the first two days and once a day for the remaining 11 days of the challenge study. Mice were humanely culled if their weight loss relative to the day of challenge decreased by 15% or more. 13 days after challenge, the challenge study was ended.

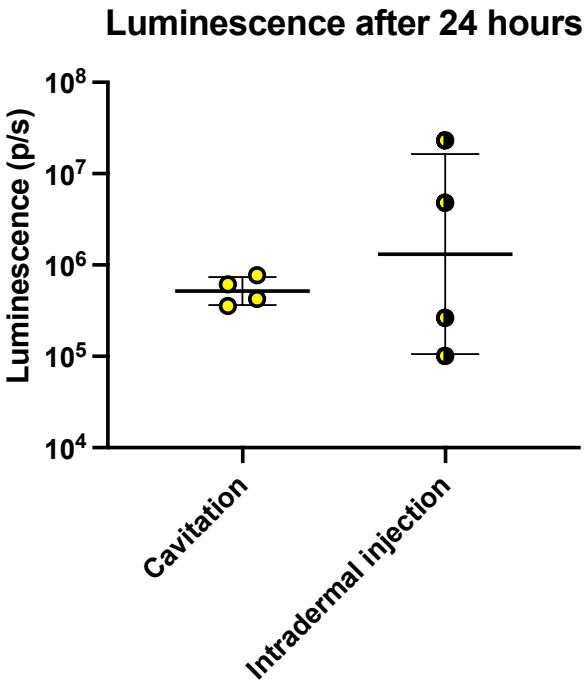
## 6.3 Results

### 6.3.1 *In vivo* for assessing pDNA delivery in DBA/2 mice

Before commencing a challenge study, the ultrasound exposure process and set-up was validated in DBA/2 mice to ensure the switch in strains had not impacted on the ability of cavitation to deliver DNA to the skin. Hence, delivery of pDNA was quantified by IVIS and qPCR, as summarised in Figures 6.2 and 6.3.




**(a)** IVIS images for all mice after 24 hours.




**(b)** Luminescence (p/s) after 24 hours

**Figure 6.2.** Groups of 4 mice were either treated with 142 µg CMV-Luc pDNA, 3G-H p-CaN and cavitation or intradermally injected with 142 µg CMV-Luc pDNA. (a) shows the IVIS image of each mouse. (b) shows the luminescence after 24 hours for each group. Geometric means $\times/\div$ geometric standard deviation are displayed. Significance was assessed with a Welch's t-test, p>0.05.

The IVIS images for the cavitation group showed comparable expression of the luciferase protein as seen in BALB/c mice (BALB/c: $5.01 \times 10^5$ vs DBA/2: $5.19 \times 10^5$, as described in Chapter 4, section 4.3.7), and good reproducibility between mice, especially compared to intradermal injection, which had a large range both in the amount of DNA present in skin after 24 hours and in terms of luciferase expression (Figures 6.2 and 6.3). This again served to emphasise the enhanced reproducibility of transcutaneous delivery. Indeed, that the technology can be ported so effectively from one strain of mice to another with such close alignment in biological outputs gives hope regarding the translatability of the approach to the human population with its diverse skin and hair characteristics. After

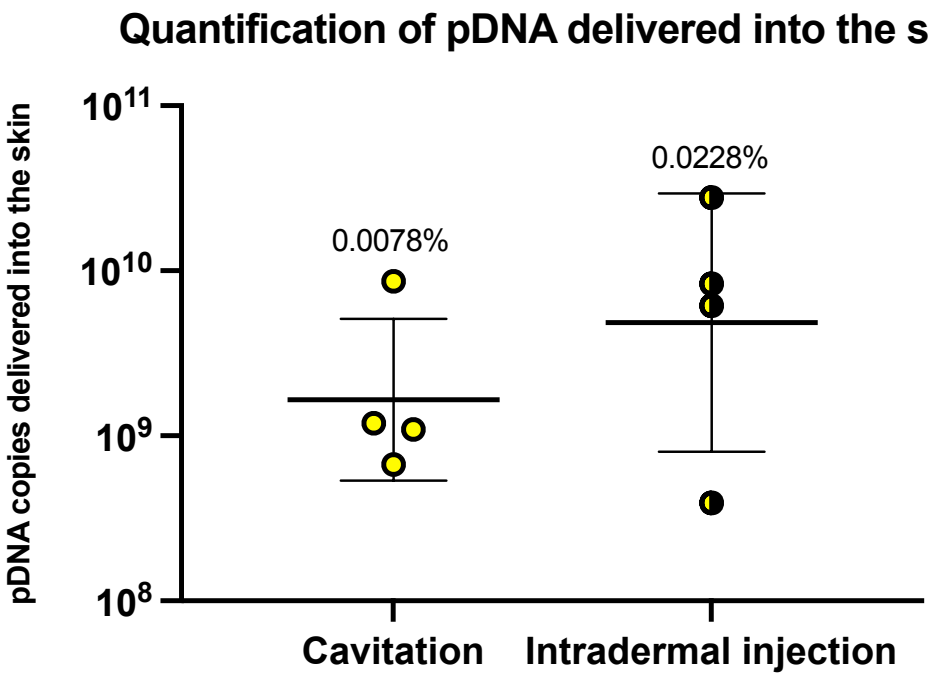



**Figure 6.3.** Quantification of CMV-Luc pDNA copies 48 hours after delivery into mouse skin via cavitation or intradermal injection. The mice were treated with formulations containing 3G-H p-CaN and CMV-Luc pDNA or intradermally injected with CMV-Luc pDNA. The individual measurements are displayed as points on the graph. Above each treatment, the percentage of the original dose is displayed. N=4 for all samples. Geometric means $\times/\div$ geometric standard deviation are displayed. Significance was assessed with a Welch's t-test, $p>0.05$.

48 hours, $1.66 \times 10^9$ copies could be detected in the skin of DBA/2 mice (0.008% of the initial dose present on the skin) (Figure 6.3). Direct comparison to 24 hour data collected in BALB/c mice is difficult but this represents a 6.8-fold reduction, in line with continued slow clearance of the DNA from the skin.

### 6.3.2 *In vivo* influenza challenge study

Having established the ability to deliver DNA transcutaneously into DBA/2 mice with 3G-H p-CaN and cavitation or I.D. injection, the strongest combinations of DNA vaccine candidates and approaches were used for the challenge study.

A dose of 142 µg of vaccine was chosen based on the DNA dose optimisation studies in sections 4.3.4 and 5.3.1, where an exponential relation was observed between DNA dose and luminescence for 20 µg to 142 µg, but no increase in luminescence was observed for 284 µg pDNA.

In chapter 5, the benefit of CMV-Perforin pDNA as an effective adjuvant for cavitation-mediated vaccination was shown. Hence, it was added to all groups to improve overall immunity. It was

also shown in chapter 5 that although the self-amplifying vector CMV-VEEV-Cal09 could not provide improved responses following cavitation-mediated delivery, it was effective when delivered by intradermal injection.

Six groups of 10 mice were treated, as summarised in Table 6.1.

**Table 6.1.** Overview of the treatment in the challenge study.

| Group signifier | Vaccine | DNA adjuvant CMV-Perforin | Administration route | Rationale |
|---|---|---|---|---|
| 1 | 50 µL S-FLU | | Intranasal | Positive control |
| 2 | 142 µg CMV-Cal09 | 142 µg | Cavitation | Optimised cavitation delivery |
| 3 | 142 µg CMV-Cal09 | 142 µg | Intradermal injection | Optimised I.D. delivery |
| 4 | 380 µg CMV-VEEV-Cal09 | 142 µg | Intradermal injection | Impact of VEEV self-amplication |
| 5 | 0.182 µg CMV-Cal09 | 0.182 µg | Intramuscular injection | I.M. control to match level delivered by cavitation |
| 6 | - | - | - | Negative control |

The mice were primed and subsequently boosted on day 21. Blood was sampled on day 14, 21, 28, 35 and 42. The anti-Cal09 antibody levels were assessed by ELISA. The ELISA results of day 42 are displayed in Figure 6.4. One mouse from the 'CMV-VEEV-Cal09 + CMV-Perforin' group was culled for procedure unrelated reasons, as well as one mouse from the S-FLU treated group.

Based on the ELISA results from Day 42, it could be observed, that 6/9 mice had generated very high levels of antibody in the self-amplifying vector group ('CMV-VEEV-Cal09 + CMV-Perforin (ID)'), which likely indicated failed injections in the remaining three mice, reflecting the difficulty of I.D. injection. In the non-self-amplifying group ('CMV-Cal09 + CMV-Perforin (ID)') a wide distribution in antibody responses could be seen, with 9/10 mice having detectable antibody levels. This fits with the theory that once the self-amplifying vector starts replicating, a high number of antigens is generated, resulting in a robust immune response. Whereas the amount of antigen generated for a non-self-amplifying vector is more closely related to the amount of pDNA delivered, which will be quite variable for intradermal injection (as seen in Figure 4.4).

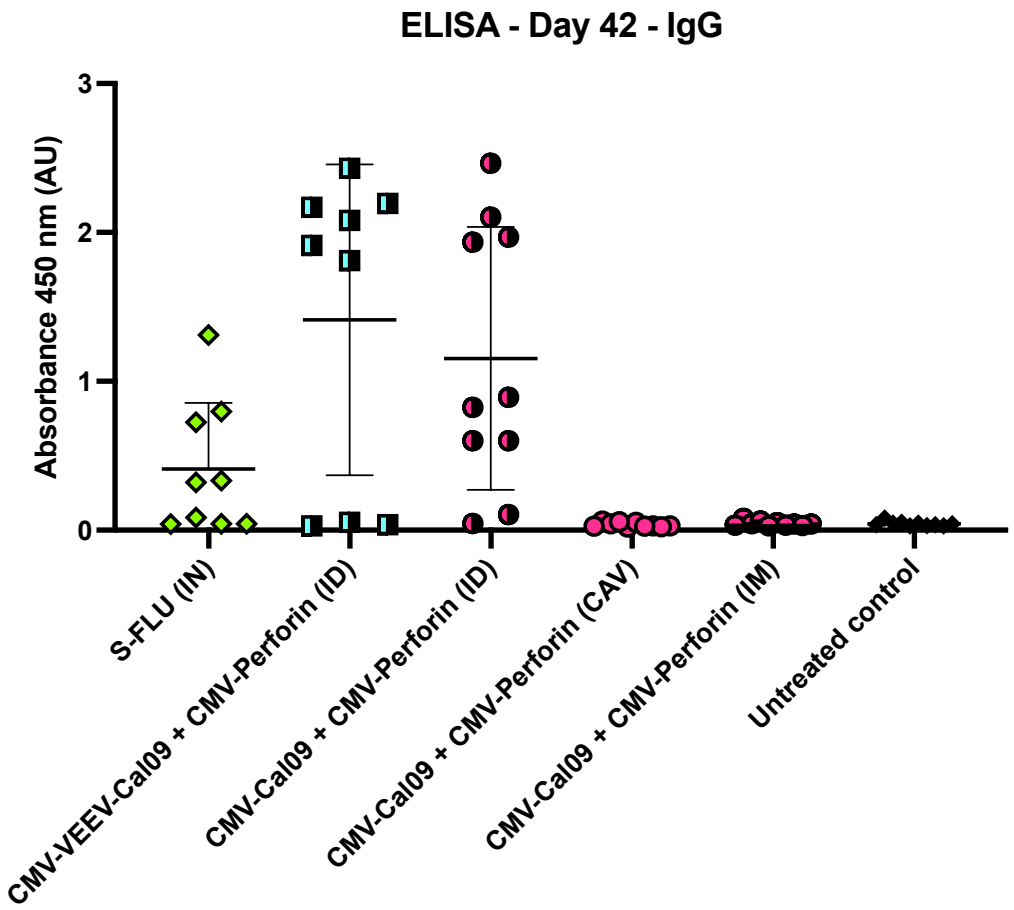



**Figure 6.4.** Summary of the anti-Cal09 HA IgG antibody levels 42 days after prime vaccination and 21 days after boosting. 6 groups are displayed. S-FLU is a positive control, which was intranasally administrated (IN). CMV-VEEV-Cal09 is a self-amplifying vector, of which 380 µg pDNA was intradermally injected. CMV-Cal09 is a non-self-amplifying vector, of which a copy-matched 142 µg was intradermally injected or delivered by cavitation or 0.182 µg was intramuscularly injected. CMV-Perforin is an adjuvant DNA vector added to each group, of which 142 µg was intradermally injected or delivered by cavitation or 0.182 µg was intramuscularly injected. The final group was an untreated control. N=10, mean and SD are displayed.

As expected, the control low amount of pDNA (based on the dose delivered by cavitation) delivered by intramuscular injection did not generate any detectable antibodies. Notably, no anti-Cal09 antibodies could be observed in the cavitation treated group. This disparity in the data produced in BALB/c mice (Figure 5.38) and DBA/2 mice was an unexpected finding. It is speculated this may be related to differences in immune system between BALB/c and DBA/2 mice. It is known from previous chapters that intradermal injection generates an IgG1/IgG2a balanced immune response, whereas cavitation-mediated vaccination results in predominantly IgG1 antibodies. It is possible DNA delivered by cavitation is processed differently by the immune system than when it is directly injected. DBA/2 mice have some notable different immune features compared to BALB/c mice [294–296], which may explain why no immune response was observed as well as provide some insights into the underlying immune response generated upon cavitation-mediated delivery. This is explored further in the discussion section of this chapter.

The positive control (S-FLU) generated low-level antibodies in 5/9 mice, as expected. The S-FLU vaccine relies on cellular immunity, rather than antibodies, to provide protection from infection. It also only has haemagglutinin present on the outside of the replication-deficient influenza virus [291], so generates relatively low levels of anti-haemagglutinin antibodies. Hence, antibody responses are not a good measure for protection for this control.

Based on these results, and stipulations within the animal project licence, 6 mice from each intradermally injected group ('CMV-Cal09 + CMV-Perforin' and 'CMV-VEEV-Cal09 + CMV-Perforin') were taken forward for challenge with influenza, as well as 6 mice from the positive control and 6 mice from the negative control. In each group, the 6 mice with the highest antibody levels were selected for challenge. Where possible, the serum samples from these mice were further analysed for titre, microneutralisation titre, isotyping and avidity.

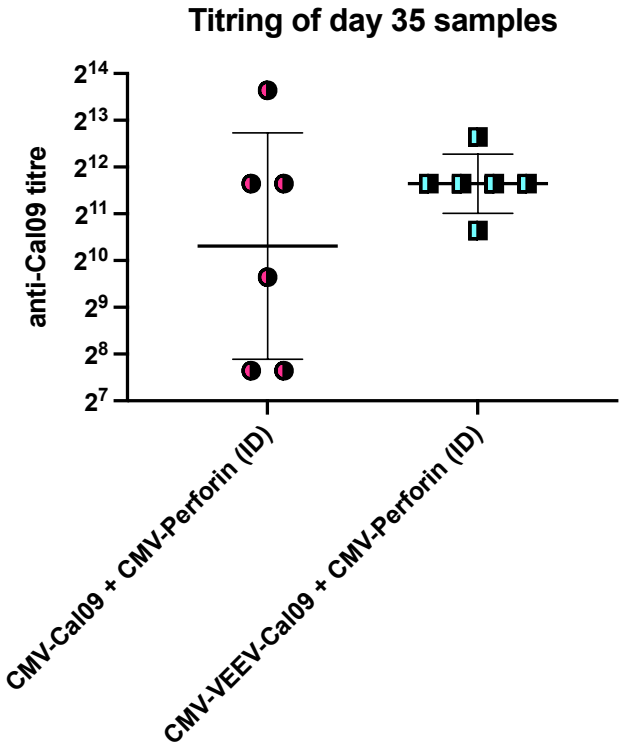



**Figure 6.5.** Titring of the anti-Cal09 HA IgG antibodies from mice intradermally injected with either 142 µg non-amplifying CMV-Cal09 and 142 µg CMV-Perforin or 380 µg self-amplifying CMV-VEEV-Cal09 and 142 µg CMV-Perforin. N=6, geometric means $\times/\div$ geometric standard deviation are displayed. Significance was assessed with a Welch's t-test, $p>0.05$.

The titring (Figure 6.5) further highlights the reproducible antibody levels generated by the self-amplifying vector, compared to the non-self-amplifying vector. There is both a marked difference in geometric means (non-amplifying: 1270 vs self-amplifying: 3200), as well as a marked difference in

geometric standard deviation (non-amplifying: 5.4 vs self-amplifying: 1.6).

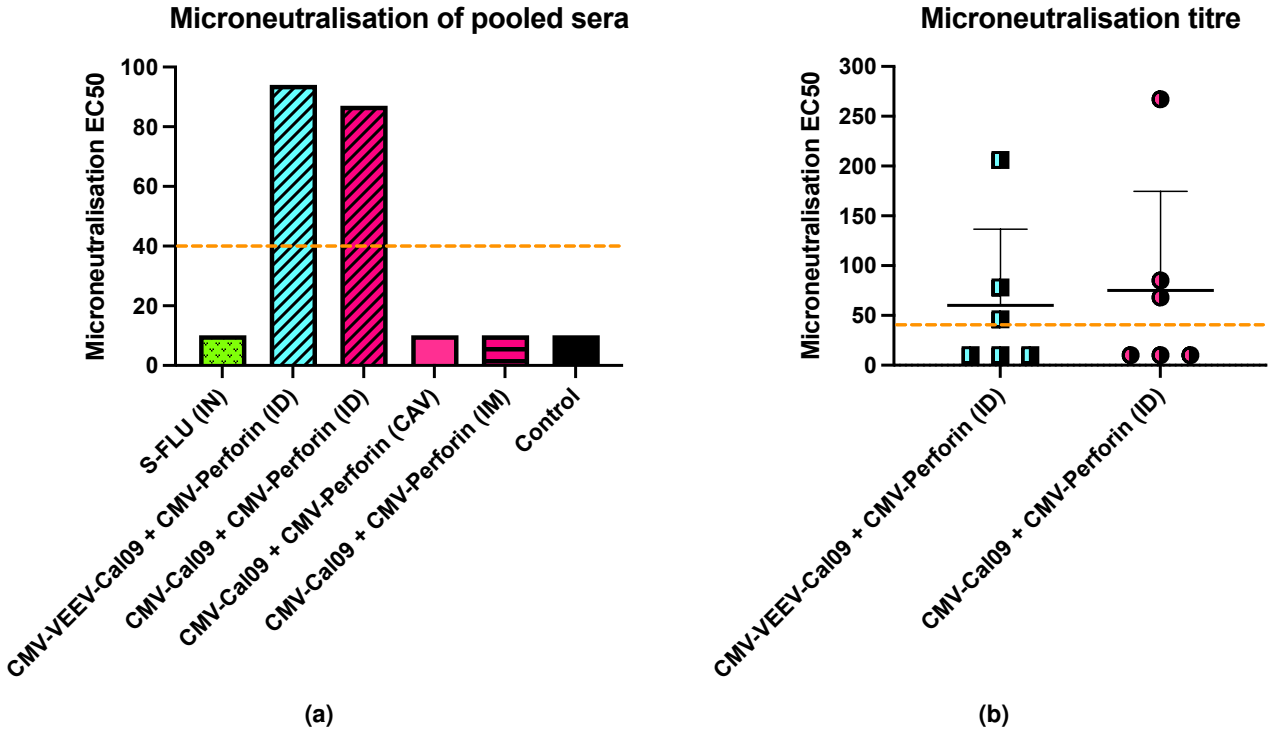
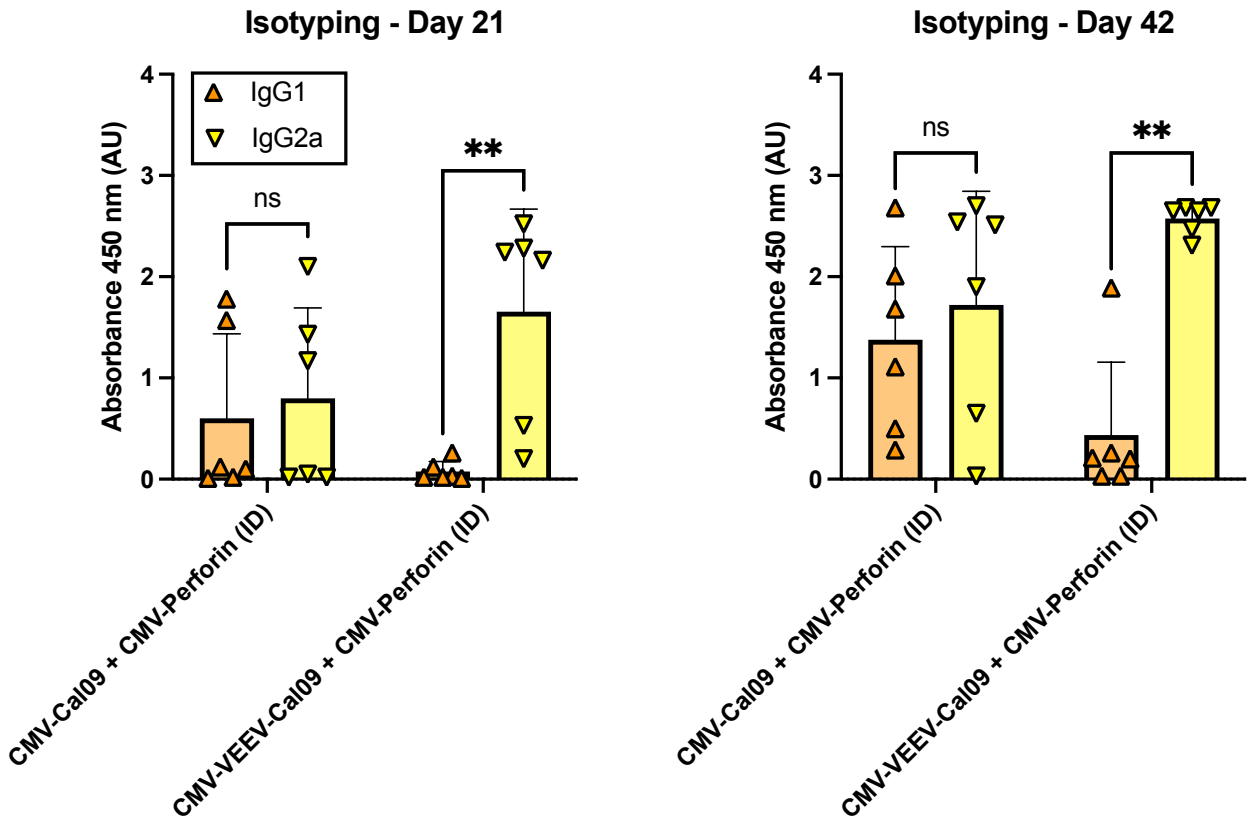



**Figure 6.6.** Microneutralisation titres, expressed as half maximal effective titre (EC50) for pooled (a) and individual (b) blood samples of the mice that were challenged taken on day 42 after prime. (a) S-FLU is a positive control, which was intranasally administrated (IN). 380 µg CMV-VEEV-Cal09 and 142 µg CMV-Perforin was intradermally injected (ID). 142 µg CMV-Cal09 and 142 µg CMV-Perforin was intradermally injected (ID) or delivered by ultrasound and 3G-H p-CaN (CAV). 0.182 µg CMV-Cal09 and 0.182 µg CMV-Perforin was intramuscularly injected (I.M.). The final group was an untreated control. The mice were homologously boosted on day 21. The limit of detection is indicated with the orange dotted line. b) 380 µg CMV-VEEV-Cal09 and 142 µg CMV-Perforin was intradermally injected (ID). 142 µg CMV-Cal09 and 142 µg CMV-Perforin was intradermally injected (ID). The mean (horizontal bar) and standard deviation (error bars) are displayed. Significance was assessed by an unpaired t-test with Welch's correction, $p>0.05$. The limit of detection is indicated with the orange dotted line.

The pooled microneutralisation titres (Figure 6.6a) further show that only the intradermally injected groups have protective antibodies, whereas the low-dose intramuscularly injected group and the cavitation-treated group, show no detectable neutralising antibodies. The pooled samples of mice injected with self-amplifying or non-amplifying pDNA show very similar EC50 titres (94 vs 87). When considering the individual blood samples of the mice selected for challenge (Figure 6.6b), both groups had 3/6 mice with titres above the detection threshold.

The blood samples of the mice selected for challenge from day 21 and day 42 were isotyped for IgG1 and IgG2a (Figure 6.7). There is a noticeable difference in the ratio of IgG1/IgG2a between the non-amplifying (CMV-Cal09 + CMV-Perforin) and the self-amplifying group ('CMV-VEEV-Cal09 + CMV-Perforin'). The self-amplifying vector appears to dramatically skew the ratio in favour of IgG2a.




**(a)** IgG1 and IgG2a levels after 21 days

**(b)** IgG1 and IgG2a levels after 42 days

**Figure 6.7.** Isotyping of anti-Cal09 HA antibodies in blood samples taken on day 21 (a) or day 42 (b) after prime vaccination. The mice were intradermally injected with 142 µg CMV-Perforin pDNA and either 142 µg CMV-Cal09 pDNA or 380 µg of self-amplifying CMV-VEEV-Cal09 pDNA. The mice were homologously boosted on day 21. A two-way ANOVA (vector x isotype) was done with a post-hoc test between isotypes for each group using the Šidák correction for multiple comparisons. ** = $p<0.005$, ns = $p>0.05$. A significant effect of isotype ($p<0.01$) and the interaction between vector and isotype ($p<0.05$) was observed for both timepoints. No significant effect of vector or subject was observed ($p>0.1$) for both days.

On day 21, little to no IgG1 can be detected in the self-amplifying group. By day 42, a highly reproducible increase in IgG1 antibodies is evident for the self-amplifying vector, but the IgG1/IgG2a ratio is still skewed towards IgG2a. For both timepoints, the isotype profile observed depended significantly on the vectors used ($p<0.05$ - day 21, $p<0.005$ - day 42). In comparison, the non-amplifying group has a much more balanced IgG1/IgG2a response, showing that although both vectors generate antibodies, the antibodies have different isotype profiles and engage with the immune system in a distinct way, perhaps as a consequence of the altered antigen expression-time profile or the danger signals caused by the VEEV self-replication mechanism.

This intriguing finding may help explain the failure of cavitation-mediated delivery to coordinate with the self-amplifying vector (as seen in Figure 5.21). As shown in Chapter 5, cavitation-mediated delivery generates predominantly IgG1 antibodies, whereas injection of the same vector generates a balanced IgG1/IgG2a response. If the response following cavitation-mediated delivery is skewed

to IgG1 antibodies (perhaps as a result of a different cell population target) and the self-amplifying vector produces a IgG2a skewed response, this may hint at why they are not compatible.

Notably when avidity was measured, a large (but not significant) increase in the mean molarity of NaSCN required to reduce ELISA antibody binding by 50% was seen in samples from the self-amplifying vector treated mice compared to samples from mice treated with non-amplifying vector (Figure 6.8). This shows further benefit of the self-amplifying vector in eliciting antibodies capable of stronger binding to the antigen.

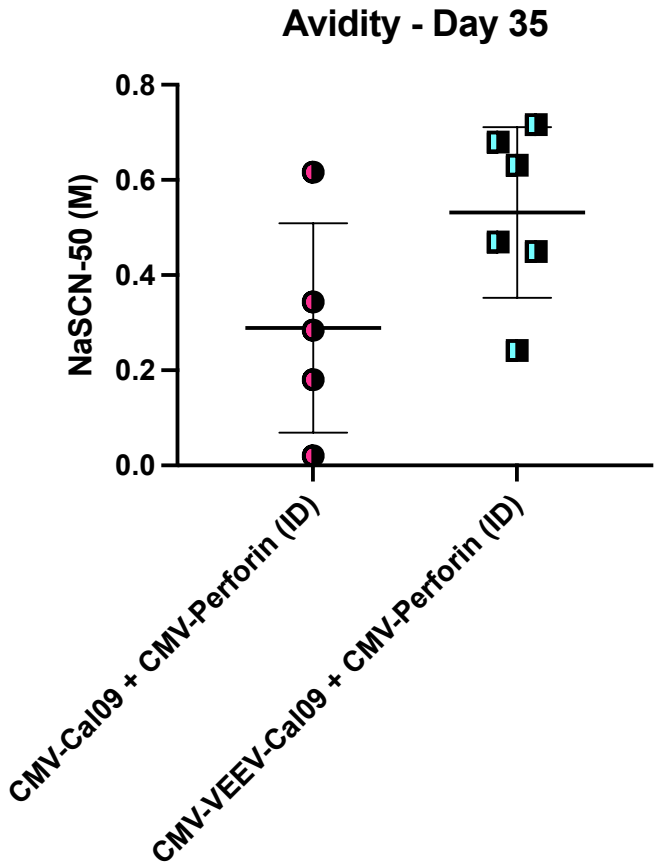



**Figure 6.8.** Avidity of anti-Cal09 HA antibodies in blood samples taken on day 35 after prime vaccination. The mice were intradermally injected with 142 µg CMV-Perforin pDNA and either 142 µg CMV-Cal09 pDNA or 380 µg of self-amplifying CMV-VEEV-Cal09 pDNA. The mice were homologously boosted on day 21. N=6 and mean and standard deviation are displayed. Significance was assessed with a Welch's t-test, $p>0.05$.

For the challenge component, 6 mice were selected from each of the following groups, based on their overall antibody levels:

- S-FLU, intranasally applied
- CMV-Cal09 + CMV-Perforin, intradermally injected

- CMV-VEEV-Cal09 + CMV-Perforin, intradermally injected
- Untreated control

Treatment of the cavitation group and the I.M. injected group could not be justified as there was no evidence of any antibody response.

Mice were challenged with 30 times the LD50-dose of the X-179A virus, which contains haemagglutinin from A/California/07/2009 (H1N1). This haemagglutinin is encoded by the CMV-Cal09 and CMV-VEEV-Cal09 vectors. Mice were checked and weighed twice daily for the first two days and then weighed daily until conclusion of the challenge study after 13 days. 15% weight loss or more was considered the humane endpoint.

In terms of survival (Figure 6.9), it can be seen that the untreated, negative control shows no survival beyond 7 days. The non-amplifying "CMV-Cal09 + CMV-Perforin" group shows slightly decreased, albeit statistically insignificant (logrank test), survival compared to the self-amplifying "CMV-VEEV-Cal09 + CMV-Perforin" group and positive control S-FLU, which both showed 100% survival.

Weight loss (Figure 6.10), a reliable indicator of overall health, evidences in more detail the difference between the treatments. Both intradermally injected groups show an increase in weight over the first two days. Subsequently, as the influenza infection progressed, a decrease in weight was seen for the untreated negative control, until all mice in this group were culled by day 7. A decrease in weight at day 7 was also seen for the non-amplifying group, where 3/6 mice lost over 7% of their body weight. In contrast, in the group treated with the self-amplifying vector, no mouse lost more than 6.5% of its body weight. Notably, this compares favourably with the S-FLU positive control group which suffered up to 9% weight loss (not displayed), showing that the self-amplifying vector provided robust protection from challenge.

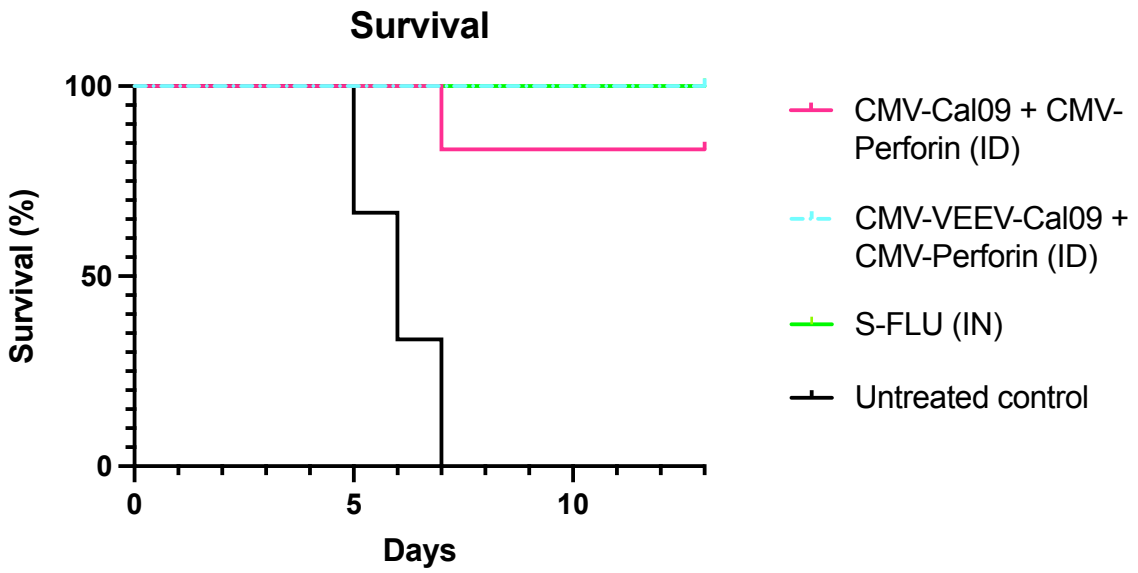



**Figure 6.9.** Survival of DBA/2 mice after intransal exposure to 30xLD50 of X-179A virus on day 50 after prime vaccination. The mice were intradermally injected with 142 µg CMV-Perforin pDNA and either 142 µg CMV-Cal09 pDNA or copy-matched 380 µg of self-amplifying CMV-VEEV-Cal09 pDNA. Mice dosed with S-FLU were used as a positive control and untreated mice as a negative control. The mice were homologously boosted on day 21. N=6.

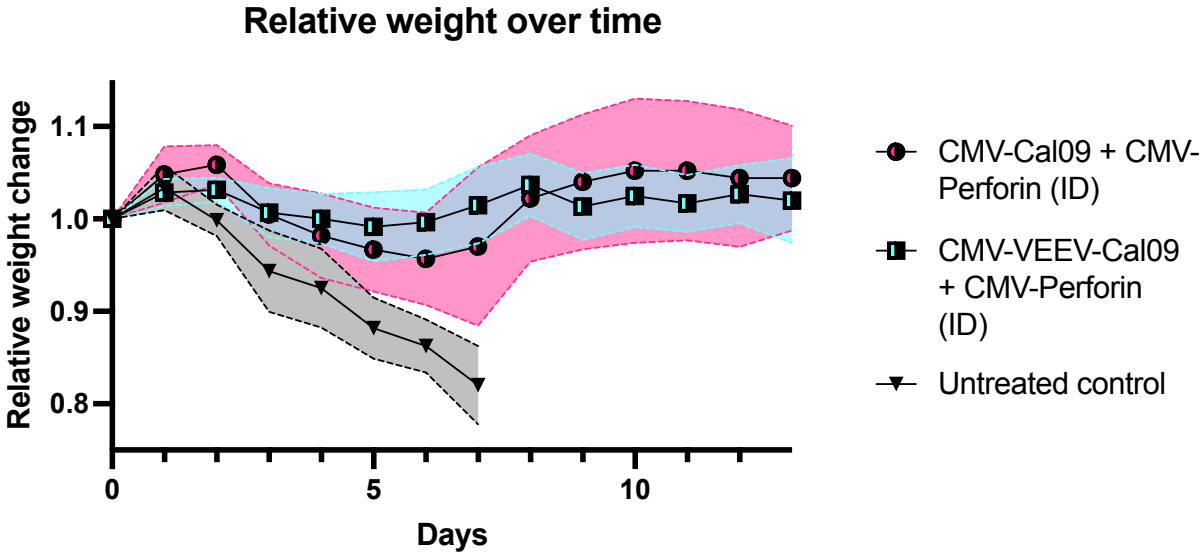



**Figure 6.10.** Relative weight changes in DBA/2 mice measured over a 13-day period after exposure to 30xLD50 of X-179A influenza virus on day 50 after prime vaccination. The mice were intradermally injected with 142 µg CMV-Perforin pDNA and either 142 µg CMV-Cal09 pDNA or 380 µg of self-amplifying CMV-VEEV-Cal09 pDNA. Untreated mice were used as a negative control. The mice were homologously boosted on day 21. N=6, line shows mean, the shaded area show the standard deviation (pink = standard deviation of the 'CMV-Cal09 + CMV-Perforin (ID)', blue region = standard deviation of the 'CMV-VEEV-Cal09 + CMV-Perforin (ID)'. Weights are calculated relative to the weight measured immediately post exposure to the virus.

## 6.4 Conclusions and Discussion

This chapter sought to bring the different strands of optimisation from previous chapters together in a challenge study. To enable the challenge study, a strain of mice was selected that was susceptible to disease upon influenza challenge. To verify DNA could still be effectively delivered into this DBA/2 strain, a pilot study was performed with luciferase-encoding pDNA. Luciferase expression was visualised after 24 hour by IVIS and DNA delivery in the skin quantified by qPCR after 48 hours. This showed comparable DNA expression and delivery as seen in BALB/c mice.

A challenge study was then designed to answer three questions. Firstly, whether delivery of a DNA vaccine by cavitation could provide equal protection to the same DNA vaccine intradermally injected. Secondly, if the low dose (0.1% of the dose in the formulation holder) delivered by cavitation would elicit a stronger immune response than intramuscular injection of that same dose. Finally, the challenge study sought to investigate if a self-amplifying vector would provide equal or greater protection than a dose-matched non-amplifying vector. The adjuvant CMV-Perforin, which has shown promise as a DNA adjuvant for cavitation-delivered DNA vaccines in Chapter 5, was added to all groups.

Unexpectedly, the group treated with pDNA and cavitation showed no detectable antibody response. As it had been demonstrated that; cavitation-mediated DNA delivery and expression had been verified in this mouse strain, the CMV-Cal09 DNA was functional (i.e. it could be expressed upon intradermal delivery) and the PCD data suggested sufficient cavitation (>3.9 μJ TASE) had been generated by the 3G-H p-CaN during 18/19 treatments, an explanation was sought in the mouse model. A deeper comparison between BALB/c mice and DBA/2 mice showed that both strains are Th2 prone upon intramuscular vaccination with a diphtheria-tetanus-acellular pertussis vaccine, with DBA/2 mice identified as more prone than BALB/c [297]. As cavitation-mediated delivery results in a Th2-skewed immune response in BALB/c mice, a similar response could have been expected in DBA/2 mice. However, DBA/2 mice differ immunologically from BALB/c mice in a number of other ways. This is useful as this makes this strain susceptible to influenza, but may also have inhibited a strong immune response following cavitation-mediated delivery from being mounted.

From isotyping of antibodies generated after cavitation-mediated delivery of pDNA in Chapters 2 and 5, it was shown that cavitation resulted in an IgG1-skewed immune response. Langerhans cells are reported to drive predominantly IgG1 responses in C57BL/6 mice [89]. Hence, it was speculated

that vaccination through cavitation-mediated delivery depends on Langerhans cells in the epidermis. DBA/2 mice have Langerhans cells in their epidermis and their distribution is similar to that in BALB/c mice [294]. However in spleens of DBA/2 mice, no dendritic cells expressing langerin are present, whereas approximately 0.25% of BALB/c mice spleen cells express intracellular langerin. In the paper by Flacher et al. describing these differences, the possible role langerin may play in antigen uptake and cross-presentation, an important process for eliciting immune responses, is also discussed [294]. This could mean that BALB/c mice are particularly good at antigen uptake and use this to generate better immune responses.

A second difference is in T cell responses. Upon Candida oral infection, DBA/2 mice recruit $\gamma\delta$ T cells at the same level as CD4+ T cells, whereas BALB/c mice recruit at least twice as many $\gamma\delta$ T cells compared to CD4+ T cells. These $\gamma\delta$ T cells were recruited more rapidly and it is believed that these T cells can play an important role in responding to pathogens [295]. The difference in T cell response is also apparent in terms of the respiratory dendritic cell subsets present in BALB/c and DBA/2 mice, where DBA/2 mice have lower frequencies of T regulator cell populations and classical lymphocytes, such as $CD3^+$ T cells and $CD19^+$ B cells. Upon stimulation of respiratory T lymphocytes, BALB/c mice produced higher levels of TNF-$\alpha$ and had higher IFN-$\gamma$ and IL-10 levels compared to DBA/2 mice [298]. Upon malarial infection, levels of IFN-$\gamma$ and IL-4 also remained lower in DBA/2 mice than in C57BL/6 mice [299]. Considering the importance of TNF-$\alpha$ and IFN-$\gamma$ in eliciting immune responses and protection from viral infection, a similar pattern in the skin could explain to some extent the lack of immune response observed in the DBA/2 mice.

A final difference is the lack of a fully functional complement system in DBA/2 mice, as they lack the murine fifth complement component [296]. The complement system has roles for both the innate and the adaptive immune system [300]. Repression of the C5 component in a mouse model of MERS-CoV infection showed a decrease in excessive inflammatory responses [301]. A study by Kim et al. also showed that vaccination with a haemagglutinin VLP vaccine in a C3 knock-out strain, thereby knocking out the complement system, resulted in substantially lower antibody responses compared to vaccination in a wildtype C57BL/6 strain (36-fold 2 weeks after boost). In particular, Kim et al. showed that the IgG1 isotype could not be detected in the C3 KO strain [302]. Hence, the compromised complement system in the DBA/2 mouse strain may have inhibited the generation of antibodies.

Overall, more work will be needed to better understand the immune route utilised by DNA delivered by cavitation into the dermal compartment. A better understanding of the facets of the immune system involved, may give more clarity on the reasons no anti-HA antibodies were seen in the DBA/2 strain.

As the cavitation-treated group showed no antibody response, comparison with the low DNA dose intramuscularly injected group was not directly possible. However, it is worth noting that the low dose injected intramuscularly elicited no antibodies either, whereas a higher dose injected intradermally did result in an observable antibody response. In Chapter 2 section 2.3.4, it was shown that intramuscular injection would be expected to result in higher antibody levels than intradermal injection, so the lack of antibodies does seem to support the hypothesis that the DNA quantity delivered by cavitation does not result in an immune response when simply injected. This could still mean that cavitation-mediated delivery of DNA shows huge dose-sparing potential. The dose-sparing potential of ultrasound-mediated delivery is also supported by Tezel et al., who showed a 10-fold lower dose of 0.9 ± 0.3 µg tetanus toxoid delivered by cavitation elicited equivalent antibody levels to 10 µg subcutenously injected [145].

The final question addressed in this chapter is whether self-amplifying DNA would provide advantages in terms of protection from disease. When anti-Cal09 HA antibody levels were titred (Figure 6.5), an initial advantage of the self-amplifying vector was evident, as the self-amplifying group showed far greater reproducibility in antibody levels generated than its non-amplifying counterpart. Both groups showed a similar pooled microneutralisation titre and had the same number of serum samples with detectable neutralising antibodies by day 42. A large difference, however, could be seen in the avidity and the isotyping of the antibodies generated. This showed that the self-amplifying 'CMV-VEEV-Cal09 + CMV-Perforin' group had a higher avidity and a much more IgG2a-skewed antibody response compared to the non-amplifying 'CMV-Cal09 + CMV-Perforin' group. As IgG2a is implicated in viral clearance [270], benefits in terms of protection would be expected from a stronger IgG2a response. This is in line with the observations in the challenge study. The self-amplifying group ('CMV-VEEV-Cal09 + CMV-Perforin') showed complete survival compared to 83% survival in the non-amplifying group ('CMV-Cal09 + CMV-Perforin'). Further benefit of the self-amplifying vector was seen in terms of symptomatic disease. The 'CMV-VEEV-Cal09 + CMV-Perforin' group showed less weight loss than both the non-amplifying group and the positive control, S-FLU.

Overall, despite a lack of immune response observed in the cavitation-treated group, the benefits of a self-amplifying vector compared to a non-amplifying vector upon intradermal injection have been demonstrated in this challenge study. This vector represents a powerful candidate for improving immunogenicity of DNA vaccines and may be part of the approach to enable DNA vaccines to reach the clinic. As this VEEV vector is designed to be amenable to cell-free large-scale production, manufacturing issues should not be a restriction to translation of such DNA-launched self-amplifying RNA. However, identifying a method of delivery that both provides an advantage over the use of N+S and aligns with the immune stimulation mode of action/cell type target will be important. Unfortunately the benefits of the self-amplification mechanism of VEEV and the benefits of cavitation-mediated delivery do not seem aligned.

# Chapter 7

# Conclusions and Future Work

## 7.1 Research overview

This thesis has explored approaches and technologies to increase the efficacy and acceptance of DNA vaccines by improving their mode of delivery and transgene expression efficiency. Chapter 1 detailed the importance of vaccination, the limitations of current vaccination strategies and how large-scale vaccination distribution, and the nature of the pathogens we face, will require new vaccination approaches. Specifically, the importance of having readily scalable and deployable technologies available to counter potentially pandemic outbreaks of rapidly evolving pathogens was emphasised. Hence, nucleotide-based vaccines have been highlighted as attractive technologies due to their quick development time, rapid production and standardised cell-free production methodologies [154]. In particular, DNA-based vaccines can offer significant advantages in terms of production and logistics due to their stability at room temperature and during delivery. However, RNA vaccines have had the upper hand due to a lack of immunogenicity achieved with current DNA vaccines delivered by currently accepted methods [303]. Notably, analysis of the literature makes a strong case that the skin is an attractive vaccination site that may enable an increased immune response and thereby allow for the more effective clinical application of DNA vaccines [304]. This is related to the skin's rich immune environment and the potential for dose sparing [99]. Interestingly, two front-runners of DNA vaccine technology, ZyCoV-D and INO-4800, both use unconventional delivery techniques into the skin: liquid jet by the Pharmajet Tropis and intradermal injection and electroporation by CELLECTRA respectively. As both liquid jet and electroporation are associated with significant discomfort for the recipient and needle-fear is still limiting vaccine uptake, there is scope for new techniques that can deliver DNA vaccines in a pain-free manner and increase their immunogenicity. Cavitation-mediated delivery was identified as a potential candidate to meet the requirements, due to its pain-free applica-

tion, its ability to enable penetration into the epidermis and its potential intrinsic adjuvant properties [145]. Of the other less invasive approaches available, microneedles are also demonstrating their potential to effectively deliver DNA into the skin [305], and are even being combined with technologies such as electroporation [306]. There is much excitement that the impressive effects seen with microneedles in animal studies are being recapitulated as clinical trials are completed [307–309]. Ultrasound-mediated cavitation has until now been limited by insufficient consistency and control of the cavitation events used to drive delivery, as well as the specialist equipment used for delivery. Indeed, a focus on nucleating cavitation without adding a cavitation agent or by using short-lived microbubbles, has meant a reliance on hard to translate ultrasound parameters and/or requirement for a two-step, 'cavitate then expose'-procedure [133, 134, 310]. However, the development of cavitation nuclei capable of sustained cavitation has opened up new possibilities for better delivery by ultrasound. It was also proposed that biodegradable cavitation nuclei that allow for both sustained cavitation and immune-stimulation could increase the immunogenicity of DNA vaccines delivered by cavitation.

Therefore, the strategy explored in this thesis combines (protein) cavitation nuclei and ultrasound to deliver DNA vaccines into the skin to elicit enhanced immune response. Progress against the aims of this thesis (see bullet points) is described in sections 7.1.1-7.1.4:

- To improve delivery and increase reproducibility for cavitation-mediated delivery of DNA into the skin *in vivo*.
- To investigate the potential of immunogenic cavitation nuclei for mediating DNA plasmid delivery as well as generating immune responses *in vivo*.
- To assess the capability of different DNA constructs in eliciting an immune response against influenza haemagglutinin protein *in vivo*.
- To evaluate the utility of combining optimised immunogenic cavitation nuclei, ultrasound-mediated cavitation and optimised DNA vectors as an effective vaccination strategy *in vivo*.

### 7.1.1 Ultrasound set-up and parameters

The first research objective, was initially explored in Chapter 2 in the context of the ultrasound set-up developed by Dr. Van Blokland and Dr. Bhatnagar [143]. This showed that negligible DNA was delivered at pressures below the threshold required to instigate cavitation. A step-wise increase

in DNA delivery was observed once cavitation was achieved (pressures $\geq$ 0.7 MPa) and this cavitation threshold was quantified as a minimal TASE value necessary for delivery (between 1.7 µJ (0.5 MPa) and 4.3 µJ (0.7 MPa)). It was also shown that despite good expression of the DNA vector, only a relatively small proportion of the available dose was delivered and just 0.03% of the original dose was present after 24 hours. However, overall a lack of reproducibility was observed and the set-up was deemed cumbersome to handle and align, which limits clinical translation. Hence, in Chapter 4 a completely new set-up was developed. This set-up (V2) inverted the coupling cone to allow for easier handling and added a pulser-receiver to allow validation of a clear ultrasound beampath to improve reproducibility. For this adapted set-up V2, four delivery parameters were optimised: p-CaN concentration, DNA concentration, pressure amplitude and treatment time. It was demonstrated that higher concentrations of cavitation nuclei resulted in more consistent cavitation over the entire treatment period. This, in turn, improved the level of delivery of, and expression from, a luciferase plasmid. In contrast, an increase in concentration of the CMV-Luc DNA plasmid had no significant effect on luciferase expression, implying the concentration of DNA is not a major limiting factor at the concentrations assessed (71 µg, 142 µg and 240 µg). However, in Chapter 5, a relationship was observed between DNA dose and expression for lower doses, implying there may be a saturation limit to the amount that can be delivered by cavitation. Further exploration of a wider range of concentrations is needed to confirm this. Interestingly, it was shown that there was also an upper limit in the TASE beyond which point luciferase expression decreased. It is proposed that the decrease in luciferase expression at high TASE values ($\geq$ 30 µJ) was likely a consequence of tissue damage, which results in a reduction in the number of viable cells capable of taking up and expressing the DNA. Hence, the treatment time was optimised to 2 min at 1.7 MPa. Previous literature on cavitation-mediated delivery has relied on a period of ultrasound exposure followed by a perhaps poorly translatable extended period of exposure to drug [133, 311], although there has more recently been a trend towards combining ultrasound treatment with drug application [141, 312], demonstrating researchers are now more cogniscent of the requirement for healthcare innovations to fit into current clinical practice. However, previous studies provide little details on observed damage and those that do generally report little to no damage *in vivo* [141, 313]. Hence, the cavitation energy and related skin damage reported here, provide further insight into factors impacting optimal DNA vaccine expression.

### 7.1.2 p-CaN

Low frequency ultrasound (20 kHz) can cause on-skin cavitation events to be generated without the need to seed the exposed area or sample with cavitation nuclei [314]. However, the addition of cavitation nuclei decreases the cavitation threshold, allowing more appropriate frequencies and lower pressure amplitudes to be used to achieve the same cavitation activity [315]. Microbubble-based cavitation does lower the cavitation threshold, but lacks the longevity of cavitation [129]. They also raise concerns about stability and co-formulation with drug, as most microbubble formulations require use within 4 hours of resuspension from dry-state [316]. Whilst polymeric cups do provide long-term stability in wet-state and longevity of cavitation response, their inert non-degradable nature means they do not provide beneficial immune stimulation and do raise concerns about duration of residence (a potential regulatory barrier [317]). In considering how the system could be enhanced, it was clear that the cavitation nuclei were a target for optimisation. Therefore the second research objective, to investigate immunogenic cavitation nuclei, was predominantly explored in chapter 3. Protein cavitation nuclei (p-CaN) are presented as a biodegradable cavitation nuclei, which can be formulated using most proteins. In total three generations of p-CaN have been validated and evaluated in this thesis (Table 7.1).

**Table 7.1.** Summary of the content of the core and synthesis of the different p-CaN formulation evaluated in this thesis.

| Name | Oil (% v/v) | Hexane (% v/v) | Cyclohexane (%v/v) | Synthesis |
|---|---|---|---|---|
| 1G p-CaN | 50 | 50 | 0 | Ultrasonic horn |
| 2G-U p-CaN | 0 | 100 | 0 | Ultrasonic horn |
| 3G-H p-CaN | 0 | 50 | 50 | Hydrodynamic shearing |

In chapter 3, it is shown that p-CaN can deliver pDNA at a similar or improved level compared to polymeric nanocups. As opposed to the inert nanocups, p-CaN can also lead to the generation of an effective immune response against the protein formulated as p-CaN, despite relatively low delivery of the protein. This was demonstrated by testing for antibodies to SARS-CoV-2 spike protein or to BSA protein, as measured in Chapter 4. Hence, it is proposed that an immune response to any target protein could be generated provided that the protein could be obtained at sufficient concentration to formulate into p-CaN. In this regard, p-CaN are a unique cavitation agent with both a physical and targeted biological effect. Notably, it was also observed that the avidity of the antibodies generated against cavitation-delivered p-CaN had the highest overall mean value compared to injection of non-

p-CaN protein and 3 of the 4 mice demonstrated higher avidity antibodies than all but one of the nine mice that were injected. This suggests additional benefit to cavitation-mediated delivery of the p-CaN formulation. It is much reported that formulation of antigenic protein into constructs which mimic the nanoscale dimensions of viruses can increase immunogenicity compared to the administration of protein in 'free' form, which may explain the immunogenic benefit of injected p-CaN. Indeed, this approach has shown success in vaccines such as RTS,S/AS01 vaccine (Mosquirix™), Human Papillomavirus Quadrivalent (types 6, 11, 16, 18) Recombinant Vaccine (Gardasil®) and NVX-CoV2373 (Nuvaxovid) to address diseases as diverse as malaria, cervical cancer and SARS-CoV-2 respectively [318–320]. It is also apparent that delivery of vaccines to the dermal compartments may enhance immunogenicity and allow dose sparing [99, 101] and that the mere application of ultrasound/cavitation to the skin can stimulate immune responses [145]. The formulation and delivery of nanoscale protein cavitation nuclei may offer exciting potential to benefit from all three of these effects. Indeed, despite only fractional delivery of BSA p-CaN by cavitation, a strong immune response could be observed in 3 out of 4 mice in section 3.3.2. More work is required to test if making p-CaN out of immunostimulatory protein would allow for the creation of a universal platform p-CaN, as the candidate chosen for this study (FLT3L [226]) could not be produced at scale in the time available.

Development of p-CaN iterations continued in chapter 4 and 5, assessing optimised parameters and with more scalable, regulatory amenable production methods demonstrating an equivalence of activity of the final product. Such consideration of scalability and amenability to production by methods with a track-record of regulatory approval is an important consideration even at the early stages of a research project. This is especially pertinent for novel nanoscale constructs which may not be supported by a long-history of previous 'like-me' approvals and a well-defined risk profile. Indeed, even for the most simple of nanoscale drug delivery agents, the liposome, the major cause of rejection by the FDA in 2016 was chemistry, manufacturing, and controls (CMC) failure [321, 322].

### 7.1.3 DNA vector optimisation

A plentiful toolbox of options exists for the enhancement of control over the level, selectivity, duration and timing of protein expression from nucleotide vectors. One of the simplest approaches to modulate expression is to modify the promoter regions which drive transcription. Hence, different constructs were assessed in two rounds of experiments to answer the third research question. In the first round, four questions were addressed, namely the effect of promoters, the effect of cell

type specific expression, the impact of DNA-based adjuvants and the importance of route of delivery. These studies showed that the use of the 'ubiquitous' CMV-promoter resulted in the highest IgG antibody response upon either I.M. or cavitation-mediated delivery. Neither the EF1$\alpha$ promoter nor the tissue-specific promoters showed an advantage. Interestingly, no antibody response was seen from the KCL27-Cal09 vector, which was designed for keratinocyte specificity (Touchlight Genetics proprietary data), upon cavitation-mediated delivery but a transient immune response was observed for the CD11c-Cal09 vector, which was designed to be specific to CD11c positive cells, which include dendritic cells [156]. This implies that cavitation-mediated delivery may specifically target or involve immune cells within the dermal layers, rather than keratinocytes. One way of addressing this in more detail could be through the delivery of reporter genes under the CMV, KCL27 or CD11c promoter and subsequent immunohistochemistry or fluorescence activated cell sorting (FACS) to specifically identify and characterise positive cells. Indeed, in preliminary experiments performed with a CMV-GFP vector and FACS, caviation-mediated delivery led to a disproportionately higher level of CD11c positive cells showing high levels of GFP expression (data not shown). This aligns well with the literature, where two mechanisms for the effectiveness for transcutaneous immunisation have been proposed: ultrasound increases permeability and the additional antigen delivered allows for an enhanced immune response, or Langerhans cells and other immune cells in the skin effectively capture the antigen and induce an immune response [323]. This second mechanism implicating Langerhans cells and other immune cells, agrees with the finding that CD11c-positive cells had relatively high levels of GFP, as well as the transient response seen under the CD11c-specific promoter.

Three adjuvants were also assessed in the first round, namely CMV-IL1$\alpha$-IL1$\beta$, CMV-IL12 and CpG-RIG1, each chosen for their potential ability to enhance the immune response to a co-delivered target-antigen. Only CMV-IL1$\alpha$-IL1$\beta$ improved antibody responses compared to CMV-Cal09 and showed a lower IgG1/IgG2a ratio, suggesting a more cellular response, but this was only in 1 out of 3 mice.

In the second round of DNA engineering, two types of DNA vector improvements were investigated. In terms of adjuvants, three DNA adjuvant vectors were explored, namely CMV-Flt3l-Fc, CMV-CD80-Fc and CMV-Perforin. These adjuvants were selected for their ability to induce a cellular immune response in previous studies [227, 228] and were co-delivered with CMV-Cal09, expressing an influenza haemagglutinin. Unfortunately, none of these adjuvants provided any advantage in terms of overall anti-Cal09 HA antibody levels upon intradermal injection. Despite a lower anti-

body titre and equal avidity, the CMV-Perforin plasmid did help generate a stronger cellular immune response to Cal09 HA protein after its I.D. co-injection with the CMV-Cal09 plasmid, as seen by a 1.4-fold increase in SFU/million cells. In contrast, when the CMV-Cal09 plasmid was co-delivered with CMV-Perforin plasmid to the skin using cavitation, an increase in anti-Cal09 HA antibody titre (10.6-fold) and avidity (1.5-fold) was seen compared to delivery of CMV-Cal09 alone. This difference between the utility of the CMV-Perforin plasmid in an I.D. and cavitation setting is possibly a consequence of the different cell types targeted by cavitation and the ability of perforin to generate DAMP signals that encourage an immune response instead of tolerance response by Langerhans cells. It is noteworthy that although quite substantial effects were seen, these proved not to be statistically significant. Further studies with higher numbers as well as FACS studies to identify positive cell populations would be required to draw firmer conclusions.

A further clue into the target cell types was given by antibody isotyping. Where intradermal injection results in a balanced IgG1/IgG2a response, cavitation consistently resulted in a bias towards IgG1 antibodies. In mice, IgG1 antibodies are associated with Th2 immune response, whereas IgG2a antibodies are associated with a Th1 immune response, which result in strong ADCC and CDC activation [193–195]. Notably, Langerhans cells have been shown to drive IgG1 responses in mice [89], hence are likely a primary immune cell type involved in generating an immune response upon cavitation-mediated delivery. Alternatively, research with gene guns has also highlighted langerin$^{+}$ dermal dendritic cells as potentially responsible for the IgG1 antibody response rather than Langerhans cells [278].

This IgG1 bias has also been previously been observed in work by Kwissa et al., which showed that intradermal injection with a gene gun resulted in IgG1/IgG2a ratio >100, whereas I.M. resulted in an IgG1/IgG2a ratio of 0.4-0.7 [209]. It has also been recorded by Feltquate et al., who saw a bias to IgG1 for both gene gun administered to the skin or muscle (IgG1/IgG2a: >10), whilst I.D. and I.M. injection resulted in IgG2a-biased antibody response (IgG1/IgG2a: 0.1-0.2). Microneedles in contrast have shown a more balanced IgG1/IgG2a response [324, 325] or even a IgG2a-skewed immune response [326]. However, little data exists on the effect of cavitation on antibody isotyping. The data presented in this thesis suggests that cavitation mimics the mechanisms of gene gun delivery more closely. A strategy of shifting the Th2 response generated by gene gun vaccination to a more Th1 response has been proposed by Schrimbeck et al. They showed that CpG sequences injected to the site of gene gun delivery of HBsAg-encoding plasmid in the 48 hours prior to 48 hours post gene gun

vaccination resulted in IgG1/IgG2a below 0.5 in BALB/c mice. They also showed that I.D. injection of 50 ng of IL-12 recombinant protein 3 hrs after gene gun immunisation reduced the IgG1/IgG2a ratio from 80 to 2-20 [327]. Such a priming strategy of the skin, would be very suitable to the p-CaN technology; a p-CaN made from IL-12 could be created and co-delivered with the pDNA encoding the desired pathogen-associated antigen.

The second improvement assessed was the utility of a self-amplifying vector. This approach represents a method to address the transient nature of expression from mRNA therapeutics by borrowing the self-amplification machinery from positive-strand RNA viruses such as VEEV [40]. This approach has shown good pre-clinical efficacy [328] and even reached phase 3 trials for SARS-CoV-2 [329]. However, reliance on RNA still raises production cost and scale-up issues and storage stability constraints. Hence, encoding and delivering the self-amplification machinery at the DNA level is an attractive approach.

In Chapter 5, a self-amplifying DNA construct, based on the non-structural proteins from VEEV [245], was created and tested. Two versions of this vector were constructed through significant cloning work: a reporter- (luciferase) and an antigen-encoding (Cal09 HA) DNA vector. The reporter gene studies revealed interesting behaviour after I.D. injection, where a lower level of expression (2.3-fold) was achieved with the self-amplifying VEEV-based construct compared to a non-amplifying vector after 24 hours, which then started to rise after 5 days resulting in substantially higher levels of expression for at least a month. However, when the self-amplifying VEEV-based vector was delivered by cavitation, a 4-fold lower level of expression after 24 hours was seen compared to the non-amplifying vector (as with I.D. delivery) but no increase in expression over time was observed. This may be related to the cell population targeted by cavitation-mediated delivery being different to that targeted by I.D. delivery. As cavitation delivers into the epidermis rather than the dermal compartment, transfected cells may not have the life span to allow for the full life-cycle of self-amplification or may silence DNA vectors more effectively. However, in an experiment using injection into the superficial dermis with plasmid DNA encoding the beta-galactosidase indicator gene to target the epidermis, expressed protein was observed in the epidermis for 3 weeks, although mRNA and DNA levels declined within the first week [330], so silencing or degradation may be more likely. Alternatively, the DNA may be processed and the cells that have taken it up migrated to other parts of the body, such as draining lymph nodes [331]. As no high level of protein expression was observed, the self-amplifying vector was not taken forward for cavitation testing.

The antigen-encoding, self-amplifying vector was taken forward for characterising the immune responses generated by this vector in combination with intradermal injection. Mice were intradermally injected with 380 µg of self-amplifying pDNA (which was copy-matched to a non-amplifying vector for comparison) and homologously boosted after 21 days. Interestingly, when anti-Cal09 HA antibody levels were plotted over time, a delay in mounting an immune response, in line with what was observed by the reporter vector, was observed. Specifically, by 29 days the response to the non-replicating vector had peaked in 3 out of 4 mice whereas the self-amplifying vector peaked at 42 days in 3 out of 4 mice. The self-amplifying vector also showed high reproducibility, with a very low geometric standard deviation around the geometric mean titre (GSD: 1.4 for self-amplifying vs 2.7 for non-amplifying), as well as a 1.34-fold higher avidity. The self-amplifying vector also generated a IgG2a-skewed IgG1/IgG2a ratio, implying stronger ADCC and CDC activation [193–195].

These raised immune responses may be a function of greater more sustained levels of antigen production and presentation and/or the life-cycle of self-amplification and the generation of dsRNA and viral protein complexes which may increase the production of 'danger signals' [246] and hence stimulate this more Th1 immune response, i.e. in much the same way adding CpG or IL-12 worked in the research of Schirmbeck et al. [327]. This Th1-biased response has also been observed upon I.M. injection of LNP-formulated self-amplifying RNA encoding the spike protein of SARS-CoV-2 [251], as well as upon I.M. injection of a self-replicating RNA co-formulated with lipid inorganic nanoparticles [332]. Commercially, self-amplifying vaccines have seen a great amount of interest and have focused on mRNA vaccines, which uses a pDNA template to generate the necessary mRNA strands. [328]. The work presented in this thesis bypasses this step, by directly introducing the very stable pDNA to the skin and co-opting the cell's own transcription machinery to generate the initial mRNA strand from which the self-replication process launches.

### 7.1.4 Influenza challenge

From the range of studies reported in Chapter 5, two approaches were deemed worthy of further investigation in Chapter 6. The combination of CMV-Perforin with CMV-Cal09 delivered by p-CaN nucleated cavitation formed one tranche of work. The use of a self-amplifying CMV-VEEV-Cal09 vector by I.D. injection formed another tranche of work. To ascertain whether the responses generated were of therapeutic relevance, studies were designed with the ultimate aim of assessing level of protection against pathogenic challenge. Hence, the aim of the challenge study was to test the most

compelling technologies and learnings from chapters 2-5 in the most stringent way possible. This involved combining the optimised cavitation nuclei, ultrasound parameters and DNA vectors to achieve an effective transcutaneous vaccination strategy (fourth research aim), as well as further probing the utility of the self-amplifying vector. As a different strain of mice, DBA/2 was required to enable the challenge with influenza strain Cal09, an initial pilot *in vivo* study was performed and showed that the same luciferase expression level could be achieved as observed in the previously used BALB/c mice.

The challenge study was then designed to answer 3 questions, namely whether a self-amplifying vector provides more protection than a non-amplifying vector, whether cavitation-mediated delivery could match intradermal injection and whether the low-dose delivered by cavitation would provide the same protection as an equivalent dose injected intramuscularly.

Despite this positive luciferase data, when the CMV-Cal09 vector and CMV-Perforin vector were co-delivered using ultrasound and BSA p-CaN cavitation nuclei, no antibodies could be detected at any time-point after treatment. Notably, sufficient cavitation was observed (>3.9 μJ TASE for 19/20 treatments), sufficient expression in the skin of the DBA/2 mouse model had been verified beforehand ($5.19 \times 10^5$ p/s) and such levels were sufficient to instigate an anti-transgene (i.e. anti-luciferase) response in BALB/c mice. It is therefore speculated that the difference in mouse model may be the underlying cause of the lack of observed raised immunity. The identified differences include a lack of langerin expression in the spleen [294], a difference in T cell responses compared to BALB/c mice [295, 298] and a lack of a fully functional complement system [296].

Flacher et al. have speculated that as langerin plays a possible role in antigen uptake, a lack of langerin in the spleen may indicate a diminished ability of effective cross-presentation of antigen [294], which could result in a muted immune response. Multiple differences in T cell populations and cytokine expression in DBA/2 mice have also been observed compared to BALB/c mice as well as strain differences upon infection [295, 298]. As T cells and cytokines play an important part in stimulating other immune cells and the expression of antibodies, a difference in T cell population may have prevented a strong immune response from being mounted. However, only specific examples exist for strain differences and no overarching immunological model exists that defines differences between BALB/c and DBA/2 mice upon transcutaneous vaccination. Finally, the complement system is compromised in DBA/2 mice. A compromised complement system has been shown to decrease antibody responses in a complement knock-out mouse strain upon vaccination with a haemagglu-

tinin VLP vaccine [302]. As cavitation-mediated delivery results in lower antibody titres compared to direct injection (Chapter 5), this decrease in antibody responses may have made the antibodies undetectable in the test system used. Further work will be needed to better define the differences between DBA/2 mice and BALB/c mice, which would hopefully inform future decisions on an appropriate animal model for testing of cavitation-mediated delivery of DNA vaccines.

As no immune response was observed in the cavitation-treated group, it was not possible to make a direct comparison with the comparitor I.M. injected mice. However, it is worth noting that no immune response was observed in these mice either. The question of whether the DNA-launched, self-amplifying vector could provide better protection than a non-amplifying vector following intradermal injection was also addressed in Chapter 6.

Despite the immunological attractiveness of the intradermal compartment as a target for vaccination, intradermal injection remains a highly variable technique often resulting in treatment failures (especially when non-condensed DNA is being delivered). These treatment failures were removed and levels of anti-Cal09 HA antibodies in the six best responders from the self-amplifying and non-amplifying groups were titred. The titring of the antibodies from these mice further emphasised the improved reproducibility of the self-amplifying vector compared to the non-amplifying vector (GSD: 2.5 vs 5.4). Also the IgG2a-skewed IgG1/IgG2a ratio was again observed (as in Chapter 5), as well as the improved avidity (as in Chapter 5). The IgG2a-bias implies a Th1 immune response and has been associated with viral clearance and better protection against disease, as well as complement activation and antibody-dependent cellular cytotoxicity [194, 195, 210, 270]. Hence, significant protective advantages are associated with eliciting an IgG2a response upon vaccination [270].

In line with animal welfare requirements, six mice from each group with sufficient antibody titre were subsequently challenged with H1N1pdm09 vaccine virus X-179A, which contains the haemagglutinin and neuraminidase of A/California/07/2009. 100% survival was observed for the group with the self-amplifying vector and positive control, whereas 83% survival was observed for the non-amplifying vector group and 0% for the negative control. The benefit of the self-amplifying vector was further emphasised in the relative weight change of the mice. In the non-amplifying group 3/6 mice lost over 7% of their body weight, whereas the self-amplifying vector group, no mouse lost more than 6.5%. Overall, the CMV-VEEV-Cal09 vector was identified as a strong candidate for improving immunogenicity of DNA vaccines. The potential for self-amplifying vectors is also supported by

data from Erasmus et al., who have shown that prime-only immunisation with a 250-µg dose spike protein-encoding self-replicating RNA co-formulated with lipid inorganic nanoparticles I.M. injected in macaques seroconverted three out of three animals [332]. A self-amplifying COVID-19 vaccine has also reached clinical trials [329]. Although only 55% efficacy against symptomatic disease was reported at phase III trials of the self-amplifying ARCT-154 vaccine, 95% protection against severe disease was described [333]. Notably, this clinical trial did show significant potential for dose-sparing with as little as 5 µg of vaccine used per dose compared to 30 µg for the BNT162b2 vaccine by Pfizer [50, 333]. The relatively low doses needed for a self-amplifying vector to have an impact may also have contributed to the strong response seen in this thesis. Indeed, nuclear delivery is a highly inefficient rate-limiting step and it has been estimated that only around 1 in 100-1000 plasmid DNA constructs reach the nucleus from the cytoplasm, a barrier mRNA does not need to cross. [41, 42]. To date although self-amplifying mRNA vaccines have made some clinical progress [328], the potential of DNA-encoded self-amplifying RNA remains relatively under-explored. This thesis is the first to report on complete protection against influenza challenge in a mouse model upon I.D. injection of a DNA-encoded, self-amplifying RNA vector and shown that a similar Th1-biased response is seen to self-amplifying mRNA.

The research presented in this doctoral thesis has therefore been the first to demonstrate:

- The utility of the V2 set-up and the optimised parameters for delivery of DNA into murine skin.
- The potential of p-CaN formulations to effectively drive the delivery of DNA into the skin, as well as generate an immune response against the protein from which they are formulated. This opens up the possibility for immunostimulatory p-CaN to be explored for improved immunogenicity of vaccines.
- The adjuvant effect of the CMV-Perforin DNA vector in improving antibody titres and avidity for cavitation-mediated delivery.
- The protection from challenge upon intradermal vaccination with the self-amplifying pDNA CMV-VEEV-Cal09 and the adjuvant pDNA CMV-Perforin.

## 7.2 Research limitations and future directions

Much work has been done in this thesis to move cavitation-delivered DNA vaccines closer to the clinic. This has included improvements in set-up, cavitation nuclei and DNA vectors. However, further steps can be taken to improve the efficacy and clinical translation of this new technology. Potential improvements and further lines of work are explored below.

### 7.2.1 Set-up

The V2 set-up described in this thesis presents a much easier to handle set-up than the V1 set-up. However, it still requires expert handling to enable successful assembly and treatment. In the literature several other set-ups have been used to deliver ultrasound to the skin. For example, cymbal arrays have been explored to enable delivery of insulin into pigs, as wearable low-frequency transducer arrays [334]. Not only can these cymbal arrays deliver transcutaneously, a 2x2 array can be less than 7 mm thick, weigh less than 22 g and allow for wide arrays that can treat larger skin areas. However, these are limited to 100 kHz [335], which is below the frequency used in this thesis and may be more effective for the delivery of the 5 kDa protein insulin than a 4 MDa DNA plasmid. The concept of these arrays could, however, be applied to this work, if larger skin areas need to be treated in humans to allow for effective delivery. Other strategies have included the application of an ultrasound horn to the skin before addition of the vaccine [145]. This strategy offers potential in terms of ease of use, as it is a handheld device, but does not utilise the convective properties of delivery by cavitation and add the complexity of a two-step procedure. The SonoPrep designed and built by Sontra Medical has been used in multiple clinical trials. This device has an ultrasound horn in a titanium housing that contains the coupling buffer and has been shown to decrease skin permeability from >200k$\Omega$-cm$^2$ to below 10 k$\Omega$-cm$^2$, which is associated with orders of magnitude increase in skin permeability to hydrophilic molecules [336]. This is a battery-powered device which allows for easy use and portability enabling easy clinical integration. Examples of its use include a clinical study on the speed of cutaneous anaesthesia onset by EMLA in combination with ultrasound pre-treatment at 55 kHz but unknown pressure for 9.0 ± 4.53 s [133]. In another clinical trial, ultrasound-permeabilisation of the skin by the SonoPrep (frequency, 53–56 kHz) (Sontra Medical Corp., Franklin, MA) followed by 5 minutes of 4% liposomal lidocaine cream decreased pain from IV cannulation. Ultrasound was applied until a threshold skin conductance was reached [311]. Also Park et al. used a commercially available ultrasound device, SONOCUBE®, at a frequency of 1.06 MHz [141], which has been specifically designed for people to use at home for cosmetic purposes. For vaccination, a portable

device such as these would allow easy clinical use, without the need for training. Hence, more work could be done to enable a set-up that is more clinically relevant and allows for a handheld device with minimal settings. It is notable that none of these devices incorporates cavitation monitoring as a feature and so the application is performed 'blind' to the amount and duration of the event believed to permit delivery.

### 7.2.2 Formulation

In this thesis, a very streamlined approach was taken to the vaccination formulation, which consisted solely of DNA, cavitation nuclei and MilliQ. However, other literature has shown that synergistic effects exist between ultrasound and other technologies, including microneedles [147], skin permeabilisation agents [337] and iontophoresis [338]. Indeed, potential exists to increase delivery of the DNA by the addition of permeabilising agents or other synergistic techniques. A potential downside of this would be the complexity and cost of bringing multimodal techniques to the clinic, as well as the additional training it may require of users.

A further optimisation that could improve clinical translation, is alteration of viscosity of the formulation. The current formulation is a liquid, which allows for the free convective flows generated by cavitation. However, a liquid placed on the skin also decreases the ease of use and a more solid patch or gel may make it simpler to use in the clinic, as it more closely mirrors current practice and would enable easy dosing.

### 7.2.3 Immunostimulatory p-CaN

Another area that was touched upon in this thesis was the immunostimulatory capabilities of p-CaN. It was shown that p-CaN can generate an immune response (Chapter 3) and Dr. Lyons has shown that p-CaN can be made from a great variety of proteins (personal communication). This opens up the possibility to make p-CaN from proteins that create an immuno-environment that is prone to a strong immune response upon expression of the antigen from the DNA. This would allow for the generation of a platform technology of immunostimulatory p-CaN that could be combined with the rapidly synthesised DNA to counter a pathogenic outbreak and prevent pandemics. Possible candidates include IL-12, FLT3L or TNF-$\alpha$, as well as pore-forming proteins that may improve delivery of the DNA. One very interesting application of the p-CaN technology would be to decrease the IgG1/IgG2a ratio from the IgG1-dominated response shown. Schirmbeck et al. have shown that I.D. injection 50 ng of IL-12 recombinant protein reduced the IgG1/IgG2a ratio from 80 to 2-20 in

combination with gene gun vaccination [327]. Such priming of the skin by IL-12 p-CaN has the potential to shift the IgG1 antibody response seen upon cavitation-mediated delivery of DNA vaccines towards IgG2a, which could result in better protection from challenge, similar to what was observed with the self-amplifying vector which has a IgG2a-skewed antibody response.

### 7.2.4 Challenge model

An interesting and unexpected observation was the lack of immunity in the DBA/2 mouse strain upon cavitation-mediated delivery of the CMV-Cal09 and CMV-Perforin vectors. No obvious explanation for this phenomenon could be identified and it suggests further research is still needed into both the mechanism that enables cavitation-mediated vaccination, as well as the search for a more appropriate challenge model. A better fundamental understanding of the delivery mechanism may also help to inform better animal models. In this work it was shown that BALB/c mice do generate an antibody response, but this mouse strain is not susceptible to influenza A/California/07/2009 (H1N1). However, they are susceptible to influenza strain A/Puerto Rico/8/1934 virus [339]. Hence, it would be interesting to investigate whether a DNA vector encoding the haemagglutinin of the A/Puerto Rico/8/1934 virus can protect mice in combination with CMV-Perforin and cavitation-mediated delivery.

### 7.2.5 Towards the clinic

This thesis has extensively used mouse models as a testbed for cavitation-mediated delivery into the skin and shown progress in parameters and formulation to improve immunogenicity. However, significant differences exist between mouse skin and humans. These differences include skin thickness, permeability, hair follicle density, immune cell profile present in the skin and dependent on the mouse model, biases towards certain immunological responses.

As transfollicular skin penetration is a possible route into the skin, the high follicular density in mouse skin may give a skewed view of the efficacy of transcutaneous vaccination in mice. However, a liposomal spray formulation containing plasmid DNA has been shown to lead to expression in both mouse and human skin [340], showcasing that it may not be limiting barrier. A more similar and popular proxy for human skin may be found in pig skin, which has shown to be able to express plasmid DNA delivered into the skin [265, 341]. Pig skin also has a more similar thickness to human skin and been shown to have similar permeability [342]. The skin thickness of the epidermis in mice has been

observed to be only three cell layers thick and less than 25 µm, whereas humans have an epidermis 6-10 cell layers thick and may be over 100 µm. Mice also have a faster epidermal turnover than humans [343]. A similar observation on skin thickness can be made for the dermis, which is 200 µm in mice and 2 mm in humans. This difference in thickness limit the extrapolation that can be made from mice to humans [344]. From an immunological point of view, the differences that are apparent in the skin include the prominence of Vγ5+ dendritic epidermal T cells (DETCs) in mouse epidermis, whereas these are not present in human skin, which relies only on langerhans cells and CD8+ T cells. Furthermore, γδ T cells play a greater role in the mouse dermal layer than in humans, which may alter the observed immunological responses [345]. Pigs, however, show greater similarities in their dendritic cells to humans, which may make them a better model for assessing transcutaneous vaccines [346].

These differences highlight the work that stands between the work presented and a clinical trial. Further work to develop this technology have been mentioned above, such as the development of a more clinically applicable device, the development of GMP standard p-CaN, which may have immunological properties, and an improved fundamental understanding of the mechanism through which immunity is generated upon ultrasound-mediated delivery of a DNA vaccines. This better fundamental understanding could then inform a better challenge model to test the current system and provide guidance for potential improvements that may be needed. To address the differences in skin permeability and thickness, *in vitro* work with pig skin could provide further clarity on the efficacy of this technology, and could build on the previous work done by Dr. Van Blokland [143]. The *in vivo* effects could be assessed in guinea pigs as a next step, which represent a rodent model with skin more similar to humans than mice [342]. This could be followed by challenge in ferrets, which represent a frequently used model in influenza research [347] and *in vivo* immunisation in pigs to assess the humoral and cellular immunity generated in an animal model with similar skin to humans. These results could then inform the necessary research in non-human primates, to provide the data to allow for a clinical trial to test this methodology in the clinic. In should be noted, however, that although the above describes one potential pathway to translation, there is no ‘ideal’ model. The preference for using mice in the studies reported in this thesis was based on the impracticality of performing large parameter identification studies in large animals such as pigs and the major issues with reproducibility experienced by Dr. Van Blokland with *ex vivo* pig skin samples. The important aspect is to understand and account for the weaknesses in whichever model is used and combine data from different models to inform efficacy and safety before progressing to the clinic.

Overall, further research remains to be done to get this technology into the clinic in terms of understanding the underlying mechanisms and improving useability. However, significant progress has been made in optimising delivery parameters, improving reproducibility and handling in the set-up for research purposes, exploring the potential of p-CaN as a novel, biodegradable and immunogenic cavitation nuclei and identifying a promising DNA adjuvant vector for cavitation-mediated delivery.

# Bibliography


[1] Strategic Advisory Group of Experts (SAGE) and others. Report of the SAGE Working Group on Vaccine Hesitancy. *World Health Organization*, 2014.

[2] Eve Dubé, Caroline Laberge, Maryse Guay, Paul Bramadat, Réal Roy, and Julie A Bettinger. Vaccine Hesitancy: An Overview. *Human Vaccines & Immunotherapeutics*, 9(8):1763–1773, 2013.

[3] WHO, UNICEF, and World Bank. *State of the World's Vaccines and Immunization*. World Health Organization, 3rd edition, 2009.

[4] Stefan Riedel. Edward Jenner and the History of Smallpox and Vaccination. In *Baylor University Medical Center Proceedings*, volume 18(1), pages 21–25. Taylor & Francis, 2005.

[5] World Health Organization. WHO Coronavirus (COVID-19) Dashboard, 2021. URL `https://covid19.who.int/`. [Accessed 8 March, 2022].

[6] COVID19 Vaccine Tracker. Approved Vaccines, 2021. URL `https://covid19.trackvaccines.org/vaccines/approved/`. [Accessed 8 March, 2022].

[7] Lu Zhang, Wei Wang, and Shixia Wang. Effect of Vaccine Administration Modality on Immunogenicity and Efficacy. *Expert Review of Vaccines*, 14(11):1509–1523, 2015.

[8] Robert L Coffman, Alan Sher, and Robert A Seder. Vaccine Adjuvants: Putting Innate Immunity to Work. *Immunity*, 33(4):492–503, 2010.

[9] Ruslan Medzhitov and Charles A Janeway Jr. Innate Immunity: Impact on the Adaptive Immune Response. *Current Opinion in Immunology*, 9(1):4–9, 1997.

[10] Yang Liu and Charles A Janeway. Cells that Present Both Specific Ligand and Costimulatory Activity are the Most Efficient Inducers of Clonal Expansion of Normal CD4 T cells. *Proceedings of the National Academy of Sciences*, 89(9):3845–3849, 1992.

[11] Karolina Palucka, Jacques Banchereau, and Ira Mellman. Designing Vaccines Based on Biology of Human Dendritic Cell Subsets. *Immunity*, 33(4):464–478, 2010.

[12] Claire-Anne Siegrist. Vaccine Immunology. *Vaccines*, 5(1):17–36, 2008.

[13] Gordon Ada. Vaccines and Vaccination. *New England Journal of Medicine*, 345(14):1042–1053, 2001.

[14] Christophe J Desmet and Ken J Ishii. Nucleic Acid Sensing at the Interface between Innate and Adaptive Immunity in Vaccination. *Nature Reviews Immunology*, 12(7):479–491, 2012.

[15] Paul Fine, Ken Eames, and David L Heymann. "Herd Immunity": A Rough Guide. *Clinical infectious diseases*, 52(7):911–916, 2011.

[16] Cornelia Betsch, Robert Böhm, Lars Korn, and Cindy Holtmann. On the Benefits of Explaining Herd Immunity in Vaccine Advocacy. *Nature Human Behaviour*, 1(3):1–6, 2017.

[17] World Health Organization et al. Vaccines against Influenza WHO Position Paper — November 2012. *Weekly Epidemiological Record*, 87(47):461–476, 2012.

[18] A Danielle Iuliano, Katherine M Roguski, Howard H Chang, David J Muscatello, Rakhee Palekar, Stefano Tempia, Cheryl Cohen, Jon Michael Gran, Dena Schanzer, Benjamin J Cowling, et al. Estimates of Global Seasonal Influenza-Associated Respiratory Mortality: A Modelling Study. *The Lancet*, 391(10127):1285–1300, 2018.

[19] Noelle-Angelique M Molinari, Ismael R Ortega-Sanchez, Mark L Messonnier, William W Thompson, Pascale M Wortley, Eric Weintraub, and Carolyn B Bridges. The Annual Impact of Seasonal Influenza in the US: Measuring Disease Burden and Costs. *Vaccine*, 25(27):5086–5096, 2007.

[20] Siddhivinayak Hirve, World Health Organization, et al. *Seasonal Influenza Vaccine Use in Low and Middle Income Countries in the Tropics and Subtropics: A Systematic Review*. World Health Organization, 2015.

[21] Pieter LA Fraaij and Terho Heikkinen. Seasonal Influenza: The Burden of Disease in Children. *Vaccine*, 29(43):7524–7528, 2011.

[22] Peter C Soema, Ronald Kompier, Jean-Pierre Amorij, and Gideon FA Kersten. Current and Next Generation Influenza Vaccines: Formulation and Production Strategies. *European Journal of Pharmaceutics and Biopharmaceutics*, 94:251–263, 2015.

[23] Janet E McElhaney. The Unmet Need in the Elderly: Designing New Influenza Vaccines for Older Adults. *Vaccine*, 23:S10–S25, 2005.

[24] Maria C Zambon. Epidemiology and Pathogenesis of Influenza. *Journal of Antimicrobial Chemotherapy*, 44:3–9, 1999.

[25] Charles J Russell, Meng Hu, and Faten A Okda. Influenza Hemagglutinin Protein Stability, Activation, and Pandemic Risk. *Trends in Microbiology*, 26(10):841–853, 2018.

[26] Steven J Gamblin and John J Skehel. Influenza Hemagglutinin and Neuraminidase Membrane Glycoproteins. *Journal of Biological Chemistry*, 285(37):28403–28409, 2010.

[27] Damian C Ekiert, Gira Bhabha, Marc-André Elsliger, Robert HE Friesen, Mandy Jongeneelen, Mark Throsby, Jaap Goudsmit, and Ian A Wilson. Antibody Recognition of a Highly Conserved Influenza Virus Epitope. *Science*, 324(5924):246–251, 2009.

[28] John Treanor. Influenza Vaccine — Outmaneuvering Antigenic Shift and Drift. *New England Journal of Medicine*, 350(3):218–220, 2004.

[29] Nicole M Bouvier and Peter Palese. The Biology of Influenza Viruses. *Vaccine*, 26:D49–D53, 2008.

[30] Stéphane Boivin, Stephen Cusack, Rob WH Ruigrok, and Darren J Hart. Influenza A Virus Polymerase: Structural Insights into Replication and Host Adaptation Mechanisms. *Journal of Biological Chemistry*, 285(37):28411–28417, 2010.

[31] Christoph Scholtissek. Source for Influenza Pandemics. *European Journal of Epidemiology*, 10(4):455–458, 1994.

[32] Fabrice Carrat and Antoine Flahault. Influenza Vaccine: The Challenge of Antigenic Drift. *Vaccine*, 25(39-40):6852–6862, 2007.

[33] World Health Organization. Ten Threats to Global Health in 2019, 2019. URL `https://www.who.int/news-room/spotlight/ten-threats-to-global-health-in-2019`. [Accessed 8 February, 2020].

[34] Jeffery K Taubenberger and David M Morens. 1918 Influenza: The Mother of All Pandemics. *Emerg Infect Dis*, 12(1):15–22, 2006.

[35] Niall PAS Johnson and Juergen Mueller. Updating the Accounts: Global Mortality of the 1918-1920 "Spanish" Influenza Pandemic. *Bulletin of the History of Medicine*, pages 105–115, 2002.

[36] Melissa A Rolfes, Brendan Flannery, Jessie R Chung, Alissa O'Halloran, Shikha Garg, Edward A Belongia, Manjusha Gaglani, Richard K Zimmerman, Michael L Jackson, Arnold S Monto, et al. Effects of Influenza Vaccination in the United States During the 2017–2018 Influenza Season. *Clinical Infectious Diseases*, 69(11):1845–1853, 2019.

[37] Vivek P Chavda, Radhika Pandya, and Vasso Apostolopoulos. DNA vaccines for SARS-CoV-2: toward Third-Generation Vaccination Era. *Expert Review of Vaccines*, 20(12):1549–1560, 2021.

[38] Department of Biotechnology (DBT) under the Ministry of Science, Technology, and Biotechnology Industry Research Assistance Council (BIRAC). DBT-BIRAC Supported ZyCoV-D Developed by Zydus Cadila Receives Emergency Use Authorization. *https://www.pib.gov.in/*, 2021. URL `https://www.pib.gov.in/PressReleasePage.aspx?PRID=1747669`. [Accessed 30 September, 2021].

[39] Karen E Gooch, Trevor RF Smith, Francisco J Salguero, Susan A Fotheringham, Robert J Watson, Mike J Dennis, Alastair Handley, Holly E Humphries, Stephanie Longet, Tom Tipton, et al. One or Two Dose Regimen of the SARS-CoV-2 Synthetic DNA Vaccine INO-4800 Protects against Respiratory Tract Disease Burden in Nonhuman Primate Challenge Model. *Vaccine*, 2021.

[40] Karl Ljungberg and Peter Liljeström. Self-Replicating Alphavirus RNA Vaccines. *Expert Review of Vaccines*, 14(2):177–194, 2015.

[41] Erin E Vaughan, James V DeGiulio, and David A Dean. Intracellular Trafficking of Plasmids for Gene Therapy: Mechanisms of Cytoplasmic Movement and Nuclear Import. *Current gene therapy*, 6(6):671–681, 2006.

[42] David A Dean, Brenda S Dean, Susanne Muller, and Louis C Smith. Sequence Requirements for Plasmid Nuclear Import. *Experimental Cell Research*, 253(2):713–722, 1999.

[43] Andrew J Geall, Ayush Verma, Gillis R Otten, Christine A Shaw, Armin Hekele, Kaustuv Banerjee, Yen Cu, Clayton W Beard, Luis A Brito, Thomas Krucker, et al. Nonviral Delivery of Self-Amplifying RNA Vaccines. *Proceedings of the National Academy of Sciences*, 109(36): 14604–14609, 2012.

[44] Elisabeth Mahase. Covid-19: UK Approves Moderna Vaccine to be Given as Two Doses 28 Days Apart, 2021.

[45] Jon A Wolff, Robert W Malone, Phillip Williams, Wang Chong, Gyula Acsadi, Agnes Jani, and Philip L Felgner. Direct Gene Transfer into Mouse Muscle In Vivo. *Science*, 247(4949):1465–1468, 1990.

[46] Yen Cu, Kate E Broderick, Kaustuv Banerjee, Julie Hickman, Gillis Otten, Susan Barnett, Gleb Kichaev, Niranjan Y Sardesai, Jeffrey B Ulmer, and Andrew Geall. Enhanced Delivery and Potency of Self-Amplifying mRNA Vaccines by Electroporation In Situ. *Vaccines*, 1(3):367–383, 2013.

[47] Bruce A Sullenger and Smita Nair. From the RNA World to the Clinic. *Science*, 352(6292): 1417–1420, 2016.

[48] Kapil Bahl, Joe J Senn, Olga Yuzhakov, Alex Bulychev, Luis A Brito, Kimberly J Hassett, Michael E Laska, Mike Smith, Örn Almarsson, James Thompson, et al. Preclinical and Clinical Demonstration of Immunogenicity by mRNA Vaccines against H10N8 and H7N9 Influenza Viruses. *Molecular Therapy*, 25(6):1316–1327, 2017.

[49] Lindsey R Baden, Hana M El Sahly, Brandon Essink, Karen Kotloff, Sharon Frey, Rick Novak, David Diemert, Stephen A Spector, Nadine Rouphael, C Buddy Creech, et al. Efficacy and Safety of the mRNA-1273 SARS-CoV-2 Vaccine. *New England Journal of Medicine*, 2020.

[50] Fernando P Polack, Stephen J Thomas, Nicholas Kitchin, Judith Absalon, Alejandra Gurtman, Stephen Lockhart, John L Perez, Gonzalo Pérez Marc, Edson D Moreira, Cristiano Zerbini, et al. Safety and Efficacy of the BNT162b2 mRNA Covid-19 Vaccine. *New England Journal of Medicine*, 2020.

[51] Laith J Abu-Raddad, Hiam Chemaitelly, Hadi M Yassine, Fatiha M Benslimane, Hebah A Al Khatib, Patrick Tang, Joel A Malek, Peter Coyle, Houssein H Ayoub, Zaina Al Kanaani, et al. Pfizer-BioNTech mRNA BNT162b2 Covid-19 Vaccine Protection against Variants of Concern After One Versus Two Doses. *Journal of travel medicine*, 28(7):taab083, 2021.

[52] Margaret A Liu. DNA Vaccines: An Historical Perspective and View to the Future. *Immunological reviews*, 239(1):62–84, 2011.

[53] Jeffrey B Ulmer, John J Donnelly, Suezanne E Parker, Gary H Rhodes, Philip L Felgner, VJ Dwarki, Stanislaw H Gromkowski, R Randall Deck, Corrille M DeWitt, Arthur Friedman, et al. Heterologous Protection against Influenza by Injection of DNA Encoding a Viral Protein. *Science*, 259(5102):1745–1749, 1993.

[54] John J Donnelly, Arthur Friedman, Douglas Martinez, Donna L Montgomery, John W Shiver, Sherri L Motzel, Jeffrey B Ulmer, and Margaret A Liu. Preclinical Efficacy of a Prototype DNA Vaccine: Enhanced Protection against Antigenic Drift in Influenza Virus. *Nature Medicine*, 1 (6):583–587, 1995.

[55] Veronica L Scott, Ami Patel, Daniel O Villarreal, Scott E Hensley, Edwin Ragwan, Jian Yan, Niranjan Y Sardesai, Paul J Rothwell, Jonathan P Extance, Lisa J Caproni, et al. Novel Synthetic Plasmid and Doggybone™ DNA Vaccines Induce Neutralizing Antibodies and Provide Protection from Lethal Influenza Challenge in Mice. *Human Vaccines & Immunotherapeutics*, 11(8):1972–1982, 2015.

[56] Lei Li and Nikolai Petrovsky. Molecular Mechanisms for Enhanced DNA Vaccine Immunogenicity. *Expert Review of Vaccines*, 15(3):313–329, 2016.

[57] Daniela S Rajão and Daniel R Pérez. Universal Vaccines and Vaccine Platforms to Protect against Influenza Viruses in Humans and Agriculture. *Frontiers in Microbiology*, 9:123, 2018.

[58] Jeffrey B Ulmer, John J Donnelly, and Margaret A Liu. Toward the Development of DNA Vaccines. *Current Opinion in Biotechnology*, 7(6):653–658, 1996.

[59] Chih-Jen Wei, Jeffrey C Boyington, Patrick M McTamney, Wing-Pui Kong, Melissa B Pearce, Ling Xu, Hanne Andersen, Srinivas Rao, Terrence M Tumpey, Zhi-Yong Yang, et al. Induction of Broadly Neutralizing H1N1 Influenza Antibodies by Vaccination. *Science*, 329(5995):1060–1064, 2010.

[60] Taufik Momin, Kevinkumar Kansagra, Hardik Patel, Sunil Sharma, Bhumika Sharma, Jatin Patel, Ravindra Mittal, Jayesh Sanmukhani, Kapil Maithal, Ayan Dey, et al. Safety and Immunogenicity of a DNA SARS-CoV-2 vaccine (ZyCoV-D): Results of an Open-Label, Non-Randomized Phase I Part of Phase I/II Clinical Study by Intradermal Route in Healthy Subjects in India. *eClinicalMedicine*, 38:101020, 2021.

[61] Cadila Healthcare Ltd. A Phase III, Randomized, Multi-Centre, Double Blind, Placebo Controlled, Study to Evaluate Efficacy, Safety and Immunogenicity of Novel Corona Virus -2019-nCov Vaccine Candidate of M/s Cadila Healthcare Limited. (Clinical trial number: CTRI/2021/01/030416) . *ctri.nic.in*, 2021. URL `http://ctri.nic.in/Clinicaltrials/showallp.php?mid1=51254&EncHid=&userName=ZyCoV-D`. [Accessed 30 September, 2021].

[62] Tina Batista Napotnik, Tamara Polajžer, and Damijan Miklavčič. Cell Death due to Electroporation - A Review. *Bioelectrochemistry*, 141:107871, 2021.

[63] Ayan Dey, TM Chozhavel Rajanathan, Harish Chandra, Hari PR Pericherla, Sanjeev Kumar, Huzaifa S Choonia, Mayank Bajpai, Arun K Singh, Anuradha Sinha, Gurwinder Saini, et al. Immunogenic Potential of DNA Vaccine Candidate, ZyCoV-D against SARS-CoV-2 in Animal Models. *Vaccine*, 39(30):4108–4116, 2021.

[64] Trevor RF Smith, Ami Patel, Stephanie Ramos, Dustin Elwood, Xizhou Zhu, Jian Yan, Ebony N Gary, Susanne N Walker, Katherine Schultheis, Mansi Purwar, et al. Immunogenicity of a DNA Vaccine Candidate for COVID-19. *Nature Communications*, 11(1):1–13, 2020.

[65] Pablo Tebas, ShuPing Yang, Jean D Boyer, Emma L Reuschel, Ami Patel, Aaron Christensen-Quick, Viviane M Andrade, Matthew P Morrow, Kimberly Kraynyak, Joseph Agnes, et al. Safety and Immunogenicity of INO-4800 DNA Vaccine against SARS-CoV-2: A Preliminary Report of an Open-Label, Phase 1 Clinical Trial. *eClinicalMedicine*, 31:100689, 2021.

[66] SA Meo, IA Bukhari, J Akram, AS Meo, and DC Klonoff. COVID-19 Vaccines: Comparison of Biological, Pharmacological Characteristics and Adverse Effects of Pfizer/BioNTech and Moderna Vaccines. *Eur Rev Med Pharmacol Sci*, pages 1663–1669, 2021.

[67] Malissa C Diehl, Jessica C Lee, Stephen E Daniels, Pablo Tebas, Amir S Khan, Mary Giffear, Niranjan Y Sardesai, and Mark L Bagarazzi. Tolerability of Intramuscular and Intradermal Delivery by CELLECTRA® Adaptive Constant Current Electroporation Device in Healthy Volunteers. *Human Vaccines & Immunotherapeutics*, 9(10):2246–2252, 2013.

[68] Sara Y Tartof, Jeff M Slezak, Heidi Fischer, Vennis Hong, Bradley K Ackerson, Omesh N Ranasinghe, Timothy B Frankland, Oluwaseye A Ogun, Joann M Zamparo, Sharon Gray, et al. Effectiveness of mRNA BNT162b2 COVID-19 Vaccine up to 6 months in a Large Integrated Health System in the USA: A Retrospective Cohort Study. *The Lancet*, 398(10309):1407–1416, 2021.

[69] Kinga Karbowniczek, Paul Rothwell, Jon Extance, Sarah Milsom, Vera Lukashchuk, Kevin Bowes, Daniel Smith, and Lisa Caproni. Doggybone DNA: An Advanced Platform for AAV Production. *Cell Gene Ther. Insights*, 3:731–738, 2017.

[70] Ian P Wicks, Meredith L Howell, Tuesday Hancock, Hitoshi Kohsaka, Tsaiwei Olee, and Dennis A Carson. Bacterial lipopolysaccharide copurifies with plasmid DNA: implications for animal models and human gene therapy. *Human Gene Therapy*, 6(3):317–323, 1995.

[71] Annalisa Ciabattini, Christine Nardini, Francesco Santoro, Paolo Garagnani, Claudio

Franceschi, and Donata Medaglini. Vaccination in the Elderly: The Challenge of Immune Changes with Aging. In *Seminars in Immunology*, volume 40, pages 83–94. Elsevier, 2018.

[72] Jean-Pierre Amorij, Wouter LJ Hinrichs, Henderik W Frijlink, Jan C Wilschut, and Anke Huckriede. Needle-Free Influenza Vaccination. *The Lancet Infectious Diseases*, 10(10):699–711, 2010.

[73] Giuseppe Del Giudice, Rino Rappuoli, and Arnaud M Didierlaurent. Correlates of Adjuvanticity: A Review on Adjuvants in Licensed Vaccines. In *Seminars in Immunology*, volume 39, pages 14–21. Elsevier, 2018.

[74] Jes Dietrich, Lars Vibe Andreasen, Peter Andersen, and Else Marie Agger. Inducing Dose Sparing with Inactivated Polio Virus Formulated in Adjuvant CAF01. *PLoS One*, 9(6):e100879, 2014.

[75] Lena Alexopoulou, Agnieszka Czopik Holt, Ruslan Medzhitov, and Richard A Flavell. Recognition of Double-Stranded RNA and Activation of NF-$\kappa$B by Toll-Like Receptor 3. *Nature*, 413 (6857):732–738, 2001.

[76] Anne Krug, Anthony R French, Winfried Barchet, Jens AA Fischer, Andrzej Dzionek, Jeanette T Pingel, Michael M Orihuela, Shizuo Akira, Wayne M Yokoyama, and Marco Colonna. TLR9-Dependent Recognition of MCMV by IPC and DC Generates Coordinated Cytokine Responses that Activate Antiviral NK Cell Function. *Immunity*, 21(1):107–119, 2004.

[77] Marc Dupuis, Kimberly Denis-Mize, Carolyn Woo, Cheryl Goldbeck, Mark J Selby, Minchao Chen, Gillis R Otten, Jeffrey B Ulmer, John J Donnelly, Gary Ott, et al. Distribution of DNA Vaccines Determines their Immunogenicity after Intramuscular Injection in Mice. *The Journal of Immunology*, 165(5):2850–2858, 2000.

[78] Angelo Mena, Marion E Andrew, and Barbara EH Coupar. Rapid Dissemination of Intramuscularly Inoculated DNA Vaccines. *Immunology and Cell Biology*, 79(1):87–89, 2001.

[79] JE Ledgerwood, Z Hu, IJ Gordon, G Yamshchikov, ME Enama, S Plummer, R Bailer, MB Pearce, TM Tumpey, RA Koup, et al. Influenza Virus h5 DNA vaccination is Immunogenic by Intramuscular and Intradermal Routes in Humans. *Clinical and Vaccine Immunology*, 19(11):1792–1797, 2012.

[80] Paul Henri Lambert and Philippe E Laurent. Intradermal Vaccine Delivery: Will New Delivery Systems Transform Vaccine Administration? *Vaccine*, 26(26):3197–3208, 2008.

[81] Mariko Egawa, Tetsuji Hirao, and Motoji Takahashi. In Vivo Estimation of Stratum Corneum Thickness from Water Concentration Profiles Obtained with Raman Spectroscopy. *Acta Dermato-Venereologica*, 87(1):4–8, 2007.

[82] Kenji Kabashima, Tetsuya Honda, Florent Ginhoux, and Gyohei Egawa. The Immunological Anatomy of the Skin. *Nature Reviews Immunology*, 19(1):19–30, 2019.

[83] Takeshi Matsui and Masayuki Amagai. Dissecting the Formation, Structure and Barrier Function of the Stratum Corneum. *International Immunology*, 27(6):269–280, 2015.

[84] Jan D Bos and Marcus MHM Meinardi. The 500 Dalton Rule for the Skin Penetration of Chemical Compounds and Drugs. *Experimental Dermatology: Viewpoint*, 9(3):165–169, 2000.

[85] Mark R Prausnitz, Samir Mitragotri, and Robert Langer. Current Status and Future Potential of Transdermal Drug Delivery. *Nature Reviews Drug Discovery*, 3(2):115–124, 2004.

[86] H Trommer and RHH Neubert. Overcoming the Stratum Corneum: The Modulation of Skin Penetration. *Skin Pharmacology and Physiology*, 19(2):106–121, 2006.

[87] William J Mulholland, Edward AH Arbuthnott, Brian J Bellhouse, J Frederick Cornhill, Jonathan M Austyn, Mark AF Kendall, Zhanfeng Cui, and Uday K Tirlapur. Multiphoton High-Resolution 3D Imaging of Langerhans cells and Keratinocytes in the Mouse Skin Model Adopted for Epidermal Powdered Immunization. *Journal of Investigative Dermatology*, 126(7): 1541–1548, 2006.

[88] Tomohiro Kubo, Yuki Uchida, Yuko Watanabe, Masahiro Abe, Akira Nakamura, Masao Ono, Shizuo Akira, and Toshiyuki Takai. Augmented TLR9-Induced Btk Activation in PIR-B–Deficient B-1 Cells Provokes Excessive Autoantibody Production and Autoimmunity. *Journal of Experimental Medicine*, 206(9):1971–1982, 2009.

[89] Takeshi Ouchi, Akiharu Kubo, Mariko Yokouchi, Takeya Adachi, Tetsuro Kobayashi, Daniela Y Kitashima, Hideki Fujii, Björn E Clausen, Shigeo Koyasu, Masayuki Amagai, et al. Langerhans Cell Antigen Capture through Tight Junctions Confers Preemptive Immunity in Experimental Staphylococcal Scalded Skin Syndrome. *Journal of Experimental Medicine*, 208(13):2607–2613, 2011.

[90] Szun S Tay, Ben Roediger, Philip L Tong, Shweta Tikoo, and Wolfgang Weninger. The Skin-Resident Immune Network. *Current Dermatology Reports*, 3(1):13–22, 2014.

[91] Xiao-Nong Wang, Naomi McGovern, Merry Gunawan, Connor Richardson, Martin Windebank, Tee-Wei Siah, Hwee-Ying Lim, Katja Fink, Jackson L Yao Li, Lai G Ng, et al. A Three-Dimensional Atlas of Human Dermal Leukocytes, Lymphatics, and Blood Vessels. *Journal of Investigative Dermatology*, 134(4):965–974, 2014.

[92] Agata Matejuk. Skin Immunity. *Archivum Immunologiae et Therapiae Experimentalis*, 66(1): 45–54, 2018.

[93] Richard Wong, Stefan Geyer, Wolfgang Weninger, Jean-Claude Guimberteau, and Jason K Wong. The Dynamic Anatomy and Patterning of Skin. *Experimental Dermatology*, 25(2):92–98, 2016.

[94] Nicola Luigi Bragazzi, Andrea Orsi, Filippo Ansaldi, Roberto Gasparini, and Giancarlo Icardi. Fluzone® Intra-Dermal (Intanza®/Istivac® Intra-Dermal): An Updated Overview. *Human Vaccines & Immunotherapeutics*, 12(10):2616–2627, 2016.

[95] Youkyung H Choi, Monica B Perez-Cuevas, Maja Kodani, Xiugen Zhang, Mark R Prausnitz, Saleem Kamili, and Siobhan M O'Connor. Feasibility of Hepatitis B Vaccination by Microneedle Patch: Cellular and Humoral Immunity Studies in Rhesus Macaques. *The Journal of Infectious Diseases*, 220(12):1926–1934, 2019.

[96] Eun Kim, Geza Erdos, Shaohua Huang, Thomas W Kenniston, Stephen C Balmert, Cara Donahue Carey, V Stalin Raj, Michael W Epperly, William B Klimstra, Bart L Haagmans, et al. Microneedle Array Delivered Recombinant Coronavirus Vaccines: Immunogenicity and Rapid Translational Development. *eBioMedicine*, 55:102743, 2020.

[97] Maya Williams, Dan Ewing, Maria Blevins, Peifang Sun, Appavu K Sundaram, Kanakatte S Raviprakash, Kevin R Porter, and John W Sanders. Enhanced Immunogenicity and Protective Efficacy of a Tetravalent Dengue DNA Vaccine using Electroporation and Intradermal Delivery. *Vaccine*, 37(32):4444–4453, 2019.

[98] Anna-Karin Roos, Sonia Moreno, Christoph Leder, Maxim Pavlenko, Alan King, and Pavel Pisa. Enhancement of Cellular Immune Response to a Prostate Cancer DNA Vaccine by Intradermal Electroporation. *Molecular Therapy*, 13(2):320–327, 2006.

[99] Robert Arnou, Patrick Eavis, Jose-Ramon De Juanes Pardo, Arvydas Ambrozaitis, Marie-Pierre Kazek, and Françoise Weber. Immunogenicity, Large Scale Safety and Lot Consistency of an Intradermal Influenza Vaccine in Adults aged 18–60 years: Randomized, Controlled, Phase III trial. *Human Vaccines*, 6(4):346–354, 2010.

[100] Richard T Kenney, Sarah A Frech, Larry R Muenz, Christina P Villar, and Gregory M Glenn. Dose Sparing with Intradermal Injection of Influenza Vaccine. *New England Journal of Medicine*, 351(22):2295–2301, 2004.

[101] Kobporn Boonnak, Jittima Dhitavat, Narumon Thantamnu, Nathamon Kosoltanapiwat, Montida Auayporn, Li Jiang, Pilaipan Puthavathana, and Punnee Pitisuttithum. Immune Responses to Intradermal and Intramuscular Inactivated Influenza Vaccine among Older Age Group. *Vaccine*, 35(52):7339–7346, 2017.

[102] Thomas Grunwald and Sebastian Ulbert. Improvement of DNA Vaccination by Adjuvants and Sophisticated Delivery Devices: Vaccine-Platforms for the Battle against Infectious Diseases. *Clinical and Experimental Vaccine Research*, 4(1):1–10, 2015.

[103] Julian Hickling and Rebecca Jones. Intradermal Delivery of Vaccines: A Review of the Literature and the Potential for Development for Use in Low- and Middle-Income Countries. *World Health Organization and Path*, 2009.

[104] JK Hickling, KR Jones, M Friede, D Zehrung, D Chen, and D Kristensen. Intradermal Delivery of Vaccines: Potential Benefits and Current Challenges. *Bulletin of the World Health Organization*, 89:221–226, 2011.

[105] Linda C Lambert and Anthony S Fauci. Influenza Vaccines for the Future. *New England Journal of Medicine*, 363(21):2036–2044, 2010.

[106] Allison Kennedy, Michelle Basket, and Kristine Sheedy. Vaccine Attitudes, Concerns, and Information Sources Reported by Parents of Young Children: Results from the 2009 HealthStyles Survey. *Pediatrics*, 127(Supplement 1):S92–S99, 2011.

[107] Mark A Jacobson, Elizabeth Sinclair, Barry Bredt, Laurie Agrillo, Douglas Black, C Lorrie Epling, Alexander Carvidi, Terence Ho, Raji Bains, Valerie Girling, et al. Safety and Immunogenicity of Towne Cytomegalovirus Vaccine with or without Adjuvant Recombinant Interleukin-12. *Vaccine*, 24(25):5311–5319, 2006.

[108] Jennifer McLenon and Mary AM Rogers. The Fear of Needles: A Systematic Review and Meta-Analysis. *Journal of Advanced Nursing*, 75(1):30–42, 2019.

[109] Timothy Callaghan, Matthew Motta, Steven Sylvester, Kristin Lunz Trujillo, and Christine Crudo Blackburn. Parent Psychology and the Decision to Delay Childhood Vaccination. *Social Science & Medicine*, 238:112407, 2019.

[110] G Frijstein, J Hortensius, and HL Zaaijer. Needlestick Injuries and Infectious Patients in a Major Academic Medical Centre from 2003 to 2010. *Neth J Med*, 69(10):465–468, 2011.

[111] A Wittmann, F Hofmann, and N Kralj. Needle Stick Injuries—Risk from Blood Contact in Dialysis. *Journal of Renal Care*, 33(2):70–73, 2007.

[112] Annette Prüss-Üstün, Elisabetta Rapiti, and Yvan Hutin. Estimation of the Global Burden of Disease Attributable to Contaminated Sharps Injuries among Health-Care Workers. *American Journal of Industrial Medicine*, 48(6):482–490, 2005.

[113] Alice Mannocci, Gabriella De Carli, Virginia Di Bari, Rosella Saulle, Brigid Unim, Nicola Nicolotti, Lorenzo Carbonari, Vincenzo Puro, and Giuseppe La Torre. How Much do Needlestick Injuries Cost? A Systematic Review of the Economic Evaluations of Needlestick and Sharps Injuries among Healthcare Personnel. *Infection Control & Hospital Epidemiology*, 37(6):635–646, 2016.

[114] Parvin Lakbala, Farbood Ebadi Azar, and Hajeb Kamali. Needlestick and Sharps Injuries among Housekeeping Workers in Hospitals of Shiraz, Iran. *BMC research notes*, 5(1):1–5, 2012.

[115] Robert J Drape, Michael D Macklin, Lori J Barr, Suzanne Jones, Joel R Haynes, and Hansi J Dean. Epidermal DNA Vaccine for Influenza is Immunogenic in Humans. *Vaccine*, 24(21): 4475–4481, 2006.

[116] Scott T Rottinghaus, Gregory A Poland, Robert M Jacobson, Lori J Barr, and Mike J Roy. Hepatitis B DNA Vaccine Induces Protective Antibody Responses in Human Non-Responders to Conventional Vaccination. *Vaccine*, 21(31):4604–4608, 2003.

[117] Sean P McBurney, Justine E Sunshine, Sarah Gabriel, Jeremy P Huynh, William F Sutton, Deborah H Fuller, Nancy L Haigwood, and William B Messer. Evaluation of Protection Induced by a Dengue Virus Serotype 2 Envelope Domain III Protein Scaffold/DNA Vaccine in Non-Human Primates. *Vaccine*, 34(30):3500–3507, 2016.

[118] Germain JP Fernando, Julian Hickling, Cesar M Jayashi Flores, Paul Griffin, Christopher D Anderson, S Rachel Skinner, Cristyn Davies, Katey Witham, Melinda Pryor, Jesse Bodle, et al. Safety, Tolerability, Acceptability and Immunogenicity of an Influenza Vaccine Delivered to Human Skin by a Novel High-Density Microprojection Array Patch (Nanopatch™). *Vaccine*, 36 (26):3779–3788, 2018.

[119] Archana V Boopathy, Anasuya Mandal, Daniel W Kulp, Sergey Menis, Nitasha R Bennett, Hannah C Watkins, Wade Wang, Jacob T Martin, Nikki T Thai, Yanpu He, et al. Enhancing Humoral Immunity via Sustained-Release Implantable Microneedle Patch Vaccination. *Proceedings of the National Academy of Sciences*, 116(33):16473–16478, 2019.

[120] Michael N Pastore, Yogeshvar N Kalia, Michael Horstmann, and Michael S Roberts. Transdermal Patches: History, Development and Pharmacology. *British Journal of Pharmacology*, 172 (9):2179–2209, 2015.

[121] Elof Eriksson, Feng Yao, Tor Svensjö, Thomas Winkler, Jaromir Slama, Michael D Macklin, Christoph Andree, Martha McGregor, Virginia Hinshaw, and William F Swain. In Vivo Gene Transfer to Skin and Wound by Microseeding. *Journal of Surgical Research*, 78(2):85–91, 1998.

[122] V Moulin, ME Morgan, D Eleveld-Trancikova, JBAG Haanen, E Wielders, MWG Looman, RAJ Janssen, CG Figdor, BJH Jansen, and GJ Adema. Targeting Dendritic Cells with Antigen via Dendritic Cell-Associated Promoters. *Cancer Gene Therapy*, 19(5):303–311, 2012.

[123] Yeu-Chun Kim and Mark R Prausnitz. Enabling Skin Vaccination Using New Delivery Technologies. *Current Topics in Microbiology and Immunology*, 351:77, 2012.

[124] Mark R Prausnitz and Robert Langer. Transdermal Drug Delivery. *Nature Biotechnology*, 26 (11):1261–1268, 2008.

[125] Joost Huibert Van den Berg. *Formulation and Delivery of Dermal DNA Vaccines*. Utrecht University, 2009.

[126] Johanna Hettinga and Robert Carlisle. Vaccination into the Dermal Compartment: Techniques, Challenges, and Prospects. *Vaccines*, 8(3):534, 2020.

[127] Claus-Dieter Ohl, Manish Arora, Roy Ikink, Nico De Jong, Michel Versluis, Michael Delius, and Detlef Lohse. Sonoporation from Jetting Cavitation Bubbles. *Biophysical Journal*, 91(11): 4285–4295, 2006.

[128] Minoru Tomizawa, Fuminobu Shinozaki, Yasufumi Motoyoshi, Takao Sugiyama, Shigenori Yamamoto, and Makoto Sueishi. Sonoporation: Gene Transfer Using Ultrasound. *World Journal of Methodology*, 3(4):39, 2013.

[129] James J Kwan, Rachel Myers, Christian M Coviello, Susan M Graham, Apurva R Shah, Eleanor Stride, Robert C Carlisle, and Constantin C Coussios. Ultrasound-Propelled Nanocups for Drug Delivery. *Small*, 11(39):5305–5314, 2015.

[130] Ryo Suzuki, Yusuke Oda, Naoki Utoguchi, and Kazuo Maruyama. Progress in the development of ultrasound-mediated gene delivery systems utilizing nano- and microbubbles. *Journal of Controlled Release*, 149(1):36–41, 2011.

[131] Kevin Ita. Recent Progress in Transdermal Sonophoresis. *Pharmaceutical Development and Technology*, 22(4):458–466, 2017.

[132] Sandra Nwokeoha, Robert Carlisle, and Robin O Cleveland. The Application of Clinical Lithotripter Shock Waves to RNA Nucleotide Delivery to Cells. *Ultrasound in Medicine & Biology*, 42(10):2478–2492, 2016.

[133] Nathaniel P Katz, David E Shapiro, Timothy E Herrmann, Joseph Kost, and Linda M Custer. Rapid Onset of Cutaneous Anesthesia with EMLA Cream after Pretreatment with a New Ultrasound-Emitting Device. *Anesthesia & Analgesia*, 98(2):371–376, 2004.

[134] Samir Mitragotri and Joseph Kost. Low-Frequency Sonophoresis: A Noninvasive Method of Drug Delivery and Diagnostics. *Biotechnology Progress*, 16(3):488–492, 2000.

[135] Rinat Lifshiz Zimon, Galya Lerman, Einat Elharrar, Tal Meningher, Aviv Barzilai, Moamen Masalha, Ramesh Chintakunta, Etili Hollander, Riki Goldbart, Tamar Traitel, et al. Ultrasound Targeting of Q-Starch/miR-197 Complexes for Topical Treatment of Psoriasis. *Journal of Controlled Release*, 284:103–111, 2018.

[136] Eloise Thomas, Jyothi U Menon, Joshua Owen, Irini Skaripa-Koukelli, Sheena Wallington, Michael Gray, Christophoros Mannaris, Veerle Kersemans, Danny Allen, Paul Kinchesh, et al. Ultrasound-Mediated Cavitation Enhances the Delivery of an EGFR-Targeting Liposomal Formulation Designed for Chemo-Radionuclide therapy. *Theranostics*, 9(19):5595, 2019.

[137] Sayan Mullick Chowdhury, Tzu-Yin Wang, Sunitha Bachawal, Rammohan Devulapally, Jung Woo Choe, Lotfi Abou Elkacem, Butrus Khuri Yakub, David S Wang, Lu Tian, Ramasamy Paulmurugan, et al. Ultrasound-Guided Therapeutic Modulation of Hepatocellular Carcinoma using Complementary MicroRNAs. *Journal of Controlled Release*, 238:272–280, 2016.

[138] Libin Chen, Tao Zhang, Shan Sun, Wenzhi Ren, Aiguo Wu, and Huixiong Xu. Ultrasound-

Mediated Cavitation Enhances EGFR-Targeting PLGA-PEG Nano-Micelle Delivery for Triple-Negative Breast Cancer Treatment. *Cancers*, 13(14):3383, 2021.

[139] J Kost, K Leong, and R Langer. Ultrasound-Enhanced Polymer Degradation and Release of Incorporated Substances. *Proceedings of the National Academy of Sciences*, 86(20):7663–7666, 1989.

[140] Rachel Myers, Megan Grundy, Cliff Rowe, Christian M Coviello, Luca Bau, Philippe Erbs, Johann Foloppe, Jean-Marc Balloul, Colin Story, Constantin C Coussios, et al. Ultrasound-Mediated Cavitation does not Decrease the Activity of Small Molecule, Antibody or Viral-Based Medicines. *International Journal of Nanomedicine*, 13:337, 2018.

[141] Donghee Park, Jongho Won, Gyounjung Lee, Yongheum Lee, Chul-Woo Kim, and Jongbum Seo. Sonophoresis with Ultrasound-Responsive Liquid-Core Nuclei for Transdermal Drug Delivery. *Skin Research and Technology*, 2022.

[142] Yaxin Hu, Yang Mo, Jianpeng Wei, Mei Yang, Xinyu Zhang, and Xin Chen. Programmable and Monitorable Intradermal Vaccine Delivery using Ultrasound Perforation Array. *International Journal of Pharmaceutics*, page 121595, 2022.

[143] Anne Charlotte van Blokland. *Instigating and Monitoring Transdermal Drug Delivery using Ultrasound-Mediated Cavitation*. PhD thesis, University of Oxford, 2018.

[144] Sunali Bhatnagar, James J Kwan, Apurva R Shah, Constantin-C Coussios, and Robert C Carlisle. Exploitation of Sub-Micron Cavitation Nuclei to Enhance Ultrasound-Mediated Transdermal Transport and Penetration of Vaccines. *Journal of Controlled Release*, 238:22–30, 2016.

[145] Ahmet Tezel, Sumit Paliwal, Zancong Shen, and Samir Mitragotri. Low-Frequency Ultrasound as a Transcutaneous Immunization Adjuvant. *Vaccine*, 23(29):3800–3807, 2005.

[146] Brenden Cheong-Qi Seah and Boon Mian Teo. Recent Advances in Ultrasound-Based Transdermal Drug Delivery. *International Journal of Nanomedicine*, 13:7749, 2018.

[147] Yeong Chae Ryu, Dong In Kim, Seung Hoon Kim, Hui-Min David Wang, and Byeong Hee Hwang. Synergistic Transdermal Delivery of Biomacromolecules using Sonophoresis after Microneedle Treatment. *Biotechnology and Bioprocess Engineering*, 23(3):286–292, 2018.

[148] Sunali Bhatnagar. *Cavitation-Enhanced Transdermal Vaccine Delivery by Ultrasound*. PhD thesis, University of Oxford, 2014.

[149] Rajvinder Karda, John R Counsell, Kinga Karbowniczek, Lisa J Caproni, John P Tite, and Simon N Waddington. Production of Lentiviral Vectors using Novel, Enzymatically Produced, Linear DNA. *Gene Therapy*, 26(3):86–92, 2019.

[150] Lina Li, Emilios K Dimitriadis, Yu Yang, Juan Li, Zhenhua Yuan, Chunping Qiao, Cyriaque Beley, Richard H Smith, Luis Garcia, and Robert M Kotin. Production and Characterization of Novel Recombinant Adeno-Associated Virus Replicative-Form Genomes: A Eukaryotic Source of DNA for Gene Transfer. *PLoS One*, 8(8):e69879, 2013.

[151] Tom Adie, Ifey Orefo, Daniel Kysh, Katalin Kondas, Shyam Thapa, Jon Extance, Tommy Duncan, and Paul J Rothwell. dbDNA™: An Advanced Platform for Genetic Medicines. *Drug Discovery Today*, 2021.

[152] C Liu, Y Xie, B Sun, F Geng, F Zhang, Q Guo, H Wu, B Yu, J Wu, X Yu, et al. MUC1- and Survivin-based DNA Vaccine Combining Immunoadjuvants CpG and Interleukin-2 in a Bicistronic Expression Plasmid Generates Specific Immune Responses and Antitumour Effects in a Murine Colorectal Carcinoma Model. *Scandinavian journal of immunology*, 87(2):63–72, 2018.

[153] Anna D Kosinska, Ejuan Zhang, Lena Johrden, Jia Liu, Pia L Seiz, Xiaoyong Zhang, Zhiyong Ma, Thekla Kemper, Melanie Fiedler, Dieter Glebe, et al. Combination of DNA Prime-Adenovirus Boost Immunization with Entecavir Elicits Sustained Control of Chronic Hepatitis B in the Woodchuck model. *PLoS Pathogens*, 9(6):e1003391, 2013.

[154] Ebony N Gary and David B Weiner. DNA Vaccines: Prime Time is Now. *Current Opinion in Immunology*, 65:21–27, 2020.

[155] Alan R Brooks, Richard N Harkins, Peiyin Wang, Hu Sheng Qian, Pengxuan Liu, and Gabor M Rubanyi. Transcriptional Silencing is Associated with Extensive Methylation of the CMV Promoter following Adenoviral Gene Delivery to Muscle. *The Journal of Gene Medicine: A Cross-Disciplinary Journal for Research on the Science of Gene Transfer and its Clinical Applications*, 6(4):395–404, 2004.

[156] Gaëlle Vandermeulen, Hervé Richiardi, Virginie Escriou, Jing Ni, Philippe Fournier, Volker Schirrmacher, Daniel Scherman, and Véronique Préat. Skin-Specific Promoters for Genetic Immunisation by DNA Electroporation. *Vaccine*, 27(32):4272–4277, 2009.

[157] ThermoFisher Scientific. pVAX1 Vector, Catalog number: V26020, 2022. URL `https://www.thermofisher.com/order/catalog/product/V26020`. [Accessed 8 March, 2022].

[158] Xiaoyin Wang, Zhongjie Xu, Zhengwei Tian, Xi Zhang, Danhua Xu, Qin Li, Junhe Zhang, and Tianyun Wang. The EF-1$\alpha$ Promoter Maintains High-Level Transgene Expression from Episomal Vectors in Transfected CHO-K1 Cells. *Journal of Cellular and Molecular Medicine*, 21(11): 3044–3054, 2017.

[159] Karin Norrman, Yvonne Fischer, Blandine Bonnamy, Fredrik Wolfhagen Sand, Philippe Ravassard, and Henrik Semb. Quantitative Comparison of Constitutive Promoters in Human ES Cells. *PloS one*, 5(8):e12413, 2010.

[160] Simone Krinner, Asli Heitzer, Benedikt Asbach, and Ralf Wagner. Interplay of Promoter Usage and Intragenic CpG Content: Impact on GFP Reporter Gene Expression. *Human Gene Therapy*, 26(12):826–840, 2015.

[161] Yanyun Jiang, Lam C Tsoi, Allison C Billi, Nicole L Ward, Paul W Harms, Chang Zeng, Emanual Maverakis, J Michelle Kahlenberg, and Johann E Gudjonsson. Cytokinocytes: The Diverse Contribution of Keratinocytes to Immune Responses in Skin. *JCI insight*, 5(20), 2020.

[162] Michaël Chopin and Stephen L Nutt. Establishing and Maintaining the Langerhans Cell Network. *Seminars in Cell & Developmental Biology*, 41:23–29, 2015.

[163] Charles A Dinarello. Immunological and Inflammatory Functions of the Interleukin-1 Family. *Annual Review of Immunology*, 27:519–550, 2009.

[164] Hiroyuki Kayamuro, Yasuo Yoshioka, Yasuhiro Abe, Shuhei Arita, Kazufumi Katayama, Tetsuya Nomura, Tomoaki Yoshikawa, Ritsuko Kubota-Koketsu, Kazuyoshi Ikuta, Shigefumi Okamoto, et al. Interleukin-1 Family Cytokines as Mucosal Vaccine Adjuvants for Induction of Protective Immunity against Influenza Virus. *Journal of Virology*, 84(24):12703–12712, 2010.

[165] Cecilia Garlanda, Charles A Dinarello, and Alberto Mantovani. The Interleukin-1 Family: Back to the Future. *Immunity*, 39(6):1003–1018, 2013.

[166] Craig S McCune and Diana M Marquis. Interleukin 1 as an Adjuvant for Active Specific Immunotherapy in a Murine Tumor model. *Cancer Research*, 50(4):1212–1215, 1990.

[167] Charles A Dinarello. Interleukin-1 in the Pathogenesis and Treatment of Inflammatory Diseases. *Blood, The Journal of the American Society of Hematology*, 117(14):3720–3732, 2011.

[168] Marjana Tomic-Canic, Mayumi Komine, Irwin M Freedberg, and Miroslav Blumenberg. Epidermal Signal Transduction and Transcription Factor Activation in Activated Keratinocytes. *Journal of Dermatological Science*, 17(3):167–181, 1998.

[169] Marcel Wüthrich, Vanessa LeBert, Kevin Galles, Jane Hu-Li, Shlomo Z Ben-Sasson, William E Paul, and Bruce S Klein. Interleukin 1 Enhances Vaccine-Induced Antifungal T-helper 17 Cells and Resistance against Blastomyces Dermatitidis Infection. *The Journal of Infectious Diseases*, 208(7):1175–1182, 2013.

[170] Fiona A Sharp, Darren Ruane, Benjamin Claass, Emma Creagh, James Harris, Padma Malyala, Manomohan Singh, Derek T O'Hagan, Virginie Pétrilli, Jurg Tschopp, et al. Uptake of Particulate Vaccine Adjuvants by Dendritic Cells Activates the NALP3 Inflammasome. *Proceedings of the National Academy of Sciences*, 106(3):870–875, 2009.

[171] Philippa Marrack, Amy S McKee, and Michael W Munks. Towards an Understanding of the Adjuvant Action of Aluminium. *Nature Reviews Immunology*, 9(4):287–293, 2009.

[172] Giorgio Trinchieri. Interleukin-12 and the Regulation of Innate Resistance and Adaptive Immunity. *Nature Reviews Immunology*, 3(2):133–146, 2003.

[173] Dennis W Metzger, Renee M McNutt, John T Collins, J Matthew Buchanan, Victor H Van Cleave, and Wesley A Dunnick. Interleukin-12 Acts as an Adjuvant for Humoral Immunity through Interferon-$\gamma$-Dependent and Independent Mechanisms. *European Journal of Immunology*, 27(8):1958–1965, 1997.

[174] U Greinert, M Ernst, M Schlaak, and P Entzian. Interleukin-12 as Successful Adjuvant in Tuberculosis Treatment. *European Respiratory Journal*, 17(5):1049–1051, 2001.

[175] Howard L Kaufman, Ken Flanagan, Christopher SD Lee, Donato J Perretta, and Heidi Horig. Insertion of Interleukin-2 (IL-2) and Interleukin-12 (IL-12) Genes into Vaccinia Virus Results in Effective Anti-Tumor Responses Without Toxicity. *Vaccine*, 20(13-14):1862–1869, 2002.

[176] Dennis M Klinman, Ae-Kyung Yi, Serge L Beaucage, Jacqueline Conover, and Arthur M Krieg. CpG Motifs Present in Bacteria DNA Rapidly Induce Lymphocytes to Secrete Interleukin 6, Interleukin 12, and Interferon Gamma. *Proceedings of the National Academy of Sciences*, 93 (7):2879–2883, 1996.

[177] Bernard P Arulanandam, Margot O'Toole, and Dennis W Metzger. Intranasal Interleukin-12 is a Powerful Adjuvant for Protective Mucosal Immunity. *The Journal of Infectious Diseases*, 180 (4):940–949, 1999.

[178] Hiroaki Hemmi, Osamu Takeuchi, Taro Kawai, Tsuneyasu Kaisho, Shintaro Sato, Hideki Sanjo,

Makoto Matsumoto, Katsuaki Hoshino, Hermann Wagner, Kiyoshi Takeda, et al. A Toll-Like Receptor Recognizes Bacterial DNA. *Nature*, 408(6813):740–745, 2000.

[179] Sven Klaschik, Debra Tross, and Dennis M Klinman. Inductive and Suppressive Networks Regulate TLR9-Dependent Gene Expression In Vivo. *Journal of Leukocyte Biology*, 85(5): 788–795, 2009.

[180] Sven Klaschik, Debra Tross, Hidekazu Shirota, and Dennis M Klinman. Short- and Long-Term Changes in Gene Expression Mediated by the Activation of TLR9. *Molecular Immunology*, 47 (6):1317–1324, 2010.

[181] Christian Bode, Gan Zhao, Folkert Steinhagen, Takeshi Kinjo, and Dennis M Klinman. CpG DNA as a Vaccine Adjuvant. *Expert Review of Vaccines*, 10(4):499–511, 2011.

[182] CL Cooper, HL Davis, ML Morris, SM Efler, AM Krieg, Y Li, C Laframboise, MJ Al Adhami, Y Khaliq, I Seguin, et al. Safety and Immunogenicity of CPG 7909 Injection as an Adjuvant to Fluarix Influenza Vaccine. *Vaccine*, 22(23-24):3136–3143, 2004.

[183] CL Cooper, HL Davis, ML Morris, SM Efler, M Adhami, AM Krieg, DW Cameron, and J Heathcote. CpG 7909, an Immunostimulatory TLR9 Agonist Oligodeoxynucleotide, as Adjuvant to Engerix-B® HBV Vaccine in Healthy Adults: A Double-Blind Phase I/II Study. *Journal of Clinical Immunology*, 24(6):693–701, 2004.

[184] Szu-Min Hsieh, Ming-Che Liu, Yen-Hsu Chen, Wen-Sen Lee, Shinn-Jang Hwang, Shu-Hsing Cheng, Wen-Chien Ko, Kao-Pin Hwang, Ning-Chi Wang, Yu-Lin Lee, et al. Safety and Immunogenicity of CpG 1018 and Aluminium Hydroxide-Adjuvanted SARS-CoV-2 S-2P Protein Vaccine MVC-COV1901: Interim Results of a Large-Scale, Double-Blind, Randomised, Placebo-Controlled Phase 2 Trial in Taiwan. *The Lancet Respiratory Medicine*, 9(12):1396–1406, 2021.

[185] Yueh-Ming Loo and Michael Gale Jr. Immune Signaling by RIG-I-like Receptors. *Immunity*, 34 (5):680–692, 2011.

[186] Hiroki Kato, Osamu Takeuchi, Shintaro Sato, Mitsutoshi Yoneyama, Masahiro Yamamoto, Kosuke Matsui, Satoshi Uematsu, Andreas Jung, Taro Kawai, Ken J Ishii, et al. Differential Roles of MDA5 and RIG-I Helicases in the Recognition of RNA Viruses. *Nature*, 441(7089):101–105, 2006.

[187] Alex JV Thompson and Stephen A Locarnini. Toll-Like Receptors, RIG-I-Like RNA Helicases

and the Antiviral Innate Immune Response. *Immunology and Cell Biology*, 85(6):435–445, 2007.

[188] MR Middleton, M Wermke, E Calvo, E Chartash, H Zhou, X Zhao, M Niewel, K Dobrenkov, and V Moreno. Phase I/II, Multicenter, Open-Label Study of Intratumoral/Intralesional Administration of the Retinoic Acid-Inducible Gene I (RIG-I) Activator MK-4621 in Patients with Advanced or Recurrent Tumors. *Annals of Oncology*, 29:viii712, 2018.

[189] Victor Moreno, Caroline Gaudy-Marqueste, Martin Wermke, Antoine Italiano, Emanuela Romano, Aurelien Marabelle, Emilee Connors, Heng Zhou, Konstantin Dobrenkov, Elliot Chartash, et al. 794 Safety and Efficacy Results from a Phase 1/1b Study of Intratumoral MK-4621, a Retinoic Acid-Inducible Gene I (RIG-I) Agonist, plus Intravenous Pembrolizumab in Patients with Advanced Solid Tumors, 2020.

[190] Cardillo G. Five Parameters Logistic Regression - There and Back Again. *Mathworks*, 2012. URL `http://www.mathworks.com/matlabcentral/fileexchange/38043`.

[191] K Oosterhuis, JH Van Den Berg, TN Schumacher, and JBAG Haanen. DNA Vaccines and Intradermal Vaccination by DNA Tattooing. *Intradermal Immunization*, pages 221–250, 2010.

[192] Sidgi Syed Anwer Abdo Hasson, Juma Khalifa Zayid Al-Busaidi, and Talal Abdulmalek Sallam. The Past, Current and Future Trends in DNA Vaccine Immunisations. *Asian Pacific Journal of Tropical Biomedicine*, 5(5):344–353, 2015.

[193] Fred D Finkelman, Joanne Holmes, Ildy M Katona, Joseph F Urban Jr, M Patricia Beckmann, Linda S Park, Kenneth A Schooley, Robert L Coffman, Timothy R Mosmann, and William E Paul. Lymphokine Control of In Vivo Immunoglobulin Isotype Selection. *Annual Review of Immunology*, 8(1):303–333, 1990.

[194] Thomas J Kipps, Peter Parham, Jenni Punt, and Leonard A Herzenberg. Importance of Immunoglobulin Isotype in Human Antibody-Dependent, Cell-Mediated Cytotoxicity Directed by Murine Monoclonal Antibodies. *The Journal of Experimental Medicine*, 161(1):1–17, 1985.

[195] GG Klaus, MB Pepys, K Kitajima, and BA Askonas. Activation of Mouse Complement by Different Classes of Mouse Antibody. *Immunology*, 38(4):687, 1979.

[196] Elsa E Kis, Gerhard Winter, and Julia Myschik. Devices for Intradermal Vaccination. *Vaccine*, 30(3):523–538, 2012.

[197] Marcelle Moura Silveira, Gustavo Marçal Schmidt Garcia Moreira, and Marcelo Mendonça. DNA Vaccines against COVID-19: Perspectives and Challenges. *Life Sciences*, 267:118919, 2021.

[198] Yuanyuan Qiu, Yi Luo, Yanli Zhang, Weicheng Cui, Dong Zhang, Junru Wu, Junfeng Zhang, and Juan Tu. The Correlation between Acoustic Cavitation and Sonoporation involved in Ultrasound-Mediated DNA Transfection with Polyethylenimine (PEI) In Vitro. *Journal of Controlled Release*, 145(1):40–48, 2010.

[199] James C Birchall, Rachel Clemo, Alexander Anstey, and Dai N John. Microneedles in Clinical Practice- an Exploratory Study into the Opinions of Healthcare Professionals and the Public. *Pharmaceutical Research*, 28(1):95–106, 2011.

[200] Yutong Lin, Lizhou Lin, Mouwen Cheng, Lifang Jin, Lianfang Du, Tao Han, Lin Xu, CH Alfred, and Peng Qin. Effect of Acoustic Parameters on the Cavitation Behavior of SonoVue Microbubbles Induced by Pulsed Ultrasound. *Ultrasonics Sonochemistry*, 35:176–184, 2017.

[201] Helga Feiszthuber, Sunali Bhatnagar, Miklós Gyöngy, and Constantin-C Coussios. Cavitation-Enhanced Delivery of Insulin in Agar and Porcine Models of Human Skin. *Physics in Medicine & Biology*, 60(6):2421, 2015.

[202] Costas D Arvanitis, Miriam Bazan-Peregrino, Bassel Rifai, Leonard W Seymour, and Constantin C Coussios. Cavitation-Enhanced Extravasation for Drug Delivery. *Ultrasound in Medicine & Biology*, 37(11):1838–1852, 2011.

[203] Enikő R Tőke, Orsolya Lőrincz, Zsolt Csiszovszki, Eszter Somogyi, Gabriella Felföldi, Levente Molnár, Róbert Szipőcs, Attila Kolonics, Bernard Malissen, Franco Lori, et al. Exploitation of Langerhans Cells for In Vivo DNA Vaccine Delivery into the Lymph Nodes. *Gene Therapy*, 21 (6):566–574, 2014.

[204] SHT Jorritsma, EJ Gowans, B Grubor-Bauk, and DK Wijesundara. Delivery Methods to Increase Cellular Uptake and Immunogenicity of DNA Vaccines. *Vaccine*, 34(46):5488–5494, 2016.

[205] John J Donnelly, Jeffrey B Ulmer, and Margaret A Liu. Immunization with DNA. *Journal of Immunological Methods*, 176(2):145–152, 1994.

[206] Simon R Best, Shiwen Peng, Chi-Mou Juang, Chien-Fu Hung, Drew Hannaman, John R Saunders, T-C Wu, and Sara I Pai. Administration of HPV DNA Vaccine via Electroporation Elicits

the Strongest CD8+ T Cell Immune Responses compared to Intramuscular Injection and Intradermal Gene Gun Delivery. *Vaccine*, 27(40):5450–5459, 2009.

[207] Jason B Alarcon, Andrea Waterston Hartley, Noel G Harvey, and John A Mikszta. Preclinical Evaluation of Microneedle Technology for Intradermal Delivery of Influenza Vaccines. *Clinical and Vaccine Immunology*, 14(4):375–381, 2007.

[208] Michael J McCluskie, Cynthia L Brazolot Millan, Robert A Gramzinski, Harriet L Robinson, Joseph C Santoro, James T Fuller, Georg Widera, Joel R Haynes, Robert H Purcell, and Heather L Davis. Route and Method of Delivery of DNA Vaccine Influence Immune Responses in Mice and Non-Human Primates. *Molecular Medicine*, 5(5):287–300, 1999.

[209] Marcin Kwissa, Jan von Kampen, Rinaldo Zurbriggen, Reinhard Glück, Jörg Reimann, and Reinhold Schirmbeck. Efficient Vaccination by Intradermal or Intramuscular Inoculation of Plasmid DNA Expressing Hepatitis B Surface Antigen Under Desmin Promoter/Enhancer Control. *Vaccine*, 18(22):2337–2344, 2000.

[210] Lin Yuan, Lihua Wu, Jian Chen, Qiang Wu, and Songhua Hu. Paclitaxel Acts as an Adjuvant to Promote both Th1 and Th2 Immune Responses Induced by Ovalbumin in Mice. *Vaccine*, 28 (27):4402–4410, 2010.

[211] Rob Noad and Polly Roy. Virus-Like Particles as Immunogens. *Trends in Microbiology*, 11(9): 438–444, 2003.

[212] MA Stanley. Imiquimod and the Imidazoquinolones: Mechanism of Action and Therapeutic Potential. *Clinical and Experimental Dermatology*, 27(7):571–577, 2002.

[213] Traci L Testerman, John F Gerster, Linda M Imbertson, Michael J Reiter, Richard L Miller, Sheila J Gibson, Tamara L Wagner, and Mark A Tomai. Cytokine Induction by the Immunomodulators Imiquimod and S-27609. *Journal of Leukocyte Biology*, 58(3):365–372, 1995.

[214] Suzanne M Garland. Imiquimod. *Current Opinion in Infectious Diseases*, 16(2):85–89, 2003.

[215] Lindy L Thomsen, Peter Topley, Maria G Daly, Sara J Brett, and John P Tite. Imiquimod and Resiquimod in a Mouse Model: Adjuvants for DNA Vaccination by Particle-Mediated Immunotherapeutic Delivery. *Vaccine*, 22(13-14):1799–1809, 2004.

[216] Chi-Mu Chuang, Archana Monie, Chien-Fu Hung, and TC Wu. Treatment with Imiquimod Enhances Antitumor Immunity Induced by Therapeutic HPV DNA Vaccination. *Journal of Biomedical Science*, 17(1):1–9, 2010.

[217] Ivan FN Hung, Anna J Zhang, Kelvin KW To, Jasper FW Chan, Can Li, Hou-Shun Zhu, Patrick Li, Clara Li, Tuen-Ching Chan, Vincent CC Cheng, et al. Immunogenicity of Intradermal Trivalent Influenza Vaccine with Topical Imiquimod: A Double Blind Randomized Controlled Trial. *Clinical Infectious Diseases*, 59(9):1246–1255, 2014.

[218] Karolina Palucka and Jacques Banchereau. Dendritic Cells: A Link Between Innate and Adaptive Immunity. *Journal of Clinical Immunology*, 19(1):12–25, 1999.

[219] Hilary J McKenna, Kim L Stocking, Robert E Miller, Kenneth Brasel, Thibaut De Smedt, Eugene Maraskovsky, Charles R Maliszewski, David H Lynch, Jeffrey Smith, Bali Pulendran, et al. Mice Lacking Flt3 Ligand have Deficient Hematopoiesis Affecting Hematopoietic Progenitor Cells, Dendritic Cells, and Natural Killer Cells. *Blood, The Journal of the American Society of Hematology*, 95(11):3489–3497, 2000.

[220] Claudia Waskow, Kang Liu, Guillaume Darrasse-Jèze, Pierre Guermonprez, Florent Ginhoux, Miriam Merad, Tamara Shengelia, Kaihui Yao, and Michel Nussenzweig. The Receptor Tyrosine Kinase Flt3 is Required for Dendritic Cell Development in Peripheral Lymphoid Tissues. *Nature Immunology*, 9(6):676–683, 2008.

[221] Eugene Maraskovsky, Ken Brasel, Mark Teepe, Eileen R Roux, Stewart D Lyman, Ken Shortman, and Hilary J McKenna. Dramatic Increase in the Numbers of Functionally Mature Dendritic Cells in Flt3 Ligand-Treated Mice: Multiple Dendritic Cell Subpopulations Identified. *Journal of Experimental Medicine*, 184(5):1953–1962, 1996.

[222] Pierre Guermonprez, Julie Helft, Carla Claser, Stephanie Deroubaix, Henry Karanje, Anna Gazumyan, Guillaume Darasse-Jèze, Stephanie B Telerman, Gaëlle Breton, Heidi A Schreiber, et al. Inflammatory Flt3l is Essential to Mobilize Dendritic Cells and for T Cell Responses during Plasmodium Infection. *Nature Medicine*, 19(6):730–738, 2013.

[223] Céline Eidenschenk, Karine Crozat, Philippe Krebs, Ramon Arens, Daniel Popkin, Carrie N Arnold, Amanda L Blasius, Chris A Benedict, Eva Marie Y Moresco, Yu Xia, et al. Flt3 Permits Survival During Infection by Rendering Dendritic Cells Competent to Activate NK Cells. *Proceedings of the National Academy of Sciences*, 107(21):9759–9764, 2010.

[224] Niroshana Anandasabapathy, Rachel Feder, Shamim Mollah, Sze-Wah Tse, Maria Paula Longhi, Saurabh Mehandru, Ines Matos, Cheolho Cheong, Darren Ruane, Lucas Brane, et al. Classical Flt3L-Dependent Dendritic Cells Control Immunity to Protein Vaccine. *Journal of Experimental Medicine*, 211(9):1875–1891, 2014.

[225] Roshan Pais, Yusuf Omosun, Joseph U Igietseme, Kohtaro Fujihashi, and Francis O Eko. Route of Vaccine Administration Influences the Impact of Fms-Like Tyrosine Kinase 3 Ligand (Flt3L) on Chlamydial-Specific Protective Immune Responses. *Frontiers in Immunology*, 10: 1577, 2019.

[226] Qi Zhou, Fang Wang, Fu Yang, Yue Wang, Xiaoying Zhang, and Shuhan Sun. Augmented Humoral and Cellular Immune Response of Hepatitis B Virus DNA Vaccine by Micro-Needle Vaccination using Flt3L as an Adjuvant. *Vaccine*, 28(5):1357–1362, 2010.

[227] Zhenzhen Ding, Hua Zhu, Laiming Mo, Xiangyun Li, Rui Xu, Tian Li, Liang Zhao, Yi Ren, Yunsheng Xu, and Rongying Ou. FLT3L and Granulocyte Macrophage Colony-Stimulating Factor Enhance the Anti-Tumor and Immune Effects of an HPV16 E6/E7 Vaccine. *Aging (Albany NY)*, 11(24):11893, 2019.

[228] Jianqiang Li, Si Chen, Jun Ge, Feng Lu, Sulin Ren, Zhiqiang Zhao, Xiuying Pu, Xiaoxiao Chen, Jiaojiao Sun, and Yueqing Gu. A Novel Therapeutic Vaccine Composed of a Rearranged Human Papillomavirus Type 16 E6/E7 Fusion Protein and Fms-Like Tyrosine Kinase-3 Ligand Induces CD8+ T Cell Responses and Antitumor Effect. *Vaccine*, 35(47):6459–6467, 2017.

[229] Tae Jin Kim, Hyun-Tak Jin, Soo-Young Hur, Hyun Gul Yang, Yong Bok Seo, Sung Ran Hong, Chang-Woo Lee, Suhyeon Kim, Jung-Won Woo, Ki Seok Park, et al. Clearance of Persistent HPV Infection and Cervical Lesion by Therapeutic DNA Vaccine in CIN3 Patients. *Nature Communications*, 5(1):1–14, 2014.

[230] Rachel Myers, Christian Coviello, Philippe Erbs, Johann Foloppe, Cliff Rowe, James Kwan, Calum Crake, Seán Finn, Edward Jackson, Jean-Marc Balloul, et al. Polymeric Cups for Cavitation-Mediated Delivery of Oncolytic Vaccinia Virus. *Molecular Therapy*, 24(9):1627–1633, 2016.

[231] Klazina Kooiman, Silke Roovers, Simone AG Langeveld, Robert T Kleven, Heleen Dewitte, Meaghan A O'Reilly, Jean-Michel Escoffre, Ayache Bouakaz, Martin D Verweij, Kullervo Hynynen, et al. Ultrasound-Responsive Cavitation Nuclei for Therapy and Drug Delivery. *Ultrasound in Medicine & Biology*, 46(6):1296–1325, 2020.

[232] Eleanor Stride, Tim Segers, Guillaume Lajoinie, Samir Cherkaoui, Thierry Bettinger, Michel Versluis, and Mark Borden. Microbubble Agents: New Directions. *Ultrasound in Medicine & Biology*, 46(6):1326–1343, 2020.

[233] Elisabeth Mahase. Covid-19: Novavax Vaccine Efficacy is 86% against UK Variant and 60% against South African Variant, 2021.

[234] Jing-Hui Tian, Nita Patel, Robert Haupt, Haixia Zhou, Stuart Weston, Holly Hammond, James Logue, Alyse D Portnoff, James Norton, Mimi Guebre-Xabier, et al. SARS-CoV-2 Spike Glycoprotein Vaccine Candidate NVX-CoV2373 Immunogenicity in Baboons and Protection in Mice. *Nature Communications*, 12(1):1–14, 2021.

[235] Moderna Inc. Moderna Ships mRNA Vaccine against Novel Coronavirus (mRNA-1273) for Phase 1 Study. *businesswire.com*, Feb 2020. URL `https://www.businesswire.com/news/home/20200224005955/en/`.

[236] Kenneth Verstraete, Sina Koch, Sevgi Ertugrul, Isabel Vandenberghe, Maarten Aerts, Gonzalez Vandriessche, Christian Thiede, and Savvas N Savvides. Efficient Production of Bioactive Recombinant Human Flt3 Ligand in E. coli. *The Protein Journal*, 28(2):57–65, 2009.

[237] Donghee Park, Jongho Won, Unchul Shin, Hyeon Park, Gillsoo Song, Jiyoung Jang, Hyunjin Park, Chul-Woo Kim, and Jong Bum Seo. Transdermal Drug Delivery using a Specialized Cavitation Seed for Ultrasound. *IEEE Transactions on Ultrasonics, Ferroelectrics, and Frequency Control*, 66(6):1057–1064, 2019.

[238] Kevin Wei, Danny M Skyba, Christian Firschke, Ananda R Jayaweera, Jonathan R Lindner, and Sanjiv Kaul. Interactions between Microbubbles and Ultrasound: In Vitro and In Vivo Observations. *Journal of the American College of Cardiology*, 29(5):1081–1088, 1997.

[239] Ashlynn LZ Lee, Chuan Yang, Shujun Gao, James L Hedrick, and Yi Yan Yang. Subcutaneous Vaccination using Injectable Biodegradable Hydrogels for Long-Term Immune Response. *Nanomedicine: Nanotechnology, Biology and Medicine*, 21:102056, 2019.

[240] Kyle T Rich, Cameron L Hoerig, Marepalli B Rao, and T Douglas Mast. Relations between acoustic cavitation and skin resistance during intermediate- and high-frequency sonophoresis. *Journal of Controlled Release*, 194:266–277, 2014.

[241] Raquel P Deering, Sushma Kommareddy, Jeffrey B Ulmer, Luis A Brito, and Andrew J Geall. Nucleic Acid Vaccines: Prospects for Non-Viral Delivery of mRNA Vaccines. *Expert Opinion on Drug Delivery*, 11(6):885–899, 2014.

[242] Norbert Pardi, Michael J Hogan, Frederick W Porter, and Drew Weissman. mRNA Vaccines — A New Era in Vaccinology. *Nature Reviews Drug Discovery*, 17(4):261–279, 2018.

[243] Deborah H Fuller and Peter Berglund. Amplifying RNA Vaccine Development. *New England Journal of Medicine*, 382(25):2469–2471, 2020.

[244] Anuj Sharma and Barbara Knollmann-Ritschel. Current Understanding of the Molecular Basis of Venezuelan Equine Encephalitis Virus Pathogenesis and Vaccine Development. *Viruses*, 11 (2):164, 2019.

[245] James H Strauss and Ellen G Strauss. The Alphaviruses: Gene Expression, Replication, and Evolution. *Microbiological Reviews*, 58(3):491–562, 1994.

[246] Han Ying, Tal Z Zaks, Rong-Fu Wang, Kari R Irvine, Udai S Kammula, Francesco M Marincola, Wolfgang W Leitner, and Nicholas P Restifo. Cancer Therapy using a Self-Replicating RNA Vaccine. *Nature Medicine*, 5(7):823–827, 1999.

[247] Zifu Zhong, Séan McCafferty, Lisa Opsomer, Haixiu Wang, Hanne Huysmans, Joyca De Temmerman, Stefan Lienenklaus, João Paulo Portela Catani, Francis Combes, and Niek N Sanders. Corticosteroids and Cellulose Purification Improve, Respectively, the In Vivo Translation and Vaccination Efficacy of sa-mRNAs. *Molecular Therapy*, 29(4):1370–1381, 2021.

[248] Zhangting Zhao, Xingyuan Ma, Ruihuan Zhang, Fabiao Hu, Tong Zhang, Yuping Liu, Myong Hun Han, Fang You, Yi Yang, and Wenyun Zheng. A Novel Liposome-Polymer Hybrid Nanoparticles Delivering a Multi-Epitope Self-Replication DNA Vaccine and its Preliminary Immune Evaluation in Experimental Animals. *Nanomedicine: Nanotechnology, Biology and Medicine*, 35:102338, 2021.

[249] Tim Beissert, Mario Perkovic, Annette Vogel, Stephanie Erbar, Kerstin C Walzer, Tina Hempel, Silke Brill, Erik Haefner, René Becker, Özlem Türeci, et al. A Trans-Amplifying RNA Vaccine Strategy for Induction of Potent Protective Immunity. *Molecular Therapy*, 28(1):119–128, 2020.

[250] Annette B Vogel, Laura Lambert, Ekaterina Kinnear, David Busse, Stephanie Erbar, Kerstin C Reuter, Lena Wicke, Mario Perkovic, Tim Beissert, Heinrich Haas, et al. Self-Amplifying RNA Vaccines give Equivalent Protection against Influenza to mRNA Vaccines but at much Lower Doses. *Molecular Therapy*, 26(2):446–455, 2018.

[251] Paul F McKay, Kai Hu, Anna K Blakney, Karnyart Samnuan, Jonathan C Brown, Rebecca Penn, Jie Zhou, Clément R Bouton, Paul Rogers, Krunal Polra, et al. Self-Amplifying RNA SARS-CoV-2 Lipid Nanoparticle Vaccine Candidate induces High Neutralizing Antibody Titers in Mice. *Nature Communications*, 11(1):1–7, 2020.

[252] Katrina M Pollock, Hannah M Cheeseman, Alexander J Szubert, Vincenzo Libri, Marta Boffito, David Owen, Henry Bern, Jessica O'Hara, Leon R McFarlane, Nana-Marie Lemm, et al. Safety and Immunogenicity of a Self-Amplifying RNA Vaccine against COVID-19: COVAC1, a Phase I, Dose-Ranging Trial. *eClinicalMedicine*, 44:101262, 2022.

[253] AM Manzoor. Chapter 1 - Introduction to Costimulation and Costimulatory Molecules in Developing Costimulatory Molecules for Immunotherapy of Diseases, 2015.

[254] Takayoshi Yamauchi, Toshifumi Hoki, Takaaki Oba, Ryutaro Kajihara, Kristopher Attwood, Xuefang Cao, and Fumito Ito. CD40 and CD80/86 Signaling in cDC1s Mediate Effective Neoantigen Vaccination and Generation of Antigen-Specific CX3CR1+ CD8+ T Cells. *Cancer Immunology, Immunotherapy*, 71(1):137–151, 2022.

[255] Ashwin C Parenky, Archana Akalkotkar, Nihal S Mulla, and Martin J D'Souza. Harnessing T-Cell Activity against Prostate Cancer: A Therapeutic Microparticulate Oral Cancer Vaccine. *Vaccine*, 37(41):6085–6092, 2019.

[256] Meng Chen, Xiangxiu Chen, Xu Song, Abaidullah Muhammad, Renyong Jia, Yuanfeng Zou, Lizi Yin, Lixia Li, Changliang He, Gang Ye, et al. The Immune-Adjuvant Activity and the Mechanism of Resveratrol on Pseudorabies Virus Vaccine in a Mouse Model. *International Immunopharmacology*, 76:105876, 2019.

[257] Doumet Georges Helou, Aurélie Mauras, François Fasquelle, Juliane Sousa Lanza, Philippe M Loiseau, Didier Betbeder, and Sandrine Cojean. Intranasal Vaccine from Whole Leishmania Donovani Antigens Provides Protection and Induces Specific Immune Response against Visceral Leishmaniasis. *PLoS Neglected Tropical Diseases*, 15(8):e0009627, 2021.

[258] Amy Haseley Thorne, Kirsten N Malo, Ashley J Wong, Tricia T Nguyen, Neil Cooch, Charles Reed, Jian Yan, Kate E Broderick, Trevor RF Smith, Emma L Masteller, et al. Adjuvant Screen Identifies Synthetic DNA-Encoding Flt3L and CD80 Immunotherapeutics as Candidates for Enhancing Anti-tumor T Cell Responses. *Frontiers in Immunology*, 11:327, 2020.

[259] Alexander C Maue, W Ray Waters, Mitchell V Palmer, Diana L Whipple, F Chris Minion, Wendy C Brown, and D Mark Estes. CD80 and CD86, but not CD154, Augment DNA Vaccine-Induced Protection in Experimental Bovine Tuberculosis. *Vaccine*, 23(6):769–779, 2004.

[260] Ilia Voskoboinik, James C Whisstock, and Joseph A Trapani. Perforin and Granzymes: Function, Dysfunction and Human Pathology. *Nature Reviews Immunology*, 15(6):388–400, 2015.

[261] Tessa Gargett, Branka Grubor-Bauk, Tamsin J Garrod, Wenbo Yu, Darren Miller, Lee Major, Steve Wesselingh, Andreas Suhrbier, and Eric J Gowans. Induction of Antigen-Positive Cell Death by the Expression of Perforin, but not DTa, from a DNA Vaccine Enhances the Immune Response. *Immunology and Cell Biology*, 92(4):359–367, 2014.

[262] Danushka K Wijesundara, Wenbo Yu, Ben JC Quah, Preethi Eldi, John D Hayball, Kerrilyn R Diener, Ilia Voskoboinik, Eric J Gowans, and Branka Grubor-Bauk. Cytolytic DNA Vaccine Encoding Lytic Perforin Augments the Maturation of- and Antigen Presentation by- Dendritic Cells in a Time-Dependent Manner. *Scientific Reports*, 7(1):1–8, 2017.

[263] Amelia J Brennan, Jenny Chia, Kylie A Browne, Annette Ciccone, Sarah Ellis, Jamie A Lopez, Olivia Susanto, Sandra Verschoor, Hideo Yagita, James C Whisstock, et al. Protection from endogenous perforin: Glycans and the c terminus regulate exocytic trafficking in cytotoxic lymphocytes. *Immunity*, 34(6):879–892, 2011.

[264] Jason Gummow, Yanrui Li, Wenbo Yu, Tamsin Garrod, Danushka Wijesundara, Amelia J Brennan, Ranajoy Mullick, Ilia Voskoboinik, Branka Grubor-Bauk, and Eric J Gowans. A Multiantigenic DNA Vaccine that Induces Broad Hepatitis C Virus-Specific T-Cell Responses in Mice. *Journal of Virology*, 89(15):7991–8002, 2015.

[265] B Grubor-Bauk, W Yu, D Wijesundara, J Gummow, T Garrod, AJ Brennan, I Voskoboinik, and EJ Gowans. Intradermal Delivery of DNA Encoding HCV NS3 and Perforin Elicits Robust Cell-Mediated Immunity in Mice and Pigs. *Gene Therapy*, 23(1):26–37, 2016.

[266] Kenneth John Chomistek and Thomai Panagiotou. Large scale nanomaterial production using microfluidizer high shear processing. *MRS Online Proceedings Library (OPL)*, 1209, 2009.

[267] Ashish C Shrestha, Danushka K Wijesundara, Makutiro G Masavuli, Zelalem A Mekonnen, Eric J Gowans, and Branka Grubor-Bauk. Cytolytic Perforin as an Adjuvant to Enhance the Immunogenicity of DNA Vaccines. *Vaccines*, 7(2):38, 2019.

[268] Alain Beck and Janice M Reichert. Therapeutic Fc-Fusion Proteins and Peptides as Successful Alternatives to Antibodies. *MAbs*, 3(5):415–416, 2011.

[269] Hanne Huysmans, Zifu Zhong, Joyca De Temmerman, Barbara L Mui, Ying K Tam, Séan Mc Cafferty, Arlieke Gitsels, Daisy Vanrompay, and Niek N Sanders. Expression Kinetics and Innate Immune Response after Electroporation and LNP-Mediated Delivery of a Self-Amplifying mRNA in the Skin. *Molecular Therapy-Nucleic Acids*, 17:867–878, 2019.

[270] Victor C Huber, Raelene M McKeon, Martha N Brackin, Laura A Miller, Rachael Keating, Scott A Brown, Natalia Makarova, Daniel R Perez, Gene H MacDonald, and Jonathan A McCullers. Distinct Contributions of Vaccine-Induced Immunoglobulin G1 (IgG1) and IgG2a Antibodies to Protective Immunity against Influenza. *Clinical and Vaccine Immunology*, 13(9): 981–990, 2006.

[271] Yeh Chen Lee, Dominic F Kelly, Ly-Mee Yu, Mary PE Slack, Robert Booy, Paul T Heath, Claire-Anne Siegrist, Richard E Moxon, and Andrew J Pollard. Haemophilus Influenzae Type B Vaccine Failure in Children is associated with Inadequate Production of High-Quality Antibody. *Clinical Infectious Diseases*, 46(2):186–192, 2008.

[272] Delphine Lechardeur, KJ Sohn, M Haardt, PB Joshi, M Monck, RW Graham, B Beatty, J Squire, H O'brodovich, and GL Lukacs. Metabolic Instability of Plasmid DNA in the Cytosol: A Potential Barrier to Gene Transfer. *Gene Therapy*, 6(4):482–497, 1999.

[273] Byong-Moon Kim, Dong-Sop Lee, Jae-Hoon Choi, Chae-Young Kim, Miwon Son, You-Suk Sun, Kwan-Hyuck Baek, Ki-Seok Park, Young-Chul Sung, and Won-Bae Kim. In Vivo Kinetics and Biodistribution of a HIV-1 DNA Vaccine After Administration in Mice. *Archives of pharmacal research*, 26(6):493–498, 2003.

[274] Eun Sung Kang, Chae Young Kim, Seon Beom Kim, Se Jin Im, Se Hwan Yang, Young Chul Sung, and Byong Moon Kim. In Vivo Kinetics and Biodistribution of HB-110, a Novel HBV DNA Vaccine, After Administration in Mice. *Archives of Pharmacal Research*, 30(3):355–360, 2007.

[275] John F Thompson, Lisa S Hayes, and David B Lloyd. Modulation of Firefly Luciferase Stability and Impact on Studies of Gene Regulation. *Gene*, 103(2):171–177, 1991.

[276] Yachun Zhang, Jie Yang, Mingming Li, Min Cui, Zhen F Fu, Ling Zhao, and Ming Zhou. A Recombinant Rabies Virus Expressing Fms-Like Tyrosine Kinase 3 Ligand (Flt3L) Induces Enhanced Immunogenicity in Mice. *Virologica Sinica*, 34(6):662–672, 2019.

[277] Vitaly Vasilevko, Anahit Ghochikyan, Nadya Sadzikava, Irina Petrushina, Mike Tran, Edward P Cohen, Patrick J Kesslak, David H Cribbs, Garth L Nicolson, and Michael G Agadjanyan. Immunization with a Vaccine that Combines the Expression of MUC1 and B7 Co-Stimulatory Molecules Prolongs the Survival of Mice and Delays the Appearance of Mouse Mammary Tumors. *Clinical & Experimental Metastasis*, 20(6):489–498, 2003.

[278] Angelika Stoecklinger, Tekalign D Eticha, Mehrnaz Mesdaghi, Adrien Kissenpfennig, Bernard Malissen, Josef Thalhamer, and Peter Hammerl. Langerin+ Dermal Dendritic Cells are Critical

for CD8+ T Cell Activation and IgH $\gamma$-1 Class Switching in Response to Gene Gun Vaccines. *The Journal of Immunology*, 186(3):1377–1383, 2011.

[279] Marc Pearton, Sang-Moo Kang, Jae-Min Song, Yeu-Chun Kim, Fu-Shi Quan, Alexander Anstey, Matthew Ivory, Mark R Prausnitz, Richard W Compans, and James C Birchall. Influenza Virus-Like Particles Coated onto Microneedles can Elicit Stimulatory Effects on Langerhans Cells in Human Skin. *Vaccine*, 28(37):6104–6113, 2010.

[280] Elena Shklovskaya, Brendan J O'Sullivan, Lai Guan Ng, Ben Roediger, Ranjeny Thomas, Wolfgang Weninger, and Barbara Fazekas de St Groth. Langerhans Cells are Precommitted to Immune Tolerance Induction. *Proceedings of the National Academy of Sciences*, 108(44): 18049–18054, 2011.

[281] Carole L Berger, Juan Gabriel Vasquez, Joshua Shofner, Kavita Mariwalla, and Richard L Edelson. Langerhans Cells: Mediators of Immunity and Tolerance. *The International Journal of Biochemistry & Cell Biology*, 38(10):1632–1636, 2006.

[282] György Fazekas, Brigitte Rosenwirth, Peter Dukor, János Gergely, and Éva Rajnavölgyi. IgG Isotype Distribution of Local and Systemic Immune Responses Induced by Influenza Virus Infection. *European Journal of Immunology*, 24(12):3063–3067, 1994.

[283] A-O Hovden, RJ Cox, and LR Haaheim. Whole Influenza Virus Vaccine is More Immunogenic Than Split influenza Virus Vaccine and Induces Primarily an IgG2a Response in BALB/c Mice. *Scandinavian Journal of Immunology*, 62(1):36–44, 2005.

[284] Clifford M Snapper and William E Paul. Interferon-$\gamma$ and B Cell Stimulatory Factor-1 Reciprocally Regulate Ig Isotype Production. *Science*, 236(4804):944–947, 1987.

[285] Manfred Kopf, Brian Abel, Awen Gallimore, Michael Carroll, and Martin F Bachmann. Complement Component C3 Promotes T-Cell Priming and Lung Migration to Control Acute Influenza Virus Infection. *Nature Medicine*, 8(4):373–378, 2002.

[286] ED Williamson, PM Vesey, KJ Gillhespy, SM Eley, M Green, and RW Titball. An IgG1 Titre to the F1 and V Antigens Correlates with Protection against Plague in the Mouse Model. *Clinical & Experimental Immunology*, 116(1):107–114, 1999.

[287] R Yuan, Arturo Casadevall, Gadi Spira, and Matthew D Scharff. Isotype Switching from IgG3 to IgG1 Converts a Nonprotective Murine Antibody to Cryptococcus Neoformans into a Protective Antibody. *The Journal of Immunology*, 154(4):1810–1816, 1995.

[288] Charles B Stauft, Chen Yang, J Robert Coleman, David Boltz, Chiahsuan Chin, Anna Kushnir, and Steffen Mueller. Live-Attenuated H1N1 Influenza Vaccine Candidate Displays Potent Efficacy in Mice and Ferrets. *PLoS One*, 14(10):e0223784, 2019.

[289] Natalie Pica, Arun Iyer, Irene Ramos, Nicole M Bouvier, Ana Fernandez-Sesma, Adolfo García-Sastre, Anice C Lowen, Peter Palese, and John Steel. The DBA. 2 mouse is Susceptible to Disease Following Infection with a broad, but limited, range of Influenza A and B Viruses. *Journal of Virology*, 85(23):12825–12829, 2011.

[290] Tiong Kit Tan, Toby PE Gamlen, Pramila Rijal, Alain R Townsend, Deborah R Gill, and Stephen C Hyde. Lung-Targeting Lentiviral Vector for Passive Immunisation against Influenza. *Thorax*, 75(12):1112–1115, 2020.

[291] Timothy J Powell, Jonathan D Silk, Jane Sharps, Ervin Fodor, and Alain RM Townsend. Pseudotyped Influenza A Virus as a Vaccine for the Induction of Heterotypic Immunity. *Journal of Virology*, 86(24):13397–13406, 2012.

[292] Mariana Baz, Kobporn Boonnak, Myeisha Paskel, Celia Santos, Timothy Powell, Alain Townsend, and Kanta Subbarao. Nonreplicating Influenza A Virus Vaccines Confer Broad Protection against Lethal Challenge. *MBio*, 6(5):e01487–15, 2015.

[293] Barbara Holzer, Sophie B Morgan, Yumi Matsuoka, Matthew Edmans, Francisco J Salguero, Helen Everett, Sharon M Brookes, Emily Porter, Ronan MacLoughlin, Bryan Charleston, et al. Comparison of Heterosubtypic Protection in Ferrets and Pigs Induced by a Single-Cycle Influenza Vaccine. *The Journal of Immunology*, 200(12):4068–4077, 2018.

[294] Vincent Flacher, Patrice Douillard, Smina Aït-Yahia, Patrizia Stoitzner, Valérie Clair-Moninot, Nikolaus Romani, and Sem Saeland. Expression of Langerin/CD207 reveals Dendritic Cell Heterogeneity between Inbred Mouse Strains. *Immunology*, 123(3):339–347, 2008.

[295] J Chakir, L Cote, C Coulombe, and N Deslauriers. Differential Pattern of Infection and Immune Response during Experimental Oral Candidiasis in BALB/c and DBA/2 (H-2d) Mice. *Oral Microbiology and Immunology*, 9(2):88–94, 1994.

[296] RA Wetsel, Daniel T Fleischer, and DL Haviland. Deficiency of the Murine Fifth Complement Component (C5). A 2-Base Pair Gene Deletion in a 5'-exon. *Journal of Biological Chemistry*, 265(5):2435–2440, 1990.

[297] Yung-Yi C Mosley, Josiah E Radder, and Harm HogenEsch. Genetic Variation in the Magnitude and Longevity of the IgG Subclass Response to a Diphtheria-Tetanus-Acellular Pertussis (DTaP) Vaccine in Mice. *Vaccines*, 7(4):124, 2019.

[298] Holger Hackstein, Andreas Wachtendorf, Sabine Kranz, Jürgen Lohmeyer, Gregor Bein, and Nelli Baal. Heterogeneity of Respiratory Dendritic Cell Subsets and Lymphocyte Populations in Inbred Mouse Strains. *Respiratory Research*, 13(1):1–13, 2012.

[299] Hanaa Y Bakir, Chikako Tomiyama-Miyaji, Hisami Watanabe, Toru Nagura, Toshihiko Kawamura, Hiroho Sekikawa, and Toru Abo. Reasons why DBA/2 Mice are Resistant to Malarial Infection: Expansion of CD3int B220+ $\gamma$ $\delta$ T Cells with Double-Negative CD4–CD8–Phenotype in the Liver. *Immunology*, 117(1):127–135, 2006.

[300] Jack Mellors, Tom Tipton, Stephanie Longet, and Miles Carroll. Viral Evasion of the Complement System and its Importance for Vaccines and Therapeutics. *Frontiers in Immunology*, 11: 1450, 2020.

[301] Yuting Jiang, Guangyu Zhao, Nianping Song, Pei Li, Yuehong Chen, Yan Guo, Junfeng Li, Lanying Du, Shibo Jiang, Renfeng Guo, et al. Blockade of the C5a–C5aR Axis Alleviates Lung Damage in hDPP4-Transgenic Mice infected with MERS-CoV. *Emerging Microbes & Infections*, 7(1):1–12, 2018.

[302] Yu-Jin Kim, Ki-Hye Kim, Eun-Ju Ko, Min-Chul Kim, Yu-Na Lee, Yu-Jin Jung, Young-Tae Lee, Young-Man Kwon, Jae-Min Song, and Sang-Moo Kang. Complement C3 Plays a Key Role in Inducing Humoral and Cellular Immune Responses to Influenza Virus Strain-Specific Hemagglutinin-Based or Cross-Protective M2 Extracellular Domain-Based Vaccination. *Journal of Virology*, 92(20):e00969–18, 2018.

[303] Michele A Kutzler and David B Weiner. DNA Vaccines: Ready for Prime Time? *Nature Reviews Genetics*, 9(10):776–788, 2008.

[304] Dominika Hobernik and Matthias Bros. DNA vaccines — How Far from Clinical Use? *International Journal of Molecular Sciences*, 19(11):3605, 2018.

[305] Yue Yin, Wen Su, Jie Zhang, Wenping Huang, Xiaoyang Li, Haixia Ma, Mixiao Tan, Haohao Song, Guoliang Cao, Shengji Yu, et al. Separable Microneedle Patch to Protect and Deliver DNA Nanovaccines against COVID-19. *ACS Nano*, 15(9):14347–14359, 2021.

[306] Dengning Xia, Rui Jin, Gaurav Byagathvalli, Huan Yu, Ling Ye, Chao-Yi Lu, M Saad Bhamla, Chinglai Yang, and Mark R Prausnitz. An Ultra-Low-Cost Electroporator with Microneedle Electrodes (ePatch) for SARS-CoV-2 Vaccination. *Proceedings of the National Academy of Sciences*, 118(45), 2021.

[307] Rohan SJ Ingrole, Erkan Azizoglu, Maria Dul, James C Birchall, Harvinder S Gill, and Mark R Prausnitz. Trends of Microneedle Technology in the Scientific Literature, Patents, Clinical Trials and Internet Activity. *Biomaterials*, 267:120491, 2021.

[308] Nadine G Rouphael, Lilin Lai, Sonia Tandon, Michele Paine McCullough, Yunchuan Kong, Sarah Kabbani, Muktha S Natrajan, Yongxian Xu, Yerun Zhu, Dongli Wang, et al. Immunologic Mechanisms of Seasonal Influenza Vaccination Administered by Microneedle Patch from a Randomized Phase I Trial. *npj Vaccines*, 6(1):1–9, 2021.

[309] Nadine G Rouphael, Michele Paine, Regina Mosley, Sebastien Henry, Devin V McAllister, Haripriya Kalluri, Winston Pewin, Paula M Frew, Tianwei Yu, Natalie J Thornburg, et al. The Safety, Immunogenicity, and Acceptability of Inactivated Influenza Vaccine Delivered by Microneedle Patch (TIV-MNP 2015): a Randomised, Partly Blinded, Placebo-Controlled, Phase 1 Trial. *The Lancet*, 390(10095):649–658, 2017.

[310] Donghee Park, Heungil Ryu, Han Sung Kim, Young-sun Kim, Kyu-Sil Choi, Hyunjin Park, and Jongbum Seo. Sonophoresis using Ultrasound Contrast Agents for Transdermal Drug Delivery: an In Vivo Experimental Study. *Ultrasound in Medicine & Biology*, 38(4):642–650, 2012.

[311] Bruce M Becker, Sara Helfrich, Elizabeth Baker, Kirsten Lovgren, P Allison Minugh, and Jason T Machan. Ultrasound with Topical Anesthetic Rapidly Decreases Pain of Intravenous Cannulation. *Academic Emergency Medicine*, 12(4):289–295, 2005.

[312] Jack Masterson, Brett Kluge, Aaron Burdette, and George Lewis Sr. Sustained Acoustic Medicine; Sonophoresis for Nonsteroidal Anti-Inflammatory Drug Delivery in Arthritis. *Therapeutic Delivery*, 11(6):363–372, 2020.

[313] Samir Mitragotri, Daniel Blankschtein, and Robert Langer. Transdermal Drug Delivery Using Low-Frequency Sonophoresis. *Pharmaceutical Research*, 13(3):411–420, 1996.

[314] Hua Tang, Chiao Chun Joanne Wang, Daniel Blankschtein, and Robert Langer. An Investigation of the Role of Cavitation in Low-Frequency Ultrasound-Mediated Transdermal Drug Transport. *Pharmaceutical Research*, 19(8):1160–1169, 2002.

[315] Sunali Bhatnagar, Heiko Schiffter, and Constantin-C Coussios. Exploitation of Acoustic Cavitation-Induced Microstreaming to Enhance Molecular Transport. *Journal of Pharmaceutical Sciences*, 103(6):1903–1912, 2014.

[316] M Schneider. Sonovue, a new ultrasound contrast agent. *European Radiology*, 9:S347–S348, 1999.

[317] Reju G Thomas, Umesh S Jonnalagadda, and James J Kwan. Biomedical Applications for Gas-Stabilizing Solid Cavitation Agents. *Langmuir*, 35(31):10106–10115, 2019.

[318] Matthew B Laurens. RTS, S/AS01 Vaccine (Mosquirix™): an Overview. *Human Vaccines & Immunotherapeutics*, 16(3):480–489, 2020.

[319] M Asif A Siddiqui and Caroline M Perry. Human Papillomavirus Quadrivalent (types 6, 11, 16, 18) Recombinant Vaccine (Gardasil®). *Drugs*, 66(9):1263–1271, 2006.

[320] Vivek Shinde, Sutika Bhikha, Zaheer Hoosain, Moherndran Archary, Qasim Bhorat, Lee Fairlie, Umesh Lalloo, Mduduzi SL Masilela, Dhayendre Moodley, Sherika Hanley, et al. Efficacy of NVX-CoV2373 Covid-19 Vaccine against the B. 1.351 Variant. *New England Journal of Medicine*, 384(20):1899–1909, 2021.

[321] Daan JA Crommelin, Josbert M Metselaar, and Gert Storm. Liposomes: the Science and the Regulatory Landscape. In *Non-Biological Complex Drugs*, pages 77–106. Springer, 2015.

[322] Yechezkel Chezy Barenholz. Doxil®—the First FDA-Approved Nano-Drug: Lessons Learned. *Journal of Controlled Release*, 160(2):117–134, 2012.

[323] Samir Mitragotri. Sonophoresis: Ultrasound-Mediated Transdermal Drug Delivery. In *Percutaneous Penetration Enhancers Physical Methods in Penetration Enhancement*, pages 3–14. Springer, 2017.

[324] Cassie Caudill, Jillian L Perry, Kimon Iliadis, Addis T Tessema, Brian J Lee, Beverly S Mecham, Shaomin Tian, and Joseph M DeSimone. Transdermal Vaccination via 3D-Printed Microneedles Induces Potent Humoral and Cellular Immunity. *Proceedings of the National Academy of Sciences*, 118(39), 2021.

[325] Dimitrios G Koutsonanos, Elena V Vassilieva, Anastasia Stavropoulou, Vladimir G Zarnitsyn, E Stein Esser, Misha T Taherbhai, Mark R Prausnitz, Richard W Compans, and Ioanna Skountzou. Delivery of Subunit Influenza Vaccine to Skin with Microneedles Improves Immunogenicity and Long-lived Protection. *Scientific Reports*, 2(1):1–10, 2012.

[326] Jae-Min Song, Yeu-Chun Kim, O Eunju, Richard W Compans, Mark R Prausnitz, and Sang-Moo Kang. DNA Vaccination in the Skin using Microneedles Improves Protection against Influenza. *Molecular Therapy*, 20(7):1472–1480, 2012.

[327] Reinhold Schirmbeck and Jörg Reimann. Modulation of Gene-Gun-Mediated Th2 Immunity to Hepatitis B Surface Antigen by Bacterial CpG Motifs or IL-12. *Intervirology*, 44(2-3):115–123, 2001.

[328] Kristie Bloom, Fiona van den Berg, and Patrick Arbuthnot. Self-Amplifying RNA Vaccines for Infectious Diseases. *Gene Therapy*, 28(3):117–129, 2021.

[329] Gábor Tamás Szabó, Azita Josefine Mahiny, and Irena Vlatkovic. COVID-19 mRNA Vaccines: Platforms and Current Developments. *Molecular Therapy*, 2022.

[330] Ulrich R Hengge, Edward F Chan, Ruth A Foster, Patricia S Walker, and Jonathan C Vogel. Cytokine Gene Expression in Epidermis with Biological Effects Following Injection of Naked DNA. *Nature Genetics*, 10(2):161–166, 1995.

[331] M Cumberbatch, RJ Dearman, CEM Griffiths, and Ian Kimber. Langerhans Cell Migration. *Clinical and Experimental Dermatology: Experimental Dermatology*, 25(5):413–418, 2000.

[332] Jesse H Erasmus, Amit P Khandhar, Megan A O'Connor, Alexandra C Walls, Emily A Hemann, Patience Murapa, Jacob Archer, Shanna Leventhal, James T Fuller, Thomas B Lewis, et al. An Alphavirus-Derived Replicon RNA Vaccine Induces SARS-CoV-2 Neutralizing Antibody and T cell Responses in Mice and Nonhuman Primates. *Science Translational Medicine*, 12(555): eabc9396, 2020.

[333] Arcturus Therapeutics. Arcturus Announces Self-amplifying COVID-19 mRNA Vaccine Candidate ARCT-154 Meets Primary Efficacy Endpoint in Phase 3 Study, 2022. URL `https://www.businesswire.com/news/home/20220420005466/en/Arcturus-Announces-Self-amplifying-COVID-19-mRNA-Vaccine-Candidate-ARCT-154-Meets-Primary-Efficacy-Endpoint-in-Phase-3-Study`. [Accessed 2 May, 2022].

[334] EJ Park, Jacob Werner, and Nadine Barrie Smith. Ultrasound Mediated Transdermal Insulin Delivery in Pigs using a Lightweight Transducer. *Pharmaceutical Research*, 24(7):1396–1401, 2007.

[335] Seungjun Lee, Robert E Newnham, and Nadine Barrie Smith. Short Ultrasound Exposure

Times for Noninvasive Insulin Delivery in Rats using the Lightweight Cymbal Array. *IEEE Transactions on Ultrasonics, Ferroelectrics, and Frequency Control*, 51(2):176–180, 2004.

[336] Jyoti Gupta and Mark R Prausnitz. Recovery of Skin Barrier Properties after Sonication in Human Subjects. *Ultrasound in Medicine & Biology*, 35(8):1405–1408, 2009.

[337] Srinivas Mutalik, Harendra S Parekh, Nigel M Davies, and Udupa Nayanabhirama. A Combined Approach of Chemical Enhancers and Sonophoresis for the Transdermal Delivery of Tizanidine Hydrochloride. *Drug Delivery*, 16(2):82–91, 2009.

[338] Seiji Tokumoto, Naruhito Higo, Hiroaki Todo, and Kenji Sugibayashi. Effect of Combination of Low-Frequency Sonophoresis or Electroporation with Iontophoresis on the Mannitol Flux or Electroosmosis through Excised Skin. *Biological and Pharmaceutical Bulletin*, 39(7):1206–1210, 2016.

[339] C Garrett Rappazzo, Hannah C Watkins, Cassandra M Guarino, Annie Chau, Jody L Lopez, Matthew P DeLisa, Cynthia A Leifer, Gary R Whittaker, and David Putnam. Recombinant M2e Outer Membrane Vesicle Vaccines Protect against Lethal Influenza A Challenge in BALB/c Mice. *Vaccine*, 34(10):1252–1258, 2016.

[340] Nuschin Meykadeh, Alireza Mirmohammadsadegh, Zhijun Wang, Etiena Basner-Tschakarjan, and Ulrich R Hengge. Topical application of plasmid dna to mouse and human skin. *Journal of Molecular Medicine*, 83(11):897–903, 2005.

[341] Ulrich R Hengge, Patricia S Walker, Jonathan C Vogel, et al. Expression of naked dna in human, pig, and mouse skin. *The Journal of Clinical Investigation*, 97(12):2911–2916, 1996.

[342] Ana M Barbero and H Frederick Frasch. Pig and guinea pig skin as surrogates for human in vitro penetration studies: a quantitative review. *Toxicology in Vitro*, 23(1):1–13, 2009.

[343] Paul A Khavari. Modelling cancer in human skin tissue. *Nature Reviews Cancer*, 6(4):270–280, 2006.

[344] Jonathan CJ Wei, Grant A Edwards, Darren J Martin, Han Huang, Michael L Crichton, and Mark AF Kendall. Allometric scaling of skin thickness, elasticity, viscoelasticity to mass for micro-medical device translation: from mice, rats, rabbits, pigs to humans. *Scientific Reports*, 7(1):1–16, 2017.

[345] Manolis Pasparakis, Ingo Haase, and Frank O Nestle. Mechanisms regulating skin immunity and inflammation. *Nature reviews immunology*, 14(5):289–301, 2014.

[346] Artur Summerfield, François Meurens, and Meret E Ricklin. The immunology of the porcine skin and its value as a model for human skin. *Molecular Immunology*, 66(1):14–21, 2015.

[347] John A Maher and Joanne DeStefano. The ferret: an animal model to study influenza virus. *Lab Animal*, 33(9):50–53, 2004.

# Appendix A

# Plasmid maps

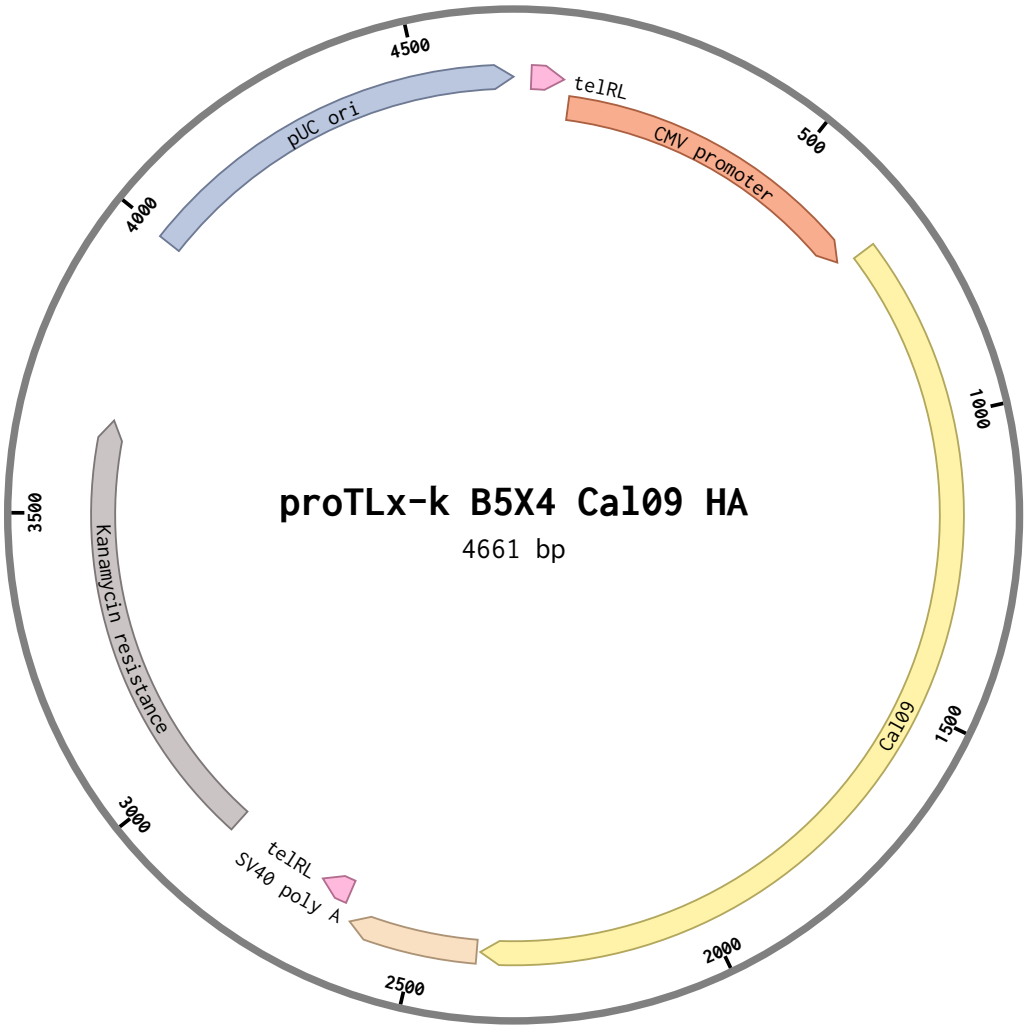



**Figure A.1.** Plasmid map of proTLx-κ B5X4 Cal09 HA

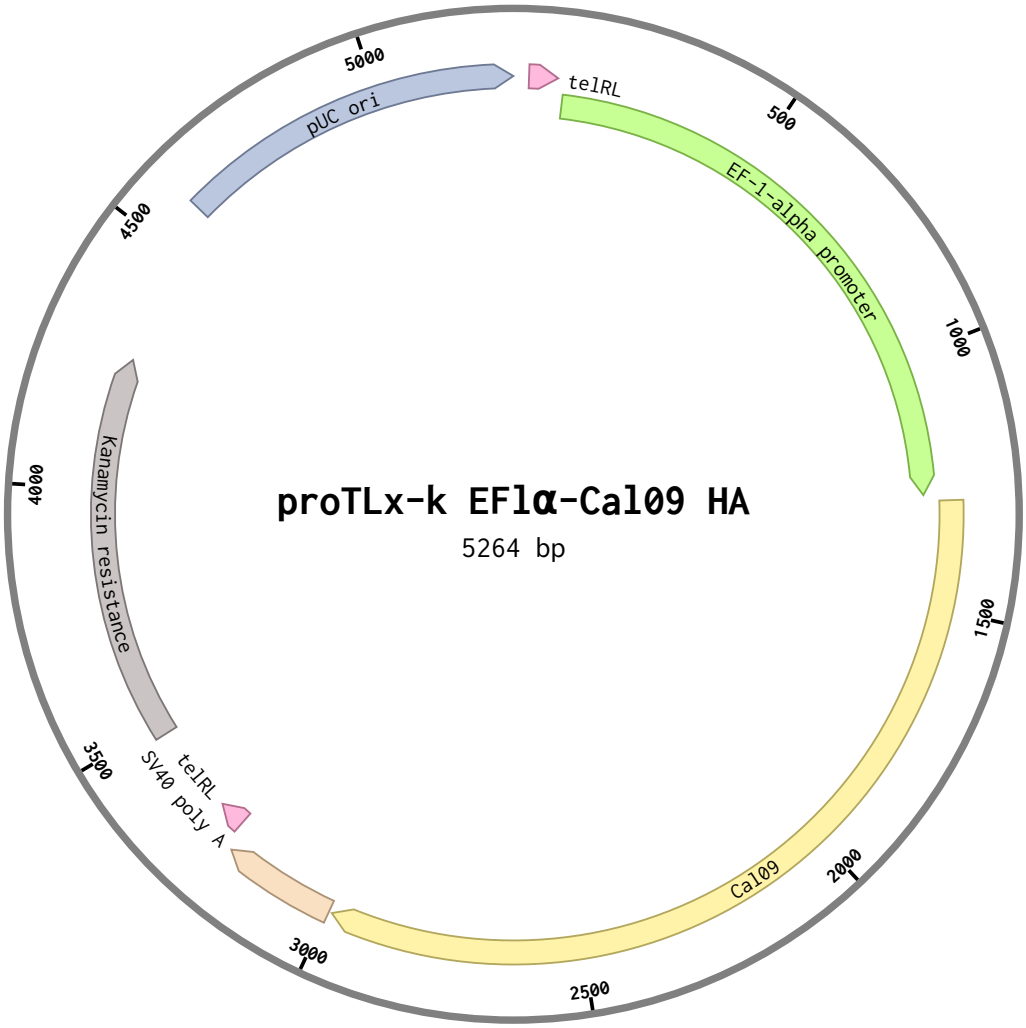



**Figure A.2.** Plasmid map of proTLx-κ EF1α-Cal09 HA

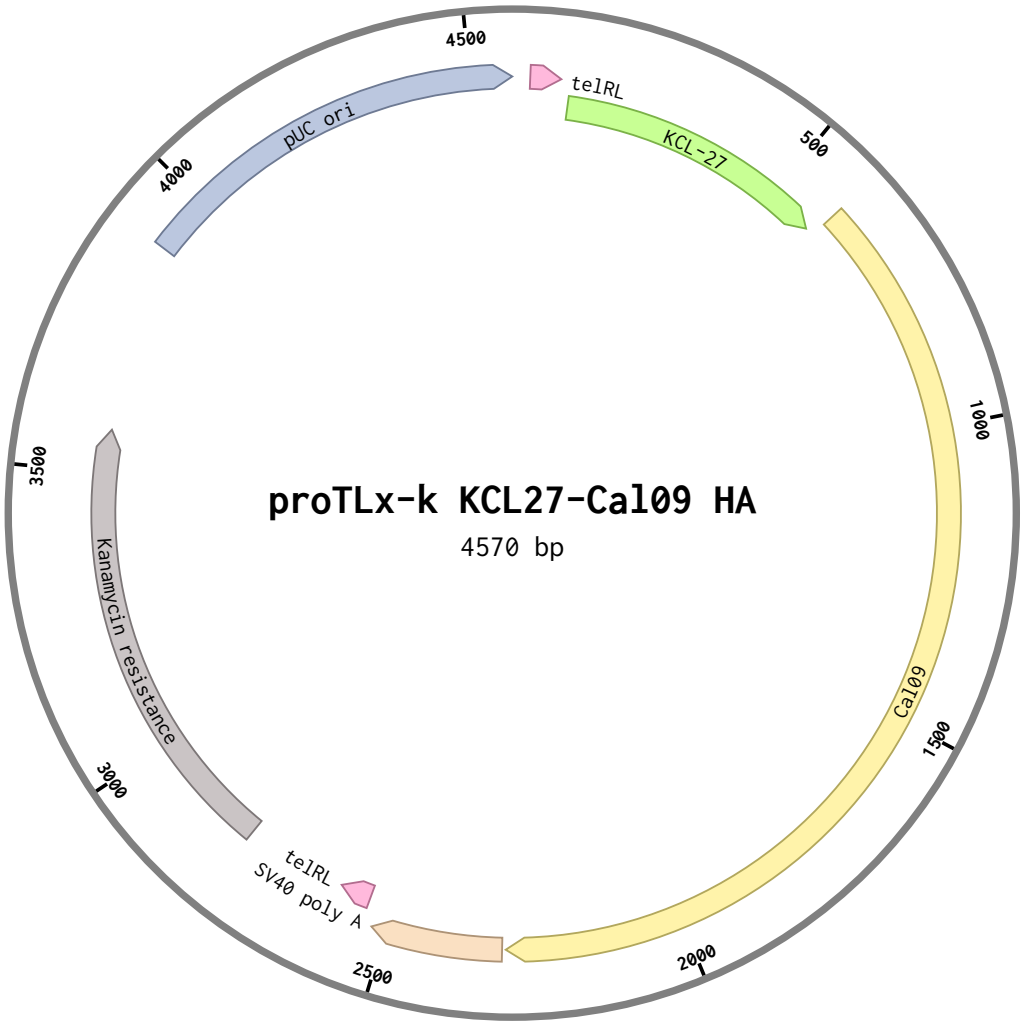



**Figure A.3.** Plasmid map of proTLx-κ KCL27-Cal09

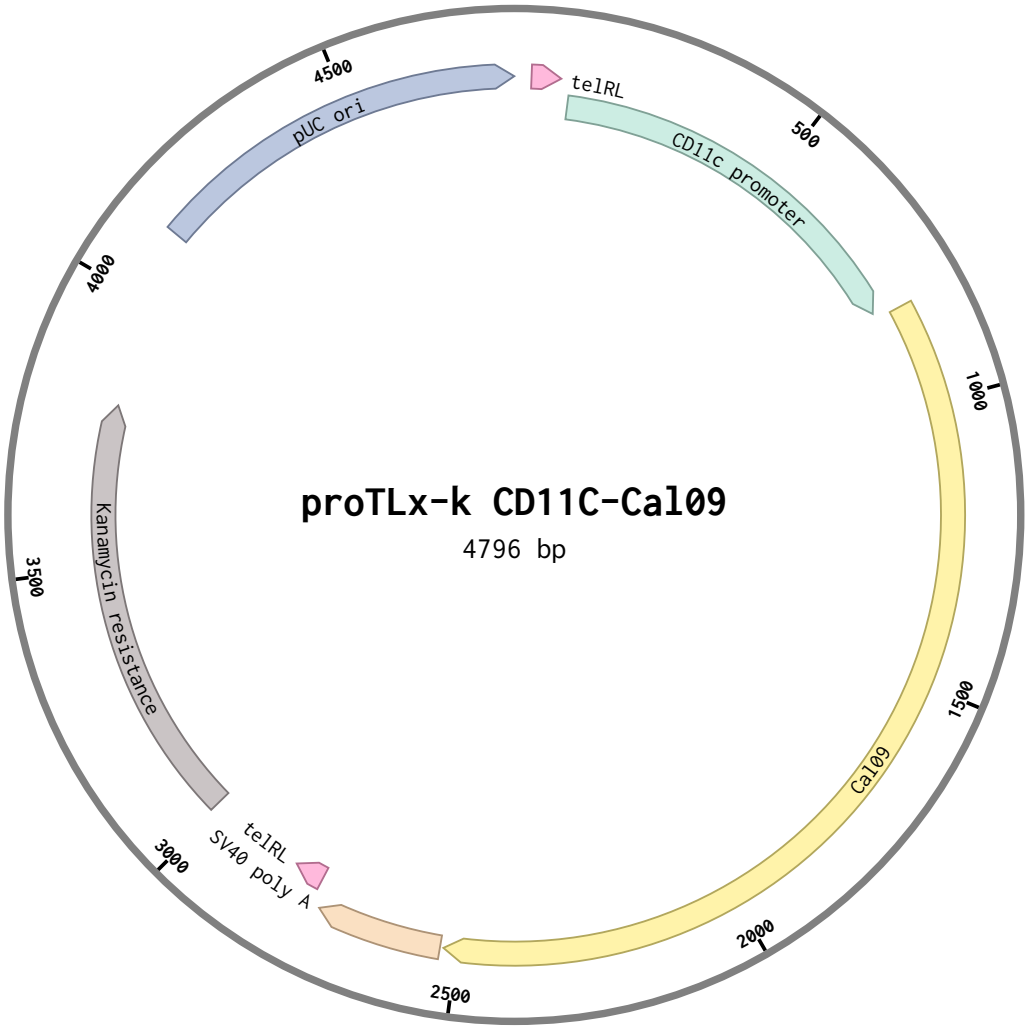



**Figure A.4.** Plasmid map of proTLx-κ CD11c-Cal09 HA

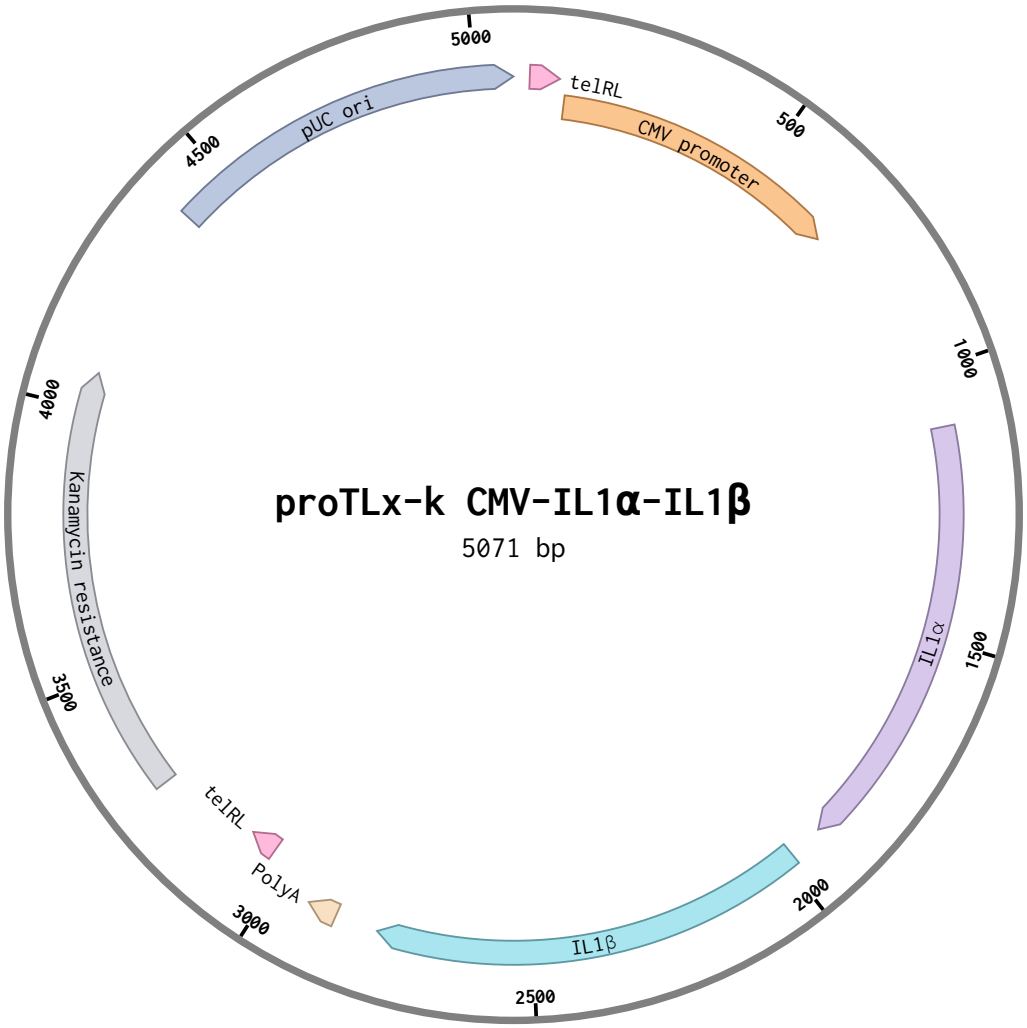



**Figure A.5.** Plasmid map of proTLx-κ CMV-IL1α-P2A-IL1β

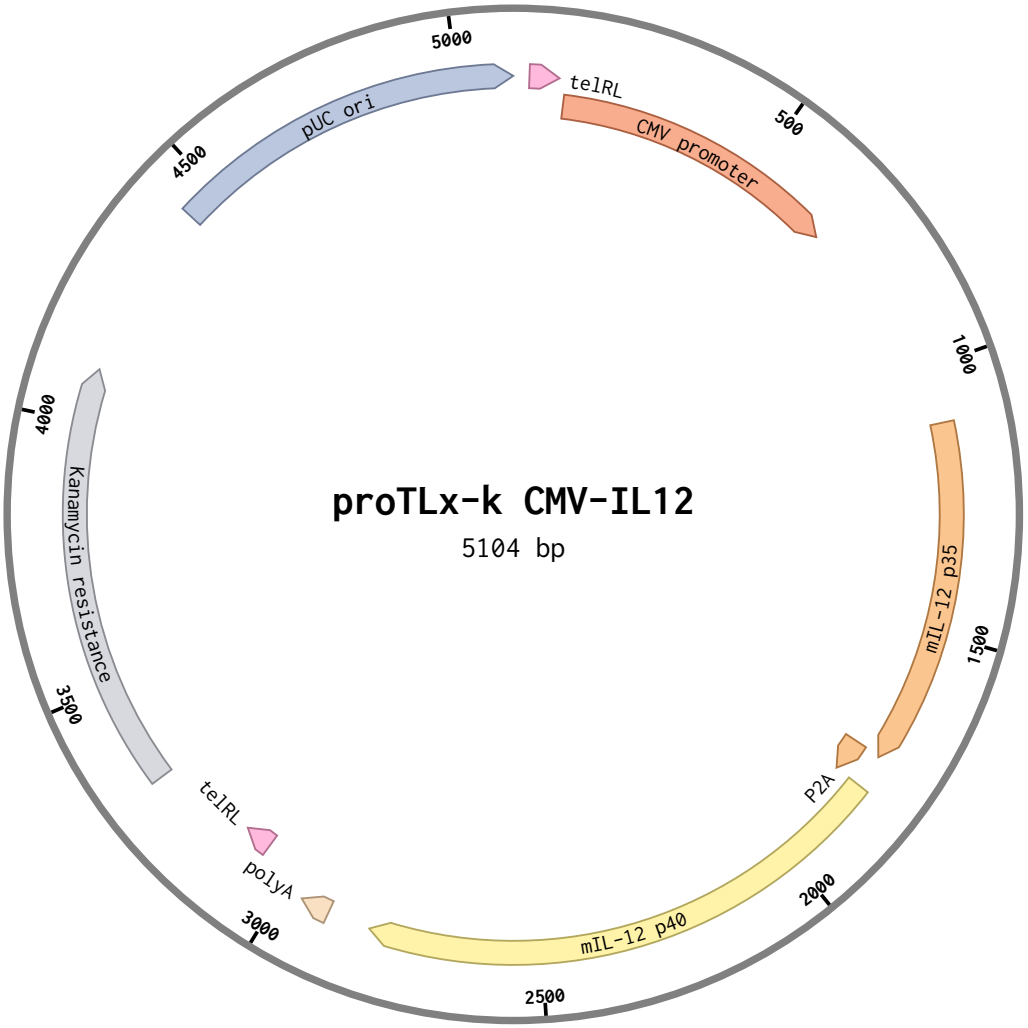



**Figure A.6.** Plasmid map of proTLx-κ CMV-IL12

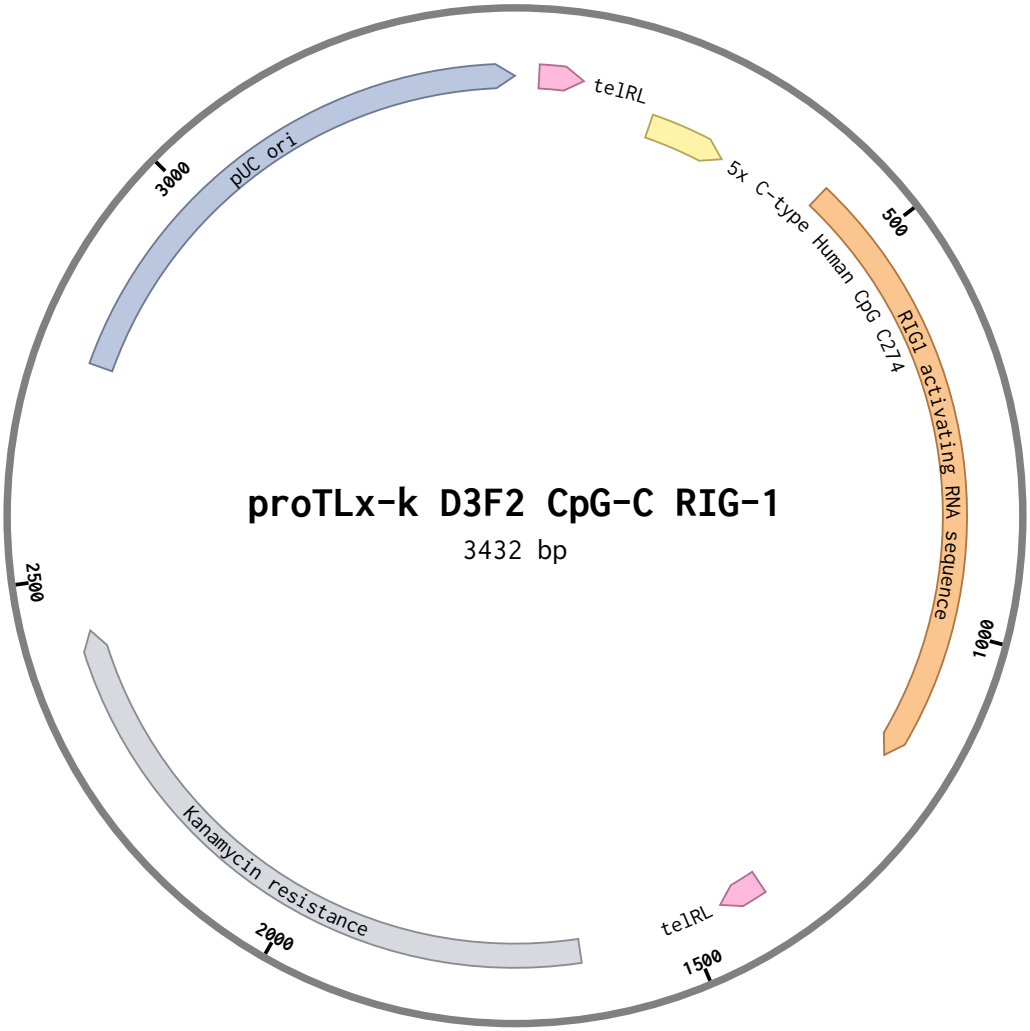



**Figure A.7.** Plasmid map of Plasmid map of proTLx-κ CpG-C RIG-I

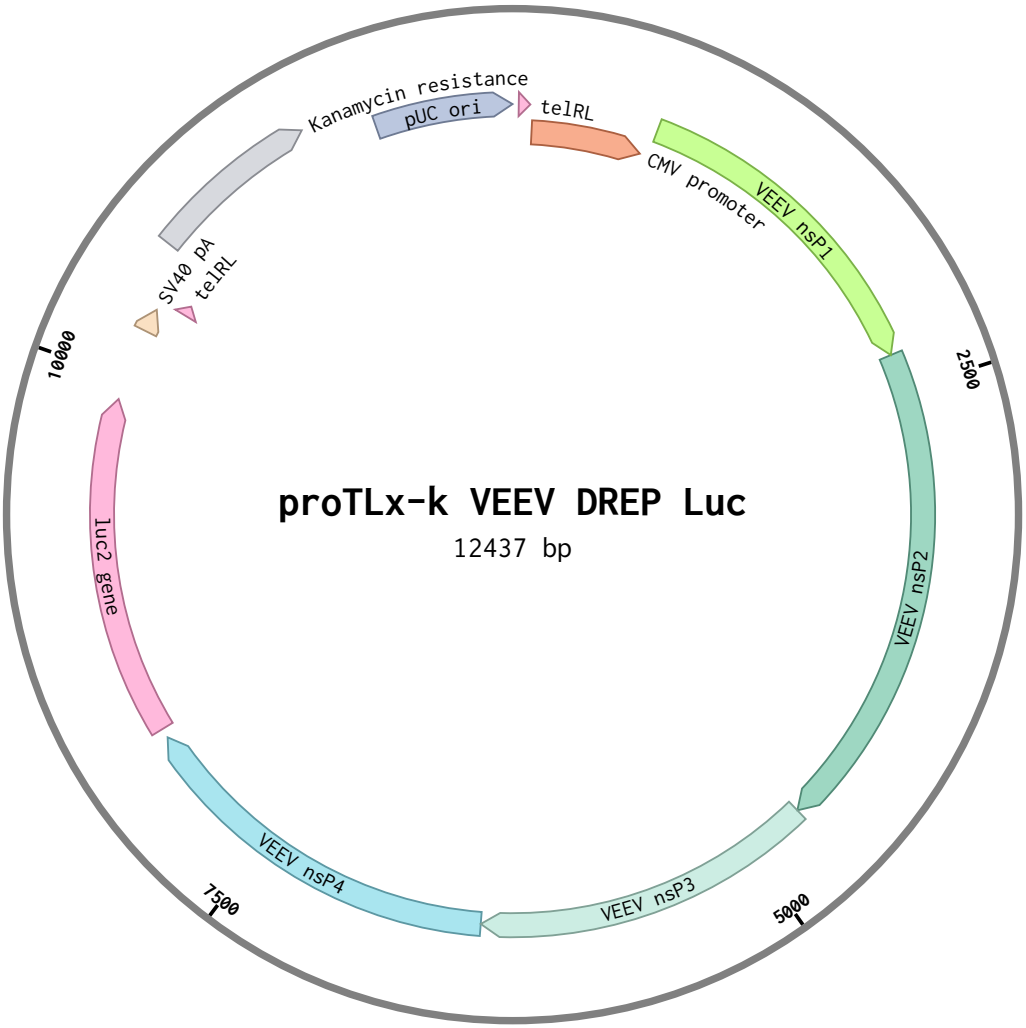



**Figure A.8.** Plasmid map of proTLx-κ VEEV DREP Luc

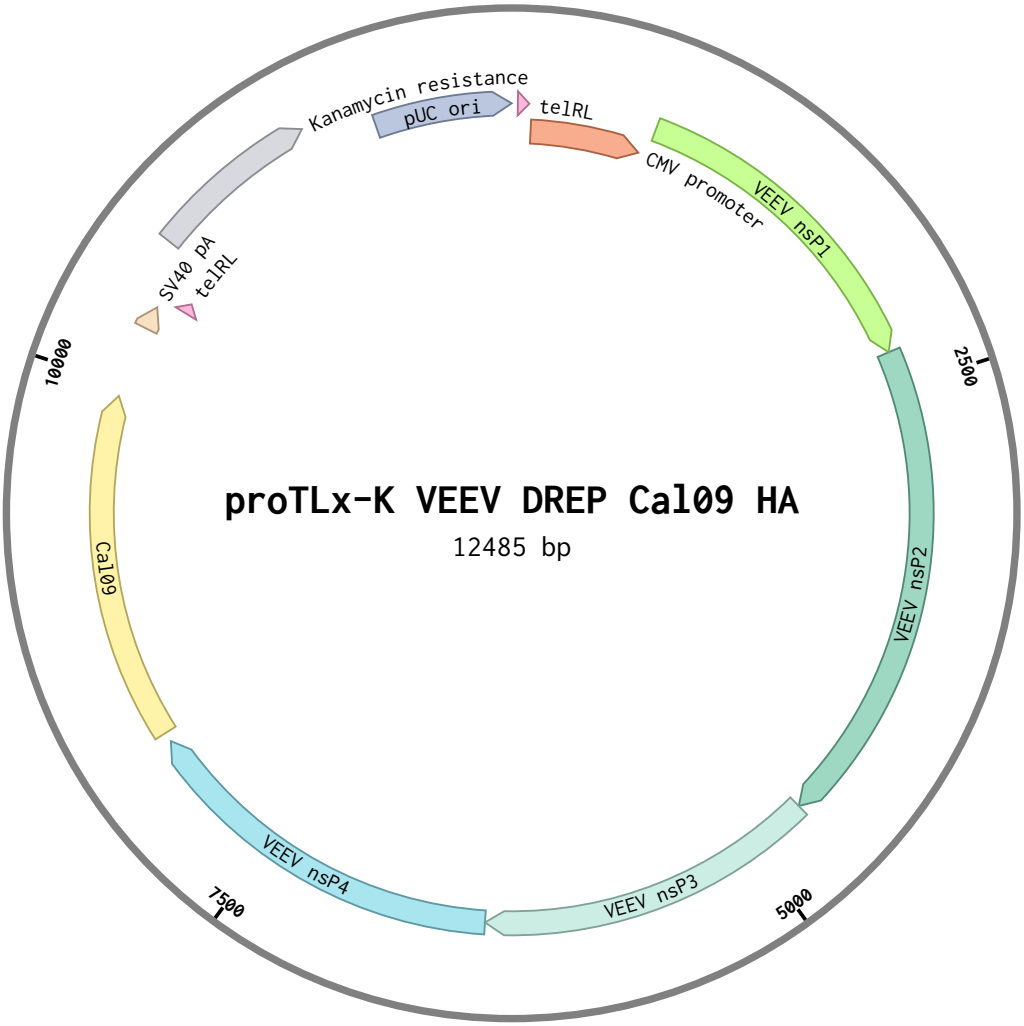



**Figure A.9.** Plasmid map of proTLx-κ VEEV DREP Cal09 HA

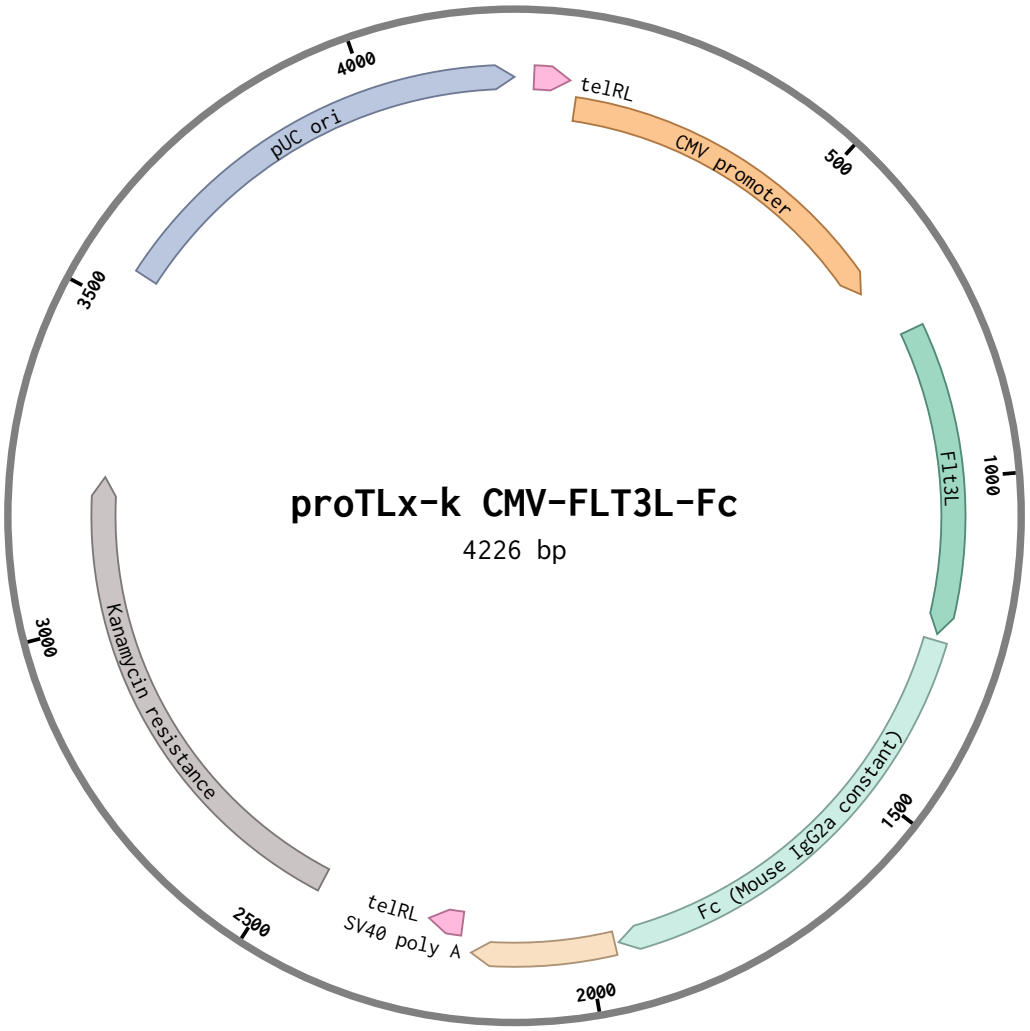



**Figure A.10.** Plasmid map of proTLx-κ CMV-Flt3l-Fc

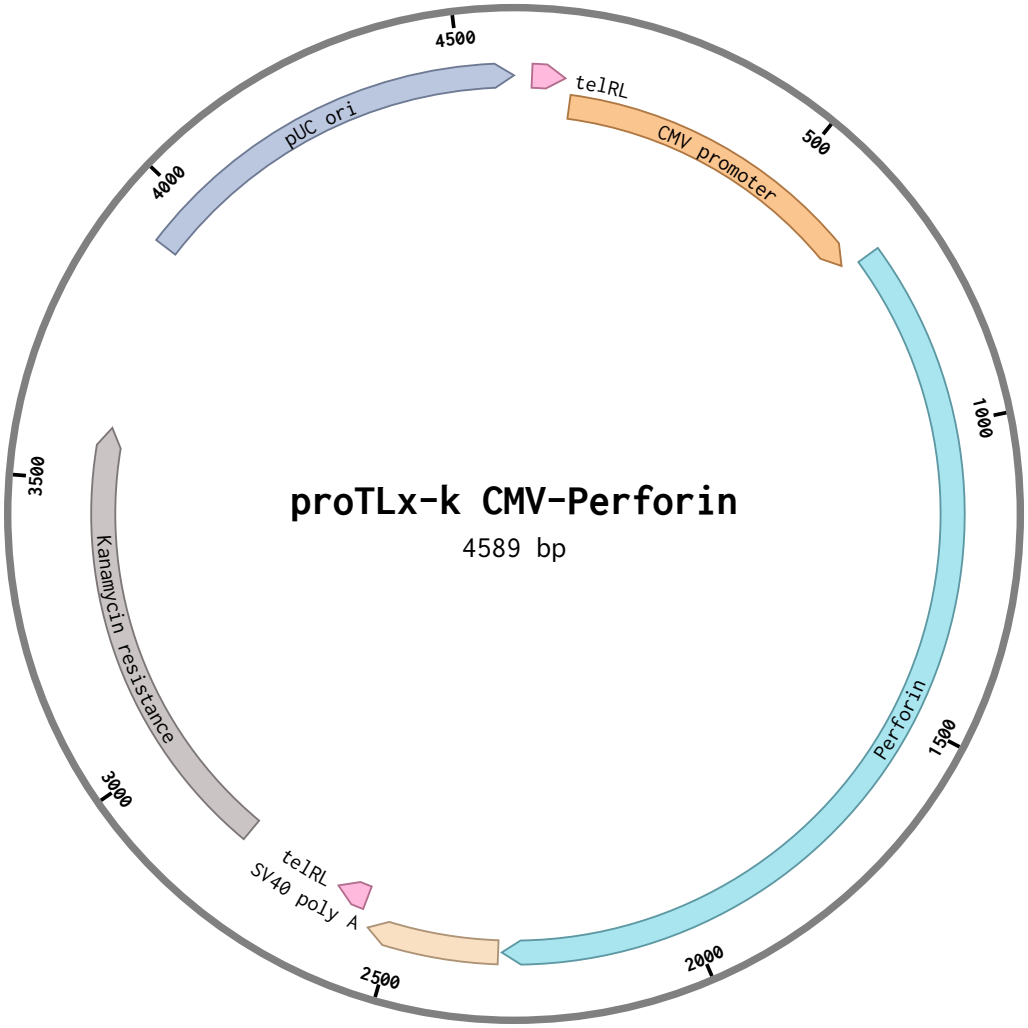



**Figure A.11.** Plasmid map of proTLx-κ CMV-Perforin

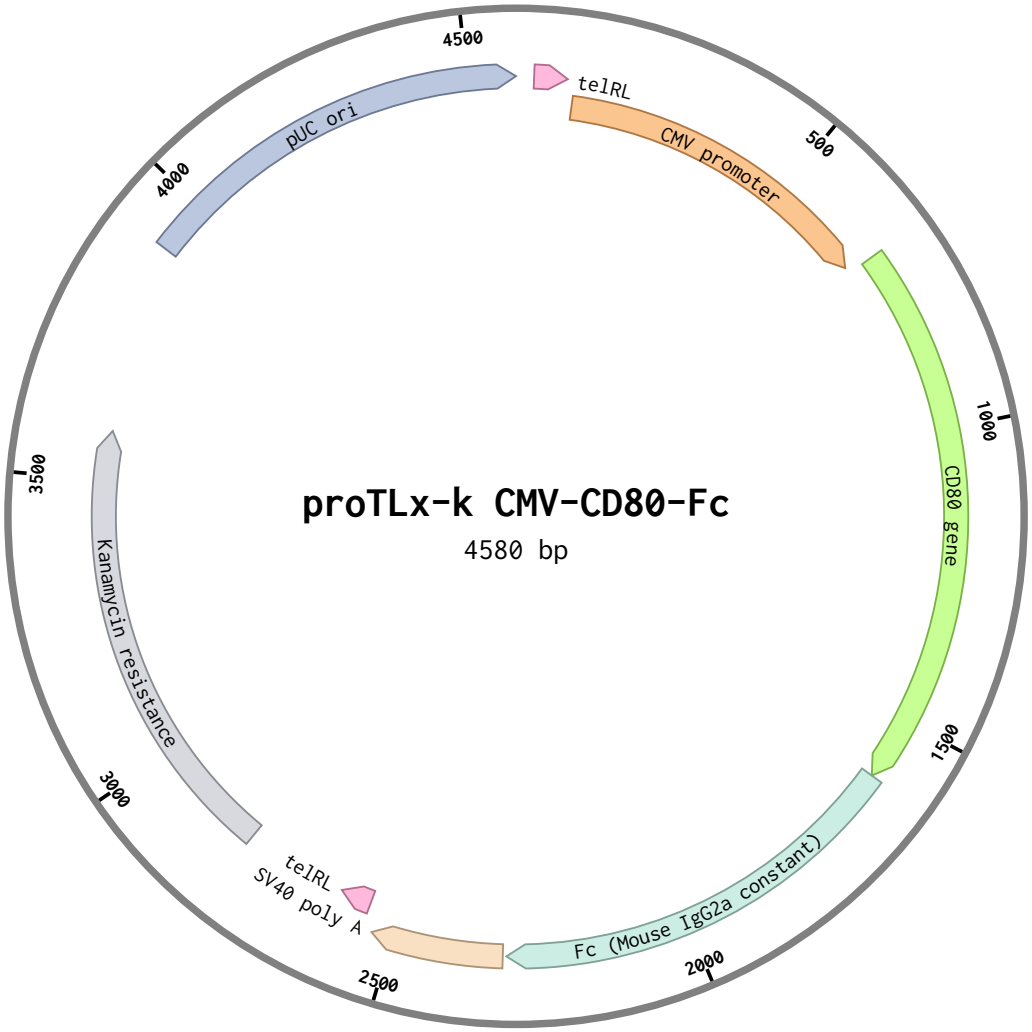



**Figure A.12.** Plasmid map of proTLx-κ CMV-CD80-Fc